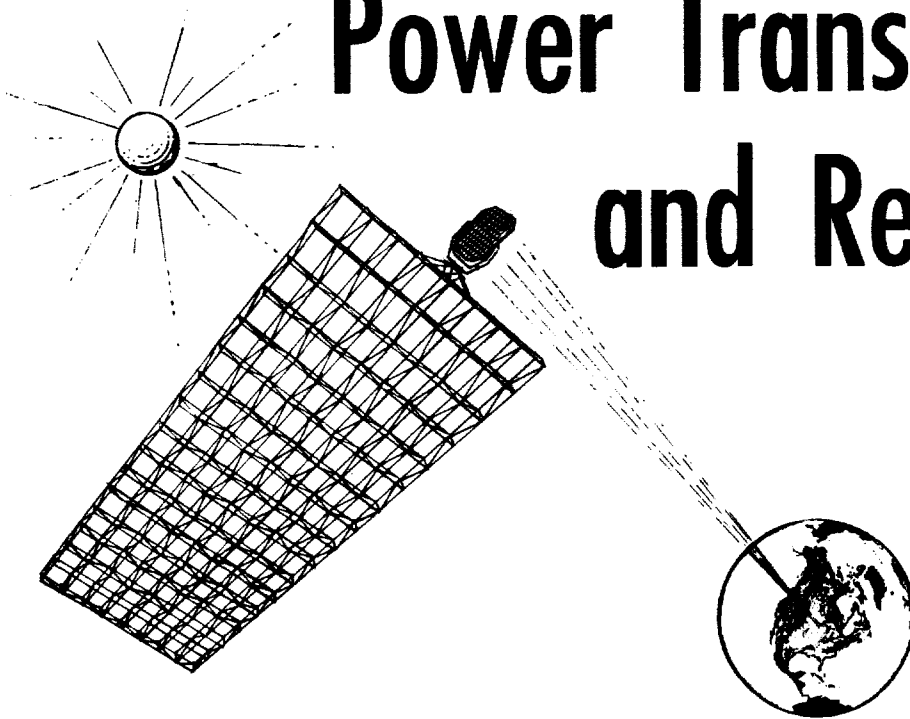


NASA Conference Publication 2141

Solar Power Satellite Microwave Power Transmission and Reception



*Proceedings of a workshop held at
Lyndon B. Johnson Space Center
Houston, Texas
January 15-18, 1980*

NASA

NASA Conference Publication 2141

Solar Power Satellite Microwave Power Transmission and Reception

*R. H. Dietz, Coordinator
Lyndon B. Johnson Space Center
Houston, Texas*

Proceedings of a workshop sponsored by
National Aeronautics and Space Administration
and held at Lyndon B. Johnson Space Center
January 15-18, 1980

NASA

National Aeronautics
and Space Administration

**Scientific and Technical
Information Office**

1980

Foreword

This publication is a compilation of the papers presented at the Solar Power Satellite (SPS) Workshop on Microwave Power Transmission and Reception held at the Lyndon B. Johnson Space Center, Houston, Texas, January 15-18, 1980. The workshop was conducted as part of the technical assessment process of the DOE/NASA SPS Concept Development and Evaluation Program. All aspects of SPS microwave power transmission and reception were addressed including studies, analyses, and laboratory investigations. Conclusions from these activities were presented as well as critical issues and recommended follow-on work. The workshop was organized into eight sessions as follows: General, Microwave System Performance, Phase Control, Power Amplifiers, Radiating Elements, Rectenna, Solid State Configurations, and Planned Program Activities. This volume primarily documents the papers presented at the six technical sessions, plus conclusions and remaining issues presented at the general session.

The workshop review panel was chaired by Dr. John W. Freeman, Rice University Professor of Space Physics and Astronomy. The review panel consisted of individuals with experience and expertise in each of the areas relevant to microwave power transmission and reception. Panel members were: Dr. Robert C. Hansen, of R. C. Hansen Inc., Professor Bernard D. Steinberg of the University of Pennsylvania, Professor Aldo V. Da Rosa of the Stanford University Radioscience Laboratory, Mr. Harry Goldie of Westinghouse, Dr. Paul J. Tallerico of the Los Alamos Scientific Laboratory, and Professor William L. Wilson, Jr. of Rice University.

The papers contained herein are a comprehensive documentation of the numerous analytical and experimental activities on the SPS Microwave Power Transmission and Reception System. It is hoped that this volume will be a useful contribution to the field of power transmission and reception.

R. H. Dietz
SPS Microwave Systems
Lyndon B. Johnson Space Center

CONTENTS

Foreword	iii
--------------------	-----

SECTION I - GENERAL SESSION

SPS Microwave System Conclusions Presented at the General Session	3
Remaining Issues - Microwave System - Presented at the General Session	4

SECTION II - SYSTEM PERFORMANCE SESSION

System Performance Conclusions By G. D. Arndt/NASA, Johnson Space Center	7
Solar Power Satellite Microwave Power Transmission System Description Executive Summary By Gordon Woodcock/Boeing Aerospace Company	18
Initial MPTS Study Results - Design Considerations and Issues . By Owen E. Maynard/Raytheon Company	28
SPS Large Array Simulation By S. Rathjen, B. R. Sperber, E. J. Nalos/Boeing Aerospace Co.	33
Achievable Flatness in a Large Microwave Power Transmitting Antenna By R. C. Ried/NASA, Johnson Space Center	43
An Active Alignment Scheme for the MPTS Array By Richard Iwasaki/Axiomatix	46
Ionospheric Power Beam Studies By Lewis M. Duncan/Los Alamos Scientific Laboratory, and William E. Gordon/Rice University	52
Proposed Experimental Studies for Assessing Ionospheric Perturbations on SPS Uplink Pilot Beam Signal By Santimay Basu, Sunanda Basu/Emmanuel College	63
Conclusions Presented at the System Performance Session	74
Remaining Issues - Environmental - Presented at the System Performance Session	76

SECTION III - PHASE CONTROL SESSION

Active Retrodirective Arrays for SPS Beam Pointing	79
By Ralph Chernoff/Jet Propulsion Laboratory	
Performance Analysis and Simulation of the SPS Reference Phase Control System	102
By W. C. Lindsey, C. M. Chie/LinCom Corporation	
Design and Breadboard Evaluation of the SPS Reference Phase Control System Concept	119
By P. M. Hopkins, V. R. Rao/Lockheed Engineering and Manage- ment Services Company, Inc.	
Coherent Multiple Tone Technique for Ground Based SPS Phase Control	129
By C. M. Chie/LinCom Corporation	
An Interferometer-based Phase Control System	139
By James H. Ott, James S. Rice/Novar Electronics Corporation	
A Sonic Satellite Power System Microwave Power Transmission Simulator	141
By James H. Ott, James S. Rice/Novar Electronics Corporation	
SPS Phase Control Studies	144
By W. W. Lund, B. R. Sperber, G. R. Woodcock/Boeing Aerospace Company	
SPS Fiber Optic Link Assessment	154
By T. O. Lindsay, E. J. Nalos/Boeing Aerospace Company	
Ionospheric Effects in Active Retrodirective Array and Mitigating System Design	159
By A. K. Nandi, C. Y. Tomita/Rockwell International	
Conclusions Presented at the Phase Control Session	169
Remaining Issues - Presented at the Phase Control Session . . .	171

SECTION IV - POWER AMPLIFIER SESSION

High Efficiency SPS Klystron Design	175
By E. J. Nalos/Boeing Aerospace Company	
High Efficiency Klystron for the SPS Application	185
By A. D. LaRue/Varian Associates, Inc.	
Analytic Investigation of Efficiency and Performance Limits in Klystron Amplifiers Using Multidimensional Computer Programs; Multistage Depressed Collectors; and Thermionic Cathode Life Studies	206
By H. G. Kosmahl/NASA, Lewis Research Center	

Progress Report on the Adapting of the Crossed-field Directional Amplifier to the Requirements of the SPS	214
By William C. Brown/Raytheon Company	
Conclusions Presented at the Power Amplifier Session	223
Remaining Issues - Presented at the Power Amplifier Session	224

SECTION V - RADIATING ELEMENTS SESSION

Reference System Description	227
By C. D. Lunden, W. W. Lund, E. J. Nalos/Boeing Aerospace Company	
The Resonant Cavity Radiator (RCR)	235
By K. G. Schroeder, R. L. Carlise, C. Y. Tomita/Rockwell International	
Evaluation of "Thick Wall" Wave Guide Element	245
By Ervin J. Nalos/Boeing Aerospace Company	
Method for Precision Forming of Low-cost, Thin-walled Slotted Waveguide Arrays for the SPS	253
By William C. Brown/Raytheon Company	
Considerations for High Accuracy Radiation Efficiency Measurements for the Solar Power Satellite Subarrays	256
By D. J. Kozakoff, J. M. Schuchardt, C. E. Ryan/Georgia Institute of Technology	
Conclusions Presented at the Radiating Elements Session	266
Remaining Issues - Presented at the Radiating Elements Session	267

SECTION VI - RECTENNA SESSION

The History of the Development of the Rectenna	271
By William C. Brown/Raytheon Company	
Rectenna System Design	281
By G. R. Woodcock/Boeing Aerospace Company, and R. W. Andryczyk/General Electric	
Rectenna Session: Micro Aspects	291
By Dr. Ronald J. Gutmann/Rensselaer Polytechnic Institute	
A Theoretical Study of Microwave Beam Absorption by a Rectenna	300
By James H. Ott, James S. Rice, Donald C. Thorn/Novar Electronics Corporation	
Rectenna Array Measurement Results	307
By Richard M. Dickinson/Jet Propulsion Laboratory	

Conclusions Presented at the Rectenna Session	317
Remaining Issues - Presented at the Rectenna Session	319

SECTION VII - SOLID STATE CONFIGURATIONS SESSION

Microwave Power Transmission System Workshop	323
By Woolsey Finnell/NASA, Marshall Space Flight Center	
Modified Reference SPS with Solid State Transmitting Antenna . .	328
By G. R. Woodcock, B. R. Sperber/Boeing Aerospace Company	
SPS Solid State Antenna Power Combiner	338
By G. W. Fitzsimmons/Boeing Aerospace Company	
Solid State Systems Concepts	348
By K. G. Schroeder, I. K. Petroff/Rockwell International	
Solid State Device Technology for Solar Power Satellite	358
By David G. Weir/RCA	
Progress Report on Solid State Sandwich Concept - Designs, Considerations and Issues	367
By Owen E. Maynard/Raytheon Company	
Conclusions Presented at the Solid State Configuration Session .	371
Remaining Issues - Presented at the Solid State Configuration Session	372

SECTION I
GENERAL SESSION

Chairman: R. H. Dietz
NASA, Johnson Space Center

SPS MICROWAVE SYSTEM CONCLUSIONS PRESENTED AT THE GENERAL SESSION

1. Microwave Power Transmission - Transferring gigawatt power levels between two points using microwaves is feasible.
2. One Antenna Vs Multiple Antennas - Each SPS microwave power transmission system should use one transmit antenna with contiguous radiating subarrays rather than multiple separate antennas.
3. Frequency - The power transmission frequency of 2.45 GHz has been determined to have advantages for power transmission and reception based on system tradeoffs including (1) transmit antenna and rectenna sizing, (2) propagation effects through the atmosphere, (3) hardware technology projections, and (4) ISM band utilization.
4. Microwave System Sizing - Transmit antenna size (1 Km), rectenna size (10 Km minor axis) and power delivered to the utility grid (5 GW) have been determined based on the minimum cost of electricity per kilowatt hour. The tradeoffs assumed a maximum thermal limit on the transmit antenna of 21 kW/m², (tube configuration), maximum power density through the ionosphere of 23 mW/cm², and the current projections of microwave system efficiencies. A microwave system using solid state power amplifiers will have a different thermal limit and different system efficiencies, resulting in different system sizes.
5. Type of Transmitting Antenna - The transmitting antenna should be a planar phased array in order to meet the requirement of maximum power transfer efficiency.
6. Type of Receiving Antenna - An SPS rectenna concept theoretically capable of recovering all RF energy impinging on its surface with direct RF-to-DC conversion provides the required maximum conversion efficiency.
7. Antenna Construction and Subarray Alignment - Construction of a 1 km diameter antenna array with a ± 1 minute flatness tolerance appears to be within the state of the art if low CTE (coefficient of thermal expansion) materials are used. Antenna subarray alignments, both initially and real-time, can be maintained to ± 3 minutes by the use of Azimuth-Elevation mounts and laser measurement techniques.
8. Power Beam Stability - Based on analytical simulations and experimental evaluations it appears feasible to automatically point and focus the power beam with minimum beam wander (± 250 m) and automatic fail safe operation (rapid beam defocusing).

REMAINING ISSUES - MICROWAVE SYSTEM
(BOTH TUBE AND SOLID STATE CONFIGURATIONS)
PRESENTED AT THE GENERAL SESSION

1. System performance
2. Noise and harmonic performance
3. Antenna transmission efficiency
4. Beam forming accuracy
5. Beam pointing accuracy
6. Power beam/pilot beam isolation
7. Mechanical alignment/tolerances
8. End-to-end system efficiency
- *9. Corona
- *10. Multipacting
- *11. Plasma
12. RFI effects on selected hardware
13. Unit costs
14. Alternate technologies
 - a. Solid state
 - b. Magnetron
15. Possible new technologies
 - a. Photoklystron
 - b. Gyrocon

*Tube configuration only.

SECTION II

SYSTEM PERFORMANCE SESSION

Chairman: Dr. G. Dickey Arndt
NASA, Johnson Space Center

SYSTEM PERFORMANCE CONCLUSIONS

G. D. Arndt

NASA - Johnson Space Center

1. System Sizing
 - o Reduced Power Levels
 - o Antenna Diameters Smaller than 1 Km

The initial sizing for the satellite power station was a 1-kilometer transmit array with 5 gigawatts of DC power out of the rectenna. There are, however, some advantages in having a smaller system size. Commercial utility companies can probably handle 1-gigawatt increments easier than 5 gigawatts; the implementation cost of 1-gigawatt system is lower; and the sidelobe radiation levels near the rectenna are lower. Disadvantages of smaller systems include lower end-to-end microwave transmission efficiency and an increase in the overall cost of electricity (mills per kilowatt-hour).

The downlink operating frequency is another trade-off consideration. The SPS reference system operates at 2.45 gigahertz, which is the center of a 100-megahertz band reserved for government and nongovernment industrial, medical, and scientific (IMS) use. This band has the advantage that all communication services operating within the 2450 ± 50 megahertz limits must accept any interference from other users. There is another IMS band at 5.8 gigahertz which should be considered. One way to reduce the terrestrial land usage requirements for the SPS rectenna is to increase the operating frequency while maintaining the same antenna size. This reduction in rectenna size must, however, be traded off against the large temporary degradation in transmission efficiency under extremely adverse weather conditions at the higher frequency.

The end-to-end microwave transmission efficiency for smaller SPS systems operating at different frequencies will not be determined. The nominal microwave transmission efficiency, from the rotary joint in the satellite to the DC/DC power interface at the output of the rectenna, is shown in figure 1. This end-to-end efficiency, for a frequency of 2450 megahertz, may be written

$$\text{Microwave Eff} = 0.805 \text{ Eff}_{\text{coll}} \times \text{Eff}_{\text{conv}} \quad (1)$$

For the reference system, $\text{Eff}_{\text{coll}} = 0.88$ and $\text{Eff}_{\text{conv}} = 0.89$, and the microwave link efficiency is 63 percent. This efficiency will be used as a reference for comparing smaller SPS systems. In equation 1, the rectenna collection efficiency Eff_{coll} is a function of incident power density and incremental rectenna area while the conversion efficiency Eff_{conv} varies only with power density. The RF-DC conversion efficiency

Figure 1. - Nominal efficiencies for the microwave system (2450 MHz)

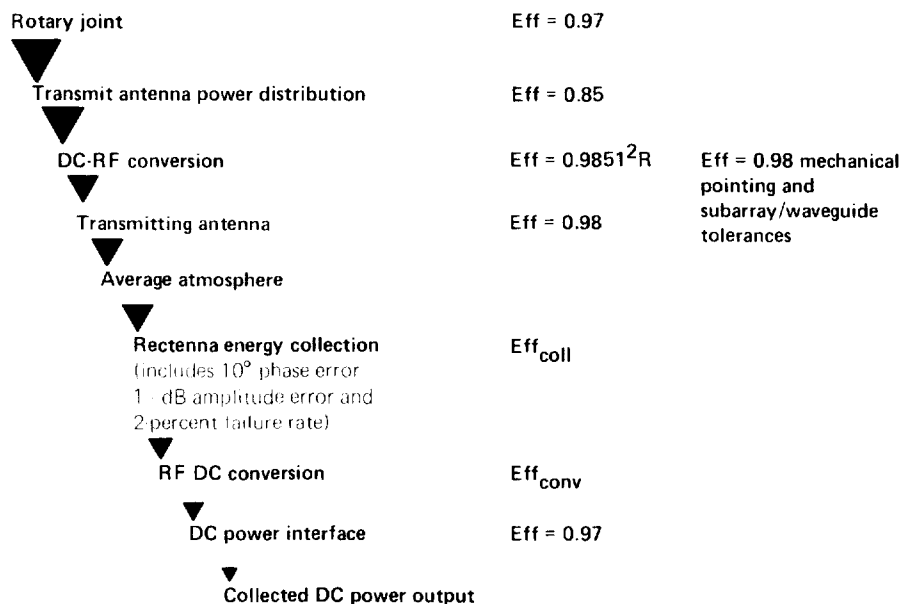
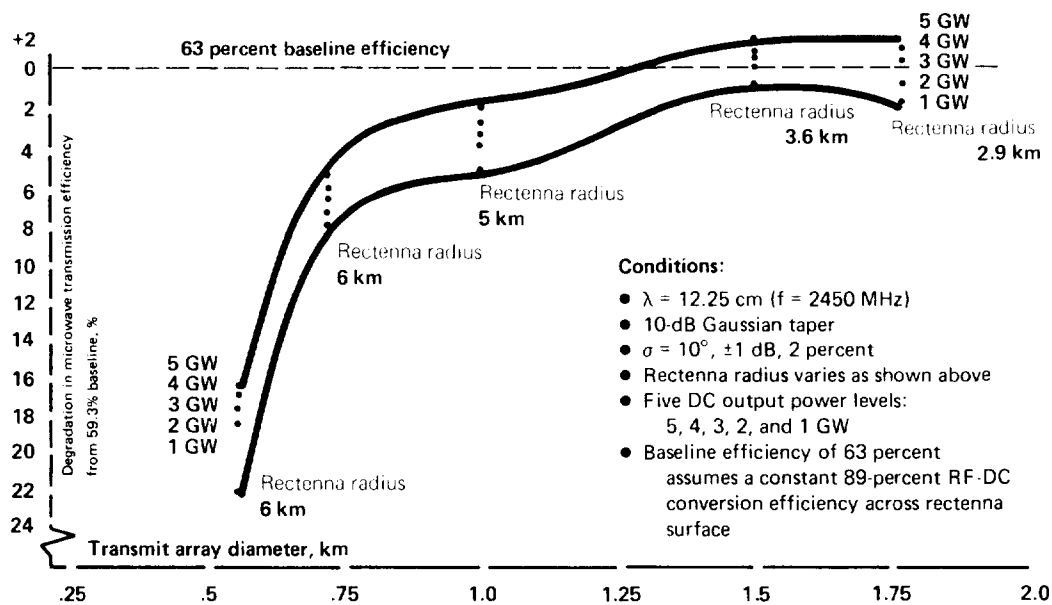


Figure 2. - SPS performance at 2450 MHz as a function of antenna size and power



depends on the input power level to the rectifying diodes connected to the half-wave dipole elements in the rectenna. During the past several years, excellent progress has been made in developing higher efficiency diodes, particularly at lower levels. This RF-DC conversion efficiency, which is the collection efficiency of the individual dipole elements times the diode rectifying efficiency, varies from 70 percent at 0.04 milliwatt per square centimeter to 90 percent at 10 milliwatts per square centimeter as a function of incident power density. These data assume a 3 percentage point improvement in the next decade over the present achievable conversion efficiency.

The degradations in end-to-end microwave efficiency for smaller SPS sizes are summarized in figures 2 and 3 for operating frequencies of 2450 and 5800 megahertz respectively. The 63 percent reference efficiency is that performance expected for a 1-kilometer, 5-gigawatt SPS system operating with a constant 89 percent RF-DC conversion efficiency in the rectenna. The difference in performance between the 5-gigawatt and the 1-gigawatt systems as shown in figure 2 is due to a reduction in rectenna conversion efficiency at the reduced power density levels associated with the 1-gigawatt system. Also, for transmit arrays with a diameter less than 1 kilometer, the power beam is dispersed over a wider area at the ground due to reductions in antenna gain. This dispersion reduces the amount of energy intercepted by the rectenna and further reduces the RF-DC conversion efficiency. The data indicate that smaller SPS powers are feasible, provided the antenna size is not reduced; that is, a 1-kilometer, 1-gigawatt SPS system will have only a 4 to 5 percent (percentage points) reduction in microwave transmission efficiency as compared to a 5-gigawatt system.

The transmission efficiency for systems operating at 5800 megahertz as given in figure 3 is interesting in that there is very little degradation in performance at the reduced power levels. The reason is that the power density levels at the rectenna are considerably higher for the 5800-megahertz systems, and hence little degradation in RF-DC conversion efficiency occurs as the power is reduced. There is also a constant degradation relative to the 59.3 percent reference efficiency due to lower efficiencies in several of the microwave subsystems operating at the higher 5800-megahertz through a heavy rain, rectennas for these systems could have intermittent power reductions unless located in dry, southwest regions.

There is a significant reduction in rectenna size at the higher frequency as shown in figure 3. If rectenna costs and land usage requirements become major factors, operating at 5800 megahertz should be seriously considered.

2. Startup/Shutdown Operations

- o Three sequences for startup/shutdown provide satisfactory performance

An SPS in synchronous orbit experiences solar eclipses by the earth, moon, and other SPS. The most important of these eclipses are by the earth, both in occurrence and duration. The satellite will be eclipsed daily by the earth for approximately six weeks during the spring and fall equinoxes, March 21 and September 21, respectively. Specifically there will be 43 eclipses centered around the spring equinox and 44 in the fall, for a total of 87 times per year. These eclipse periods will vary each day, with the time building up to a maximum of 75 minutes at the equinox. Except for the first and last days of each series, the satellite is totally eclipsed.

Because of switching conditions and transients in the DC power distribution system, the microwave system will be brought up (or shutdown) in controlled increments, rather than having on-off switching of 7 GW of power. The resultant microwave radiation patterns can vary greatly, depending upon the sequencies used for energizing the antenna. The beam patterns have been evaluated in order to reduce the environmental effects of the microwave radiation from the antenna under transient operating conditions.

Let us now examine what happens to the solar array during an eclipse. Both the solar cells and the structures will cool off quickly. The structure will drop to 70⁰K (-335⁰F) during the longest (72 minutes) occult period (Ref. 5). The solar cell temperature drops from its normal operating value of 310⁰K to 110⁰K at the end of 70 minutes. After emerging from the earth's shadow, cell temperatures rise quickly, particularly if the cells are open-circuited. A solar cell's output is a function of temperature and the cells will produce a higher output power for a few minutes until the temperature stabilizes. Since the voltage regulation to the klystron tubes is +5%, the tubes cannot be energized until near steady-state operating temperatures are reached in the solar array.

The operational procedure would be to open-circuit the solar cells prior to emergence from occultation, close to the DC power circuits in the solar array after the solar cell temperatures have stabilized near 310⁰K (a few minutes depending the length of the eclipse period), and then sequentially energize the klystron tubes in an optimum manner to minimize radiation effects.

The pattern characteristics for the main beam, sidelobes, and grating lobes were examined for eight types of energizing configurations which include:

1. Random - the antenna is starting at the center and progressing outward
2. Concentric rings - starting at the center and progressing outward
3. Concentric rings - beginning at the outer and progressing to the center
4. Line strips - center to the outside edge
5. Line strips - outside edge to the center

Figure 3. - SPS performance at 5800 MHz as a function of antenna size and power

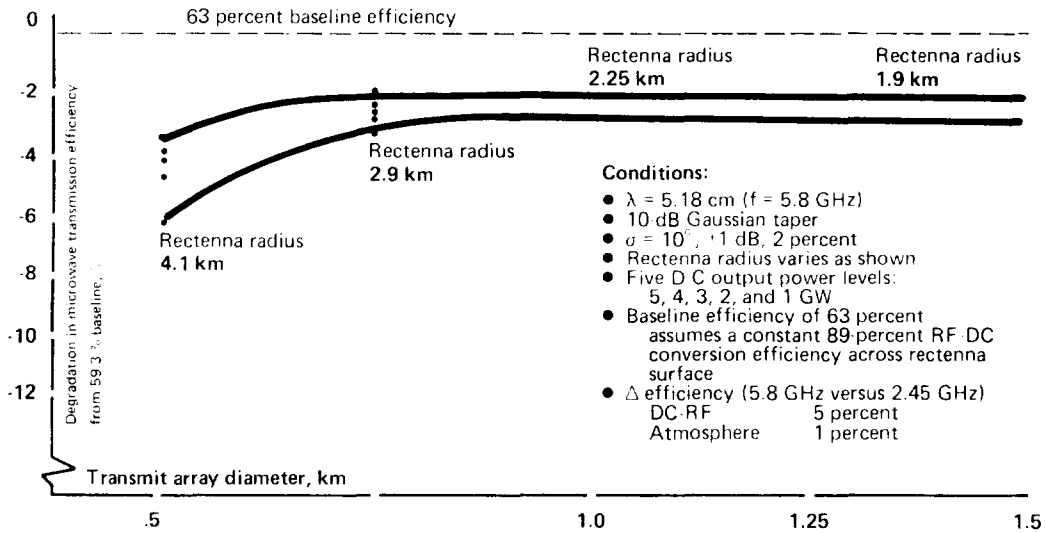
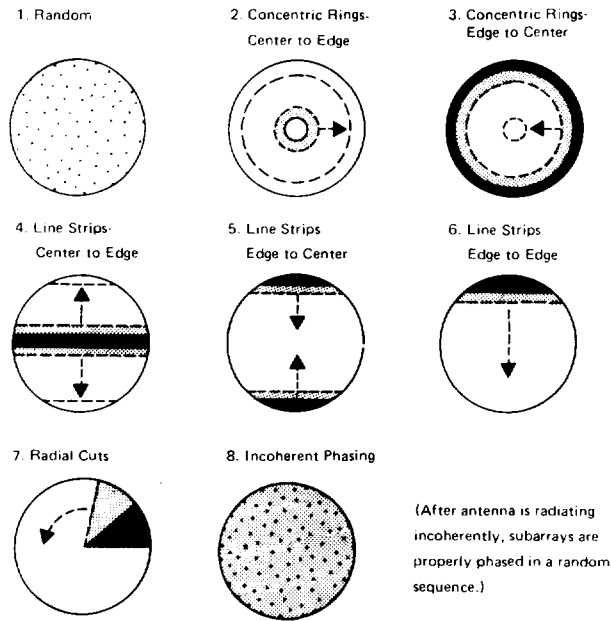


Figure 4. - Antenna startup/shutdown configurations



Note: Increments of 10% power are used for all sequences. Antenna illumination is a 10 dB gaussian taper.

Figure 5. Sidelobe Patterns for the Random Sequence

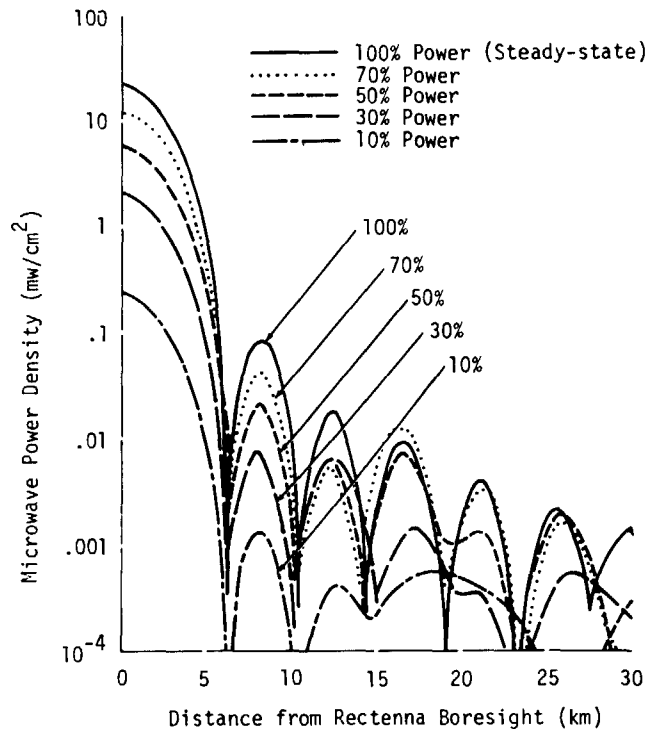
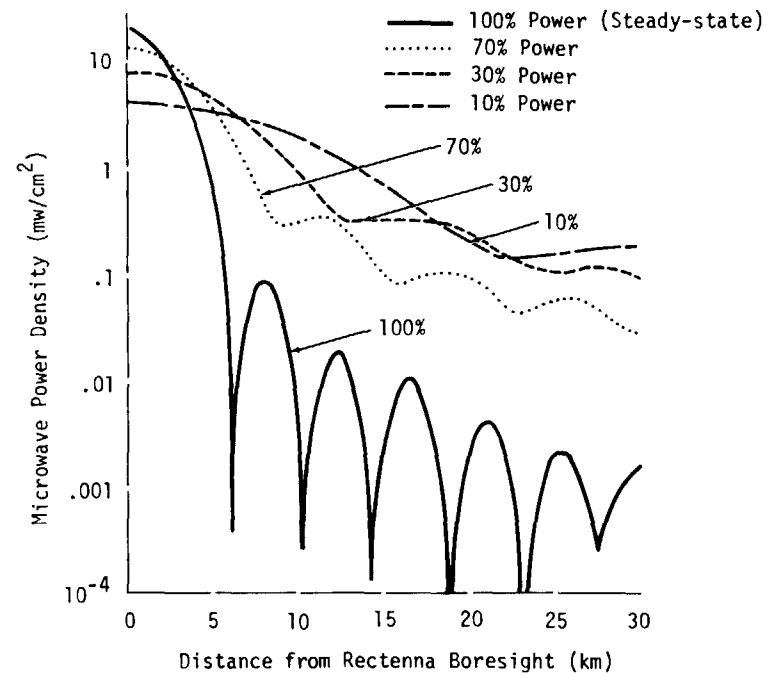


Figure 6. Sidelobe Patterns for Line Strips- Edge to Edge



6. Line strips - edge-to-edge
7. Radial cuts
8. Incoherent phasing

In each of these sequences shown in figure 4, the amount of antenna power is increased in ten discrete steps. For each of the configurations the reference error tolerances for random amplitude and phase errors throughout the antenna are included. The results are obtained through computer programs which simulate the 7220 subarrays as individual radiators properly phased together.

To briefly summarize the results, three sequences provided satisfactory performance in that the resultant sidelobe levels during startup/shutdown were lower than the steady-state levels present during normal operations. These three sequences were:

- o random
- o incoherent phasing
- o concentric rings - center to edge

As an example of the performance of the random sequence, the random startup is well-behaved in that the partial power patterns closely resemble the full power characteristics, only reduced in amplitude as shown in figure 5. As the radiated power is decreased the effective antenna area decreases, and the far sidelobe levels increase. The peaks and nulls of the sidelobes remain spatially stationary as the antenna radiating area changes.

An example of a poor startup/shutdown sequence is shown in figure 6, i.e., line strips - edge to edge. By taking successive vertical strips at one edge of the antenna and progressing to the other edge, the peaks and nulls of the sidelobes moves inward towards the rectenna with additional power. These patterns have sidelobe levels several orders of magnitude greater than for steady-state. In conclusion a proper choice of sequences should not cause environmental problems due to increased microwave radiation levels during the short time periods of energizing/de-energizing the antenna.

3. Antenna/Subarray Mechanical Alignments
 - o Alignment requirements determined by grating lobe peaks and scattered power levels
 - o Antenna alignment requirement is 1 min or 3 min depending upon phase control configuration.

There are two types of mechanical misalignments: (1) a systematic tilt of the entire antenna structure produced by attitude control system errors, and (2) a random tilt of the individual subarrays produced by antenna bending or subarray alignment errors. The rectenna collection efficiency (which is an indication of the amount of scattered power) as a function of systematic (structure) and random (subarray) tilts is shown in figure 7. It is interesting to note that the two tilts have the same degradation in collection efficiency per arc

Figure 7. - Antenna tilt (min)

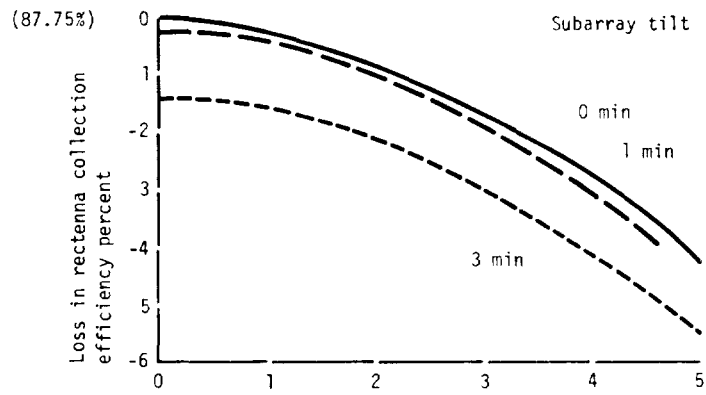
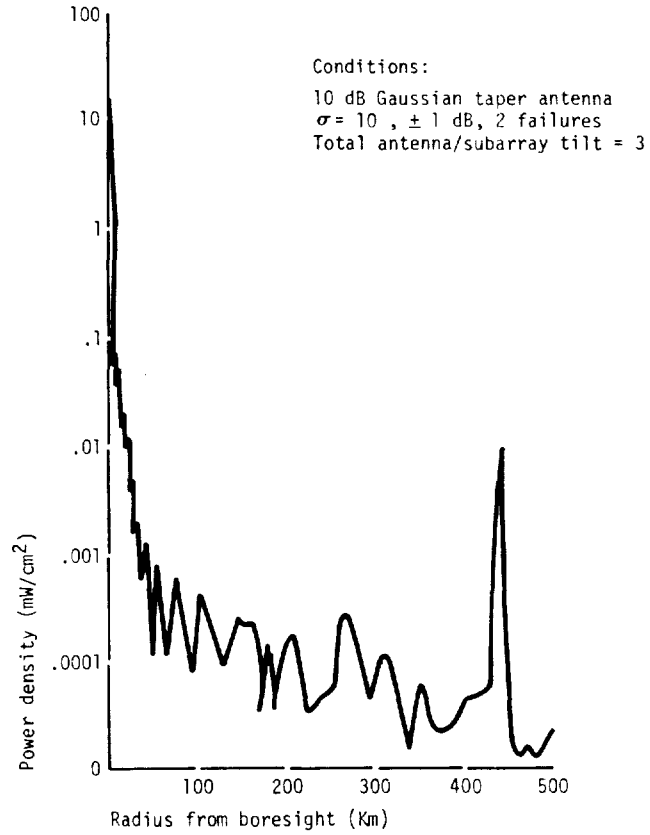


Figure 8. - Peak density for sidelobes and grating lobe as a function of range from rectenna.



minute of misalignment. It will be shown later that the systematic tilt has an order of magnitude greater effect on grating lobe levels than the random tilts.

The antenna and subarray/power module misalignments produce well-defined grating lobes. The grating lobes occur at spatial distances corresponding to angular directions off-axis of the antenna array where the signals from each of the subarrays add in-phase. When the mechanical boresights of the subarrays are not aligned with the pilot beam transmitter at the rectenna, the phase control system will still point the composite beam at the rectenna; however, some of the energy will be transferred from the main beam into the grating lobes. The grating lobes do not spatially move with misalignment changes but their amplitudes are dependent upon the amount of mechanical misalignment. The distance between maxima for the grating lobes is inversely proportional to the spacings between phase control centers on the transmit antenna. If the phase control is provided to the 10.4 meter X 10.4 meter subarray level, grating lobe peaks occur every 440 Km. If the phase control system is extended down to the power module level, the grating lobes will be spatially smeared and the peaks greatly reduced in amplitude. This improvement in grating lobe pattern would be due to differences in spacings between the power tubes within the antenna. An example of the first grating lobe peak for a total antenna/subarray tilt of 3.0 arc-minutes is shown in figure 8.

Based upon environmental considerations, the grating lobes are constrained to be less than $.01 \text{ mw/cm}^2$. The total mechanical alignment requirements for both the subarrays and the total antenna can be determined from this constraint. The amplitudes of the grating lobes for phase control to the power module level and an antenna tilt of 1 min is shown in figure 9. The locations and spacings of these grating lobes across the continental United States with the rectenna centrally located are shown in figure 10.

Conclusions from the antenna simulation studies are:

- (1) Systematic (antenna) tilt has an order of magnitude greater effect on grating lobe peaks than random (subarray) tilt.
- (2) The systematic tilt must be less than 1 min for phase control to the 10 meter square subarray level and 3 min for phase control to the power module level in order for the grating lobe peaks to meet the guideline of $.01 \text{ mw/cm}^2$.
- (3) Random (subarray) tilt is limited to 3 min in order to maintain a 2% or less drop in rectenna collection efficiency. The random tilt has a profound impact on the amount of scattered microwave power but only a very small contribution to the grating lobe peaks.

4. Scattered Microwave Power

o System error parameters have been defined to minimize scattered power

Figure 9. - Grating lobe peaks for 10 meter subarrays and phase control 10 power modules (tubes)

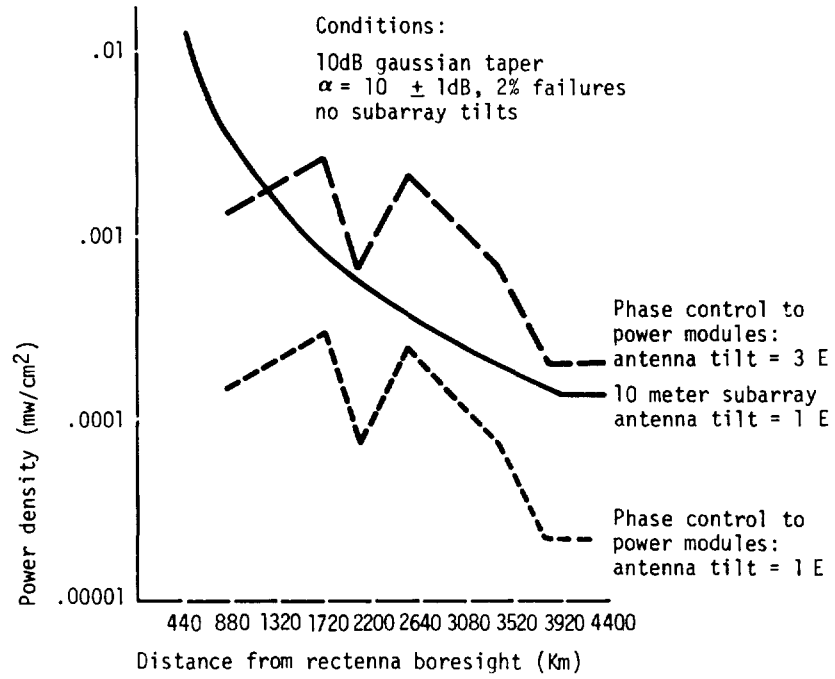
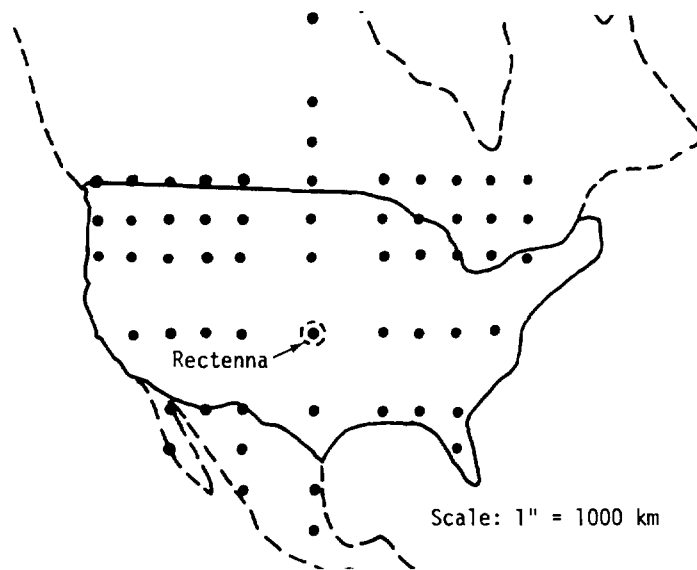


Figure 10. - Grating locations for a single beam.



The relative importance of the electrical and mechanical tolerances on the rectenna collection efficiency is summarized in figure 11. The baseline error parameters are $\sigma = 10^0$ rms phase error, + 1 dB amplitude error, 2% failures, .25 inch mechanical gap between the 10. meter X 10. meter subarrays, antenna tilt < 1 min (attitude control) and subarray tilt < 3 min. The scattered microwave power is the extra power lost (not incident upon the rectenna) due to the error tolerances. The rectenna would intercept 95.3% of the total power transmitted by a perfect system; the error tolerances reduce this amount of received power to 86.0% of the transmit power.

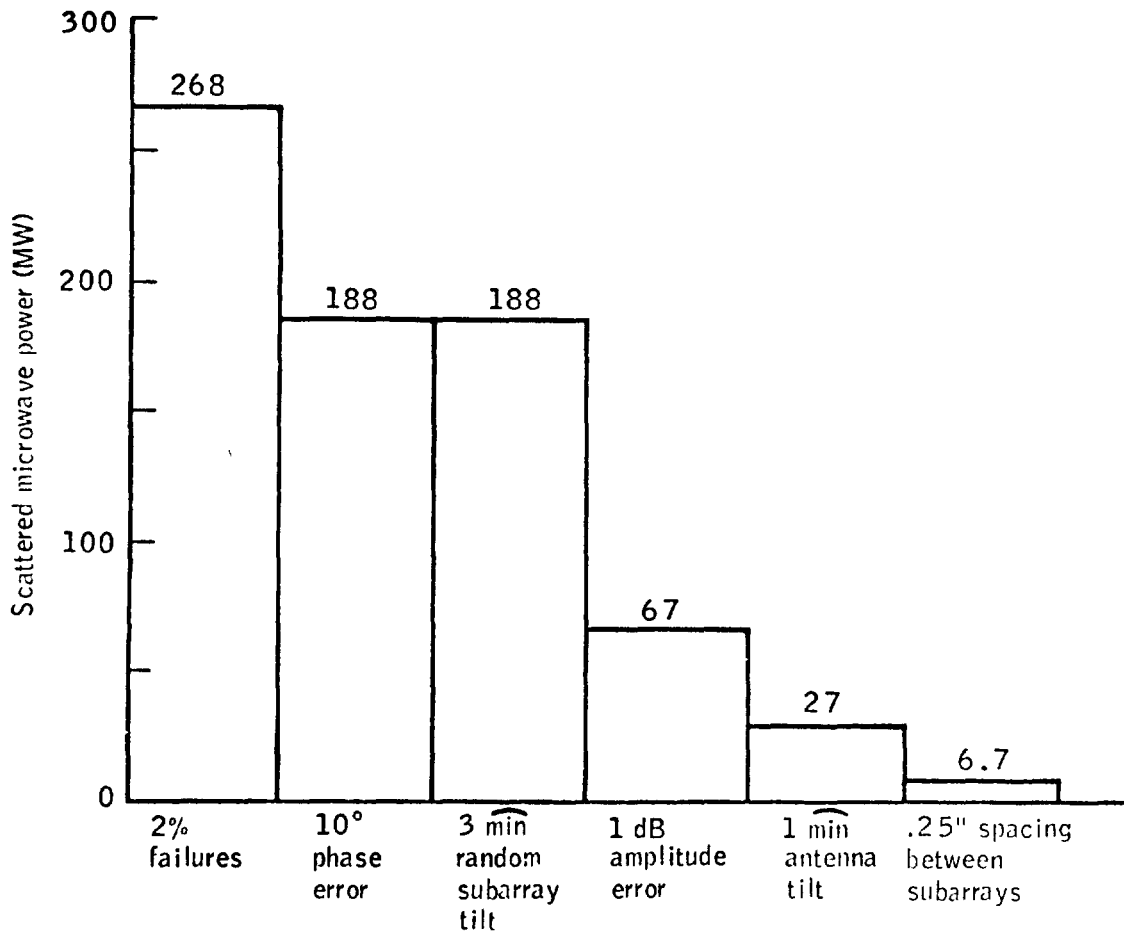


Figure 11 - Scattered microwave power due to electrical and mechanical errors. (10 meter subarray).

**SOLAR POWER SATELLITE
MICROWAVE POWER TRANSMISSION
SYSTEM DESCRIPTION EXECUTIVE SUMMARY**

By Gordon Woodcock/Boeing

BACKGROUND

The idea of beaming baseload electric power from solar power satellites in space to utility receivers on Earth originated with experiments in microwave power beaming to small helicopters by W. C. "Bill" Brown of Raytheon in the 1960's. Peter Glaser's proposal for a Satellite Solar Power Station in 1968 included a conceptual system for microwave power beaming to deliver the solar energy to Earth.

The first NASA study of SPS was performed for the Lewis Research Center by A. D. Little, Grumman, Raytheon, and Spectrolab. That study, completed in 1972, selected 2450 MHz as the transmission frequency and determined that apertures on the order of 1 km at the satellite and 10 km at the ground receiver would provide efficient energy transfer. At that time it was estimated that 10,000 megawatts could be delivered through a single transmission link of this size. Subsequent studies, using a provisional intensity limit at Earth of 23 mw/cm², somewhat less efficient dc-to-RF conversion efficiency, and more thorough thermal analyses, have reduced the single-link maximum power to 5000 megawatts.

The frequency selection of the original study was based on preliminary optimizations of energy transfer efficiency and cost. Higher frequencies lead to smaller apertures (and less power per link), but suffer additional atmosphere absorption and are expected to yield slightly lower dc-RF and RF-dc conversion efficiencies. Lower frequencies require larger apertures; the reference aperture is already uncomfortably large in the eyes of many reviewers. Present frequency allocations include industrial bands at 2450 and 5800 MHz. The present reference system has selected the lower of these two frequencies; preliminary analyses of the 5800 MHz option showed slightly higher costs if the same intensity limits were observed, but the 23 mw/cm² limit might well be raised at the higher frequency.

Frequency allocation for SPS was discussed at the 1979 WARC; no frequency was assigned but it was ruled that the U.S. could have such an assignment if the SPS is proven environmentally safe by further research.

SYSTEM SIZING

Selection of the microwave system power level is a problem of constrained optimization. The relevant constraints are illustrated in Figure 1. The most important factors are:

(1) Inefficiencies in conversion of dc electric power to microwave power result in waste heat that must be rejected to space by thermal radiation. The amount of heat that can be rejected per unit area is proportional to the fourth power of the absolute temperature of the heat rejection apparatus. Most of the heat appears at the RF amplifiers; the rejection capability is thus limited by the temperature limits of the amplifiers. This could be altered by refrigeration equipment (allowing heat to be rejected at temperatures above the amplifier limits) or by a large-scale heat transport system (allowing the heat rejection area to be larger than the transmitter aperture area). These alternatives have been avoided in the SPS reference systems in the interests of simplicity. For the reference system employing Klystron amplifiers, the heat rejection temperature is approximately 350C (=623K) permitting a thermal rejection capability of 4.5 kw/m² after emissivity and geometric factors are accounted. The net efficiency of the reference system is about 83% resulting in an RF power limit of about 22 kw/m². It should be mentioned that the design of the reference system allows heat rejection only from the back side of the transmitter. Some of the alternate systems, notably solid-state transmitters, may be designed to reject heat from both sides. The solid-state system is, however, limited to heat

rejection temperatures on the order of 100C and is, therefore, limited to RF power densities roughly 1/4 those of the reference system.

(2) The maximum RF power intensity is in the ionosphere. This limit has presently been set at 23 mw/cm² based on theoretical considerations of ionosphere heating by the beam. The limit is quite uncertain and could be set higher or lower as a result of further research. (Preliminary results of heating tests suggest the possibility of a higher limit, but these results are not conclusive at present.) If the ionosphere limit can be raised, other factors, such as the tolerance of birds that may fly through the beam, may become important. This constraint sets the maximum power per unit area that can be derived from the receiving antenna. The average, of course, is less.

(3) The maximum allowable sidelobe level (RF intensity outside the receiving site controlled area) may affect aperture illumination factors. The transmitter aperture is nonuniformly illuminated to reduce sidelobes and improve link efficiency. Under certain assumptions one can show that a Gaussian amplitude taper is optimal. (For finite apertures the Gaussian must be truncated.) Other illumination tapers with similar shape yield nearly the same results. In any event it is necessary to quantize the actual illumination taper to conform to the various permitted subarray configurations (see below). An important tradeoff is the degree of truncation of the taper. The truncation is normally expressed as the ratio of center intensity to edge intensity. For example, a 10-db taper (the reference) indicates a factor of 10 reduction of intensity from center to edge. The greater the taper, the higher the link efficiency and the less the sidelobe intensity, as shown in Figure 2. The figure also shows the actual quantized taper as compared to the ideal truncated Gaussian.

One might think that the more taper the better, but there are adverse factors. Greater taper leads to (a) More beam spread as shown in Figure 3; (b) A smaller value of average-to-peak intensity at both the receiver and transmitter, as shown in Figure 4. Therefore, more taper leads to lower link power and larger apertures, both tending to increase system cost per kilowatt of generating capacity. These effects offset the cost reduction from increasing efficiency; there is an economically optimal illumination taper. For the reference system, the optimum is 10 db and the taper was selected on this basis.

The level of the first sidelobe that results from the reference taper and center beam intensity limit is about 0.1 mw/cm². As this is below present microwave exposure limits in the U.S., the sidelobe level did not enter into the illumination taper selection. If standards below 0.1 mw/cm² are applied to SPS then the reference taper may have to be adjusted to comply. As an example, a taper of 17 db (assuming no change in center beam strength) will place the first sidelobe level at 0.01 mw/cm². The system power output is reduced to about 4500 megawatts, the transmitter aperture increases to 1.2 km, and the ideal aperture-to-aperture efficiency increases from .965 to .990. As a result, the system cost per kilowatt is increased slightly.

The transmitter-receiver aperture product may be expressed as $2\tau R\lambda$, where τ is a factor dependent on the transmitter illumination function, R is the range, and λ is the wavelength. As noted, the aperture-to-aperture beam efficiency is also dependent on the illumination function. For a given efficiency in the SPS range of interest, i.e. 0.8, the minimum value of τ will result from a truncated Gaussian amplitude taper with the transmitter phase front focused at the receiver (for typical SPS transmitters, a planar wavefront gives essentially equivalent results). If one is willing to accept larger values of τ , more flexibility is available for controlling the beam characteristics at the receiver. One may, for example, improve the average-to-peak intensity ratio as illustrated in Figure 5. This could reduce the rectenna land use by a factor on the order of 2, a very important prospect for improved ability to site rectennas in more densely populated areas. These beam-shaping features have not been incorporated in the present reference system, but merit serious consideration in the future.

Systems smaller than the reference can be designed. Figure 6 is a parametric map of variation in a unit cost function with link power and transmitter aperture. This particular map represents systems for which the maximum sidelobe intensity is constrained to 0.01 mw/cm² (the reference system is at 0.1) and the cost-optimal system is sized at about 4500 megawatts with a 1.2-km transmitter as discussed above. (The power figures on the chart are input power to the transmitter and should be multiplied by a link efficiency of about 60% to derive net output power on the ground.) Systems with power rating less than the reference incur a cost penalty that is modest down to a power level of about 2500 megawatts, and increases more rapidly below that level.

TRANSMITTER ARRANGEMENT

The power transmitter is illustrated in Figure 7. It is a large planar phased array made up of subarrays mounted on a two-tier (primary and secondary) structure. Each of the 7220 subarrays includes from four to thirty-six klystron power amplifiers and associated control electronics. The quantized variation in the number of klystrons per subarray, and hence power density, provides an approximation to a 9.54 db, truncated Gaussian power illumination taper.

The subarrays are supported by the secondary structure, in turn supported by the primary structure. DC power from the solar array is fed to the subarrays through power processing and protective switch gear. About 15% of the power is processed to alternate voltages and regulated as necessary. The remainder is provided directly to the klystrons. All power is connected through interrupters and disconnect switches for fault isolation.

The reference phase distribution system distributes a coherent reference clock signal to all subarrays. This signal and the uplink (pilot) signal are phase conjugated at each klystron power amplifier to provide low-level RF drive signals of the correct phase. These signals are amplified to about 5 watts by solid-state preamplifiers and fed to each klystron; the klystron RF power output is approximately 70 kw each.

The antenna mechanical pointing includes star sensors and control moment gyros that aim the antenna toward its ground station to an accuracy of about one minute of arc. Computation is provided by the information management and control system; ground commands to correct residual aiming errors can be input through the communications system if necessary. Continuous desaturation of the CMG's is provided by a feedback loop that commands the antenna turntable drive. Low-pass filters and a compliant antenna mechanical suspension permit the CMG' to retain fine pointing control authority.

The antenna maintenance equipment includes crew provisions and mobility systems to support periodic removal and replacement of failed equipment.

The primary structure is a pentahedral truss made up of 1.5 meter tribeams fabricated in space by a beam machine. Feedstock for the beam machine is a graphite filamentary composite thermoplastic material shipped from Earth in roll and/or nested form. The beam elements are protected with thermal control and ultraviolet screen coatings and by selective multilayer insulation in the area where the transmitter head dissipation creates a thermal environment that would otherwise exceed the temperature capability of the material. Beam sections are terminated in centroidal fittings with mechanical attachments that include joint-slop takeup provisions to maximize structure rigidity.

The secondary structure provides a bridge on the MPTS primary structure and provides the base for mounting the transmitter subarrays, which are installed on a three point mount. The basic element is a 10.4 meter beam, 2.5 meters in depth, space fabricated from graphite composite

materials. The secondary structure is continuous around the perimeter of the antenna. In one direction the member spacing between rows is the width of one subarray and is the width of two subarrays in the orthogonal direction. Relationships between primary and secondary structures and subarrays are shown in Figure 8.

Each subarray includes 120 radiating waveguide "sticks" each 60 wavelengths in total length. The sticks geometry is selected so that the stick wavelength is twice the stick width, yielding a subarray 10.43 meters square. The arrangement of klystrons and RF power distribution waveguides is selected to minimize continuous stick length subject to the constraint that each stick be an integral number of wavelengths. Shorts within the sticks set the length of each radiating element. Pertinent discussions are given in the descriptive sketch. Minimizing stick length provides 3 advantages:

- o Reduced sensitivity to temperature
- o Greater slot offset, reducing scattering loss sensitivity to tolerances in slot offset
- o Reduced RF I²R losses

All of the subarray configurations are schematized in Figure 9. All geometries except the 4 x 4 employ a split klystron output to cut active stick length in half. This cannot be done for the 4 x 4 configuration because 60 is not evenly divisible by 8.

The subarray distribution and radiating waveguides are assumed fabricated from graphite/aluminum metal matrix composites. The structure members are a high-temperature graphite plastic-matrix composite. Solid-state components are mounted on the radiating waveguide assembly under multilayer insulation so that the radiating waveguide serves as a cold plate. In addition, thermal insulation is used to force the klystron heat rejection system to radiate only out the back face of the antenna, alleviating the thermal environment for the solid-state components.

The MPTS power distribution system provides power transmission, conditioning, control, and energy storage for all elements mounted on the antenna side of the rotary joint. The antenna is divided into 228 power control sectors, each of which provides power to approximately 440 Klystrons. The Klystrons require power at 9 different voltage levels. Two of the Klystrons' depressed collectors require the majority of the supplied power and are supplied directly from dedicated portions of the satellite power generation system. The rest of the Klystron supplied power and the power required for other power consuming equipment mounted on the power transmission structure is provided by DC/DC converters. Switch gear is provided for power control and fault protection. System disconnect switches are provided for equipment isolation for maintenance purposes.

Aluminum sheet conductors are used for power transmission from the interface subsystem to the power sector control substations and are routed along structural elements on the antenna primary structure farthest from the radiating waveguides. Round aluminum conductors provide power transmission from the substations to the antenna RF subarrays. Flexible connections are used to route power across the elevation joint between the antenna yoke and the antenna. Each power sector substation includes the required DC/DC converter, switchgear, disconnects, and energy storage. Figure 10 shows the circuit diagram.

The Power Transmission System Attitude Control System provides fine control of antenna mechanical aiming. Control Moment Gyros (CMG's) are used to generate torques required for this fine control. Control of the CMG's is accomplished using the signals derived from pointing errors determined from the phase control system. Rough pointing to acquire the phase control signal is accomplished using star scanners to control the CMG's.

The CMG's are located on the back side of the Primary Structure and are 12 in number for each transmitting antenna. A feedback loop from the Antenna Attitude Control System to the SPS mechanical rotary joint allows the rotary joint to apply torque to the antenna to continuously desaturate the antenna CMG's. This torque is supplied through a highly compliant mechanical joint so that the natural frequency of the antenna in its mechanical supports is below the control frequency bands for the CMG's controlling antenna attitude.

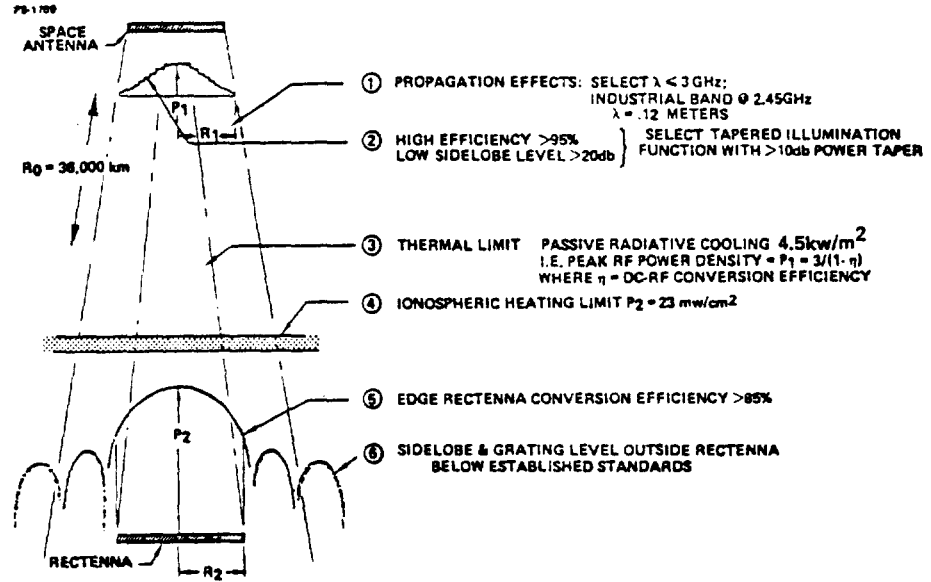


Figure 1: Design Constraints In Microwave Beam Link

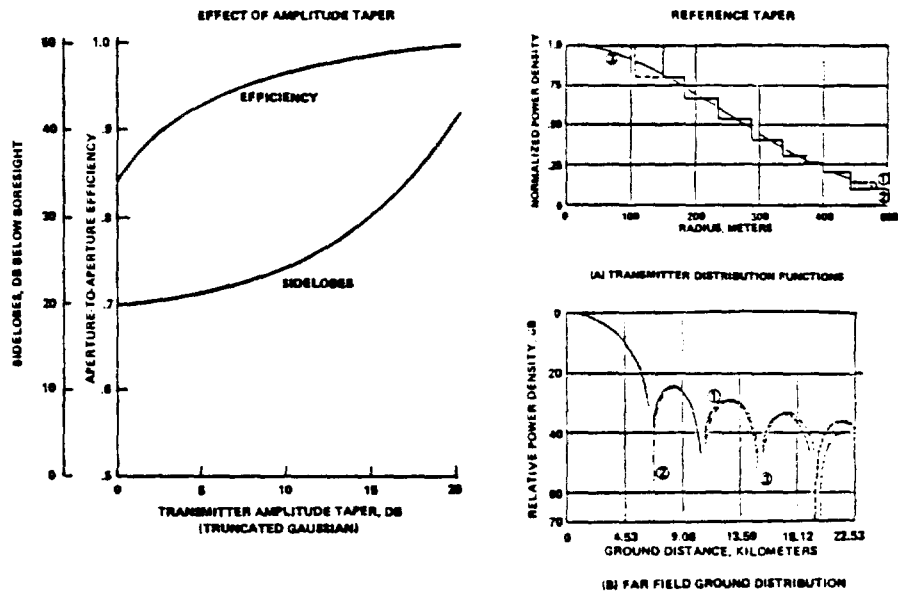


Figure 2: Power Transmitter Illumination Taper Factors

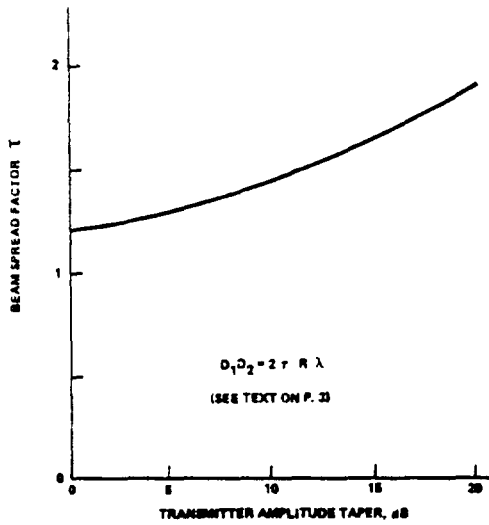


Figure 3: Beam Spreading

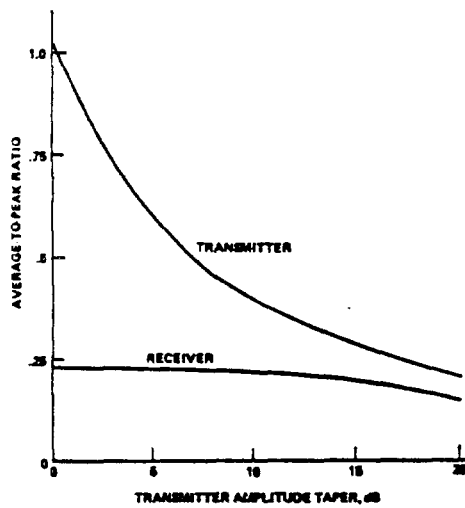


Figure 4: Intensity Ratios

INFLECTED BESSEL K=4.35

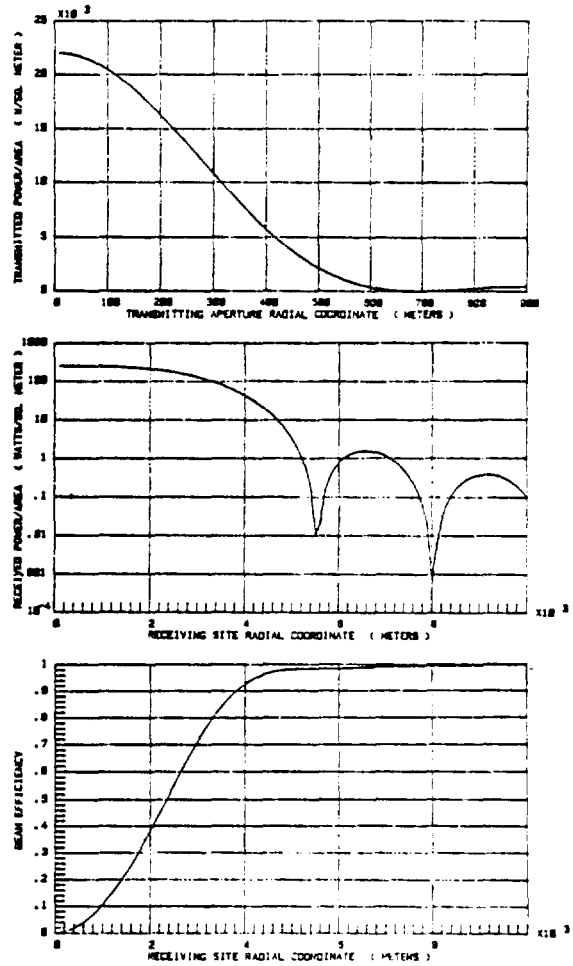
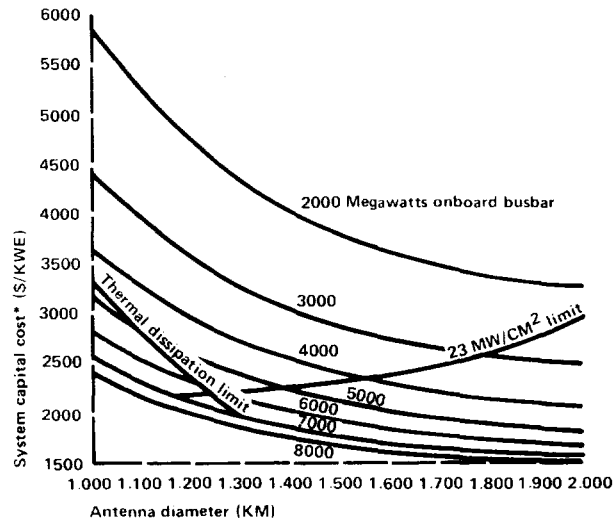


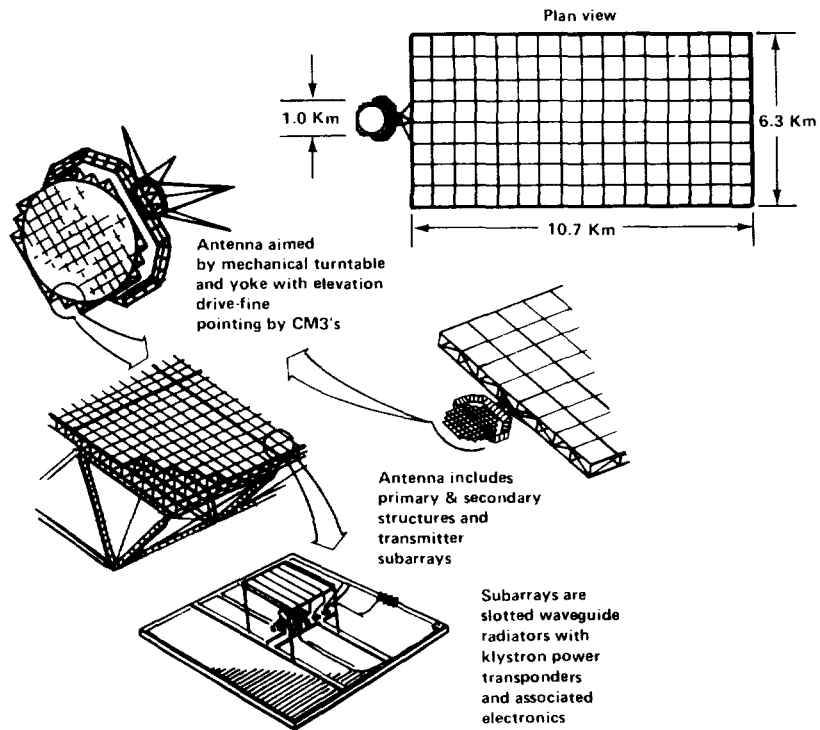
Figure 5: Use of Larger Aperture To Improve Average Ground Receiver Intensity

Figure 6. Transmitter constraints determine minimum cost design point.



* Assumes beam diameter rectenna

Figure 7. - Power transmitter.



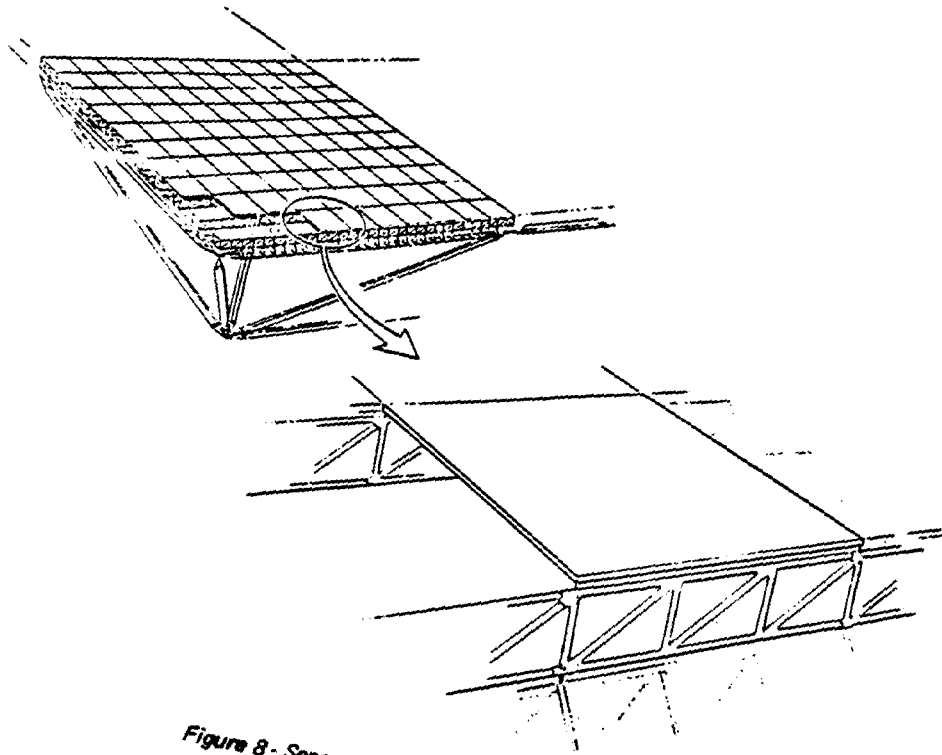
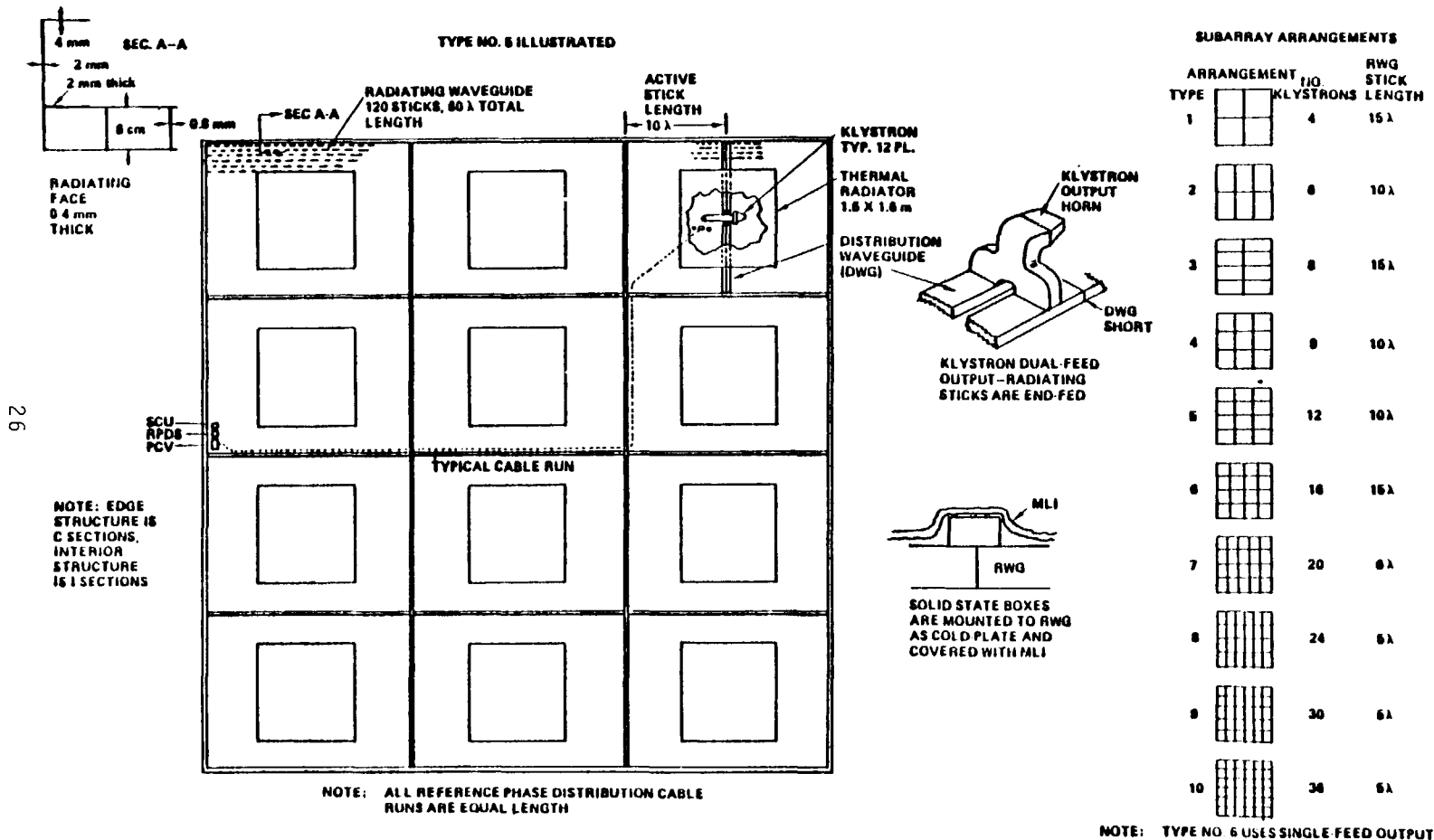


Figure 8 - Secondary Structure



26

Figure 9: Transmitter Subarrays

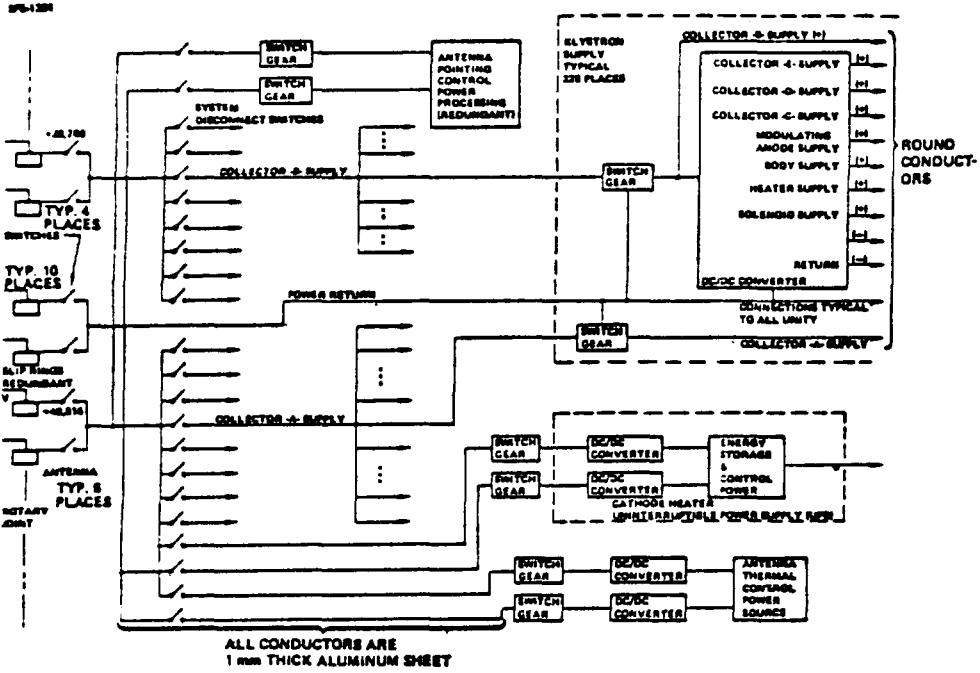


Figure 10 - Power Distribution

INITIAL MPTS STUDY RESULTS
- DESIGN CONSIDERATIONS AND ISSUES -

Owen E. Maynard
Raytheon Company, Equipment Division

Presented At

System Performance Session of the SPS Microwave Systems Workshop
15-18 January 1980

Lyndon B. Johnson Space Center, Houston, Texas

ABSTRACT

Progress in analysis, design and technology demonstration performed over the 1964-1979 time period is reviewed. Emphasis is on identifying the documentation for detail beyond the scope of the presentation and summarizing what was determined and, in retrospect, how firm those determinations appear to be. Twelve specific subsystems and technology areas are reviewed. Relevant issues or considerations are discussed and their resolution or status is presented.

Introduction and Background

Investigations of Microwave Power Transmission System (MPTS) concepts by Raytheon over the last 15 years are summarized in the attached figure. They began with, Item (1), investigations by Bill Brown in powering a high altitude platform by converting DC power on the ground to RF microwave power, transmitting it to a rotary wing platform, converting the RF power to DC, driving a rotary wing through a DC motor, controlling the platform in azimuth and elevation with a beam-riding autopilot for the helicopter. This work pointed out the potential of microwave power transmission and again Bill Brown continued to pursue this and other applications, including the Orbit-to-Orbit Transmission of Item (2), over the years.

This MPTS approach was adopted as part of Dr. Peter Glaser's Power from Space concept. Raytheon in-house investigations and reviews in the 71-72 time period determined that the concept of Microwave Power Transmission from Space was sufficiently sound to warrant further investigation and commitment of resources.

The key issues identified by the Raytheon committee review were:

- (a) Major steps must be taken to assure that the billions of diodes in the ground-based rectenna are sufficiently reliable to support a long life of approximately 30 years.
- (b) The entire MPTS concept must be advanced rather rapidly.

Item (a) has been pursued primarily by operating the diodes at power levels well below their time critical levels and by employing fail safe concepts where known failure modes result in open circuits and do not precipitate other failures. Item (b) has been pursued as aggressively as national support will permit. Good management practice normally would not support strong dependence on a few individual performers, however the issue is really most significant in

that tube technology is suffering from lack of interest in the academic community and in the technology community in general in favor of solid state approaches. The high power handling capability of tubes over solid state was considered to be a major factor. The maturity of tube technology permitted the definition of concepts with no known failure modes, passive waste heat dissipation limited by topology considerations and by the relatively high allowable temperatures for associated magnets as compared to solid state junctions. The efficiency of the device was considered a key item. An 80% efficient device results in twice as much inefficiency and waste heat dissipation required as a 90% efficient device and low allowable temperature limits compound the problem further. High power density on orbit was considered to be fundamental to low cost and the delivery of large amounts of power to the ground.

Major System Studies

Arthur D. Little, Inc., Grumman Aerospace Corporation, Spectrolab, Inc. and Raytheon conducted integrated in-house investigations, Item (3), of the SPS concept and contracted with NASA Lewis Research Center for a Feasibility Study of SPS, Item (4), in the 1971-72 time period. The major MPTS issues included RFI and biological considerations and the Office of Telecommunications Policy was briefed and consulted in the early period. The frequency had been established at 2.45 GHz (the ISM band) by the early studies and the study for NASA Lewis Research Center indicated that 3.3 GHz would be near optimum from the RFI point of view. Later studies by Raytheon for Lewis Research Center indicated that 2.2 GHz was near optimum from the SPS point of view, however RFI to other users of the spectrum was considered an adverse factor and the 2.45 GHz ISM band was again identified as the near optimum from many points of view.

The transmitting antenna diameter was consistently in the 1 km diameter region and the ground rectifying antenna was in the 10 km diameter region.

Biological limits for national and international applications for exposure outside the protected primary beam was assumed to be nominally 0.1 mW/cm². It was recognized that extensive investigation may show this to be an incorrect assumption and that in the limit it may be either higher or lower. Truncated Gaussian taper for the transmitting antenna was considered fundamental to the concept to maintain low sidelobes and to provide the flexibility in the concept for more or less taper as the dictates of biological limits required. The effects on life forms within the main beam were considered to be of concern, warranting in-depth investigation. The need for flexibility in the concept to control the main beam power density was therefore indicated. The trend toward less than low-cost-optimum levels began since the primary way of controlling main beam power density was to reduce transmitted power density and/or total transmitted power.

Microwave Power Transmission System Studies, Item (5), for NASA Lewis Research Center in the 74-75 period were most extensive and detailed, providing the basic relationships among performance, weight and cost. The scope was considered to be full breadth covering all the known issues. The depth was limited by time and effort that was considered appropriate for this first major investigation of the MPTS. The detailed results are reported in the four-volume report Microwave Power Transmission System Studies (NASA CR-134886, ER75-4368). A Satellite Power System Technology Risk Assessment was performed which identified in a level 5 breakdown the technology areas as they relate to microwave power transmission. The risk rating criteria categories were again at 5 levels: 1 - In Use, 2 - In Development, 3 - On the Technology Frontier, 4 - Conceptual and 5 - Invention. The configuration and technical approach

was modified to not require any Invention. There were 24 items in Category 4 requiring further investigation, advanced technology development and demonstrations. Relatively standard technology development was considered to be required in all other areas.

The 24 critical items as presented in order of priority and discussed in Volume 4 of ER75-4368 are:

- | | |
|-------------------------------|-------------------------------------|
| 1. DC-RF Converters & Filters | 13. Radio Frequency |
| 2. Materials | 14. Support Modules |
| 3. Phase Control Subsystems | 15. Orbital Assembly Operations |
| 4. Waveguide | 16. Reliability |
| 5. Structure | 17. Solar Electric Propulsion Stage |
| 6. Manufacturing Modules | 18. Transportation Operations |
| 7. Remote Manipulators | 19. SPS Flight Mechanics |
| 8. Biological | 20. Operations and Maintenance |
| 9. Attitude Control | 21. Power Source |
| 10. Ionosphere | 22. Heavy Lift Launch Vehicle |
| 11. Power Transfer | 23. Socio-economic Considerations |
| 12. Switch Gear | 24. Re-Supply |

A Critical Technology and Ground Test Program was described in Section 13 of ER75-4368. The 48 kW Klystron and the 5 kW Crossed Field Directional Amplifier (CFDA) were considered to be the leading tube contenders, with the Amplitron version of the CFA having the highest potential performance, lowest weight, longest life and lowest cost; however, there was significant uncertainty regarding CFDA noise. The study included a major effort by Shared Applications and Raytheon Equipment Division for the Klystron and significantly less effort for the less complex Amplitron. It was recognized that the Crossed Field Amplifier should be the subject of advanced development before selection could be made.

Environmental effects relative to propagation and phase control were discussed in NASA CR-134886, Section 3. This covered Atmospheric Attenuation and Scattering Ionospheric Propagation, Ionospheric Modification by High Power Irradiation & Faraday Rotation Effects. Subsequent data and investigations in this area have necessitated updating as reported in Items (11), (17) and (18).

The purpose of Item (9) was to provide a total set of qualitative relationships between areas requiring investigation and the viable approaches for investigation. Nine major points of focus in ground based study, technology development, analysis and test were identified. This was provided to both MDAC and GAC in support of Item (10). Item (12) was provided in response to a series of issues relating to whether or not a rational program with intermediate steps could be formulated that would give progressive confidence that would support authorizations to proceed on a continuous but step-wise basis. This identified a 10-step program that although outdated indicates the characteristics required.

Studies under ECON for NASA-MSFC of Item (11) included the rationale for the ground power density region of interest between 20 and 50 mW/cm². It was further indicated that 23 mW/cm² was a reasonable value for reference purposes.

The Rectenna Technology Study, Item (14), by Bill Brown of Raytheon provided further detail on the rectenna for Boeing.

The investigations into SPS and alternate technologies of Item (15) began to identify the basis for direct comparison of SPS with other approaches for base power. Raytheon Equipment Division worked in a consultant role to identify the several sources of relevant information.

The SPS Pilot Beam and Communication Link Study, Item (17), provided relevant sizing approaches and data in those areas that were not addressed in previous activities. Interpretation of the results of this study in the area of ionospheric effects, as expressed by others working in the area of ionospheric modeling and phase control, were inconsistent with Raytheon's understanding of the problem and a draft Technical Note of Item (18), SPS Pilot Beam Ionospheric Effects Discussion of Critical Issues, was distributed to personnel working in the ionospheric modeling and phase control areas. Details from this T.N. will be included in the oral presentation.

The Solid State SPS Microwave Generation and Transmission Study, Item (19), and the Magnetron Tube Assessment Program will be reported on in other appropriate sessions.

Major Demonstrations and Technology Developments

The Reception-Conversion Subsystem (RXCV) for Microwave Power Transmission System effort of Item (6) will be reported on in other appropriate sessions. It was vitally important in that it constituted a major positive step in credibility with the technical community. The high RF to DC efficiencies (> 80%) demonstrated in the field and the high DC to DC efficiencies (54%) demonstrated and certified by JPL in the laboratory constituted progress that created significant interest in and belief by the technical community.

The RF to DC Collector/Converter Technology Development, Item (7), will be reported on in other appropriate sessions. It extended the RF to DC efficiency data to low power levels and provided significant advancement in understanding of possible approaches to fabrication for low cost.

The Design and Fabrication of Crossed Field Amplifiers, Item (8), will be reported on in other appropriate sessions. Although this development was limited to a Phase I activity, it along with major contributions by R. Dickinson of JPL provided insight that precipitated Item (16). The Raytheon in-house work in Item (16) was followed by a program under contract from JPL to investigate the magnetron directional amplifier and will be reported on in other appropriate sessions. This work is a very significant system level contribution in that it has brought the most familiar microwave oven magnetron into contention, contrary to the belief that the Amplitron and Klystron were the leading contenders as reported under Item (5). This is hopefully indicative of simple but imaginative approaches that may evolve in each of the SPS areas of overall concept and technology.

The Magnetron Tube Assessment, Item (20), will be reported on in other appropriate sessions. This assessment is most important in the system performance area in that it is the investigation of an alternate technology that is relatively mature, lightweight, highly efficient and relatively simple from both the device and interface with the power grid points of view.

Relevant technologies under consideration and development, Item (13), are being investigated by Raytheon.

RAYTHEON'S PARTICIPATION IN SOLAR POWER SATELLITE PROGRAM RELATED WORK - SYSTEM STUDIES AND TECHNOLOGIES

DESCRIPTIVE TITLE	PRIOR TO 1970	PERIOD OF PERFORMANCE										CUSTOMER	PRIME	SUB	RELATED REPORT NUMBER		
		70	71	72	73	74	75	76	77	78	79					80	81
1 Microwave Powered Helicopter	1964													USAF	Raytheon		RADC-TR-65-188
2 Orbit-to-Orbit Power Transmission	1969													NASA-MSFC	Raytheon		PT-4601
3 MPTS in Satellite Solar Power Station														In-House			ER72-4038
4 Feasibility Study of SPS														NASA-LeRC	Arthur D. Little	Raytheon Grumman Spectrolab	NASA CR-2357
5 Microwave Power Transmission System Studies														NASA-LeRC	Raytheon	Shared Applic's & Grumman	NASA CR-134886
6 Reception-Conversion Subsystem (RXCV) for Microwave Power Transmission System														NASA	JPL	Raytheon	ER75-4386
7 RF to DC Collector/Converter Technology Development														NASA-LeRC	Raytheon		NASA CR-135194
8 Design and Fabrication of Crossed Field Amplifier														NASA-LeRC	Raytheon		NASA CR-159410
9 Areas of Investigation Relationships to Development Approaches														In-House			
10 Space Station System Analysis Study														NASA-MSFC NASA-JSC	GAC MDAC	Raytheon Raytheon	
11 Space Based Solar Power Conversion and Delivery System Study														NASA-MSFC	ECON	Raytheon	ECON 77-145-1 S/C ECON-0003
12 Satellite Power System Development Plan Summary														In-House			
13 DOD Applications & DARPA Advanced Technology Development (Relevant Space Based Investigations)														SAHSD RADC	TR//GAC Raytheon	Raytheon	
14 SPS System Evaluation Phase III - Rectenna Technology Study														NASA-JSC	Boeing	G.E. Raytheon	D180-24635-1 PT-5155
15 SPS & Alternate Technology Comparisons														ANL	UE&C Inc.	Consultant	UE&C-ANL-79031
16 Crossed Field Directional Amplifiers For Use in the Solar Power Satellite														In-House			
17 SPS Pilot Beam & Communication Link Study														NASA-MSFC	Raytheon		NASA-33157
18 SPS Pilot Beam Ionospheric Effects Discussion of Critical Issues														In-House			Draft 6/79
19 Solid State SPS Microwave Generation and Transmission Study														NASA-MSFC	Raytheon		
20 Magnetron Tube Assessment														NASA-MSFC	Raytheon		

SPS LARGE ARRAY SIMULATION

S. Rathjen B. R. Sperber, E. J. Nalos, Boeing Aerospace Company

1.0 INTRODUCTION

The computer simulation has been developed with the objective of producing a flexible design and verification tool for the SPS reference design. The computer programming efforts have been directed primarily to beam pattern analysis. The following reasons have been specified as the purpose of the computer programs: verification of the reference design, definition of feasible departures such as quantized distributions, the study of far-out sidelobe roll-off characteristics, the analysis of errors and failures, illumination function analysis to develop beam patterns for efficient collection, and beam shaping synthesis to meet environmental constraints.

2.0 ARRAY SIMULATION PROGRAMS

Three types of computer simulations have been developed to study the SPS microwave power transmission system (MPTS). The radially symmetric array simulation is low cost and is utilized to investigate general overall characteristics of the spacetenna at the array level only. "Tiltmain," a subarray level simulation program, is used to study the effects of system errors which modify the far-field pattern. The most recently designed program, "Modmain," takes the detail of simulation down to the RF module level and so to date is the closest numerical model of the reference design.

Early in the computer program development stage, radially symmetric array simulations were written to model various power taper distributions and to compare their beam efficiencies.

The radially symmetric simulations have been used to study a variety of spacetenna distribution functions enabling comparisons of the on-axis power densities, the far field patterns, and their associated beam efficiencies.

The "Tiltmain" array simulation is much more complex than the circularly symmetric simulation due to the fact that "Tiltmain" models the spacetenna as comprised of 7220 subarrays. In "Tiltmain," the ground-grid is specified as a planar circular area where the electric fields are determined. The field at any particular point on the grid is computed using scalar wave equations with approximations that make them accurate in the Fresnel Zone. The equations are not valid for the very near field, but give very good results in the Fresnel Zone, $D^2/\lambda > R > 2D^2/\lambda$, and the far field $R > 2D^2/\lambda$ where D is the diameter of a circular spacetenna or the diagonal of a rectangular spacetenna, λ is the wavelength of the transmission signal, and R is the range from the spacetenna to the ground-grid. The electric field at any particular point is determined by calculating the field from each subarray in the spacetenna to the given grid point and then summing all the fields to give the total field at that grid point.

The total power collected by the ground-grid is calculated by multiplying the power density at a point by the incremental area associated with that point to give the power over that area, and then summing up the power from each sample. Efficiencies with respect to the total power collected on the ground-grid and with respect to the total input power of the orbiting spacetenna are calculated at incremental grid distances out of the specified diameter.

"Modmain" is the most complex simulation of the MPTS to date in that the spacetenna is modelled not only as 7220 subarrays (as in "Tiltmain") but each subarray is modeled as a composition of RF transmitter modules. "Modmain" models over 100,000

modules and simulates phase errors, amplitude errors, failures, and systematic as well as random tilt.

The "Tiltmain" simulation was unable to model below the subarray level because its program structure caused data storage limitations problems; "Modmain" is structured in such a way as to overcome this disadvantage. Previously, the amplitude and phase of each subarray was stored in an array and recalled for each ground point. With "Modmain" the amplitude and phase of every module is not stored but the contribution of a module at each ground point is calculated and stored before moving on to the next module where the contribution is added to the previous ground point contributions.

3.0 REFERENCE DESIGN VERIFICATION

The computer programs have been used to investigate different antenna aperture illumination functions. An optimized aperture distribution will maximize the RF power intercepted by the ground rectenna and minimize the sidelobes and grating lobes. The types of illumination functions investigated include: Gaussian, cosine on a pedestal, uniform, reverse phase, inflected Bessel, and quadratic on a pedestal. Each of these was evaluated in terms of maximum power density at the transmit array and the rectenna, sidelobe levels, beam shape, and beam efficiency. Several Taylor series tapers were also explored with general results indicating that sidelobe levels decrease as the amount of taper increases.

Figure 1 shows five spacetenna distribution functions and the required spacetenna size and power densities to produce the same peak power density on the ground and the same size main beam. Figure 2 depicts the five far-field patterns showing the relative levels of the sidelobes. It was found that a 10 dB Gaussian taper has the best performance and that when quantized into at least eight levels produced nearly the same results as a theoretical continuously variable function. From antenna layout considerations, a 10-step, 10 dB Gaussian taper was then chosen for the aperture illumination (See Figure 3). The farther out sidelobes were compared for the continuous and ten-step quantized Gaussian tapers. The results show very little difference between the two cases.

In order to verify the energy distribution at distances far away from antenna boresight, it was necessary to determine the roll-off characteristics of the entire antenna. This was done by a numerical integration technique applied to the radiation pattern of the 10 dB Gaussian taper distribution. It was established that the sidelobes rolled off at 30 dB/decade of angle. This coincidentally is the roll-off rate of a uniform circular aperture. Next, the error plateaus were computed from the assumed error magnitudes and the number of subarrays associated with three different subarray sizes. The aperture efficiency was also obtained by numerical integration. Next the subarray roll-off characteristics were obtained by numerically integrating the square aperture distribution for each of 19 different cuts over a 45° sector of θ . These cuts were then averaged at each θ . The resultant subarray sidelobes also roll off at 30 dB/decade of angle. There is an additional error plateau associated with the randomly scattered power by each slot in the subarray. This second plateau will in theory roll off in accordance with the radiation pattern of the slot.

The lowest integral element in the MPTS is the klystron module, composed of a klystron, its feed and radiating waveguides, thermal control, solid state driver and RF control, power distribution, power return, and the support structure. The factors in selecting the klystron module sizes include: RF power density and thus the thermal environment, ease of quantizing the spacetenna aperture distribution, and awareness of klystron module interfaces. The high power density at the center of the beam is generated by 36 klystrons, each rated 70 KW, radiating RF from an area slightly larger than 108 m² (area of subarray). The 36 klystrons are organized into a 6 by 6 matrix. At the edge of the 10 dB tapered antenna a

subarray should have 3.60 klystrons. Since 3.60 is not an integer number, each edge subarray has 4.0 klystrons formed into a 2 by 2 matrix. Matrix configurations were similarly established for each power density step in the taper. Due to the klystron module system interfaces and the thermal limitations, the smallest possible size module is 1.5 by 1.5 meters.

The reference system calls for phase control at the klystron module level. Current thinking defines this level rather than phase control at the subarray level because of the belief that the modules cannot be assembled together accurately enough to retain a uniform phase front. The uniform phase front for the subarray could not be achieved due to the tilt of the modules and the distributed phase errors which occur within the subarray. Figure 4 shows the comparison between subarray and klystron module phase control level as a function of random tilt. The peak power density on the Earth is closely correlated to the beam efficiency and so Figure 4 shows that the klystron module phase control level is significantly better than subarray level control.

Simulations made to compare phase control level as a function of random phase error is shown in Figure 5. The results indicate a range of values for both systems, meaning that for 10^0 of random phase error both phase control systems have a random range of values statistically which are equal as would be expected.

Grating lobes are peaks in radiation occurring at angular directions off axis of the spacetenna where the signals from each of the subarrays add in-phase. The lobe amplitudes are a function of the mechanical alignment of the modules and the spacetenna pointing whereas the spatial position of the lobes is dependent upon the modules sizes. When there is no mechanical misalignment (no tilt of modules or spacetenna), the grating lobes appear to be split because the peaks of the "array factor" fall directly in the nulls of the subarray pattern. As tilt occurs, the peaks move out of the nulls, quickly increasing their amplitude because of the steep slope of the subarray pattern nulls. Figure 6 shows a comparison between grating lobe amplitudes for module and subarray phase control levels when two arc minutes of spacetenna tilt is simulated. Once again phase control at the module level shows a significant advantage over control at the subarray level.

4.0 SHAPED BEAM SYNTHESIS

In order to improve the overall collection efficiency by increased beam flatness out to the rectenna edge as well as provide an additional means of sidelobe control, beam synthesis with resultant phase reversals at some portions of the spacetenna was considered. These phase reversals are obtained by a fixed phase shifter at the klystron input and represent a first step towards a continuously variable phase distribution across the spacetenna, should this be more desirable. The results indicate that it is possible to synthesize a pattern that is considerably more flat-topped than the 10 dB Gaussian or other patterns that we have investigated. The price paid for this improvement is increased spacetenna size or a larger rectenna.

It is possible to increase the flatness of the beam without limit with arbitrarily large apertures and large numbers of beam components. Figure 7 compares the 10 dB Gaussian taper with the reverse phase taper and the continuous phase synthesis. The comparison shows the differences in the amplitude and phase illumination tapers across the spacetenna as well as the far-field patterns. Results show that reshaped beam pattern with "squared" main beams are possible but at the expense of larger transmit antennas or larger rectennas.

The idea of adding a suppressor ring to the spacetenna was investigated in the hope of significantly reducing the first sidelobe level. Figure 8 presents the results of this

study. The upper left diagram shows the layout of the spacetenna with its uniform distribution out to 0.72 times the normalized radius and the suppressor ring of width W . The diagram on the upper right shows the linear relationship between beam efficiency and the first sidelobe level as the ring width changes. $.98 R_0$ means that the width of the suppressor ring is bound by the edges $.98 R_0$ and R_0 . Looking at the lower right diagram shows the effect of changing the phase of the suppressor ring as well as the ring width. From this diagram it may be concluded that an in-phase ring is better than one which is out of phase. The lower left diagram shows the far-field pattern produced for the suppressor ring case where the inside edge of the suppressor ring is at $.94 R_0$. Although the first sidelobe is lower by about 5 dB than the case without a suppressor ring a significant loss in beam efficiency accompanies this achievement.

A dual suppressor ring case was looked into with a 10 dB taper rather than the uniform illumination and a larger spacetenna radius of 2 km. Figure 9 presents the illumination across the large array with the ring closest in out-of-phase by 180° and the second ring in-phase with the array. The far-field pattern for this case is shown in Figure 10 with a sidelobe level about the same as the referenced design but a main beam radius which is about 2.35 Km less.

A study was made to look at using defocusing and phase taper for beam shaping. Cases where the beam was focused at infinity showed much lower peak power density and much broader beams. These results indicate that reshaped beams with reduced peak levels are possible at the expense of larger spacetennas or rectennas.

Quadratic phase taper was utilized to look at shaped beam synthesis. In Figure 11, the far-field patterns for 4 cases with uniform amplitudes and different quadratic phase tapers are compared. As θ max increases the on-axis power density decreases (see Figure 11) and the beam efficiency decreases significantly (see Figure 12). Figures 13 and 14 show the far-field patterns and efficiencies for quadratic phase taper with the Gaussian rather than the uniform amplitude taper. These results show that the reference Gaussian taper without quadratic phase error is the most efficient pattern. Figure 15 presents a table which shows how the quadratic phase taper may be utilized to design alternate SPS systems.

5.0 SPS SYSTEM SIMULATION

In this final section three types of SPS system simulations are described: a) Incoherent phasing, b) startup/shutdown operations, and c) multiple beams. Incoherent phasing was simulated to investigate the effect of complete phase control failure. The results show that the far-field pattern takes on a constant value in the rectenna and sidelobe region. The constant value is about $.003 \text{ mw/cm}^2$ over 5 dB below the Russian exposure level.

Computer simulations were utilized by JSC to investigate the performance of the MPTS during startup/shutdown operations. (See paper by G. D. Arndt and L. A. Berlin entitled "Microwave System Performance For A Solar Power Satellite During Startup/Shutdown Operations" on p. 1500 in Vol. II of the Proceedings of the 14th Intersociety Energy Conversion Engineering Conference.) Three sequences are recommended—random, incoherent phasing, and concentric rings-center to edge. The use of incoherent phasing is attractive in that it allows the antenna to be energized in any sequence. In conclusion the question of energizing the antenna has several practical solutions and should not present environmental problems.

The possibility of transmitting several power beams from an SPS has intrigued various researchers for some time. Recently, some computer runs were made to verify the capability of transmitting multiple beams using a modified version of the large array program TILTMAT. The scheme used to generate the beams was the simplest possible

one imagineable; namely, splitting the main beam along an axis by spatially modulating the illumination function by a factor $\cos(k r \sin \theta)$ when: $k = 2\pi/\lambda$, r = subarray displacement from center, θ = beam split angle. Results of a simply split 6.5 G.W. reference Gaussian are shown on Figure 16, and are as predicted except for the central lobe which did not diminish as the split angle was increased to 6×10^{-4} radians. The central peak may be due to an in-phase residual component in the spatial modulation or a grating lobe effect. Understanding and eliminating the central peak will be among our future efforts along with investigating various other multiple beam effects.

6.0 CONCLUSION

The computer simulations described have proven to be powerful versatile tools in the prediction of RF performance of the space solar power satellite. They are continually being refined and their use is being extended into the planning of initial experimental verification of the array performance.

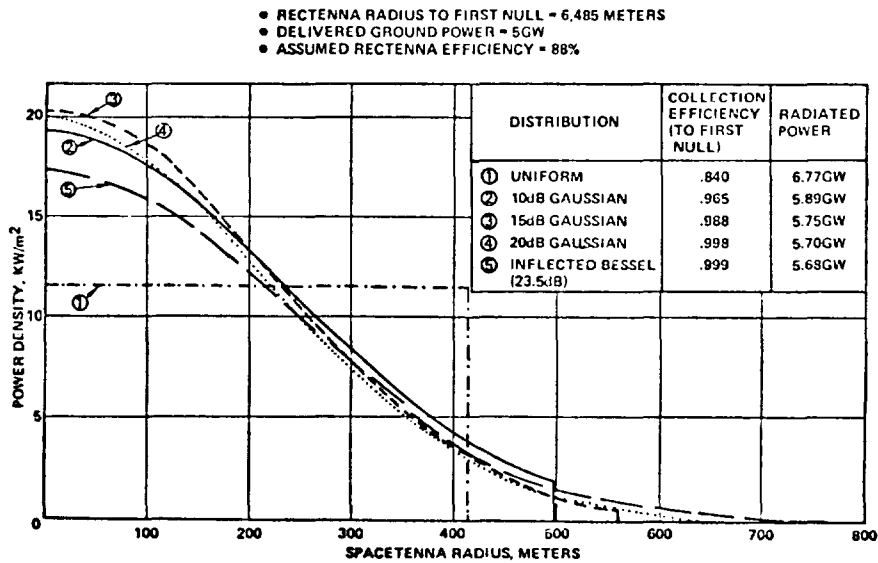


FIGURE 1

FIGURE 2

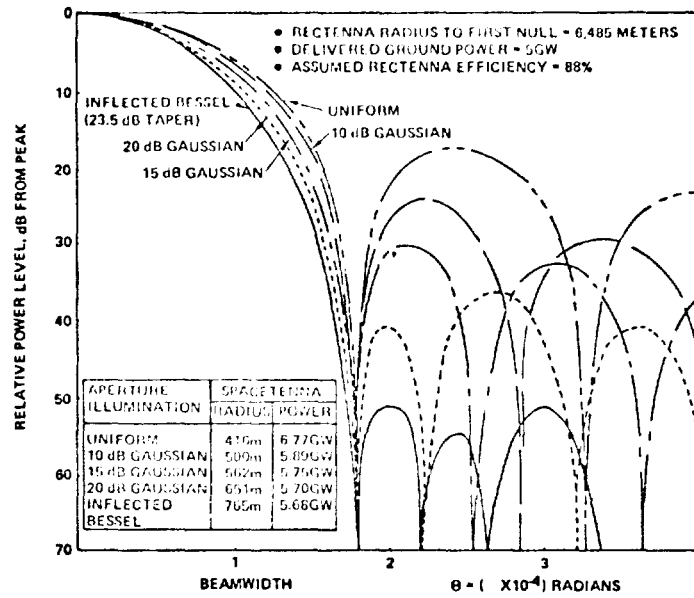


FIGURE 3

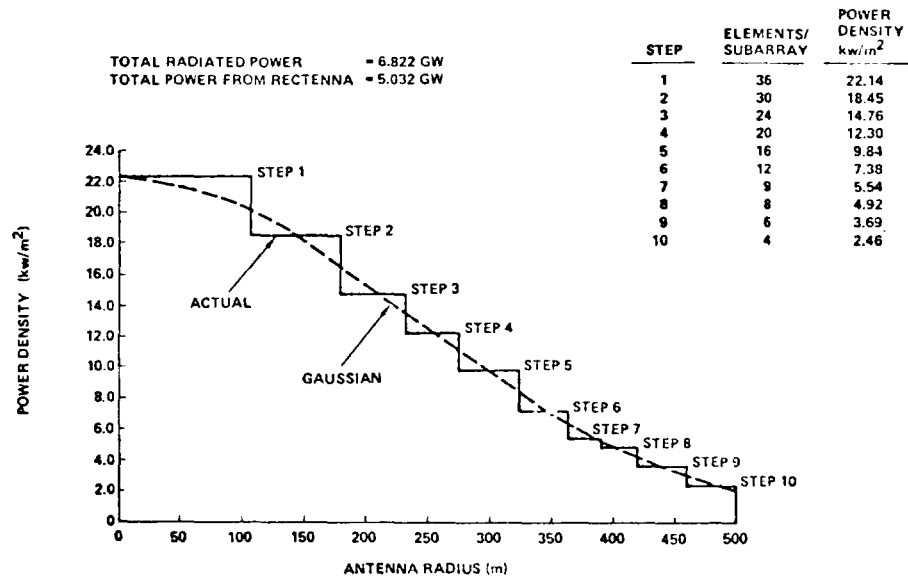
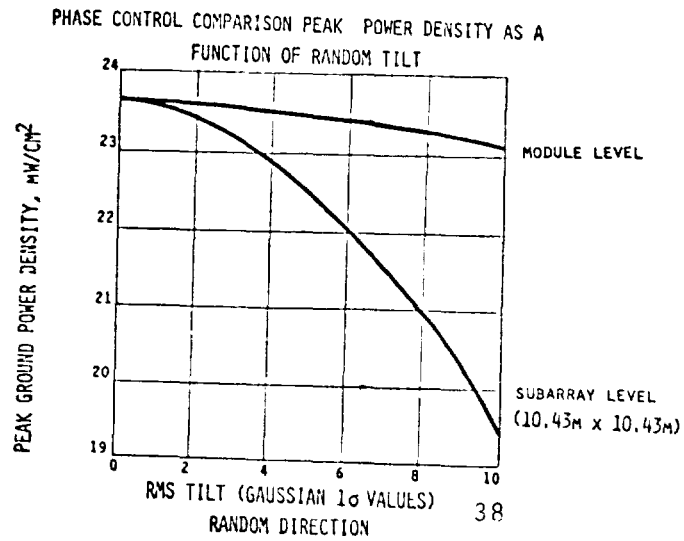


FIGURE 4



PHASE CONTROL LEVEL COMPUTER SIMULATION

FIGURE 5

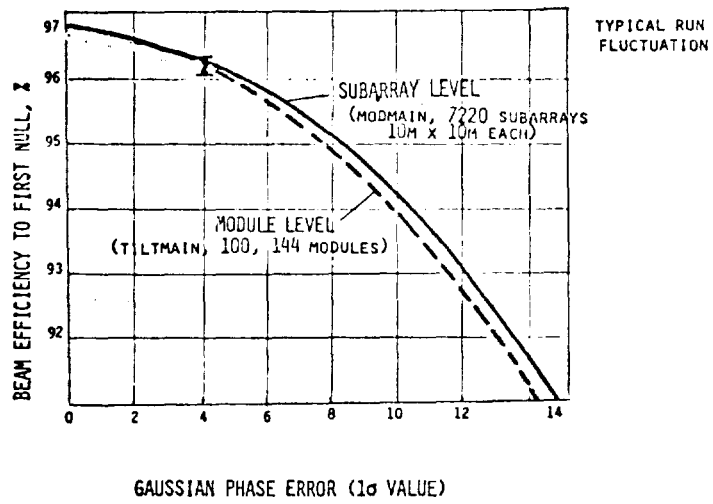


FIGURE 6

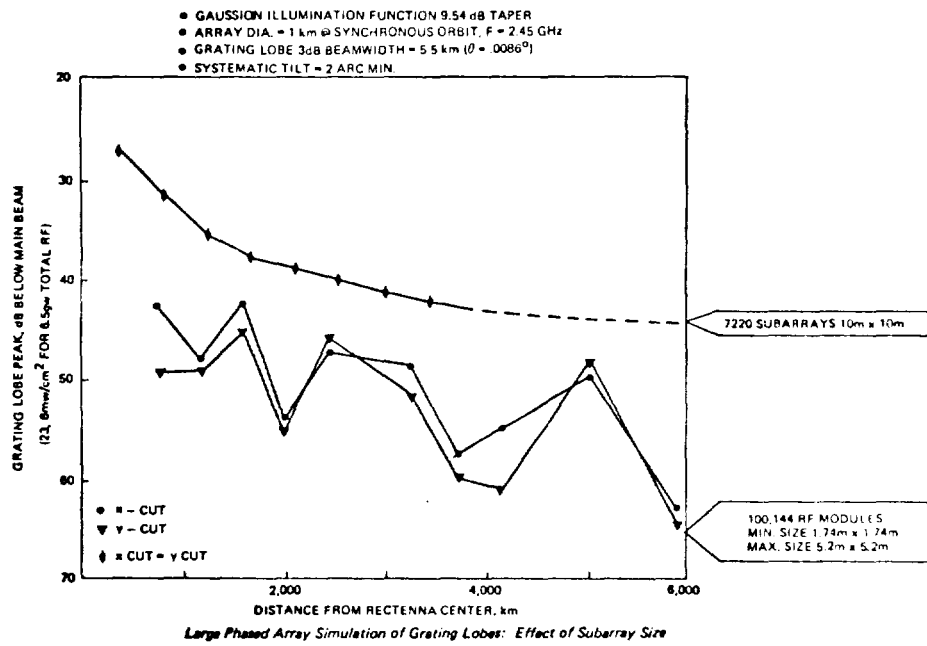
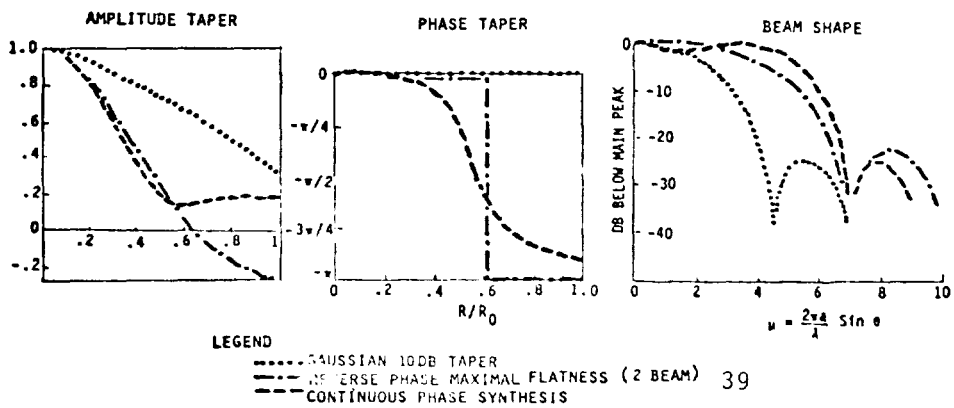


FIGURE 7



SPS Shaped Beam Synthesis

FIGURE 8

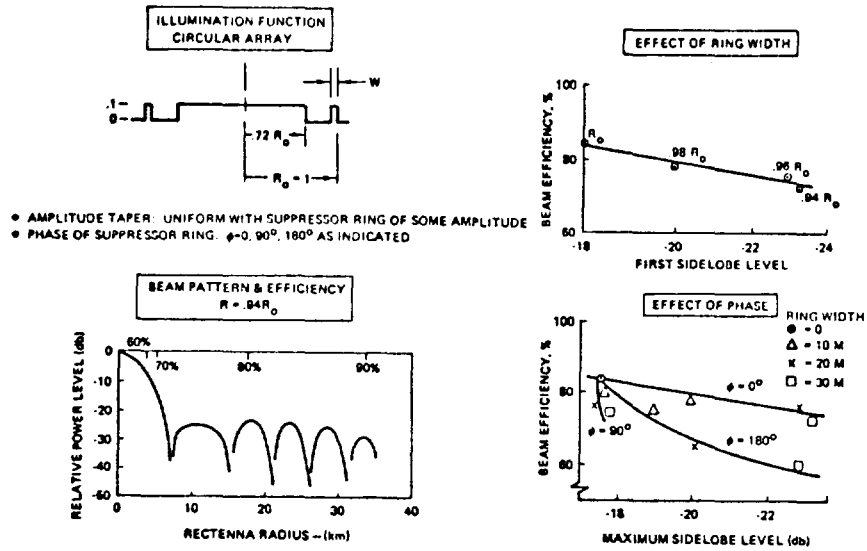


FIGURE 9

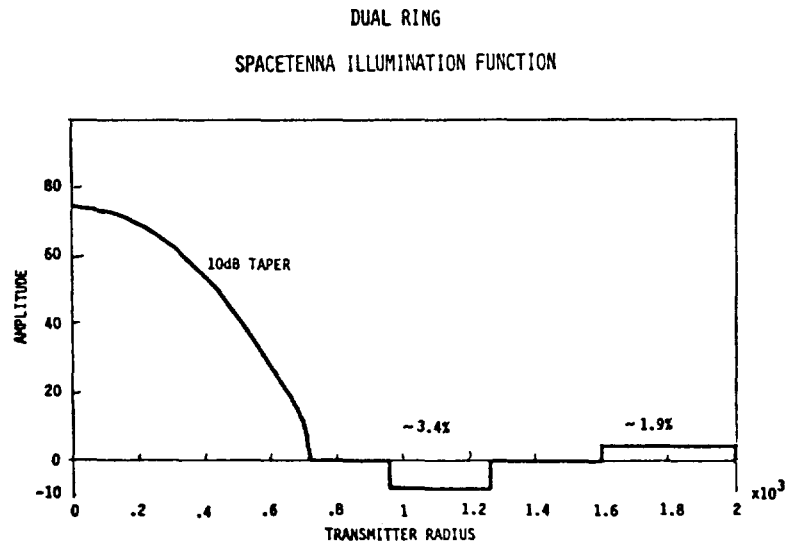
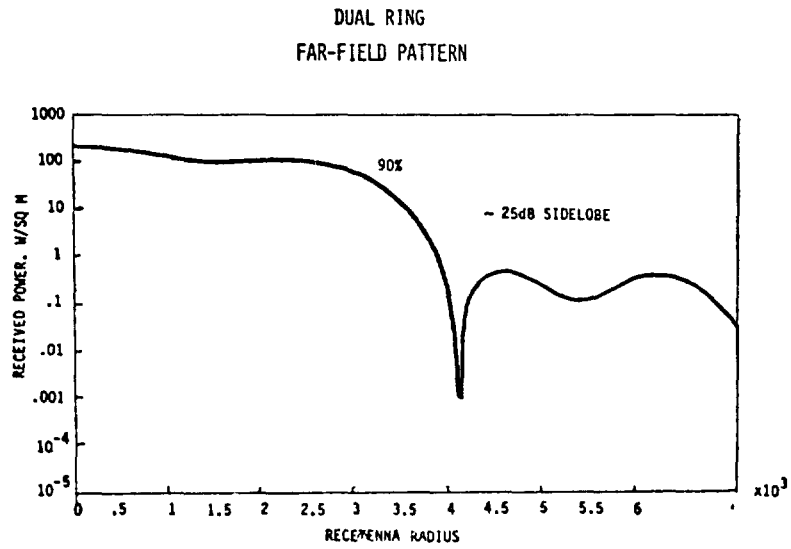


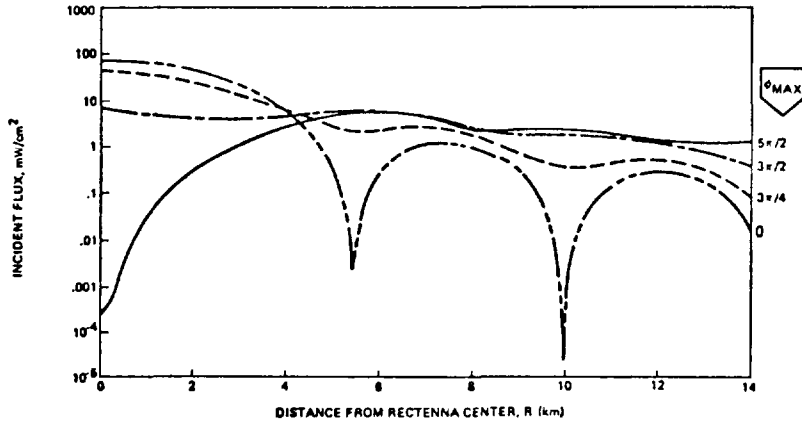
FIGURE 10



SPS Shaped Beam Synthesis

AMPLITUDE TAPER - UNIFORM
 PHASE TAPER - QUADRATIC $\theta = \theta_{MAX} (R/R_0)^2$
 SPACE ANTENNA 1 KM DIA., 2.45 GHz 22kw/m² 5GW

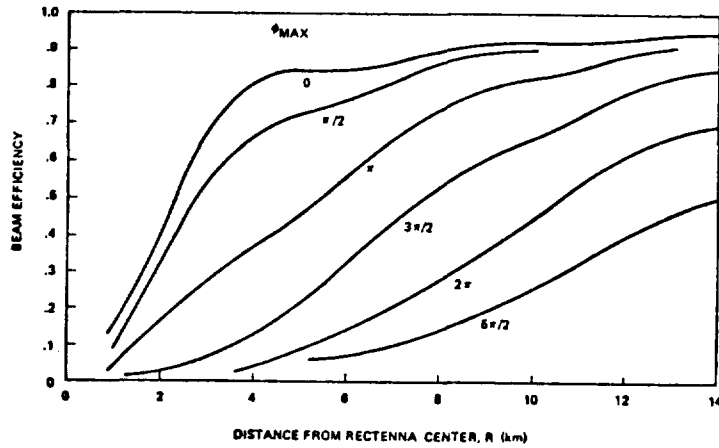
FIGURE 11



SPS Shaped Beam Synthesis

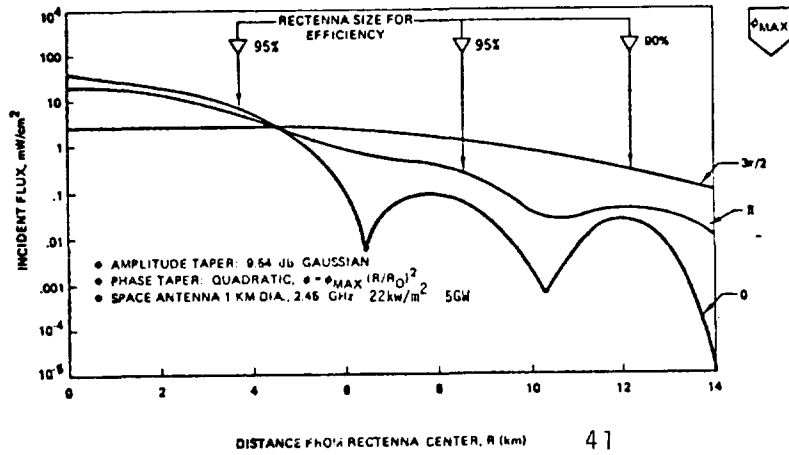
• AMPLITUDE TAPER: UNIFORM
 • PHASE TAPER: QUADRATIC, $\theta = \theta_{MAX} (R/R_0)^2$
 • SPACE ANTENNA 1 KM DIA., 2.45 GHz

FIGURE 12



SPS Shaped Beam Synthesis

FIGURE 13



SPS Shaped Beam Synthesis

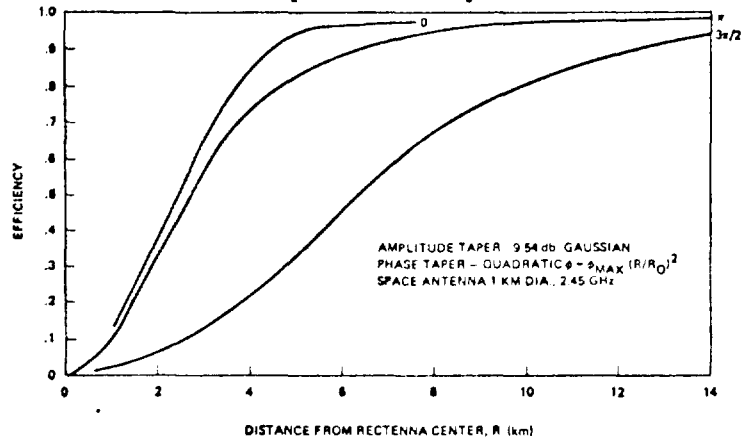


FIGURE 14

ALTERNATE SPS DESIGNS USING BEAM DEFOCUSING QUADRATIC PHASE TAPER $\phi = \phi_{MAX} (R/R_0)^2$

5GW 1KM 22KW/M ²					← KLYSTRON BASELINE 5GW
ϕ_{MAX}	PEAK ON AXIS POWER mW/CM ²	RECTENNA DIAM. KM	POWER FLUCTUATION CR. TO EDGE	EFFICIENCY %	
0	23	10KM	23:1	97	
1.2π	5.8	22	35:1	95	
3π/2	2.1	28	48:1	92	
10GW 1.4KM 22KW/M ²					← POTENTIAL 10GW KLYSTRON DESIGN
1.2π	23	15.7KM	35:1	95	
2GW 1.5KM 5KW/M ²					← SOLID STATE SPS (BOEING)-2GW
1.2π	20 5.8	6.7 14.7	23:1 35:1	97 95	
4GW 2.1KM 5KW/M ²					← POTENTIAL SPS 4GW DESIGN
1.2π	20	10.5	35:1	95	

FIGURE 15

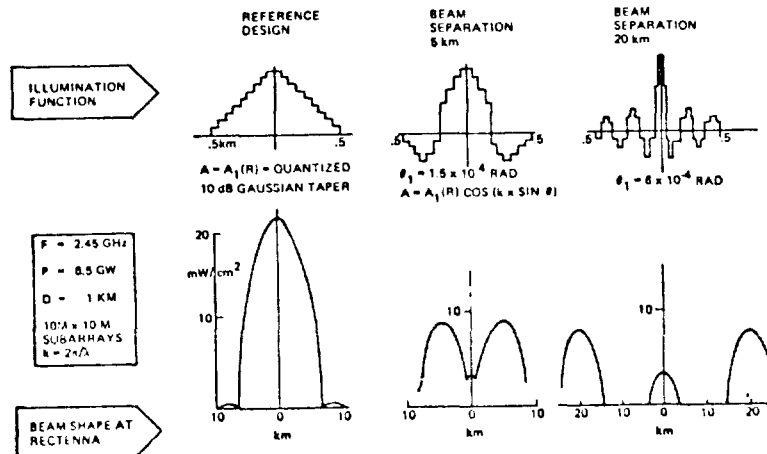


FIGURE 16

ACHIEVABLE FLATNESS IN A LARGE MICROWAVE POWER TRANSMITTING ANTENNA

By R. C. Ried/NASA Johnson Space Center

SUMMARY

The efficient and practical operation of a large aperture planar phased array for the transmission of microwave power requires accurate mechanical pointing and minimal structural deformation. The Solar Power Satellite (SPS) has a definite advantage for satisfying tight mechanical requirements due to the benign external load environment of space. Potential distortion associated with the thermal environment has led to consideration of low coefficient of thermal expansion (CTE) structural materials to minimize this effect.

An evaluation of the achievable flatness in a large microwave power transmitting antenna has been performed by F. Leinhaupel and associates¹. This study considered manufacturing and assembly tolerances, maneuvering and environmental accelerations as well as thermal distortion. Quantitative results required consideration of a specific microwave power transmission system (MPTS), SPS configuration and structural material. The configuration which was evaluated was basically a dual reference SPS system with pseudoisotropic GY-70/X-30 (graphite epoxy) as a representative dimensionally stable composite for the structural material. This particular material was selected due to the availability of statistical material property data and because of experience with manufacturing and assembly tolerances which have been achieved.

The loads, accelerations, thermal environments, temperatures and distortions were calculated for a variety of operational SPS conditions along with statistical considerations of material properties, manufacturing tolerances, measurement accuracy and the resulting loss of sight (LOS) and local slope distributions. The basic result of the study is that a LOS error and a subarray rms slope error of two arc minutes can be achieved with a passive system. This encompasses all manufacturing errors, thermal distortions, static structural loads and dynamic

movement resulting from transient loads.

Significant specific results of this study include:

- Existing materials measurement, manufacturing, assembly and alignment techniques can be used to build the MPTS antenna structure, orders of magnitude larger than current space systems.

- Manufacturing tolerance can be critical to rms slope error. Study results show that the slope error budget can be met with a passive system. As a backup approach, initial active alignment can be used to correct the interface between prime and secondary structures and/or between secondary and subarray structures. Tolerance then is limited by measurement accuracy and actuator resolution.

- Structural joints without free play are essential in the assembly of the large truss structures. Joint "slop" as contrasted to joint tolerance, can be eliminated by bonding or welding. Joint tolerance is a small part of overall strut length, and makes a minor contribution to slope error.

- The material properties of GY-70/X-30 pseudoisotropic graphite/epoxy composite were used as representative of strength, modulus and CTE. Variation in material properties, particularly for CTE, from part to part is more significant than the actual value. The design can accommodate predictable length changes and still achieve the required flatness. The uncertainty in CTE leads to the thermal distortion that degrades performance. However, thermal distortion is small over the range of operating temperatures and material properties not as well regulated as those of GY-70/X-30 will meet requirements.

Although the results of this study are applicable to a particular configuration, it is evident that the MPTS structure represents a reasonable extension of the present state-of-the-art. Furthermore, the probability is high that the accuracy requirements can be achieved with a passive system.

REFERENCE

1. Achievable Flatness In A Large Microwave Power Antenna Study, General Dynamics Conair Division Report No. CASD-NAS-79-011, under Contract No. NAS9-15423, Tech. Monitor F. J. Stebbins, August 1978.

AN ACTIVE ALIGNMENT SCHEME FOR THE MPTS ARRAY

By

Richard Iwasaki
Axiomatix
Los Angeles, California

In order to maximize the efficiency of the microwave power transmission system (MPTS), the surface of the array antenna must be extremely flat, which is difficult to achieve using passive techniques over the 1 km dimensions of the array. In order to achieve and maintain this required flatness, a rotating laser beam used for leveling applications on earth has been utilized as a reference system. A photoconductive sensor with a reflective collecting surface is used to determine the displacement and polarity of any misalignment and automatically engage a stepping motor to drive a variable-length mechanism to make the necessary corrections. Once aligned, little power is dissipated since a nulling bridge circuit that centers on the beam is used, an important alignment feature since even laser beams broaden considerably at 1 km distances. A three-point subarray alignment arrangement is described which independently adjusts, in the three orthogonal directions, the height and tilt of subarrays within the MPTS array and readily adapts to any physical distortions of the secondary structure (such as that resulting from severe temperature extremes caused by an eclipse of the sun). Finally, it is shown that only one rotating laser system is required since optical blockage is minimal on the array surface and that it is possible to incorporate a number of redundant laser systems for reliability without affecting the overall performance.

1.0 ROTATING LASER BEAM REFERENCE SYSTEM

A commercially available rotating laser system, the Laser Level, appears to satisfy many of the requirements for achieving flatness over a very large area. A key element for achieving flatness is the use of a pentaprism for attaining exact perpendicularity about the rotating axis. A unique feature of the pentaprism is the automatic compensation of any tilting resulting from errors such as misaligned bearing surfaces.

The Helium-Neon laser source must use a collimator to minimize the inherent beam broadening, a limiting factor for defining alignments at long distances. It is estimated that the beam diameter expands from 1 mm at the laser to 3 inches at 500 m, and the sensor system must be able to accommodate this wide range of beam diameters.

2.0 OPTICAL SENSORS

A photoconductive sensor configuration has been devised to attain alignment with the center of a laser beam, for any laser beam diameter. The basis for this design is the use of a nulling-bridge detector circuit that utilizes symmetry about the separation (about 0.1 mm) of two colinear photoconductive strips which total five inches in length. The conductivity of the photoconductor increases with laser beam illumination so that equal illumination results in identical resistance and therefore a null in the resistive bridge. This null condition, when properly biased, dissipates very little power.

If the two colinear strips are asymmetrically illuminated as a result of the beam center being offset, however, the nulling condition is lost and a voltage imbalance occurs. The magnitude and polarity of this voltage imbalance can be used to drive an electric motor to realign the sensors as part of a negative feedback loop until null is again realized.

The 0.1 mm separation permits operation close to the rotating laser system, whereas the 5 inch overall length easily accommodates the 3 inch diameter laser beam at extremities of the array. Tapering of the tips of the photoconductive strips near the gap will compensate for relative signal strength changes by providing a variable resistance along the strip. Further improvements in the laser light collection

efficiency can be obtained by using optical matching by protective thin film coatings and by shaping the glass supporting structure into a paraboloidal or semi-circular shape and metallizing it to form a reflective surface.

Redundancy can be readily implemented by having multiple adjacent photoconductive strips, each driving separate variable length motors. Using a pin-and-socket arrangement, these multiple photoconductive sensors can be as easily replaced as vacuum tubes.

The locations of the three photoconductive sensors required to align each subarray are just above the attachment points, which are referred to as the three point support.

3.0 THREE POINT SUBARRAY MOUNT

In order to reduce the number of adjustments required to align the subarrays, a three point mount with a single support has been studied. The entire subarray is attached to any secondary structure configuration by only a single sturdy support. This single support can readily adapt to any tilting arising from physical distortions of the secondary structure by simply adjusting the height of the subarray.

The initial alignment procedure, during fabrication, can use the rotating laser beam reference plane to adjust the position of the single support mount. Installation consists of sliding this mount into a keyed slot built into the secondary structure and centering the beam on the photoconductive sensor located at the center of the subarray where the single support is attached. The two orthogonal tilting directions are controlled by two variable length struts which form a triangular truss with the support and subarray. Each tilting direction is independent of the other so that iterative adjustment procedures are avoided. During fabrication, an astronaut would visibly align the photoconductive sensors above the struts within the laser beam reference plane, and subsequent adjustments would be implemented by the active alignment instrumentation.

4.0 OPTICAL SENSOR POSITIONING

The use of a rotating laser beam reference system requires that a clear field of view to all sensors is desirable such that only one laser system is necessary to align all the subarrays. Since there are supporting structures located beneath the subarrays, obviously the flat radiating surface of the array is a better choice.

If the rotating laser system is in the center of the array and the optical sensors are 0.125 inches wide, then the closest sensors 7.1 m away would subtend an angle of 0.05° . Sensors located at farther distances would subtend even smaller angles. For example, the second set 11.2 m away subtends 0.03° . Using the square symmetry of the array, it is possible to illuminate all of the sensors by offsetting the laser at least 0.125 inches from the exact center. Larger width photoconductive sensors can be used and would correspondingly subtend larger angles, but the offset concept is still valid. Adjustable position sockets for the photoconductive sensors can provide some flexibility in the event of inadvertent blockage.

If redundant rotating laser systems are used, a common baseplate is recommended to ensure that both reference planes are coincident. Multiple laser systems (with pentaprisms assumed to be 2 cm wide) placed 1 m apart in line with the service corridors discussed in section 6.0 will not obscure the required field of view of each other.

Electromagnetic interference arising from the microwave power radiated from the array is reduced by the normal orientation of the photoconductive sensor to the array and its 5 inch length, which, on the basis of a dipole on a ground plane, has minimal coupling effects. Also, the metallizing of the sensor, with the possible addition of wire grids on the exposed optical face, should not permit interference. The effective cavity formed by the metallized sensor is also non-resonant to the radiated microwave frequency. Therefore the placement of the sensors on the array face is not unreasonable.

5.0 VARIABLE LENGTH MECHANISMS

In developing the concepts for an active alignment system, two of the dominating criteria were to use simple designs and attempt to

incorporate redundancy provisions suitable for operation in space, especially in view of the reluctance of using electric motors for long duration missions.

The variable length mechanism, which is basically a worm gear drive driven by a stepping motor, is the only electromechanical device used for this active alignment scheme. The redundant variable length mechanisms are short segments serially located along the strut, each independently driven by a separate photoconductive sensor nulling bridge circuit. If for some reason one motor or the bearings of one variable length mechanism fails, then the other redundant systems intrinsically maintain the variable length capability. And if multiple failures occur, replacement of the entire strut consists of removing and installing only two pins in a U-clamp arrangement.

The center support attachment is unique in that it uses a universal ball joint about which the subarray can readily pivot in any direction. The side orthogonal support struts, designated arbitrarily as azimuth (Az) and elevation (El), pivot about the axis formed by the central universal ball joint and the opposite side strut attachment point. Since three points in space define a plane and if these three photoconductive sensors align themselves to the laser beam reference plane, then the subarray is considered aligned. And on a macroscopic scale, if all subarrays are aligned, the array itself is aligned.

Since worm gear drives move by the rotation and translation along a pitched thread, the actual physical movement can be made quite small by means of gearing ratios and stepping motors. Further, by geometrical considerations of the triangular struts, the actual amount of tilting for a given amount of variable length change is quite small. Therefore an extremely high degree of resolution is achievable in adjusting the orientation of the subarray and therefore the array itself. Once this premise is accepted, then it is easy to imagine that the design engineers can extend the concept so that the desired practical resolution is feasible, by the proper choice of pitched threads and the specifications for the stepping motor.

6.0 MAINTENANCE SERVICE CORRIDORS

One aspect of the three-point support is the existence of a square matrix of service corridors or passageways directly under the subarrays for rapid accessibility for necessary repairs. A service vehicle traversing these corridors will be at most only half a subarray dimension away from any position in the array. In addition, since there are only three supports per subarray, the supporting under-structure is not cluttered.

The matrix of corridors also presents the possibility of incorporating a shadow-masking alignment monitoring scheme using 170 laser beams on two adjacent sides passing through strategically placed apertures under the subarrays and incident on detecting sensors on the opposite side. Misalignment is indicated by the loss of signals in both intersecting laser beams, thereby immediately locating the source of the problem.

7.0 MONOPULSE POINTING SYSTEM

A related topic of discussion to the alignment scheme is the accurate pointing of the MPTS array towards the effective location of a pilot beam, which may vary due to refractive variations of the ionosphere. One method which might be considered is a monopulse tracking system that senses the phase differentials of an encoded pilot beam and points the array in the proper direction. Although this scheme will not permit rapid compensation, if the ionospheric fluctuations are slow, the pointing accuracy will be adequate such that instantaneous fine pointing adjustment by an auxiliary retrodirective pilot beam phase reference system is possible.

Four receiving antennas, mounted within a microwave baffle to reduce coupling effects to the radiated microwave power, located at the extremities of the array, will allow active tracking of the pilot beam source located at the rectenna.

IONOSPHERIC POWER BEAM STUDIES

LEWIS M. DUNCAN

LOS ALAMOS SCIENTIFIC LABORATORY

WILLIAM E. GORDON

RICE UNIVERSITY

23 MW/CM²

A POWER DENSITY LEVEL OF 23 MW/CM² HAS ACHIEVED THE STATUS OF A FIRM DESIGN SPECIFICATION BASED ON THEORETICAL CALCULATIONS OF A THRESHOLD FOR MICROWAVE-IONOSPHERE NONLINEAR INTERACTION (THERMAL RUNAWAY).

THERMAL RUNAWAY IS NO LONGER A VALID THEORETICAL CONCEPT ALTHOUGH FOR COMPARABLE POWER DENSITIES ENHANCED ELECTRON HEATING IS OBSERVED TO CHANGE THE ELECTRON TEMPERATURE BY A FACTOR OF TWO OR THREE, BUT NOT BY AN ORDER OF MAGNITUDE.

THERE IS, SO FAR, NO EXPERIMENTAL EVIDENCE TO SUPPORT 23 MW/CM² AS AN UPPER LIMIT.

THE QUESTION TO BE POSED AND ANSWERED IS AT WHAT POWER DENSITIES IS THE IONOSPHERE MODIFIED IN A WAY THAT PRODUCES UNACCEPTABLE COMMUNICATION EFFECTS AND/OR ENVIRONMENTAL IMPACTS?

ARECIBO TEST RESULTS

CASE 1 HEATING WAVE PENETRATED THE IONOSPHERE

FREQUENCY	OHMIC HEATING AS A FRACTION OF 5 GW SPS HEATING	DIAMETER OF HEATED VOLUME RELATIVE TO SPS HEATED VOLUME	CROSS SECTION FOR FIELD-ALIGNED SCATTER IS LESS THAN
6-10 MHz	1%	3.00	$4 \times 10^{-3} \text{M}^2$
430 MHz	40%	0.10	$4 \times 10^{-3} \text{M}^2$
2380 MHz	5%	0.01	10^{-3}M^2

ARECIBO TEST RESULTS

CASE 2 HEATING WAVE REFLECTED BY THE IONOSPHERE (NOT THE SPS CONDITION)

PLASMA INSTABILITIES ARE EXCITED BY THE HF HEATER WAVE LEADING TO FIELD-ALIGNED STRIATIONS THAT SCATTER RADIO WAVES.

FIELD-ALIGNED RADIO-SCATTERING CROSS-SECTIONS UP TO 10^3M^2 .

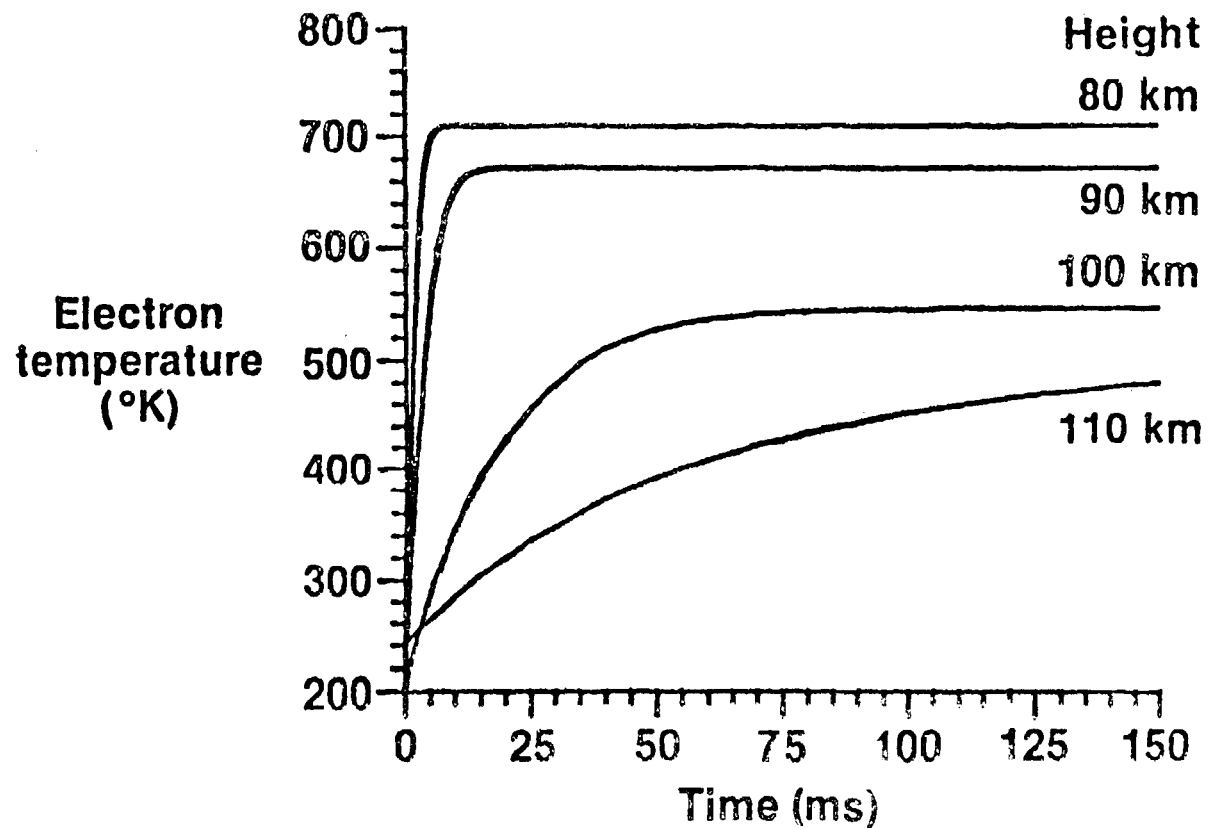
SINCE THE EXCITATION OF THESE INSTABILITIES REQUIRES A MATCHING OF THE HEATER FREQUENCY TO THE IONOSPHERIC PLASMA FREQUENCY, A CONDITION THAT IS NOT MET BY THE SPS, THEY WILL NOT BE EXCITED. NO OTHER INSTABILITIES ARE PRESENTLY KNOWN THAT THE SPS FREQUENCY WILL EXCITE.

THE SIMULTANEOUS ILLUMINATION OF THE IONOSPHERE BY THE SPS FREQUENCY AND A SECOND FREQUENCY SEPARATED BY ABOUT 15 MHz OR LESS COULD PRODUCE THE INSTABILITIES DESCRIBED ABOVE.

ENHANCED ELECTRON HEATING BY THE SPS BEAM

- (1) WILL INCREASE ELECTRON TEMPERATURES BY UP TO A FACTOR OF THREE OR MORE, MOSTLY IN THE LOWER IONOSPHERE.

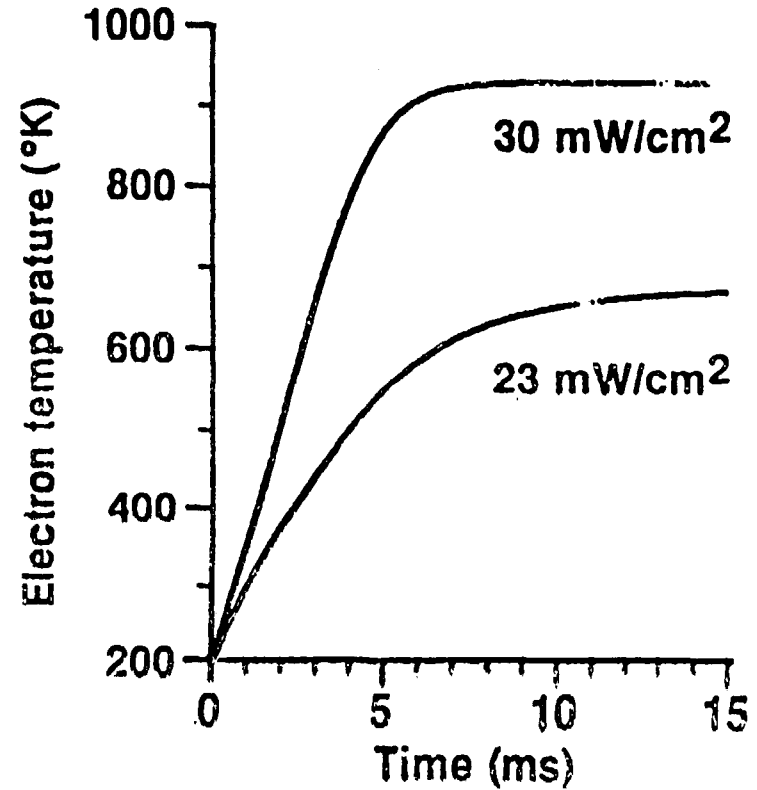
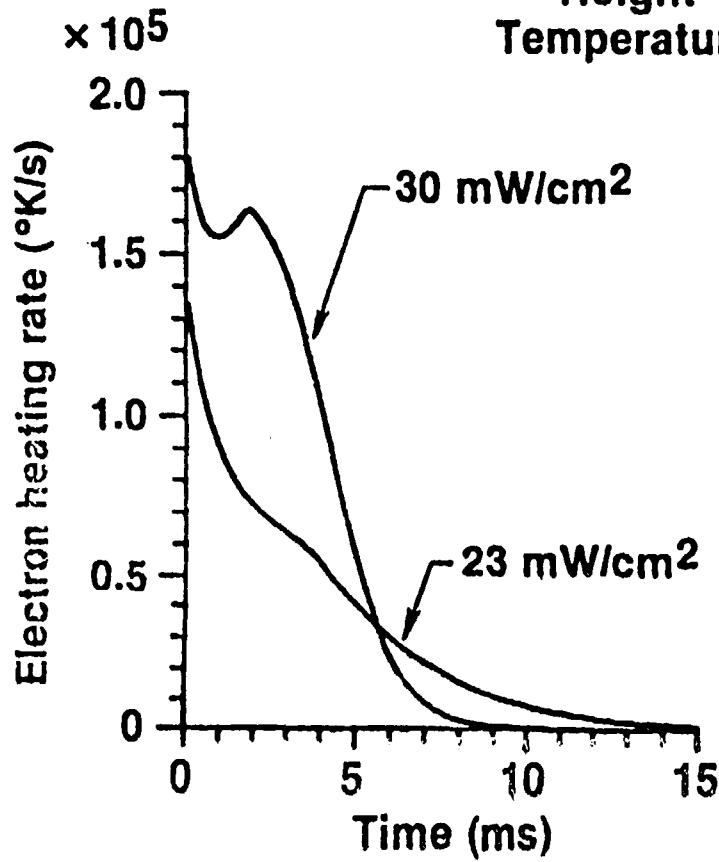
Power flux = 23 mW/cm²
Frequency = 2450 MHz
Standard midlatitude atmosphere



ENHANCED ELECTRON HEATING BY THE SPS BEAM

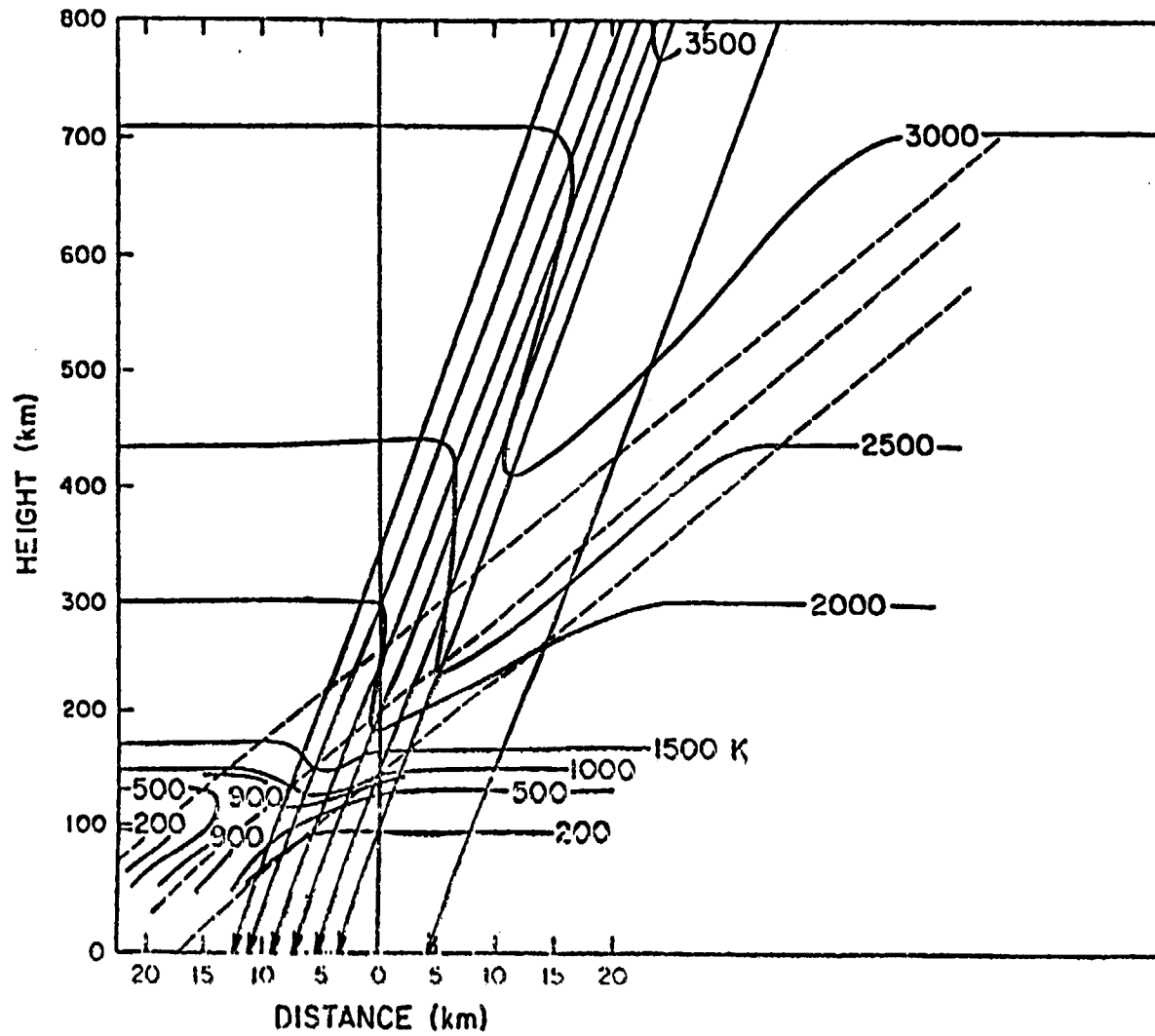
(2) IS PREDICTED TO BE DEPENDENT ON THE INCIDENT POWER DENSITY.

Frequency = 2450 MHz
Height = 90 km
Temperature = 187°K.



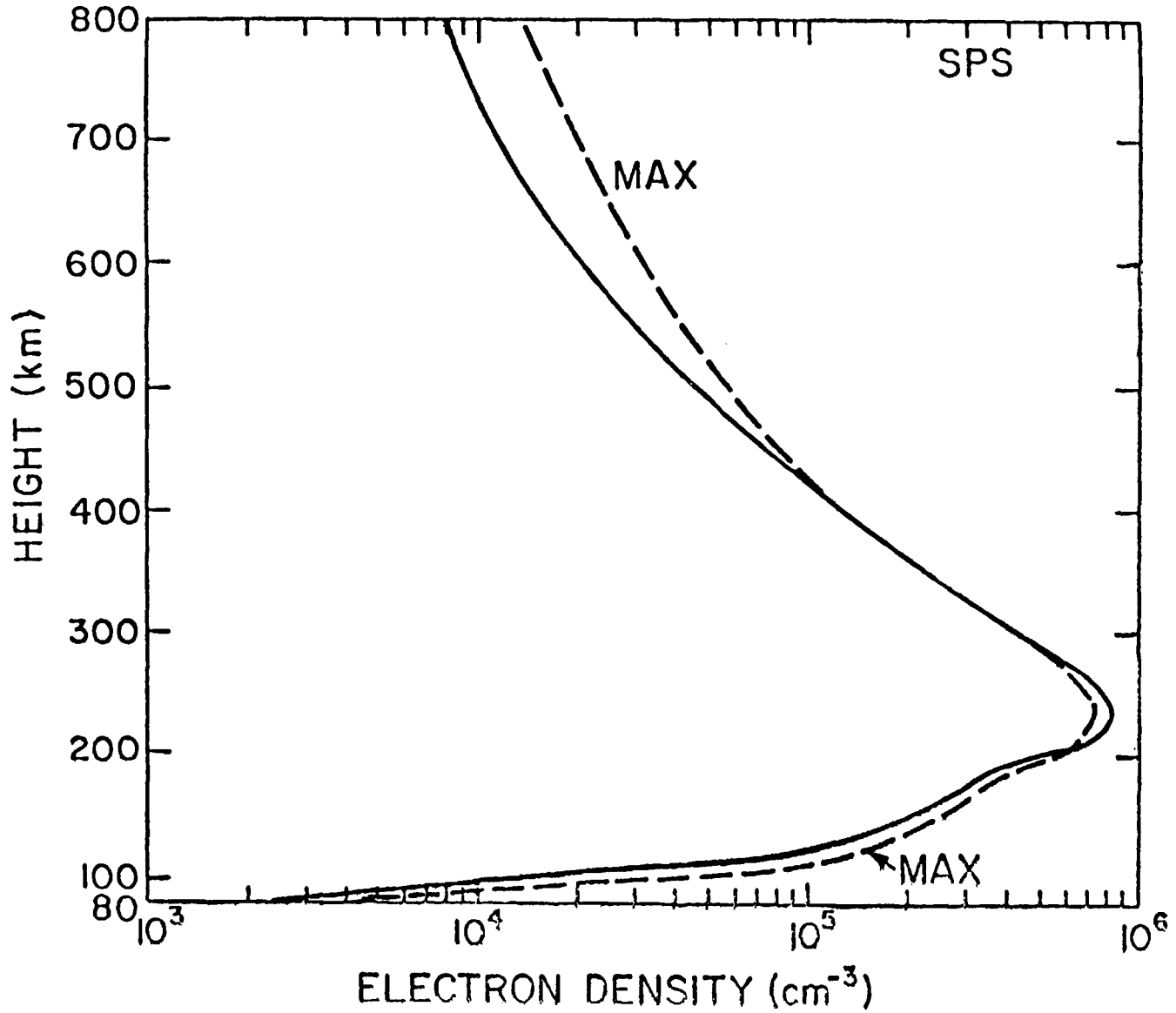
ENHANCED ELECTRON HEATING BY THE SPS BEAM

(3) WILL INCREASE ELECTRON TEMPERATURES IN AND NEAR THE BEAM BY SMALL FACTORS.

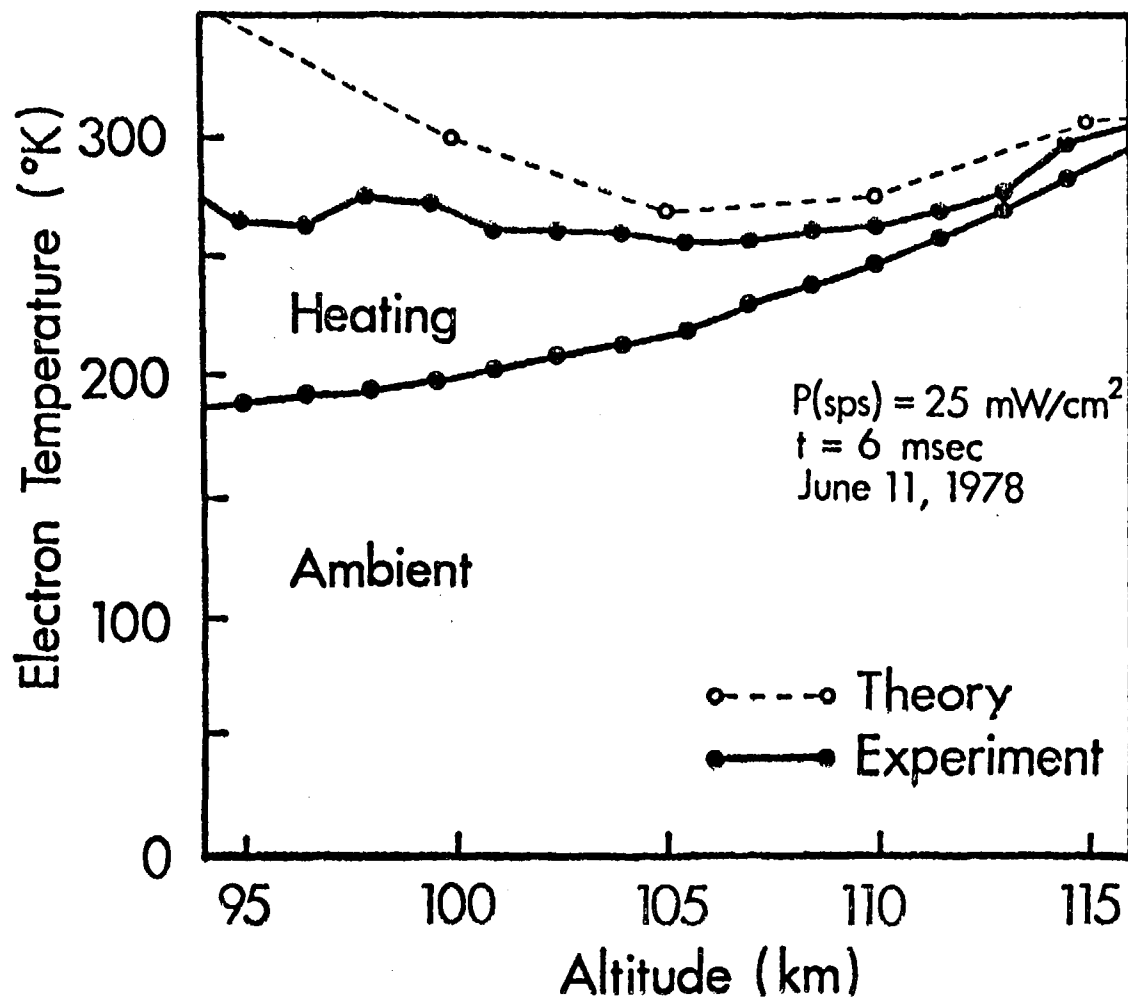


ENHANCED ELECTRON HEATING BY THE SPS BEAM

(4) WILL CHANGE THE ELECTRON DENSITY IN THE BEAM BY SMALL AMOUNTS.



OBSERVATIONS OF ENHANCED ELECTRON HEATING AT ARECIBO ARE CLOSE TO, BUT BELOW,
THE PREDICTED INCREMENTS.

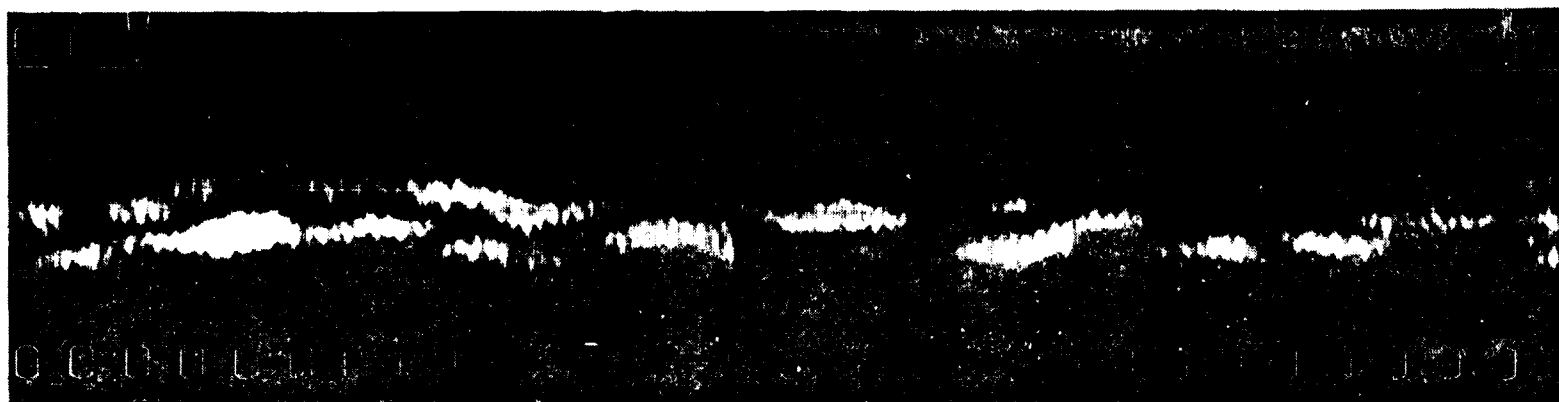


COMPARISON OF 5800 MHz AND 2450 MHz

<u>MEDIUM</u>		<u>2450 MHz</u>	<u>5800 MHz</u>
IONOSPHERE		1 KW	0.25 KW
NEUTRAL ATMOSPHERE AT 60° ELEVATION ANGLE		90 MW	100 MW
RAIN (25MM/HR OVER 20 KM PATH IN BEAM)		45 MW	1.450 GW
HAIL (1.93 CM DIAMETER HAILSTONES, 10 KM PATH THROUGH THE BEAM)	DRY	0.2 GW	1.7 GW
	WET	2.7 GW	4.99 GW

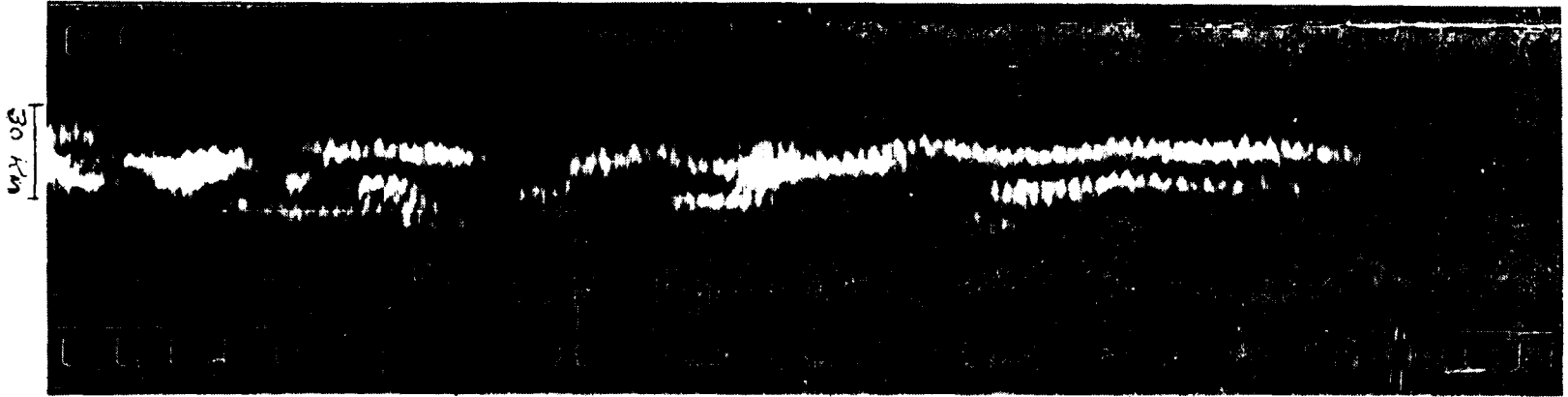
RADAR ECHOES FROM FIELD-ALIGNED STRIATIONS

61



RADAR ECHOES FROM FIELD-ALIGNED STRIATIONS

62



1 SEC

PROPOSED EXPERIMENTAL STUDIES FOR ASSESSING IONOSPHERIC
PERTURBATIONS ON SPS UPLINK PILOT BEAM SIGNAL

Santimay Basu and Sunanda Basu
Emmanuel College
Boston, MA 02115

Introduction

The microwave beam of the proposed Solar Power Satellite (SPS) at geosynchronous altitude is to be formed and directed by phase information derived from a pilot signal at 2.45 GHz transmitted from ground and received in a number of module locations on the SPS antenna. The frequency of the pilot signal has been chosen to be sufficiently low as to avoid the effects of strong scattering by turbulence in the neutral atmosphere and yet high enough to avoid any possible refractive effects caused by the ionized upper atmosphere. However, the ionosphere is known to contain irregular variation of concentration due to natural processes and the downlink microwave beam has also been predicted to interact with the ionosphere to cause artificial irregularities (Perkins and Valeo, 1974; Perkins and Roble, 1978; Duncan and Behnke, 1978). Thus the uplink pilot signal has to propagate through the ionosphere containing natural and possibly some artificial irregularities. In view of the fact that microwave signals from communication satellites suffer considerable perturbations both in intensity and phase in the equatorial and auroral zones there has been some concern that the uplink pilot signal may suffer perturbations with possible consequences to the formation of the downlink high power microwave beam. While there may exist some satisfaction regarding the SPS site location at midlatitudes avoiding the intense belt of equatorial and auroral irregularities, there is evidence for the occurrence of ionospheric irregularities at midlatitudes causing considerable perturbations of signal intensity at VHF and even at GHz. Though these effects due to natural irregularities are usually smaller at midlatitudes as compared to the equatorial zone, the effective perturbations at midlatitudes may become magnified if a geostationary satellite acquires finite orbital inclination. The generation of artificial irregularities by ionospheric heating in the underdense mode and the effects thereof on transionospheric microwave propagation remain totally

unexplored from the experimental standpoint. In the following sections we shall provide some evidence of the occurrence of natural irregularities at midlatitudes based on scintillation measurements by the use of VHF and GHz transmissions from geostationary satellites and satellite in-situ measurements. We shall then provide an outline of our proposed measurements related to the detection, lifetime and drift of artificial irregularities generated by ionospheric heating in the underdense mode.

Formulation of the Problem

Figure 1 illustrates that in the presence of fluctuations of ionospheric electron concentration confined within a layer of thickness L_e , an incident plane wave undergoes phase fluctuations as it emerges from the layer. For small phase fluctuations, the emerging wavefront contains only phase perturbations without any fluctuations in intensity. As the wavefront propagates towards the observer's plane, phase mixing occurs and thereby spatial intensity fluctuations also develop. In the presence of a relative motion between the propagation path and the irregularities, the spatial variations of intensity and phase sweep past the observer's receiving system giving rise to temporal variations in phase and intensity called phase and intensity scintillations. In the practical situation, such as for the SPS case, or radio wave scintillation measurements, the ionospheric irregularities between the transmitter and the receiver are located in the far zone of the transmitter so that the radiation can be well approximated by a spherical wave. On the other hand, the beam nature of the wave has to be considered when the irregularities are located in the near zone of the transmitter as frequently encountered in optical propagation (Ishimaru, 1978). In the case of spherical wave propagation between a transmitter and receiver separated by a distance L and the scatterers at a variable distance η from the transmitter the correlation functions of intensity (I) and phase (ϕ) over the receiving plane in the weak-scatter regime are given by:

$$\begin{aligned}
 B_I(L, \rho) &= \langle I(L, \rho_1) I(L, \rho_2) \rangle \\
 &= (2\pi)^2 \int_0^L d\eta \int_0^\infty \kappa d\kappa J_0(\kappa\eta\rho/L) |H_r|^2 \phi_n(\kappa)
 \end{aligned} \tag{1}$$

$$\begin{aligned}
B\phi(L, \rho) &= \langle \phi(L, \rho_1) \phi(L, \rho_2) \rangle \\
&= (2\pi)^2 \int_0^L d\eta \int_0^\infty \kappa d\kappa J_0(\kappa\eta\rho/L) |H_i|^2 \phi_n(\kappa) \quad (2)
\end{aligned}$$

where

ρ - dimension transverse to propagation path
 κ - irregularity wave number
 $\phi_n(\kappa)$ - irregularity wave number spectrum
 k - wave number of the propagating wave

$$|H_r|^2 = k^2 \sin^2 |\eta(L-\eta)\kappa^2/2kL|$$

$$|H_i|^2 = k^2 \cos^2 |\eta(L-\eta)\kappa^2/2kL|$$

The variance of intensity and phase may be obtained by putting $\rho = 0$ in equations (1) and (2). These equations may be used to obtain the respective variances from a knowledge of the irregularity spectrum. In solving the equations for the ionospheric case, it must be considered that the irregularities in the inertial subrange cause the diffraction effects as distinct from the case of geometrical optics. Measurement of variances and temporal spectra allow a determination of the strength of turbulence which may then be used to derive the structure functions of phase and intensity. In principle, direct measurements of phase and intensity correlations are possible using the spaced receiver technique with variable baselines.

Strong Ionospheric Irregularities at Midlatitudes

At Ramey Air Force base near Arecibo, Puerto Rico, nighttime scintillation events accompanied by long period (30 mins to 1 hour) variations of total electron content have been routinely observed (Kersley et al., 1979; Basu et al., 1979). The top panel in Figure 2 shows the temporal (local time = UT-4.5 hours) variations of total electron content measured with a radio polarimeter by the use of 137 MHz transmissions from geostationary satellite, SMS-1. The bottom panel shows that the fluctuations in total electron content were accompanied by intensity scintillations in excess of 15 dB.

Satellite in-situ observations have also revealed existence of such large and small scale structure near Arecibo. The

solid line in Figure 3 shows the spatial variation of ion concentration, N (or electron concentration for charge neutrality at F region heights) recorded by the ion drift meter on board the Atmosphere Explorer E satellite. The AE-E data has been kindly made available to us by W.B. Hanson. The ion concentration is sampled 16 times per sec. The irregularity amplitude $\Delta N/N$ computed from 3-sec intervals of N data are indicated by the circles. The satellite altitude, longitude, magnetic local time and latitude are indicated in the diagram. Long period spatial variations of electron concentration, as well as, steep horizontal gradients at a latitude close to that of Arecibo may be noted. Such steep gradients are accompanied by small scale irregularities with amplitudes exceeding 10%. Such levels of irregularity amplitude ($\Delta N/N$) and ambient density (N) provides ΔN values which can explain observed scintillation events near Arecibo shown in Figure 2 if we assume a layer thickness of about 100 km (Basu and Basu, 1976).

In Figure 4 we show a case of similar perturbations of total electron content accompanied by 1 dB fluctuation of intensity at 1.7 GHz (Fujita et al., 1978). Such levels of GHz scintillation activity with a maximum of 2.3 dB are often observed near the June solstice at Kashima, Japan with ETS-II satellite, for which the propagation path is nearly aligned with the earth's magnetic field. It may be of interest to note that the magnetic dip location of Kashima is nearly identical to that of Arecibo although the geographic latitude is higher than Arecibo. An equivalent enhancement of scintillation activity may be encountered at U.S. sites such as, Boulder or Arecibo, if the geostationary satellite acquires finite orbital inclination. Such large amplitude natural irregularities may cause phase perturbations at the SPS frequency. Their effects on both the pilot and power beams should be carefully assessed.

Proposed Measurement of Phase and Intensity Scintillation Effects During Ionospheric Heating

We have made plans to perform several experiments in conjunction with RF ionospheric heating both in the overdense and underdense modes at Arecibo and at Platteville. In December, 1979, we had planned to make use of the Arecibo heating facility and perform ground and airborne measurements of the effects of ionospheric heating. Figure 5 shows the observing geometry, the shaded region indicating the heated volume at 5 MHz. From Roosevelt Roads, Puerto Rico, we planned to receive the 249 MHz transmissions from LES-9 and obtain the variance and temporal spectra

of phase and intensity scintillations at that frequency. In view of the finite orbital inclination of LES-9 satellite, the locus of the intersection of the propagation path with 300 km ionospheric height lies within the heated volume between 06-10 UT. In addition, the AFGL Airborne Ionospheric Observatory agreed to provide supporting measurements of phase and intensity scintillations using LES-9 and Fleetsatcom satellites (Figure 5) 6300 Å airglow and ionosonde measurements. The Fleetsatcom satellite was chosen to probe the ionosphere outside the heated volume and detect the presence of naturally occurring irregularities. The aircraft was also expected to scan the heated region to define the extent of the perturbed volume. Simultaneous diagnostic incoherent scatter measurements from Arecibo Observatory were requested for determining the electron concentration and temperature.

Unfortunately, the Arecibo Heating Facility could not be made operational in December, 1979 so that the above experiments had to be postponed. However, we have drawn up a back-up plan for similar experiments using the LES-8 satellite in conjunction with the heating facility at Platteville during Feb-March, 1980 (Rush et al., 1979). In addition to some of the experiments outlined above, we have planned to include spaced receiver scintillation measurements to obtain ionospheric drift. We also propose to set up an observing station such that a field aligned propagation path can be viewed through the heated volume. These measurements will provide an estimate of the phase and intensity structure functions. Experimental support for the above program will be provided by Dr. J. Aarons of AFGL. At a later date, we shall utilise the phase coherent spread spectrum signals from NAVSTAR-GPS satellites at 1575 MHz and 1227 MHz to make accurate phase scintillation measurements in the GHz range. These results are expected to provide a direct input to the design of the SPS system. However, it is essential that the heating facilities at Arecibo and Platteville be upgraded as proposed by Gordon and Duncan (1978) and Rush et al., (1979) to meet the SPS power density levels at F-region altitudes before accurate experimental results can be provided for predicting SPS ionospheric and telecommunication systems impact.

This work was partially supported by National Science Foundation Grant No. ATM 78-25264 and Air Force Geophysics Laboratory Contract F19628-78-C-0005.

References

- Basu, S. and S. Basu, Geophys. Res. Lett., 3, 681, 1976.
- Basu, S., S. Basu, S. Ganguly and J.A. Klobuchar, Simultaneous Incoherent Scatter and Scintillation/Total Electron Content Observations in the Mid-latitude Ionosphere, presented at National Radio Science Meeting, URSI, Boulder, Colorado, November, 1979.
- Duncan, L.M. and R.A. Behnke, Phys. Rev. Lett., 41, 998, 1978.
- Fujita, M., T. Ogawa and K. Koike, J. Atmos. Terr. Phys., 40, 963, 1978.
- Gordon, W.E. and L.M. Duncan, NASA Report No. NAS9-15212, July, 1978.
- Ishimaru, A., Wave Propagation and Scattering in Random Media, Academic Press, New York, 1978.
- Kersley, L., J. Aarons and J.A. Klobuchar, J. Geophys. Res., 1979 (in press).
- Perkins, F.W. and E.J. Valeo, Phys. Rev. Lett., 32, 1234, 1974.
- Perkins, F.W. and R.G. Roble, J. Geophys. Res., 83, 1611, 1978.
- Rush, C.M., J.C. Carroll and E.J. Violette, Report No. NTIA-TM-79-27, U.S. Dept. of Commerce, October, 1979.

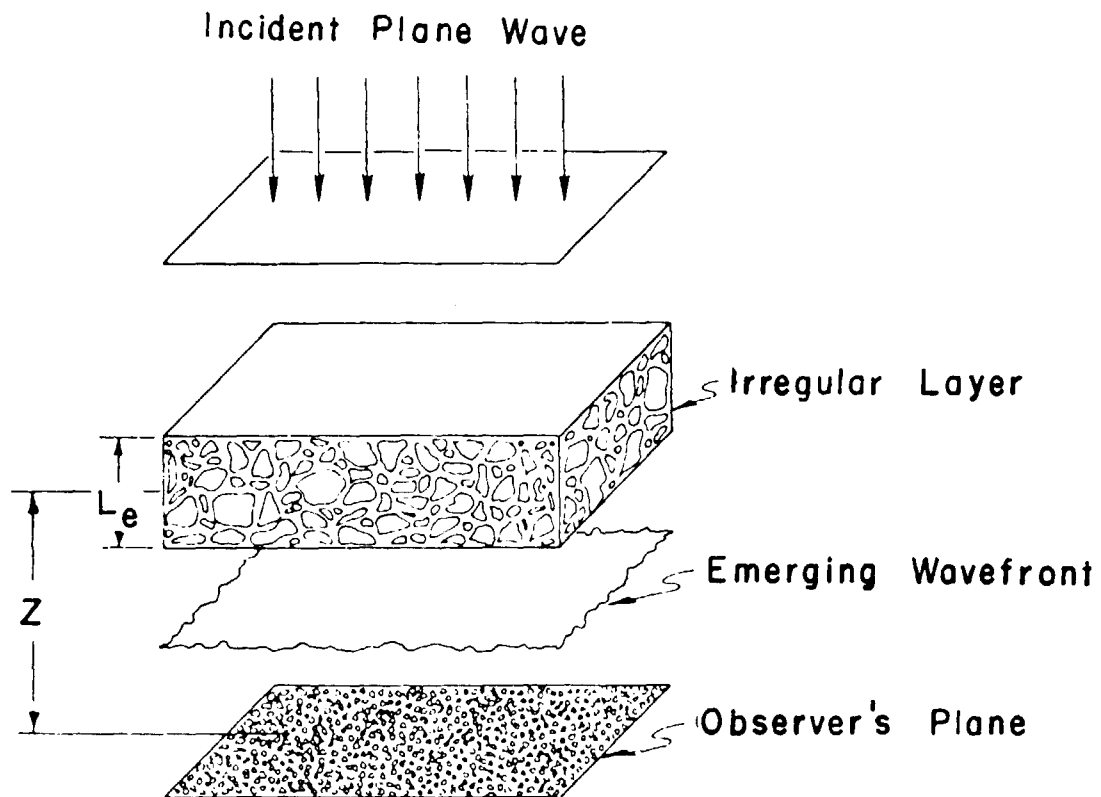


Figure 1. Geometry of the scintillation problem.

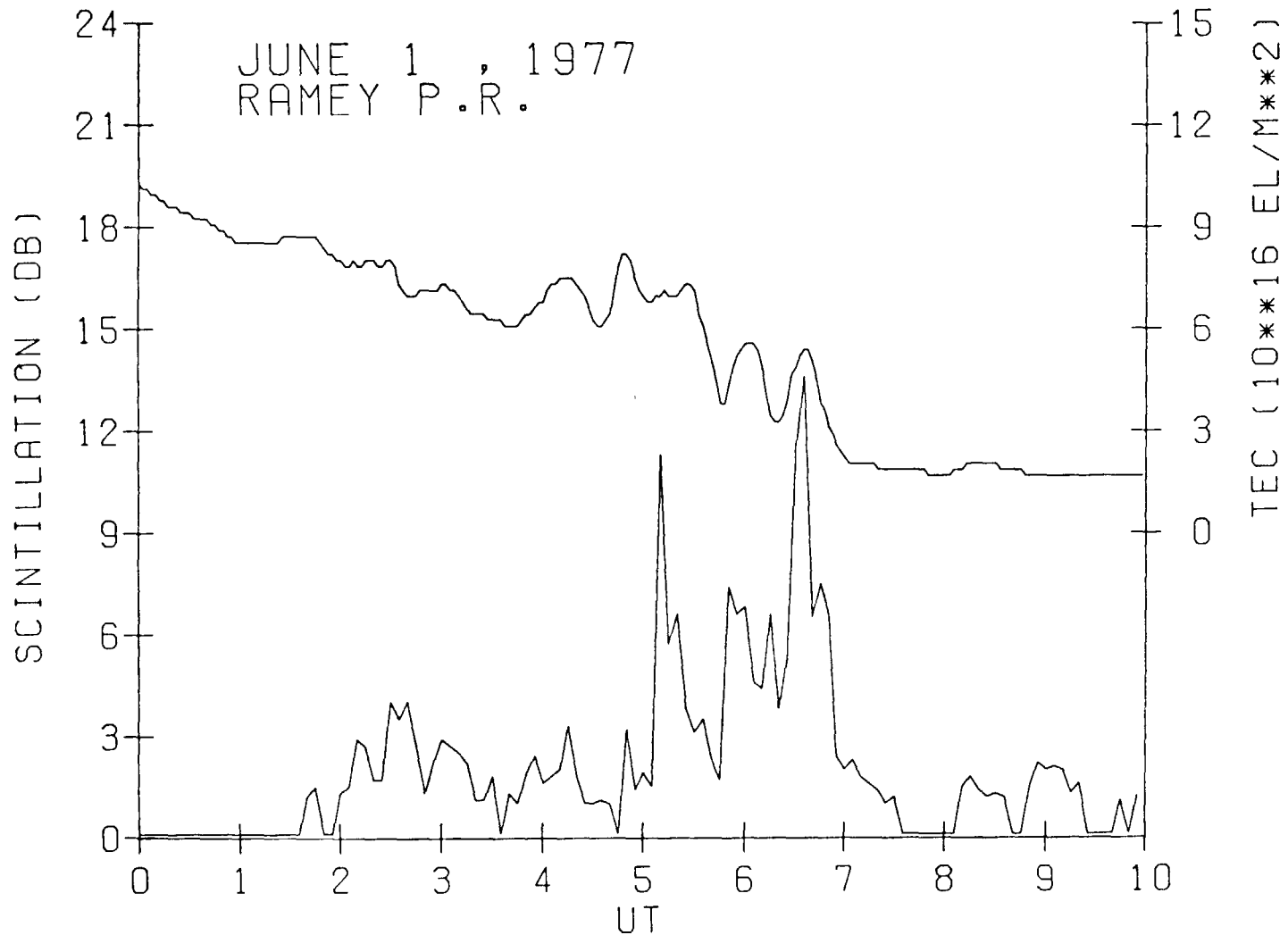


Fig. 2. Total electron content (top panel) and scintillation (lower panel) measurements obtained at Ramey Air Force Base, P.R., using SMS-1 at 137 MHz on June 1, 1977 showing large amplitude scintillations correlated with content fluctuations. This diagram was made available by J.A. Klobuchar of AFGL.

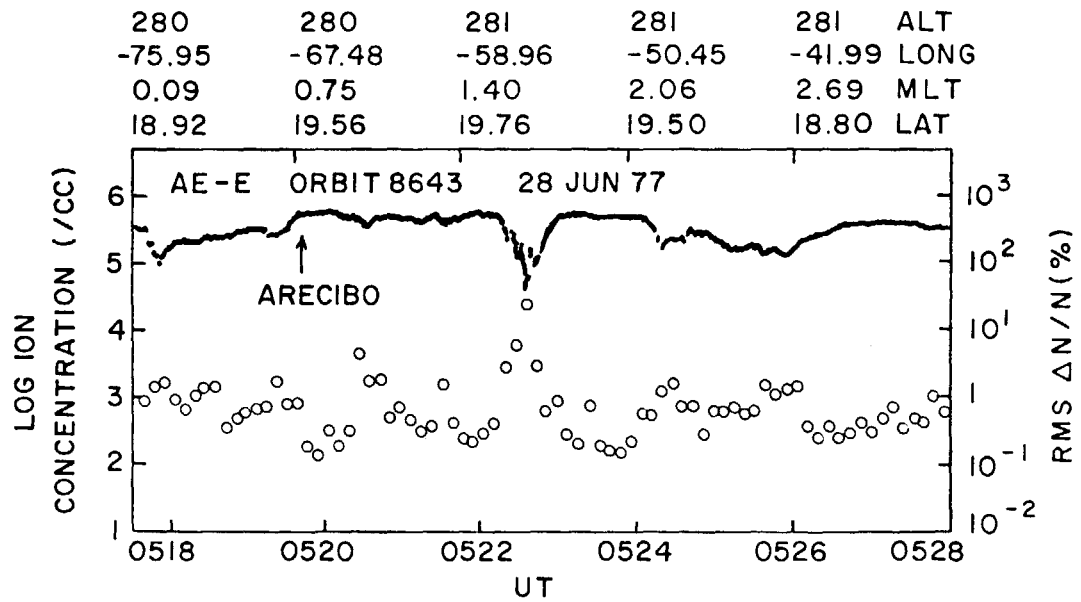


Figure 3. Atmospheric Explorer E orbit near Arecibo showing large amplitude irregularities.

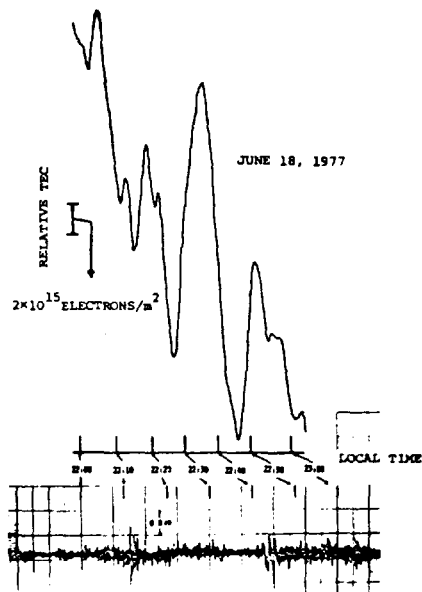


Figure 4. Example of nighttime scintillation (lower) and irregular variation of TEC (upper) observed at Kashima on June 18, 1977.

SATELLITE POSITIONS FOR DEC. 20, 1979
 300km INTERSECTIONS FROM ROOSEVELT ROADS, P. R.

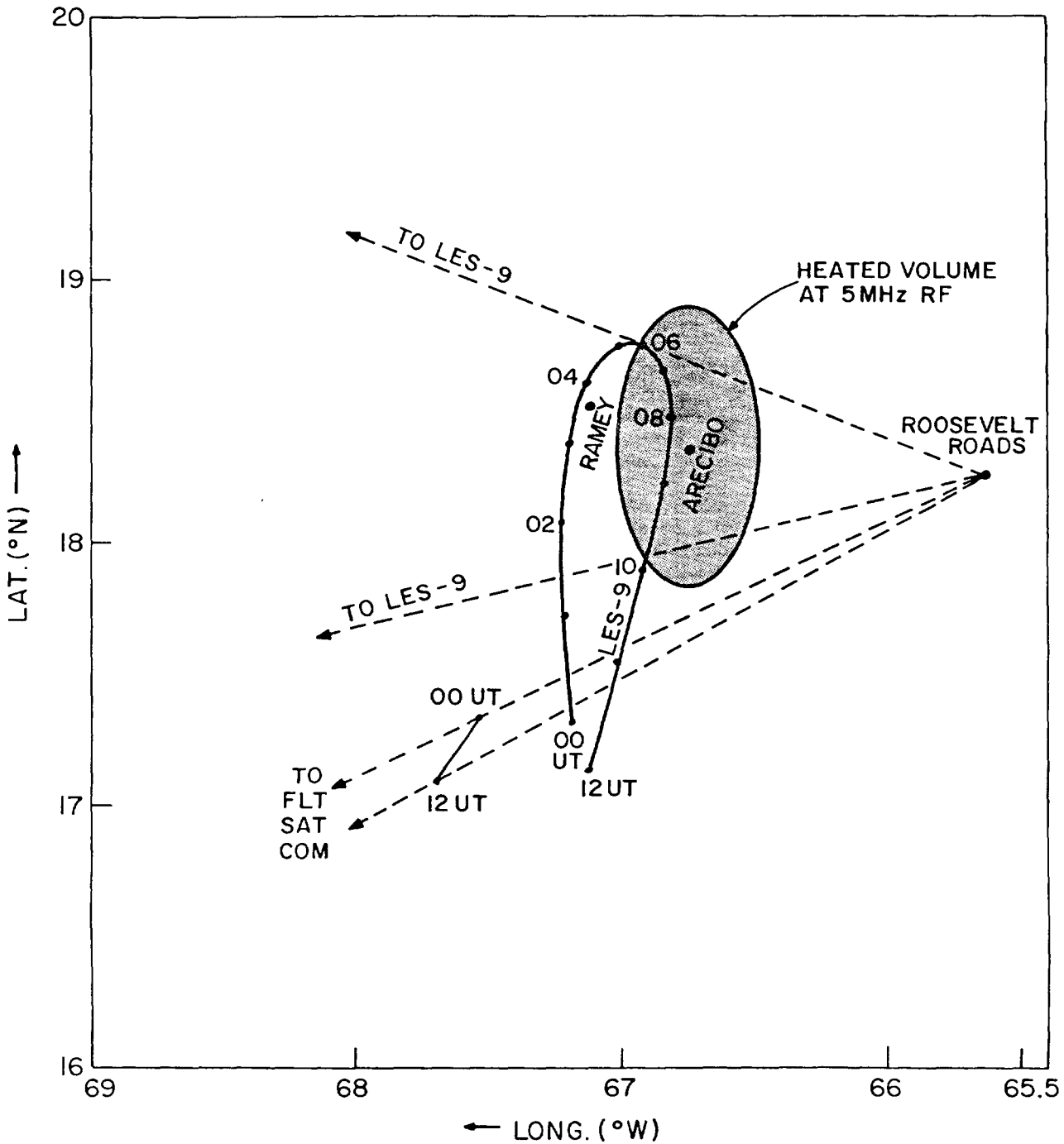


Figure 5. Observing geometry of LES-9 and Fleetsatcom satellites during proposed ionospheric heating from Arecibo.

CONCLUSIONS PRESENTED AT THE SYSTEM PERFORMANCE SESSION

1. Performance Based on System Sizing
 - a. Reduced power levels (< 5GW) will have only small degradations in microwave transfer efficiency.
 - b. Antennas with less than 1 Km diameter at 2450 MHz quickly degrade in microwave transmission efficiency as the size decreases.
2. Antenna Illumination - a 10-step, 10dB gaussian taper is the optimum antenna illumination for rectenna collection efficiency, given the 21 kW/m² and 23 mW/m² constraints.
3. Antenna/Subarray Mechanical Alignments
 - a. Antenna/subarray mechanical alignment is constrained by the allowable peak grating lobe levels (assumed to be $\leq .01$ mW/cm²) and the allowable scattered power levels.
 - b. Antenna alignment is constrained to ≤ 1 min. for phase control at the 10-meter per side subarray size and ≤ 3 min. for phase control to the power module (tube) level (average 3 meters per side subarray size).
 - c. The subarray size of 10m X 10m, based on microwave system requirements, represents a good compromise between conflicting mechanical and electronic requirements. Larger subarrays (e.g. 18m X 18m) would require motor-driven screwjacks, whereas smaller subarrays (e.g. 4m X 4m) would complicate the phase control electronics and construction and maintenance requirements.
4. Startup/Shutdown Operations - Three possible sequences for antenna startup/shutdown operations will provide sidelobe peak levels outside of the rectenna boundaries less than those experienced during normal steady-state operations.
5. Sources of Scattered Microwave Power - The greatest contributors to lost or scattered microwave power are, in order of importance:
 - Tube failures - 268 MW, based on a maximum of 2% tube failures at any one time
 - Phase errors - 188 MW, based on 10° RMS phase error
 - Subarray tilt - 188 MW, based on ± 3 min. subarray misalignment
 - Amplitude error - 67 MW, based on ± 1 dB amplitude error across the surface area fed by one klystron tube
 - Antenna tilt - 27 MW, based on ± 1 min. antenna misalignment
 - Subarray spacings - 6.7 MW, based on 0.25-inch gap spacing between mechanical subarrays.

SYSTEM PERFORMANCE CONCLUSIONS (CONTINUED)

6. Initial theoretical studies indicate that Faraday rotation induced by the ionosphere will not be a problem.

REMAINING ISSUES - ENVIRONMENTAL - PRESENTED AT THE SYSTEM PERFORMANCE SESSION

1. Validity of the present ionospheric transmission limit of 23 mW/cm^2
2. Effects of heating/disturbing the ionosphere on communications
3. Effects of heating/disturbing the ionosphere on performance of microwave system
4. Electromagnetic compatibility
 - a. Radiated noise/harmonics at SPS
 - b. Reradiated noise/harmonics at rectenna

SECTION III

PHASE CONTROL SESSION

Chairman: Jack W. Seyl
NASA, Johnson Space Center

Active Retrodirective Arrays
for SPS Beam Pointing

Ralph Chernoff
Jet Propulsion Laboratory

I. INTRODUCTION

The basic requirement of the SPS beam pointing system is that it deliver a certain amount of S-band ($\lambda = 12.5$ cm) power to a 9.6 km diameter receiving antenna ("rectenna") on the ground. The power is transmitted from a 1.0 km diameter antenna array on the SPS, which is, for a rectenna at about ± 40 deg. latitude, some 37.5×10^6 km distant. Figure 1 shows the "pointing loss", i.e. the relative loss of intercepted power, as a function of pointing error. With perfect pointing the rectenna intercepts 93.5% of the SPS beam, but Figure 1 shows that this falls to 92.6% (1.0% pointing loss) when the pointing error (displacement of peak of beam from rectenna center) is 0.66 km, and 91.6% (2.0% loss) when it is 0.90 km; i.e., pointing loss increases roughly as the square of the pointing error for small errors.¹ 0.66 km is equivalent to $0.66/37.5 \times 10^3 = 17.6$ microradians angular error. At the present time ARA's appear to be the best bet to realize this very stringent beam pointing requirement.

An active retrodirective array (ARA) transmits a beam towards the apparent source of an illuminating signal called the pilot (Figure 3). "Active" implies that the array produces, not merely reflects, RF power. Retro-directivity is achieved by retransmitting from each element of the array a signal whose phase is the "conjugate" of that received by the element. Assuming that the phase of the pilot signal received by the kth element of the array at time t is

$$\phi_k(t) = \omega (t - r_k/c), \quad (1)$$

where r_k is the distance from the kth element to the source of the pilot signal, we define the conjugate of ϕ_k to be

$$\phi_k(t)^* = \omega'(t + r_k/c) + \phi_0 \quad (2)$$

where ϕ_0 is an arbitrary phase offset which must, however, be constant over

¹. Figure 1 is calculated from two computer programs recently developed at JPL. The first computes the the exact far field power density from a series expansion of the radiation integral for a circular aperture with Gaussian illumination, and the second numerically integrates that power density over the rectenna for various values of the pointing error. The far field program assumes an exact, continuous, Gaussian illumination without phase or amplitude errors. It should not be confused with the program previously developed by W.F. Williams of JPL for the express purpose of simulating the effects of such errors, and which (for that very reason) consumes far more computer time than the present program.

the entire array. In order to do this, each element of the array must be equipped with a phase conjugation circuit (PCC). The phase of the signal received from the k th element by a receiver located at the pilot source ($r = 0$) at time t is

$$\phi_k(t,0) = \omega'(t + r_k/c - r_k/c) + \phi_0 = \omega' t + \phi_0. \quad (3)$$

Thus the contributions to the field at $r = 0$ from the various elements of the array are all in phase at that point, which means that the beam points toward the pilot source. Note that this definition does not require that the transmitted frequency, ω' , be the same as the pilot frequency. We will, in fact, assume that $\omega' \neq \omega$, as it normally must be in order to provide input-output isolation, but retrodirectivity will still result if the propagation medium is reciprocal and non-dispersive. Note also that the elements of the ARA need be neither equally spaced nor coplanar. The array pattern will, of course, suffer if the array geometry is too irregular, but it will still be retrodirective. Note finally, that the pilot signal wavefront need not be spherical; the ARA will still be retrodirective even if the pilot wavefront is distorted by an inhomogeneous medium provided that the medium is slowly varying (changes negligibly within a round trip light time). In sum, the only necessary conditions for the proper operation of an ARA are that the propagation medium be reciprocal, non-dispersive and slowly varying. The ARA's relative insensitivity to dimensional and propagation medium perturbations makes it highly suitable to the SPS (as well as to a number of other space applications).

An ARA is, to a high degree, inherently failsafe in that failure of the pilot signal results in the immediate collapse of the downlink beam due to the destruction of the phase coherence of the elements of the array. The residual ground level intensity due to the n incoherent signals radiated by an ARA in the absence of a pilot is of order $p/2n$ (depending somewhat on the illumination taper) where n is the number of ARA elements and p is the peak intensity of the beam during normal ARA operation, i.e. in the presence of a pilot signal. For the SPS reference system, $p = 23 \text{ mW/cm}^2$ and $n = 7200$, so $p/2n$ is about 0.002 mW/cm^2 , which is well below levels presently considered hazardous.

II. ARA DESIGN PROBLEMS AND SOLUTIONS

A. Phase Reference Distribution

From (1) and (2) we see that phase conjugation amounts to advancing the phase of an input signal by an amount equal to its delay. The phase conjugation circuit (PCC) must, therefore, be provided with a phase reference against which to measure that delay. If we locate each PCC at its associated ARA element as in Figure 1, then it is clear that we must transmit the phase reference to each PCC from some central source via transmission lines of equal phase delay modulo 2π . But it may be difficult to do this if the transmission lines are very long. For example, consider the 1.0 km diameter SPS ARA described above operating at S-band ($\lambda = 12.5 \text{ cm}$). If the master phase reference is located at the center of the disk, the transmission lines to elements at the periphery will be 500 m long. If we wish to keep the phase

delay in this line constant to within $\pi/10$ radians, its length must not vary by more than $\pm\lambda/20$ cm, or a relative change no greater than $\pm 1.2 \times 10^{-5}$.

Fortunately, we can avoid the whole problem by locating all PCC's at the reference source rather than at their respective elements. This method of providing the phase reference, called "central phasing", is illustrated in Figure 3, which, for the sake of clarity, shows only two elements of the ARA. The phase reference for this ARA is the pilot signal received by the 0-th, or reference, element. The pilot signal received by the κ th element is transmitted to its associated PCC located at the reference element via the transmission line and diplexer, 2PLX. The PCC conjugates the entire phase delay, i.e. the sum of the space delay, $\omega r_{\kappa}/c$, and the transmission line delay, $\omega 2k_0/c_L$, where c_L is the phase velocity of the line, and transmits that conjugate signal back down the same transmission line to the κ th element, which retransmits it. Its phase at that point is $\omega'(t + r_{\kappa}/c) + \phi_0$ which is exactly what it would be were the PCC located at the κ th element rather than at the reference element. Thus the length of the transmission line is immaterial provided only that: 1) the line is dispersionless, and 2) its length is constant with time. Clearly, central phasing is just a simple extension of the phase conjugation principle.

Locating all the PCC's in one small volume very near the reference element may be difficult if the array contains thousands of elements. A modification of the central phasing idea using a tree topology in which the phase reference is regenerated at each node will be required in such large arrays. This is illustrated in Figure 4. Each branch of the tree consists of a PCC, located near the node, and an element of the ARA at the end of a transmission line. A phase reference supplies all the PCC's connected to a node. At the initial node, this is the reference element of the array. At subsequent nodes, it is a phase reference regenerator (PRR). The PRR combines samples of the pilot and conjugate signals at an element to reproduce the original reference. Specific ways of doing this will be described in the discussion of PCC's in Subsection B below.

The dashed boxes in Figure 4 contain all the circuit elements located at a node. Since the signal paths within these node assemblies are unilateral, their phase delays must be carefully balanced in order to avoid phase error buildup at successive nodes. In order to assure the stability of the phase delay balance, these assemblies must be uniform and compact. Critical applications may require temperature stabilization of some active elements.

The number of nodes in a tree is relatively small even for an ARA of several thousand elements. For example, if we have six branches at each node, then a tree of only five nodes suffices for an array of 9331 elements. PRR's are required only at the first through fourth order nodes of this tree. A PRR at a fourth order node is the last in a chain of four PRR's connecting the PCC's at that fourth order node to the reference element of the ARA. The error in the value of the phase reference produced by this last PRR is the sum of the errors arising in all the PRR's in the chain. If these errors arise from independent and identical random processes in each PRR, then the probable error of the output of the last PRR is $\sqrt{4} (PE)^2 = 2 (PE)$ is the probable error of each PRR. Thus the error buildup due to repeated regeneration of the phase reference is moderate even for large arrays.

B. Phase Conjugation Circuits

A very simple phase conjugation circuit (PCC) is shown in Figure 5. Since its input and output frequencies are the same ($\omega'=\omega$), this circuit is impractical because of isolation problems. Shifting the output frequency may solve the isolation problem, but we may, depending on how the shifting is done, find that the transmitted beam is no longer retrodirected. For example, the output frequency of this PCC can be shifted simply by slightly offsetting the frequency of the phase reference by $\Delta\omega$. The result is a sort of approximate phase conjugation which, in a planar ARA, causes a pointing error (called "squint") given by

$$\Delta\theta = -\frac{\Delta\omega t}{\omega} \tan\theta, \quad (4)$$

where θ is the scan angle (angle between direction of arrival of the pilot signal and the normal to the array). $\Delta\omega$ has a practical lower bound due to the imperfect isolation of real diplexer filters. Therefore, $\Delta\theta$ may be too large for applications requiring both very precise pointing and a wide scan range.

In order to avoid these difficulties we would like to have exact, frequency shifting PCC's, i.e. PCC's that satisfy our definition, Eq. (2), of phase conjugation where $\omega' \neq \omega$. One such exact PCC is shown in Figure 6. This one uses a phase locked loop which both conjugates the phase and translates the frequency of the input signal. Mixer M2 is an upconverter while M1 is a downconverter. The conjugate relation,

$$\phi_1^* = R (2 \phi_0 - \phi_1) = R \omega \left(t + \left(\frac{1}{c}\right) (r_1 - 2 r_0) \right), \quad (5)$$

where $R = 1/(1 \pm 2/n)$, follows immediately from the phase lock condition. The circuit is practical for $n \geq 4$. The \pm sign in the expression for R reflects the fact that two stable operating states are theoretically possible. Which state actually occurs depends upon the locking range of the VCO. Also, an n-fold phase ambiguity may occur due to the practical difficulty of synchronizing the "divide by n" devices in the various PCC's, but it can be easily shown that this ambiguity is removed (modulo 2π) if the PCC output frequency is multiplied by a multiple of n-2. Since the PCC would normally be designed to operate at frequencies much lower than the 2.45 GHz SPS downlink frequency, the additional requirement that its output frequency be $2450/m(n-2)$, where m and n-2 are arbitrary positive integers, is not unduly restrictive.

The phase reference regenerator (PRR) for the circuit of Figure 6 may take various forms. One of these is illustrated by the circuit shown in Figure 7 which recovers the phase reference ϕ_0 by the proper combination of the conjugate, $\phi_1^* = R (2 \phi_0 - \phi_1)$, and the pilot signal, ϕ_1 . Note that three mixers are required here, not just two; we cannot add two signals of the same frequency in a single mixer because the upper sideband would then have the same frequency as the second harmonic of the strong signal. We must add the pilot signal to the output of M1 in two stages, M2 and M3, in order to remove this "degeneracy".

PCC's and PRR's are, as noted above, usually IF circuits, while the pilot is a microwave signal. We must somehow accurately transfer the phase information in the pilot signal to the IF input signal to the PCC. A receiver which does this is called a coherent receiver. The best known coherent receiver is the phase-locked receiver shown in Figure 8a. The average, or slowly varying, part of the pilot signal phase is divided by $n + 1$, the ratio of the microwave to IF frequency. A simpler, and much cheaper, kind of coherent receiver is shown in Figure 8b. The pilot signal for this receiver must consist of two carrier signals or "tones" transmitted from the same pilot antenna. These tones can be the upper and lower sidebands produced by balanced modulation. The IF output of the "two-tone receiver" in Figure 8b is simply a doubled version of the modulation, which contains the phase information in each of the pilot tones divided, again, by the pilot/IF frequency ratio. In Figure 8b, we assume that the LO frequency, f_L , lies between those of the two pilot tones, f_1 and f_2 , so that mixer M1 produces the two lower sidebands $f_1 - f_L$, $f_L - f_2$. These are separated by bandpass filters, and one of them is amplified to a level sufficient to serve as the LO for M2. M2 is an upconverter. Hence, its output phase is

$$\phi_i = (\phi_1 - \phi_L) + (\phi_L - \phi_2) = \phi_1 - \phi_2. \quad (6)$$

Since

$$\phi_1 = \omega_1 (t - r/c),$$

and

$$\phi_2 = \omega_2 (t - r/c),$$

Eq. (4) gives

$$\phi_i = (\omega_1 - \omega_2) (t - r/c),$$

in fulfillment of our requirement that the IF phase be an accurate representation of the pilot signal phase (or phases) uncontaminated by the phase of extraneous signals (the LO phase in this case).

Note that f_L in Figure 8b must not be exactly half way between f_1 and f_2 , because then $f_1 - f_L$ would be equal to $f_L - f_2$ which would produce degeneracy in mixer M2. f_L need not be between f_1 and f_2 , but if it isn't, mixer M2 must be a downconverter. The limiter in Figure 8b is required to avoid phase offset changes in the mixer M2 produced by changes in its input level.

C. Pointing Errors in ARA's

1) Doppler Errors: Doppler errors arise in two ways: first, from the radial velocity v_0 of the reference element with respect to the pilot source, and second, from the difference $v_k - v_0$ between the radial velocities of the k th and reference elements. In [1, appendix A] we derive an expression for $\delta\phi_{jk}$, the difference in phase between the contributions to the field at the pilot source, as a function v_0 , v_j and v_k for $j, k = 1, \dots, n$. Perfect retrodirection is, of course, equivalent to $\delta\phi_{jk} = 0$ for all pairs of elements j and k .

Considering first the error due only to the radial motion of the reference element, we get

$$\delta\phi_{jk} = \left(\frac{2\omega v_o}{c}\right) (\tau_k - \tau_j), \quad (5)$$

where

$$\tau_i = \left(\frac{1}{c}\right) r_i(t - \tau_i), \quad i = j, k$$

is the phase-delay time for the signal from the i th element arriving at the pilot source ($r = 0$) at time t . For a planar array

$$\tau_k - \tau_j = \left(\frac{1}{c}\right) a_{jk} \sin \theta,$$

where a_{jk} is the distance between the j th and k th elements, and θ is the scan angle, i.e. the angle of incidence of the pilot signal (Fig. 9). In [1, appendix A] we show that the transmitted beam points in the direction θ' given by

$$\sin \theta' = \left(1 + \frac{2v_o}{c}\right) \sin \theta \quad (6)$$

which gives

$$\Delta\theta = \theta' - \theta = \left(\frac{2v_o}{c}\right) \tan \theta. \quad (7)$$

Equation (7) is just the squint error due to the two-way Doppler shift

$$\Delta\omega = -\left(\frac{2v_o}{c}\right)\omega.$$

To get some idea of the magnitude of this error, apply (7) to the SPS ARA described in Section I. Its allowable pointing error is 17.6×10^{-6} rad. Therefore, assuming $|\theta| < 45^\circ$ (much larger than the scan angles specified in ARA preliminary designs), (7) gives

$$\max |v_o| = 2640 \text{ m/s.}$$

The actual radial velocities of geosynchronous satellites are much smaller than this (less than 1.0 m/s in most cases), so we need not worry about "Doppler squint" for SPS.

The expression for the differential Doppler error is

$$\delta\phi_{ok} = \left(\frac{2\omega}{c}\right) \tau_{k0} (v_o - v_k), \quad (8)$$

where τ_{k0} is the transmission line delay between the k th and reference elements. Since it depends on the value of each v_k rather than just v_o , the effects of differential Doppler are far more various than that of simple translational Doppler. In the absence of information on the various physical properties of the ARA structure and on its attitude control system, we have no way of knowing what steady-state or transient motions of the ARA are possible, and therefore, no way of applying (8). The best we can do is to calculate bounds on $|v_o - v_k|$ based on a reasonable bound for τ_{k0} and an arbitrary $|\delta\phi_{ok}|$ bound. A bound for $\tau_{k0} = l_{k0}/c_L$ is $\tau_{k0} < 3D/2c$, which results if we assume that $l_{k0} < D$, the dimension of the ARA, and $c_L > (2/3)c$. Let $\delta\phi$ be the

allowable phase error. Then from (8)

$$|v_o - v_k| \leq \frac{\lambda c (\delta\phi)}{6\pi D},$$

which says that the upper bound for the differential Doppler is proportional to the approximate beamwidth λ/D as well as to $\delta\phi$. Using the SPS antenna as an extreme example again, assume $D = 1000$ m, $\lambda = 0.125$ m, and $\delta\phi = 0.1\pi$. Then $|v_o - v_k| \leq 625$ m/s. Since such large relative velocities would be most unusual for any spacecraft, a differential Doppler will rarely, if ever, be significant.

2) Aberration Error: It can be shown [1, appendix B] that the transverse component v_T of the ARA relative to the pilot source produces a pointing error

$$\Delta\psi = -\frac{2v_T}{c}. \quad (9)$$

We shall call this error an "aberration" because it is essentially the same phenomenon as an astronomical aberration: the small annual oscillation in the apparent position of stars due to the earth's orbital motion. Equation (9) is just twice the astronomical value, as one might expect from the fact that retrodirectivity is a two-way light path process, while the light from a star reaches the earth by a direct one-way path.

In Fig. 10 we assume that the spacecraft carrying the ARA moves with uniform velocity v with respect to the pilot source. Equation (9) is obtained by applying the coordinate transformations of special relativity twice: first to obtain the angle of incidence of the pilot signal with respect to the ARA, and the second to obtain the angle of incidence of the retrodirected signal with respect to the pilot source.

The aberration error is negligible for geosynchronous satellites. For the 1.0-km diameter ARA of the SPS, the maximum allowable error, 17.6×10^{-6} rad, would be exceeded only by

$$v_T = 17.6 \times 10^{-6} (3 \times 10^8) = 2640 \text{ m/s},$$

whereas $v_T < 10$ m/s for the typical geosynchronous satellite.

3) Effect of Transmission Line Mismatches: Our previous analysis of central phasing (Section II-A) assumed that the phase shift produced by a transmission line of length l is simply $-\beta l$ for a signal of frequency $\omega = v_o\beta$, where the phase velocity v_o is assumed to be independent of ω . But this result does not take into account the effect of multiple internal reflections in the line due to mismatches at its junctions with the diplexers at either end. When we do so (1, pp. 18-20), we find that the resulting error in the phase of the conjugate signal is approximately

$$\Delta\phi_b(l) = \arg(T_{1b}T_{2b}) - \frac{\omega_b}{\omega_a} \arg(T_{1a}T_{2a}) \quad (10)$$

where T_{1a} , T_{1b} are the voltage transmission coefficients at one end of the line at the pilot ω_a and conjugate ω_b frequencies, respectively, and T_{2a} , T_{2b} are the corresponding coefficients at the other end.

4) Multipath Effects: Multipath causes pointing errors in much the same way transmission line mismatches do. The received signal, either pilot or retrodirected, is the vector sum of a direct signal plus one or more signals each of which reach the receiving antenna after one or more reflections from the surroundings. The effect is to perturb the phase of the received signal. This would be harmless if $\omega_b = \omega_a$, for then reciprocity would assure exactly the same phase perturbation of the retrodirected signal received back at the pilot source no matter how complicated the multipath situation. But since $\omega_b \neq \omega_a$, reciprocity does not hold and phase errors result. Except in the very simplest cases, multipath effects are too difficult to calculate. Their presence can be inferred, however, by an irregular variation of the pointing error with a scan angle. We will see such evidence of multipath below in data obtained for a breadboard ARA.

5) Ionospheric Effects

Since they violate two necessary conditions for the operation of ARA's, ionospheric dispersion and time fluctuations are potential sources of pointing error. Ionospheric dispersion per se produces negligible pointing errors even at very high electron densities, but the variation of density across the region of the ionosphere traversed by the pilot signal may cause differential phase errors across the ARA aperture. These inhomogeneities of the ionosphere cause the scintillations occasionally observed in communication satellite signals. Their effect on ARA performance is now being investigated by Dr. A.K. Nandi of Rockwell and others. The possibility that absorption of SPS downlink power by the ionosphere may promote inhomogeneities is a further complication. Some ionospheric heating experiments have been made in this connection, but realistic simulation of this effect is impractical due to the huge volume and power of the SPS beam. The effect of a disturbed ionosphere on ARA performance is the chief unresolved problem in pointing the SPS beam. However, we can certainly say that no beam pointing system is immune to ionospheric effects, and no system so far proposed offers any better hope for dealing with it than does the ARA.

III. EXPERIMENTAL RESULTS

A. X-Band ARA

A two-element X-band ARA breadboard was built and tested by the author at the Jet Propulsion Laboratory. The purpose of the breadboard was to demonstrate exact phase conjugation and central phasing, both of which, as we saw above, would be necessary features of very large ultraprecise ARA's.

The PCC used in this breadboard is just that of Fig. 6 for $n = 4$, so that the frequency translation ratio is $R = 2$. Since this array has only two elements, both of which must transmit a conjugate signal, one of the elements must serve as reference element both for the other element and for itself.

The antenna range setup is shown in Fig. 11. The ARA is mounted on the antenna positioner on the right which rotates only in azimuth. The two ARA elements are identical rectangular horns mounted at the same height $23.2 \lambda_T = 82.4$ cm apart, where $\lambda_T = 3.55$ cm is the transmitted wavelength. The 3-dB beamwidth of the horns is about 30° . The rack on the left is the pilot source. A test receiver diplexed to the pilot horn provides the signal for the pattern recorder. The distance between the ARA and the pilot source is about 10 m. A considerable amount of absorbing material is required to minimize reflections in this very compact range.

The ARA pattern is shown as the dashed curve in Fig. 12; i.e., this curve is the output of the test receiver diplexed to the pilot horn as a function of ARA rotation in azimuth. An interferometer pattern (solid curve), produced by driving both elements from the same source at $f_T = 8434.04$ MHz, is superimposed on the ARA pattern by way of comparison. If the ARA were perfectly retro-directive, the dashed curve would be the envelope of the interferometer pattern over the entire scan, but, as we can see, this is true only within about $\pm 5^\circ$ of broadside. The main reason for the increasing departure from perfect retro-directivity for scan angles greater than 5° is the increase in the multipath contribution to the signals received by both the ARA horns and the diplexed pilot horn at large scan angles. The effect of multipath is probably aggravated by amplitude-to-phase conversion in the ARA electronics. This conclusion is qualitatively supported by the fact that retrodirectivity dramatically improved when 1) the setup was reoriented to minimize reflections from nearby buildings, and 2) absorbing panels and material were placed in front of and on the reflecting surfaces as shown in Fig. 11.

The central phasing concept is incorporated into the ARA breadboard by connecting the second element to its PCC at the reference element by a coaxial line. A line stretcher included in this coaxial line enabled us to make an experimental check of that concept. The results of changing the line length are shown in Fig. 13. The ARA patterns for the indicated line-length changes were recorded in top-to-bottom time sequence starting with the zero line-length change ($\Delta l = 0$ in) pattern as a datum. The other two $\Delta l = 0$ patterns (between 2 in and 3 in and between 3 in and 4 in) were run as checks on thermal drift.

We see from Fig. 13 that $\Delta l < 2$ in does not appreciably affect the retro-directivity of the ARA, while extending Δl to 3 in almost completely destroys it. The similarity of the three $\Delta l = 0$ patterns shows that thermal drift is not a factor in these measurements. The fact that $\Delta l = 2$ in = 1.43 wavelengths at $f_T = 8.434$ GHz shows that central phasing is highly effective in spite of the poorly matched rudimentary diplexers used in this breadboard.

B. 8 Element S-Band ARA

Figure 14 is a block diagram of the 8 element ARA now being built at JPL. Its transmitted frequency will be the same as that of the SPS, 2.45 GHz. It will employ the phase locked PCC of Figure 6 with $n = 8$ ($R = 4/3$), and the two-tone receiver of Figure 8b. A phase reference regenerator (PRR) similar to that of Figure 7 will be incorporated in the rudimentary, 2-node, central phasing tree. Preliminary bench tests have verified satisfactory performance of the PRR. Tests of this breadboard ARA are scheduled for this summer.

References

1. JPL Publication 78-20, "Large Active Retrodirective Arrays for Space Applications," Jet Propulsion Laboratory, Pasadena, CA.

SPS BEAM POINTING LOSS

10 dB GAUSSIAN TAPER

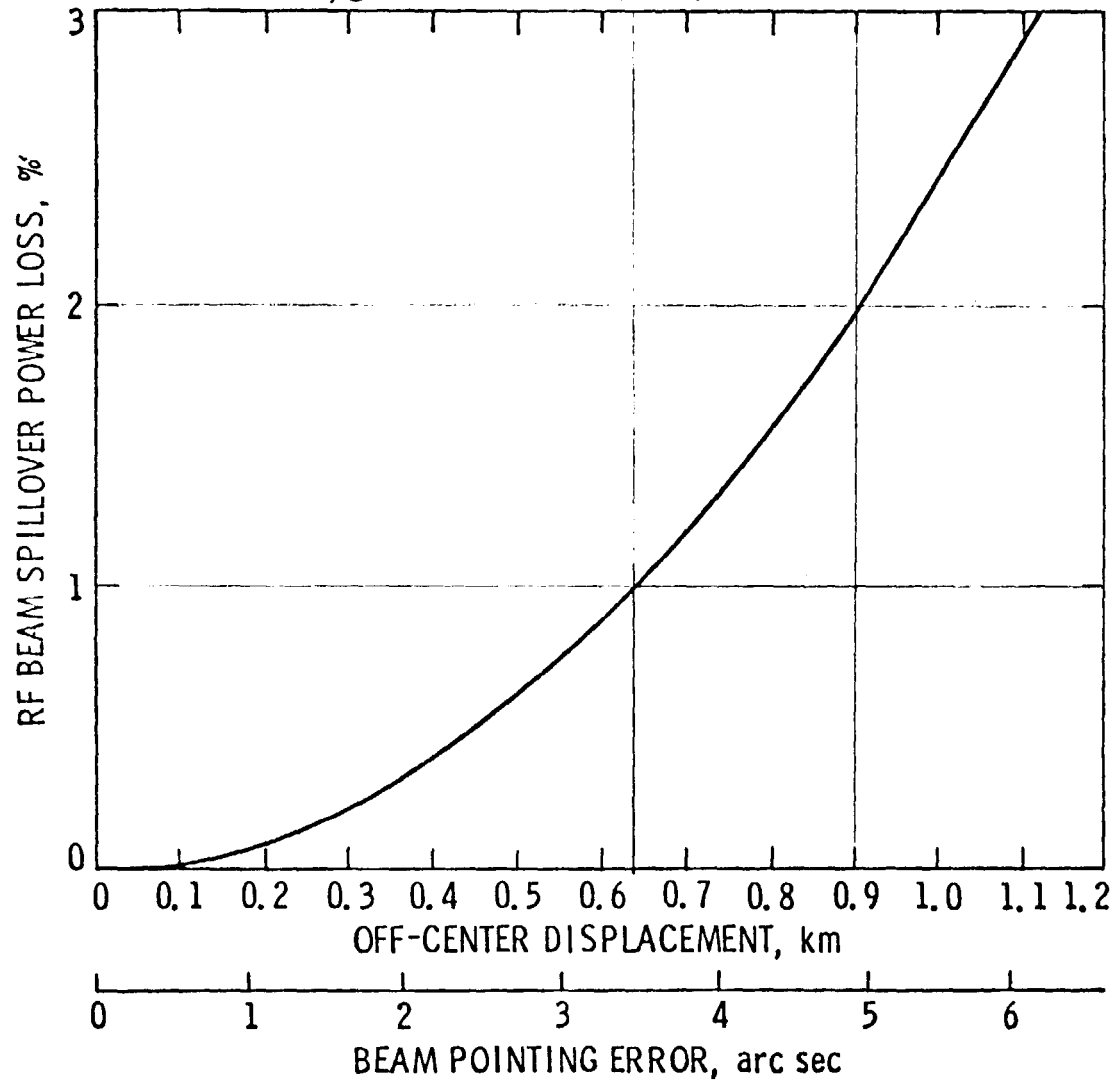


Figure 1.

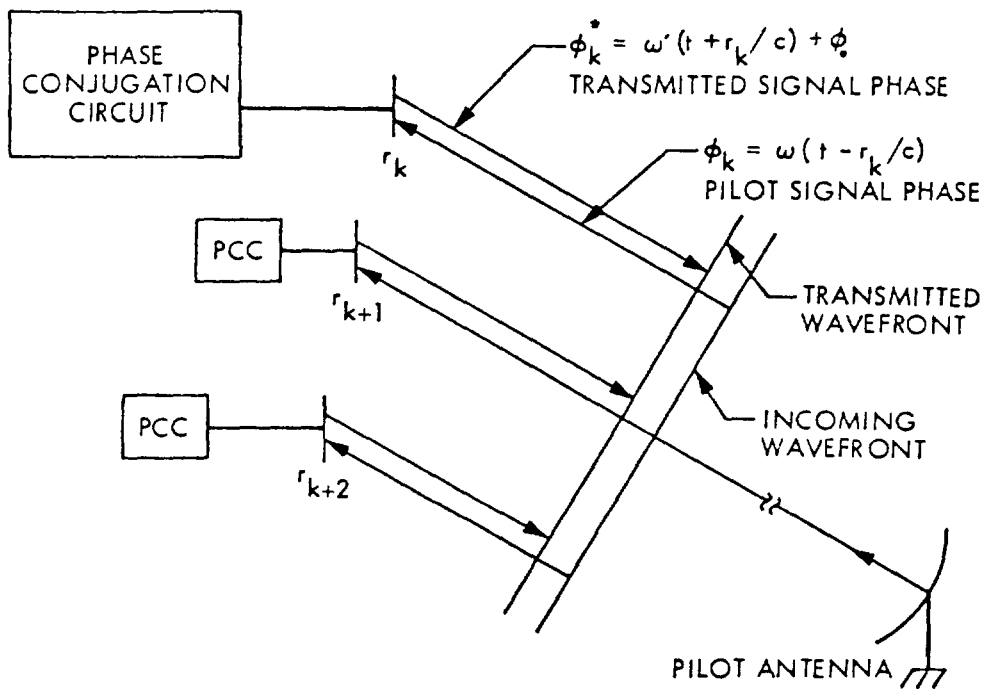


FIGURE 2 ACTIVE RETRODIRECTIVE ARRAY

$$[\phi_1(t)]^* = \omega'(t + \frac{r_1}{c} + \frac{l_{10}}{C_L}) + \phi_0$$

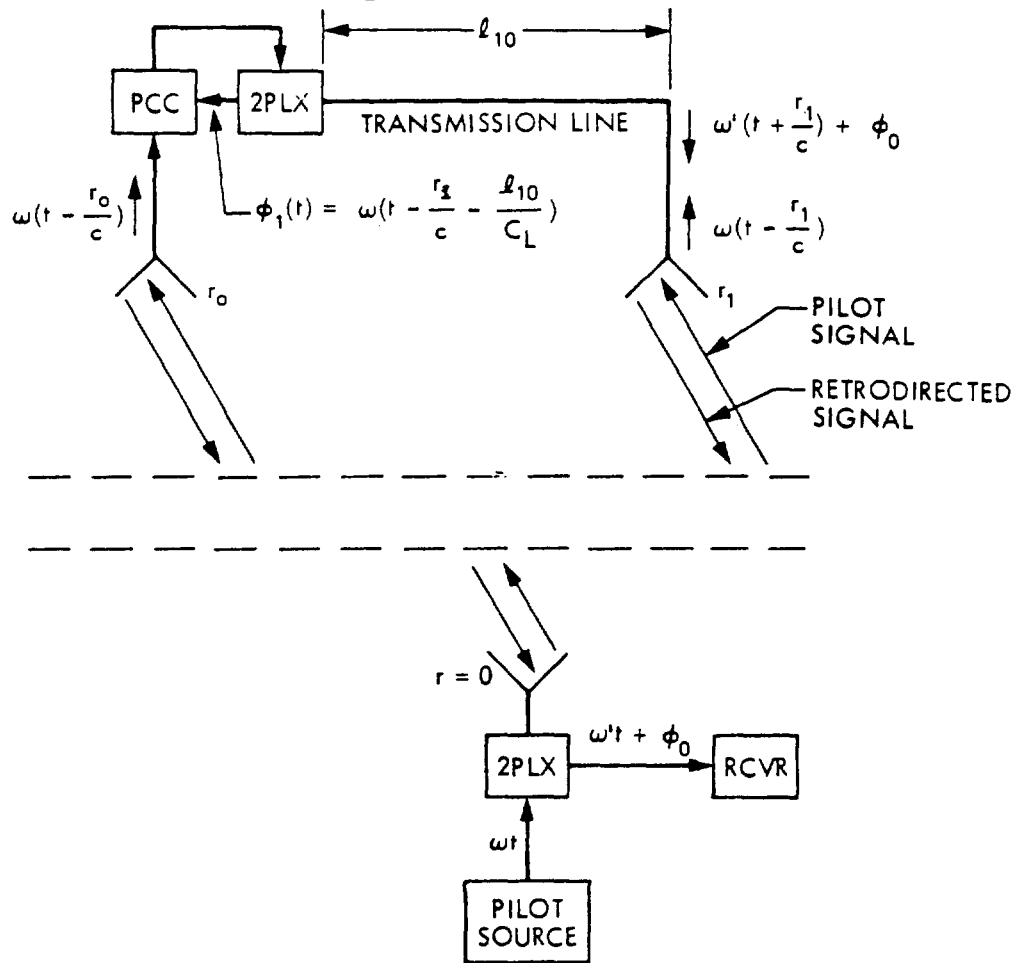


FIGURE 3 CENTRAL PHASING

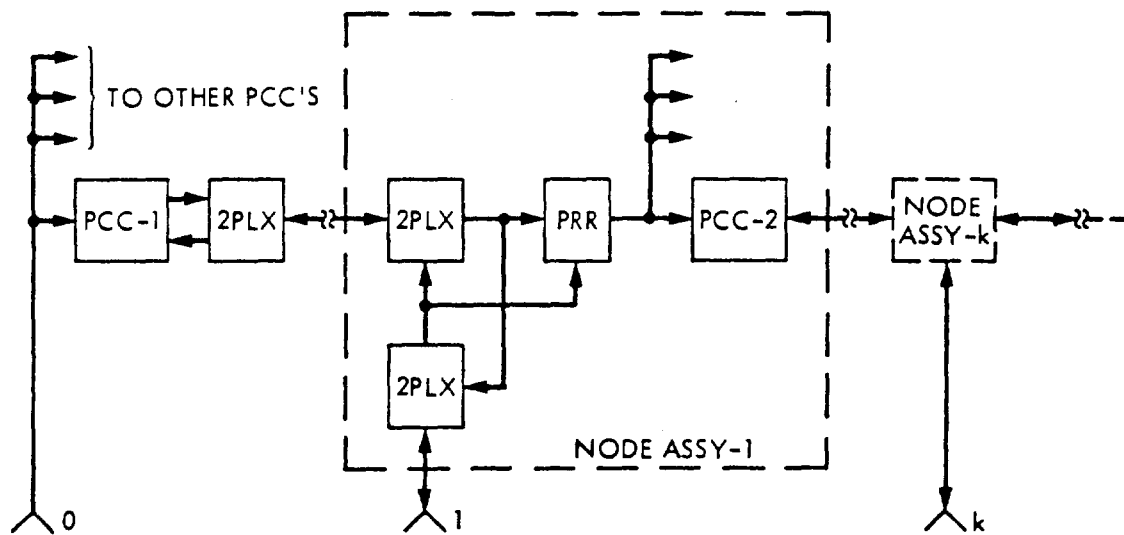


FIGURE 4. TREE STRUCTURE FOR CENTRALLY PHASED ARA

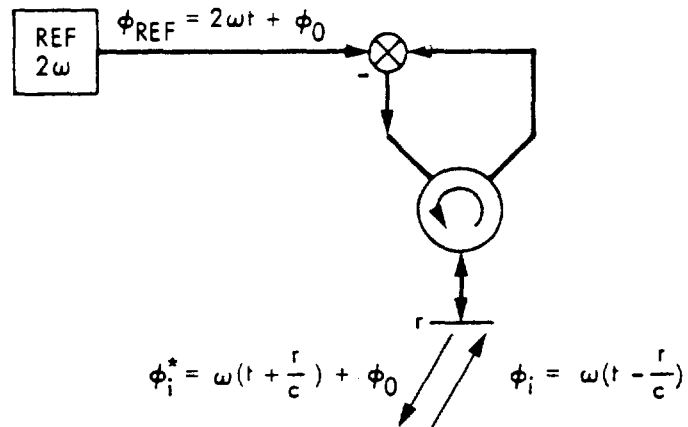


FIGURE 5. SIMPLE PHASE CONJUGATING CIRCUIT

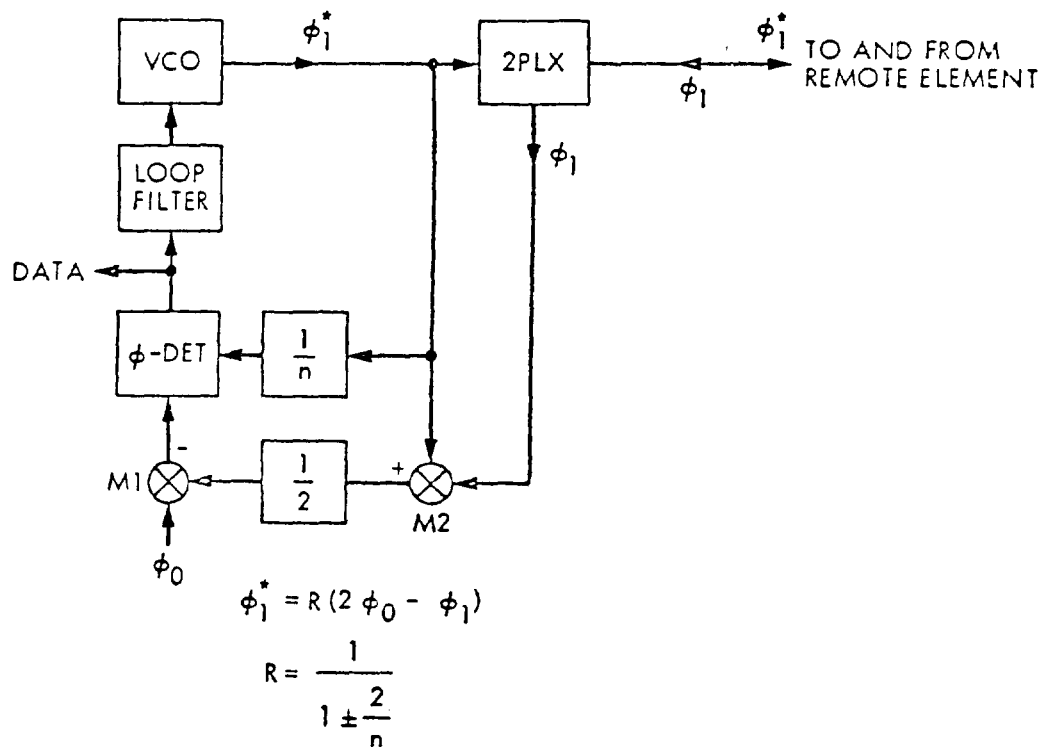


FIGURE 6. EXACT PCC: PHASE LOCKED LOOP TYPE

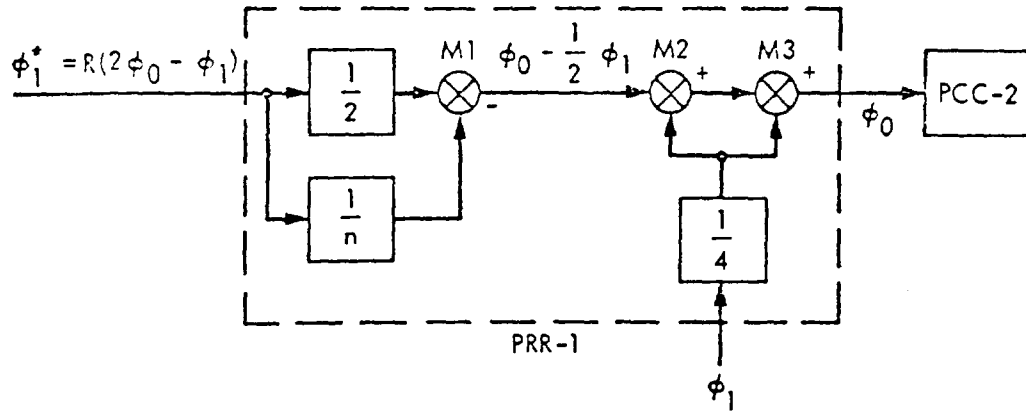
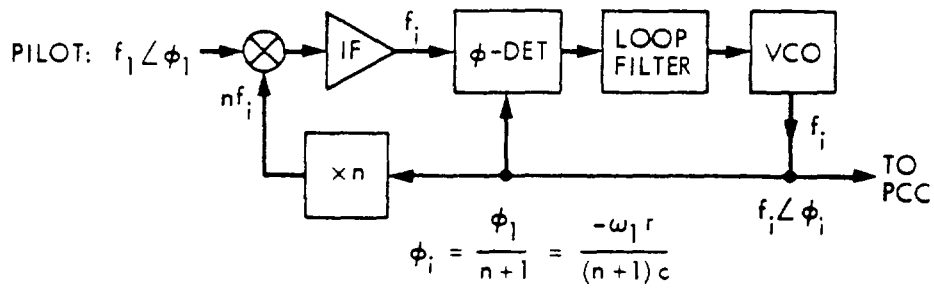
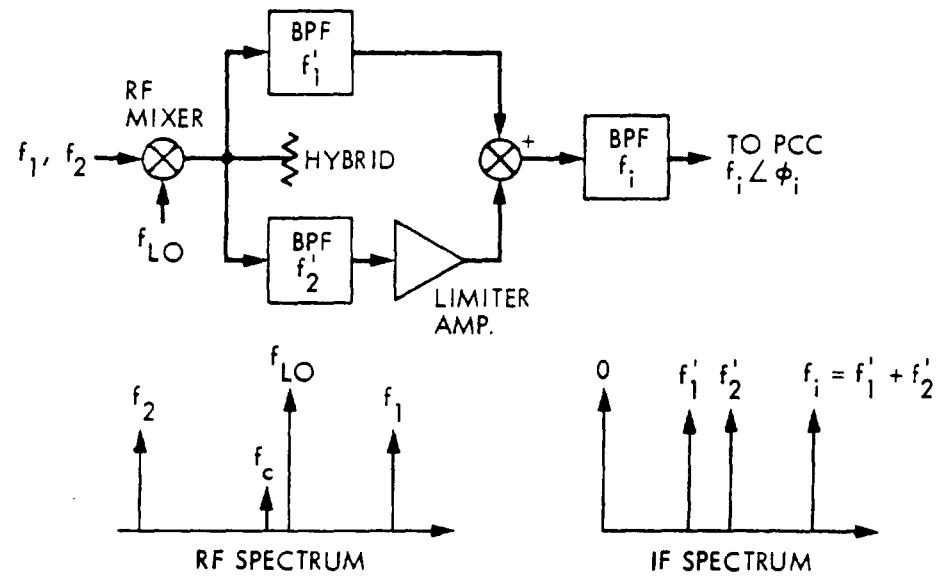


FIGURE 7. PHASE REFERENCE REGENERATOR (PRR) FOR PCC OF FIGURE 6



PHASE LOCKED LOOP RECEIVER

(a)



$$f'_1 = f_1 - f_{LO}$$

$$f'_2 = f_{LO} - f_2$$

$$f_i = f'_1 + f'_2 = f_1 - f_2$$

$$\phi_i = \phi_1 - \phi_2 = (\omega_2 - \omega_1) \frac{r}{c}$$

TWO TONE RECEIVER

(b)

FIGURE 8. ARA RECEIVERS

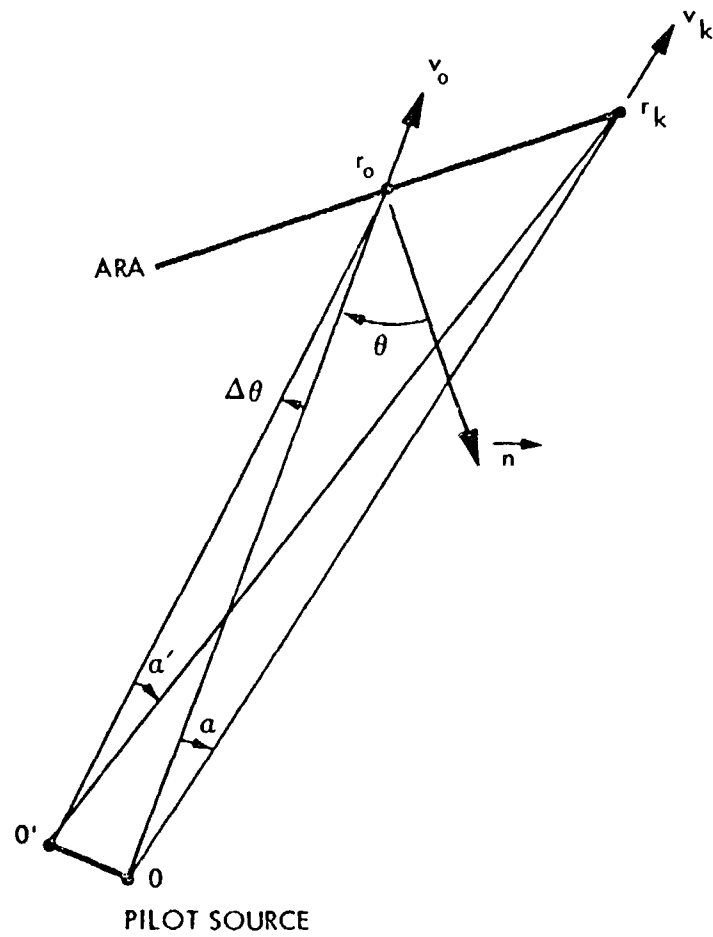


FIGURE 7. DOPPLER POINTING ERROR

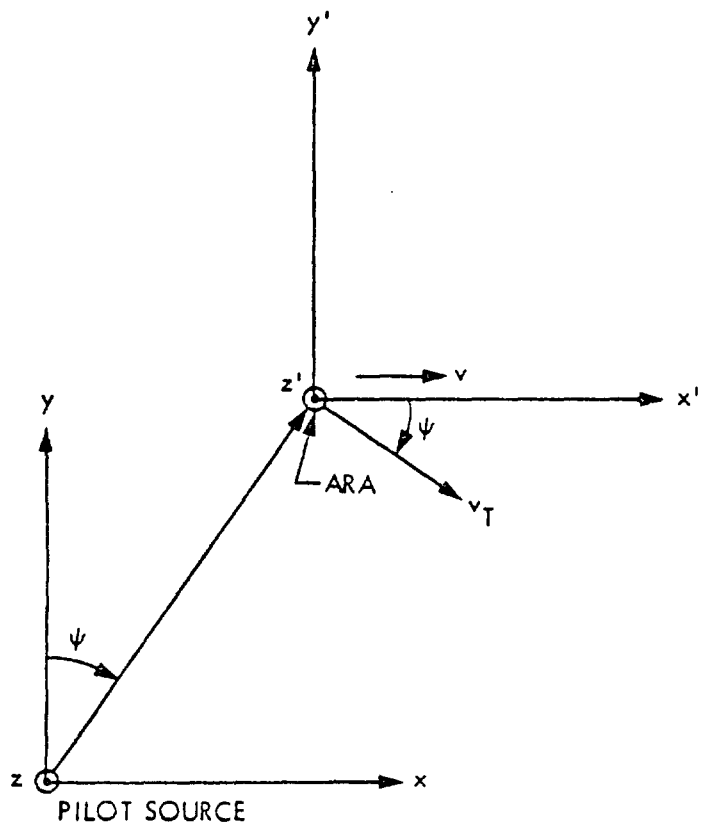


FIGURE 10. ABERRATION POINTING ERROR

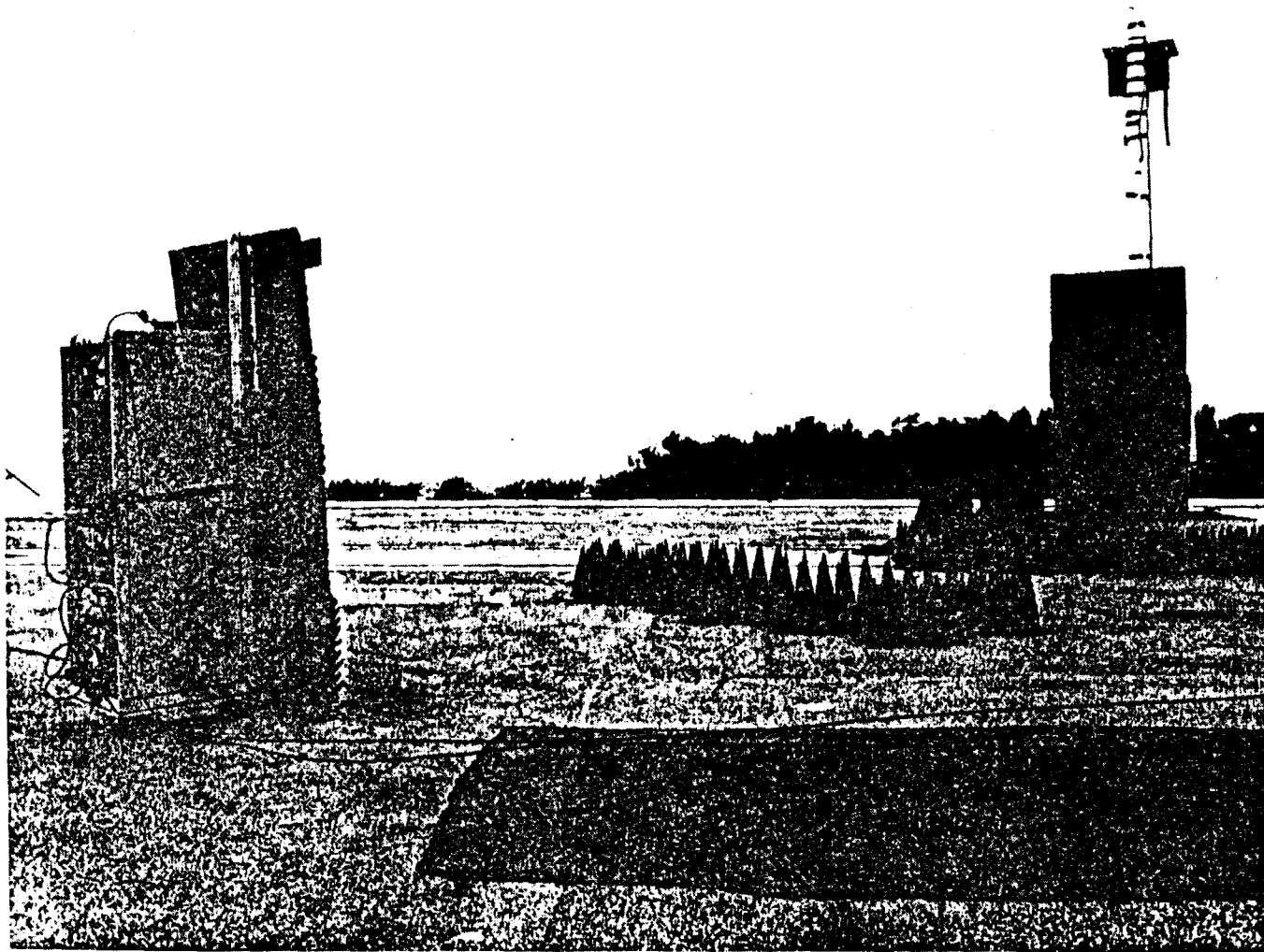
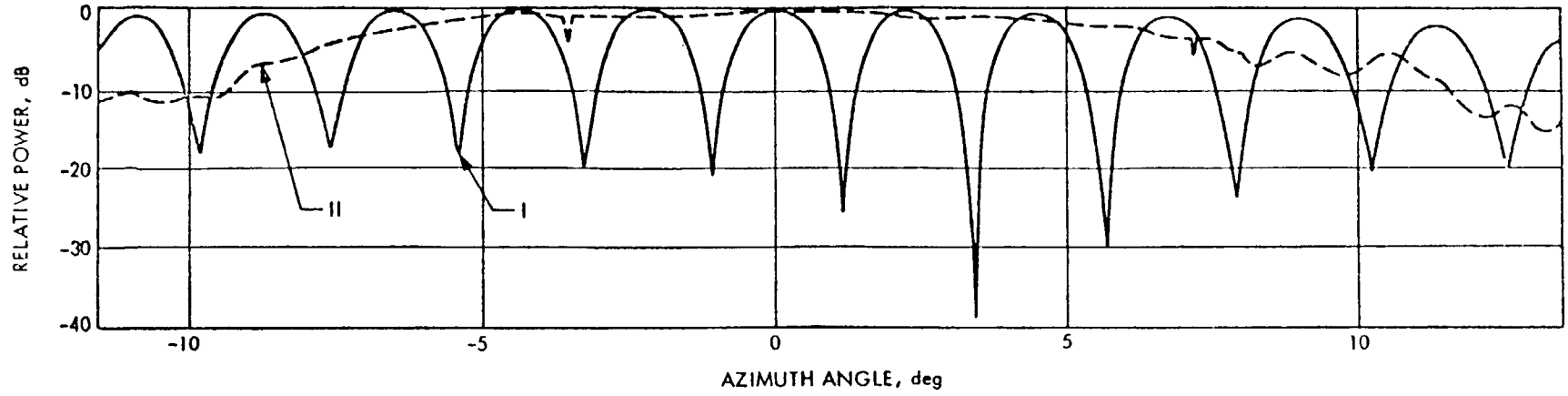


Figure 11. Antenna Range Set-up



LEGEND:

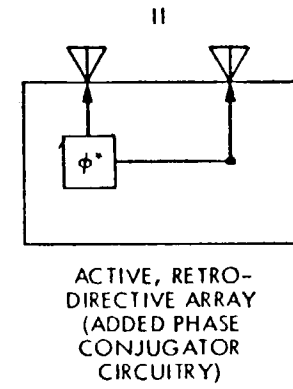
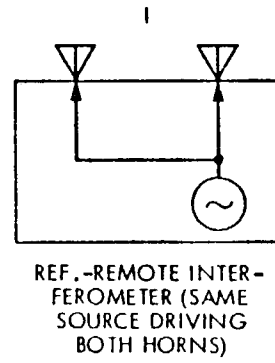
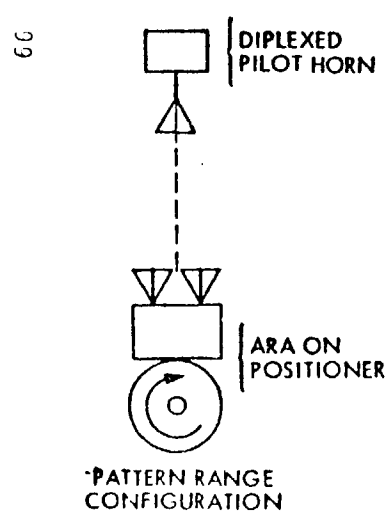


FIGURE 12. RETRODIRECTIVE ARRAY PATTERN

001

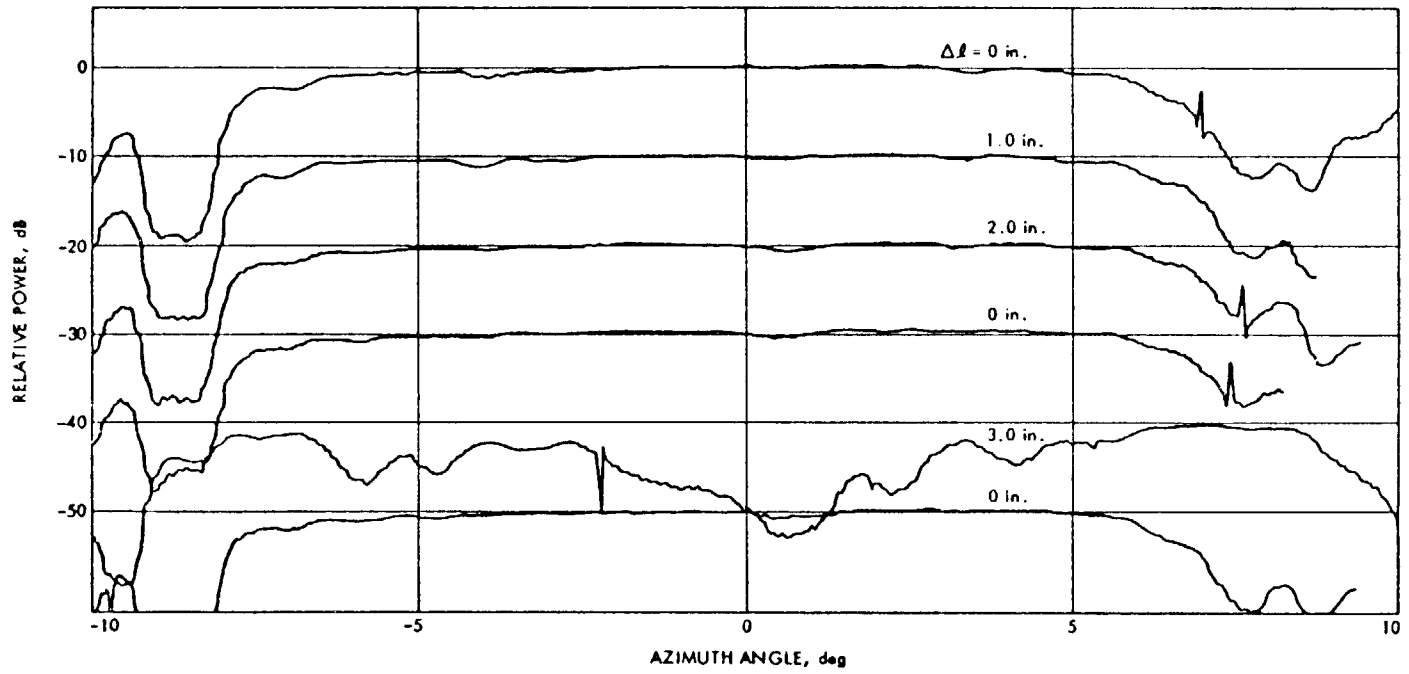
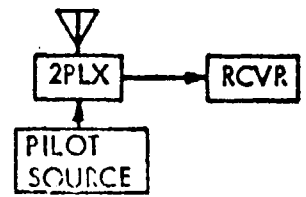
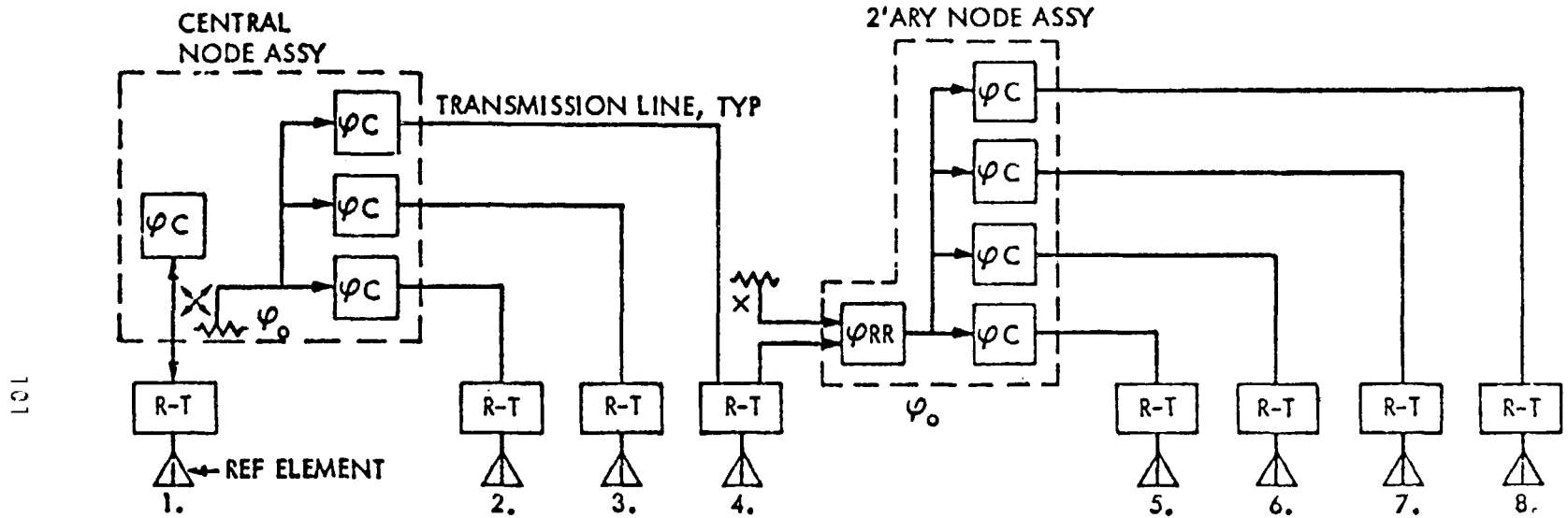


FIGURE 13. ARA BREADBOARD: EFFECT OF LINE LENGTH CHANGES

BEAMED RF POWER TECHNOLOGY 8-ELEMENT EXPERIMENTAL ACTIVE RETRODIRECTIVE ARRAY (ARA) BLOCK DIAGRAM



LEGEND:
 R-T = RCVR-XMTR-DIPLEXER ASSY
 ϕ_C = PHASE CONJUGATOR
 ϕ_{RR} = PHASE REFERENCE REGENERATOR
 ϕ_0 = REFERENCE PHASE
 2PLX = DIPLEXER

Figure 14.

PERFORMANCE ANALYSIS AND SIMULATION OF
THE SPS REFERENCE PHASE CONTROL SYSTEM*

W. C. Lindsey and C. M. Chie
LinCom Corporation

ABSTRACT

This short paper provides a summary overview of the SPS reference phase control system as defined in a three phase study effort (see Refs. 1-5). It serves to summarize key results pertinent to the SPS reference phase control system design. These results are a consequence of extensive system engineering tradeoffs provided via mathematical modeling, optimization, analysis and the development/utilization of a computer simulation tool called SOLARSIM.

1.0 INTRODUCTION

The SPS reference phase control system investigated under contract to the Johnson Space Center is reviewed in Section 2. The next section is devoted to the analysis and selection of the pilot signal and power transponder. The SOLARSIM program development and the simulated SPS phase control performance are treated in Section 4.

2.0 THE SPS CONCEPT AND THE REFERENCE PHASE CONTROL SYSTEM

Figure 2.1 illustrates the major elements required in the operation of an SPS system which employs retrodirectivity as a means of automatically pointing the beam to the appropriate spot on the Earth. From Figure 2.1 we see that these include: (1) the transmitting antenna, hereafter called the spacetenna, (2) the receiving antenna, hereafter called the rectenna, and (3) the pilot signal transmitter. The rectenna and pilot signal transmitter are located on the Earth. The purpose of the spacetenna is to direct the high-power beam so that it comes into focus at the rectenna. The pilot signal, transmitted from the center of the rectenna to the spacetenna, provides the signal needed at the SPS to focus and steer the power beam.

As seen from Fig. 2.1 the SPS phase control system is faced with several key problems. They include: (1) path delay variations due to imperfect SPS circular orbits, (2) ionospheric effects, (3) initial beam forming, (4) beam pointing, (5) beam safig, (6) high power amplifier phase noise effects, (7) interference (unintentional and intentional), etc.

2.1 SPS Transmitting System Concept

From the system engineering viewpoint, the SPS transmitting system which incorporates retrodirectivity is depicted in Fig. 2.2. As seen

*This work was performed at LinCom Corporation for NASA Johnson Space Center Houston, TX, under contract NAS 9-15782.

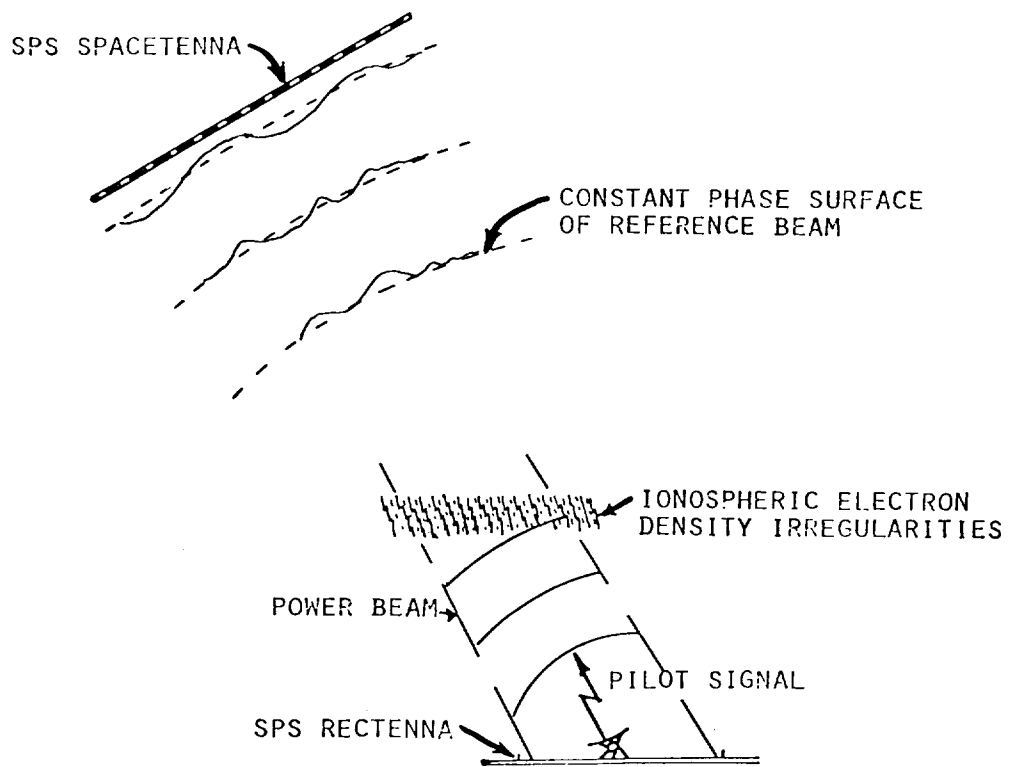


Figure 2.1. Space Based Solar Power Satellite and Earth Based Energy Collection System Concept.

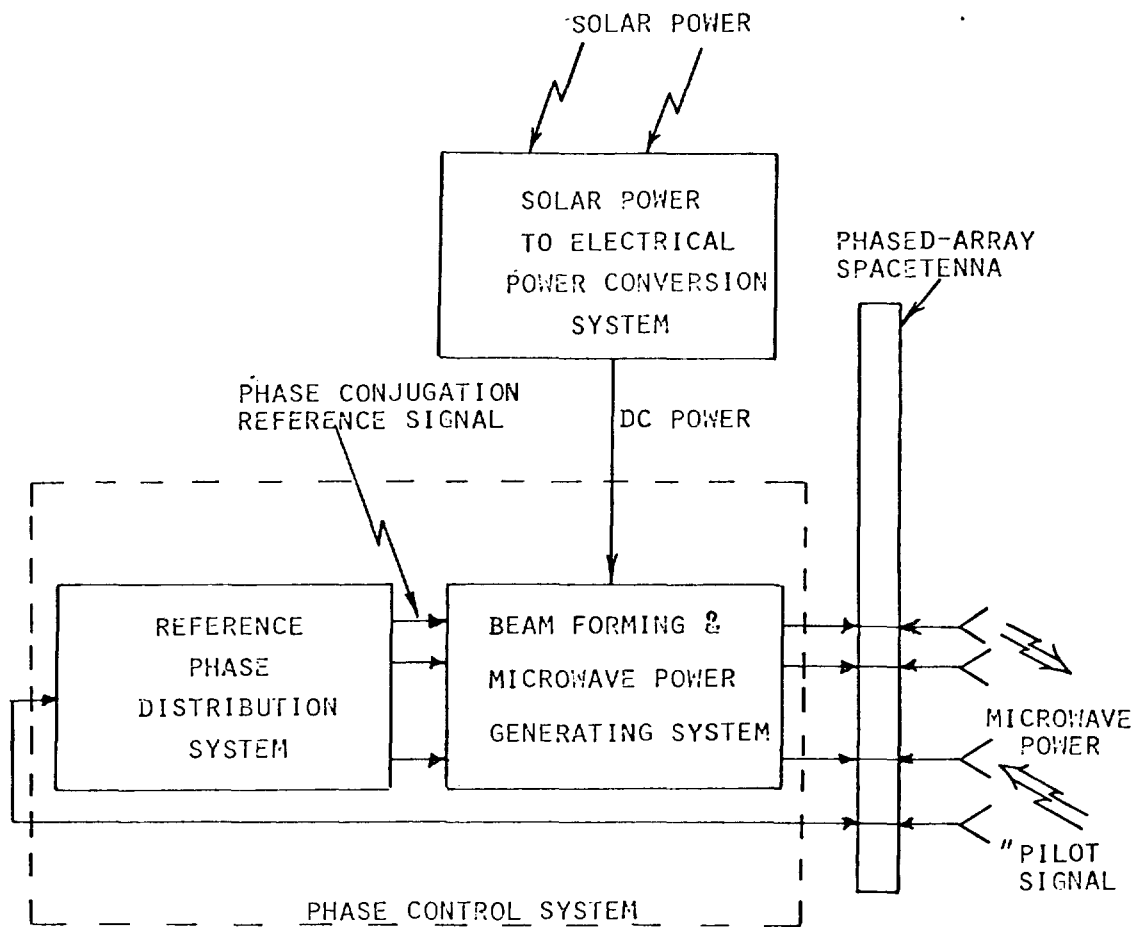
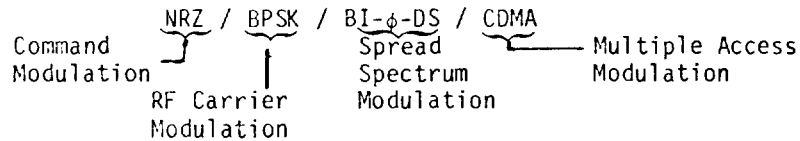


Figure 2.2. Solar Power Satellite (SPS) Transmission System (Phase Conjugation).

from Fig. 2.2 the SPS Transmission System consists of three major systems: (1) The Reference Phase Distribution System, (2) The Beamforming and Microwave Power Generating System, and (3) The Solar Power to Electrical Power Conversion System.

2.2 Reference System SPS Pilot Waveform

The reference system SPS pilot waveform utilizes: (1) NRZ command modulation, (2) split phase, direct sequence pseudo-noise or spread spectrum modulation, BI- ϕ -DS. This combined data-code modulation is used to bi-phase modulate (BPSK) the RF carrier. Multiple access in the SPS network is to be achieved via code division multiple access techniques (CDMA). Thus the baseline SPS pilot waveform is characterized via four modulation components summarized by the symbols:



A functional diagram indicating the mechanization of the pilot transmitter is shown in Fig. 2.3. As illustrated the data clock and code clock are coherent so that the uplink operates in a data privacy format. The purpose of the spread spectrum (SS) code generator is several fold. First it provides link security, second it provides a multiple access capability for the operation of a network of SPSs, and third, the anti-jamming protection is provided for both intentional radio frequency interference (RFI) and unintentional RFI such as those arising from a neighboring SPS on the adjacent orbit. Proper choice of this code modulation will also provide the needed isolation between the uplink and the downlink, since a notch filter can be placed around the carrier frequency at the SPS receiver input to blank out the interferences without destroying the uplink signal (see pilot signal spectrum in Fig. 2.3). The selection of the PN code parameters to achieve the code isolation and processing gain required will be addressed in Section 3.

2.3 Reference Phase Control System

The reference phase control system concept was presented in detail in Ref. 3; its major features are summarized in this section. Based upon earlier study efforts (Refs. 3,4), a phase control system concept has been proposed which partitions the system into three major levels. Figure 2.4 demonstrates the partitioning and represents an expanded version of Fig. 2.2. The first level in Fig. 2.4 consists of a reference phase distribution system implemented in the form of phase distribution tree structure. The major purpose of the tree structure is to electronically compensate for the phase shift due to the transition path lengths from the center of the spacetenna to each phase center (PCC) located in each subarray. In the reference system, this is accomplished using the Master Slave Returnable Timing System (MSRTS) technique. The detailed mathematical modeling and analysis of the MSRTS technique is provided in Ref. 4. Based upon extensive tradeoffs

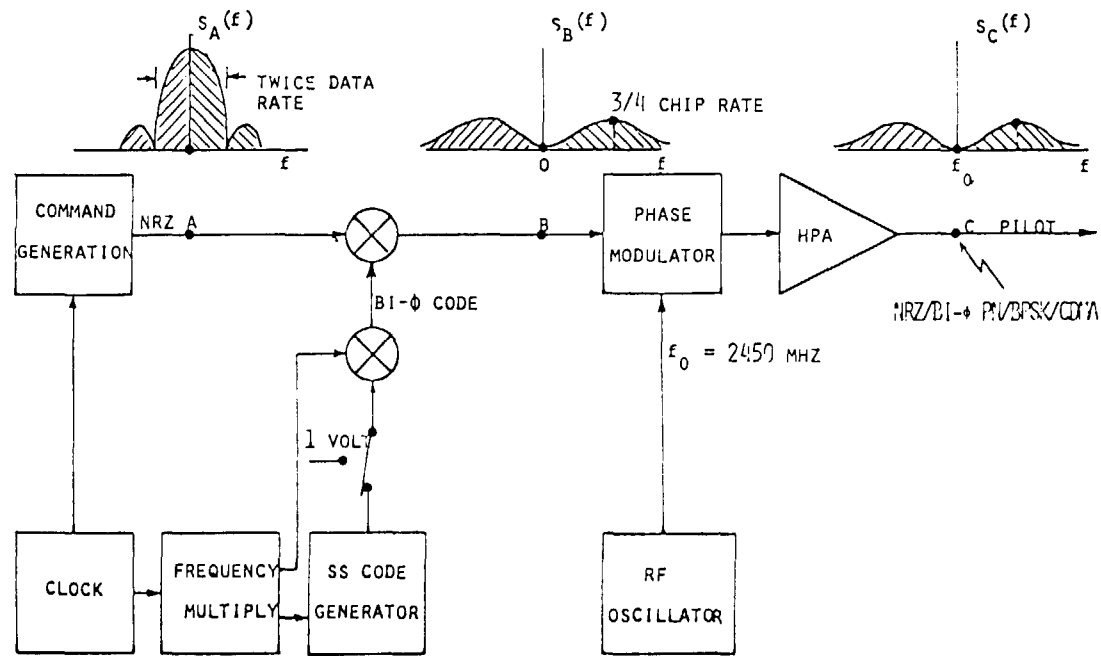


Figure 2.3. Reference System Pilot Signal Transmitter Functional Diagram.

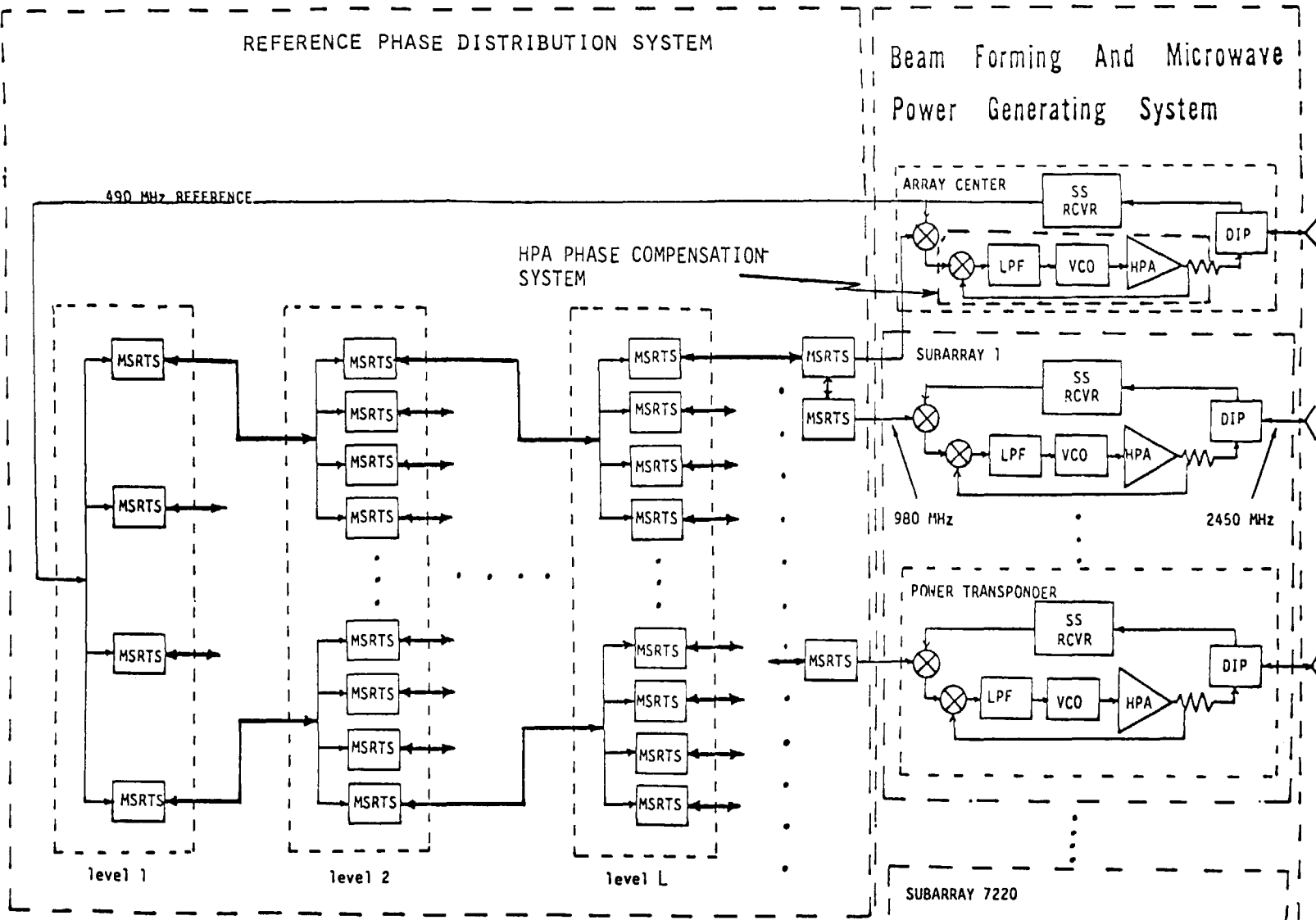


Figure 2.4. Reference Solar Power Satellite Transmission System.

using SOLARSIM and appropriate analysis during the Phase II study, a four level tree is selected to be the reference phase distribution system configuration.

The second level is the Beam Steering and Microwave Power Generation System which houses the SPS Power Transponders. This transponder consists of a set of phase conjugation multipliers driven by the reference phase distribution system output and the output of a pilot spread spectrum receiver (SS RCVR) which accepts the received pilot via a diplexer connected to a separate receive horn or the subarray itself. The output of the phase conjugation circuits serve as inputs to the third level of the phase control system. The third level of phase control is associated with maintaining an equal and constant phase shift through the microwave power amplifier devices while minimizing the associated phase noise effects (SPS RFI potential) on the generated power beam. This is accomplished by providing a phase-locked loop around each high power amplifier.

2.4 Reference System SPS Power Transponder

In addition to distributing the constant phase reference signal over the spacetenna, a method for recovering the phase of the received pilot signal is required. Figure 2.5 represents the functional diagram of the SPS power transponder. This includes the pilot signal receiver, phase conjugation electronics and the high power amplifier phase control system.

In the mechanization of the SPS power transponders, two receiver "types" will be required; however, most of the hardware will be common between two receivers. One receiver, the Pilot Spread Spectrum Receiver, is located at the center of the spacetenna or the reference subarray. It serves two major functions: (1) acquires the SS code, the carrier and demodulates the command signal, (2) provides the main input signal to the Reference Phase Distribution System.

The second receiver "type" will be located in the Beam Forming and Microwave Power Generating System. Its main purpose is to phase conjugate the received pilot signal and transpond power via the j-th spacetenna element, $j = 1, 2, \dots, 101, 552$.

In the case that data transmitting capability is not implemented for the pilot signal, the Costas loop can be replaced by a CW loop. This avoids the need for provisions to resolve the associated Costas loop induced phase ambiguity.

3.0 PILOT SIGNAL DESIGN AND POWER TRANSPONDER ANALYSIS

The key technical problem areas concerning the reference phase control system design and specifications are the SPS pilot signal design and power transponder analysis. Figure 3.1 illustrates the radio frequency interference (RFI) scenario.

The interferences are generated by different mechanisms: (1) self jamming due to the power beam leakage from the diplexer/circulator; (2) mutual coupling from adjacent transponders, (3) thermal noise and (4)

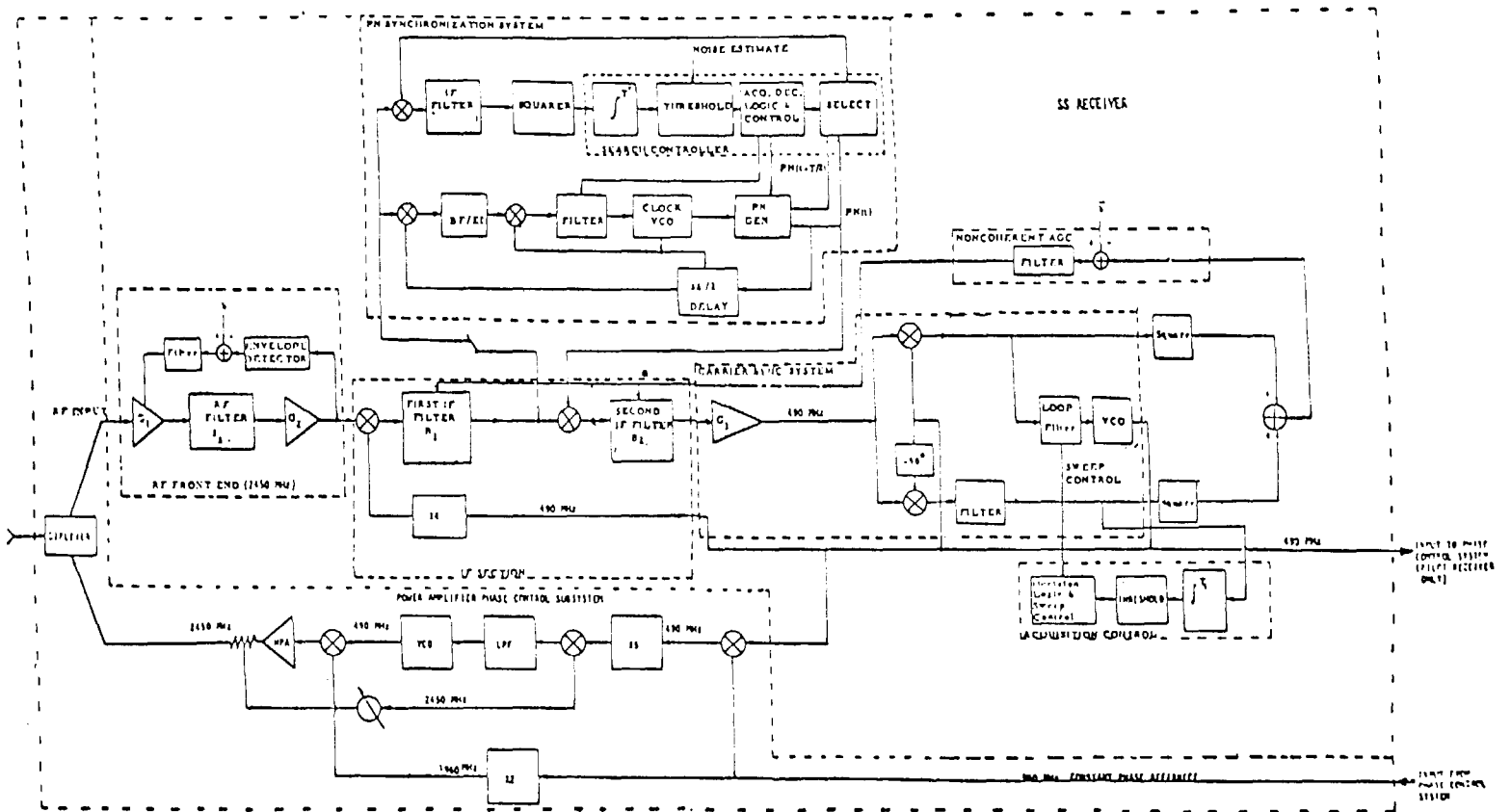
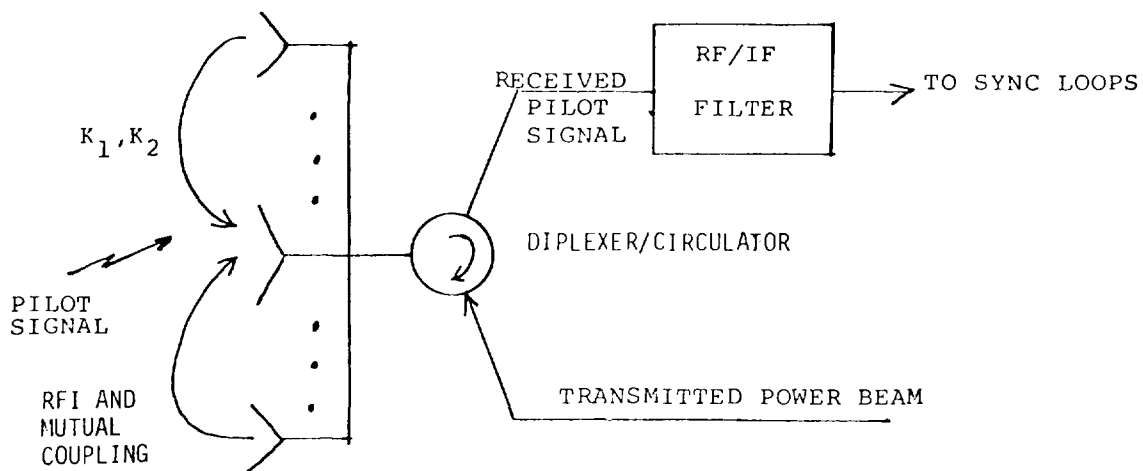
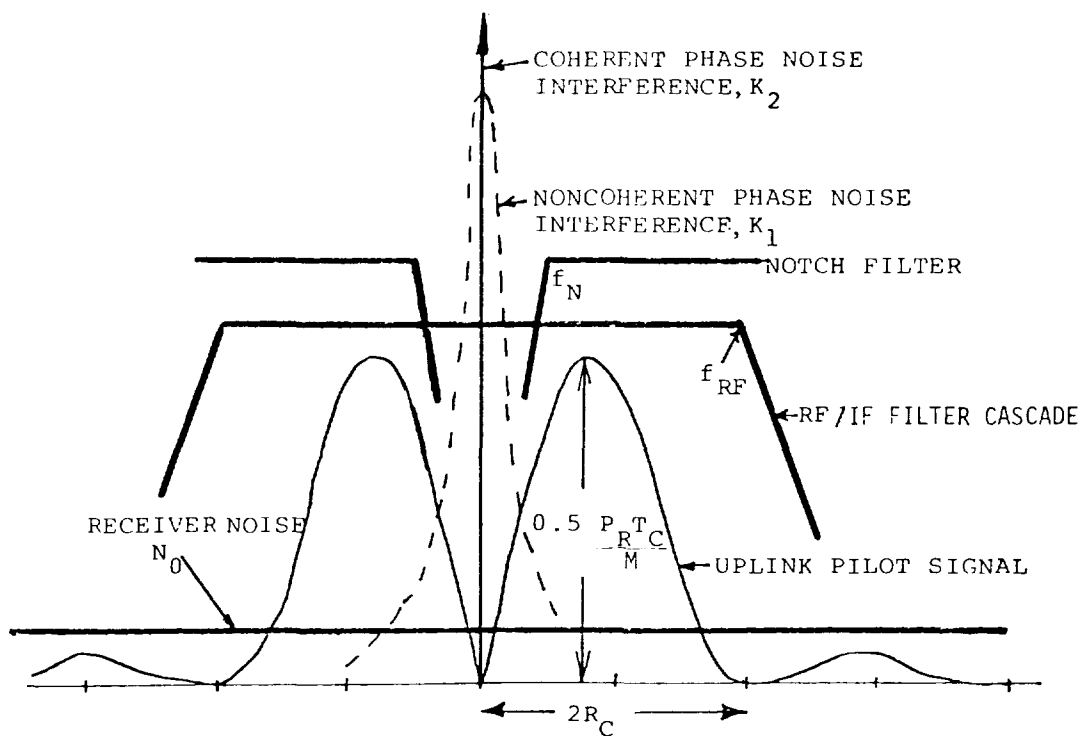


Figure 2.5. Central SPS Power Transponder Located at Spacetenna Center.



(a) SPS Power Transponder Front End (Conceptual)



(b) Signal and Noise Spectrum

Figure 3.1. Signal and Noise Spectrum into SPS Transponder.

interference from adjacent SPSs. The signal and interference spectrum at the input to the SPS transponder is depicted in Fig. 3.1. In general, the combined phase noise interference from the power beams consists of a coherent and a noncoherent term. Depending on the mechanization of the antenna structure and diplexer/circulator characteristics, these terms are associated with gains K_1 and K_2 . Note that the phase noise interferences are concentrated around the carrier frequency (2450 MHz). The uplink pilot signal on the other hand has no power around this frequency. Its power spectrum peaks at $f = 0.75 R_c$, with a value proportional to the produce of the received power (P_r) and the PN chip rate (R_c), and inversely proportional to the PN code length (M). The parameters R_c and M are related to the processing gain of the PN spread signal and determines its interference suppression capability. The RF filter characteristic is mainly determined by the waveguide antennas, which have bandwidths ranging from 15 to 45 MHz depending on the array area. Our goal is to optimally select (1) the pilot signal so that it passes the RF filter with negligible distortions, and (2) a practical notch filter that rejects most of the phase noise interferences. When this is done, one can be assured that the reconstructed pilot signal phase after the sync loops is within a tolerable error for the retrodirective scheme.

3.1 Pilot Signal Parameter Selection

SOLARSIM is developed to enable performance tradeoffs of pertinent design parameters such as pilot signal transmitter EIRP, PN code requirement, chip rate and RF front end characteristics (notch filter). The computer model is based upon a mathematical framework which includes the analytical models for power spectral density of the pilot signal, various sources of interference, the RF front end, the PN tracking loop and the pilot tracking loop. The resulting design values are provided in a later section.

3.2 Power Transponder Analysis

Analytical models are developed for the SPS transponder tracking loop system that include: (1) the PN despreader loop, (2) the pilot phase tracking (Costas) loop and (3) the PA phase control loop. The phase reference receiver that feeds the phase distribution system is also modeled. Various sources of potential phase noise interferences are identified and their effects on the performance of the individual loops are modeled. In particular, a model of the phase noise profile of the klystron amplifier based on a specific tube measurement is introduced. Important implications on the PA control loop design are also addressed.

An analytical model for evaluating the overall performance of the SPS transponder is given. The phase fluctuation at the output of the transponder is shown to be directed related to the various noise processes through the closed-loop transfer functions of the tracking loops. These noise processes are either generated externally to the transponder circuitry such as ionospheric disturbances, transmit frequency instability, or externally such as receiver thermal noise, power beam interferences, data distortions, VCO/mixer phase noise and the phase variations introduced by the reference distribution tree.

3.3 Summary of Results

The important findings and preliminary specifications the transponder design parameters and results based upon SOLARSIM and the analytical models discussed in Sections 3.1 and 3.2 can be summarized as follows:

- EIRP = 93.3 dBW
- PN Chip Rate ~ 10 Mcps
- RF filter 3 dB cutoff frequency ~ 20 MHz
- Notch filter 3 dB cutoff frequency ~ 1 MHz
- Notch filter dc attenuation ~ 60 dB
- PN Code period ~ 1 msec
- Costas loop phase jitter < 0.1 deg for 10 Hz loop bandwidth
- Channel Doppler is negligible
- Klystron phase control loop bandwidth ≥ 10 kHz

In arriving at these design values, we have used extensively the capabilities of SOLARSIM to perform the necessary tradeoffs. Figure 3.2 represents a typical design curve generated via SOLARSIM and used to pick the RF filter 3 dB cutoff frequency. The details and other tradeoffs performed are documented in Ref. 5, Vol. II.

The preliminary results are generated using a tentative model of RFI with coupling coefficients $K_1 = K_2 = 20$ dB. Explicitly, we assumed that the transponder input sees a CW interference with power equal to 0.65 KW and a phase noise (1/f type) interference at about 20 W. Of course, when these values are changed significantly, our predictions have to be modified. For this reason, the development and verification of an acceptable model for the effects of mutual coupling on the phase array antenna based upon the "near field" theory is extremely important and essential in the near future.

A maximum-length linear-feedback shift register sequence, i.e., m-sequences generated by a 12 stage shift register with a period equal to 4095 is recommended as the spread spectrum code. In the code division multiple access situation, the theoretical optimal solution is to use the set of 64 bent function sequences of period 4095, enabling as much as 4095 simultaneous satellite operation of the SPS network. The bent sequences are guaranteed to be balanced, have long linear span and are easy to initialize. However, the set of maximum length sequence of period 4095, though suboptimal, may suffice. This depends of course on the code partial correlation requirement and the number of satellites in the network. The design detail is discussed in Ref. 5, Vol. II.

At this point our results indicate that it is feasible to hold the antenna array phase error to less than one degree per module for the type of disturbances modeled in this report. However, there are irreducible error sources that are not considered herein and their effects remain to be seen. They include: (a) reference phase distribution errors, (b) differential delays in the RF path.

4.0 SPS PERFORMANCE EVALUATION VIA SOLARSIM

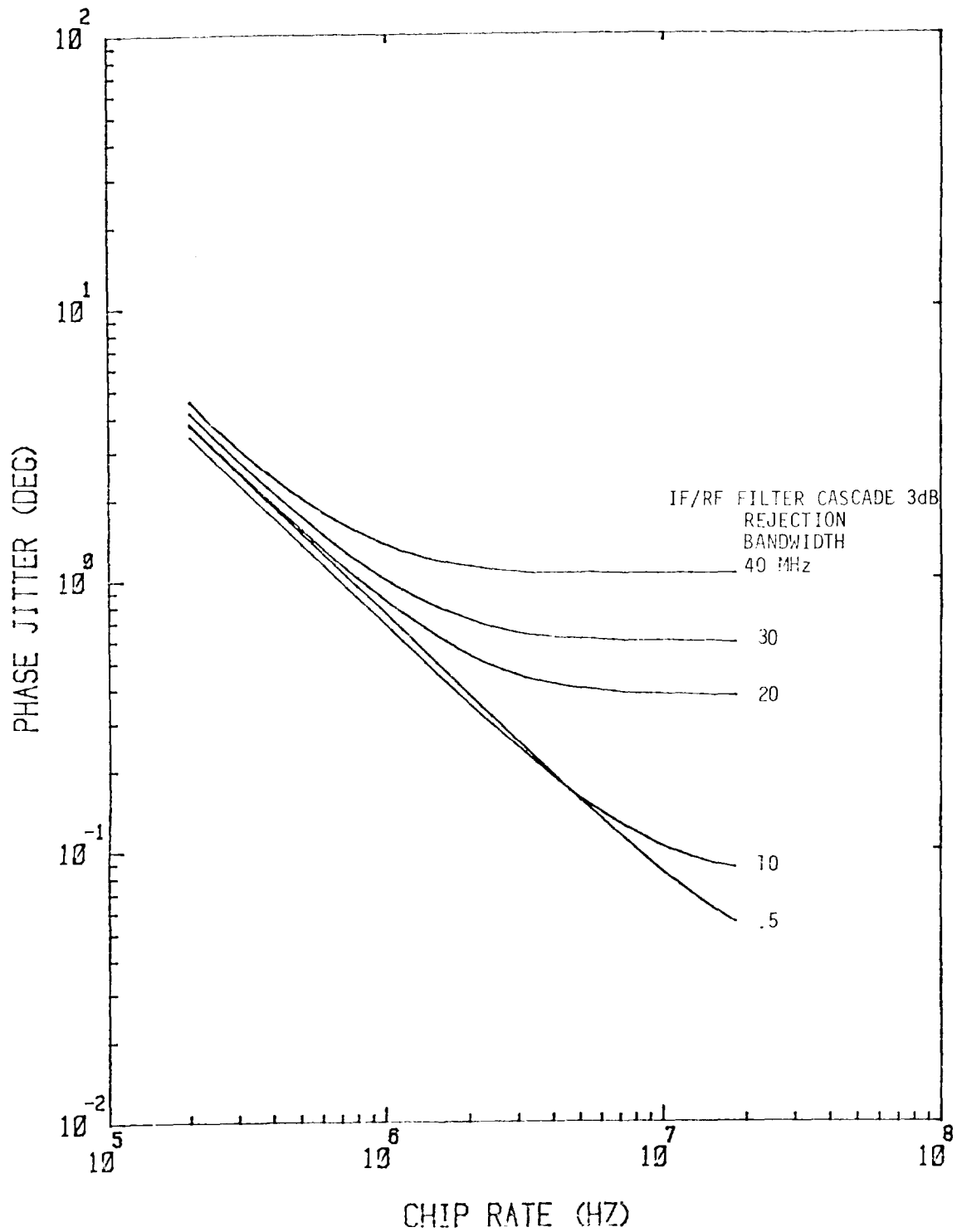


Figure 3.2. Effect of Varying Notch Filter Frequency Cutoff.

Because of the complicated nature of the problem of evaluating performance of the SPS phase control system and because of the multiplicity and interaction of the problems as they relate to subsystem interfaces, the methods of analysis and computer simulation (analytical simulation) have been combined to yield performance of the SPS system. The result is the development of SOLARSIM--a computer program package that allows a parametric evaluation of critical performance issues. The SOLARSIM program and its various subroutines have been exercised in great detail to provide system engineering tradeoffs and design data for the reference system. In what follows, we shall focus on the key results obtained from one of the SOLARSIM subroutines, viz., POWER TRANSFER EFFICIENCY.

4.1 System Jitters and Imperfections Modeled in POWER TRANSFER EFFICIENCY

The system jitters and imperfections can be grouped into two main classes: (1) jitters arising due to spacetenna electrical components which include such effects as the amplitude jitter and the phase jitters of the feed currents and (2) jitters arising due to the mechanical imperfections of the spacetenna which include the subarray tilts (mechanical pointing error), tilt jitters and the location jitters. The location jitters include the transmitting and receiving elements and arise from the misplacement of the radiating elements.

4.2 Definition of Power Transfer Efficiency

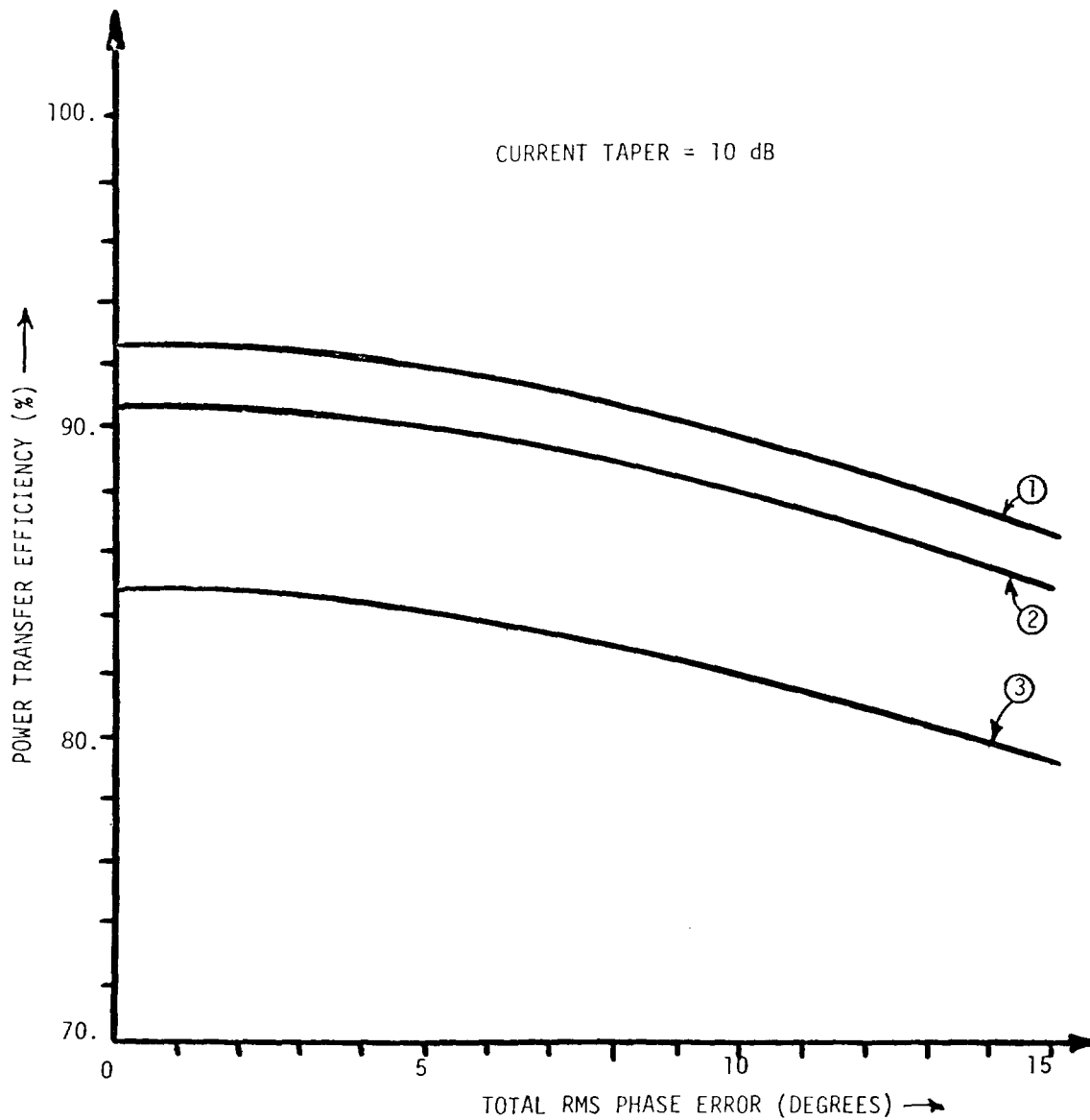
The power transfer efficiency adopted is defined by:

$$\text{POWER TRANSFER EFFICIENCY} = \frac{\text{Power Received by the 10 km Diameter Rectenna}}{\text{Total Power Radiated by the Spacetenna}}$$

This definition is convenient because the multiplying constants due to the propagation through the medium cancel out from the numerator and denominator.

4.3 Effects of System Imperfections on SPS Efficiency

Figures 4.2 - 4.3 summarize the effects of the various system imperfections on the SPS power transfer efficiency obtained through SOLARSIM. In Figure 4.1, the power transfer efficiency is plotted against the total phase error produced by the SPS phase control system. For a mechanically perfect system with no location jitters and mechanical pointing errors or jitters (curve ①), the total rms phase error is restricted to less than 10^0 at RF to yield a 90% efficiency. Curve ② depicts the influence of the mechanical pointing error (assumed to be 10' with a jitter of 2') when the location jitters are absent. As can be seen from the figure, for a total phase error of 10^0 the power transfer efficiency of the spacetenna drops down to 87.3%. When the location jitters of 2% of lambda is added for the transmitting and receiving elements, this number drops down to 82.0% (see Curve ③). It is expected that the SPS system will operate in the region between Curve ① and ③. In this case, the power transfer efficiency will be less than 90% for a typical rms phase error of 10 degrees.



LEGEND

- ① MECHANICAL POINTING ERROR (MPE) = 0, LOCATION JITTER (LJ) = 0, JITTER ON MECHANICAL POINTING = 0
- ② MPE = 10', LJ = 0, JITTER ON MPE = 2'
- ③ MPE = 10', LJ = 2% of λ , JITTER ON MPE = 2'

Figure 4.1. SPS Power Transfer Efficiency vs Phase Error.

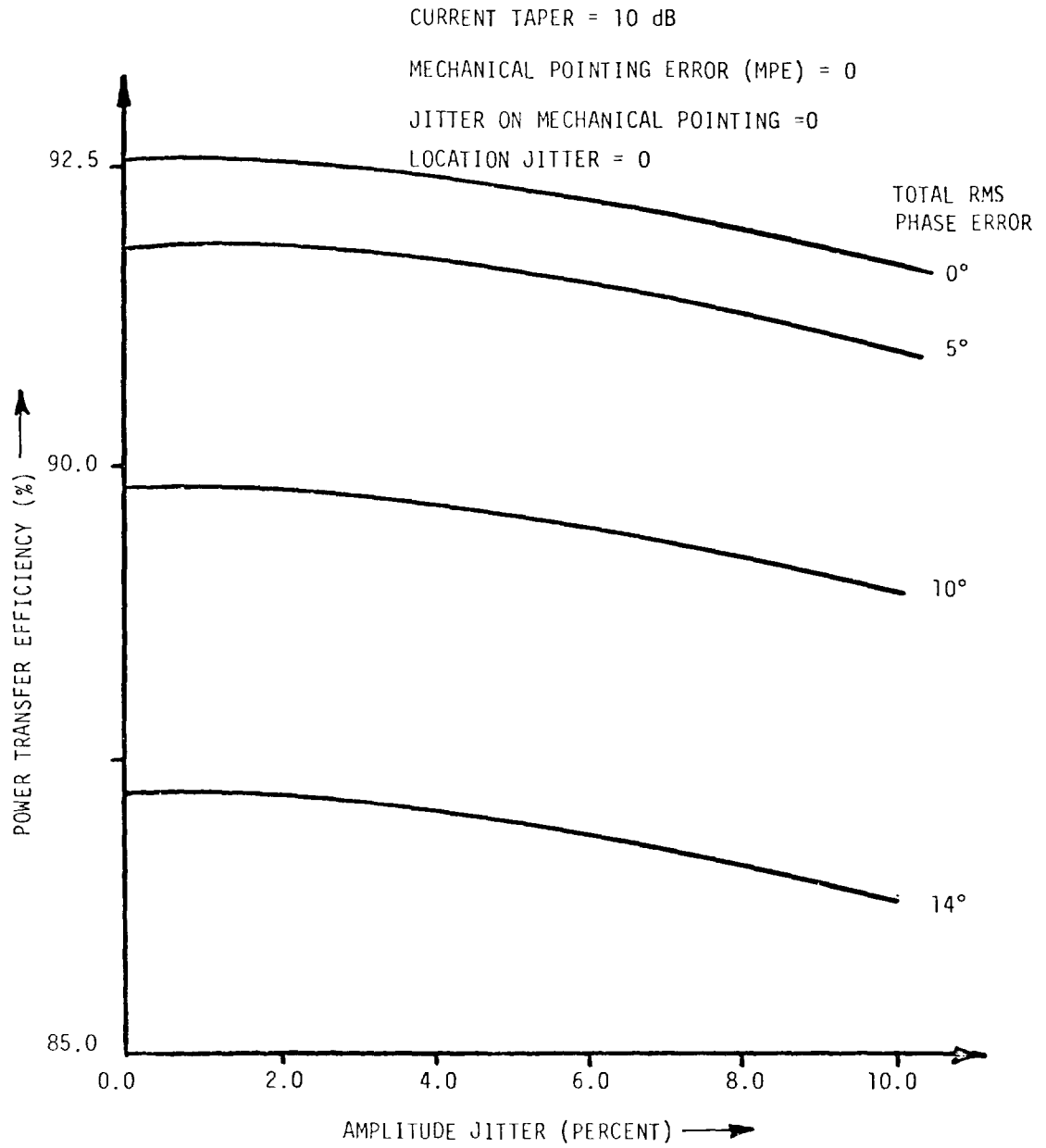


Figure 4.2. Effect of Amplitude Jitter on SPS Power Transfer Efficiency.

CURRENT TAPER = 10 dB
MECHANICAL POINTING ERROR = 0
JITTER ON MECHANICAL POINTING = 0
PHASE JITTER = 0

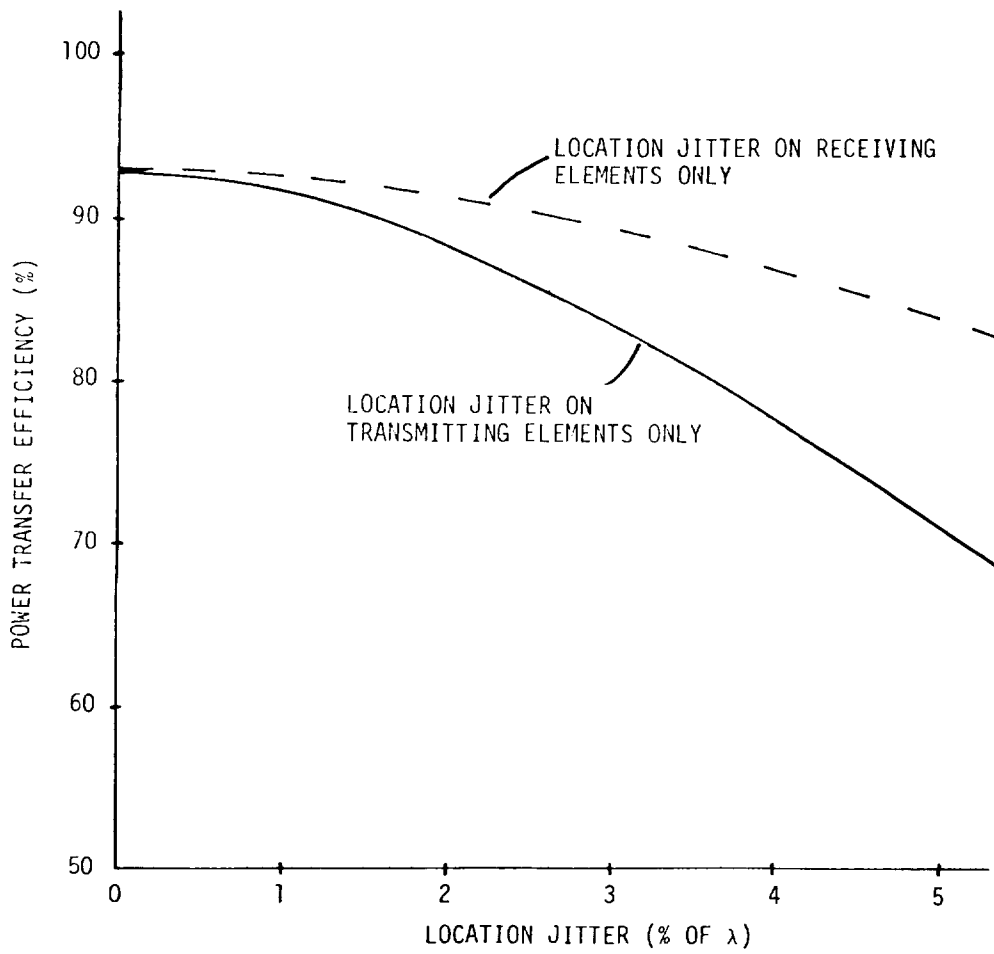


Figure 4.3 Effect of Location Jitters on the Otherwise Perfect SPS.

4.3.1 Current Amplitude Jitter

The effect of the current amplitude jitter is shown in Fig. 4.2 for a mechanically perfect system. As can be seen from the figure, for an amplitude jitter of 5%, the power transfer efficiency of the mechanically perfect spaceteenna with the current phase jitter of 0° is 92.3%. This value drops to 91.63% for the total phase error of 5° and to 89.57% for a total phase error of 10° . One can conclude that the power transfer efficiency is relatively insensitive to the amplitude jitters.

4.3.2 Location Jitters

Figure 4.3 investigates the effects of location jitters on the power transfer efficiency of an otherwise perfect SPS. As can be seen from the figure, the degradation of efficiency is severe: for a location jitter on each radiating element of $2\% \lambda$ the power transfer efficiency drops to 88.3%. As a comparison, Fig. 4.1 shows that for a rms phase error of 7° ($2\% \lambda = 7.2$) the efficiency is down to 91.2%. It is noticeable that the effect produced by location jitters on the receiving (conjugating) elements is comparable to the effect produced by the phase error. This is true because both these effects enter into the transmission system at the same physical point, i.e., the center subarray. On the other hand, power transfer efficiency is rather sensitive to the location jitter on the radiating elements.

REFERENCES

1. Lindsey, W. C., and Kantak, A. V., "Automatic Phase Control in Solar Power Satellite Systems," Prepared for NASA/JSC, TR-7809-0977, September 1977, LinCom Corporation, P.O. BOX 2793D, Pasadena, CA.
2. Lindsey, W. C., "A Solar Power Satellite Transmission System Incorporating Automatic Beam Forming, Steering and Phase Control," prepared for NASA/JSC, TR-7806-0977, June 1978, LinCom Corporation, P.O. BOX 2793D, Pasadena, CA.
3. Lindsey, W. C., and Kantak, A. V., "Automatic Phase Control in Solar Power Satellite Systems," Prepared for NASA/JSC, TR-7802-0977, February 1978, LinCom Corporation, P.O. BOX 2793D, Pasadena, CA.
4. Lindsey, W. C., Kantak, A. V., Chie, C. M., and Booth, R. W. D., "SPS Phase Control System Performance Via Analytical Simulation, Phase II," Prepared for NASA/JSC, TR-7903-0977, March 1979, LinCom Corporation, P.O. BOX 2793D, Pasadena, CA.
5. Lindsey, W. C., Kantak, A. V., and Chie, C. M., "SPS Phase Control Performance Via Analytical Simulation Phase III," Vols. I-IV, Prepared for NASA/JSC, TR-0180-0779, January 1980, LinCom Corporation, P. O. BOX 2793D, Pasadena, CA.

DESIGN AND BREADBOARD EVALUATION OF THE SPS
REFERENCE PHASE CONTROL SYSTEM CONCEPT

P. M. Hopkins and V. R. Rao

Lockheed Engineering and Management Services Company, Inc.

1. INTRODUCTION

Efficient operation of a very large phased array such as the proposed solar power satellite [1], requires precision focusing and pointing of the power beam; i.e., the power beam must have a planar wavefront directed precisely at the center of the target antenna (rectenna). To maintain such a power beam requires real-time phase compensation at each subaperture in order to adjust for structural deformations and other transitory factors. In the current solar power satellite (SPS) baseline, the spaceborne antenna (Space-tenna) is an active retrodirective array [2], [3]. A pilot signal transmitted from the center of the rectenna is phase-conjugated at each subaperture (power module) of the spacetenna, thereby assuring that the radiated composite wave is focused on the target. This scheme requires a large amount of precision electronic circuitry on the spacetenna. Specifically, pilot receivers must be located at each power module and an adaptive distribution network is required in order to provide a properly phased reference signal at each conjugator [4], [5].

In order to verify theoretical and simulation results, a project was initiated by the Tracking and Communication Systems Department of Lockheed Electronics Company to design, develop, and test a breadboard system comprising a pilot receiver and transmitter, phase distribution system, and power transponder. This breadboard system is to be used in the Electronic Systems Test Laboratory (ESTL) at the Johnson Space Center. The total breadboard system will include one pilot transmitter, one pilot receiver, nine phase distribution units, and

two power transponders. It will be shown in the following sections of this paper that with this complement of equipment, segments of a typical phase distribution system can be assembled to facilitate the evaluation of significant system parameters.

The major objectives of the project are to determine the achievable accuracy of a large phase distribution system, the sensitivity of the system to parameter variations, and the limitations of commercially available components in such applications.

2. ACCOMPLISHMENTS

The design and development of a breadboard Master-Slave Returnable Timing System (MSRTS) was the first objective of the project. Nine units were planned; three were completed and used for prototype evaluation tests. Six remaining units are in final assembly.

2.1 MSRTS BREADBOARD

The MSRTS breadboard system is of a modular design with three major elements. These are the Phase Tracking Unit (PTU), the Interface/Return Unit (IRU) and the Main Frame. Modular construction permits the equipment to be configured in various ways as required to model portions of the proposed SPS phase distribution tree network. A simplified functional diagram of a single MSRTS stage is shown in Figure 1. Figure 2 shows the tree distribution structure for which the breadboard MSRTS is designed.

The major components of the PTU are Voltage Controlled Oscillator (VCO), loop filter, circulator, mixers and a phase detector. The phase lock loop circuitry is used to advance the phase of VCO to compensate for the effect of the delay introduced by the path between nodes of a tree structure.

At the IRU, two functions are performed. First, a portion of the received reference signal is returned to the preceding PTU via the single interconnecting cable. This return signal arrives at the PTU with a phase delay proportional to the line length. The delay is measured in the phase detector

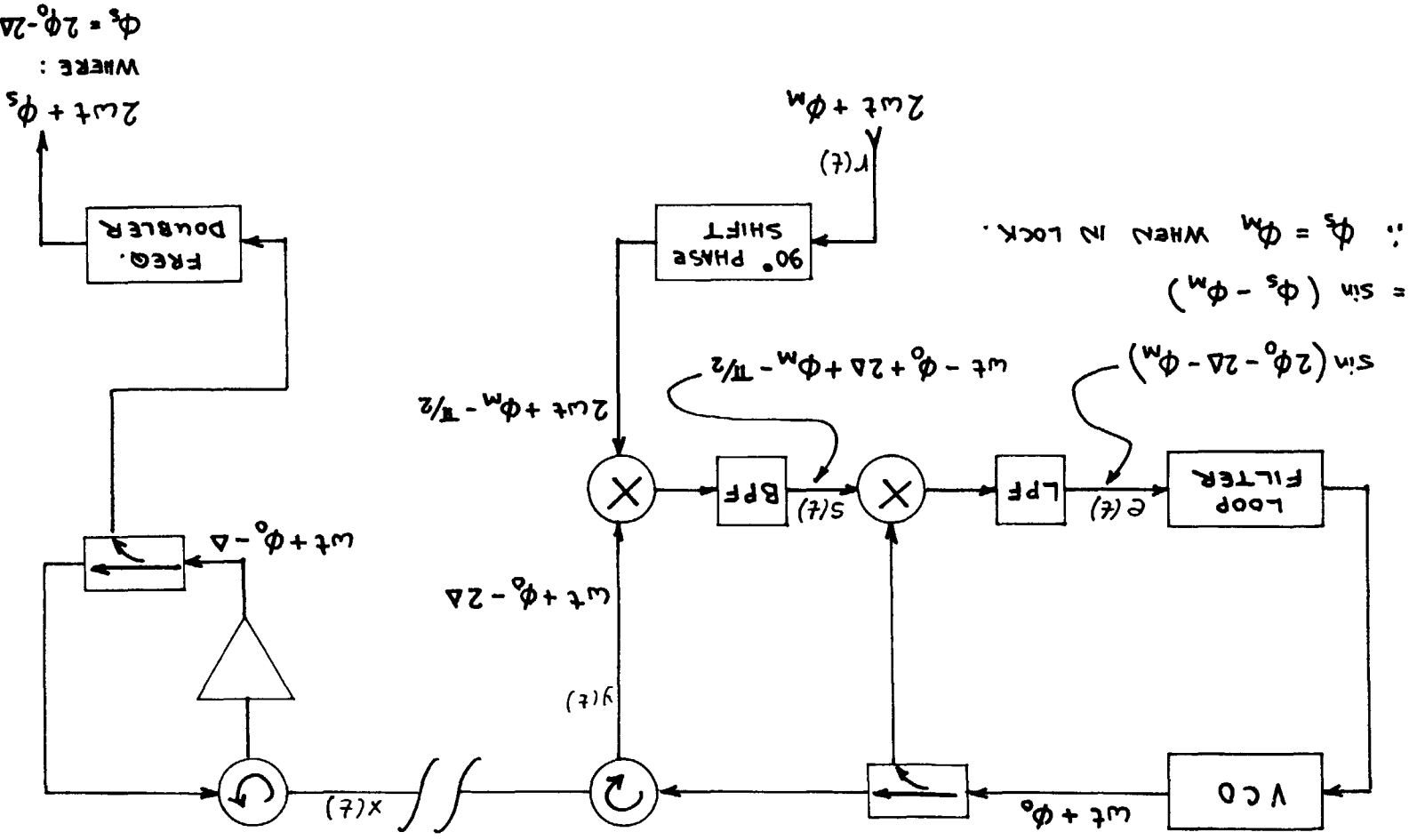


Figure 1. Simplified functional diagram of MSRTS.

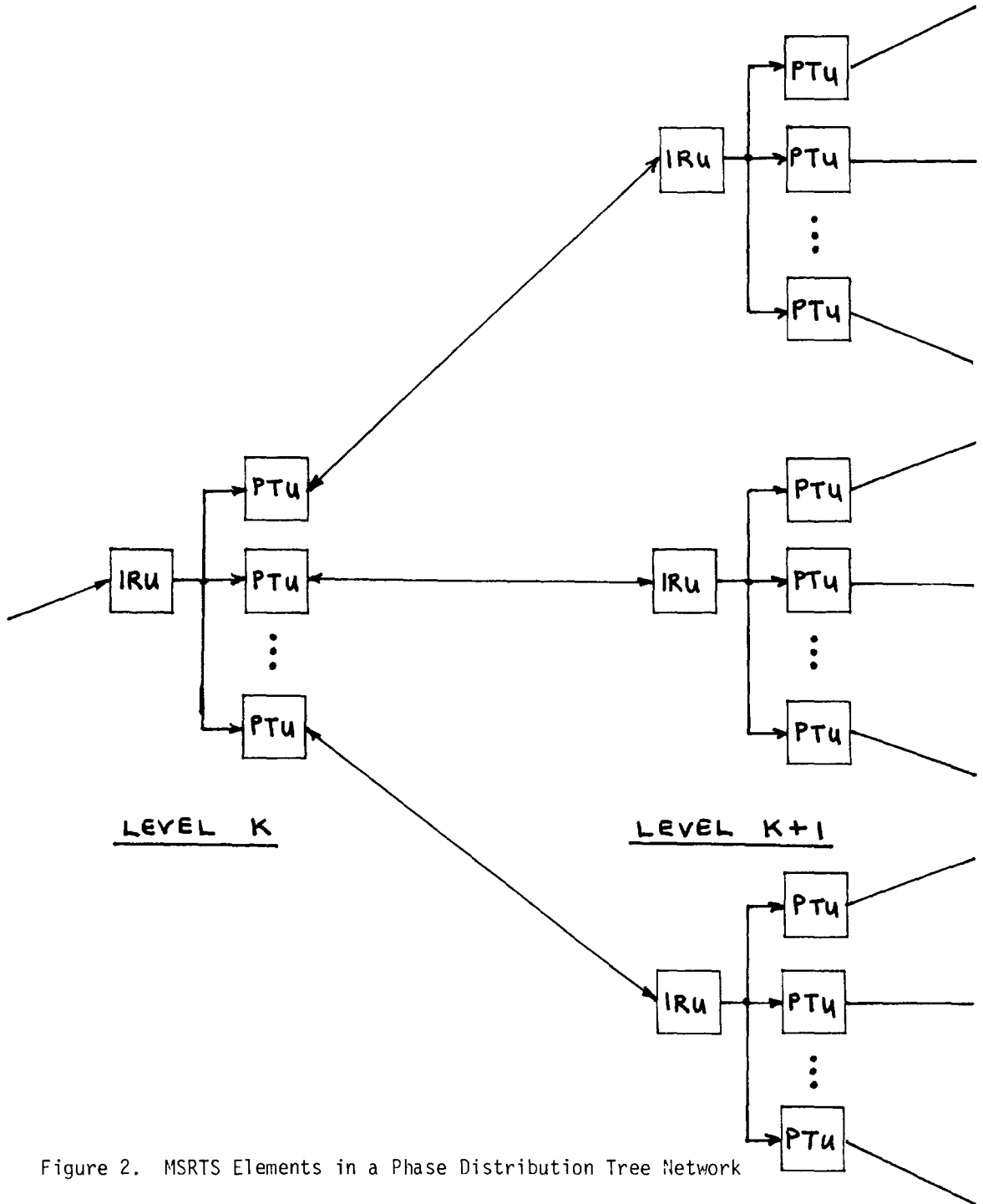


Figure 2. MSRTS Elements in a Phase Distribution Tree Network

of the PTU, and the VCO phase is appropriately adjusted so that the reference phase is correct at the IRU input. Second, the reference signal at the IRU is doubled in frequency to match the reference input to the PTU. When the PTU is phase locked, the phase of the IRU output signal is the same as the phase of the preceding PTU input signal, within the accuracy limitations of the hardware. Each IRU can provide up to four outputs.

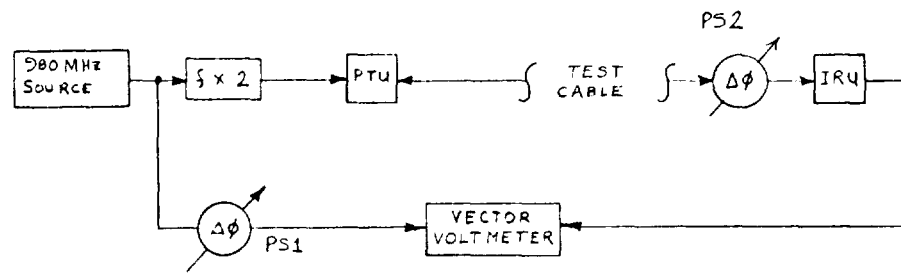
The Main Frame contains supplies and a patch panel that facilitates the interconnection between PTU's and IRU's mounted in separate mainframes. Each mainframe is capable of supporting a total of three PTU's and/or IRU's.

2.2 MSRTS BREADBOARD TEST RESULTS

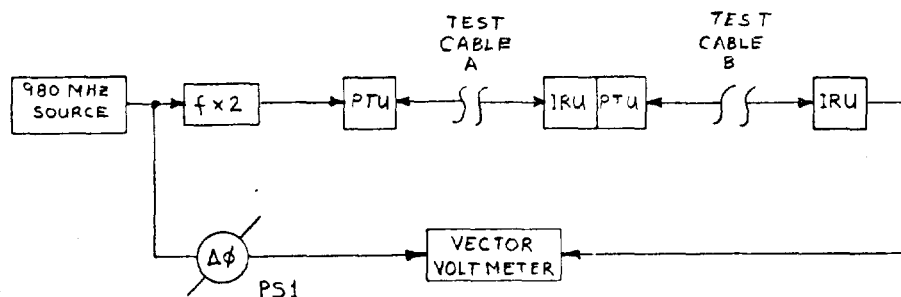
Three prototype MSRTS breadboard units were used in a variety of test configurations to evaluate the accuracy of phase control and the effects of component imperfections. These test configurations included those shown in Figure 3.

For example, the three-node series network of Figure 3c was tested with 30 different cable combinations, using RG-14 coaxial cable in lengths between 200 and 250 feet (60 - 80 meters); that is, after initial adjustment of the test configuration with zero phase error on the vector voltmeter, 30 different combinations of cables were substituted for Test Cables A and B. For each combination, the resulting phase error was measured and recorded. The results are presented in the histogram of Figure 4, which indicates a standard deviation of error of 4.2° . This experiment is intended to demonstrate the accuracy of the breadboard MSRTS with arbitrary cable lengths. It is important to note that the cables were not cut to precise measurements.

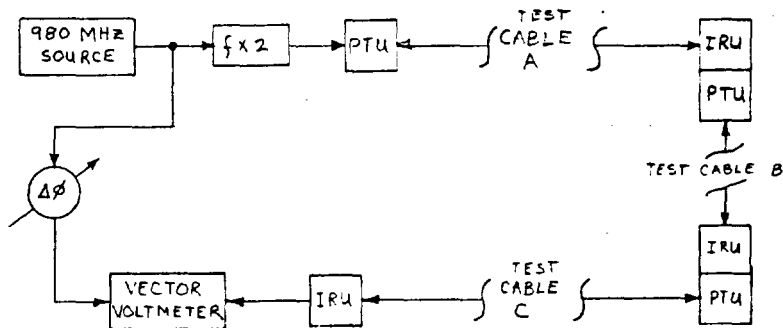
Another type of phase error measurement was made with the configuration of Figure 3a. Minor variations in electrical line length were introduced by means of a phase shifter (PS2). The phase error at the vector voltmeter was initially nulled with PS2 set to zero. Then PS2 was varied from 0 to 180° , equivalent to a half-wave variation in cable length. The resulting phase error is shown in Figure 5.



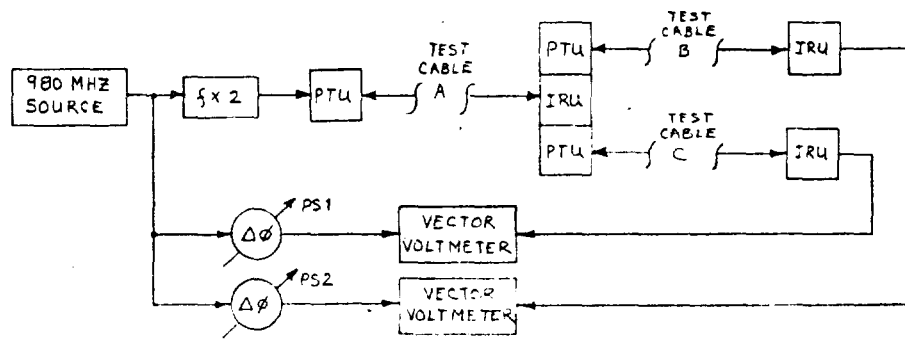
a) TWO-NODE



b) THREE-NODE SERIES



c) FOUR-NODE SERIES



d) FOUR-NODE WYE

Figure 3. MSRTS Breadboard Test Configuration

STANDARD DEVIATION OF 30 TRIAL SAMPLE = 4.2 DEGREES

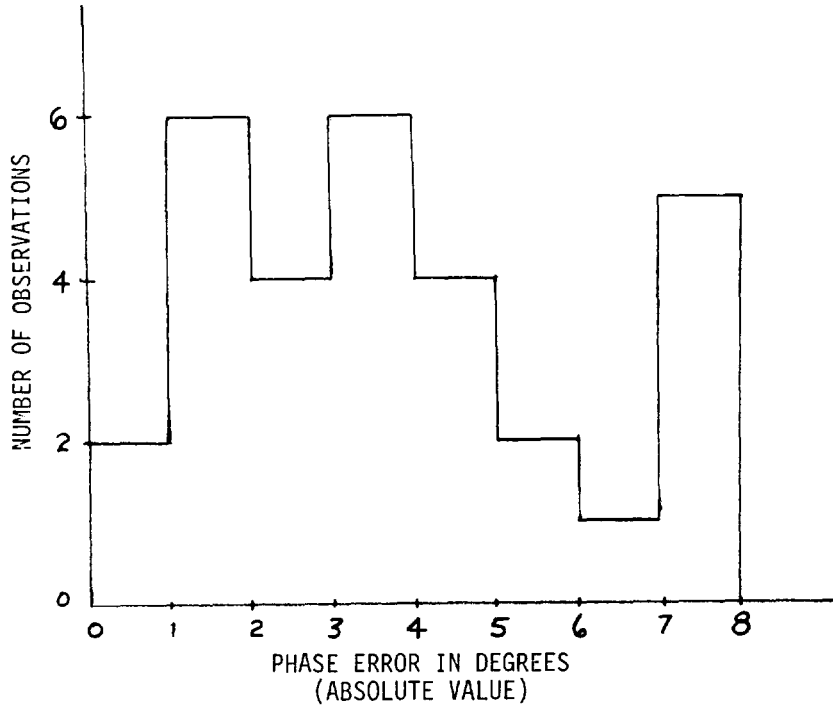


Figure 4. Histogram of Three-Node Test Results

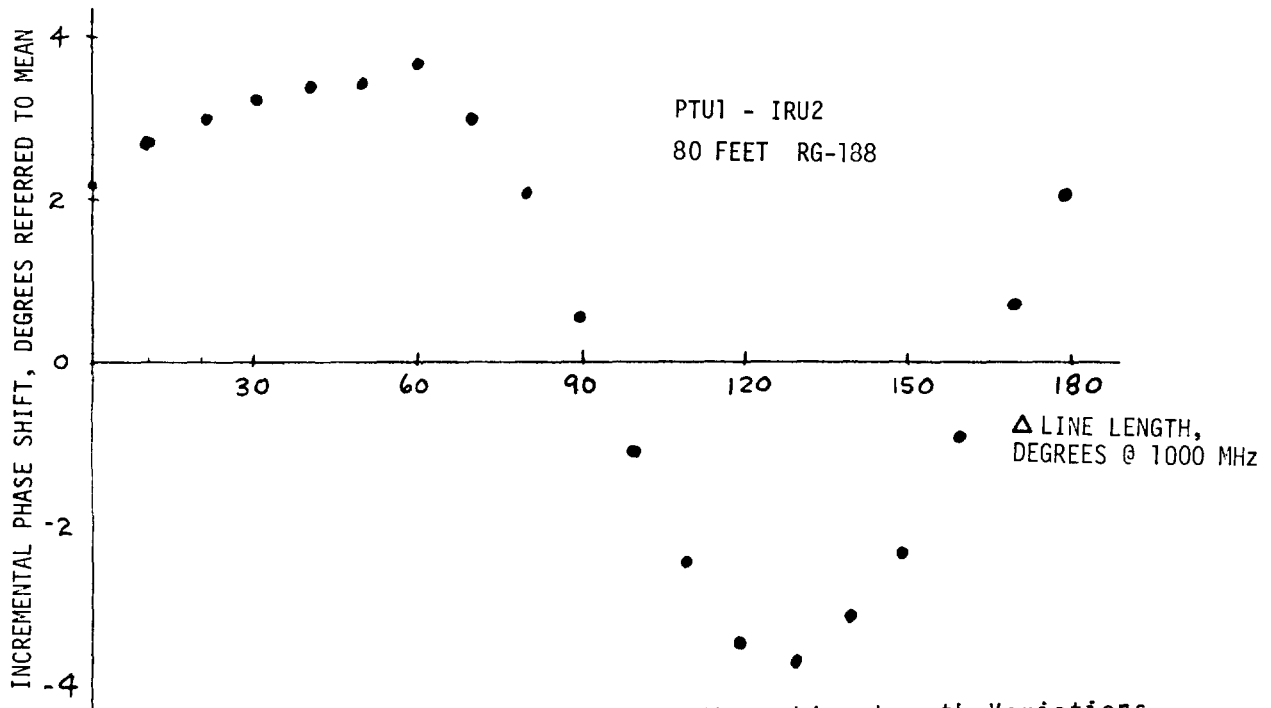


Figure 5. Phase Error Versus Minor Line Length Variations.

2.3 INTERPRETATION OF TEST RESULTS

A detailed report of the MSRTS breadboard test results has been prepared [6]. The conclusions from that report are summarized in the following:

- Satisfactory performance can be obtained using readily available components under closely controlled conditions.
- Commercially available components exhibit non-ideal behavior which is critical to MSRTS performance, e.g. port-to-port isolation of mixers and circulators was not sufficient to prevent extraneous signals which can cause phase errors. These effects can be minimized with compensating networks.

3. CONTINUING DEVELOPMENT

The breadboard MSRTS will be used as part of a larger breadboard system which models the total SPS phase control concept. A pilot transmitter will generate a pseudonoise (PM) code-modulated spread spectrum pilot carrier at 2450 MHz. A central pilot receiver will phaselock to the pilot carrier and provide a reference for the MSRTS. At the final level of the MSRTS tree, each IRU will provide a reference phase signal for a power transponder. Each power transponder will receive the pilot carrier, phase-conjugate, and retransmit. The ESTL breadboard system, shown functionally in a typical test configuration in Figure 6, will consist of the following units.

- One Pilot Transmitter
- One Central Pilot Receiver
- Nine MSRTS Elements
- Two Power Transponders
- One Klystron Power Amplifier

These units can be interconnected in various test configurations. Tests will be performed to evaluate the feasibility of the MSRTS phase control concept and to determine the sensitivity of the phase control system to variations in system parameters. In addition, techniques for suppressing the phase noise of the klystron power amplifier will be investigated.

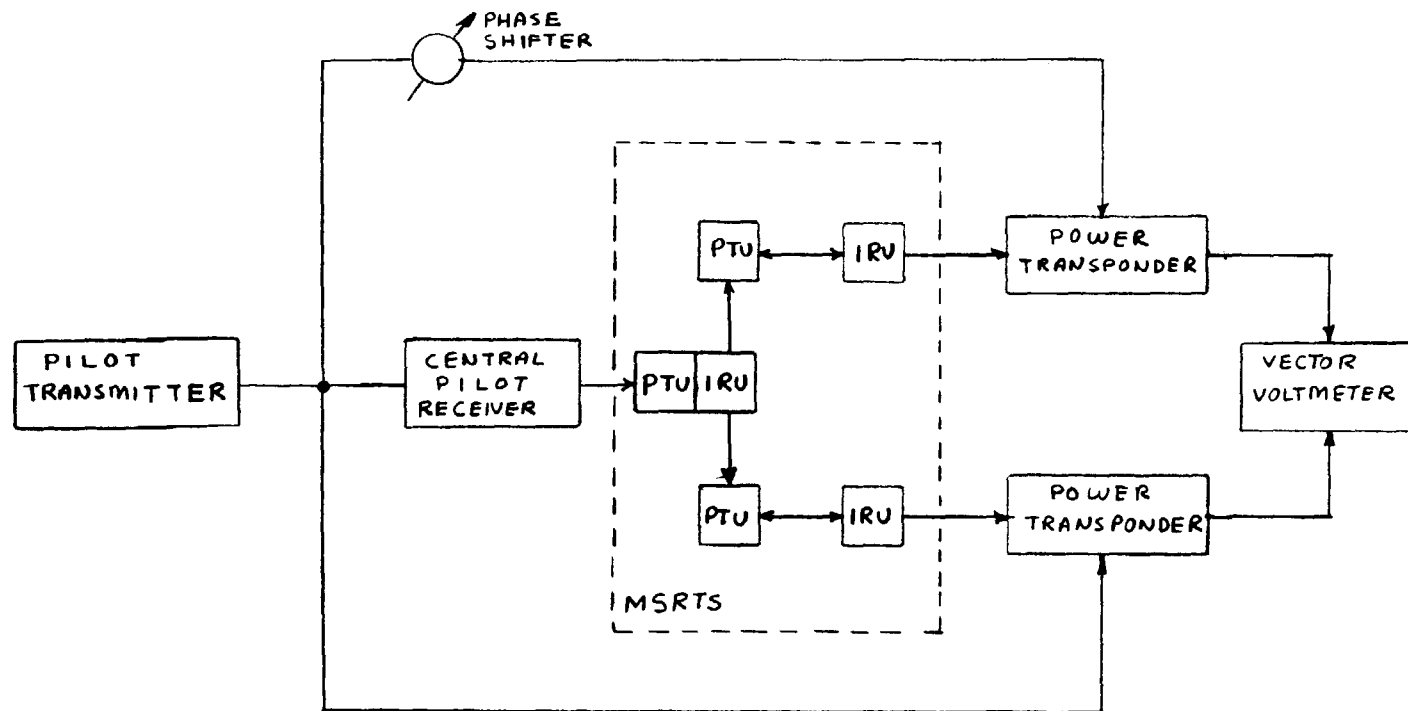


Figure 6. Breadboard SPS Phase Control System in Typical Test Configuration

Design and development of the ESTL breadboard system will be completed by March 1980. The test and evaluation program will be completed by July 1980.

4. ACKNOWLEDGEMENTS

The work described in this paper was performed under NASA Contract Number NAS 9-15800. The design, development, and initial testing of the breadboard MSRTS was done by Dr. James C. Vanelli of Lockheed Electronics Company, Inc.

5. REFERENCES

1. "Initial Technical, Environmental and Economic Evaluation of Space Solar Power Concept." NASA Lyndon B. Johnson Space Center, Houston, Texas, JSC-11568, August 31, 1971.
2. Skolnick, M. I. and King, D. D.: "Self-Phasing Array Antennas." IEEE Transactions on Antennas and Propagation, Volume AP-12, pp. 142-149, March 1964.
3. Ghose, R. N.: "Electronically Adaptive Antenna Systems." IEEE Transactions on Antennas and Propagation, Volume AP-12, pp. 161-169, March 1964.
4. Lindsey, W. C. and Kantak, A. V.: "Automatic Phase Control in Solar Power Satellite Systems." Lincom Technical Report TR-7802-0977, February 15, 1978.
5. Lindsey, W. C.: "A Solar Power Satellite Transmission System Incorporating Automatic Beamforming, Steering and Phase Control." Lincom Technical Report TR-7806-0977, 1978.
6. Vanelli, J. C.: "Design and Testing of a Master-Slave Returnable Timing System for the Solar Power Satellite." Lockheed Electronics Company, Houston, Texas, LEC-10474/EE7-79-714, December 1979.

COHERENT MULTIPLE TONE TECHNIQUE FOR
GROUND BASED SPS PHASE CONTROL*

C. M. Chie
LinCom Corporation

1.0 Introduction

The ground based phase control concept has been under study at LinCom as an alternative approach to the reference SPS phase control system (See Refs. 1,2,3). The details of the ground based phase control system study are documented in Ref. 4. In this short paper we summarize the coherent multiple tone technique used for the ground based phase measurement waveform design and phase control system.

2.0 Ground-Based Phase Control Concept

The ground based phase control system achieves beam forming by adjusting the phases of the individual transmitters on board SPS. The phase adjustments are controlled by ground commands. To specify the correct amount of adjustments, the phases of the power beams from each individual transmitter arriving at the rectenna center must be measured, the appropriate corrections determined (to ensure that all power beams arrive at the same phase) and relayed to the SPS. The proposed scheme to be considered is sequential in nature, i.e., the phase measurement is performed one at a time for each individual transmitter at approximately one-second intervals (measurement time allocated is 10 μ sec). The phase corrections are updated once every second. A 10-bit phase quantization for the corrections giving 0.35° resolution is envisioned. The uplink command data rate is on the order of 10 Mbps. The functional operation of the ground-based phase control concept is summarized in Fig. 1. As evident from the figure, the key issues that need to be addressed are:

*This work was performed at LinCom Corporation for the NASA Johnson Space Center, Houston, TX, under Contract No. NAS9-15782.

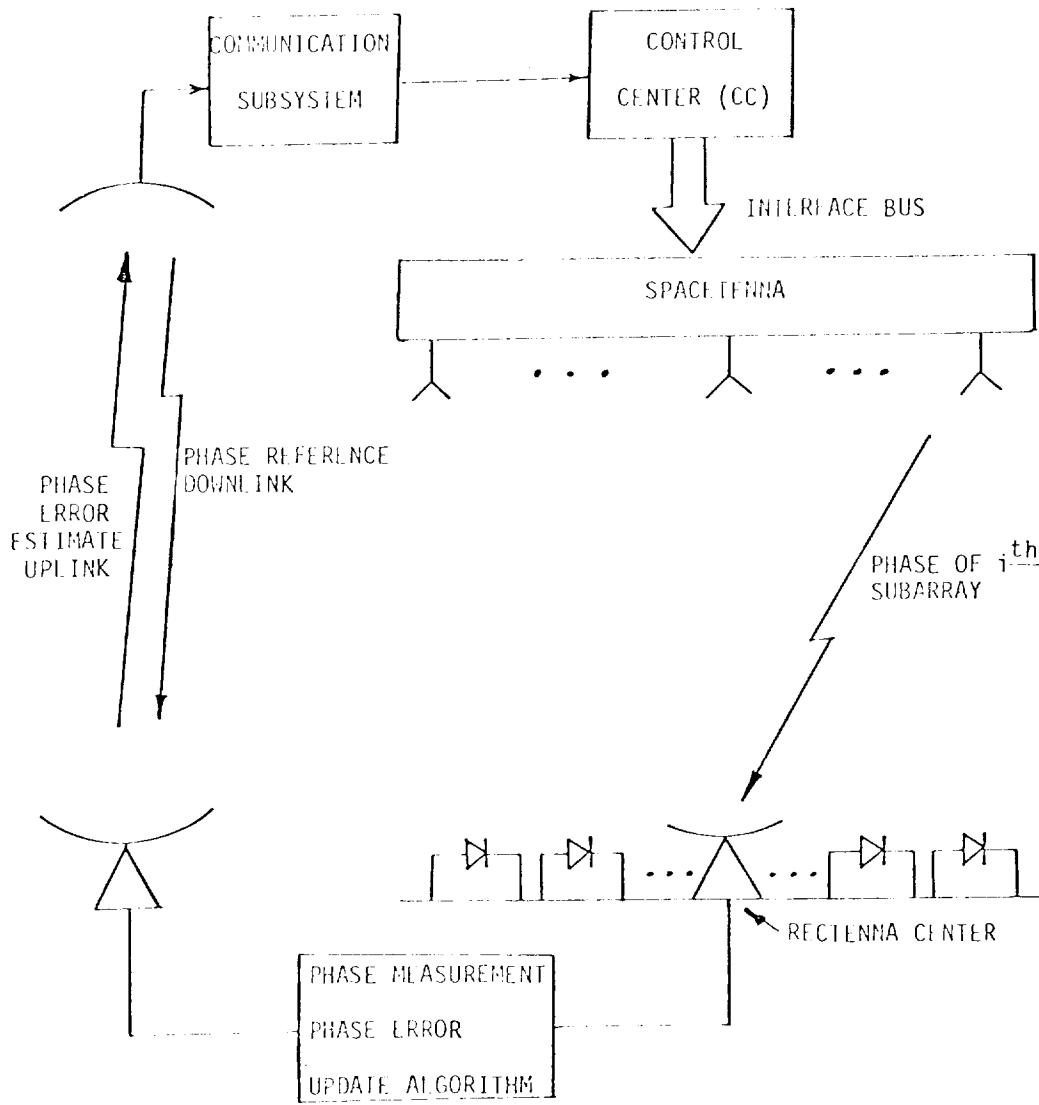


Figure 1. Ground Based Phase Control System Concept with Major Functional Blocks.

- (1) measurement waveform design and selection,
- (2) phase measurement pilot reference design and selection,
- (3) uplink phase corrections command link format and design, and
- (4) system synchronization techniques.

3.0 Two-Tone Phase Measurement Scheme with Coherent Subcarrier

In the basic two-tone measurement scheme, two side tones at $f_0 \pm \Delta f$ are transmitted from the satellite to the ground receiver. A phantom carrier can be reconstructed from the sidetones by passing the signal through a squaring circuit. The output will then have a CW component with frequency $2f_0$ and a phase component equal to $(\phi_1 + \phi_2)$, where ϕ_1 and ϕ_2 are the channel induced phase shifts at $f_0 + \Delta f$ and $f_0 - \Delta f$, respectively. This phase shift is very close to double the one that would have occurred if the downlink signal were a single sinusoid at frequency f_0 . If we divide the $2f_0$ component by two, we obtain the average phase $\frac{\phi_1 + \phi_2}{2}$. Unfortunately, the divide by two circuit results in a $0^\circ - 180^\circ$ ambiguity.

4.0 Four-Tone Phase Measurement Scheme

The four-tone measurement scheme given in Fig. 2 is a simple modification of the two-tone scheme. Basically, we first use frequencies at $f_0 \pm 2\Delta f$ for phase error measurement with introduces π ambiguity. Then we use frequencies at $f_0 \pm \Delta f$ for ambiguity resolution. The scheme works as follows. The transmitted signal at the input to the transmitting antenna is (neglecting multiplicative constants)

$$s_1(t) = \cos\left[\omega_0\left(1 + \frac{\ell}{N}\right)t + \left(1 + \frac{\ell}{N}\right)\theta_i + \frac{2\pi k \ell}{N}\right] \\ + \cos\left[\omega_0\left(1 - \frac{\ell}{N}\right)t + \left(1 - \frac{\ell}{N}\right)\theta_i - \frac{2\pi k \ell}{N}\right] \quad \ell = 0, 1, 2$$

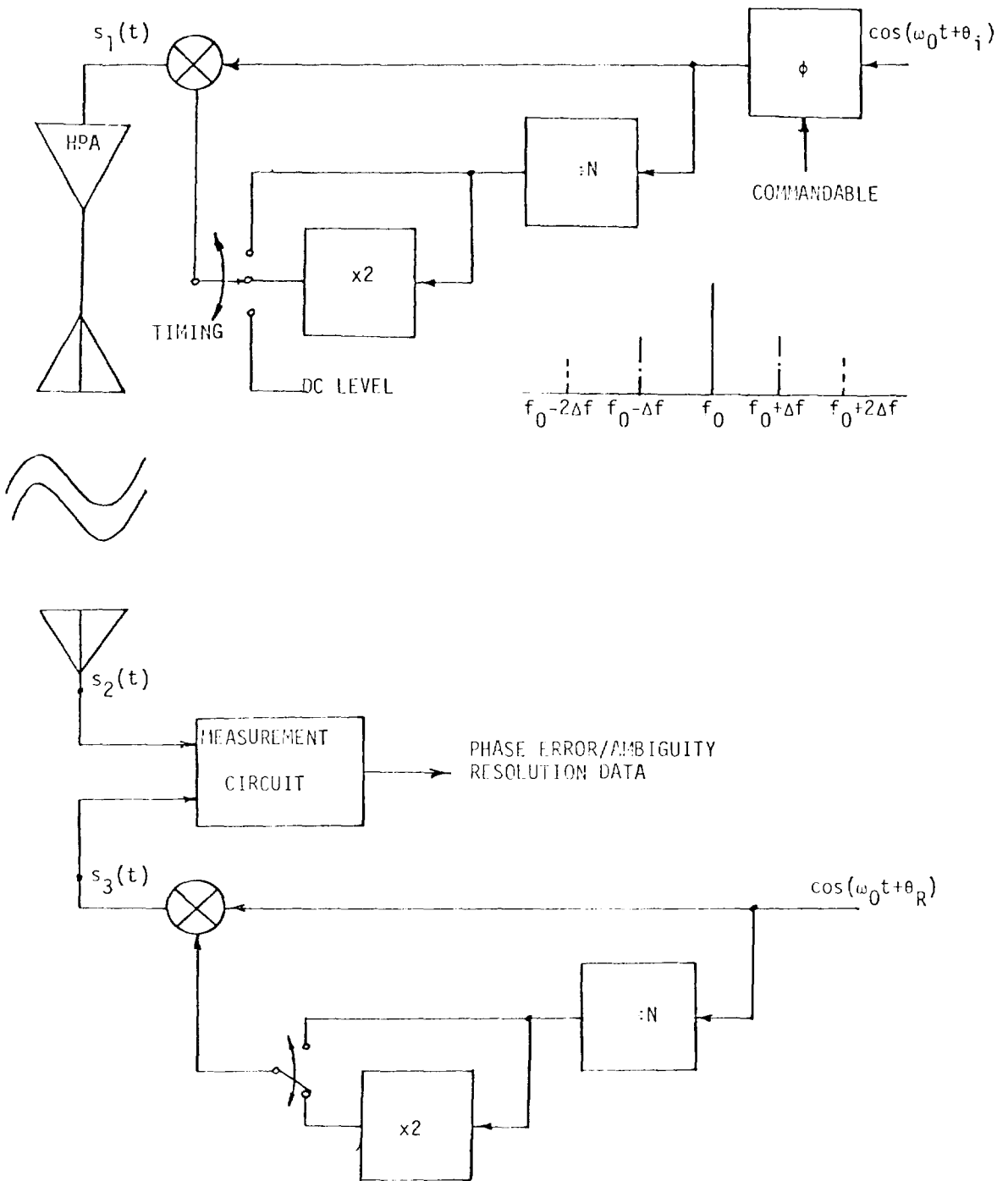


Figure 2. Four-Tone Phase Measurement Scheme.

where θ_i includes the commandable phase shift, $\frac{2k\pi}{N}$ is the ambiguity introduced by the divide by N circuit, $f = \frac{f_0}{N}$, and $\ell = 0,1,2$ depending on whether the PM is in the power mode (1), ambiguity resolution mode (2), or phase error measurement mode (3). At the receiver on the ground,

$$s_2(t) = \cos[\omega_0(1 + \frac{\ell}{N})t + (1 + \frac{\ell}{N})\theta_i + \frac{2\pi k\ell}{N} + \varphi_+(\ell)] \\ + \cos[\omega_0(1 - \frac{\ell}{N})t + (1 - \frac{\ell}{N})\theta_i - \frac{2\pi k\ell}{N} + \varphi_-(\ell)]$$

where $\varphi_+(\ell)$ and $\varphi_-(\ell)$ are the phase shifts introduced by the channel.

The reference signal $s_3(t)$ is given by

$$s_3(t) = \cos[\omega_0(1 + \frac{\ell}{N})t + (1 + \frac{\ell}{N})\theta_R + \frac{2\pi \ell m}{N}] \\ + \cos[\omega_0(1 - \frac{\ell}{N})t + (1 - \frac{\ell}{N})\theta_R - \frac{2\pi \ell m}{N}]$$

where θ_R is the phase of the ground reference, and $\frac{2\pi m}{N}$ is the ambiguity introduced by the ground divide by N circuit. If the operations are synchronized, we can then measure up to modulo 2π at the output of the measurement circuit, the phases

$$\varphi_+(\ell) + (1 + \frac{\ell}{N})(\theta_i - \theta_R) + \frac{2\pi \ell}{N}(k-m) = \phi_+(\ell) + 2\pi M_+(\ell) \quad (1)$$

$$\varphi_-(\ell) + (1 - \frac{\ell}{N})(\theta_i - \theta_R) - \frac{2\pi \ell}{N}(k-m) = \phi_-(\ell) + 2\pi M_-(\ell) \quad (2)$$

Actually, in (1) and (2), $\phi_+(\ell)$ and $\phi_-(\ell)$ are the measured phases and $M_+(\ell)$ and $M_-(\ell)$ are integers so that the absolute values of $\phi_+(\ell)$ and $\phi_-(\ell)$ can be restricted to π . Note that we are interested in determining $[\varphi_+(\ell) + \varphi_-(\ell)]/2$ modulo 2π . For $\ell=2$, we know from (1) and (2) that

$$\frac{\varphi_+(2) + \varphi_-(2)}{2} = \frac{\phi_+(2) + \phi_-(2)}{2} + [M_+(2) + M_-(2)]\pi - (\theta_i - \theta_R) \quad (3)$$

Now if we can resolve whether $[M_+(2) + M_-(2)]$ is even or odd, we can determine $[\varphi_+(2) + \varphi_-(2)]/2 + (\theta_i - \theta_R)$ modulo 2π . This information is

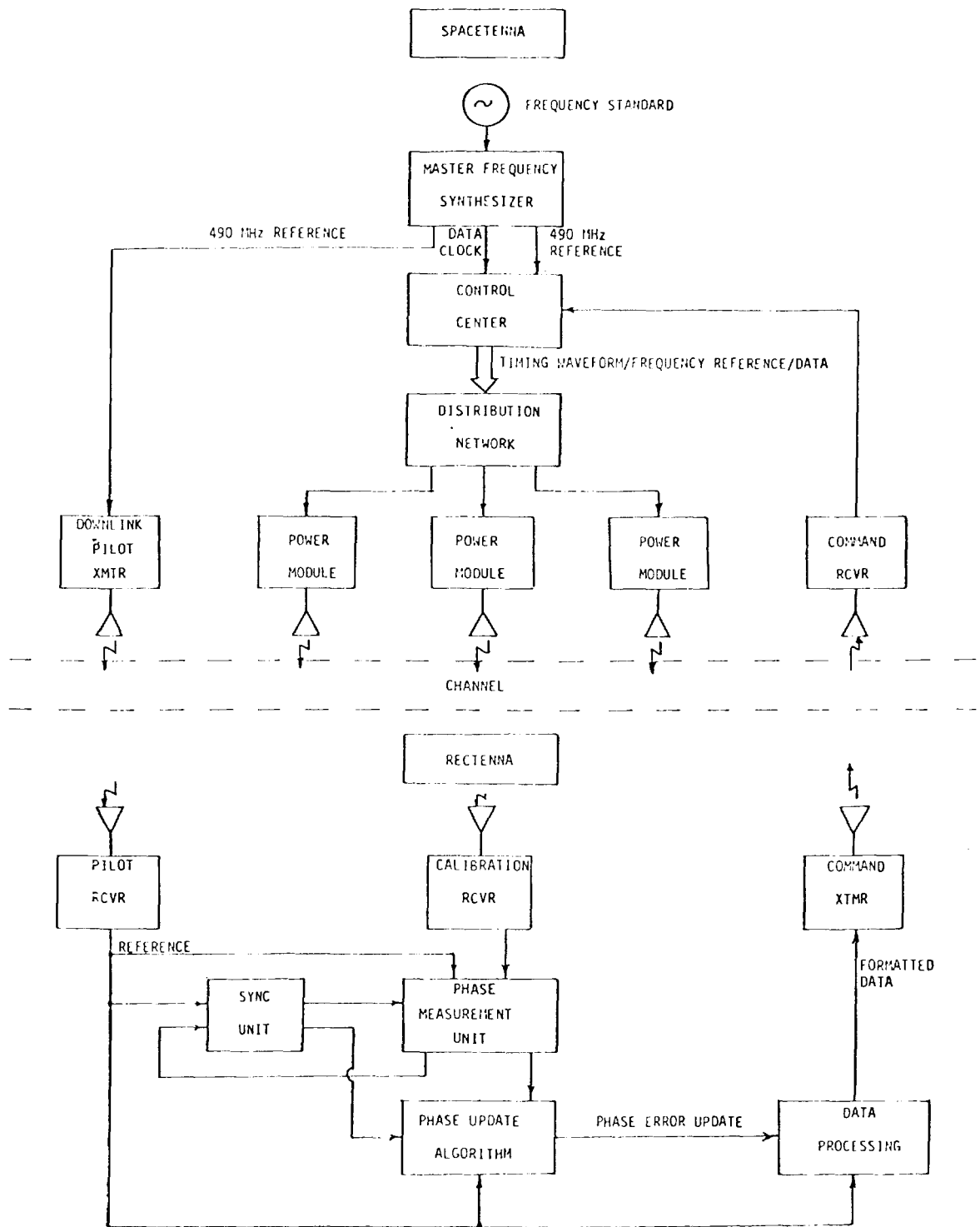


Figure 3. SPS Ground Based Phase Control Functional Block Diagram Showing System Timing Hierarchy.

provided by comparing

$$\varphi_+(1) - \varphi_-(1) = -\frac{2}{N}(\theta_i - \theta_R) - \frac{4\pi}{N}(k-n) + \phi_+(1) - \phi_-(1) + [M_+(1) - M_-(1)]2\pi \quad (4)$$

$$\frac{\varphi_+(2) - \varphi_-(2)}{2} = -\frac{2}{N}(\theta_i - \theta_R) - \frac{4\pi}{N}(k-n) + \frac{\phi_+(2) - \phi_-(2)}{2} + [M_+(2) - M_-(2)]\pi \quad (5)$$

If Δf is designed properly ($\Delta f < 50$ MHz) the left hand side of (4) and (5) are nearly equal. See Ref. 4 for a discussion on ionospheric effects. Equating (4) and (5) we have

$$\frac{\phi_+(2) - \phi_-(2)}{2} + [M_+(2) - M_-(2)]\pi \equiv \phi_+(1) - \phi_-(1) \pmod{2\pi} \quad (6)$$

Since we can measure $\phi_+(2)$, we can determine from (6) whether $[M_+(2) - M_-(2)]$ is odd or even. This then determines whether $[M_+(2) + M_-(2)]$ is odd or even, since $[M_+(2) - M_-(2)] + [M_+(2) + M_-(2)] = M_+(2)$ must be even. With this information, we can solve for $[\varphi_+(2) + \varphi_-(2)]/2 + (\theta_i - \theta_R)$ modulo 2π in (3).

5.0 Baseline System for Ground-Based Phase Control

The implementation of the ground-based phase control concept is determined by the phase control waveform designs employed. Based on our waveform selections, functional subsystems to implement the ground-based phase control concept are identified and functionally represented. The resultant ground-based phase control functional block diagram is depicted in Fig. 3 and includes:

- Satellite Signal Processing
 - Time-Frequency Control
 - Processing Control Center
 - Signal Distribution Network
 - Processing Power Module
 - Downlink Pilot Transmitter

- Uplink Command Receiver
- Ground Based Signal Processing
 - Pilot Beacon Receiver
 - Calibration Receiver
 - Phase Measurement Unit
 - Synchronization Unit
 - Phase Update Algorithm
 - Data Processing Unit
- Uplink Command Transmitter

The ground-based system envisioned employs satellite based frequency/timing reference with an IF frequency of 490 MHz. A 4-tone measurement scheme using frequencies at $2,450 \pm 9.57$ MHz and $2,450 \pm 19.14$ MHz is selected. Each power module devotes 10 μ sec per second for phase correction measurement, representing a minimal loss in total power transmitted. Two frequencies are chosen for the downlink and one frequency for uplink; the downlink pilot signal center frequency is set at 4.9 GHz.

Our preliminary investigation indicates that the effects of power beam interference and thermal noise on the phase measurement error can be controlled to a tolerable level. The ground based system can also function if the ionosphere is nonturbulent in nature and the satellite's tilt rate is limited to $0.5 \widehat{\text{min}}/\text{sec}$.

6.0 Limiting Factors of the Feasibility of Ground-Based Phase Control System

The feasibility of the ground-based phase control concept becomes unclear if the conditions on the ionosphere and the satellite motion are not met. The ground-based phase control system can only correct for random phase fluctuations which have a correlation time that is large

compared with 1.25 sec. The noise components which are faster than 1.25 sec is uncompensated for and result in a degradation on transmission efficiency. Unfortunately, measured ionosphere data which is suitable for the SPS system is not readily available. (Most data are concerned with spatial correlations rather than temporal correlations. Also, most data are measured from low orbit satellites rather than geostationary satellites.) The other limiting factor is the statistical behavior of the random pointing error exhibited by the spaceteenna. Again, the fast component of this error is not corrected for and it contributes to efficiency degradation. At this point, we feel that the development and specification of models for ionospheric phase disturbance and satellite motion is essential. It is hoped that our findings can serve as a guideline for any parallel efforts in studying these two factors.

REFERENCES

1. Lindsey, W. C., and Kantak, A. V., "Automatic Phase Control in Solar Power Satellite Systems," Prepared for NASA/JSC, TR-7809-0977, September 1977, LinCom Corporation, Pasadena, CA.
2. Lindsey, W. C., "A Solar Power Satellite Transmission System Incorporating Automatic Beam Forming, Steering and Phase Control," Prepared for NASA/JSC, June, 1978, LinCom Corporation, Pasadena, CA.
3. Lindsey, W. C., and Kantak, A. V., "SPS Phase Control System Performance via Analytical Simulation," Prepared for NASA/JSC, February, 1979, LinCom Corporation, Pasadena, CA.
4. Chie, C. M., "A Ground Based Phase Control System for the Solar Power Satellite," Prepared for NASA/JSC, January, 1979.

AN INTERFEROMETER-BASED PHASE CONTROL SYSTEM

James H. Ott
James S. Rice
Novar Electronics Corporation, Barberton, Ohio

ABSTRACT

An interferometer-based phase control system for focusing and pointing the SPS power beam is discussed. The system is ground based and closed loop. One receiving antenna is required on earth. A conventional uplink data channel transmits an 8-bit phase error correction back to the SPS for sequential calibration of each power module. Beam pointing resolution is better than 140 meters at the Rectenna.

INTRODUCTION

Key to focusing and pointing the SPS power beam is the maintenance of precise phase relationships among the transmitted signals of each Spacatenna subarray. Specifically, the signals transmitted by each power module must arrive at the center of the Rectenna in phase. This results in a power beam having a planar wavefront pointed at the center of the Rectenna. However, structural deformations in the Spacatenna can, if not compensated for, alter the phases of the power module signals at the Rectenna by altering the path lengths of the signals between the power modules and the Rectenna. In addition, variations within the Spacatenna circuitry can also alter the phases of the signals.

Novar Electronics Corporation has developed an interferometer-based phase control system.¹ This approach, which we call Interferometric Phase Control (IPC), has three significant characteristics which differentiate it from the Reference System retrodirective approach.

1. Interferometric Phase Control is a ground based closed loop system.
Unlike in the retrodirective approach, the phase correction information is obtained on earth by measuring the resultant power transmission of the Spacatenna power modules and comparing them against a reference.
2. The Spacatenna's power modules are calibrated sequentially.
A signal from a reference transmitter near the center of the Spacatenna is sequentially phase compared with a calibration transmission of each of the power modules.
3. During normal power transmission, the frequency of each power module is shifted slightly during phase calibration.
Maintenance of a properly focused and pointed power beam can be accomplished concurrently with the normal transmission of power from the SPS by using frequencies for calibration which are different from the power beam frequency.

SYSTEM DESCRIPTION

On or near the Rectenna site, an antenna called the Phase Measurement Antenna (PMA) receives the transmission from the Spacatenna Reference Transmitter (SRT) and the particular power module being phase tuned (calibrated). Analysis of these signals provides sufficient information to generate a phase error correction term which is sent up to the on-board phase control circuitry, shown in Figure 1, of the power module undergoing calibration.

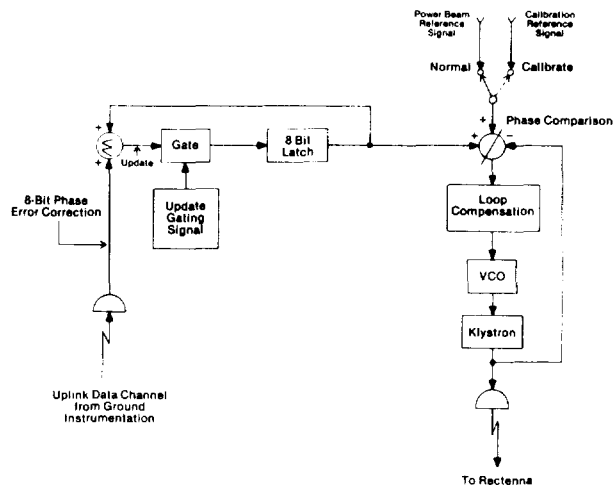


FIGURE 1
POWER MODULE PHASE CONTROL CIRCUITRY

Phase Tuning During Normal Power Transmission

Simultaneous with the transmission of the power beam, coherent signals at three different frequencies are transmitted from the Spacatenna. Two of these signals are transmitted from the SRT, which is located near the center of the Spacatenna, and one is transmitted from the power module being phase tuned, as shown in Figure 2. The two signals transmitted from the SRT are respectively called s_1 and s_{r1} , and the signal transmitted by the power module being phase tuned is called s_2 . The frequency of s_1 is midway between that of s_{r1} and s_2 so that the beat frequency of s_1 and s_2 is the same as that of s_1 and s_{r1} .

At the PMA, simple mixing and filtering circuitry detects two difference frequency signals. One signal is due to s_1 and s_2 . The other, which is called a phase reference signal, is that due to s_1 and s_{r1} . These two beat frequency signals are then phase compared.

The phase comparison gives the phase difference between the two beat frequency signals which is a function of z-axis deformations* in the power module being phase tuned plus biases in the phase feed network of the SPS. Certain components of the phase difference change with a change in frequency, others do not. Since the power module being phase tuned is transmitting at a frequency different from the power beam frequency, it is necessary to distinguish between these frequency dependent and frequency independent components in order to determine the phase

*deformations in a direction toward or away from the Rectenna.

IONOSPHERIC EFFECTS

correction that will be correct at the power beam frequency. This is done by shifting s_{r1} and s_2 to a different set of frequencies, according to a phase ambiguity error avoidance criterion, and making a second phase difference measurement. These two phase difference measurements are numerically adjusted by -2π , 0 , or $+2\pi$ according to a second phase ambiguity error avoidance criterion. These two numerically adjusted phase differences provide sufficient information to calculate the phase error correction² transmitted back to the SPS power module being phase tuned. This phase error correction can be made with an 8-bit binary word sent to the SPS via a data channel. An 8-bit accuracy produces a phase resolution of $360^\circ : 2^8 \approx 1.4^\circ$. This is sufficient to give a power beam pointing resolution better than 140 meters at the Rectenna.

A tradeoff exists between satellite bandwidth requirements and the power module updating rate which is limited by filter settling times. It is anticipated that the frequency separation between s_1 , s_2 , s_{r1} and the power beam will be on the order of 1 MHz. At these frequency separations, the update interval for an entire Spacetenna could be on the order of a few seconds. It is possible that this will be fast enough to correct for any changes that will occur at the Spacetenna due to deformations, thermal effects, etc.

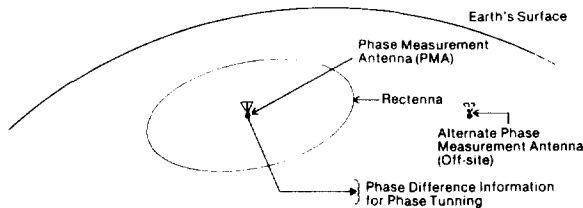
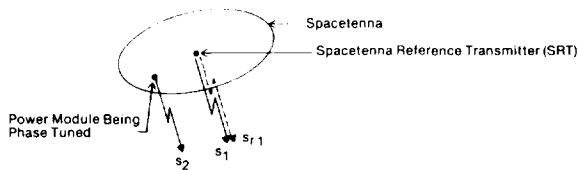


FIGURE 2
INTERFEROMETRIC PHASE CONTROL
-Pictorial representation of relationship between space-
tenna signals and ground instrumentation.

Phase Tuning During Startup

It is also possible to use this interferometer technique to phase tune the power modules at the power beam frequency during initial startup or maintenance. This would be necessary to calibrate the phase tuning system used during normal power transmission for any phase vs. frequency nonlinearities. In this case, the measured phase difference is the phase error correction.

With the ground based closed loop interferometer phase control approach, ionospheric effects are limited to phase errors introduced into the space-to-earth transmission path only.

Although, the PMA is shown to be at the center of the Rectenna, it is not necessary that it be located there or even within the Rectenna site. Off-site measurement has the advantage that the signals being phase tuned do not have to pass through an ionosphere that may be subjected to undetermined heating effects by the power beam.

An important advantage of Interferometric Phase Control is its inherent ability to make use of statistical error reduction techniques to minimize any ionospheric effects. This includes time averaging and/or spatial averaging using several on and off-site phase measurement antennas.

PREDICTION OF DEFORMATION DYNAMICS/MAPPING

It should be pointed out that once the Spacetenna has been initially phase tuned, learning curves or adaptive modeling techniques could be used to predict the dynamics of Spacetenna structural deformations. With such predictions, it is felt that the capability would then exist to phase tune the entire Spacetenna based on frequency measurements of only a "few" key power modules and occasional measurements of the rest. By adding two additional receiving antennas on the earth so that there are three earth antennas spaced a few kilometers apart and not in a straight line, additional phase measurements can be made. These measurements provide information to "map" the face of the Spacetenna, that is, to determine the relative distance, direction and motion of each power module with respect to the SRT. This provides the capability for performing a transverse modal analysis, from the earth, of select samples of power modules on the face of the Spacetenna. In addition, the interferometer phase control technique provides the ability to automatically identify defective power modules.

CONCLUSIONS

Interferometric Phase Control (IPC) was originally developed as a closed loop, ground control approach for focusing and steering the power beam because of Novar's concern over effects that the ionosphere might have on the pilot beam of the retrodirective system. IPC could provide a useful adjunct to the retrodirective system to mitigate phase biasing problems with the retrodirective system and to provide a backup system if there are times when the atmosphere/ionosphere precludes use of a retrodirective system. Until definitive studies have been completed on the atmospheric/ionospheric effects on the retrodirective system, Novar recommends the simultaneous development of power beam control techniques using both the retrodirective approach and IPC.

REFERENCES

1. J. H. Ott and J. S. Rice: "Digital SPS Phase Control Using Traveling Wave Interferometry" Novar Electronics Corporation Technical Report, October, 1978.
2. Ibid., p. 32.

A SONIC SATELLITE POWER SYSTEM MICROWAVE POWER TRANSMISSION SIMULATOR

James H. Ott
 James S. Rice
 Novar Electronics Corporation, Barberton, Ohio

ABSTRACT

A simulator is described which generates and transmits a beam of audible sound energy mathematically similar to the SPS power beam. The simulator provides a laboratory means for analysis of ground based closed loop SPS phase control and of ionospheric effects on the SPS microwave power beam.

INTRODUCTION

Novar Electronics Corporation is in the final stages of constructing and testing a Satellite Power System Microwave Transmission Simulator. In a ground based laboratory environment, the simulator generates and transmits a beam of audible sound energy which is mathematically similar to the microwave beam which would transmit energy to earth from a Solar Power Satellite.

SIMULATOR DESCRIPTION

Figure 1 shows the major functional parts of the simulator. The Sonic Spacetenna (Figure 2) is 1.3 meters in diameter and contains 3200 independent transmitting elements. These elements are connected in a 64 row by 64 column matrix. Each column is driven by a driver which multiplexes each of the 64 rows 32,000 times per second. This enables the simulator's computer to control the amplitude, phase, and frequency of each of the 3200 transducers. The simulator is designed to transmit a coherent sonic power beam at 12 kHz. Any illumination taper, e.g., Gaussian, can be programmed and the resultant ground pattern studied. A computer, RAM Memory, 300 MB disc drive, and line printer are incorporated to provide a very high degree of experimental flexibility.

SIMULATOR CAPABILITIES

A unique feature of Novar's Sonic Simulator is its ability to provide actual photographs of the transmitted power beam. Figure 3 shows a scanning system which provides an intensity modulated raster of the sonic beam. By adding a phase signal to the intensity modulator, the phase coherence can also be photographed. This technique, developed at Bell Labs in the early 1950's will provide photographic records similar to Figure 4.

As soon as the Sonic Simulator is operational (mid-February, 1980), its initial use will be to generate a collimated coherent sonic beam to verify that the beam divergence and sidelobe characteristics are in satisfactory agreement with the aperture illumination equations which have been used to define the SPS microwave beam.

The concept of "ground based" phase control implies a closed loop phase control system which makes corrections in deviations in SPS beam pointing and focusing from ground based measurements of the received power beam. In other words, ground based phase control is a servo control system which like any servo system has a measureable transfer function, frequency response, step response, noise factor, resolution, loop stability, etc. Novar is using its

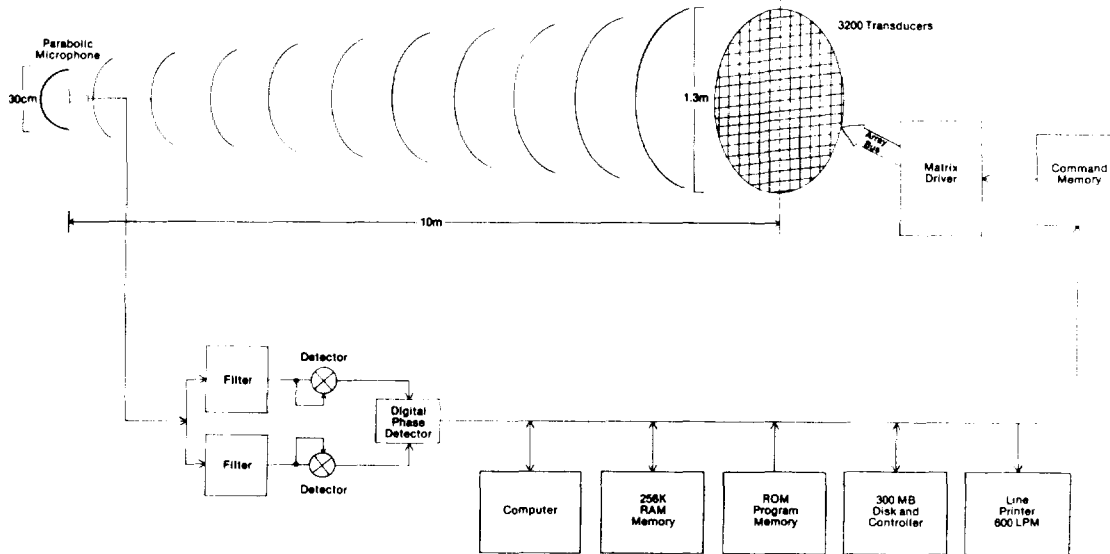


FIGURE 1
 SONIC SPS PHASE CONTROL SIMULATOR
 MAJOR FUNCTIONAL BLOCKS

interferometer phase control technique to focus and point the sound beam. The open and closed loop characteristics of the Sonic Simulator will be measured. A descriptive servo loop diagram and transfer function will be developed and all measured characteristics will be tested for agreement with control system theory. The next step will then be to analyze and mitigate the effects of unwanted interfering inputs such as air currents in the laboratory and the reflection of the sonic beam off walls.

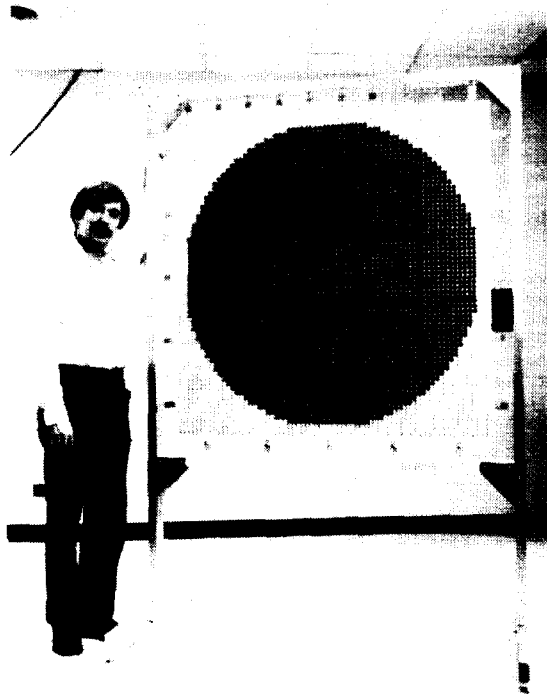


FIGURE 2
SONIC SPACETENNA

The Sonic Simulator can be readily forced to deal with the same noise characteristics as the ionosphere would introduce into the real world SPS phase control system. This would be accomplished by altering the propagation of the simulator's sonic beam through the use of sculptured reflecting surfaces and controlled air turbulence.

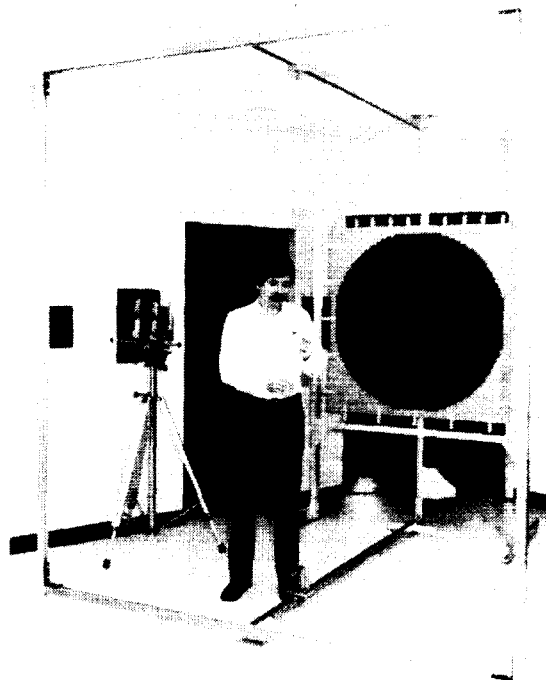


FIGURE 3
PHOTOGRAPHIC SCANNING SYSTEM

A precision mechanical scanning system provides an actual photograph of the sonic beam. The camera lens remains open in a darkened room while the sound-to-light modulator (device being pointed at) provides a light output proportional to the intensity of the sonic beam. The modulator is scanned up and down and forward and backward to provide a photograph of a cross section of the beam.

Ionospheric effects will impact an SPS Phase Control System similar to the way that noise and offset error impact any closed loop servo system. Therefore, conventional control system synthesis techniques should be able to reduce SPS phase control errors due to ionospheric effects.

Analytical techniques will be developed to permit the validation of these sonic propagation models against measured ionospheric parameters. This would, for example, lead to the quantitative correlation of ionospheric electron density patterns with the sound reflecting surface's roughness and placement.

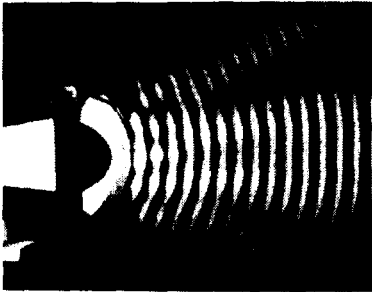
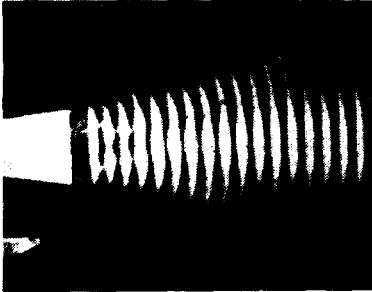


FIGURE 4
REPRESENTATIVE PHOTOGRAPH OF A MECHANICALLY
SCANNED SONIC BEAM (Bell System Technical Journal,
1951)

CONCLUSIONS

It is expected that a number of conclusions can be provided regarding the applicability of the sonic simulation technique to the future development of the SPS power transmission system. If conclusions are favorable, we would expect that the sonic simulator will provide a low cost alternative to many of the time consuming orbiting satellite experiments that would otherwise be necessary.

REFERENCE

1. W. E. Kock and F. K. Harvey, "A Photographic Method for Displaying Sound Waves and Microwave Space Patterns," Bell System Technical Journal, Vol. 30, July 1951, pp. 564-587.

SPS PHASE CONTROL STUDIES

W. W. Lund, B. R. Sperber, G. R. Woodcock
Boeing Aerospace Company

1.0 INTRODUCTION

To properly point and form the SPS microwave power beam, the outputs of the power amplifiers in the transmitting array must be phased in a specific and coherent fashion. The purpose of the SPS phase control system is to bring this about reliably.

A number of different phase control schemes can be, and have been, envisioned. The one selected for the SPS baseline system is a retrodirective CW phase conjugating system using a spread spectrum uplink signal and a reference phase signal that is distributed via fiber optics. The basis of this selection is relative technical simplicity and requisite assurance of success.

The operational principle of the retrodirective phase control system is that if a signal E_{Received} , described by

$$E_{\text{Received}} = \cos(\omega t + \theta_{\text{ref}} + \theta_{\text{rec}}) \quad (1)$$

is received, a phase conjugated signal

$$E_{\text{Transmitted}} = \cos(\omega t + \theta_{\text{ref}} - \theta_{\text{rec}}) \quad (2)$$

is transmitted. If this is done all over the transmitting aperture, the resulting beam will leave in the inverse direction of the incoming pilot beam.

Problematic technical aspects in implementing the scheme above are that the received and transmitted frequency spectra are dissimilar and that the reference phase θ_{ref} against which the received phase θ_{rec} is measured must be the same all over the transmitting array. (Regarding tolerable systematic phase shift, it may be noted that a phase shift of 3×10^{-2} radians will scan the beam approximately 40 meters.)

Transmitter noise, receiver noise and pilot beam power determine how close the pilot beam frequencies of the spread-spectrum uplink can be to the downlink. Studies at Boeing and elsewhere have yielded values for this offset in the range of 5 to 50 MHz. In the case of the most recent Boeing pilot link study, the network of considerations used was as shown on Figure 1, yielding the characteristics of the final system as a function of transmitting frequency notch filter cutoff frequency f_c , pilot beam receiving aperture and desired signal to noise of the received pilot signal shown on Figure 2.

For accurate pointing it is important that the received pilot signal be scaled to generate the transmitted downlink signal instead of merely translated. I.e., if the downlink frequency is f_0 , the pilot frequency is $f_0 + \Delta f = \omega/2\pi$ and the received field is given by Equation (1), the downlink should be:

$$E_{\text{transmitted}} = \cos \left[f_0 (f_0 + \Delta f)^{-1} (\omega t + \theta_{\text{ref}} - \theta_{\text{rec}}) \right], \quad (3)$$

instead of

$$E_{\text{transmitted}} = \cos \left[(\omega - 2\pi\Delta f)t + \theta_{\text{ref}} - \theta_{\text{rec}} \right]. \quad (4)$$

The reason for this is that if frequencies are not scaled but translated by some amount Δf , the transmitted beam is incorrectly steered off the pilot beam axis by an amount W . W depends on the transmitting aperture tilt θ , the range of R and the transmitting frequency f according to the "squint" formula:

$$W = R \theta \Delta f f_0^{-1} . \quad (5)$$

For the baselined spread spectrum pilot signal Δf is effectively 0.

Selection of the specific spread spectrum uplink signal scheme and the decoding of the uplink at the receiver is pending further study of ways to mitigate ionospheric and tropospheric distortions of the uplink wavefront. The basic problem is that the index of refraction in the beam propagation path depends on the atmospheric pressure, composition, temperature and the degree of ionization; and in the troposphere the index of refraction increases with increasing density while in the ionosphere the opposite is true. A secondary problem is geometry: if there is only a single pilot beam just a small central portion of the propagation path through the troposphere and ionosphere is sampled. Finally, the effects of the power beam on the temperature and density of the ionosphere must not interfere with phase control or beam pointing.

The effect of phase errors on the transmitted beam is to distort the wavefront. The effect of average phase errors can be treated as a function of position in classical optical fashion to get beam offset, defocusing, astigmatism, distortion and similar quantities. The effect of random RMS phase errors $\bar{\delta}^2$, assumed not a function of position, is to reduce the main beam efficiency by the factor

$$\eta_{\text{random}} = e^{-\bar{\delta}^2} \quad (6)$$

Because in general there is a residual on-axis $\bar{\delta}^2$ over a single phase controlled area proportional to that area, the above equation qualitatively illustrates the reason for the recent change in the baselined level of phase control from the sub-array level to the klystron power module level. The approximately factor of 10 average decrease in phase controlled area contributed to a smaller effective $\bar{\delta}^2$. The revenues from the extra received power of the now more efficient power beam over a satellite lifetime were found to adequately compensate for the increased phase control system cost. Other benefits associated with phase control to the module level include increased pointing accuracy and decreased waveguide tuning mismatches.

2.0 BASELINE PHASE CONTROL SYSTEM DESCRIPTION

The baselined phase control system, illustrated on Figure 3, consists of 101,552 klystron module level power amplifier phase control subsystems, as shown on Figure 4, and an 816-2/3 MHz reference phase distribution network of fiber optical cables and master slave returnable timing system repeater units as shown in Figure 5.

The reference phase distribution tree (to be described in more detail in the next section) has four levels culminating at the klystron module with no more than a 1:36 output branching, and constitutes most of the physical and operational (but not functional) complexity of the system. Its purpose is to provide identical phase reference phase signals to all klystron modules for use in conjugating the pilot to get the power downlink.

The klystron power amplifier phase control subsystems contain the phase control system's functional complexity insofar as they each receive and decode the

spread spectrum pilot link signal, make any necessary corrections, conjugate it using the 816-2/3 MHz reference phase signal from the phase distribution tree and actively compensate for phase shifts suffered in the power amplifier and waveguide feed networks.

Fiber optic cabling was chosen over conventional coax for the reference phase distribution because of its lower mass, lower signal attenuation, and the fact that it has no short circuit failure mode. It also has lower phase delay and costs less. However, the phase delay variations are not low enough to eliminate the need of feedback (i.e., returnable timing systems) on all but the subarray (Level 4) reference phase control tree level. At the lowest level the length is so short that temperature induced variations in phase shift are judged to be tolerable.

NASA-funded technology development work at Boeing is currently developing 980 MHz fiber optic transmitters and receivers for SPS use. The expected successful completion of these and their demonstration with a 1 km cable should substantially verify that fiber optic technology can distribute the reference phase:

3.0 BASELINE SYSTEM RELIABILITY AND REDUNDANCY

It is clear that any reference phase control system that refers phases to central points has critical links when system reliability is considered. Because of this, the most central units in the reference system have been made redundant and autonomous.

The baseline transmitting array has three autonomous master reference phase receivers, which each transmit a reference phase signal via separate and redundant fiber optic cable links to each of twenty active Level 1 sector phase distribution units. (See Figure 7) These units select valid phase control signals and distribute them via redundant fiber optic cables to twenty Level 2 (group) distribution units. The group distribution units in turn tree the signal out further to 19 subarrays each. At the subarray, a last distribution unit sends the signal to each klystron module, where it is used as a reference for conjugation of the phase control pilot signal receiver output. The klystron is held in proper relation to the conjugated pilot beam signal by a control loop of its own that compensates for its internal phase shifts with temperature, time, and voltage.

An analysis of the basic reliability of the baseline configuration was performed by G.E. under subcontract to Boeing. The element reliabilities and basic configuration assumed are shown in Figures 7 and 8. For purposes of analysis the phase control system was considered as four segments. The first segment starts at the master reference receivers and continues through the sector reference distribution unit's selection switch SW_1 . The second segment is from the output of SW_1 to the output of the subarray group signal splitter B_{1g} . A third segment runs from this splitter through to the output of the subarray splitter B_{mn} . Finally, the last segment was analyzed from the B_{mn} output to the klystron input.

4.0 COSTS

Reference phase control system element costs, estimated by standard aerospace avionics cost estimating methodology from the computerized Boeing Program Cost Model data base. After estimation of the first unit cost on the basis of platform, function and service factors the costing methodology used was to discount the per unit cost on a 70% learning curve through the 1000th unit. After this was assumed to saturate and per learning unit costs were constant. Table I summarizes characteristics of the phase control system units on board subarrays, while Table II summarizes the segments of the reference phase distribution system at levels above the subarray level.

The primary results of the cost estimations are that the phase control system costs total well under \$100 million and are dominated by the costs of the phase control pilot beam receivers. With more detailed reference satellite phase control system specifications there can be a requisite reduction in cost uncertainties. However, it should be noted that substantial (factor of two or more) reductions in phase control system cost are unlikely because current aerospace and electronic industry technology routinely deals with production runs such as those required for the SPS phase control system on equipment of comparable complexity.

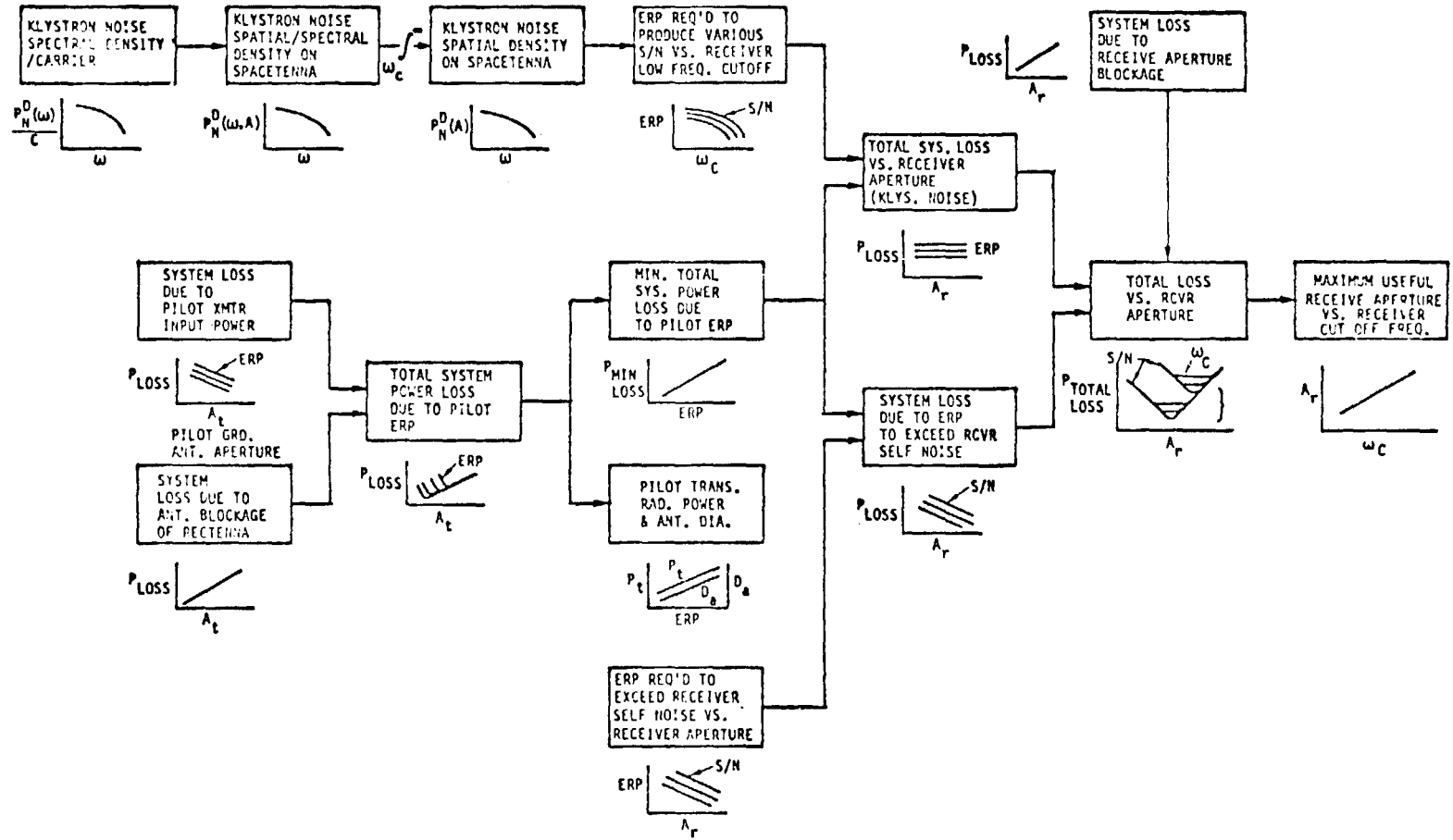


FIGURE 1. PILOT LINK ANALYSIS FLOW CHART

Table I. Intrarray Phase Control System
Production Cost Characteristics

<u>Subarray Type</u>	<u>Number of Klystrons</u>	<u>Subarrays of This Type</u>	<u>PCR Mass (kg)</u>	<u>PCR Cost (\$)</u>	<u>RPDS Mass (kg)</u>	<u>RPDS Cost (\$)</u>	<u>Length Cable (m)</u>	<u>Cable Mass (kg)</u>	<u>Cable Cost (\$)</u>
1	4	1028	4.4	2240	1.0	595	33	3.7	73
2	6	1052	6.6	3360	1.0	595	49	5.4	108
3	8	612	8.8	4480	1.0	595	61	6.9	138
4	9	664	9.9	5040	1.0	595	72	8.0	160
5	12	900	13.2	6720	1.0	595	95	10.6	212
6	16	784	17.6	8960	1.0	595	132	14.5	290
7	20	628	22.0	11200	1.0	595	167	18.2	365
8	24	644	26.4	13440	1.0	595	197	21.6	433
9	30	632	33.0	16800	1.0	595	232	26.0	521
10	36	276	39.6	20160	1.0	595	296	32.5	649
TOTAL		7220	112 T	\$57M	7 T	\$4M		91 T	\$1M

Table II. Intersubarray Phase Control System
Production Cost Characteristics

<u>Item</u>	<u>No. Req'd.</u>	<u>Avg. Unit</u>	<u>Per SPS (M)</u>
Master Reference Receiver and Reference Phase Transmitter	3	424K	1.272
Cables	60	4.6K	0.276
Slave Repeaters	400	25.1K	10
Level 2 Cables	380	2.5K	0.95

\$12.5M

Level 3 cables are common with area-subarray data harness (see WBS 1.1.3)

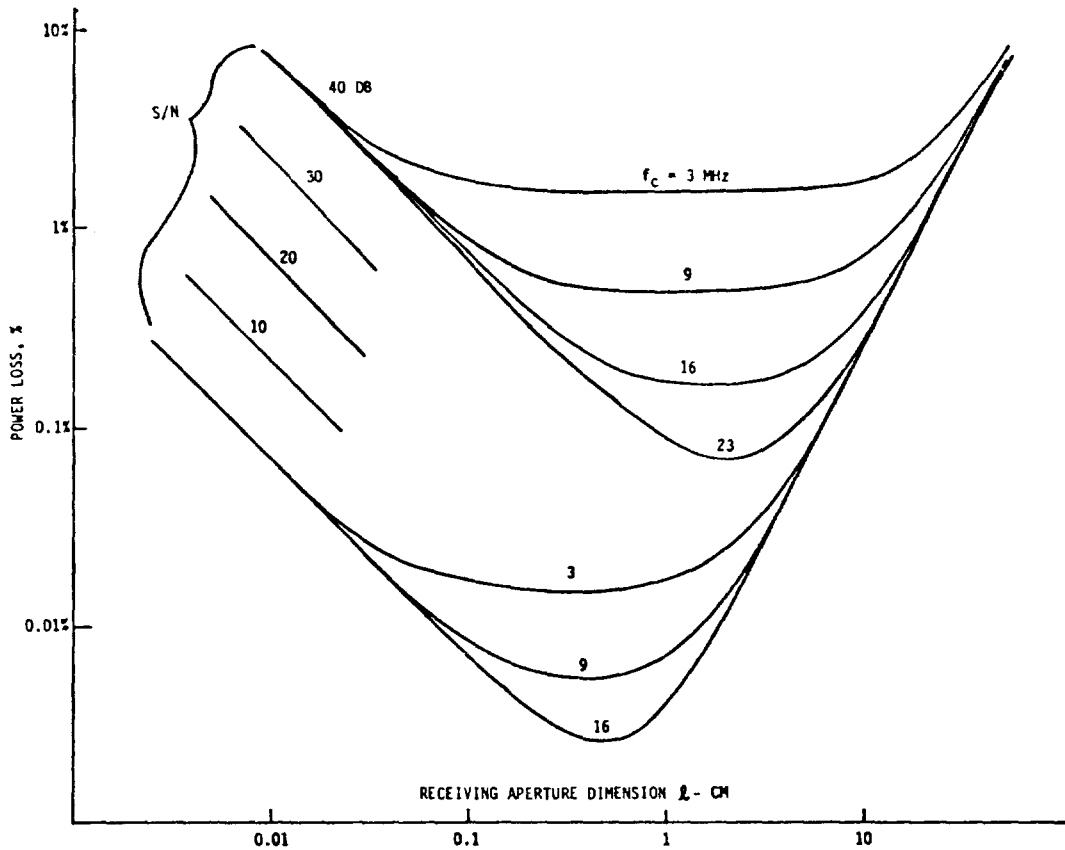


FIGURE 2. TOTAL SYSTEM LOSS VS. RECEIVE APERTURE.

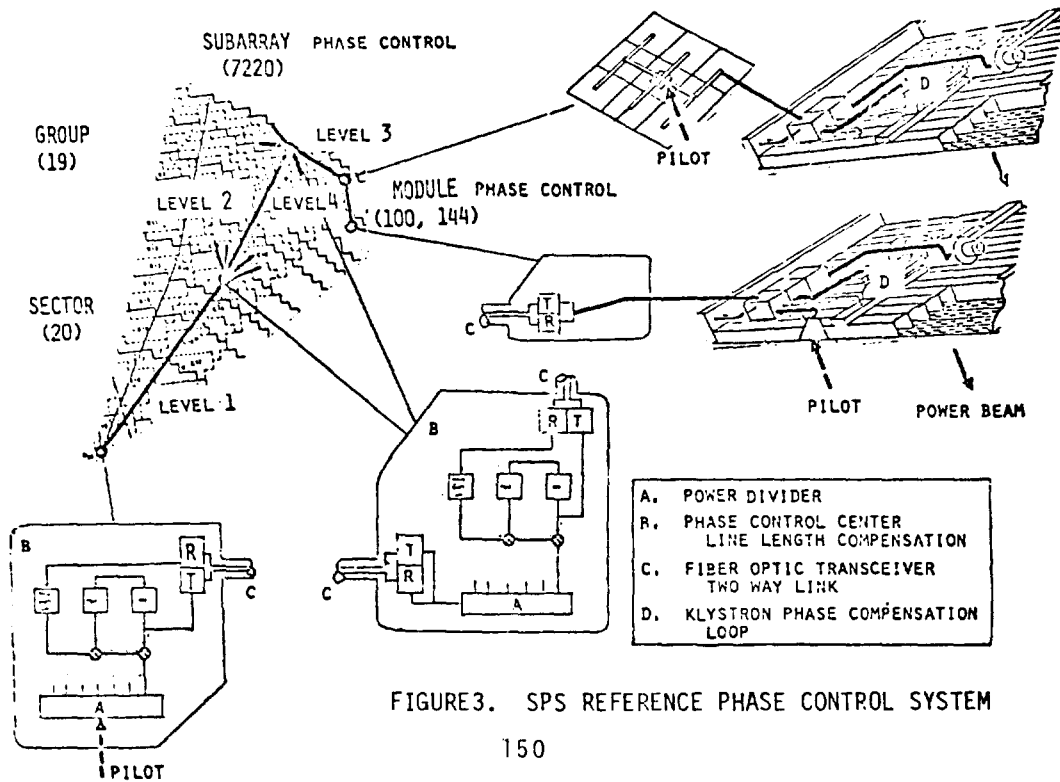


FIGURE 3. SPS REFERENCE PHASE CONTROL SYSTEM

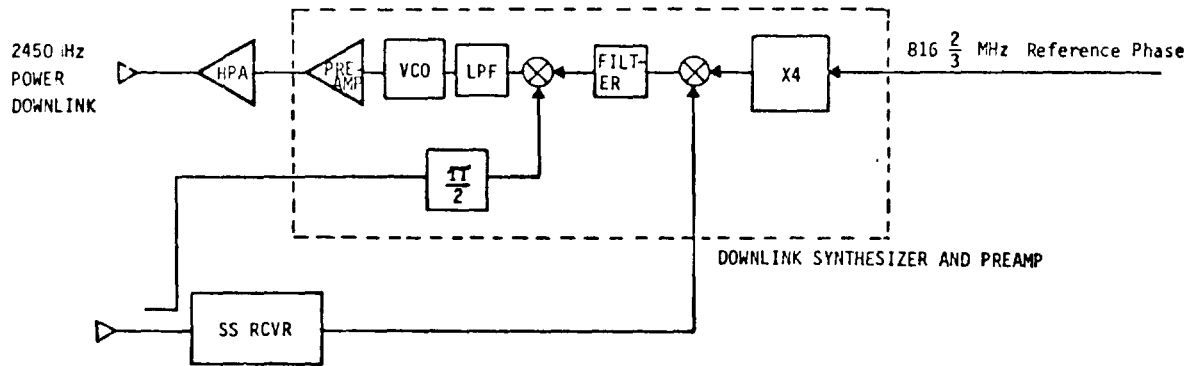


FIGURE 4. POWER AMPLIFIER PHASE CONTROL SUBSYSTEM

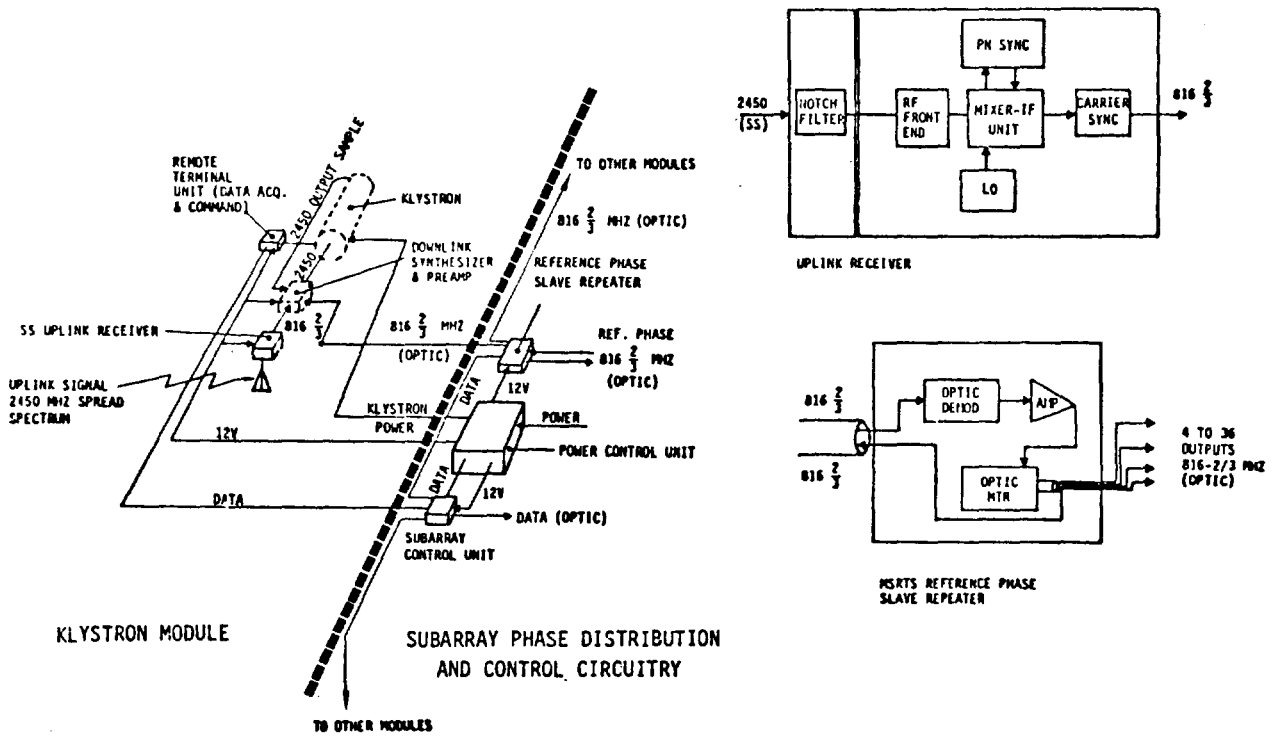


FIGURE 5. SUBARRAY CONTROL CIRCUITS

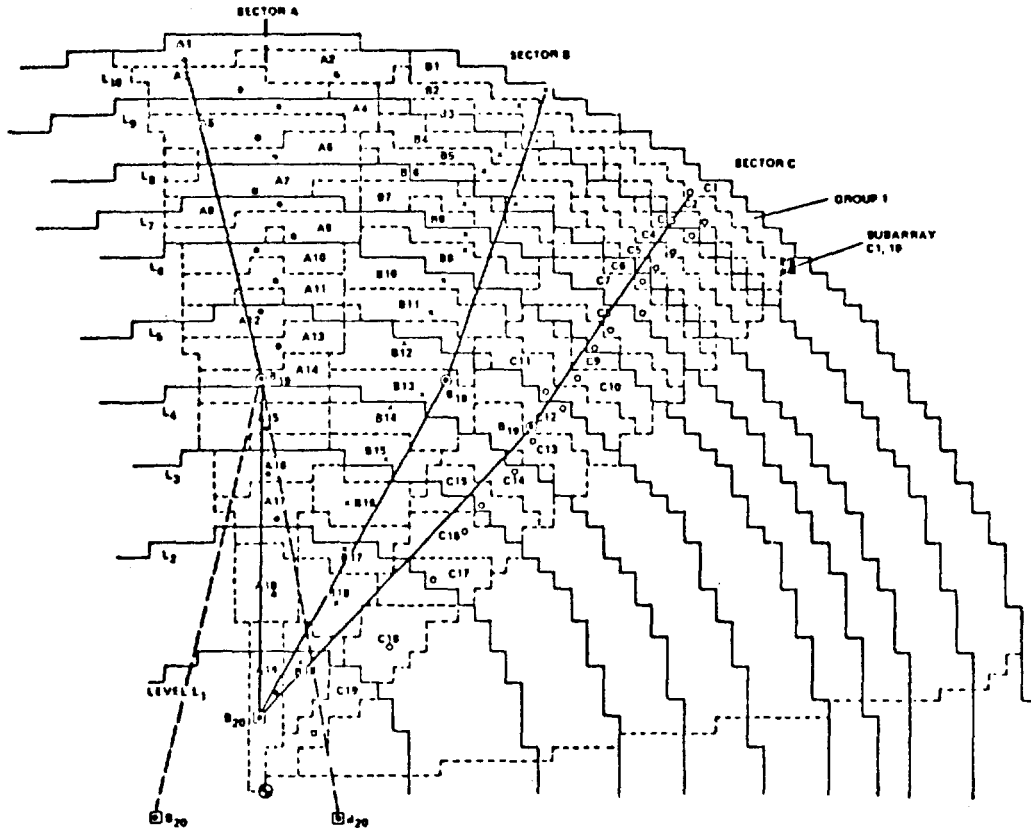


FIGURE 6. LOCATION OF REFERENCED PHASE REPEATER STATIONS OF SECTORS AND GROUPS

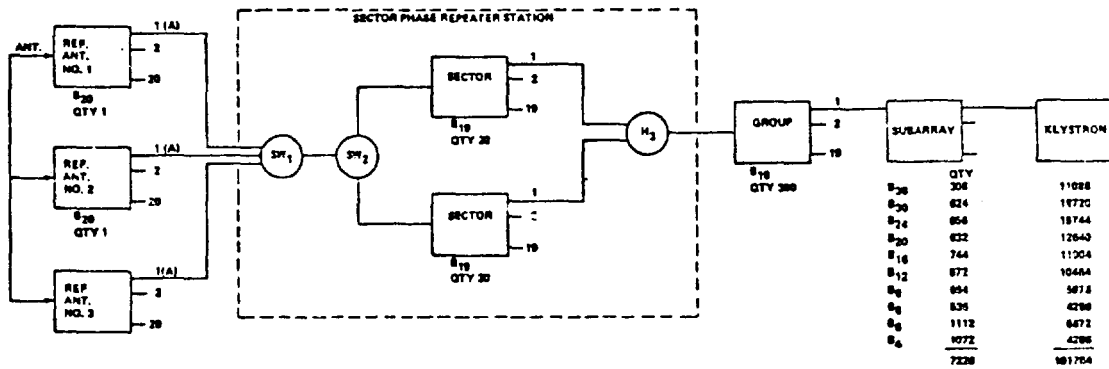


FIGURE 7. REDUNDANCY CONCEPT OF PHASE DISTRIBUTION NETWORK

SPS FIBER OPTIC LINK ASSESSMENT

T. O. Lindsay, E. J. Nalos
Boeing Aerospace Company

1. INTRODUCTION

Fiber optic technology has been tentatively selected in the SPS baseline design to transmit a stable phase reference throughout the microwave array. Over a hundred thousand microwave modules will be electronically steered by the phase reference signal to form the power beam at the ground receiving station. The initially selected IF distribution frequency of the phase reference signal has been set at 980 MHz or a submultiple of it.

Fiber optics offers some significant advantages in view of the SPS application. Optical transmission is highly immune to EMI/RFI, which is expected to be severe when considering the low distribution power (<1mW). In addition, there will be savings in both mass, physical size, and potentially in cost.

2. FIBER OPTIC LINK VERIFICATION PROGRAM

2.1 TASK DESCRIPTION

The purpose of the present program is to demonstrate feasibility of a fiber optic link at 980 MHz for SPS application. The specific tasks are: 1) Analyze existing optical fibers for use in the phase distribution fiber/optic link with emphasis on phase change effects and ability to transmit high frequency IF signals; i.e., low attenuation and adequate bandwidth; 2) Analyze suitable optical emitters and detectors to determine feasibility of operation and usage at 980 MHz; 3) Select and purchase optical emitters, detectors, and fibers for link development; 4) Design and construct impedance matching systems for matching the optical emitter and detector to laboratory equipment; and 5) Assemble and test a two-way link at 980 MHz consisting of matched detectors, emitters, and a two-fiber cable of minimum length of 200 meters.

In the present phase control system for SPS, a two-way link is required in the phase distribution system at each level to achieve phase compensation for phase changes induced by temperature changes and other property changes in the electronic circuit.

2.2 FIBER OPTIC LINK DESIGN

The results of the component selection for the fiber optic link are summarized in Table 1 below.

TABLE 1: COMPONENT SELECTION FOR FIBER OPTIC TEST LINK

Component	Type	Features	
Emitter	GaAlAs Multi-Mode Injection Laser Diode	1. Moderate cost 2. High power 3. High modulation bandwidth	
	GaAlAs Single-Mode Injection Laser Diode*	1. High power 2. High coupling eff. 3. High bandwidth 4. Low distortion	5. Low threshold 6. High reliability 7. Narrow spectral width
	Light Emitting Diode (LED)	1. No threshold current 2. Low distortion 3. Low cost 4. Stable operating point	

TABLE 1: COMPONENT SELECTION FOR FIBER OPTIC TEST LINK (Continued)

Component	Type	Features
Detector	Silicon Avalanche Photodiode*	1. Gain - BW product \approx 80 GHz 2. High RCVR S/N 3. Moderate cost
	Silicon PIN Photodiode	1. Low bias voltage 2. Stable operating point 3. Low cost
Fiber	Step-index glass Multi-mode	1. Low cost 2. Low attenuation
	Graded-index glass Multi-mode*	1. Moderate cost 2. High bandwidth 3. Low attenuation
	Step-index glass Single-mode	1. Extremely high bandwidth 2. Low attenuation 3. Poor coupling efficiency

As a result of the investigations, multi-mode graded index fiber was chosen due to its high bandwidth, low attenuation, availability, and high coupling efficiency with injection laser diodes; single-mode injection laser diode was selected for its high bandwidth, high output, and excellent linearity; and an avalanche photodiode was selected because of its high bandwidth and superior sensitivity.

The link will operate at a wavelength of 820 nm where present laser diodes and avalanche photodiodes are readily available and offer good reliability. Fiber attenuation, although not minimum, reaches an acceptable value at 820 nm also.

The injection laser diodes were purchased from Nippon-Electric in Japan; the two-fiber cable was obtained from Siecor (fibers manufactured by Corning Glass Works); and the avalanche photodiodes from RCA.

One of the problems to be solved for the 980 MHz feasibility link was to develop simple, but effective, signal coupling techniques for the emitter and detector. The approach chosen is illustrated schematically in Figure 2. The use of the 47Ω resistor in series with the injection laser diode causes approximately 50Ω to be seen by the driver amplifier and it also aids in converting the driver output to a current source which is needed by the diode for linearity. The output signal current from the avalanche photodiode flows directly into the 50Ω input impedance of the laboratory amplifier. In both cases, the dc biasing networks are isolated from the signal paths by shorted quarter-wave microstrip techniques.

2.3 EXPERIMENTAL RESULTS

The results of an initial test to couple 980 MHz through a sample link are shown by Figure 2. The fiber length was 300 meters and the type is similar to that to be used in the two-way link development. Results are listed for two values of detector biasing. The output voltage waveforms were monitored using a sampling oscilloscope and, in both cases, the trace was stable and noise-free.

The test setup was similar to that shown in Figure 3. The emitter and detector modules are towards the right foreground shown with a length of coiled fiber optic cable. Laboratory equipment includes a 980 MHz frequency synthesizer, a vector voltmeter, oscilloscope, preamplifier, and biasing and monitoring equipment.

The emitter and detector modules used in the initial test are shown in Figure 4a and 4b. The thermal environment aboard the SPS is expected to be widely variable with values anticipated between -50°C and $+150^{\circ}\text{C}$. Therefore, a major subject of interest involves the variation in propagation time through a fiber as temperature is changed. Propagation time is directly related to the transmitted phase and is known to be affected by thermal expansion and refractive index variation. Data was also taken to determine the magnitude of the phase variation versus temperature as illustrated in Figure 6. The phase sensitivity is not low enough to obviate the need for phase compensation except possibly for the shortest (last) level of phase distribution.

For a one-way link length of 200 meters, the transmitted phase would vary approximately 2.5 degrees for every $^{\circ}\text{C}$ of temperature change at 980 MHz. This rate is acceptable with the present phase control system because of the two-way link length compensation. The two lengths of fiber will be adjacent for the total link, providing accurate tracking and matching.

At the outer levels of the phase reference distribution network, the link lengths average <10 meters and comprise over 90% of all of the elements. It may be possible to eliminate the return link in such cases as the phase shift will be greatly reduced for the short runs, averaging 0.125 degrees of shift per $^{\circ}\text{C}$.

As fiber optic technology progresses, longer wavelengths should be investigated where bandwidth and attenuation characteristics are superior for fused silica fibers. It is anticipated that phase shift sensitivity may be reduced at longer wavelengths because of dispersive changes in the refractive index. Fiber optics represent a promising approach for the phase distribution system for the SPS and merit further development to realize their full potential.

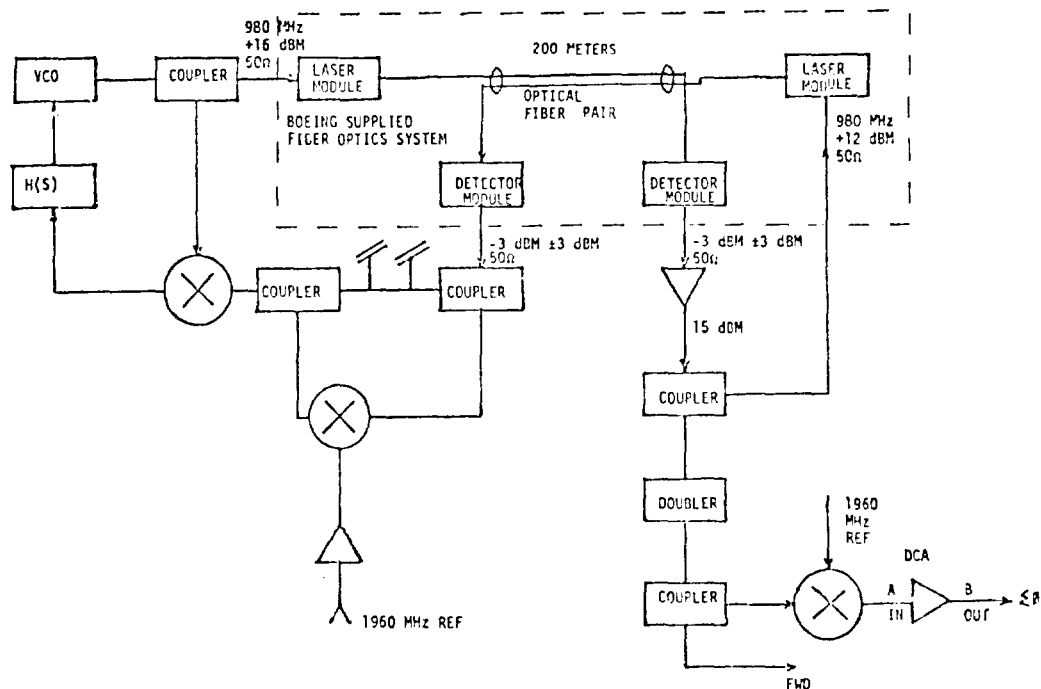
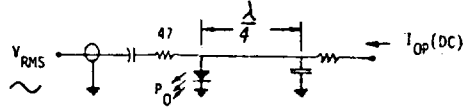


FIGURE 1 TEST CONFIGURATION FOR 2 WAY FIBER OPTIC LINK.

EMITTER MODULE:

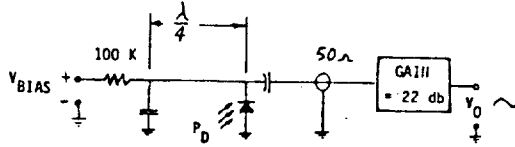
$I_{THRESH} = 60 \text{ ma}$
 $I_{OP} = 67 \text{ ma DC}$
 $V_{MOD} = 0.7 \text{ V RMS}$
 $P_0 = 262 \mu\text{Watts}$



DETECTOR MODULE:

V_{BIAS}	185 Volts	315 Volts
V_0	71 MV RMS	283 MV RMS
P_D	19.1 μ Watt	19.1 μ Watt

Out



FIBER: CORNING JVPO
 Length = 303 Meters
 Atten = 3.9 db/km @ 900 nm
 BW = 870 MHz-km
 N.A = 0.218

FIGURE 2 FIBER OPTIC LINK DESIGN SPECIFICATIONS

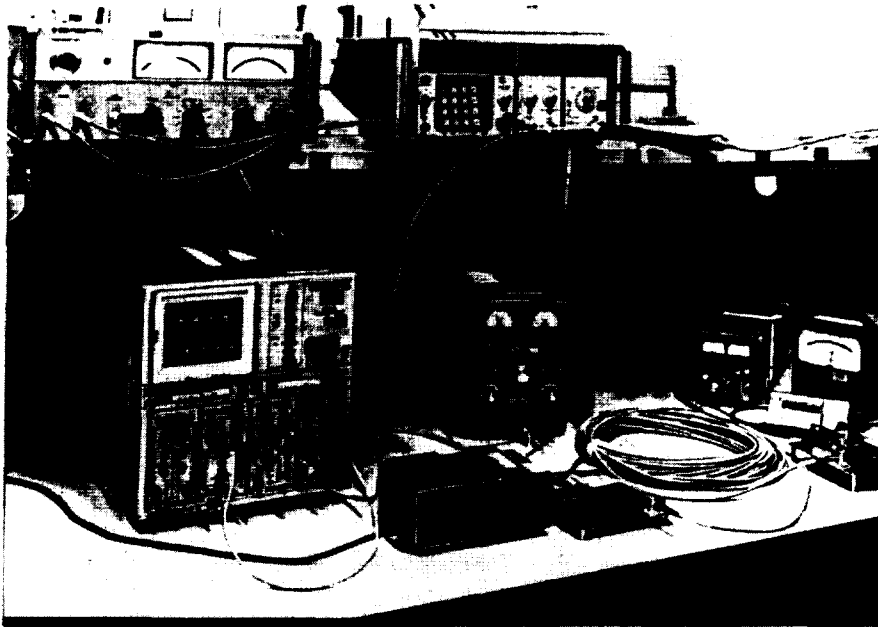


FIGURE 3 INITIAL 980 MHz LINK TEST SETUP

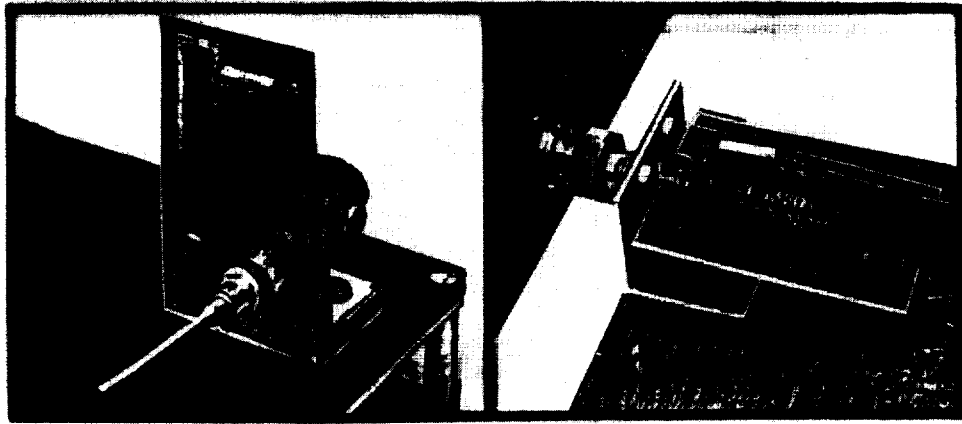


FIGURE 4A EMITTER MODULE BOARD. FIGURE 4B DETECTOR MODULE BOARD

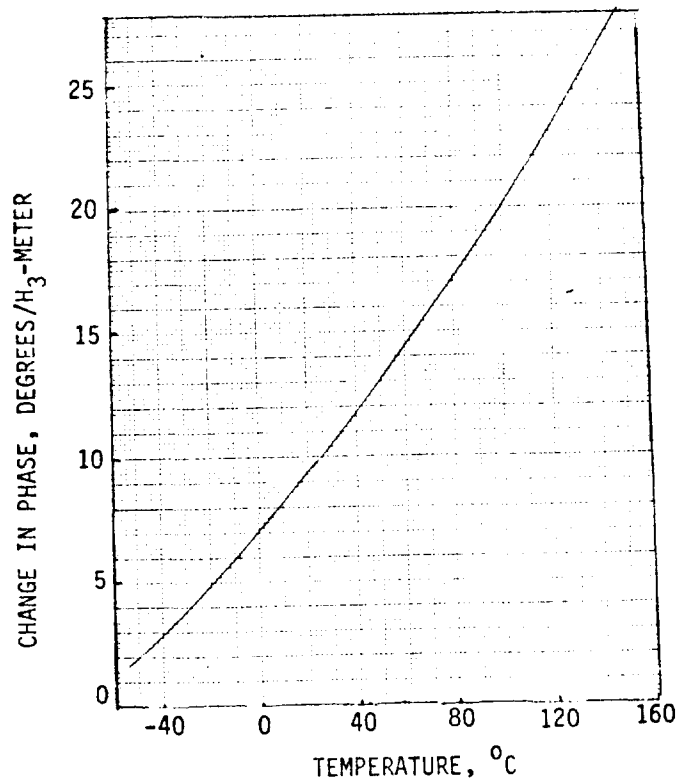


FIGURE 5 PHASE CHANGE OF GRADED INDEX FIBER vs. TEMPERATURE

- CORNING FIBER 303 METERS LONG
- FREQUENCY 980 MHZ

IONOSPHERIC EFFECTS IN ACTIVE RETRODIRECTIVE ARRAY
AND MITIGATING SYSTEM DESIGN

A. K. Nandi and C. Y. Tomita
Rockwell International

Abstract

The operation of an active retrodirective array (ARA) in an ionospheric environment (that is either stationary or slowly-varying) is examined. The restrictions imposed on the pilot-signal structure as a result of such operation are analyzed. A 3-tone pilot beam system is defined which first estimates the total electron content along paths of interest and then utilizes this information to aid the phase conjugator so that correct beam pointing can be achieved.

I. INTRODUCTION

In order to make the solar power satellite system perform correctly, it is necessary to point the high power downlink beam towards a specific point on ground. The downlink beam is narrow and pointing accuracy requirements are stringent. One way of achieving this objective is to use the retrodirective array such that the down-going power beam points in the same direction from which a ground-originated pilot signal came. In this approach, the downlink wavefront is obtained by conjugating the phases of various segments of the uplink (pilot) wavefront. For operational reasons, the uplink and downlink frequencies cannot be identical. Both the uplink and downlink wavefronts are required to travel through the ionosphere. The object of this note is to examine system operation constraints imposed by the ionosphere and find possible remedies. The discussion that follows is based on the assumption that the ionosphere is stationary or slowly-varying. Also, heating effects on the medium due to the downlink power beam are not taken into account.

II. IONOSPHERIC EFFECTS ON SINGLE-TONE PILOT BEAM

It is well-known that an important feature of the retrodirective array is that the down-coming beam is phase coherent when it arrives at the source.¹ This statement is rigorously correct only if the propagation medium is non-dispersive spatially homogeneous and temporally stable. In case of the ionosphere, one or more of the above conditions are violated. Under certain conditions, beam pointing error can occur and phase coherence at the source can be lost.

Consider the situation shown in Figure 1. Assume the uplink and downlink frequencies are given by f_u and f_D , respectively ($f_u \neq f_D$). The (path-dependent) phase shift at f_u on one particular radio link can be written as²

$$\phi(f_u) = \frac{2\pi f_u L}{c} - \frac{b}{2\pi f_u c} \int_0^L N d\ell \quad (1)$$

where

$$b = \frac{e^2}{2 \epsilon_0 m}; \quad e = \text{electron charge, } m = \text{electron mass,}$$
$$\epsilon_0 = \text{free-space permittivity}$$

$$= 1.6 \times 10^3 \text{ mks}$$

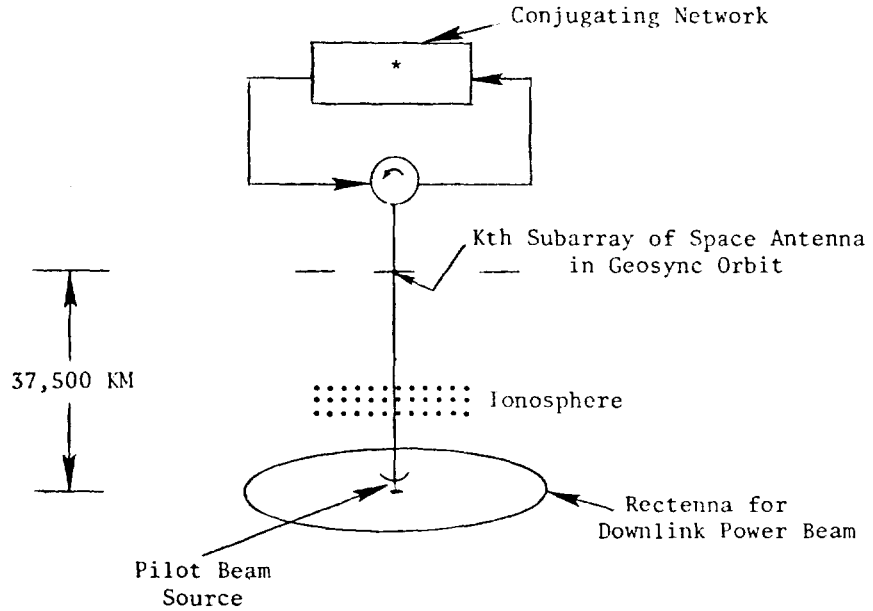


Figure 1.

L is the physical path length involved and $\int_0^L N d\ell$ is the integrated electron density along the path under consideration ($\approx 10^{17} - 10^{19}$). Note the second quantity on the right hand side of Equation (1) accounts for ionospheric effects on a CW tone. On using appropriate constants, one can write

$$\begin{aligned} \phi(f_u) &= \frac{2\pi f_u L}{c} - 40.5 \times \frac{2\pi}{f_u c} \int_0^L N d\ell \\ &= \frac{2\pi f_u L}{c} - \frac{K_u}{f_u} \end{aligned} \quad (2)$$

Since one is interested in knowing the phase shift at f_D , a reasonable estimate of the phase can be obtained by multiplying $\phi(f_u)$ by f_D/f_u (this estimate becomes increasingly accurate as $f_u \rightarrow f_D$). Thus,

$$\begin{aligned} \bar{\phi}(f_D) &= f_D/f_u \times \phi(f_u) \\ &= \frac{2\pi f_D L}{c} - \frac{K_u}{f_u^2} \cdot f_D \end{aligned} \quad (3)$$

On conjugating this phase, one obtains

$$\bar{\phi}^*(f_D) = -\frac{2\pi f_D L}{c} + K_u \frac{f_D}{f_u^2} \quad (4)$$

The downlink signal at the transmitting end can be written as

$$S_{\text{down}}^T(t) = \cos \left[\omega_D t + 2\pi f_D \frac{L}{C} - K_u \frac{f_D}{f_u^2} \right] \quad (5)$$

The downlink signal at the receiving end is given by

$$S_{\text{down}}^R(t) = \cos \left[\omega_D t - \left(K_u \frac{f_D}{f_u^2} - \frac{K_D}{f_D} \right) \right] \quad (6)$$

For a temporally stable ionosphere and ignoring second-order effects, one can set $K_u = K_D$ in Equation (6) and obtain

$$S_{\text{down}}^R(t) = \cos \left[\omega_D t - K_u \left(\frac{f_D}{f_u^2} - \frac{1}{f_D} \right) \right] \quad (7)$$

If, in addition, the propagation medium is assumed non-dispersive, then the second term on the right hand side of Equation (7) involving K_u could be equated to zero. In the present situation, this kind of assumption is highly unrealistic. Note in Equation (7), K_u applies to a particular radio path and will, in general, be different on different paths because of ionospheric inhomogeneity. A consequence of this fact is that the phase coherence (at source) property of the downlink signal mentioned earlier does no longer hold good. Furthermore, if a coherent phase perturbation occurs due to some ionospheric large-scale features (such as a wedge), then even a beam pointing error is possible. The magnitude of these effects need to be evaluated for worst-case ionospheric conditions. The two tone pilot beam system which aims at alleviating some of the ionospheric problems mentioned above is discussed next.

III. TWO-TONE PILOT BEAM SYSTEM

If two tones (symmetrically situated around the downlink frequency) are used on the uplink transmission, then under appropriate conditions an average of the phases of the uplink tones can be taken to be a good estimate of the phase at the downlink frequency. The idea here is that the phase errors caused by a stationary ionosphere can be largely eliminated by this approach. Let f_1 and f_2 be the two tones constituting the pilot beam and symmetrically located around the downlink frequency f_D . The choice of the offset Δf is based on conflicting requirements and is not discussed here.

Using the notation as before, for a given link one can write

$$\phi(f_1) = 2\pi f_1 \frac{L}{C} - \frac{40.5}{f_1} \times \frac{2\pi}{C} \int_0^L N \, d\ell = \phi_1 \quad (8)$$

and

$$\phi(f_2) = 2\pi f_2 \frac{L}{C} - \frac{40.5}{f_2} \times \frac{2\pi}{C} \int_0^L N \, d\ell = \phi_2 \quad (9)$$

Then

$$\begin{aligned} \bar{\phi} &= \frac{\phi(f_1) + \phi(f_2)}{2} \\ &= 2\pi f_D \frac{L}{C} - \frac{40.5}{f_D} \times \frac{2\pi}{C} \int_0^L N \, d\ell; \quad \left| \frac{\Delta f}{f_D} \right| \ll 1 \\ &= \phi(f_D) \end{aligned} \quad (10)$$

Table 1. Number of Ambiguities (η) Vs. Δf

Δf MHz	f_1 GHz	f_2 GHz	$10^{19} \frac{e1/m^2}{\eta}$	$10^{18} \frac{e1/m^2}{\eta}$	$\int N d\ell$
100	2.350	2.550	92	9.2	
50	2.400	2.500	45	4.5	
10	2.440	2.460	8.9	0.89	
5	2.445	2.455	4.4	0.44	
1	2.449	2.451	0.9	0.09	

It is clear from Table i that in order to avoid ionospheric ambiguity for the strongest concentration under consideration, Δf should not exceed 1 MHz. Other operational constraints render such a choice unacceptable.

In what follows, a 3-tone approach due to Burns and Fremouw is used to resolve the ambiguity problem.³ It is based on a direct measurement of $\int N d\ell$ along the paths of interest and then using this information to estimate the path related phase shift at the downlink frequency f_D .

Consider a frequency-amplitude pattern as shown in Figure 2 where the three uplink tones f_1 , f_2 and f_3 are coherent at ground. Indeed, the three tones can be generated by a low-deviation phase-modulated transmitter. Thus, using equations similar to Equation (8) for three frequencies f_1 , f_2 and f_3 , one can write

$$\begin{aligned} \delta\phi_A &= \phi_2 - \phi_1 \\ &= \frac{2\pi}{C} \left\{ (f_2 - f_1) L - 40.5 \times \int N d\ell \times \left(\frac{1}{f_2} - \frac{1}{f_1} \right) \right\} \end{aligned} \quad (13)$$

and

$$\begin{aligned} \delta\phi_B &= \phi_1 - \phi_3 \\ &= \frac{2\pi}{C} \left\{ (f_1 - f_3) L - 40.5 \times \int N d\ell \times \left(\frac{1}{f_1} - \frac{1}{f_3} \right) \right\} \end{aligned} \quad (14)$$

The second difference of phase shift is given by

$$\begin{aligned} \delta_2\phi &= \delta\phi_A - \delta\phi_B \\ &= \frac{2\pi}{C} \times 40.5 \times \int N d\ell \times \left[\frac{2}{f_1} - \frac{1}{f_3} - \frac{1}{f_2} \right] \end{aligned} \quad (15)$$

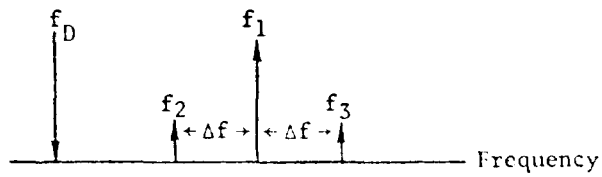


Figure 2.

For suitably chosen Δf , one obtains

$$\delta_2\phi \approx -\frac{2\pi}{C} \times 40.5 \times \int N \, d\ell \times \frac{2 \Delta f^2}{f_1^3} \quad (16)$$

Suppose one needs to avoid a 360° ambiguity in $\delta_2\phi$ for values of $\int N \, d\ell$ less than 10^{19} . From Equation (16), one easily finds

$$\Delta f^2 \approx -\delta_2\phi \times f_1^3 / \left(\frac{2\pi}{C} \times 40.5 \times 2 \times \int N \, d\ell \right) \quad (17)$$

Let

$$\begin{aligned} f_1 &= 2.45 + 0.153125 \text{ (this choice will be justified later)} \\ &= 2.603125 \text{ GHz} \end{aligned} \quad (18)$$

Then

$$\begin{aligned} \Delta f^2 &\approx (2\pi) \times (2.6 \times 10^9)^3 \times C / (2\pi \times 81 \times 10^{19}) \\ &= 0.651 \times 10^{16} \end{aligned}$$

or

$$\Delta f \approx 80.6 \text{ MHz} \quad (19)$$

Thus, with $\Delta f \leq 80.6$ MHz and assuming that $\delta_2\phi$ can be measured, then $\int N \, d\ell$ can be calculated rather easily from Equation (16). An implementation that measures $\delta_2\phi$ with relative ease is shown in Figure 3.

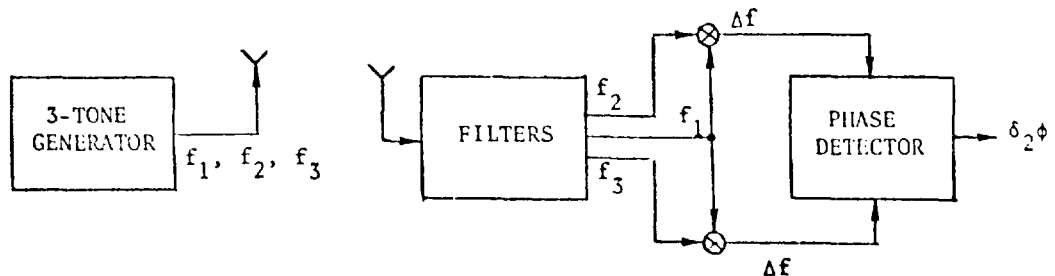


Figure 3. Measurement of $\delta_2\phi$

Reordering Equation (16), one easily obtains

$$\begin{aligned}\hat{N} &= \text{computed value of } \int N \, d\ell \\ &= \frac{f_1^3}{2 \Delta f^2} \times \frac{C}{2\pi} \times \frac{1}{40.5} \times (-\delta_2 \phi)_{\text{measured}} \\ &= \alpha \cdot (-\delta_2 \phi)_{\text{measured}}\end{aligned}\tag{20}$$

For $f_1 = 2.603$ GHz and $\Delta f = 80.0$ MHz, one can compute

$$\alpha = 1.6 \times 10^{18}\tag{21}$$

Based on S/N ratio considerations, the accuracy of the \hat{N} computation in Equation (20) is determined by the accuracy of $\delta_2 \phi$ measurement and is given by

$$\alpha_{\hat{N}} = \alpha \cdot \sigma_{\delta_2 \phi}\tag{22}$$

Once an estimate of $\int N \, d\ell$ for a given link is found, one needs to perform several steps of signal processing starting with the phase at f_1 and finishing with the conjugated phase at f_D . These steps are shown in Figure 4.

It is fair to point out that the conjugator used is a modified version of the one in Reference 1. With the additional boxes, the new conjugator clearly takes into account steady-state ionospheric effects.

For the present configuration, the uplink and downlink frequencies are related by the equation*

$$\frac{n}{n+2} \cdot f_1 = f_D$$

or

$$f_1 = \frac{n+2}{n} f_D\tag{23}$$

For $f_D = 2.45$ GHz and $n = 32$, one obtains

$$f_1 = 2.603125 \text{ GHz (see Equation (18)).}$$

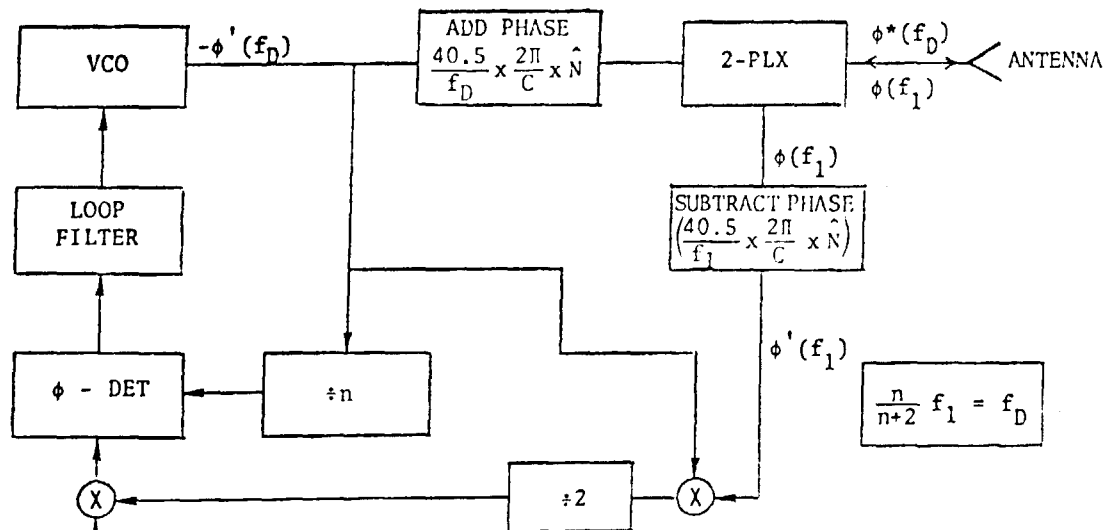
It is interesting to examine the output $\phi^*(f_D)$ of the conjugator in Figure 4. On taking differentials, one obtains

$$\Delta \phi^*(f_D) = \frac{40.5}{f_D} \times \frac{2\pi}{C} (1 - f_D^2/f_1^2) \Delta \hat{N}\tag{24}$$

One using $f_D = 2.45$ GHz and $f_1 = 2.603$ GHz, the above equation simplifies to

$$\Delta \phi^*(f_D) = 3.95 \times 10^{-17} \Delta \hat{N}\tag{25}$$

*Note the mode of operation indicated here is different from that in Ref. 1.



$$\begin{aligned} \phi_o(f_1) &= \text{Ref Phase} \\ &= \omega_1 \frac{L_0}{C} - \frac{40.5}{f_1} \times \frac{2\pi}{C} \times \int_0^{L_0} N \, d\ell \\ &= \text{Constant at all subarrays} \end{aligned}$$

$$\begin{aligned} \phi(f_1) &= \omega_1 \frac{L}{C} - \frac{40.5}{f_1} \times \frac{2\pi}{C} \times \int_0^L N \, d\ell \\ \phi^*(f_D) &= -\phi'(f_D) + \frac{40.5}{f_D} \times \frac{2\pi}{C} \times \hat{N} \\ &= \frac{n}{n+2} [2\phi_o(f_1) - \phi'(f_1)] + \frac{40.5}{f_D} \times \frac{2\pi}{C} \times \hat{N} \\ &= \text{const.} - \omega_D \frac{L}{C} + \frac{40.5}{f_D} \times \frac{2\pi}{C} \left[\hat{N} \left(1 - \frac{f_D^2}{f_1^2}\right) + \frac{f_D^2}{f_1^2} \int_0^L N \, d\ell \right] \end{aligned}$$

Figure 4. Modified Chernoff Conjugator

so that

$$\hat{\Delta N} = 2.53 \times 10^{16} \times \Delta \phi^*(f_D) \quad (26)$$

Suppose one requires an rms accuracy of 10° ($= .174$ rad) on $\phi^*(f_D)$. Then the required accuracy on N is given by

$$\begin{aligned} \sigma_{\hat{N}} &= 2.53 \times 10^{16} \times .174 \\ &= 4.41 \times 10^{15} \end{aligned} \quad (27)$$

On going back to Equation (22), one finds

$$\begin{aligned} \sigma_{\delta_2} &= \sigma_{\hat{N}}/\alpha, \quad \alpha = 1.6 \times 10^{18} \\ &= 2.76 \times 10^{-3} \end{aligned} \quad (28)$$

Squaring the quantity on the right hand side of Equation (28) and on using some results in Reference 3, one obtains a value for (P_R/σ^2) .** Thus,

$$\begin{aligned} P_R/\sigma^2 &= (S/N) \text{ ratio at the receiver sketched in Figure 3} \\ &= \frac{8}{\text{Var}(\delta_2 \phi)_{\text{opt}}} \\ &= \frac{8}{7.62 \times 10^{-6}} \\ &= 1.05 \times 10^6; \text{ i.e., } 60 \text{ dB} \end{aligned}$$

As far as Figure 4 is concerned, several comments are in order. Firstly, the use of the same \hat{N} for both uplink and downlink phase compensations need justification. Secondly, the conjugator suffers from divider ambiguity problems. This makes it necessary to phase conjugate at IF and then suitably multiply the conjugator output frequency to 2.45 GHz. Preliminary design of a 3-tone conjugator operating at IF has been completed and will be reported elsewhere.

V. CONCLUSION

An attempt has been made above to incorporate the role of the ionosphere in ARA system design. A conjugator has been sketched that compensates for steady-state ionospheric effects. Work is currently in progress to evaluate the magnitudes of ionospheric wedge effects. Based on (limited) available data² and because of geometry considerations (the proximity of the ionosphere to the rectenna), it appears unlikely that any compensation towards ionospheric effects would be necessary. However, in order to make a definite conclusion, more data on wedge structure are desirable. In addition, this problem needs examination in the light of ionospheric heating effects due to the downlink power beam.

** P_R is the total 3-tone signal power received and σ^2 is the noise power out of any one of the tone filters that have identical bandwidths.

REFERENCES

1. Chernoff, R. C., "Large Active Retrodirective Array for Space Application," IEEE Trans. on Antennas and Propagation, pp 489-496, July 1979.
2. Lawrence, R. S., Little, C. G., and Chivers, H. J., "A Survey of Ionospheric Effects Upon Earth-Space Radio Propagation," Proc. IEEE, pp 4-27, January 1964.
3. Burns, A. A. and Fremouw, E. J., "A Real-Time Correction Technique for Transionospheric Ranging Error," IEEE Trans. on Antennas and Propagation, pp 785-790, November 1970.

CONCLUSIONS PRESENTED AT THE PHASE CONTROL SESSION

1. Need for Phase Control System

An electronic phase control system is required to focus and steer a coherent narrow power beam. (Conventional electromechanical pointing techniques are not adequate due to antenna flatness and pointing accuracy required).

2. Performance Conclusions

a. Beam misalignment (pointing error) is acceptable when 10° RMS phase error is achieved and antenna/subarray mechanical alignment requirements are maintained.

b. Upward bound on phase error is determined by acceptable economic losses in scattered power rather than beam pointing errors or environmental factors.

c. Based on system performance requirements of 10° RMS phase error the power lost from the main beam is less than 3% and the beam pointing error is less than ± 250 meters with 99% probability.

d. Phase control to the smallest transmitter area (power module for the reference system), reduces the grating lobe peaks and relaxes subarray mechanical alignment and antenna positioning constraints.

e. Phase control to the power module level is economically sound based on cost trade-offs between phase control electronics and main beam power losses.

3. Retrodirective Phase Control Concepts

a. Conclusions

- (1) Implementation/performance for 10° RMS phase error appears to be within the state-of-the art based on analytical simulations and experimental (laboratory) evaluations.
- (2) Secure operation can be achieved (coded pilot signal).
- (3) Doppler effects are not a problem.
- (4) Biases in distribution system present a potentially serious calibration problem
- (5) Ionospheric effects on phase control are uncertain and could affect further system definition.

- (6) The retrodirective phase control concept has the features of fast response automatic phase tracking/adjustment; automatic/rapid fail safe operation (dephasing occurs in milliseconds and diffuses power beam to $.003 \text{ mW/cm}^2$ density levels); a complex phase distribution system and critical performance for efficient power transmission (distributed and centralized techniques).

4. Ground Based Phase Control Concepts

a. Conclusions

- (1) Implementation/performance appears feasible, based on analytical studies.
- (2) Secure operations can be provided with coded command channel.
- (3) Ionospheric effects on phase control performance are uncertain and could affect further system definition.
- (4) Biases in distribution system can be adjusted out during normal operations (part of the phase control loop).
- (5) The ground based phase control concept has the features of closed loop phasing (measures phase at ground and commands phase adjustments via communication link); slower responses than retrodirective (.25 second delay due to geosynchronous transit time); and the dephasing process is slower than retrodirective (may require additional beam safing measures).

5. Hybrid (Retrodirective and Ground Based) Phase Control

Based on limited investigations it appears that the best features of both the retrodirective and ground based phase control concepts can be incorporated into a hybrid system.

REMAINING ISSUES - PRESENTED AT THE PHASE CONTROL SESSION

1. Phase error buildup in distribution system
2. Array topology for distribution system (phase error buildup vs. reliability)
3. Proof of phase distribution concept
4. Power signal interference on pilot signal receiver
5. Phase conjugation accuracy
6. Effects of ionospheric/atmospheric disturbances
7. Accuracy of beam formation, pointing
8. Failure effects on beam forming and pointing
9. RFI of power module due to phase lock loop around P.A.
10. Alternate concepts (ground based)

SECTION IV

POWER AMPLIFIER SESSION

Chairman: Louis Leopold
NASA, Johnson Space Center

HIGH EFFICIENCY SPS KLYSTRON DESIGN
E. J. Nalos, Boeing Aerospace Company

1. Introduction

Considerable data has now been accumulated on the feasibility of an 80-85% high power klystron design from previous studies. The most likely compact configuration to realize both high efficiency and high gain (~ 40 dB) is a 5-6 cavity design focused by an electromagnet. A refocussing section will probably be required for efficient depressed collector operation. An outline of a potential klystron configuration is given in Figure 1. The selected power output of 70 kW CW resulted from a maximum assumed operating voltage of 40 kV. The basic klystron efficiency cannot be expected to exceed 70-75% without collector depression. Although impressive gains have been achieved in raising the basic efficiency from 50% to 70% or so with a multi-stage collector, the estimated efficiency improvement due to 5-stage collector at the 75% level is only about 8%, resulting in an overall efficiency of about 83%. These estimates need to be verified by experiment, since the velocity distribution of the spent klystron beam entering the collector is not precisely known. It appears that the net benefit of a 5-stage collector over a 2-stage collector is between 1.5 - 3.5 kW per tube. This has the double benefit of less electrical power to be supplied as well as less thermal power in the collector to be dissipated. Table 1 indicates an estimated energy balance in the klystron which leads to the above estimates. A modulating anode is incorporated in the design to enable rapid shutoff of the beam current in case the r.f. drive should be removed. In this case, the collector would become overheated since it would receive the full beam power.

2. Depressed Collector Design

One of the greater uncertainties in the design is the velocity distribution of electrons in the output gap, particularly for a high basic efficiency tube. Experimental verification will be required for the selection of proper depressed voltages at each collecting electrode. Varian has reported that about 10% of the electrons develop twice the d.c. beam voltage in a 50% efficient tube. We estimate that this will be reduced to perhaps 2% for an 80-85% efficient tube. To obtain initial specifications for the collector supply, an estimate was made of the possible voltage ratios required, as indicated in Figure 2.

3. Voltage Regulation

The requirements on the modulating anode and body voltage are dictated primarily by phase fluctuations. At 40 kV, $\phi \approx 3000^\circ$ and at 41 kV, this calculation yields 2972° . Thus, $d\phi/dt = -37^\circ$ per kV. If a 10° phase error were allowable in the klystron, this would translate into a regulation requirement of $\pm .67\%$ at 40 kV, provided that klystron-to-klystron phase errors are not correlated. Although it is likely that voltage fluctuations on all klystrons on a given d.c. - d.c. converter will go up and down together, the time delays in distribution, of the order of fractions of microseconds, will make them appear as though they were uncorrelated at a given instant at all klystron terminals. With this in mind, the initial regulation requirement on the modulating anode and body supply was set at 0.5%. Since it is contemplated to include the klystron in a phase compensation loop, it may be possible to relax this requirement when the loop performance is verified.

4. Electron Beam Focusing Design

The focusing options for the klystron include: (1) solenoid ElectroMagnetic (EM) focusing, (2) Multiple-pole electromagnetic focusing with periodic field reversals, introducing the possibility of Permanent Magnet (PM) implementation, (3) Periodic Permanent Magnet (PPM) focusing used successfully on low and medium power tubes (mostly TWT's); and 4) Combined PM/PPM focusing wherein the PM section at the output is used to retain good efficiency and good collimation in the high power r.f. region. The low risk approach of (1) was recommended in order to achieve the highest efficiency, but R&D efforts in a combined PM/PPM approach should be investigated for possible later incorporation.

In order to achieve a conservative design, we have initially selected a capability of achieving 1,000 Gauss in the solenoid when operating at 300°C. Selecting a minimum ID dimension compatible with directly winding the solenoid on the tube involves a trade study of the required solenoid power and weight as a function of solenoid OD. Figure 3 shows the trade of solenoid power and weight with coil OD.

It is anticipated that the solenoid will consist of copper sheet with glass-like insulation between layers, wound directly on the tube body. With factory adjusted cavity tuning, there will be no protruding tuners. It is possible that the solenoid may be used for baking out the tube in space.

As a matter of interest, the performance parameters of a 50 KW PM focused klystron were estimated in Table 2. With the design assumptions postulated, it does not appear to offer any advantages over an efficiently focused solenoid design.

5. Design Approach to Long Life

The objective of SPS is the achievement of 30 year life and since the main component of the MPTS system is the r.f. transmitter, its consideration is of paramount importance. The major transmitter elements which contribute to life are summarized in Table 3. The achievement of uniform tube-to-tube performance will require stringent materials control, well defined construction techniques, and special design features such as temperature compensated cavity frequency control.

An initial risk assessment of the unknowns on the space environment have led us to favor a closed envelope approach as a reference design. Some of the concerns with open envelope operation near the Shuttle vehicle deal with outgassing from non-metallic skin of heavy molecules and absorbed volatile species: cabin leaks (oxygen); fuel cell flash evaporators (water vapor); Vernier control rocket engine exhaust; and main rocket engine outgassing (water vapor). The degree to which such contaminants can be localized, and the pumping speed of space, etc., have yet to be determined.

The NASA objective of 30 year life, in the light of current experience and understanding, thus has to be based on the following phased approach:

- . Conservative Design:
 - Emission; R.F., Thermal and Stress: Derating
- . Determination of Appropriate Manufacturing Procedures
- . Adequate Protective Features
 - Modulating Anode
 - System Monitoring Requirements

5.2 Tube MTBF Considerations

Ideally, a failure model of the transmitter would be desired, in which no failures occurred until wearout mechanisms set in; i.e., avoidance of early mortality. To some degree this can be achieved by a burn-in procedure to identify and remove infant mortality victims. It is anticipated that with the reference design tube, partial or full bakeout in space will be feasible, avoiding the need to perform costly burn-in on the ground. Also, with mass production, automated manufacture, good quality control, and maintenance, infant mortality can be minimized.

With roughly $N = 100,000$ tubes, if a maximum of 2% of all klystrons are allowed to fail at scheduled SPS shutdown, (every 6 months), the required tube MTBF would be approximately

$$\frac{(.02N)}{N} (\text{Tube MTBF}) = 6 \text{ months} - .5 \text{ years; i.e., MTBF} = (50)(.5) = 25 \text{ years.}$$

This is compatible with the reference klystron design; however, a more refined reliability model needs to be developed, of which the exponential failure model is but one case corresponding to a constant failure rate. With proper burn-in procedures, and as better understanding of failure modes is developed, the SPS klystron may require a much lower MTBF to meet the above criteria. With a proper burn-in period, infant mortality failures can be avoided and failures shifted toward cathode wearout limitations. The required burn-in period for current space qualified TWT's is of the order of 1,500 hours. Further understanding of the required tube MTBF under these conditions will evolve with the ground based development program implementation.

6. Klystron Tube Protection

The tube interacts with the subarray through the waveguide feed system. The primary requirement is maintenance of a good r.f. match under all conditions. During initial processing or if mismatched, either external or internal arcing may occur. Commercial waveguide components are available to visually detect arcs and use a trigger signal to disconnect the tube rapidly, in this case by connecting the modulating anode to cathode. This can occur in much less than 1 μ sec, adequate to prevent damage.

With loss of r.f. drive, the entire electron beam power appears at the collector. The conventional klystron is designed to handle this power. In our case, the collector is designed to handle only the spent electron beam after normal r.f. interaction. If the loss of r.f. drive is sensed at the klystron input, the modulation-anode power supply will be used to shut off the electron beam.

The most likely region of dc arcing is between cathode structure and modulation-anode and between the modulating anode and the r.f. circuit. In the event of an arc, the energy stored in the modulation-anode power supply RC circuit is discharged. Ordinarily the arc extinguishes after a brief interval and normal tube performance is restored automatically. Should some unknown fault cause persistent non-clearing arcing, arc logic could be designed to sense repeated loss of r.f. output and to shut down the modulation-anode power supply.

- . Adequate Test Program on Ground
 - Failure Mode Identification
 - Infant Mortality Elimination - Burn-in
- . Understanding of Space Environment
 - Processing in Space
 - Open Envelope Operation
- . Definition of Maintenance Philosophy
 - Allowable Down Time
 - In-place Repair Feasibility
- . Development of Improved MTBF Analytical Model
- . Space Test Verification

There are promising developments in transmitter life which lend some credibility to the 30 year life objective. For instance, the best ten high power klystrons running on the BMEWS system have seen 9 years of life and are still running. With proper burn-in procedures, current space based TWT's are being qualified for 7 years life. Over 100 such tubes currently in space have been running for well over 2 years. It is our expectation that within the SPS development time-frame, tube MTBF's approaching 30 years with the suggested design approach will be feasible. It is important to recognize that significant life test programs on the ground will be required not only for cathodes, but the entire r.f. envelope.

5.1 Cathode Design

The mechanisms limiting thermionic cathode life are primarily evaporation rate of the cathode material, cathode matrix properties, and impurities. The cathode-tube interaction is paramount in realizing long life, regardless of how good the cathode may be in a diode test. The approach to realize 30 year life must be based on minimizing tube-cathode interactions through conservative design, good beam focusing and proper selection of materials to minimize poisoning gases produced by electron bombardment. The most likely candidates, based on present knowledge, are either a tungsten matrix cathode operating at a temperature of slightly above 1000°C or a nickel matrix cathode operating at about 800°C. The lower temperature would be preferable from the life point of view but factors such as migration and reactivation feasibility tend to favor the higher temperature cathode. Our current assessment, based on discussions with the tube industry suggests that it would probably be unwise to utilize some of the newer cathodes until sufficient life test data has been accumulated. Encouragement with respect to long life in thermionic cathodes can be derived from the work at Bell Telephone Laboratories on the so-called Coated Powder Cathode (CPS), which is in use on long life repeaters, capable of 50,000 hours life at current densities approaching 1 amp/cm², much higher than those proposed for the SPS Klystron (<.2 amps/cm²).

Persistent repeated nonclearing rf arcing in the klystron rf load or output system may result in tube damage. The rf arc logic protection circuit is designed to sense reflected rf power caused by the arcing and to shut down the modulation-anode power supply pending correction of the problem.

7. Operation Under Reduced Voltage

One advantage of the klystron is the fact that efficiency does not deteriorate significantly with voltage. The effect of solar cell voltage degradation on klystron power output is indicated in Figure 4 for the condition that the klystron characteristics remain on the V-I portion of the solar cells corresponding to maximum d.c. output. This condition can only be achieved if the perveance of the tube is slightly changed. If the modulating anode is mounted on a diaphragm, such an adjustment could be made. This feature would also be useful for adjustment of tube-to-tube uniformity. It is seen that if the solar cells are not refurbished, the efficiency remains high, but the power output drops significantly. On this basis, it was decided to refurbish solar cells and not require the transmitter to adjust perveance for solar cell optimal matching.

8. Klystron Power Output Trade Study

The reference klystron represents an initial point design within the given NASA guidelines. It is intended primarily as a vehicle to demonstrate its potential in the SPS application. If the operating voltage at GEO can be increased to a value above 40 kv other klystron power levels become of interest.

One of the advantages of the linear beam amplifier such as a klystron is the fact that the different interaction regions, i.e., beam formation, r.f. interaction, and beam collection are physically separate and hence distribute the thermal stresses over a large area. The most critical portion of the klystron from the thermal point is the output gap. The output gap interception for two typical values of beam transmission (95% and 98%) is indicated in Figure 5. The capability of the output gap to handle this interception is given for two values of heat rejection capability: 0.25 and 0.5 kw/cm² of area. This could be either heat pipe cooling or pumped fluid cooling.

It is seen that for a 4% beam interception and $W = 0.25 \text{ kw/cm}^2$, the maximum beam voltage is about 67 kv, corresponding to a power level in excess of 200 kw. If the perveance were increased from $S = 0.3$ to 0.5×10^{-6} , still within the regime of potentially high efficiency, this power level would correspond to 580 kw. This has encouraged us to investigate two additional point designs, at 250 kw and at 500 kw, respectively, the parameters for which are summarized in Table 4.

The efficiency including solenoid power is somewhat higher than that for the reference design. It is worth noting that even with a longer tube, the efficiency increases by about 2% points due to lower incremental solenoid requirements at higher power. The specific mass decreases from about 0.8 kg/kw at 70 kw to less than 0.4 kg/kw at 500 kw CW. Thus, it appears advantageous to consider a higher power klystron design should the voltage constraints permit it.

The cost of a single klystron tube is estimated from the cost trends in Figure 6. For a 70 kw CW tube, the mass production cost is estimated at \$2800. The acquisition cost of r.f. tubes and 10-year replacement cost of spares, based on a projected transportation cost to space of \$60 per kg, for a system output of 6 GW RF in space, are summarized in Table 5. The transportation costs comprise about 47 to 62% of the total cost. Again, with the assumptions made, it appears advantageous to go to as high power per tube as possible. As the ground-based development program proceeds, the results of these trade studies will be used in updating the present baseline design, not only for the klystron transmitter candidate, but for other transmitters as well.

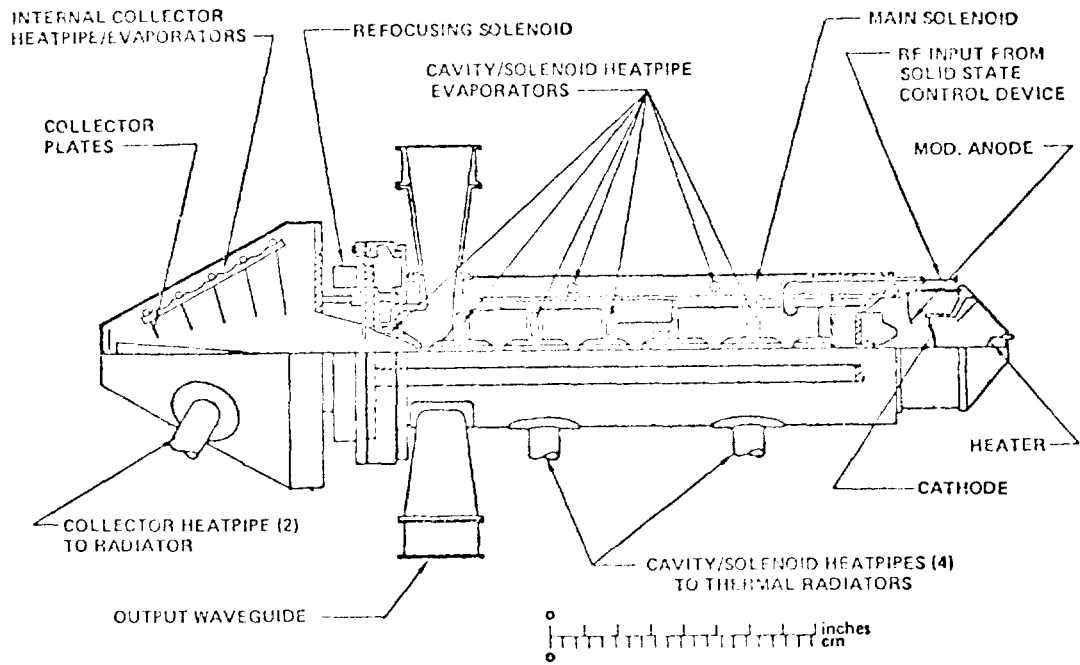


Figure 1 Reference Klystron Configuration

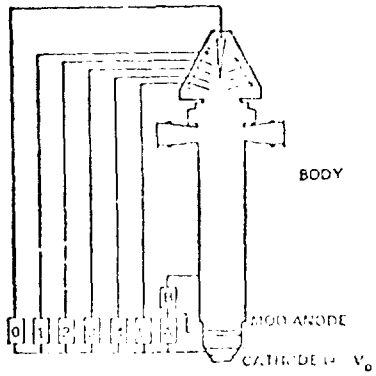
Table 4 Energy Balance in Reference Klystron Design

	2-SEGMENT COLLECTOR	5 SEGMENT COLLECTOR
BEAM POWER	92.62 Kw	92.62 Kw
RF LOSS IN DRIVER CAVITIES	.40 Kw	.40 Kw
RF POWER PUTPUT ¹	70.66 Kw	70.66 Kw
OUTPUT CAVITY RF LOSS	2.19 Kw	2.19 Kw
OUTPUT INTERCEPTION LOSS ²	1.62 Kw	1.62 Kw
POWER ENTERING COLLECTOR	17.75 Kw	17.75 Kw
COLLECTOR RECOVERY	7.10 @ 40%	10.65 @ 60%
THERMAL LOSS IN COLLECTOR	10.65 Kw	7.1 Kw
NET BEAM POWER	85.52 Kw	81.97 Kw
EFFICIENCY EXC. SOLENOID	82.6%	86.2%
NET EFFICIENCY ³	81.2%	84.6%

1. ELECTRONIC EFFIC. (.73) x OUTPUT CIRCUIT EFFICIENCY (.97) x REMAINING POWER (92.22 Kw)

2. BASED ON 4% INTERCEPTION @ $V_0/3$ (.33%) and 2 $V_0/3$ (.7%) i.e., .0178 $V_0 I_0$

3. INCLUDING 1.5 Kw FOR SOLENOID AND HEATER POWER.



ESTIMATED CURRENT & VOLTAGE DISTRIBUTIONS

COLLECTOR CONFIGURATION	3 SEGMENT			5 SEGMENT		
	V/V ₀	I/I ₀	P/P ₀	V/V ₀	I/I ₀	P/P ₀
MOD. ANODE SUPPLY	.5	-.01	-.019	.5	-.01	-.019
MOD. ANODE LOSS	0	-.01	-.019	0	-.01	-.019
SPIN. ELECT. SUPPLY	0	.02	-.01	0	.02	-.01
COLLECTOR #1	.16	.02	.017	.16	.02	.017
COLLECTOR #2	.19	.01	.006	.19	.01	.006
COLLECTOR #3	.25	.05	.016	.25	.05	.016
COLLECTOR #4	-.01	-.01	-.019	-.01	-.01	-.019
COLLECTOR #5	-.01	-.01	-.019	-.01	-.01	-.019
TOTAL		1.0	1.34		1.0	1.34
EFFICIENCY IMPROVEMENT			1.63			1.13
ESTIM. EFFICIENCY DECREASED (20% REDUCED COLLECTOR LOSS)			0.245			0.215

Figure 2. Reference Klystron Depressed Collector Design

COPPER SOLENOID 3" ID, 1000 GAUSS, 16.5" LONG

- ASSUMES POWER GENERATION @ 3.5 kw AND PASSIVE HEAT REJECTION @ 6.2 kw/kw (125°C).
- AS ABOVE, WITH 3.86 kw/kw FOR 300°C HEAT REJECTION.

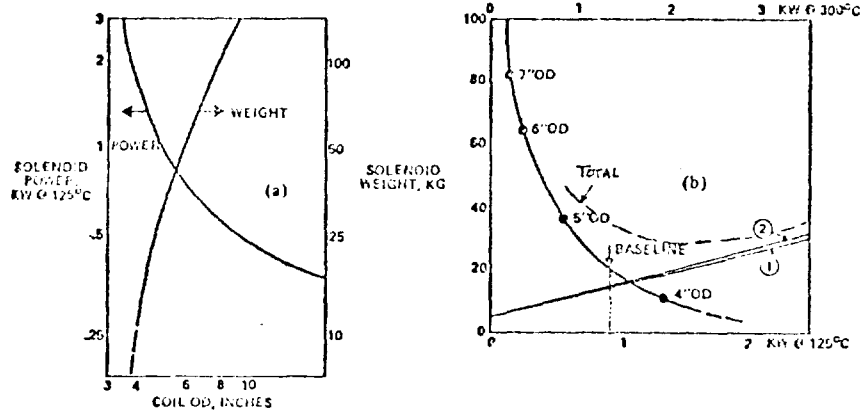


Figure 3 Solenoid Design for High Power Klystron

Table 2 50 KW Permanent Magnet Klystron Design

VOLTAGE/CURRENT	3KV, 1.81 AMP'S
PERVEANCE/BEAMPOWER	S = .244, P ₀ = 69KW
ELECTRONIC EFFICIENCY	0.75
CIRCUIT EFFICIENCY	0.97
RF POWER OUTPUT	50KW
HEATER POWER	1KW
DRIVER RF LOSSES	.005V ₀ I ₀ = .3KW
OUTPUT INTERCEPTION LOSS	.025V ₀ I ₀ = 1.72KW
RF OUTPUT CAVITY LOSS	.03(50) = 1.50KW
POWER INTO COLLECTOR	15.48KW
COLLECTOR THERMAL INPUT	8.51KW REMOVED @ 500°C

PASSIVE COOLING -

RADIATOR & HEAT PIPES LIQUID METAL CYCLE @ 2.2/1.5KG/KW FOR 275°C
@ .94/1.4KG/KW FOR 500°C

WEIGHT ESTIMATE

TUBE & POLEPIECES	12.0KG	o SPECIFIC WEIGHT = .78 TO .83 KC/KW
COLLECTOR - 5 SEGMENT	6.0	
MAGNETS	7.5	o EFFICIENCY = 80.7%
RADIATOR DISTANCE	0 - 1 METER	
COOLING @ 275°C	5.4 8.0KG	
COOLING @ 500°C	4.2 8.0KG	
TOTAL WEIGHT	35.1 41.5KG	

Table 3- Features Affecting Transmitter Life

- BEAM FORMATION**
 - CATHODE MANUFACTURING MATERIAL PROCESSING
 - EMISSION SUPPRESSION FROM SURFACES
 - CATHODE BASE MATERIAL PURITY - POISONING MECHANISM
 - EVAPORATION RATES FROM IMPREGNATED CATHODES
 - HEATER WARMUP
 - BURN-IN PERIOD - NO INFANT MORTALITY
- BEAM FOCUSING**
 - SOLENOID DESIGN/MATERIALS - SPACE BAKEOUT FEASIBILITY AND CONTROL
 - MAGNETIC CIRCUIT MATERIAL SELECTION SmCo_5 , ALNICO, FLUX CONDUCTORS
- RF CIRCUIT**
 - COPPER ALTERNATIVES FOR CAVITIES
 - PROPERTIES OF LOSSY INTERNAL CERAMICS
 - OUTPUT WINDOW POWER LIMITS BeO , Al_2O_3
- BODY AND COLLECTOR**
 - LEAKAGE OF INSULATORS
 - SUPPRESSION OF SECONDARY EMISSION
- EXTERNAL**
 - LEAD AND CONNECTOR COMPATIBILITY

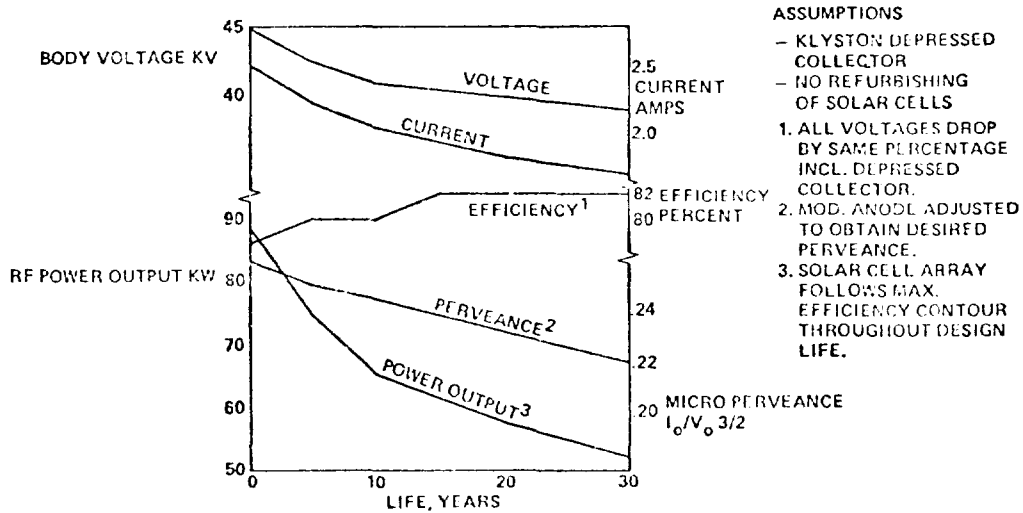


Figure 4 Klystron Performance When Optimally Matched to Solar Cell Output

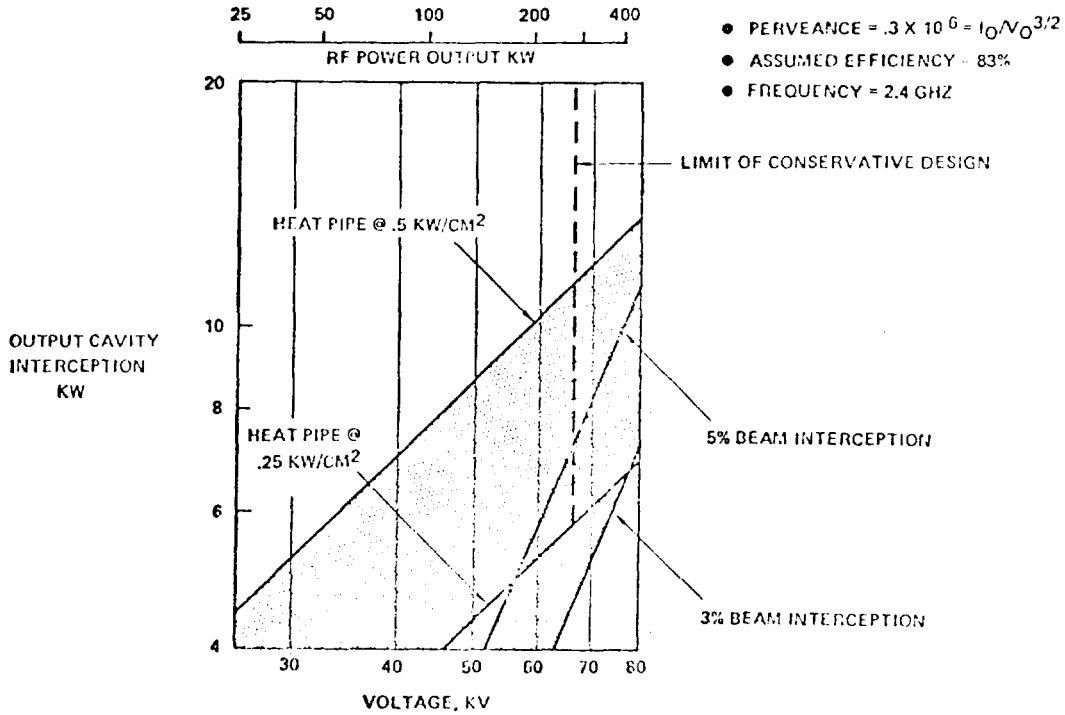


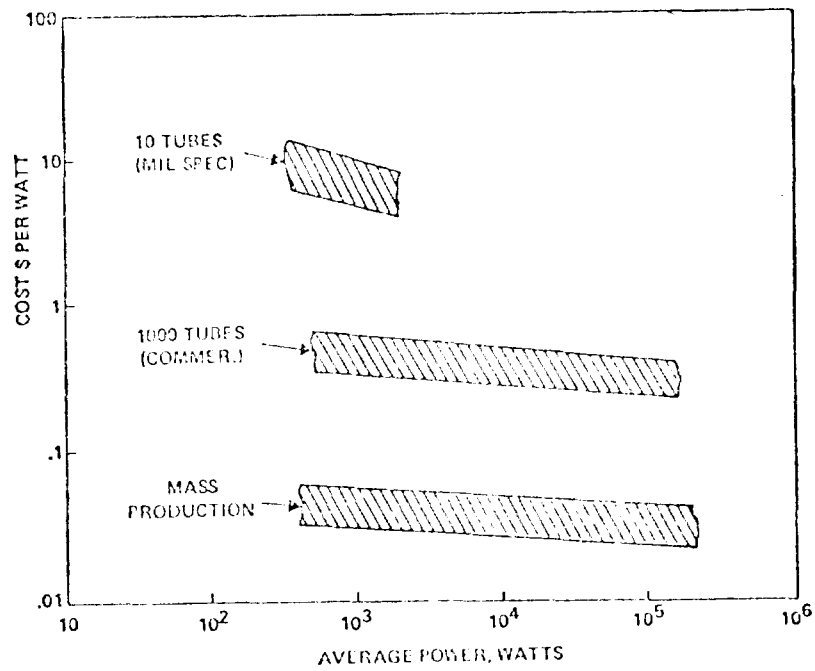
Figure 5. High Power CW Limitations of High Efficiency Klystron

Table 4 Alternate High Power Klystron Designs

POWER VOLTAGE/CURRENT PERVEANCE $K \times 10^6$ RF SECTION LENGTH $\sim \sqrt{V_0}$	70.6kw 42kv/2.2amps .25 16.5in		250kw 65kv/5amps .30 20.5in		500kw 80kv/8.2amps .36 22.8in	
	WEIGHT, kg	POWER, kw	WEIGHT	POWER	WEIGHT	POWER
TUBE WEIGHT, CAVITY, SEALS, BODY ETC. $\sim 1.2 \sqrt{V_0}$	10kg		15kg		16.6kg	
COLLECTOR WEIGHT (EST.) $\sim V_0 I_0$	7.0kg		13.2kg		18.7kg	
SOLENOID (EST.) @ 300°C, 1 KGAUSS, $P \sim B^2 \times L \sim \sqrt{V_0} K$	20kg	2kw	24.8kg	2.98kw	27.9kg	3.98kw
HEATER AND REFocusing COIL RF LOSSES		1.0kw 4.2kw		1.50kw 14.7kw		2.0kw 29.8kw
RADIATOR AND HEAT PIPES	0	1m	0	1m	0	1m
WEIGHT AND POWER DISSIP'N REQ'D @ 300°C	9.5	14.5	7.2kw	25.3 33.6	19.2kw	47.3 72.0 35.8
WEIGHT AND POWER DISSIP'N REQ'D @ 500°C	4.9	9.3	9.9kw	16.7 32.1	34.1	33.8 64.9 69.0
TOTAL WEIGHT KG	51.4	60.8	95.0	123.7	144	199.8
SPECIFIC WEIGHT KG PER KW	.727	.860	.380	.425	.268	.400
EFFICIENCY INC. SOLENOID	80.51%		82.43%		82.67%	

LEGEND:

- SOLENOID FOCUSING, FIVE STAGE COLLECTOR, 45% RECOVERY.
- RF LOSSES AT INPUT, OUTPUT, PLUS 4% INTERCEPTION LOSS TOTAL 4.45% OF $V_0 I_0$
- USEFUL RF OUTPUT = $.7029 V_0 I_0$
- COLLECTOR THERMAL DISSIPATION = $.105 V_0 I_0$
- COLLECTOR POWER RECOVERED = $.0860 V_0 I_0$
- EFFICIENCY = 83.4% EXCLUDING SOLENOID
- HEAT PIPES (W/O METER) + RADIATOR WEIGHT ESTIMATED @ 2.01/1.32kg/kw @ 300°C (BODY AND SOLENOID)
- @ .94/1.45kg/kw @ 500°C (COLLECTOR)
- S BAND DESIGN WITH SOLENOID @ 200°C ID = 3" OD = 4 1/2"



(b) COST VARIATION WITH POWER LEVEL AND QUANTITY

Figure 6 Cost Trends in High Power CW Transmitters

Table 5. RF Transmitter Acquisition & 10 Year Replacement Cost

SPS-1546

CANDIDATE	POWER PER UNIT, kW	NUMBER PER SYSTEM	ACQUISITION COST		REPLACEMENT COST		SPECIFIC COST \$/kW	SPECIFIC WEIGHT	MASS		TRANS. PORT COST	SYSTEM COST		
			PER UNIT \$K	PER SYSTEM \$M	MTBF, YEARS	REPLACEMENTS MONTH			INITIAL ACQON	10 YR REPLACEMENT				
1	50	120x10 ³	2.7	324	28	357	116	70	.8	4.8	1.7	203	102	830
2	70	55,000	2.8	238	26	272	91	40	.75	4.76	1.8	206	108	723
3	250	24,000	7.0	168	24	84	70	28	.4	2.4	1.0	144	60	441
4	500	12,000	10	120	20	50	60	20	.3	1.6	.9	108	54	341

LEGEND

CANDIDATE

- 1, 1M FOCUSED KLYSTRON 38kv
- 2, 1M FOCUSED KLYSTRON 42kv
- 3, 1M FOCUSED KLYSTRON 65kv
- 4, 1M FOCUSED KLYSTRON 80kv

TRANSPORT COST AT \$ 60 1/2 TO ORBIT

EXPONENTIAL FAILURE RATE

PASSIVE COOLING

NO BURN IN COSTS INCLUDED

HIGH EFFICIENCY KLYSTRON FOR THE SPS APPLICATION

By A. D. LaRue, Varian Associates, Inc.

INTRODUCTION

Proposed satellite power stations, where solar energy is to be converted to microwave energy and beamed to earth to be converted to ac power, will require large numbers of high efficiency microwave devices. A total microwave tube operating efficiency of 85% has often been mentioned as the minimum acceptable. It has been estimated that one percentage point in tube efficiency is roughly equivalent to two hundred million dollars in installation costs for a single satellite power station.

During the past several years interest has centered on the klystron as a possible source of microwave energy in the satellite power station because of high power output (50 to 70 kW), high gain (40 to 50 dB), low noise (-181 dB/Hz or greater) referenced to the carrier, ease of phase control, and potential for very long life. While the state-of-the-art operating efficiency of the klystron is lower than that of the crossed field tube, it may be possible to enhance klystron efficiency through the use of collector depression, that is by recovering energy from the spent electron beam after microwave amplification.

Any study of the SPS klystron at Varian starts with the VKS-7773 experimental 50 kW S-band tube tested at 74.4% base efficiency.¹ This tube was the culmination of efficiency studies covering klystron electron beam microperveances in the range of 1.0 to 0.5 micropervs. The lower value was used in this high efficiency klystron. Design considerations for the SPS klystron use the VKS-7773 as a design bench mark. Theoretical studies indicate likely modifications that should yield some increase in klystron base efficiency. Study of the efforts of a number of workers in the field of depressed collectors, moreover, suggests that the recovery of energy still present on the electron beam after microwave amplification may lead to a total efficiency of close to 85%.

This paper discusses these matters and others in some detail. Subjects considered include efficiency, noise, harmonics, cooling, and life. The mod-anode, to be employed for beam control, and the depressed collector, used in spent electron beam energy recovery, are described.

THE VKS-7773 KLYSTRON

The VKS-7773 experimental klystron cw amplifier was tested at 50 kW power output and 74.4% tube base efficiency when operated at 28 kV and 2.4

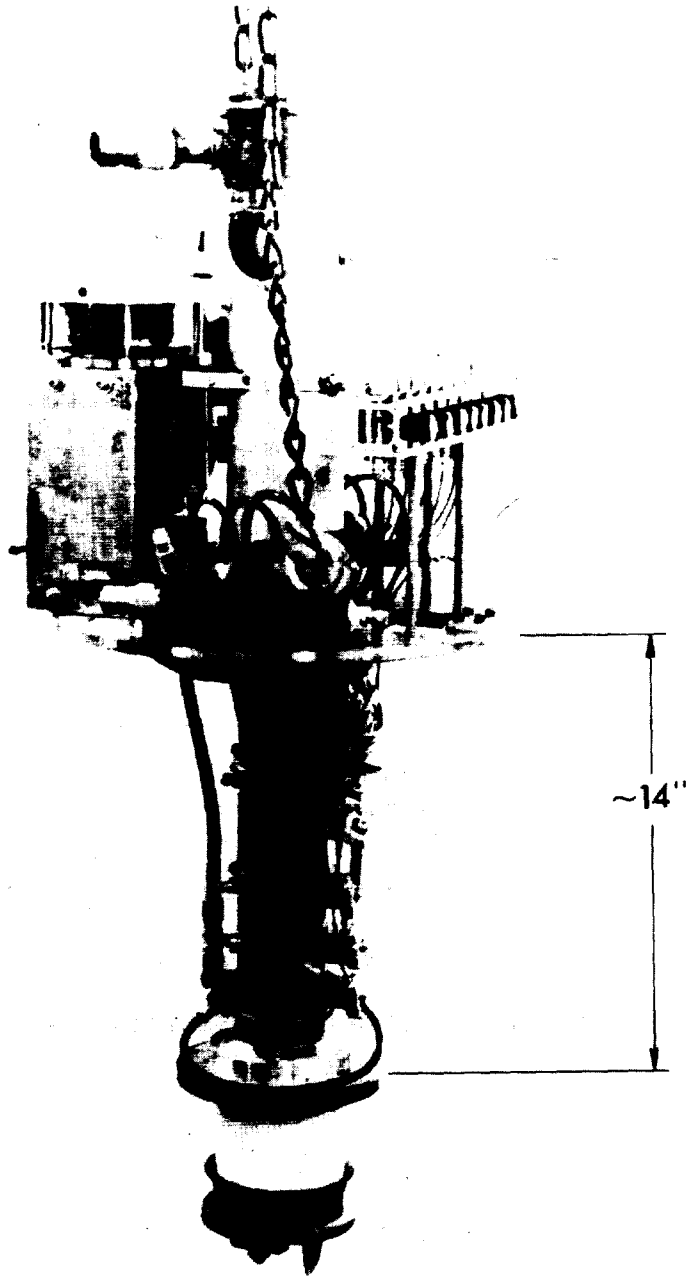
amperes beam current in the 1970 tests described by Erling Lien of Varian.¹ Figure 1 is a photograph of the klystron. The tube used a 0.5 microperv electron gun (bottom of picture), seven resonant cavities (within the 14" length between magnetic polepieces), and a standard water-cooled collector (top of picture). The resonant cavity structure employed two second harmonic cavities. These contributed to the electron beam bunching process and high electronic efficiency. They also permitted use of a relatively short resonant cavity system. The klystron was tunable within the frequency range 2425-2475 MHz. A waveguide output and standard pillbox rf output window were employed. Separate water cooling systems were used on the klystron body, output cavity, and collector to permit analysis of power dissipation throughout the klystron. RF power output was determined through this power analysis, combined with beam power, calibrated coupler, and calorimetric water load measurements.

Figure 2 shows the power output and base efficiency observed with the VKS-7773 CW klystron as a function of beam voltage. Over the beam voltage range from 20 to 28 kV, power output varied from 21 to 50 kW. Base efficiency was above 70% even at the lower beam voltage, reaching 74.4% at 28 kV.

After microwave amplification, the spent beam of the VKS-7773 still has about 14.3 kW of energy, ordinarily dissipated in the collector. If a depressed collector were used to recover a portion of this energy, the overall efficiency could be increased. Figure 3 shows the total klystron efficiency as a function of collector recovery efficiency for this case. If half of the spent beam energy were recovered, overall efficiency would be 85%.

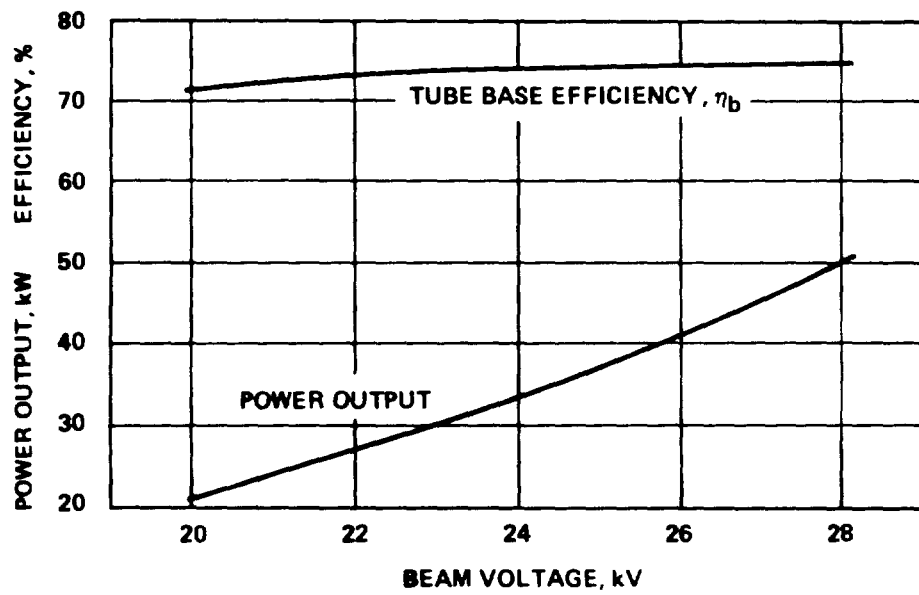
NEW HIGH EFFICIENCY DESIGN

Table 1 shows principal operating characteristics of the VKS-7773 experimental CW klystron amplifier and those of a new design aiming at higher operating efficiency. The VKS-7773 was designed to employ a 0.5 micropervance electron beam. This choice stemmed from computer work on designs using 0.5 to 1.0 microperv electron beams. Theory predicts high electronic conversion efficiency, the efficiency with which rf energy is coupled from the electron beam into the resonant output cavity, for low electron beam micropervance. Use of a low electron beam micropervance



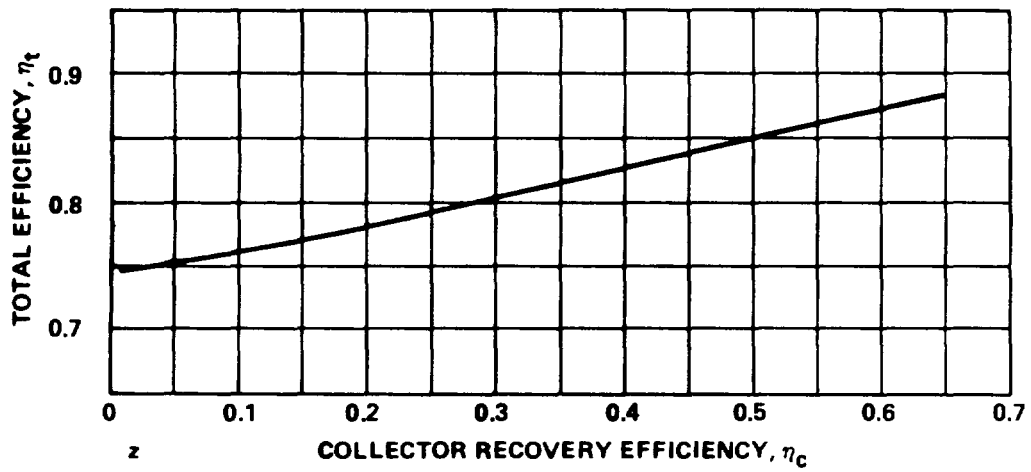
VKS-7773 EXPERIMENTAL HIGH EFFICIENCY KLYSTRON CW AMPLIFIER

FIGURE 1



VKS-7773, POWER OUTPUT AND EFFICIENCY VS BEAM VOLTAGE

FIGURE 2



VA-7773, TOTAL EFFICIENCY WITH A DEPRESSED COLLECTOR

FIGURE 3

means employment of a high voltage and low current beam, or a high impedance beam. For the SPS klystron, interest has centered primarily on 50 kW power output designs having electron beam microperveances in the range of 0.2 to 0.35 micropervs. Considerable study has also been applied a 70 kW power output klystron, some thoughts to a 300 kW tube. The example of the table is a 52 kW power output klystron using a 0.3 microperveance electron beam. Extrapolation of computer data leading to the VKS-7773 klystron design and study of a report on the evaluation of rf output energy extraction by Kosmahl and Albers² indicates an electronic conversion efficiency between 0.77 and 0.82 for this case. If one assumes a value of 0.79 and applies a 0.98 circuit efficiency, the efficiency with which rf energy is coupled from the output cavity to the useful load, then the tube base operating efficiency, product of the two, is 0.77.

Table 1
Klystron CW Amplifier Operating Characteristics

	<u>VKS-7773</u>	<u>New Design</u>
Frequency, GHz	2.45	2.45
Tuning, MHz	± 25	Fixed
Beam Voltage, kV	28	35
Mod-Anode Voltage, kV	--	17
Gun μ perveance	0.5	0.85
Beam μ perveance	0.5	0.3
Beam Current, A	2.4	1.96
Power Output, kW	50	52
Base Efficiency, η_b , %	74	77
Collector Efficiency, η_c , %	--	51*
Total Efficiency, η_t , %	--	85*
Saturated Gain, dB	50	50
Brillouin Field, B, Gauss	465	349

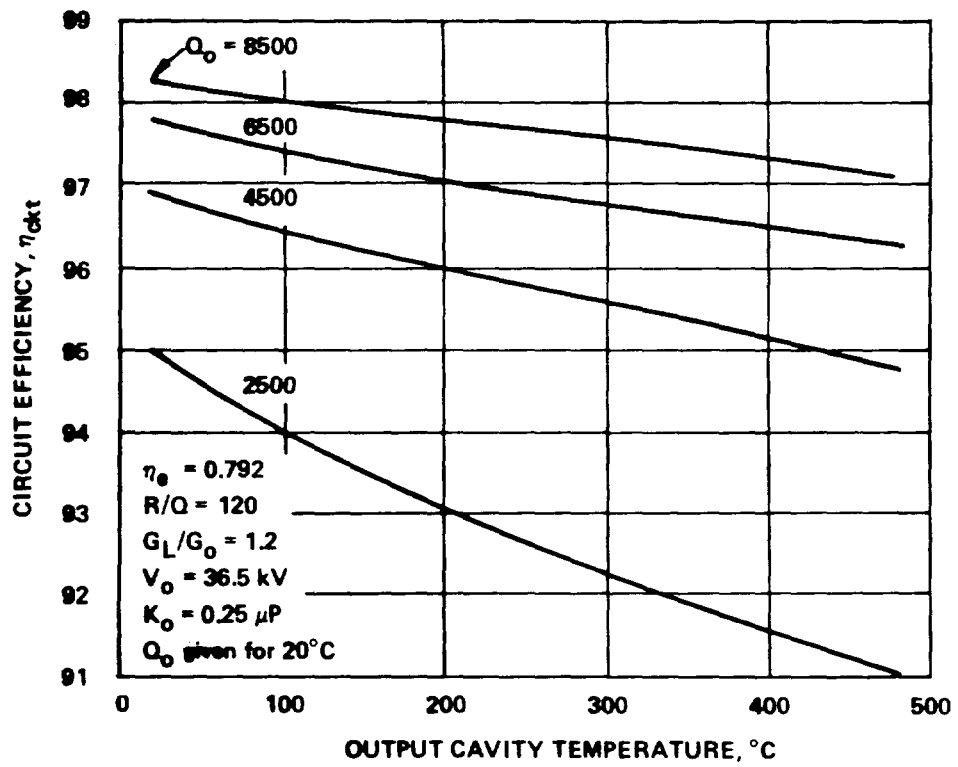
*With depressed collector assembly

RF output circuit efficiency declines with reduced electron beam microperveance, and losses increase in the rf output cavity. The net efficiency benefit from the employment of a low microperveance electron beam is limited by this fact, and an optimum condition exists, evidently within the range of 0.2 to 0.35 electron beam microperveance. For the SPS klystron, this region has been studied only from a theoretical viewpoint. The necessary experimental verification has yet to be undertaken.

The operating temperature of the rf output cavity of the SPS klystron is quite important, because a high temperature will cause a decline in circuit efficiency. The effect is quite pronounced in resonant structures of moderate unloaded Q (Q_0). A structure having an unloaded Q of 2500 at 20°C would experience a loss of circuit efficiency of about three percentage points when heated to 300°C. If the 20°C unloaded Q were 8500, the loss in circuit efficiency at 300°C would be less than one percentage point. These relationships are shown in Figure 4. Unloaded Q values of 7000 to 8000 should be possible in the SPS klystron rf output cavity through design techniques described in a NASA report of work by Dr. G. M. Branch³, in which Q's of about 6500 were obtained in C-band resonant cavities.

DEPRESSED COLLECTOR

Depressed collectors have been studied by various workers over the past twenty years or more^{4,5}. Depressed collector recovery efficiencies as high as 84% have been reported in relatively low power and low to moderate base efficiency microwave linear beam tubes⁶. As tube base efficiency increases, it becomes more and more difficult to realize high collector recovery efficiency, because the spent electron beam of the more efficient tube contains electrons having a wide spread of energy and of both axial and radial velocities. A large population of relatively low energy slow electrons must exist. Collector recovery efficiency in such a case may be greatly improved through use of an electron beam refocusing section between the rf output cavity and the depressed collector entrance. A NASA report describes theoretical work by Branch and Neugebauer⁷ on electron beam refocusing. The refocusing section reduces the spread in electron radial velocities and preprocesses the beam for entry into the depressed collector region at suitable angles with respect to the axis so that more effective electron sorting may be achieved.



CIRCUIT EFFICIENCY VS OUTPUT CAVITY TEMPERATURE

FIGURE 4

Depressed collectors have taken various forms in the past. Probably the most successful to date is the Kosmahl design^{5,6}, known as the "Depressed Electrostatic Collector". Figure 5 is an example of a multistage depressed electrostatic collector. The illustration is intended only for purposes of explanation. The rf output cavity (not shown) would be on axis at the bottom of the drawing, and the spent electron beam would enter the electron beam refocusing section here and proceed upwards.

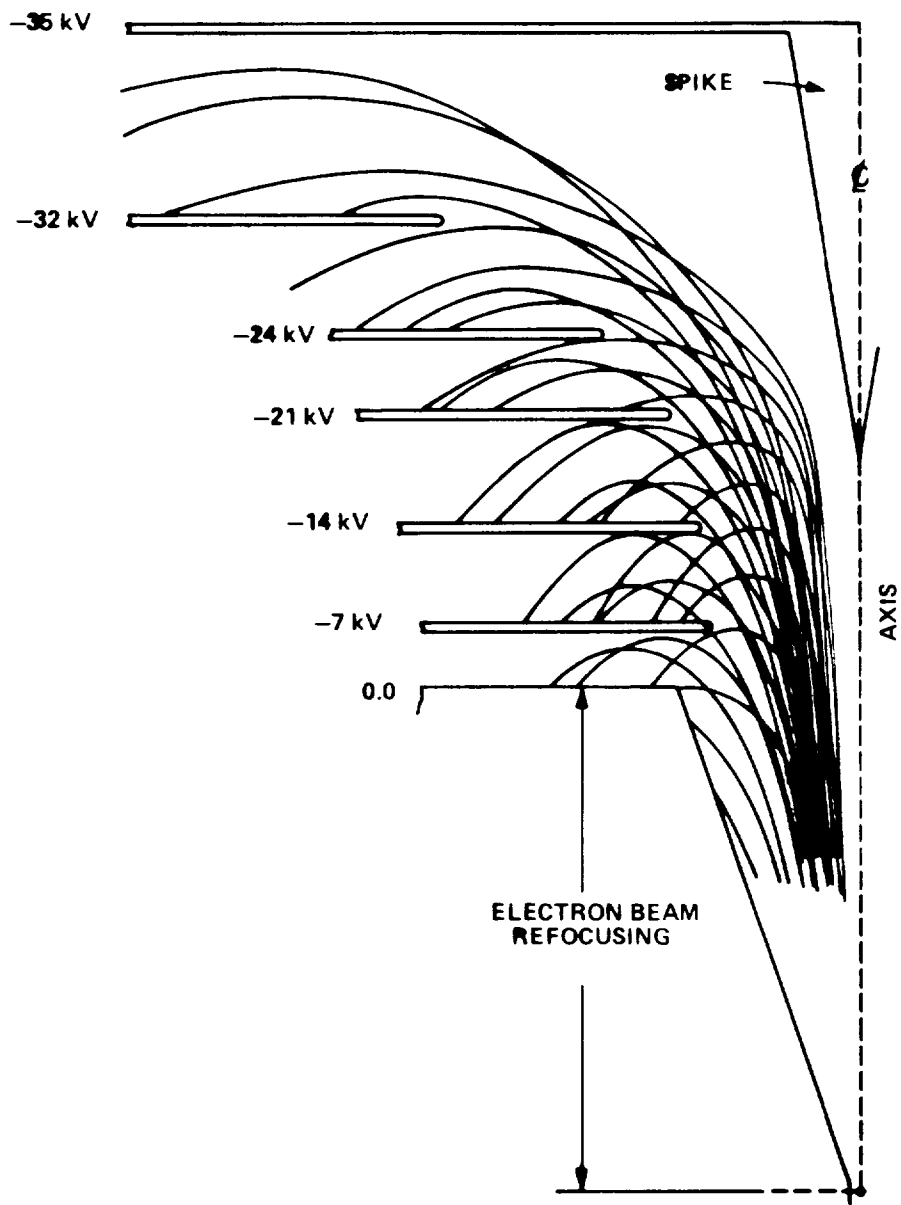
The main magnetic electron beam focusing field collapses suddenly along the axis, and all electrons in the beam experience an increase in radial velocity upon entering the refocusing section. A relatively small auxiliary magnetic focusing field is used in the refocusing section to form a magnetic "plateau". The electron beam expands, develops reduced and more nearly uniform radial velocity, and enters the main collector at angles suitable for electron sorting and collection.

Upon entering the main collector the electron beam comes within the influence of a dispersing spike at cathode potential. The beam is collected for the most part on the backs of the collecting plates, the sides away from the direction of the entering beam. The plates are biased at suitable voltages, and the collector current from each is returned to the respective power supply.

None of the details of a design for an SPS klystron depressed electrostatic collector have been worked out. Such a design will require computer analytical work and experiment. Depressed collector test models must follow design work on the basic klystron.

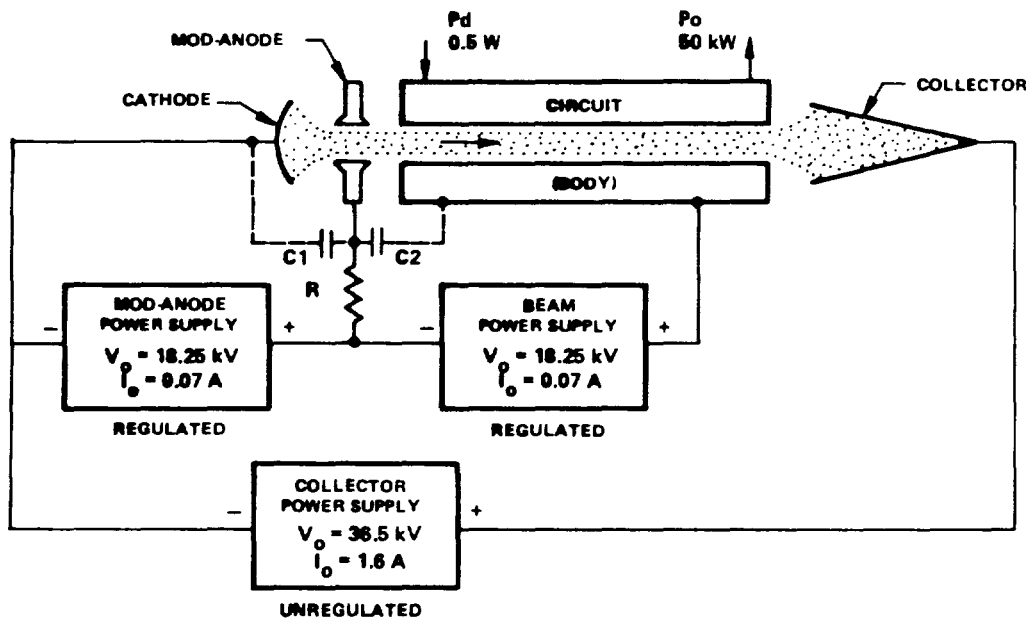
THE MOD-ANODE

The modulating anode (mod-anode) is widely used in high power klystron electron gun design. This feature offers several advantages for the SPS klystron. Figure 6 illustrates a typical mod-anode arrangement, simplified for purposes of explanation. In this case the 50 kW power output klystron employs a 0.25 micropervance electron beam operating at 36.5 kV and 1.67 amperes. The mod-anode operates at half the full beam voltage and controls the level of beam current injected into the rf circuit. Post acceleration raises the electron beam to full voltage. The mod-anode is a nonintercepting electrode. It controls beam current without intercepting beam current. Body current in this example is 0.07 amperes. The mod-anode and



**EXAMPLE OF MULTISTAGE
DEPRESSED ELECTROSTATIC COLLECTOR**

FIGURE 5



SIMPLIFIED DIAGRAM ILLUSTRATING THE KLYSTRON MOD-ANODE

FIGURE 6

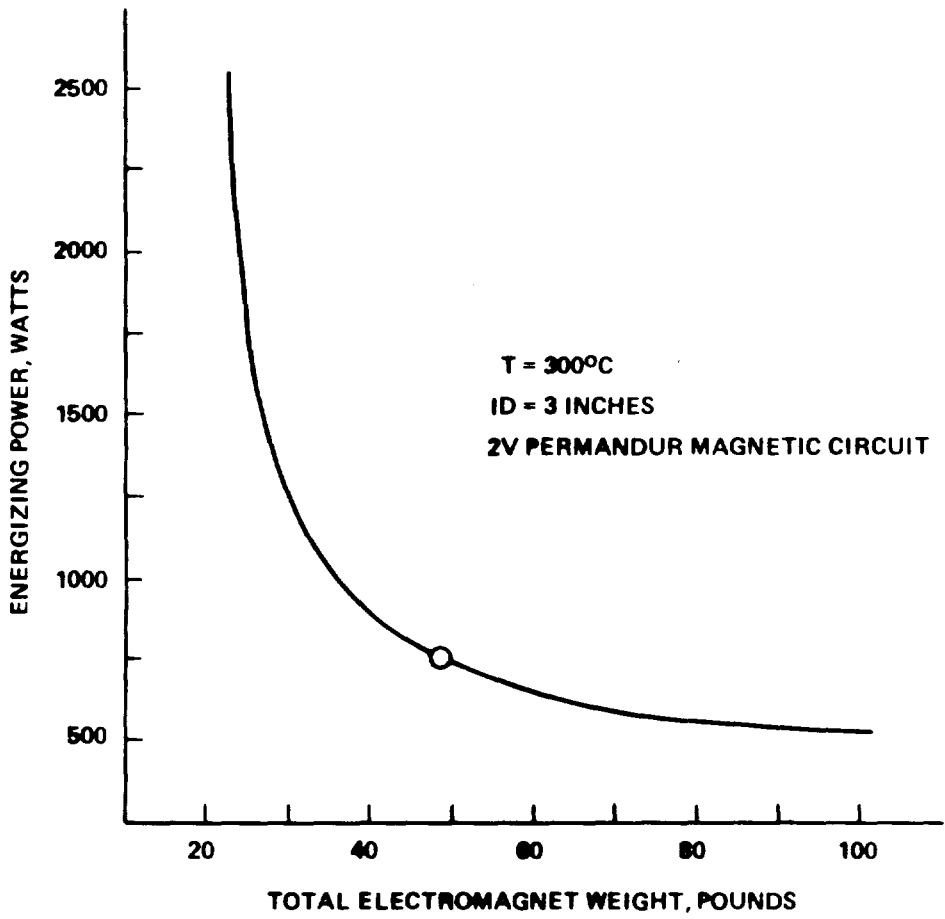
beam power supplies furnish this current. These power supplies are well-regulated to insure good phase stability on a short term basis from klystron input to output. The collector power supply furnishes 1.6 amperes of beam current. This power supply need not be so well regulated.

One of the advantages of mod-anode is that the electrode divides the total beam voltage, thereby reducing the voltage appearing between any two adjacent electrodes. A second advantage rests in the control of beam current, and therefore of power output. Still a third advantage relates to occasional arcing in the cathode to mod-anode region, a possibility in any new klystron. Since the mod-anode does not intercept electron beam current, it may be isolated from the mod-anode and beam power supplies by a relatively large impedance. A resistance is shown in the illustration, though some combination of resistance and inductance may prove to be superior with the SPS klystron. Now, should an arc occur between cathode and mod-anode, the capacitance C1 discharges through the arc, and the fault then quickly clears. The effect on klystron performance is a very brief interruption of beam current and power output and prompt resumption of normal operation in a very short time. Such occasional arcing and brief temporary interruption of normal klystron operation is observed with many new high power klystrons equipped with mod-anode electron guns.

ELECTROMAGNET

The use of a low microperveance electron beam means use of a high voltage low current beam, a circumstance that tends to reduce magnetic focusing field requirements. A major impact on electromagnet size, weight, and power may be effected through reduction of the inside diameter to the minimum. Figure 7 illustrates calculations made for the minimum electromagnet ID presently viewed as possible for the new 52 kW SPS klystron described in Table 1. The optimum design is in the region of the knee of the curve. The circled point, for example, represents a 49 pound electromagnet requiring 750 watts to provide an 875 Gauss magnetic field, two and one-half times theoretical Brillouin.

The hypothetical design operates at a maximum temperature of 300°C and includes allowance for heat pipe cooling structures. Weight of the magnetic poles and return path is kept relatively low through use of 2V-Permandur for this circuit. This material is an iron-vanadium-cobalt alloy having a



SPS KLYSTRON ELECTROMAGNET: ESTIMATED WEIGHT VS POWER TRADE-OFF

FIGURE 7

magnetic working level of 22,000 Gauss and a Curie point of 980°C. The high magnetic working level means that small magnetic cross-sections are satisfactory in the magnetic polepieces and return path. The high Curie point implies excellent magnetic stability at lower operating temperatures.

The 3 inch minimum ID of the electromagnet will require that the unit be assembled as an integral part of each klystron, at least in early sealed off versions of the tube. There is a distinct possibility that electro-magnetic-derived beam focusing will be necessary only over the rf output end of the klystron, with permanent magnet focusing (using samarium-cobalt magnets) being employed with the first few cavities. Electromagnetic power and weight may be halved by this technique. The possibility should be explored during SPS klystron development.

KLYSTRON NOISE

Klystron noise power output is viewed as stemming from shot noise in the electron beam. This noise "signal" appears at the input resonant cavity interaction gap, like any rf drive signal, modulates the carrier, and is amplified by the klystron. In the SPS klystron the circuit bandwidth is quite narrow, and noise output is confined to small low level sidebands close to the carrier.

Figure 8 shows the results of a computation of klystron noise power spectral density for a 50 kW power output 50 dB gain SPS klystron. The rf drive signal is assumed to be monochromatic and free of noise. The data includes both AM and FM noise contributions expressed in dBW/Hz.

Klystron noise power output measurements are typically made relatively close to the carrier through a technique described in an IEEE MTT article by Klaus H. Sann.⁸ An outstanding feature of the technique is cancellation of the carrier by means of microwave circuitry, thus permitting close to carrier noise measurements.

The SPS klystron per se will likely be very "quiet" compared to the rf drive signal applied to the klystron input. Computed klystron and amplified oscillator-driver noise powers are shown in Figure 9. A logarithmic abscissa is used better to show close-to-carrier noise. The possible noise power spectral densities for three oscillator-drivers are illustrated. The data shows only an equivalent FM noise deviation for each case. AM noise contributions are relatively much smaller.

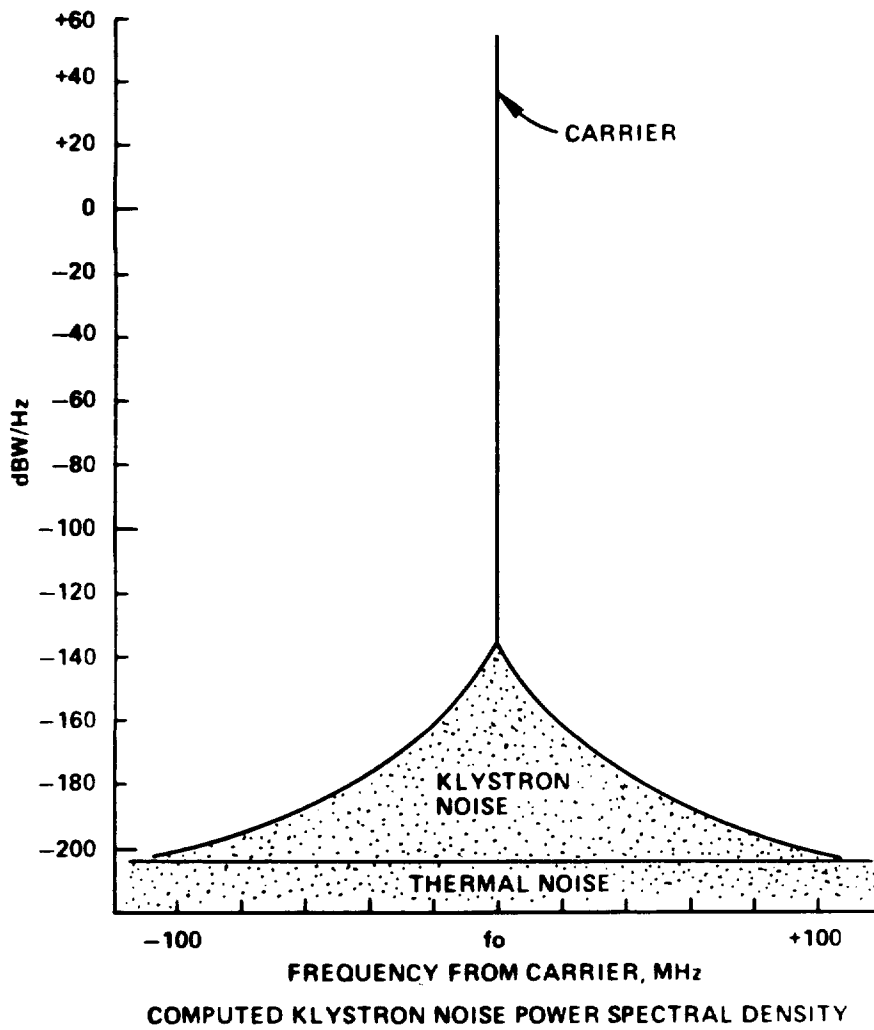
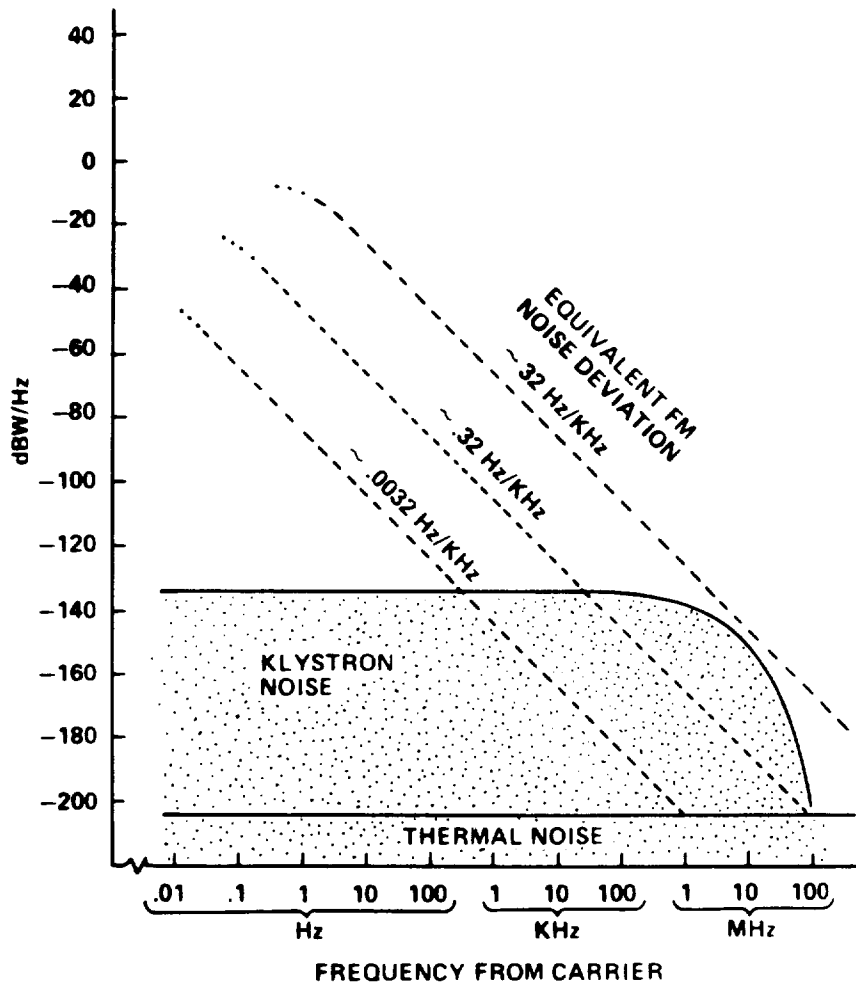


FIGURE 8



COMPUTED NOISE POWER SPECTRAL DENSITY FOR KLYSTRON AND FOR THREE OSCILLATOR DRIVERS

FIGURE 9

KLYSTRON HARMONICS

The second harmonic of the SPS klystron should be close to 30 dB or more down from fundamental klystron power output. Higher order harmonics may be somewhat further down, though little experimental verification is at hand. Harmonic measurements are difficult because of the many possible modes of propagation. The subject has been studied by many workers over the years ^{9,10}.

Klystron harmonic levels may require external attenuation in the SPS installation. Three practicable types of high power filters may be considered; the leaky wall waveguide, lossy "tee", and reactive stub array. An estimated attenuation of these filters to second through sixth harmonics is shown in Table 2. The leaky wall waveguide and reactive stub array have less and less effect as order of harmonic increases, because attenuation with these filters is active at or close to the waveguide walls. The lossy "tee", on the other hand, is more effective as order of harmonic increases, though attenuation of the lower order harmonics is less. Since the leaky wall waveguide filter is large and bulky, some combination of simpler lossy "tee" and reactive stub array seems indicated.

Table 2
Estimated Attenuation of Harmonic Filters

<u>Harmonic</u>	<u>3 ft Lossy Leaky Wall</u>	<u>Lossy "Tee"</u>	<u>Reactive Stub Array</u>
2nd	60 dB	8 dB	40 dB
3rd	40 dB	10 dB	30 dB
4th	15 dB	12 dB	20 dB
5th	10 dB	14 dB	10 dB
6th	5 dB	16 dB	5 dB

KLYSTRON COOLING

Table 3 outlines an estimate of klystron cooling requirements for the 52 kW power output klystron of Table 1. To sum up; approximately 3.5 kW of waste power from the klystron body must be dissipated at a maximum tube element temperature of 300°C or thereabouts; approximately 7 kW of waste

power from the collector plates may be dissipated at a maximum tube element temperature of 600°C or higher.

Table 3
Estimate of Klystron Cooling Requirements
(Po = 52 kW, Ko = 0.3 μP)

<u>Klystron Element</u>	<u>Power, Watts</u>	<u>Maximum Temperature</u>
Heater	100	
Electromagnet	750	
RF Driver Cavities	887	
RF Output Cavity	1758	
	Subtotal	
	3495	< 300°C
Collector Plates	6938	> 600°C
	Total	
	10433	

The collector plates in this case are designed to handle only the waste power remaining in the spent electron beam after microwave amplification. With loss of rf drive power, the electron beam must be turned off at once. The mod-anode may be used as a control electrode for the purpose.

Since radiative cooling must be used for dissipation, heat must be conducted from tube elements to suitable radiators. At the present time, the most likely method for achieving this appears to be through use of heat pipe systems.

TUBE LIFE

The desired life of the microwave tube device to be used in the SPS system is 30 years or more. Life histories of most microwave tubes fall far short of this figure. One high power klystron, the Varian VA-842, has shown potential for a comparable operating life. The VA-842 is a 75 kW average power output and 1.25 MW peak power output pulsed UHF klystron. The

operating pulse width is 2.0 milliseconds. The electron gun design includes a mod-anode. Cathode emission density and operating temperature are moderate.

Table 4 shows data extracted from the USAF "Electron Inventory Report" of 30 June 1979. Four VA-842 klystrons, all still running, have accumulated operational life figures of from about 14.1 to 16.5 years. Three other long-lived tubes are listed as failing after approximately 11.1 to 13.8 years.

Table 4
VA-842 Klystron Life Data

Long-Lived VA-842 Klystrons

<u>S/N</u>	<u>Status</u>	<u>Hours</u>	<u>Years</u>
408	Still Running	144,883	16.5
393	Still Running	139,993	16.0
374	Still Running	133,469	15.2
511	Still Running	123,384	14.1
317	Failed 12/75	121,303	13.8
332	Failed 8/76	108,777	12.4
505	Failed 12/74	102,259	11.7

Calculated MTBF (68 tubes) = 37,748 hours

Data from USAF "Electron Inventory Report", 30 June 1979

The calculated mean time before failure (MTBF) for 68 VA-842 klystron failures in use during the period 1964 to 1979 is 37,748 hours.

One key to long klystron life appears to be low cathode emission density and moderate operating temperature. Use of a heated cathode is not a deterrent to long life. Heater problems with VA-842 klystrons have been insignificant.

CONCLUSIONS

Starting with the Varian VA-7773 klystron, state-of-the-art computations indicate that the basic efficiency may be improved by a few percentage points from 74% to possibly as high as 79% by lowering the electron beam microperveance to a value in the range of 0.2 to 0.35 micropervs, where the optimum product of electronic times circuit efficiency may be obtained. While improvement over known VKS-7773 performance would be modest, the relative importance of each percentage point in operating efficiency may justify the effort.

With a minimum acceptable microwave device efficiency of 85%, the additional efficiency points may possibly be realized through collector depression and recovery of energy from the spent electron beam. The achievement of 85% total efficiency will be a formidable task, yet the efforts of several workers^{4,5,6,7} suggest that sufficient energy may be recovered by this means. If the many advantages of the klystron are to be applied, the importance of each point in efficiency would seem to require the investigation of collector depression.

Table 5 summarizes the advantages of the high efficiency klystron cw amplifier for space applications.

Table 5
Advantages of High Efficiency Klystron CW Amplifier
for Space Applications

1. High Gain Amplifier, 40 to 50 dB
2. High Power Output, 50 kW or more
3. High Efficiency, ~85% with collector depression
4. Low Noise Output Narrow bandwidth klystron
5. Low Harmonic Output Typically -30 dB or more from carrier
6. Long Life Potential ~16.5 years on record with one klystron type
7. Ease of Control and Protection with Mod-Anode Electron Gun Design

BIBLIOGRAPHY

Efficiency

1. Erling L. Lien, "High-Efficiency Klystron Amplifiers", Publication of Eighth International Conference on Microwaves and Optical Generation and Amplification, pp 11-21 to 11-27, September 1970.
2. Kosmahl and Albers, "Three-Dimensional Evaluation of Energy Extraction in Output Cavities of Klystron Amplifiers", IEEE Transactions on Electron Devices, Vol. ED-20, No. 10, October 1973.
3. Dr. G. M. Branch, "Circuit Efficiency Enhancement Studies at 12 GHz", NASA Lewis Research Center Contract NAS3-11533, May 29, 1970.

Depressed Collector

4. A. Saharian, "Multisegment Depressed-Collector for High Power Klystrons," MIT Lincoln Laboratory, Air Force Contract AF 19(628)-500 (ARPA Order 85), June 16, 1964.
5. Neugebauer and Mihran, "Multistage Depressed Electrostatic Collector for Magnetically Focused Space Borne Klystrons", NASA Lewis Research Center Contract NAS3-11532, Sept. 14, 1970.
6. Koshahl and Ramins, "An 82 to 84 Percent Efficient, Small Size, 2 and 4 Stage Depressed Collector for Octave Bandwidth High Performance TWTs," NASA Lewis Research Center Technical Memoranda NASA TM X-73572, December 6, 1976.
7. Branch and Heugebauer, "Refocusing of the Spent Axisymmetric Beam in Klystron Tubes", NASA Lewis Research Center Contract NAS3-8999, June 30, 1972.

Noise Measurements

8. Klaus H. Sann, "The Measurement of Near-Carrier Noise in Microwave Amplifiers", IEEE Transactions on Microwave Theory and Techniques, Vol. MTT-16, No. 9, September 1968.

Harmonic Measurements

9. Forrer and Tomiyasu, "Effects and Measurements of Harmonics in High Power Waveguide Systems", IRE National Convention Record, pt 1, pp 263-269, 1957.
10. J. J. Taub, "A New Technique for Multimode Power Measurement", IRE Transactions on Microwave Theory and Techniques, Vol. MTT-7, pp 469-502, November 1962.

ANALYTIC INVESTIGATION OF EFFICIENCY AND PERFORMANCE
LIMITS IN KLYSTRON AMPLIFIERS USING MULTIDIMENSIONAL
COMPUTER PROGRAMS; MULTI-STAGE DEPRESSED COLLECTORS; AND
THERMIONIC CATHODE LIFE STUDIES.

by

H. G. Kosmahl
NASA Lewis Research Center

Introduction

In 1972 this author together with L.U. Albers performed an extensive parametric investigation of the extraction of energy in output gaps of klystron amplifiers, using our own 3-D computer programs. Due to complexity of the program which used a hydrodynamic, axially and radially deformable disk-ring model and the resulting long computing time we limited our investigation, Ref. 1, to the output gap, by far the most important and difficult part of the klystron interaction. As inputs best results from independent studies at G.E. by T. Mihran, Ref. 2 and at Varian, Ref. 3, by E. Lien were used to initiate the starting conditions for the electrons and the RF voltage using our program. Although this method of computation is less exact than processing the entire klystron interaction in 3-Dimensions we verified that, for a confined flow focused beam throughout the penultimate cavity, radial velocities remain very small and the beam is highly laminar. It was, therefore, concluded that possible errors resulting from treating only the output cavity in 3-D would remain small.

Discussion of Results

We proceed now with the discussion of the computer results. Figure 1 shows the cross-section of the ring model used in computations and the degree of complexity and care applied to compute accurately the radial and axial deformation of the rings and the space charge forces. The price paid for this effort - the computing time - was felt to be justified for the one time verification. Figure 2 shows typical axial and radial space charge functions. In agreement with basic theory the radial functions obey Gauss' law inside the beam and the axial space charge force is zero at the tunnel wall $r=a$.

Efficiency

Let us now turn to the discussion of computed efficiencies. Figure 3 shows a plot of efficiency versus $\beta_e a$ for two bunching levels, $i_1 = 1.81 I_0$ and $i_1 = 1.64 I_0$, $B = 2.5 X B_{BR}$, and 0.5μ perveance. The voltage swings α are 1.10, 1.05, and 1.0, respectively. The $1.81 I_0$ bunching is characterized by a very compact bunch with a small velocity spread and absence of a typical antibunch disk since the maximum velocity past the output gap is only $1.14 u_0$. As can be seen from the plots, the efficiency seems to decrease linearly with increasing $\beta_e a$ with a slope of approximately 2.5 percent points efficiency loss for each 0.1 radian increase in $\beta_e a$. Note that b/a , β_e , and 2.1 were held constant and only a was permitted to increase. Thus at large $\beta_e a$ values the aspect ratio b/a is

small; the RF fields penetrate deeper into the tunnels than in cases of narrow tunnels. We observed that many disks were caught in the long fringes and experienced a post-acceleration when the RF field reverses its phase. This phase reversal is also responsible for the increase in current interception that is marked in percentage points, since the radial RF fields action changes from converging into diverging. Computations at $\beta_e a > 1$ were not continued due to a rapid increase in interception to impractical levels.

The above finding of increasing η with decreasing $\beta_e a$ is confirmed by a number of new experimental results in high-efficiency klystrons and TWT designs, mainly at Varian (3), but it seems to disagree with the estimates of Mihran (4), and the very early finding by Cutler (5). It should be remembered that Mihran's conclusions were based on the behavior of rigid disks and did not treat the energy extraction, while Cutler's experiments with helical structures cannot be considered representative of a solid wall tunnel and a discrete gap with regard to RF and space-charge fields. The author knows that the constant bunching level assumed for computing the straight lines of Figure 3 cannot be strictly realized in practical designs. The value $\beta_e a = 0.5$ is probably as small as can be realized at high frequencies and further decrease in $\beta_e a$ would only increase the demands upon the focusing fields to excessive levels.

A physical explanation for the behavior presented in Figure 3 was recently found by researchers at Varian, notably E. Lien, who showed that a favorable conversion of second harmonic bunching into fundamental bunching takes place at small values $\beta_e a$.

Another important selection criteria for high efficiency designs is the choice of perveance which, in turn, is a measure of space charge forces in the beam. Large space charge increases the degree of the velocity spread in beams of all tube types and also decreases the efficiency of depressed collectors. If we again assume constant bunching, then Figure 4 demonstrates clearly the destructive effects of increasing perveance on the electronic efficiency of the output gap. Note also the increase of interceptions. On the other hand, to achieve high overall efficiency, the circuit efficiency, η_{K} must be as high as possible which requires larger values of perveances. Thus, a compromise is required. This author suggested a value around 0.25 μ perv. as most reasonable selection.

Still another selection must be made concerning the length of the output gap. The results are plotted in Figure 5 with θ_0 , the output gap length in radius, as parameter and the output voltage α_{out} as abscissa. Fortunately, within a range of $\theta_0 = 20^\circ$ to 40° , η remains insensitive to gap length.

Parametric Optimization of the Output Gap Performance

If one assumes, as we did throughout this paper, that the quality and magnitude of the bunching used in this study was very close to a practical optimum, then it should be possible to perform a parametric computer optimization of the electronic klystron efficiency. Note that the value of $l_1/I_0 = 1.81$ obtained by E. Lien is close to the theoretical limit $l_1/I_0 = 2$ and that this design resulted in a very compact bunch and absence of a typical antibunch disk since

the maximum velocity past the output gap was only $1.14u_0$. With this justification we proceed to discuss Figure 6 which is the most important result of this study.

Figure 6 is a summary of some of our computations executed for disk distribution and klystron design parameters as supplied by Mihran from General Electric and Lien from Varian. Our results are plotted with solid and dotted lines as η versus phase. Available for comparison were results published by Mihran et al. (2) and by Varian (3), both with one-dimensional programs. The top circle indicates an 83 percent value as computed by Lien (3), (and private communication) who measured 75 percent with 2 percent RF interception and the triangle, an 82 percent value as computed by Mihran et al. (2) Note that both investigators used almost identical bunching levels with, however, different $\beta_e a$ values of 0.485 and 0.75, respectively. Disregarding at first interception (which cannot be computed with one-dimensional models) it is seen from Figure 6 that Lien's number is about 3 percent and Mihran's about 10 percent points higher than our result (which indicates 6 percent current interception at $\eta = 0.806$). The strong dependence of η on $\beta_e a$ is evident. A more sensible evaluation is possible if not only measured and computed efficiencies but also interceptions are compared. Turning now to Table 1 which summarizes measured (by Lien) and computed (author's program) results, excellent agreement in efficiencies is evident. At $\alpha = 1.08$ the agreement in interception is also very good and becomes less good with decreasing α where measurements indicate some residual interception while our program indicates none.

It is believed that this difference is more due to the "nonideal" features of tubes than to program errors. Also, the level of interception in Lien's klystron was very small to begin with.

A comparison between Mihran's measurements of $\eta = 0.62$ with our computations was not possible because Mihran's measurements were carried out at a perveance of 0.72×10^{-6} instead of 0.5×10^{-6} and disk distribution for the higher perveance was not available.

In computing the above cases the correct field distribution between the tunnel tips, as discussed in Ref. 6, was used. The detail is illustrated in Figure 7, case (C) where the ratio of the E_z field at the tunnel tips to that in a middle of the gap at $r=a$ was approximately 2.5. Using the correct, actual field and not the uniform one is important for the trajectories of slow electrons moving close to $r=a$.

Conclusions

A very accurate mathematical model and computer program for the computation of electronic interaction, electron trajectories, interceptions, and efficiency was developed for the output cavity of a klystron amplifier. It is concluded that one-dimensional programs yield efficiencies that are approximately 10 percent points too high at η levels > 0.7 . It has been confirmed that $\eta \approx 0.75$, with a few percent interception, is possible and that $\eta \approx 0.8$ could be obtained with 6 percent "ideal" interception. With the augmentation by a novel depressed collector, overall efficiencies of 80-85 percent seem possible. A very important conclusion is the result that η increases linearly with decreasing $\beta_e a$, at least in the range $0.4 < \beta_e a < 1.0$. Another important conclusion is that efficiency increases initially with interceptions. At $\eta > 0.7$ transverse velocities of many rings are comparable to axial components and exit angles up to 30° were observed.

Multi-Stage Depressed Collectors

The combination of LeRC developed Multi-Stage Depressed Collectors (MDC) and Spent Beam Refocusing Schemes has led to demonstration of highest collector and overall efficiency when applied to TWT's with moderate electronic efficiencies ($\eta_e < 25\%$), Ref. 7. MDC efficiencies in excess of 97% were measured on dc beams of medium perveance ($0.5 \mu \text{ perv}$) and more than 85% MDC efficiency on spent beams with 20% electronic efficiency. This author developed simple relations for predicting the MDC and the overall efficiency, η_{ov} , for TWT's in Ref. (8):

$$\eta_{col} = \eta_{DC} \left[1 - \frac{1}{N-1} \frac{f(\mu \text{ perv}) \sqrt[3]{\eta_e \cdot \mu \text{ perv}}}{2 - f(\mu \text{ perv}) \cdot \sqrt[3]{\eta_e \cdot \mu \text{ perv}}} \right]. \quad (1)$$

$$\eta_{ov} = \frac{\eta_{ck} \cdot \eta_e}{1 - \eta_{col} + \eta_{col} \left(\eta_e + \frac{P_{INT}}{P_o} \right) + \frac{P_{SOL}}{P_o}} \quad (2)$$

(Pint, Psol designate, respectively, the intercepted and solenoid power).

These relations may be derived, Ref. (8), from a more basic relation derived by this author, also in Ref. (8), for the smallest (normalized) energy of an electron in the spent beam of a helical TWT:

$$\frac{V_{min}}{V_o} = 1 - f(\mu \text{ perv}) \cdot \sqrt[3]{\eta_e \cdot \mu \text{ perv}} \quad (3)$$

The factor $f(\mu \text{ perv})$ is a simple function of the perveance ranging from $f(0) = 1.26$ to $f(2) = 0.8$ for helical TWT's. It assumes different (from those quoted above) but as yet unknown values for coupled cavity TWT's and klystrons. Relation (3) holds also below saturation and does not contain any small signal quantities. Were $f(\mu \text{ perv})$ known for klystrons it could be then applied to eqs. (1) and (2).

During the earlier days of our collector work at LeRC we did some collector work in conjunction with klystrons of microperv .75 at C-Band and 0.5 at Ku band and $\eta_e \approx 40\%$. Highest then achieved collector efficiencies were approximately 65% resulting in overall efficiencies of about only 50% due to interception and poor circuit efficiencies (less than 90%). A klystron with 80% electronic efficiency has a very unfavorable velocity spread that will make the design of a MDC even more difficult because of the presence of majority of rings at the output whose velocities are $< 0.2 u_o$. This author doubts that a MDC efficiency of more than 50% could be practically realized. This

fact plus the presence of interception, circuit losses ($\eta_{ck} \approx 0.95$), the solenoid power and a complex power supply are likely to limit the effective RF output efficiency to below 85%.

Cathodes

Cathode performance and cathode life are the main limiting factors to the reliability and long life of microwave amplifiers. The Microwave Amplifier Group at LeRC was and is, for this reason, engaged and committed to testing and analyzing high performance impregnated tungsten matrix cathodes since 1971. Figure A shows the results of long life tests, carried out in real tubes at a density of $2A/cm^2$ on a large number of samples. At $2A/cm^2$ the standard Philips B-cathode has a useful life of about 40,000 hours. The M cathode, the most promising and interesting of the matrix type cathodes, is expected to perform for 8-10 years at $2A/cm^2$ judging from the recorded performance to date. Since the SPS klystron would require a cathode loading density of only 1 or less A/cm^2 , commensurate with a true cathode temperature of about $980^\circ C$, an educated guess would lead us to an estimated life of perhaps 20 years. Actual test results of this duration are, of course, not available at all and great caution must be exercised in making predictions for system life exceeding 15 years.

References

1. H.G. Kosmahl and L.U. Albers: " Three-Dimensional Evaluation of Energy Extraction in Output Cavities of Klystron Amplifiers. IEEE - TRANS on E.D., Vol. ED-20, No. 10, October 1973, pp. 883-890.
2. T.G. Mihran, G.M. Branch, and G.J. Griffin, "Design and Demonstration of a klystron with 62 percent efficiency," IEEE TRANS on E.D., Vol. ED-18, pp. 124-133, Feb. 1971.
3. E. Lien, " High Efficiency Klystron Amplifier," presented at the 8th Int. Conf. Microwave and Optical Generation and Amplification, Amsterdam, The Netherlands, Sept. 1970.
4. T.G. Mihran, "The Effect of Drift Length, Beam Radius and Perveance on Klystron Power Conversion Efficiency." IEEE Trans. on E.D., Vol. ED-14, pp. 201-206, April 1967.
5. C. C. Cutler, "The Nature of Power Saturation in Traveling Wave Tubes," Bell System Tech. Journal, Vol. 35, pp. 841-876, July 1956.
6. H. G. Kosmahl and G.M. Branch. "Generalized Representation of Electric Fields in Interaction Gaps in Klystrons and Traveling Wave Amplifiers." IEEE Trans. E.D., Vol. ED-20, pp. 621-629, July 1973.
7. IEEE - Transactions on E.D., Vol. ED-26, October 1979, pp. 1589-1598 and 1662 - 1664
8. H.G. Kosmahl, "How to Quickly Predict the Overall TWT and the Multistage Depressed Collector Efficiency." IEEE Trans. on E.D. Vol. ED-27, March 1979

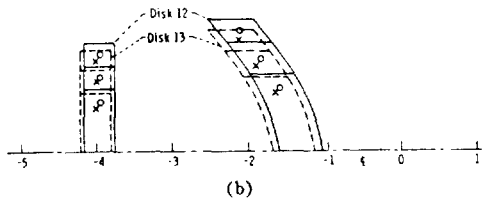


Fig. 1. (a) Effect of source ring on reference ring. (b) Typical overlapping and deformation of disks 12 and 13. Crosses and circles indicate centers of rings. Position -4 is prior and position -2 past the output gap.

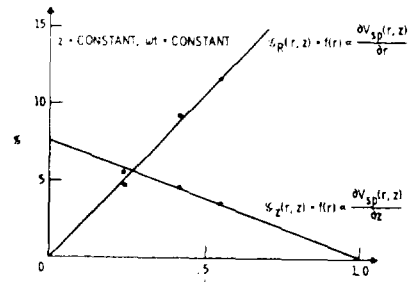


Fig. 2. Typical axial and radial space-charge functions of the beam in the output gap.

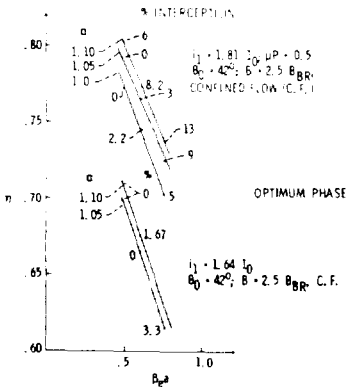


Fig. 3. Efficiency versus $\beta_e a$ with voltage swing α_0 as parameter. Current interception is listed in percent points.

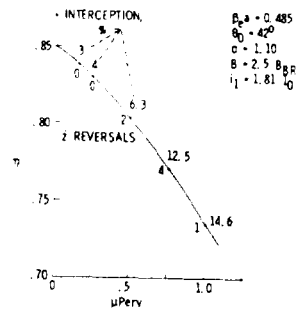


Fig. 4. Efficiency versus perveance assuming constant bunching level. Interceptions and velocity reversals are listed at computed points.

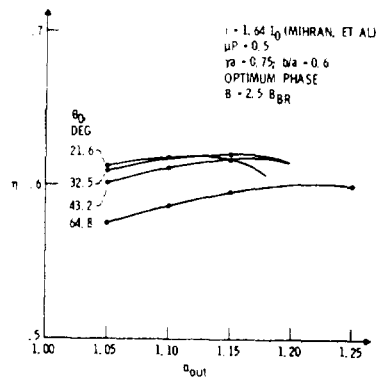


Fig. 5. Efficiency versus output voltage $\alpha = \delta/\epsilon_0$ with output gap angle θ_0 as parameter, phase adjusted for highest efficiency.

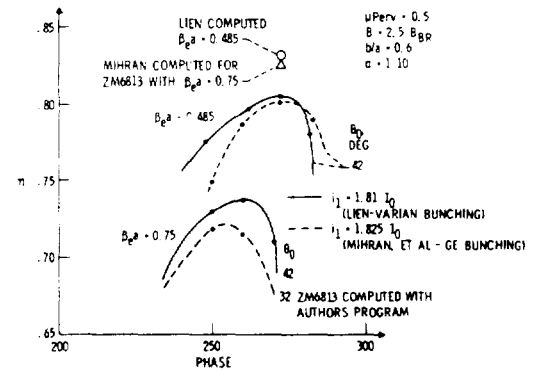


Fig. 6. Internal conversion efficiency computed with authors program for General Electric and Varian high-efficiency designs.

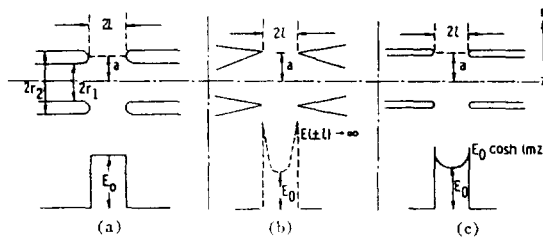


Fig. 7. Electric fields for three differently shaped tunnel tips. (a) Constant field ($E_0 = \text{constant at } r = a$); blunt tips and relatively

TABLE I
COMPARISON BETWEEN MEASURED EFFICIENCIES AND INTERCEPTIONS FOR A VARIAN DESIGN
 $I_1 = 1.81 I_0$; $B_e a = 0.485$; $\mu \text{perv} = 0.5$

α	Measured (Lien) percent		Authors' Computed percent	
	η	Interception	η	Interception
1.08	0.751	1.9	0.775	1.5
0.953	0.705	1.6	0.709	0.5
0.603	0.681	1.4	0.679	0

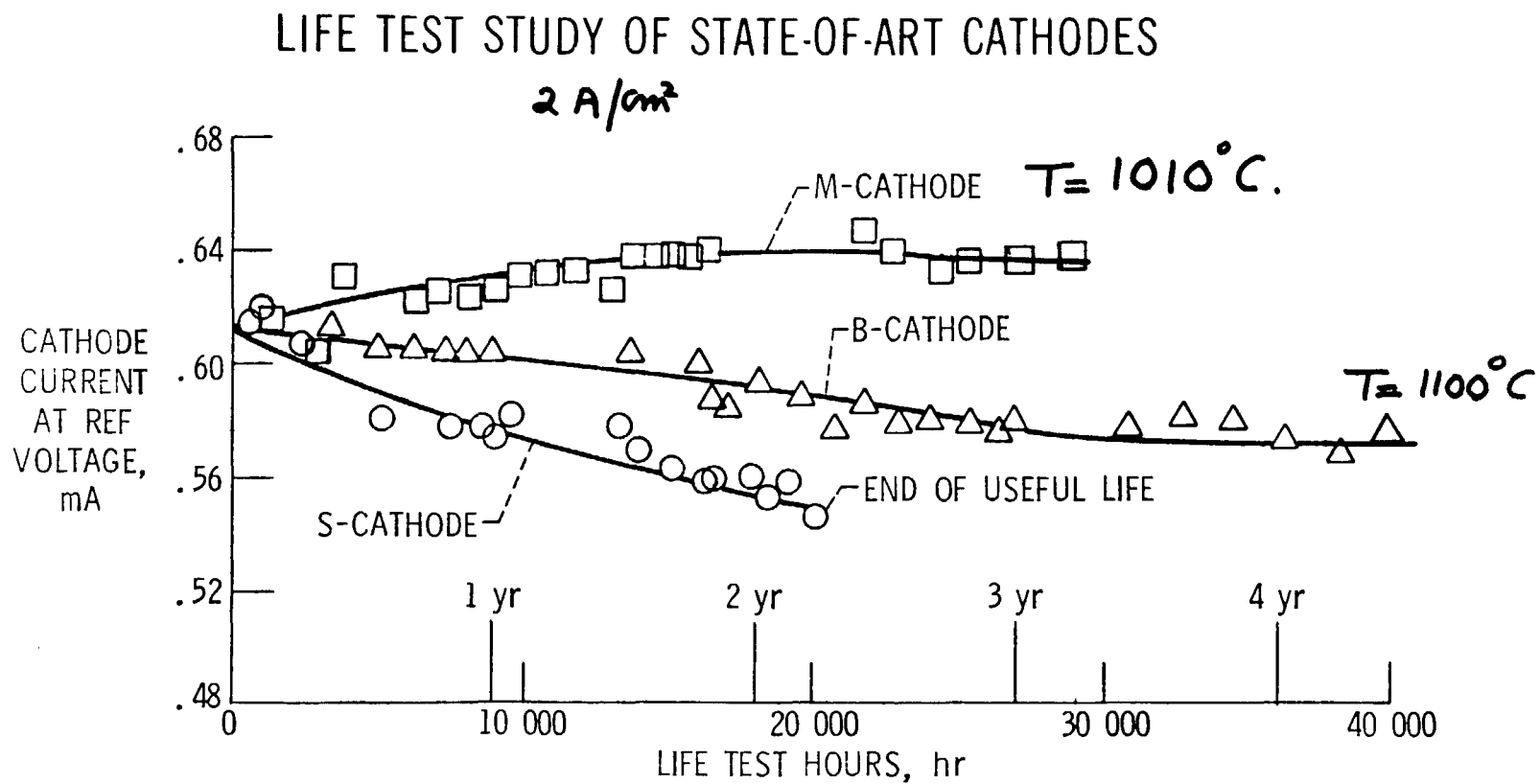


Fig. 8. Life Test Study of State-of-Art Cathodes.

PROGRESS REPORT ON THE ADAPTING OF THE CROSSED-FIELD
DIRECTIONAL AMPLIFIER TO THE REQUIREMENTS OF THE SPS

William C. Brown
Raytheon Company

Presented at the MICROWAVE POWER AMPLIFIER SESSION OF THE SPS MICROWAVE SYSTEMS WORKSHOP
January 15-13, 1980, Lyndon B. Johnson Space Center, Houston, Texas

ABSTRACT

Progress in adapting the crossed-field directional amplifier to the SPS is reviewed with special emphasis upon (1) recent developments in controlling the phase and amplitude of the microwave power output, (2) a perceived architecture for its placement in the subarray, and (3) recent developments in the critical pivotal areas of noise, potential cathode life, and efficiency.

Introduction and Background

The first proposed use of the crossed-field directional amplifier in the solar power satellite dates back to 1969 and 1970.¹ Since then there have been a number of successive discoveries and developments resulting in an ever-increasing better fit between the device and the severe requirements that are imposed upon the generator by the SPS.

First proposed by the author in the form of a 200 to 400 kW liquid cooled amplatron¹, the crossed-field device approach was soon changed to a passively cooled amplatron in the power range of five to ten kW because of the high desirability of passive cooling in the SPS satellite as pointed out by O.E. Maynard.² Such a tube was designed and the first phase of its development completed.³

In 1975 R.M. Dickinson of JPL proposed that because of its high efficiency, simplicity, relatively low mass, and already established high production volume and low cost, the microwave oven magnetron be incorporated into a directional amplifier package and considered for the SPS. While subsequently investigating this approach the author made two important discoveries: the first, that the microwave oven magnetron, when operated with a ripple-free DC power source and with no externally applied filament power, has an extremely high signal to noise ratio⁴; the second, that under these conditions the carburized thoriated tungsten cathode can be operated at such low temperatures that a potential life of more than 50 years is indicated under the high-vacuum and highly controlled operating conditions in space.^{5,6}

The potential role of the magnetron directional amplifier in the SPS is now being further evaluated under a NASA-MSFC contract.⁷ This investigation first involves an extension of the laboratory data base on the magnetron directional amplifier utilizing the microwave oven magnetron. This data, when combined with information obtained from other sources, will then make it possible to accurately define the projected characteristics of a higher powered version of the magnetron directional amplifier for SPS use, and to define a program of technology development that would result in the development of such an amplifier.

Because of the basic similarities of the magnetron and amplatron in their construction configurations and performance characteristics it is found that much of the experience gained in adapting the amplatron to SPS use is directly applicable to a similar adaptation

of the magnetron directional amplifier.

The current study involves a penetrating look at all of the interfaces associated with the magnetron directional amplifier. At least one level of higher integration must be examined, and in some instances, more. The study has progressed far enough to yield a specific architecture that is shaped by these interfaces and that appears to have many attractive features.

One of the most important developments of the current activity is the precise control of both the amplitude and phase of the microwave power output from the amplifier by feedback control systems utilizing phase and amplitude references. The method by which amplitude is controlled is of overall SPS system interest in that it can be adapted to match the entire microwave generating system to the solar photovoltaic area at the point of maximum operating efficiency.

The material which follows is intended to provide the reader with: (1) a brief summation of those features of the crossed-field device that are of a desirable nature for the SPS; (2) a comparison of the amplatron and the magnetron directional amplifier for orientation purposes; (3) knowledge of the recently established architecture of the subsection of the subarray into which the amplifier is placed; (4) an introduction to the recently developed method for accurately controlling the phase and the amplitude of the microwave power output; (5) discussions of several very important pivotal areas relating to noise, tube life, and efficiency and (6) a summation of areas of concern needing additional attention.

Features of the Crossed-Field Microwave Generator that are Desirable for the SPS

- High Efficiency: Overall efficiencies in excess of 85% have been demonstrated in an off-the-shelf magnetron used for industrial microwave heating and in certain laboratory models of the amplatron. An efficiency in excess of 80% at power levels (3 kW) low enough to utilize passive cooling has also been obtained.
- High Signal to Noise Ratio: Random noise level in a 1 MHz band down 100 dB or more at frequencies above and below carrier frequency by more than 10 MHz. The noise level may be lower because instrumentation is the limitation.
- Potential Life of 50 Years or More: Such life is possible by operating at low emission current densities that allow the low operating temperatures that have a proven association with extremely long life of carburized thoriated tungsten cathodes.

- Low Ratio of Mass to Microwave Power Output: The current estimate by the author is 0.4 kilograms per kilowatt of microwave power at the tube output. This includes the weight of the passive radiator but not the buck boost coils which are considered a power conditioning function.
- Accurate Control of the Phase and Amplitude of the Microwave Power Output: By use of a set of phase and amplitude references and a set of phase and amplitude sensors the phase can be controlled to within ± 1 degrees and amplitude to within $\pm 3\%$.
- Potential to Perform the Bulk of the System Power Conditioning Requirements: The buck-boost coils necessary for output amplitude control of the magnetron can take on the added function of adjusting the input of the microwave system to operate at the optimum output voltage for the solar array.
- Minimal X-Ray Radiation: The crossed-field tube energy conversion mechanism generates negligible radiation, permitting maintenance functions during operation of the SPS.
- Only One Voltage and Two Terminals Required for Normal Microwave Tube Operation: Auxiliary power is required for a few seconds to heat up the cathode and initiate emission.
- Simplicity of Construction: The crossed-field device, particularly in its magnetron form, is very simple in construction.
- High Degree of Maturation in Production and Cost: Currently, more than two million magnetrons that closely resemble a similar tube for the SPS are manufactured annually for the microwave oven.

Definition of Crossed-Field Directional Amplifiers - Comparison of Amplitron and Magnetron Directional Amplifier

A directional amplifier is defined as a device which passes energy in both directions but which amplifies in only one direction. There are at least three ways, as shown in Figure 1, in which a crossed-field device may be used as a directional amplifier. The first is in a self-contained device called the amplitron.^{8,9} The amplitron is unique among the devices in that it needs no assist from auxiliary devices to obtain its directional amplification. It is a relative broadband device and has a very small phase change from input to output as a function of a change in frequency, magnetic field, or DC current level as compared with other crossed-field directional amplifiers and linear beam tubes, as well. This feature is advantageous in many applications where a high degree of phase stability is needed. The device does have limited gain of about 10 dB. The device is widely used in radar systems.

The second way is the combination of a magnetron oscillator and ferrite circulator which converts the magnetron oscillator into an amplifier with a bandwidth over which gain can be obtained.¹⁰ The bandwidth is dependent upon the level of the drive relative to the level of the power output of the device. Typically, a bandwidth of 15 MHz can be obtained at 2.45 GHz with a gain of 20 dB while 5 MHz is possible with a gain of 30 dB. At these gains and within these bandwidths, the efficiency will remain high and nearly constant. The very high signal-to-noise ratio is independent of bandwidth and gain.

The total range of phase shift within the device as the drive frequency is shifted over this bandwidth is approximately 180°. The center of the frequency range over which amplification occurs is at a frequency dependent upon the operating current level of the tube, the temperature of the tube envelope, and other secondary factors.

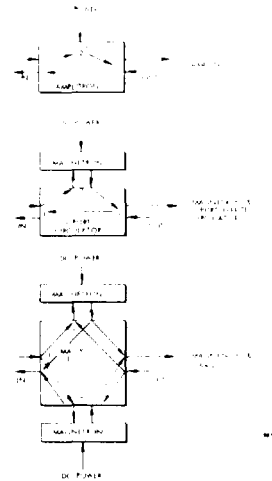


Figure 1. Directional Amplifier Approaches Utilizing Crossed-Field Devices.

As shown in Figure 1, the principle can also be carried out by means of a "magic T" or, synonymously, a 3 dB hybrid, an alternative method originally suggested for the SPS by R.M. Dickinson. A matching of the characteristics of the two tubes is required in the hybrid, but a ferrite circulator is not required.

It should be noted that the operating theory of the directional amplifier is well established.¹⁰ They are often called "reflection amplifiers" or "locked oscillators". The principle is probably more often employed for solid state amplifier devices than for vacuum tubes.

It is important to realize that the magnetron device and the amplitron are very closely related so that development work that is done on one may be directly applicable to the other, as indeed is the case in the SPS. A set of scaling laws and design equations apply equally well to both devices in establishing their power level, voltage and current inputs, efficiency, cathode size, and other basic parameters. Both devices even use the same slow wave circuit, with which the electrons interact. However, the manner in which connections are made to this internal circuit is the basis of distinguishing these devices. As shown in Figure 2, the circuit is made reentrant in the magnetron and one output connection is made to the device, while the internal circuit in the amplitron is cut and the ends of it matched to external transmission lines.

Overall Architecture of the Subarray Employing the Magnetron Directional Amplifier

Physically placing the microwave generator in the subarray and making the proper allowances for its many electrical and mechanical interfaces with other components

and with space itself introduces the perennial systems design problem of making all the parts fit. This problem is currently being worked on as a necessary part of the MSFC study to project the characteristics of the magnetron directional amplifier and to define the technology development program to fully develop the magnetron directional amplifier.⁷

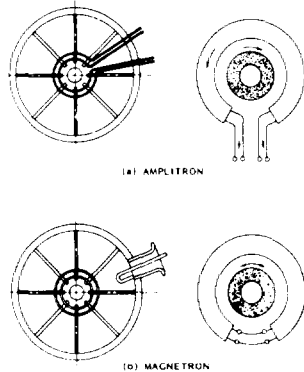


Figure 2. Diagram Illustrating the Basic Differences of Construction and Operation Between the Amplitron and the Magnetron.

It is believed that the development of the subsection shown in Figure 3 represents a substantial advancement toward the ultimate solution of this problem. The design recognizes and solves the following problems:

1. The microwave generators must dispose of their heat directly to space by operating at temperatures in the 200° to 300°C range. On the other hand, solid state devices which may be needed for many purposes cannot reliably operate at temperatures higher than 150°C and lower temperatures are preferable.

The design takes care of this problem by having the generators radiate heat in only one direction. Heat normally radiated toward the face of the array is largely reflected by a thin insulation blanket. There is also a substantial temperature drop across the thin walled waveguide construction. The solid state devices are located either on the face of the slotted waveguide array or in the slots immediately back of the face which are a property of the proposed method for fabrication of the thin-walled slotted waveguides radiators. Such components may be easily attached to heat radiating sinks on the front surface, if need be.

2. Phase and amplitude sensors, phase and amplitude references, and electronics associated with the control loops for phase and amplitude control must be incorporated. The architecture of Figure 3 provides the means of putting both the references and sensors for both amplitude and phase at the point where they are needed most-right at the radiating surface of the antenna. All solid state devices that are associated with the control electronics are located in the same area where they can be operated in a relatively cool environment.

In the architecture the phase and amplitude references are fed from the backbone of the subarray through flat ducts welded to the surface of the slotted waveguide arrays. These ducts serve an additional function in that they are very effective stiffeners of the thin aluminum faces of the waveguide array. However, the fact that these ducts run all the way to

the edge of the subarray governs the number of tubes and area of slotted waveguide array that are in the subsection. Thus, the whole subsection may be considered as a plug-in unit and this concept replaces the earlier held concept that each tube and its slotted waveguide array section represented a plug-in unit.

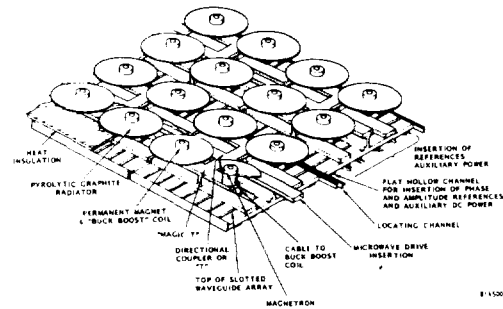


Figure 3. Assembly Architecture for the Magnetron Directional Amplifier in the Antenna Subarray. Two Subsections are Shown. Microwave Drive and All References and Auxiliary Power are Inserted from the "Backbone" of the Subarray. The Array has Two Distinct Temperature Zones. The Top is Used to Radiate the Heat. The Bottom is Used for Mounting of Solid State Components.

3. Interface with the microwave drive source. In Figure 3 the microwave drive source is not shown but it is derived from another magnetron directional amplifier identical to the ones directly attached to the waveguide radiators. At a gain level of 20 dB, one magnetron directional amplifier can drive between 50 and 100 other magnetron directional amplifiers. The microwave drive for any one subsection, as shown, is delivered to the intended tube through a waveguide which runs the length of the subsection and serves all the tubes. The energy may be siphoned off by a number of different techniques including directional couplers and the standing wave techniques used in the design of the slotted waveguide radiators.

After the power is taken off the central waveguide feed it enters one port of a "magic T", or alternatively, one of the ports of a ferrite circulator (not shown). Two magnetrons with matched performance are placed at either end of the Magic T, unequally separated in distance from the center by a quarter wavelength. The combined power of these generators then comes out of the fourth port of the device directly into the slotted waveguide array.

4. One of the interesting features of this architecture is that the cathode and magnetic circuits are operated at ground potential. This permits the power for initial heating of the filament and for energizing the buck-boost coils on the magnetron to be operated at ground potential. The anode and its radiator are isolated from ground potential by means of alumina ceramics which also support the anode and the magnetic circuit. The output of the magnetron is a coaxial probe which excites the waveguide without physical contact and therefore can remain at anode potential.

5. Sources of auxiliary power. Not shown in Figure 3 but located along the spine feeding the subsection array are sources of the auxiliary DC power needed

for the phase and amplitude control systems and for the transient heating of the filament for starting purposes. The amounts of power that are needed are relatively small, characteristically five or ten watts for each magnetron directional amplifier. This power is most easily obtained by tapping off a portion of the microwave power from the magnetron directional amplifier that drives the subsection array, then performing the desired impedance transformations at microwave frequency and rectifying the output with the highly efficient type of rectifiers that are used in the rectenna. The auxiliary power is then distributed to the individual magnetron directional amplifiers in the subsection array through the flat conduits located on the slotted waveguide array surface.

Incorporation of Phase and Amplitude Tracking in the Magnetron Directional Amplifier

The output phase of any microwave generator in the SPS, regardless of kind, must be carefully controlled in order that it not appreciably impact the overall phase budget of the subarray which must include many other factors. Open ended control for the magnetron directional amplifier and klystron is not feasible and probably only marginally feasible for the amplifron. For the magnetron directional amplifier and klystron this control must utilize a low level phase reference at the output, a comparator circuit to compare the phase of the generator output with the reference phase and to generate an error signal, and a feedback loop to make a compensating phase adjustment at the input.

The control of the output amplitude in the face of many factors that tend to change that amplitude is also essential for generating an efficient microwave beam. In the case of a crossed-field device the output amplitude can be controlled to a predetermined value by another control loop which makes use of small electromagnets that can be used to boost or buck the residual field provided by permanent magnets.

The amount of power required to compensate for expected variations in the permanent-magnet field with temperature and life, and minor changes in the dimensions of the tube with life are very small. With additional power, but still reasonable in the context of power dissipation from other causes, this arrangement can also adjust the operation of the microwave generator array to the most efficient operating point of the solar photovoltaic array. This would be very difficult by any other means of power conditioning because the output of the solar cell array is DC and the direct transformation from one DC voltage to another is not possible without resistive losses. Indirect methods such as transformation to high frequency AC, then an AC voltage change by transformers, and then back to DC again by rectification would appear to be highly impractical in this application where huge powers, very low mass requirements, and difficulty of dissipating the inevitable losses in the transformation process prevail.

It is of importance to note that the magnetron directional amplifier will be operating in an efficiency-saturated mode so that modest changes in operating voltage will have only a minor impact upon operating efficiency. Thus the optimized efficiency of the solar cell array will predominate in the combined operating efficiency of solar array and microwave generators.

The overall schematic for the combined phase and amplitude control of the magnetron directional amplifier is shown in Figure 4. Also shown is how this control can be related to the overall power

absorption by the solar cell array. A central computer establishes the most efficient operating point (maximum power output) of the solar cell array and then adjusts the reference power output of the banks of magnetron directional amplifiers, making certain of course not to err on the side of asking for more power than is available from the array.

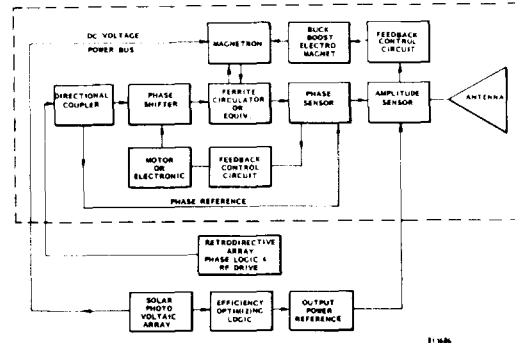


Figure 4. Schematic Diagram of Phase and Amplitude Control of Output of Magnetron Directional Amplifier. The Packaged Unit is Enclosed in Dotted Line. Relationship to SPS Overall System is Indicated Outside of Dotted Line.

The phase and amplitude tracking system requires a set of references and a set of sensors. These references and sensors are located at the front face of the slotted waveguide array where the most accurate sensing of the phase and amplitude can be made and where the solid-state sensing and control devices can find a temperature environment that they can tolerate.

The amplitude reference is a DC voltage whose value can be remotely controlled from a central source. The amplitude sensor is a crystal detector coupled to the slotted waveguide array. It provides a DC voltage which is compared with the DC voltage reference. The error voltage, after suitable gain, establishes a current in the buck-boost coils which changes the magnetic field, which in turn changes the magnetron current to change the power output of the magnetron in a direction to minimize the error voltage.

The phase control system makes use of a phased-controlled signal from a central source, a sample of the output power, and a balanced detector which compares their phases. The error signal can be used to operate a number of different types of phase shifters positioned in the input side of the magnetron directional amplifier.

A test bed, shown in Figure 5, has been constructed to check out the proposed control system. For most laboratory measurements a resistive microwave load is substituted for the slotted waveguide. The sensors are located in the waveguide approach to the load. Although the evaluations of the control systems are not complete, the initial information indicates that they behave as predicted.

Noise Emission Properties of the Amplifron, Magnetron, and Magnetron Directional Amplifier

The lack of historic data on the noise performance of CW crossed-field devices and the consequent inability to predict their behavior in the SPS application where the noise level of the transmitter is

a highly critical issue understandably became a major factor in the preliminary selection of a generator approach in the reference design. In the recent time frame people within the SPS microwave system community have become aware of the very low noise data that has been obtained from the microwave oven magnetron^{4,5} which is now serving as a scaled-down version of an SPS magnetron and to a lesser degree they are aware of the low noise data that was obtained from the amplitrone development.³

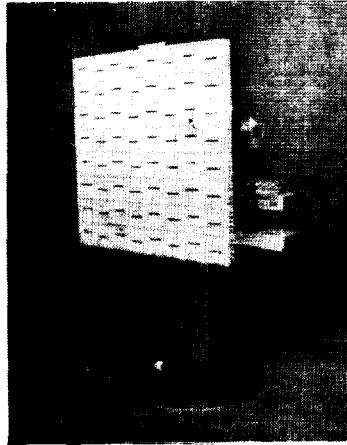


Figure 5. Test Bed for the Phase and Amplitude Tracking Investigation, Shown with Slotted Waveguide Load as an Option.

The early lack of data in this area is understandable when it is considered that the production of random noise outside of an area immediately around the signal (where it is important in communication or doppler radar applications) has been of little concern or interest in the past. However, just the converse is true in the SPS application where the high power level of the transmitter makes it mandatory to have very high ratios of carrier signal to random noise everywhere but immediately close to the carrier. Even after the importance of this noise was realized it was necessary to make special noise measuring setups to obtain more sensitive measurements of noise. In these setups the carrier signal was greatly attenuated in order to allow the noise to be visible as exhibited on a sensitive spectrum analyzer.

Many measurements of signal to noise ratio over frequency ranges of as much as ± 1000 MHz either side of the carrier have been made on magnetron directional amplifiers with this equipment.⁴ A typical set of measurements is shown in Figure 6.⁴ The data was taken both with normal external power applied to the filament and with no external power applied. The reader's attention is to be focused on the very high signal to noise ratio that is obtained over a frequency sweep of 200 MHz with no external power applied. The signal to noise ratio is 100 dB for a 1 MHz band of noise. This corresponds to a signal to noise ratio of 130 dB per 1 KHz of noise which is greater than the 125 dB quoted for the klystron in the reference design. Sweeps of ± 1000 MHz around the carrier also exhibit equally large signal to noise ratios. The reader is reminded that with these signal to noise levels even a 10 gigawatt transmitter would be radiating only one watt of noise for each megahertz of the

frequency spectrum.

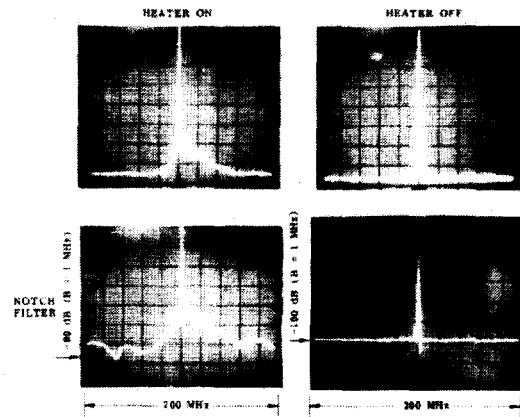


Figure 6. Spectrum of Locked Magnetron.

The signal to noise level may be substantially better than 100 dB/MHz because the measurements are still limited by equipment sensitivity. The sensitivity is currently being increased by 20 dB so that signal to noise ratios of as great as 120 dB/MHz can be measured.

It should be noted that while these noise measurements were made with a device gain of approximately 20 dB, the noise behavior remains independent of gain at high gain levels. At high gain levels the drive source appears as a small reflection factor (0.1 for a gain of 20 dB) and this has a negligible impact upon the behavior of the tube.

It should also be noted that these low noise measurements have been observed on magnetrons made by different manufacturers and in different time periods, but not on all magnetrons that have been randomly selected. However, no studies of a statistical nature have been made nor probably should be made until more sensitive measuring equipment is available. And it may be more effective to devote any limited future effort to better understanding the sources of noise in the magnetron.

There is currently no government support of any investigation into the sources of noise in the crossed-field device. However, Raytheon Company did carry on a modest effort in this area in 1979 in which special external probing equipment was built to examine the fine structure of magnetron operation with the hope of determining some of the factors that greatly impact the noise performance. Some of these results are very interesting but a discussion of their logic and implications would be so lengthy and involved that it would be outside the scope of this summary article.

Measurements of close-in phase modulation noise added by the magnetron directional amplifier¹¹ were also made when it was operating with a gain of approximately 20 dB. These measurements indicated a carrier-to-noise level that was typically 115 dB for a 1 KHz band of noise in the range of 10 KHz to 100 KHz removed from the carrier frequency. This represents excellent performance.

The discussion is now turned to harmonic generation. In this area there was no particular issue between the crossed-field and klystron device

approach since it is known that both of these devices along with all other classes of microwave generators produce harmonics. It was apparent, however, that there was little data on the quantitative level of these harmonics in any device, partly for the reason that it is difficult to make such measurements in waveguide where the harmonics usually become accessible.

However, a method of making measurements in a small coaxial line and water load attached immediately to the output of the magnetron and matched into it with a normal loaded Q, thus avoiding the problem of multiple mode propagation, was employed. Measurements made on two representative tubes, designated as #11 and #12, are given below.¹²

Frequency	HARMONIC LEVELS	
	#11 *dbc	#12 *dbc
f_o	0	0
$2 f_o$	-71	-69
$3 f_o$	< -97	-85
$4 f_o$	-86	-93
$5 f_o$	-62	-64

*dbc - decibels below carrier level

These findings are somewhat better than had been anticipated. The unexpected anomaly of the significant energy at the 5th harmonic is an indication of the difficulty of the a priori assessment of the more complicated characteristics of any microwave generator that may be designed for the SPS.

Investigation into the Designing of Magnetrons with Cathode Life of 50 Years

It is well known from the theory and experience associated with properly carburized thoriated tungsten cathodes that such cathodes can have extremely long life if they are operated at low temperatures in a good vacuum.^{13,14} An investigation of the application of this knowledge to the design of long life cathodes for SPS magnetrons was precipitated by a question raised by a NASA representative about the life of tubes with carburized thoriated tungsten cathodes that had exhibited very high signal to noise ratio when power from the external heater source was set to zero.⁶ The resulting investigation not only indicated that very long life can be achieved but also led to the discovery of an apparently overlooked feedback mechanism in the magnetron that maintains the emitting surface of the cathode at a temperature just sufficient to supply the needed current that flows from the cathode to the anode.¹⁵ This mechanism assures that the tube will determine its own long life, independent of external circumstances with the exception of compromised high vacuum and demand for increased anode current beyond the design value.

The investigation that was made began with the use of an optical pyrometer to observe the brightness temperature of the magnetron cathodes through optically transparent windows in specially constructed tubes. The arrangement is shown in Figure 7. The tube is fitted inside of a magnetic solenoid so that the magnetic field and therefore the operating voltage of the tube can be varied. Most measurements were made without the application of any external heater power to the filament.

It was observed that the only parameter that had a significant impact upon the cathode temperature was anode current. It had previously been assumed, for

example, that cathode bombardment power would increase with greater magnetic field and greater power input. By contrast, it was observed that when the anode current was held constant and the magnetic field varied over a range of two to one to give an increase of power input by approximately the same amount, the cathode temperature remained the same to within $\pm 10^\circ\text{C}$, or not much greater than the resolution of the optical pyrometer.

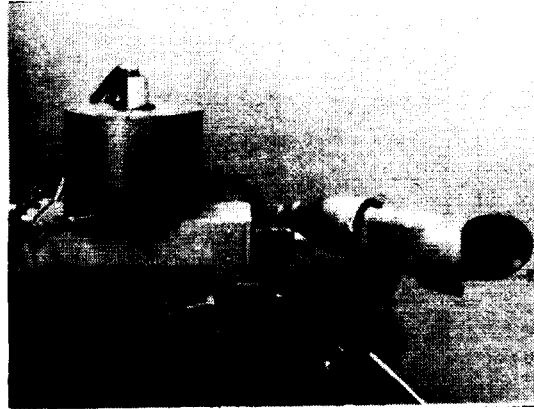


Figure 7. Test Arrangement for Viewing the Temperature of the Filament-Type Cathode in the Microwave Oven Magnetron as a Function of Anode Current, Applied Magnetic Field, and Microwave Load. Optical Pyrometer is in the Right Foreground. Transparent Window is Visible Outside of Solenoid-Type Electromagnet.

The variation of cathode temperature with anode current is shown in Figure 8. The slope of this curve is nearly the same as that obtained from the Richardson-Dushman equation which predicts temperature limited emission density as a function of true temperature. If the Richardson equation is matched to the true temperature of 1896° Kelvin that corresponds to a brightness temperature of 1500°C, then a reasonable value for the constant A of the equation is obtained. The emission as a function of temperature may then be obtained and as the three points on Figure 8 indicate follows closely the experimental data.

It has been established from life test evaluations that the life of a carburized tungsten cathode is a very steep function of the operating temperature. The difference between life at 2000°K and 1900°K is a factor of ten.

From the great body of design data that is based upon many laboratory investigations as well as life test data, an operating temperature of 1900° Kelvin is associated with a potential life of 500,000 hours or more than 50 years, as derived from the curves and the notes on Figure 9, if the cathode is made from 0.040 inch diameter wire that is 50% carburized.^{13,14} This is a reasonable design and a reasonable operating temperature for a cathode that could be used in a magnetron designed for SPS use.

Of course, life test data for 50 years is not available. But the design data of Figure 7 would have predicted a life of 130,000 hours for each of a lot of 12 tubes manufactured by Machlett for use in the WWV transmitter. The filament wire was 0.035 inch in diameter and 20% carburized, and the tubes were run at 1950° Kelvin. The 12 tubes had a total running

time of 850,000 hours and there had been no failures when the equipment was retired from service. Some of the tubes had been operated at 86,000 hours or 2/3 of the predicted life. Considering that there were no failures among the 12 tubes this test would indicate that the use of Figure 7 is conservative practice.

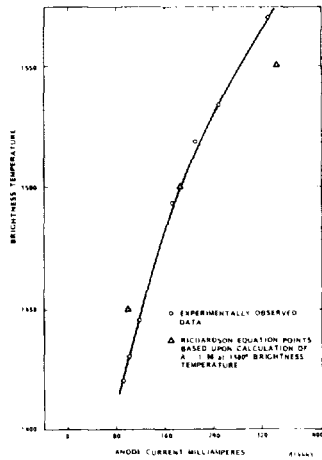


Figure 8. Cathode Brightness Temperature and Associated Points of Temperature Limited Emission as Function of Anode Current in the Microwave Oven Magnetron.

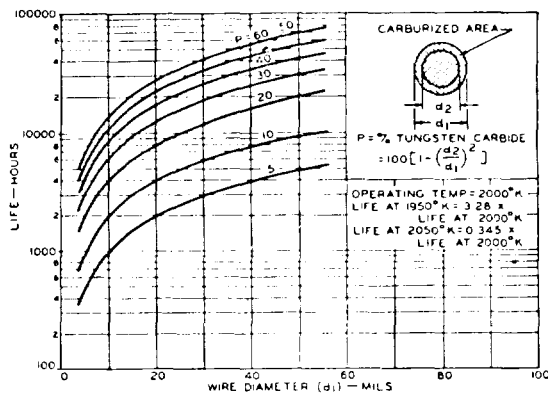


Figure 9. Thoriated-Tungsten Filament Life Curves as Function of Wire Diameter and % Carburization. Note Increase or Decrease in Life as Function of Temperature as Noted.

These tubes were also high power and high voltage tubes, similar to the projected SPS magnetron and subject to the same cathode failure mechanisms if the vacuum inside of the tube were not sufficiently good.

The conclusion is that a very good argument can be made for extremely long cathode life in the proposed SPS magnetron. The argument is based upon observations of low operating cathode temperatures in operating magnetrons, an internal mechanism that will automatically keep the cathode temperature as low as possible over closely controlled operating conditions in the SPS, an enormous body of experience and information on the carburized thoriated tungsten cathode that is well documented in published papers and books and the correlation of the long life of the Machlett tubes with predicted life.

Crossed-Field Device Efficiency

Crossed field electron tubes of the magnetron and amplatron type are properly recognized as the most efficient of microwave generator devices. But the highest electronic efficiency, defined as the efficiency with which DC power is converted into microwave power, is associated with a high ratio of the magnetic field B to a design parameter B_0 which is proportional to frequency as shown in Figure 10. But the theoretical electronic efficiency is always degraded to some degree by the circuit efficiency, and can be degraded by improper design of the interaction area and other design parameters as well. When the B/B_0 ratio is high and the tube otherwise properly designed the measured electronic efficiency has exceeded 90% as exhibited by the commercially available 8684 magnetron. For reasons largely related to the physical size and cost of the permanent magnet, crossed-field devices are almost always designed in the range of B/B_0 of four to six. This is true of the microwave oven magnetron whose operating characteristics have recently been intensively evaluated.

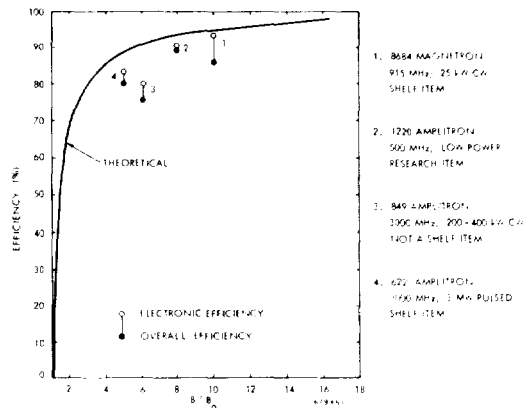


Figure 10. Magnetron Efficiency as a Function of B/B_0 Ratio.

However, the microwave oven magnetron can have its permanent magnet removed and be operated in an electromagnet. When this has been done the measured overall efficiency can be considerably increased as shown in Figure 11. The measurement of $82 \pm 1\%$ efficiency was carefully measured after extensive preparation and precaution and then a balance was made between the DC power input and the sum of the microwave power output and the power dissipated in the anode as an additional precaution.¹⁶ After taking a carefully measured circuit efficiency of 95% into account, the electronic efficiency was computed to be

9. W.C. Brown, "The Platinotron: Amplitron and Stabilotron", in E.C. Okress, *Crossed-Field Microwave Devices*, Vol. 2, Academic Press, 1961, pp. 165-209.
10. E.E. David, "Phasing by RF Signals" in E.C. Okress, *Crossed Field Microwave Devices*, Vol. 2, Academic Press, 1961, pp. 375-399.
11. Microwave Beamed Power Technology Improvement, JPL Contract #955104, with Raytheon, Monthly Progress Report #10 for April 1979.
12. Microwave Beamed Power Technology Improvement, JPL Contract #955104, with Raytheon, Monthly Progress Report #14 for August 1979.
13. W.H. Kohl, "Handbook of Materials and Techniques for Vacuum Devices" Reinhold Publishing Corp, 1967, pp. 487-491.
14. Ayer, R.B., "High-power Industrial Vacuum Tubes Having Thoriated Tungsten Filaments," *AIEE Trans.*, 72, Pt. 1, 121-125, (May 1953).
15. "Microwave Beamed Power Technology Improvement," JPL Contract #955104 with Raytheon Monthly Progress Report #5 for Nov. 1978.
16. "Microwave Beamed Power Technology Improvement," JPL Contract #955104 with Raytheon Monthly Progress Report #10 for April 1979.

CONCLUSIONS PRESENTED AT THE POWER AMPLIFIER SESSION

1. Power Amplifier/Microwave System Tradeoffs

- a. Based on present assumptions of microwave system requirements and projected performance of various microwave power amplifiers, the klystron offers a feasible approach for SPS microwave power generation, the amplitron appears to be less suitable, and the magnetron should continue to be investigated to better understand its performance characteristics relative to SPS applications.
- b. Based on SPS microwave system applications, it is desirable to have maximum power output and gain consistent with other microwave system parameters

2. Klystron Conclusions

- a. The klystron power amplifier has the attractive features of high gain (40-50 dB) low drive power required from the phase control system, high power (50-70 kW), low noise characteristics, and fewer tubes per antenna requiring phase control.
- b. Cathode lifetime and its maintenance implications is a major concern for the SPS.
- c. Efficiencies of 75% at S-band and a power output of 50 kW have already been recorded. The application of depressed collectors have increased tube efficiencies. It appears likely that 85% can be achieved.
- d. A heatpipe cooling system is required for heat rejection.

3. Amplitron Conclusions

Projected performance of amplitrons is less attractive for SPS applications because of low power (5 kW), low gain (7 dB), higher noise levels, higher drive power required from the phase control system, and more tubes per antenna requiring phase control. The amplitron is less complex and passive cooling techniques appear to be within the state-of-the-art.

4. Magnetron Conclusions

Because of recent projections in performance characteristics (low noise, high efficiency and moderate gain) magnetrons warrant continued investigations. The magnetron is also less complex and hence the maintenance implications appear to make it more attractive.

REMAINING ISSUES PRESENTED AT THE POWER AMPLIFIER SESSION

1. High RF-DC conversion efficiency (\geq 85%)
2. Reliability
3. Amplifier RFI (noise, harmonics, filtering requirements)
4. Other operating parameters (temperature, gain)
5. Proof of thermal cooling concept
6. Specific weight
7. High volume manufacturing techniques
8. Precision manufacturing
9. Design for ease of maintenance
10. Design of power supply/power amplifier for stable operation
11. Depressed collectors
12. Investigation of circuit protection devices
13. Launch/Transportation packaging considerations
14. Metals/materials research (magnets, cathodes)

SECTION V

RADIATING ELEMENTS SESSION

Chairman: James S. Kelley
NASA, Johnson Space Center

REFERENCE SYSTEM DESCRIPTION

By C. D. Lunden, W. W. Lund, E. J. Nalos/Boeing Aerospace Company

1.0 SPS ANTENNA ELEMENT EVALUATION

The SPS transmitting array requires an architecture which will provide a low weight, high efficiency and high structural rigidity. Several candidate antenna configurations include the parabolic dish, the parabolic cylinder, the lens and the waveguide slot array. As discussed below, the waveguide slot array is preferred over the other options.

Parabolic dishes are widely used on earth. For SPS application, they could be readily laid up in six-foot diameters with lightweight graphite-epoxy materials. On the other hand, the area efficiency of such an array is relatively low. Moreover, a zero spillover feed configuration is not presently apparent.

An array of parabolic cylinders with line-source feeds could give better area efficiency than an array of dishes, but would suffer from feed blockage.

A lens, using lightweight waveguide structures, with zero blockage behind-the-lens feedhorns can have high efficiency and little spillover, but the SPS center-to-edge illumination tapers would give a spatial "lumpiness" which would produce undesirable grating lobes in the far-field pattern.

As noted above, waveguide slot arrays constitute the most desirable option. Consequently, such an array has been chosen for the SPS. Waveguide slot arrays offer high efficiency, uniform illumination, and are fairly lightweight. Bandwidths of such arrays are narrow, typically 1/2-2%. Although this does not directly impact the SPS, which transmits power at a single frequency of 2.45 GHz, the narrow bandwidth does constrain the thermal and mechanical tolerances of the antenna.

2.0 SLOTTED WAVEGUIDE MODULE DESIGN VERIFICATION

2.1 EXPERIMENTAL PROGRAM

The purpose of this program is to better define the electronic aspects of an SPS specific waveguide slot array. The specific aims of the program are as follows:

- o To build a full-scale half-module, 10 stick, array, the design parameters for which are to be determined by analytical considerations tempered by experimental data on a single slotted radiating stick.
- o To experimentally evaluate the completed array with respect to antenna pattern, impedance and return loss.
- o To measure swept transmission amplitude and phase to provide a data base for design of a receiving antenna.

2.2 ARRAY CONFIGURATION

The first step in module design is to fix the gross dimensions, including the module length and width, and the dimensions of the radiating sticks and the feed waveguide. Because the feedguide is a standing wave device in which the coupling slots must be spaced by $\lambda_g/2$, where λ_g is the guide wavelength, and because λ_g is a function of waveguide width, the radiating stick and feedguide dimensions are not independent.

The SPS baseline design calls for a half-module of ten 1.6 m long sticks of 6 cm x 9 cm cross-section. For these dimensions, at the SPS frequency, the feedguide dimensions are also 6 cm x 9 cm. To assess the desirability of the baseline configuration, the ohmic losses of several alternative configurations of equal area were calculated. The I^2R losses for these are plotted in Figure 1 as functions of radiating stick

in the loss curve is quite shallow. Also, the values of the minima do not appear to be very configurationally sensitive. On the other hand, it was determined in the course of this study that end-feeding of the feedguide may afford somewhat lower loss than expected of the baseline configuration which utilizes center-feeding.

Based on the above considerations, it was decided to configure the experimental module according to the baseline design. The commercially manufactured waveguide which most nearly approximates the baseline guide, is WR-340, with dimensions of 4.32 x 8.64 cm. Because this was not available in sufficient quantity, WR-284 waveguide was used instead for the developmental module. Because this waveguide is narrower than the baseline, and because it would be used for both the radiating sticks and the feedguide, the design frequency of the developmental module was increased from 2.45 GHz to 2.86 GHz. With 6061 Aluminum feedguide, the ohmic losses in the module are expected to be less than 1%.

2.3 WAVEGUIDE STICK DESIGN

The design of the waveguide stick entails the assignment of values to both the slot offset from the waveguide centerline and the slot length. The slot length, l , is chosen so that the slot is resonant at the design frequency. The slot offset is chosen to give the desired slot conductance. This is determined by impedance matching considerations. Thus, for a waveguide stick containing N identical shunt slots, the desired value of normalized slot conductance, g , is just $g = 1/N$.

For a single isolated stick, the choice of slot length and slot offset is relatively straightforward. The slot length is given to good approximation by $l = \lambda_0/2$, where λ_0 is the free-space wavelength. The conductance and slot offset are related to sufficient accuracy by a well known equation.

Tentative radiator stick dimensions in WR-284 waveguide are:

Slot Spacing	3.0 inch	Slot Offset	.187 inch
Slot Length	1.98 inch	Slot Normalized	.055
Slot Width	.125 inch	Conductance	
		Number of Slots	18 or 20

Where several sticks are placed in close proximity, however, as they are in the SPS module, the design problem is exacerbated by mutual coupling between the sticks. That is, the slots in any particular stick are now loaded by the slots in the neighboring sticks and will necessarily exhibit resonant frequencies and conductances which differ significantly from those predicted by single stick equations.

The changes in stick behavior due to mutual coupling effects are shown in Figure 2. Here, both the resonant frequency and the reflection coefficient of a single stick at resonance change noticeably in the presence of a second stick. A theoretical analysis of this problem, based on an adaptation of a mutual coupling analysis for an array of dipoles (L. Stark, Radio Science 1, 361, 1966) is shown in Figure 3. As might be expected, the effects converge rather rapidly, suggesting that a particular slot does not interact to any significant extent with other slots that are more distant than third or fourth neighbors. Figure 3 also shows that mutual coupling effects are also present between neighboring slots of a single stick.

Because of the mutual coupling problem, the choice of slot length and offset has been pursued in an iterative manner beginning from the single stick analytical values. Data for several iterations with two waveguide sticks, are shown in Table 1. Because the slot offsets, once machined, are fixed, stick impedance in these data was varied by changing the number of slots by the means of a sliding short in the waveguide. Adjacent

sticks were fed in-phase using home built four-hole directional couplers machined in one end of each stick, permitting swept return-loss/coupling measurements without interference by guide flanges.

2.4 FEED GUIDE DESIGN

The radiating waveguide sticks are fed in-phase by a feed waveguide whose axis is perpendicular to those of the radiating sticks. Like the radiating sticks, the feedguide supports a standing wave. The power is coupled from the feedguide to each radiating stick through a resonant (length = $\lambda_0/2$) coupling slot which is inclined to the feedguide axis. The transformed radiating stick impedance seen by the feedguide is proportional to $\sin^2 2\theta$, where θ is the inclination angle. The phase of the power coupled to the stick is inverted as the coupling slot is reflected in the feedguide axis. For maximum power transfer to the 10 radiating sticks, each stick must present an impedance to the feedguide of one-tenth the feedguide characteristic impedance. This dictates a rather small coupling slot inclination of about 7°. To maintain proper phasing of the radiating sticks, the coupling slots are alternately reflected in the feedguide axis.

Tentative feed stick dimensions in WR-284 6061 aluminum waveguides for the 1/2-module are:

Slot Spacing	3.0 inch	Slot Normalized Resistance	.10
Slot length	2.0 inch	Slot Number	10.
Slot Width	.125 inch		
Slot Offset Angle	7.		

3.0 RECEIVING TECHNIQUES EVALUATION

The receiving antenna receives a pilot signal from earth with phase information to keep all modules in-phase. Symmetry considerations argue for the pilot signal to originate from the center of the SPS earth receiving array. Ionospheric phase shift and Faraday rotation call for the pilot signal to be centered on the SPS power frequency with the phase information in symmetrically disposed sidebands. The purposes of the receiving techniques evaluation were to:

- o Conduct a shared antenna versus separate receiving antenna analysis to determine feasible pilot beam budget and receiving antenna constraints due to power module.
- o Design and select a pilot-beam receiving antenna techniques compatible with a power beam array which must allow simultaneous transmission of an S-Band carrier and reception of the anticipated pilot-beam spread-spectrum signal.

The pilot beam link analysis established that very small low gain pilot receiving antenna elements imbedded in the transmitting array are significantly superior to any scheme of diplexing, because: (1) The total system power losses are two orders of magnitude lower with a separate antenna than with any state-of-the-art diplexing device; (2) The small antenna, due to its inherent broad bandwidth, is fully compatible with a spread spectrum signal; whereas the transmit array is not, (3) The small, low gain antenna represents a much lower development risk than a diplexing device.

Also from the pilot beam link analysis, formalisms have evolved from which to determine values of pilot transmitter power and antenna aperture, as well as pilot receiving antenna aperture. The transmitter power and aperture depend foremost upon the requisite pilot link effective radiated power, ERP. The ERP, in turn, depends upon the signal-to-noise requirement of the pilot link receiver; and hence, the noise environment in which the receiving system must operate. Consequently, the ERP requirements were found to be extremely sensitive to the cut-off frequency of a required receiver I.F. notch filter.

The relationship between transmitting antenna diameter and system power loss (efficiency) is shown in Figure 4. This relationship is not monotonic due to the fact that increasing the antenna diameter produces two opposing effects. It reduces the amount of pilot transmitter power required to produce the requisite ERP, while simultaneously increasing the degree of rectenna blockage. At low diameters, the transmitter power effect dominates, and the loss decreases with increasing diameter; whereas, at larger diameters, rectenna blockage becomes most important, and the system loss increases with increasing diameter. Thus, for a particular ERP, there is a rather limited set of pilot transmitter power/aperture combinations which gives minimum system loss.

The relationship between system losses and pilot-link receiving aperture is shown in Figure 5. For small apertures, an increase in aperture reduces system losses due to a decrease in the required ERP. At large apertures, the system losses increase with increasing aperture, due to receiving antenna blockage of the spacetenna. The specific nature of this relationship depends on the required signal-to-noise ratio, S/N, in the pilot receiver, and also on the bandwidth, f_c , of the intermediate frequency notch-filter. As S/N is increased, the pilot ERP must increase, and so also must the system losses. As f_c is decreased, more of the power transmitter noise spectrum is passed by the receiver I.F. This increase in noise must be overcome by an increase in pilot link transmitter power.

As shown in Figure 5, the optimum receiving aperture, under any foreseeable conditions, is quite small. Consequently, the pilot-link receiving antenna requirement can be satisfied by a simple dipole or slot antenna. Adaptations of these to the SPS array are shown in Figure 6. The slot antenna is inserted in a notch cut in the outer portion of adjacent waveguide narrow walls. The dipole is positioned at a distance $\lambda_0/4$ above the array by a small rigid coax feed, which like the slot, is slipped through a hole in the waveguide walls. These antennas may be dimensioned either to be resonant or non-resonant. The aperture of the resonant structure is larger, but so also is the effect on the impedance of the neighboring transmitting-antenna radiating slots. To the extent that the lower aperture can be tolerated, the non-resonant structure is preferred.

An important consideration in the pilot link design is the isolation of the pilot receiver from noise inherent to the high-power down-link signal. With the dipole, isolation can be improved by rotating the antenna so that it is cross-polarized to the power transmitting antenna. An alternate noise-cancelling scheme utilizes two dipoles per receiving antenna, as shown in Figure 6. These are separated by $\lambda_0/4$ and can therefore be connected to pass, as would a directional coupler, radiation coming from the earth, while rejecting that which is earthbound.

One of the candidate receiving antennas in Figure 6, the slot, or "credit-card" receiving antenna, has been built and sweep-tested. It consists of a 1.75" x .062" teflon-glass microcircuit board shorted around three edges to form a low-impedance waveguide cavity.

4.0 ANTENNA EFFICIENCY MEASUREMENTS

The antenna pattern will be measured on one of the six antenna ranges at Boeing. Besides observing the far-field rule $R > 2D^2/\lambda > 180$ ft., high paths and sharp-beam range illuminators will be employed to minimize multipath errors. For the ranges at the Boeing Developmental Center, multipath errors at beam-center are estimated to be well under $\pm .1$ db. Gain is measured using a Scientific Atlanta SA-1740 Precision Amplifier-Receiver, and SA-12-1/70 Standard gain horn. Measurement accuracies are estimated as follows:

Standard-gain Horn (Δ gain)	+ .2 db
Match	+ .2 db
Switch mismatch differences between two positions	+ .2 db
Receiver/mixer linearity	+ .2 db
Total RSS Value	+ .4 db or + 9% in power

By hardwiring the SPS array to the standard gain horn, with their beams pointed near 90° apart to avoid crosstalk, the rf switch and its inherent uncertainty can be eliminated.

The antenna efficiency is obtained from the experimental measurement of gain, G , with respect to a reference horn, and directivity, D . Since the directivity is the gain of a lossless antenna, the ratio of these values represents the efficiency of the antenna. The gain is obtained from the measured value of incremental gain above a calibrated standard horn. The directivity is expressed as the ratio of the maximum radiation intensity, U_{max} to the average radiation intensity \bar{U} , which is given by $\bar{U} = 1/4\pi \int U(\theta, \phi) d\Omega$.

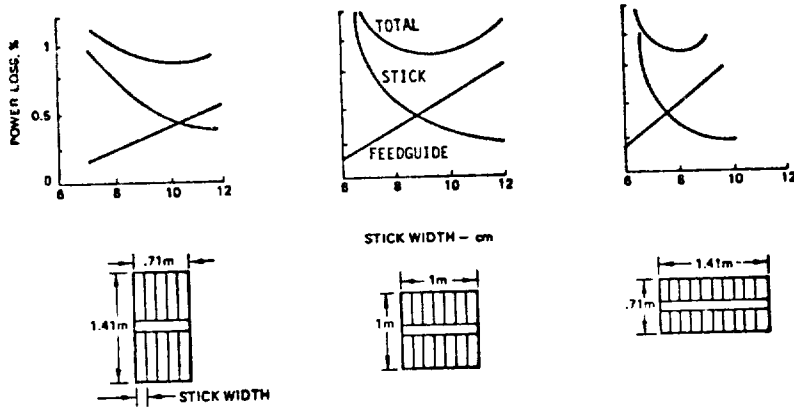
The directivity measurement is carried out separately by rotating the antenna continuously through selected azimuth and elevation angles and integrating the far field contributions over a solid sphere, thus obtaining the directivity with reference to an isotropic radiator as $D = U_{max}/\bar{U}$.

The efficiency is obtained from the ratio of two separately measured experimental values, $\eta = G/D$. With currently available antenna range accuracy, this measurement is typically determined to + .4 db accuracy. The resulting efficiency value will give an indication of ohmic losses in the waveguide feed system and in the radiating sticks. In the SPS baseline design, this loss is estimated to be less than 0.1 db, and the antenna range measurement will thus provide a crude verification only.

TABLE: 1 ITERATIVE DESIGN PROCEDURE FOR RADIATING STICK PARAMETERS

STICK NUMBER	NO. OF SLOTS ¹ FOR BEST MATCH		SLOT ³ OFFSET	SLOT LENGTH	COMMENT
	SINGLE STICK	WITH ² NEIGHBOR			
1	22	20	.18"	2.04"	RESONANCE @ 2900 MHz SLOT TOO LONG
2	16	14	.20"	1.94"	RESONANCE @ 2880 MHz SLOT TOO SHORT TOO MUCH CONDUCTANCE PER SLOT
3	18	16	.187"	1.98"	RESONANCE AT 2875MHz
4	18	18	.180"	2.00"	EXPECT 2860 MHz ⁴

1. SLIDING SHORT MEASUREMENT: VSWR AT RESONANCE < 1.1
2. NON-DUPLICATE STICKS ARE USED TO APPROXIMATE MUTUAL COUPLING EFFECT
3. AFFECTS PRIMARILY SLOT CONDUCTANCE
4. DESIRED FREQUENCY FOR FEED GUIDE TO BE IDENTICAL TO RADIATING STICK GUIDE (WR240)



- NOT SENSITIVE TO MODULE ASPECT RATIO
- NOT VERY SENSITIVE TO WAVEGUIDE SIZE
- STICK STANDING WAVES SUGGEST END FEEDING PREFERABLE

Figure 1 : RF Module P^2R Optimization

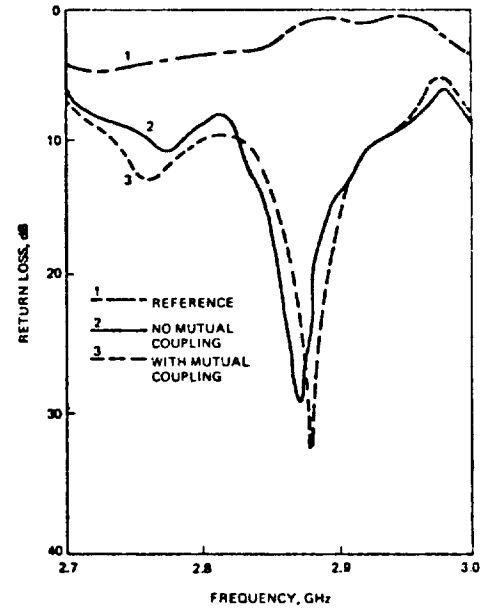


Figure 2: Effect of Mutual Coupling - Two Stick Measurement

ANALYTICAL EXPRESSION¹

$$\frac{Y}{Y_0} = \frac{4 \cdot S_y \cdot S_H \cdot (1 - \omega^2)}{b \cdot \lambda^2 \left[1 + \omega^2 \right] + \left(\frac{a}{2b} \right)^2} = \omega^2 \left(\frac{1}{2} \sqrt{1 + \frac{\lambda^2}{2b^2}} \right) \sin^2 \left(\frac{\pi x}{a} \right)$$

WHERE

$$m = n - k$$

$$n = \sum_{i=1}^m \left[\frac{\sin \left(\frac{\pi y_i}{S_y} \right)}{\frac{\pi y_i}{S_y}} \right]^2 \left[\frac{\sin \left(\frac{\pi x_i}{S_H} \right)}{\frac{\pi x_i}{S_H}} \right]^2 \left[\left(\frac{a}{S_H} \right)^2 + 1 \right]$$

$$m = |n - 4|$$

$$m \neq 0 \neq n \neq 0, \left[\frac{\pi y}{S_y} \right]^2 + \left[\frac{\pi x}{S_H} \right]^2 + \sqrt{\left(\frac{a}{S_H} \right)^2 + 1} \left(\frac{\pi y}{S_y} \right)^2$$

1 = % THE NUMBER OF NEIGHBORING SLOTS CONSIDERED IN THE 'Y' PLANE
 k = % THE NUMBER OF NEIGHBORING SLOTS CONSIDERED IN THE 'X' PLANE

a = GUIDE I.D. WIDTH k = SLOT OFFSET
 b = GUIDE I.D. WIDTH x = SLOT OFFSET
 c = GUIDE I.D. HEIGHT b = SLOT WIDTH
 S_y = SLOT 'Y' PLANE SPACING y = SLOT SHUNT ADMITTANCE
 S_H = SLOT 'X' PLANE SPACING Y₀ = GUIDE CHARACTERISTIC

1. MODIFICATION OF STARK'S DIPOLE EXPRESSION TO SLOTS

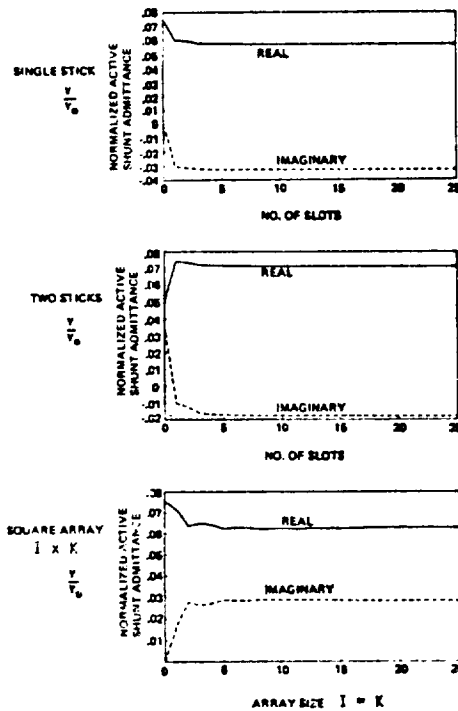


Figure 3: Estimate of Mutual Coupling in SPS Slotted Waveguide Array

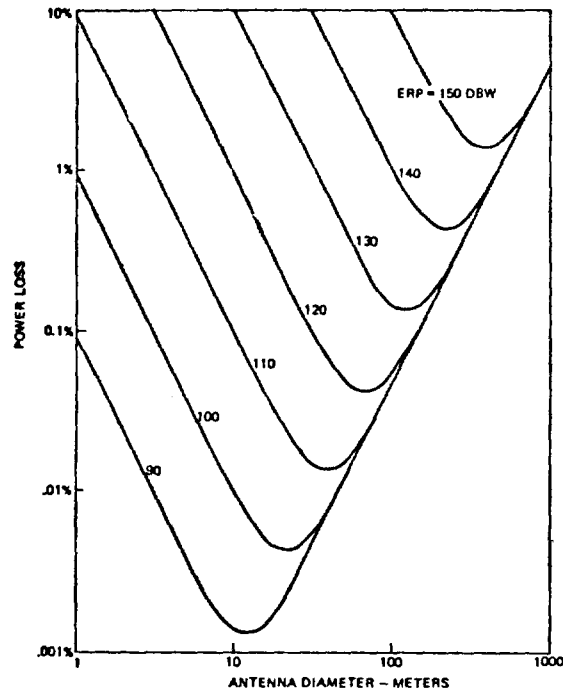


Figure 4 System Power Loss Vs. Pilot Transmit Antenna Diameter and ERP Required

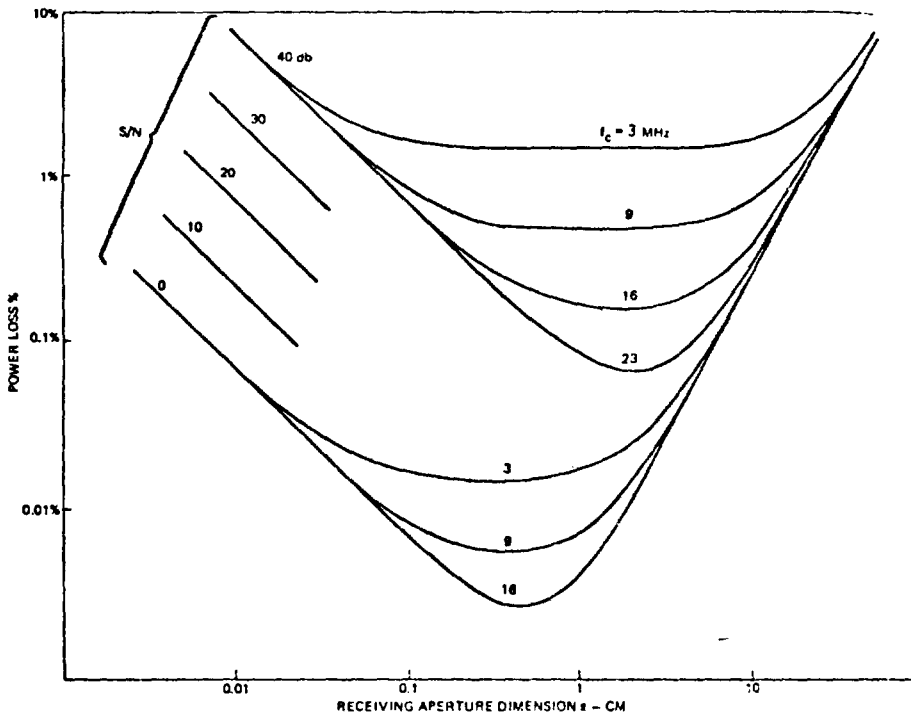


Figure 5 : Total System Loss Vs. Receive Aperture

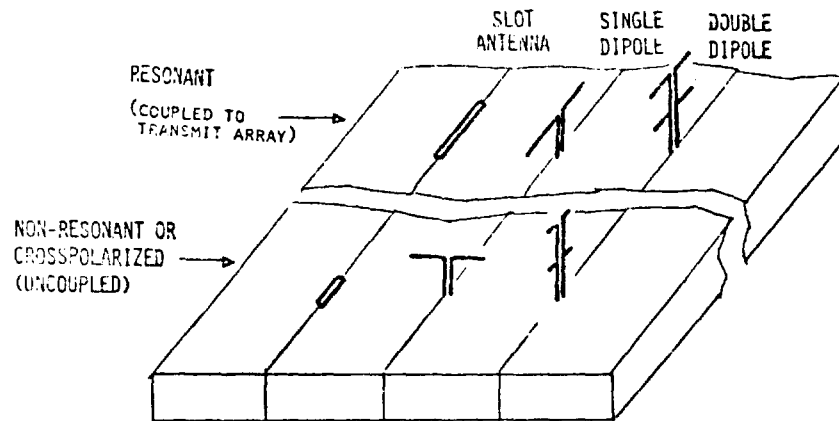


FIGURE 6: POTENTIAL SPS PILOT-LINK RECEIVING ANTENNA CONFIGURATIONS. THE DOUBLE DIPOLE CONFIGURATIONS AFFORD PARTIAL NOISE CANCELLATION.

THE RESONANT CAVITY RADIATOR (RCR)

K. G. Schroeder, R. L. Carlise, C. Y. Tomita, Rockwell International

1. INTRODUCTION

The fundamental theory of MW antenna operation and basic array technology development status was used in the design of the 1-km diameter 5-Gw SPS microwave antenna. However, the aperture size and the high efficiency requirements make the MW antenna extremely complex. Studies have shown that the slotted waveguide array is one of the most efficient radiators for the antenna. Subsequent analyses have shown that the temperature interface between waveguides and dc-RF conversion tubes can cause severe thermal design problems on the array. An alternate design, the Resonant Cavity Radiator, is described here.

2. RADIATING ELEMENT DESIGN

2.1 Basic RCR Principle

Conventional waveguide designs such as the TE_{10} mode waveguide slotted array make tube installation fairly complex. To solve the resultant temperature interface problem and possibly increase the RF efficiency of the radiator, Rockwell developed the resonant cavity radiator (RCR). The RCR is a resonant cavity box excited with the TE_{10} mode. Physically, the RCR is a conventional standing waveguide radiator with the common walls removed. The RCR has three significant potentials. They are:

1. Improvement in efficiency.
2. Lighter weight.
3. Simpler structure which allows the RCR to be integrated with the RF tube to alleviate the thermal interface problem.

2.2 RCR Theoretical Attenuation Estimates

The loss mechanisms of the RCR can be best explained by comparison to conventional arrays. The typical flat plate antenna array is formed by placing side-by-side several sections of rectangular waveguide as shown in Figure 1.

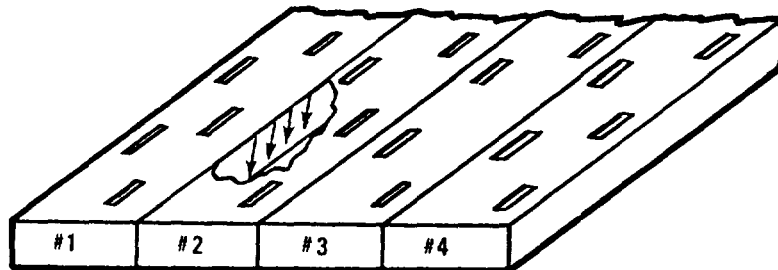


Figure 1. Typical TE_{10} SWR Array

The mode that propagates down each waveguide is the dominant TE₁₀. The mode designation simply describes a particular electric-magnetic field configuration that satisfies Maxwell's equations. A portion of the top wall in waveguide No. 2 in Figure 1 is cut away to show the current flowing in the side wall. Not shown is the adjacent currents flowing in waveguide No. 1. These currents (waveguide No. 1) are flowing in the opposite direction and because the system is symmetrical, they are of equal magnitude. If the side walls are removed as in the RCR, these two equal and opposite currents cancel. Since conduction losses are simply I²R losses, any reduction in surface currents will make the antenna array more efficient.

The closed-form analytical expression for conduction losses for a silver-plated RCR supporting the TE_{m,0} modes is given as:

$$\alpha_c = \frac{2.8738 \times 10^{-4}}{b \sqrt{1 - \left(\frac{m\lambda}{2a}\right)^2}} \left[1 + \frac{2b}{a} \frac{m\lambda^2}{2a} \right] \frac{\text{dB}}{\text{meter}} \quad (1)$$

For an "a" dimension of 4.460 inches and a "b" dimension of 2.130 inches (11.319 cm by 5.40 cm) the loss calculated from the above equation is tabulated in Table 1. This shows that for a typical array length of 2.5 meters, a TE₇₀ RCR has the potential of saving 4.3 x 10⁶ watts of power. Weight savings in the MW antenna is achieved by two design features: (1) the RCR is designed with no side walls with the exception of the cavity walls, and (2) it can be designed to be structurally integrated with a magnetron or klystron heat dissipator because of the simplicity of the structure.

2.3 Typical Integration Between RCR and Tube

Figure 2 shows a typical anode heat radiator integrated with the RCR bottom. The area required for heat dissipation computed by Rockwell indicates that the RCR has more than sufficient area to dissipate the excess heat. In the aperture high-density area, only 0.76 percent of the total RCR area is required to replace a 48-cm magnetron anode. The RCR bottom wall can be constructed of pyrolytic graphic composite, or equivalent, and plated for high RF conduction. The plating technique of pyrolytic graphite to operate at extremely high temperatures should be investigated in future studies. The potential weight savings of the RCR is then the removal of the side walls and the weight reduction achieved by incorporating heat dissipation in the waveguide bottom wall. The integrated assembly also provides techniques for solving the high-temperature interface problem. It should be noted that the RCR may offer other advantages for ease of maintenance and assembly.

Table 1: Theoretical Power Saving of RCR Over Conventional Standing Wave TE₁₀ Slotted Arrays

Mode	(α) dB/Meter	Loss Differential for 2.5m (dB)	Power Savings 5-GW/Base
TE _{1,0}	8.068×10^{-3}	-	
TE _{2,0}	7.193×10^{-3}	.00218	2.51×10^6
TE _{3,0}	6.901×10^{-3}	.00291	3.35×10^6
TE _{4,0}	6.755×10^{-3}	.00328	3.77×10^6
TE _{5,0}	6.668×10^{-3}	.00350	4.02×10^6
TE _{6,0}	6.609×10^{-3}	.00364	4.19×10^6
TE _{7,0}	6.567×10^{-3}	.00375	4.3×10^6
TE _{8,0}	6.530×10^{-3}	.003845	4.42×10^6
TE _{10,0}	6.490×10^{-3}	.00394	4.53×10^6

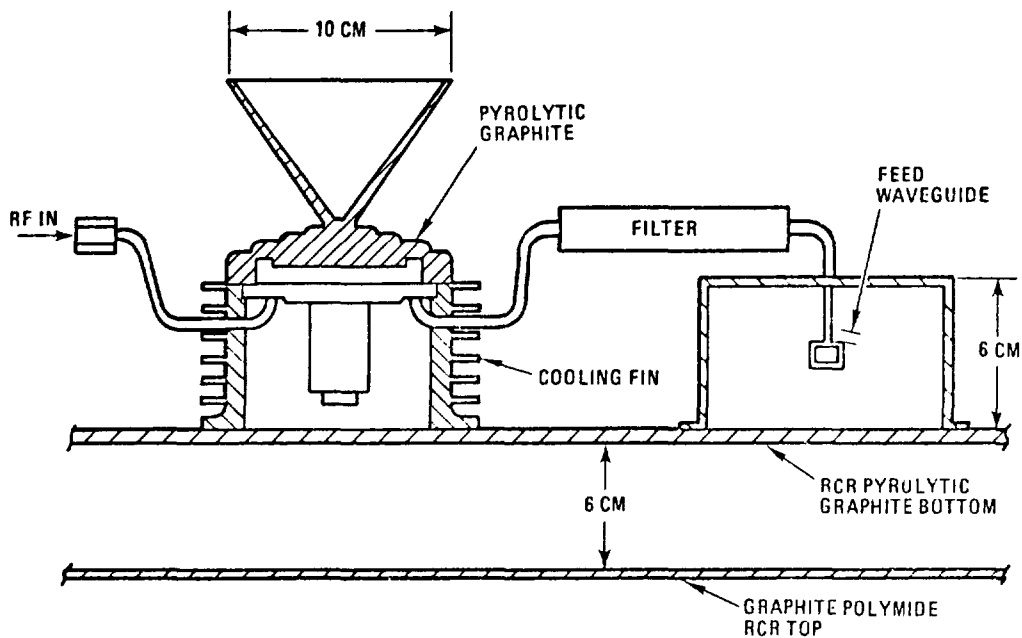


Figure 2. Magnetron Modified Heat Sink (Input-Output Connections May be Different)

2.4 Measurement Results

One of the primary uncertainties with the RCR is the suppression of higher order modes. One of the easiest ways of detecting higher order mode existence is by observing radiation patterns. Higher order modes will collimate in off-boresight locations, causing null filling and higher sidelobes. Rockwell developed special feed techniques which led to the reduction of higher order modes. To prove the technique does suppress higher order modes, scaled tests were conducted. A TE₇₀ RCR shown in Figure 3 was fabricated and tested with results shown in Figures 4 and 5. The RCR was uniformly excited for -13 dB peak sidelobe level. Measured sidelobe levels in the E and H planes were -13 dB for good correlation. Off-axis patterns also were taken at predicted higher order mode locations. No existence of higher order mode propagation was found. These tests were performed on a limited scale; however, it definitely proves that the RCR has a potential for a major breakthrough in array technology. Efficiency verification tests will be performed by Rockwell to verify theoretical predictions.

3. SUBARRAY DESIGN

Rockwell's design of the MPTS transmit array consists of 6993 subarrays, each 10 meters square. The optimum size of the subarray is a function of the electronic scanning range of the antenna. A small subarray allows more electronic scanning range; however, the total number of electronic scanning circuits increases with the increased number of subarrays. With a subarray larger than 10 meters square, the pointing requirements of the subarray is extremely tight, therefore undesirable. The baseline subarray size of 10m by 10m requires the subarray to be pointed to within ± 1 arc minutes for less than 0.5-percent loss. Typical power plots in dB and percent of the subarray is shown in Figures 6 and 7. A typical subarray may consist of 20 to 50 RCR's, depending on the power density of the subarray.

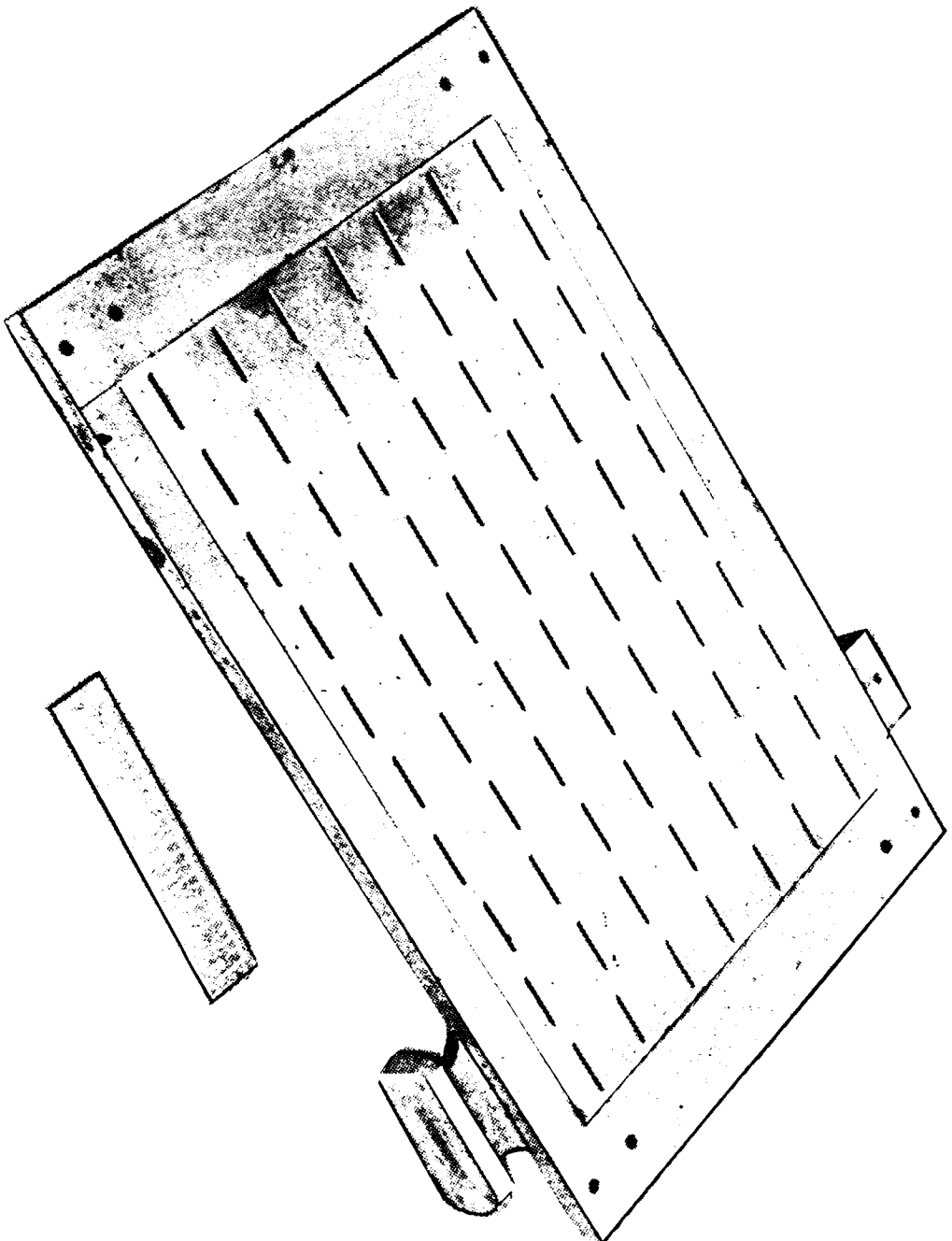


Figure 3. Experimental RCR

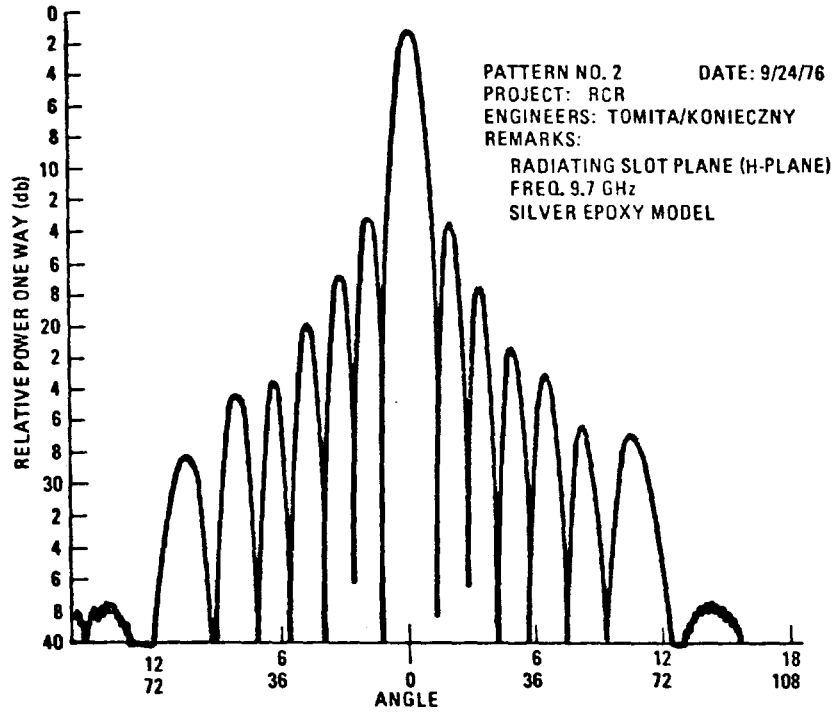


Figure 4. RCR H-Plane Pattern

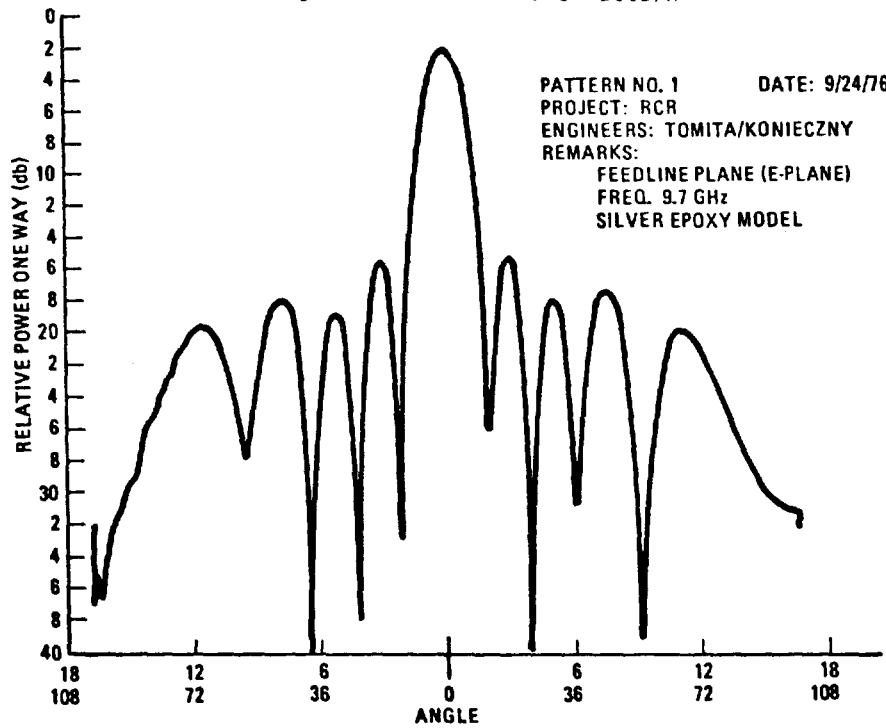


Figure 5. RCR E-Plane Pattern

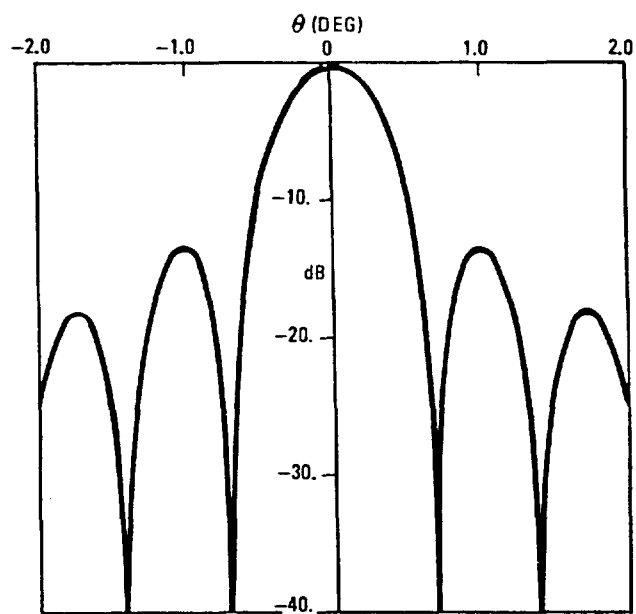


Figure 6. Far-Field Radiation Pattern
(10-Meter Square Subarray)

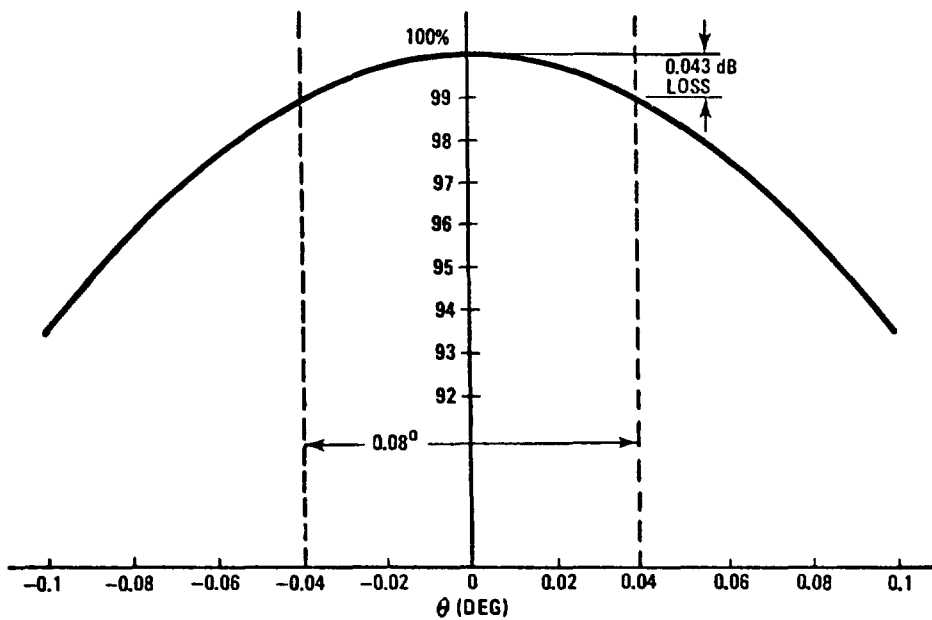


Figure 7. 10-Meter Square Element Factor

4. TUBE SUBARRAY INSTALLATIONS

One of the prime advantages of the RCR is its adaptability to numerous magnetron or klystron tube installations. Rockwell has studied various tube/RCR integrated and non-integrated concepts to determine potential solutions to the weight and high-temperature interface problem. Figures 8 through 11 illustrate various magnetron and klystron mounting techniques to the RCR. Figure 8 which shows magnetron mounting, illustrates the configuration where the back face of the RCR is integral to the magnetron. It should be recognized that these techniques are advanced and unproven; however, it offers the MPTS antenna designer alternative installation concepts. The simplicity of the RCR for maintenance also is shown in Figure 8. The RCR modes for various installation concepts will vary as a function of the power density or structural integrity. In the low density areas such as shown in Figure 9, a TE_{70} RCR may be used. In the higher density areas of the array a TE_{30} RCR can be used. The interconnecting feed lines of the RCR as shown in Figures 9 through 11 represent implementation of the old version of Rockwell's phased array retrodirective network. Separate pilot and reference pick-up antennas are used in the new phase control system, similar to the one described in connection with the solid-state concepts.

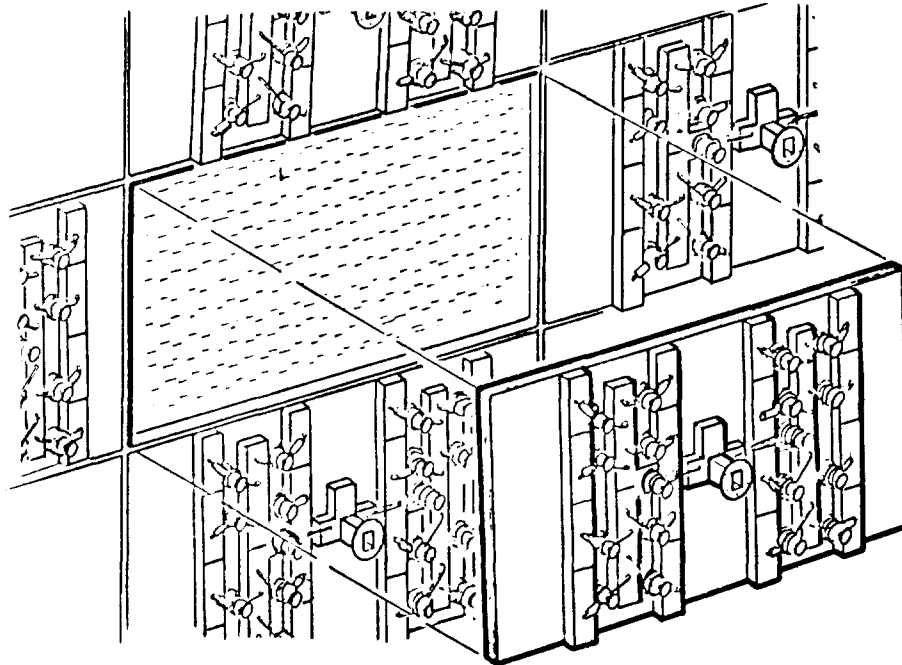


Figure 8. RCR Element Maintenance

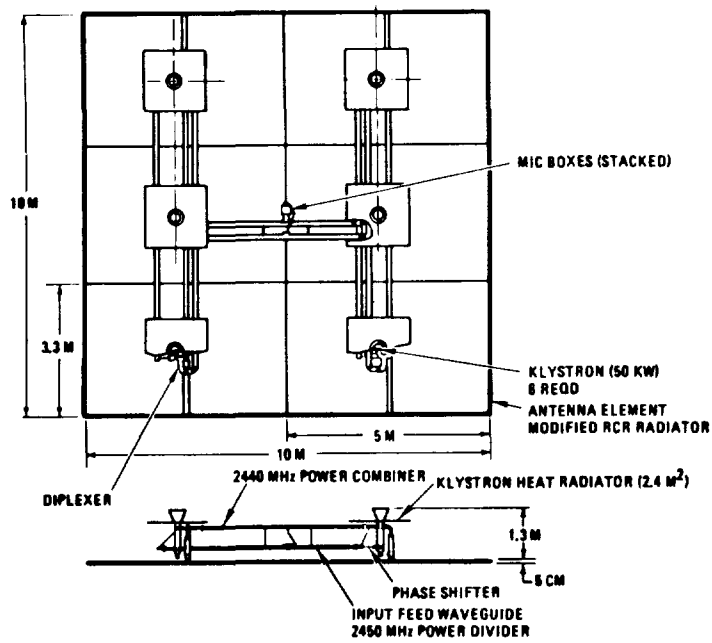


Figure 9. Low-Density 10-Meter-Square Subarray

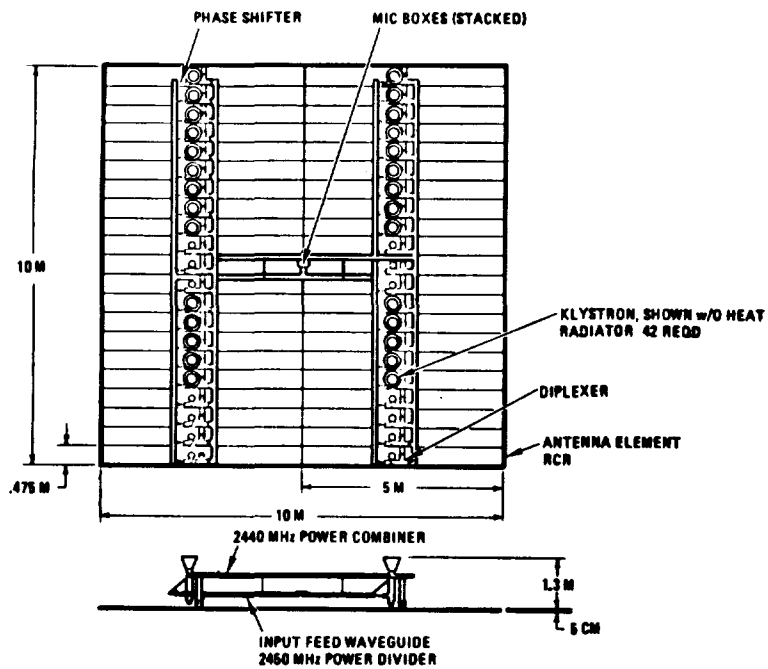


Figure 10. High-Density 10-Meter-Square Subarray

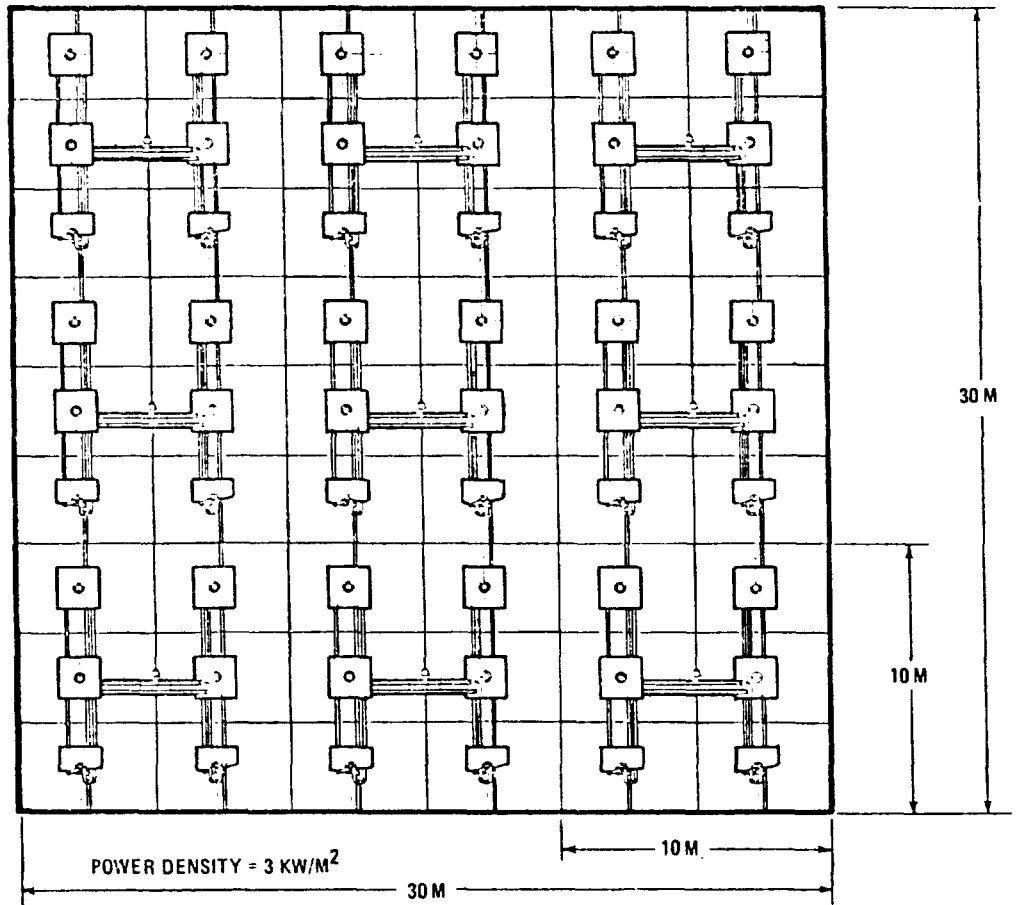


Figure 11. Low-Density 30-Meter-Square Layout Array

EVALUATION OF "THICK WALL" WAVE GUIDE ELEMENT
By Ervin J. Nalos, Boeing Aerospace Company

1.0 SPS ANTENNA ELEMENT EVALUATION

The SPS transmitting array requires an architecture which will provide a low weight, high efficiency and high structural rigidity. Several candidate antenna configurations include the parabolic dish, the parabolic cylinder, the lens and the waveguide slot array. As discussed below, the waveguide slot array is preferred over the other options.

Parabolic dishes are widely used on earth. For SPS application, they could be readily laid up in six-foot diameters with lightweight graphite-epoxy materials. On the other hand, the area efficiency of such an array is relatively low. Moreover, a zero spillover feed configuration is not presently apparent.

An array of parabolic cylinders with line-source feeds could give better area efficiency than an array of dishes, but would suffer from feed blockage.

A lens, using lightweight waveguide structures, with zero blockage behind-the-lens feedhorns can have high efficiency and little spillover, but the SPS center-to-edge illumination tapers would give a spatial "lumpiness" which would produce undesirable grating lobes in the far-field pattern.

As noted above, waveguide slot arrays constitute the most desirable option. Consequently, such an array has been chosen for the SPS. Waveguide slot arrays offer high efficiency, uniform illumination, and are fairly lightweight. Bandwidths of such arrays are narrow, typically 1/2-2%. Although this does not directly impact the SPS, which transmits power at a single frequency of 2.45 GHz, the narrow bandwidth does constrain the thermal and mechanical tolerances of the antenna.

2.0 SLOTTED WAVEGUIDE MODULE DESIGN VERIFICATION

2.1 EXPERIMENTAL PROGRAM

The purpose of this program is to better define the electronic aspects of an SPS specific waveguide slot array. The specific aims of the program are as follows:

- o To build a full-scale half-module, 10 stick, array, the design parameters for which are to be determined by analytical considerations tempered by experimental data on a single slotted radiating stick.
- o To experimentally evaluate the completed array with respect to antenna pattern, impedance and return loss.
- o To measure swept transmission amplitude and phase to provide a data base for design of a receiving antenna.

2.2 ARRAY CONFIGURATION

The first step in module design is to fix the gross dimensions, including the module length and width, and the dimensions of the radiating sticks and the feed waveguide. Because the feedguide is a standing wave device in which the coupling slots must be spaced by $\lambda_g/2$, where λ_g is the guide wavelength, and because λ_g is a function of waveguide width, the radiating stick and feedguide dimensions are not independent.

The SPS baseline design calls for a half-module of ten 1.6 m long sticks of 6 cm x 9 cm cross-section. For these dimensions, at the SPS frequency, the feedguide dimensions are also 6 cm x 9 cm. To assess the desirability of the baseline configuration, the ohmic losses of several alternative configurations of equal area were calculated. The I^2R losses for these are plotted in Figure 1 as functions of radiating stick

in the loss curve is quite shallow. Also, the values of the minima do not appear to be very configurationally sensitive. On the other hand, it was determined in the course of this study that end-feeding of the feedguide may afford somewhat lower loss than expected of the baseline configuration which utilizes center-feeding.

Based on the above considerations, it was decided to configure the experimental module according to the baseline design. The commercially manufactured waveguide which most nearly approximates the baseline guide, is WR-340, with dimensions of 4.32 x 8.64 cm. Because this was not available in sufficient quantity, WR-284 waveguide was used instead for the developmental module. Because this waveguide is narrower than the baseline, and because it would be used for both the radiating sticks and the feedguide, the design frequency of the developmental module was increased from 2.45 GHz to 2.86 GHz. With 6061 Aluminum feedguide, the ohmic losses in the module are expected to be less than 1%.

2.3 WAVEGUIDE STICK DESIGN

The design of the waveguide stick entails the assignment of values to both the slot offset from the waveguide centerline and the slot length. The slot length, l , is chosen so that the slot is resonant at the design frequency. The slot offset is chosen to give the desired slot conductance. This is determined by impedance matching considerations. Thus, for a waveguide stick containing N identical shunt slots, the desired value of normalized slot conductance, g , is just $g = 1/N$.

For a single isolated stick, the choice of slot length and slot offset is relatively straightforward. The slot length is given to good approximation by $l = \lambda_0/2$, where λ_0 is the free-space wavelength. The conductance and slot offset are related to sufficient accuracy by a well known equation.

Tentative radiator stick dimensions in WR-284 waveguide are:

Slot Spacing	3.0 inch	Slot Offset	.187 inch
Slot Length	1.98 inch	Slot Normalized	.055
Slot Width	.125 inch	Conductance	
		Number of Slots	18 or 20

Where several sticks are placed in close proximity, however, as they are in the SPS module, the design problem is exacerbated by mutual coupling between the sticks. That is, the slots in any particular stick are now loaded by the slots in the neighboring sticks and will necessarily exhibit resonant frequencies and conductances which differ significantly from those predicted by single stick equations.

The changes in stick behavior due to mutual coupling effects are shown in Figure 2. Here, both the resonant frequency and the reflection coefficient of a single stick at resonance change noticeably in the presence of a second stick. A theoretical analysis of this problem, based on an adaptation of a mutual coupling analysis for an array of dipoles (L. Stark, Radio Science 1, 361, 1966) is shown in Figure 3. As might be expected, the effects converge rather rapidly, suggesting that a particular slot does not interact to any significant extent with other slots that are more distant than third or fourth neighbors. Figure 3 also shows that mutual coupling effects are also present between neighboring slots of a single stick.

Because of the mutual coupling problem, the choice of slot length and offset has been pursued in an iterative manner beginning from the single stick analytical values. Data for several iterations with two waveguide sticks, are shown in Table 1. Because the slot offsets, once machined, are fixed, stick impedance in these data was varied by changing the number of slots by the means of a sliding short in the waveguide. Adjacent

sticks were fed in-phase using home built four-hole directional couplers machined in one end of each stick, permitting swept return-loss/coupling measurements without interference by guide flanges.

2.4 FEED GUIDE DESIGN

The radiating waveguide sticks are fed in-phase by a feed waveguide whose axis is perpendicular to those of the radiating sticks. Like the radiating sticks, the feedguide supports a standing wave. The power is coupled from the feedguide to each radiating stick through a resonant (length = $\lambda_0/2$) coupling slot which is inclined to the feedguide axis. The transformed radiating stick impedance seen by the feedguide is proportional to $\sin^2 2\theta$, where θ is the inclination angle. The phase of the power coupled to the stick is inverted as the coupling slot is reflected in the feedguide axis. For maximum power transfer to the 10 radiating sticks, each stick must present an impedance to the feedguide of one-tenth the feedguide characteristic impedance. This dictates a rather small coupling slot inclination of about 7° . To maintain proper phasing of the radiating sticks, the coupling slots are alternately reflected in the feedguide axis.

Tentative feed stick dimensions in WR-284 6061 aluminum waveguides for the 1/2-module are:

Slot Spacing	3.0 inch	Slot Normalized Resistance	.10
Slot Length	2.0 inch	Slot Number	10.
Slot Width	.125 inch		
Slot Offset Angle	7.		

3.0 RECEIVING TECHNIQUES EVALUATION

The receiving antenna receives a pilot signal from earth with phase information to keep all modules in-phase. Symmetry considerations argue for the pilot signal to originate from the center of the SPS earth receiving array. Ionospheric phase shift and Faraday rotation call for the pilot signal to be centered on the SPS power frequency with the phase information in symmetrically disposed sidebands. The purposes of the receiving techniques evaluation were to:

- o Conduct a shared antenna versus separate receiving antenna analysis to determine feasible pilot beam budget and receiving antenna constraints due to power module.
- o Design and select a pilot-beam receiving antenna techniques compatible with a power beam array which must allow simultaneous transmission of an S-Band carrier and reception of the anticipated pilot-beam spread-spectrum signal.

The pilot beam link analysis established that very small low gain pilot receiving antenna elements imbedded in the transmitting array are significantly superior to any scheme of diplexing, because: (1) The total system power losses are two orders of magnitude lower with a separate antenna than with any state-of-the-art diplexing device; (2) The small antenna, due to its inherent broad bandwidth, is fully compatible with a spread spectrum signal; whereas the transmit array is not, (3) The small, low gain antenna represents a much lower development risk than a diplexing device.

Also from the pilot beam link analysis, formalisms have evolved from which to determine values of pilot transmitter power and antenna aperture, as well as pilot receiving antenna aperture. The transmitter power and aperture depend foremost upon the requisite pilot link effective radiated power, ERP. The ERP, in turn, depends upon the signal-to-noise requirement of the pilot link receiver; and hence, the noise environment in which the receiving system must operate. Consequently, the ERP requirements were found to be extremely sensitive to the cut-off frequency of a required receiver I.F. notch filter.

The relationship between transmitting antenna diameter and system power loss (efficiency) is shown in Figure 4. This relationship is not monotonic due to the fact that increasing the antenna diameter produces two opposing effects. It reduces the amount of pilot transmitter power required to produce the requisite ERP, while simultaneously increasing the degree of rectenna blockage. At low diameters, the transmitter power effect dominates, and the loss decreases with increasing diameter; whereas, at larger diameters, rectenna blockage becomes most important, and the system loss increases with increasing diameter. Thus, for a particular ERP, there is a rather limited set of pilot transmitter power/aperture combinations which gives minimum system loss.

The relationship between system losses and pilot-link receiving aperture is shown in Figure 5. For small apertures, an increase in aperture reduces system losses due to a decrease in the required ERP. At large apertures, the system losses increase with increasing aperture, due to receiving antenna blockage of the spacetenna. The specific nature of this relationship depends on the required signal-to-noise ratio, S/N, in the pilot receiver, and also on the bandwidth, f_c , of the intermediate frequency notch-filter. As S/N is increased, the pilot ERP must increase, and so also must the system losses. As f_c is decreased, more of the power transmitter noise spectrum is passed by the receiver I.F. This increase in noise must be overcome by an increase in pilot link transmitter power.

As shown in Figure 5, the optimum receiving aperture, under any foreseeable conditions, is quite small. Consequently, the pilot-link receiving antenna requirement can be satisfied by a simple dipole or slot antenna. Adaptations of these to the SPS array are shown in Figure 6. The slot antenna is inserted in a notch cut in the outer portion of adjacent waveguide narrow walls. The dipole is positioned at a distance $\lambda_0/4$ above the array by a small rigid coax feed, which like the slot, is slipped through a hole in the waveguide walls. These antennas may be dimensioned either to be resonant or non-resonant. The aperture of the resonant structure is larger, but so also is the effect on the impedance of the neighboring transmitting-antenna radiating slots. To the extent that the lower aperture can be tolerated, the non-resonant structure is preferred.

An important consideration in the pilot link design is the isolation of the pilot receiver from noise inherent to the high-power down-link signal. With the dipole, isolation can be improved by rotating the antenna so that it is cross-polarized to the power transmitting antenna. An alternate noise-cancelling scheme utilizes two dipoles per receiving antenna, as shown in Figure 6. These are separated by $\lambda_0/4$ and can therefore be connected to pass, as would a directional coupler, radiation coming from the earth, while rejecting that which is earthbound.

One of the candidate receiving antennas in Figure 6, the slot, or "credit-card" receiving antenna, has been built and sweep-tested. It consists of a 1.75" x .062" teflon-glass microcircuit board shorted around three edges to form a low-impedance waveguide cavity.

4.0 ANTENNA EFFICIENCY MEASUREMENTS

The antenna pattern will be measured on one of the six antenna ranges at Boeing. Besides observing the far-field rule $R > 2D^2/\lambda > 180$ ft., high paths and sharp-beam range illuminators will be employed to minimize multipath errors. For the ranges at the Boeing Developmental Center, multipath errors at beam-center are estimated to be well under $\pm .1$ db. Gain is measured using a Scientific Atlanta SA-1740 Precision Amplifier-Receiver, and SA-12-1770 Standard gain horn. Measurement accuracies are estimated as follows:

Standard-gain Horn (Δ gain)	+ .2 db
Match	+ .2 db
Switch mismatch differences between two positions	\pm .2 db
Receiver/mixer linearity	+ .2 db
Total RSS Value	\pm .4 db or \pm 9% in power

By hardwiring the SPS array to the standard gain horn, with their beams pointed near 90° apart to avoid crosstalk, the rf switch and its inherent uncertainty can be eliminated.

The antenna efficiency is obtained from the experimental measurement of gain, G , with respect to a reference horn, and directivity, D . Since the directivity is the gain of a lossless antenna, the ratio of these values represents the efficiency of the antenna. The gain is obtained from the measured value of incremental gain above a calibrated standard horn. The directivity is expressed as the ratio of the maximum radiation intensity, U_{max} to the average radiation intensity \bar{U} , which is given by $\bar{U} = 1/4\pi \int U(\theta, \phi) d\Omega$.

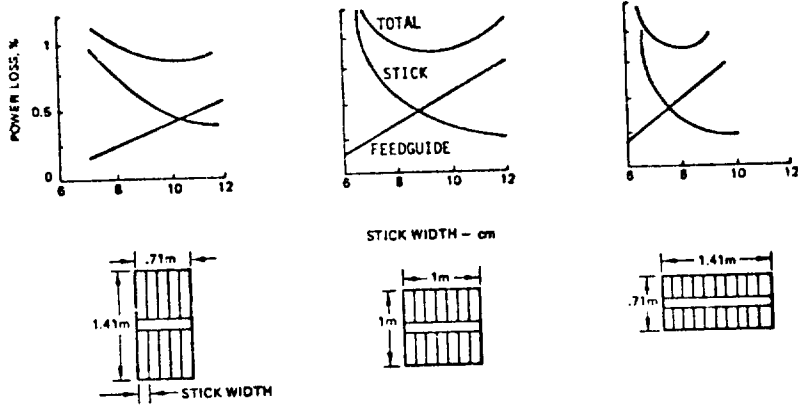
The directivity measurement is carried out separately by rotating the antenna continuously through selected azimuth and elevation angles and integrating the far field contributions over a solid sphere, thus obtaining the directivity with reference to an isotropic radiator as $D = U_{max}/\bar{U}$.

The efficiency is obtained from the ratio of two separately measured experimental values, $\eta = G/D$. With currently available antenna range accuracy, this measurement is typically determined to \pm .4 db accuracy. The resulting efficiency value will give an indication of ohmic losses in the waveguide feed system and in the radiating sticks. In the SPS baseline design, this loss is estimated to be less than 0.1 db, and the antenna range measurement will thus provide a crude verification only.

TABLE: 1 ITERATIVE DESIGN PROCEDURE FOR RADIATING STICK PARAMETERS

STICK NUMBER	NO. OF SLOTS ¹ FOR BEST MATCH		SLOT ³ OFFSET	SLOT LENGTH	COMMENT
	SINGLE STICK	WITH ² NEIGHBOR			
1	22	20	.18"	2.04"	RESONANCE @ 2800 MHz SLOT TOO LONG
2	16	14	.20"	1.94"	RESONANCE @ 2860 MHz SLOT TOO SHORT TOO MUCH CONDUCTANCE PER SLOT
3	18	16	.197"	1.98"	RESONANCE AT 2875MHz
4	18	18	.180"	2.00"	EXPECT 2860 MHz ⁴

1. SLIDING SHORT MEASUREMENT: VSWR AT RESONANCE < 1.1
2. NON-DUPLICATE STICKS ARE USED TO APPROXIMATE MUTUAL COUPLING EFFECT
3. AFFECTS PRIMARILY SLOT CONDUCTANCE
4. DESIRED FREQUENCY FOR FEED GUIDE TO BE IDENTICAL TO RADIATING STICK GUIDE (WR240)



- NOT SENSITIVE TO MODULE ASPECT RATIO
- NOT VERY SENSITIVE TO WAVEGUIDE SIZE
- STICK STANDING WAVES SUGGEST END FEEDING PREFERABLE

Figure 1 : RF Module P²R Optimization

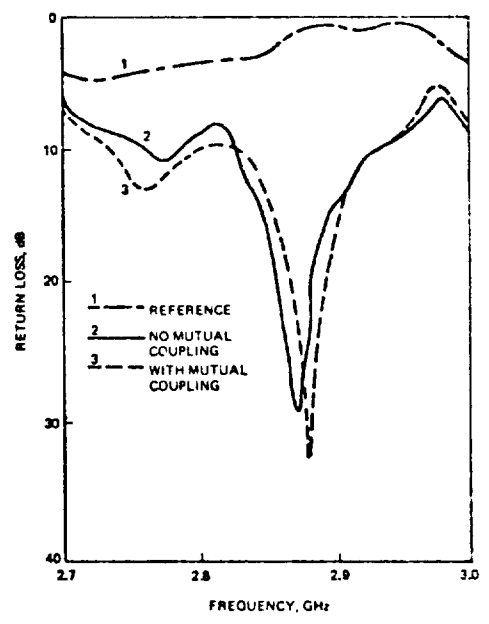


Figure 2: Effect of Mutual Coupling - Two Stick Measurement

ANALYTICAL EXPRESSION¹

$$\frac{y}{y_0} = \frac{4 \sin^2 \beta_c s_H (1 - \cos) \cos^2 \left(\frac{\pi}{2} \sqrt{1 - \frac{\lambda^2}{2b^2}} \right) \sin^2 \left(\frac{\pi x}{a} \right)}{2 \lambda^2 \left[1 + \cos^2 \left(\frac{\pi}{2} \sqrt{1 - \frac{\lambda^2}{2b^2}} \right) \right]}$$

WHERE

$$m = n = k$$

$$w = \sum_{l=1}^L \left[\frac{\sin \left(\frac{\pi y_l}{s_c} \right)}{\frac{\pi y_l}{s_c}} \right]^2 \left[\cos \left(\frac{\pi x_l}{2s_H} \right) \right]^2 \left[\left(\frac{\pi x_l}{s_H} \right)^2 + 1 \right]$$

$$m = l = n = k$$

$$m \neq 0, a \neq 0, \left[\frac{\sin \left(\frac{\pi y}{s_c} \right)}{\frac{\pi y}{s_c}} \right]^2 \left[1 - \left(\frac{\pi x}{2s_H} \right)^2 \right] \sqrt{\left(\frac{\pi x}{s_H} \right)^2 + \left(\frac{\pi y}{s_c} \right)^2}$$

1 = X THE NUMBER OF NEIGHBORING SLOTS CONSIDERED IN THE 'S' PLANE
 k = X THE NUMBER OF NEIGHBORING SLOTS CONSIDERED IN THE 'W' PLANE

b = GUIDE I.D. WIDTH x = SLOT OFFSET
 a = GUIDE I.D. WIDTH X = SLOT OFFSET
 b = GUIDE I.D. HEIGHT s = SLOT WIDTH
 s_c = SLOT 'S' PLANE SPACING y = SLOT SHUNT ADMITTANCE
 s_H = SLOT 'W' PLANE SPACING y₀ = GUIDE CHARACTERISTIC

1. MODIFICATION OF STARK'S DIPOLE EXPRESSION TO SLOTS

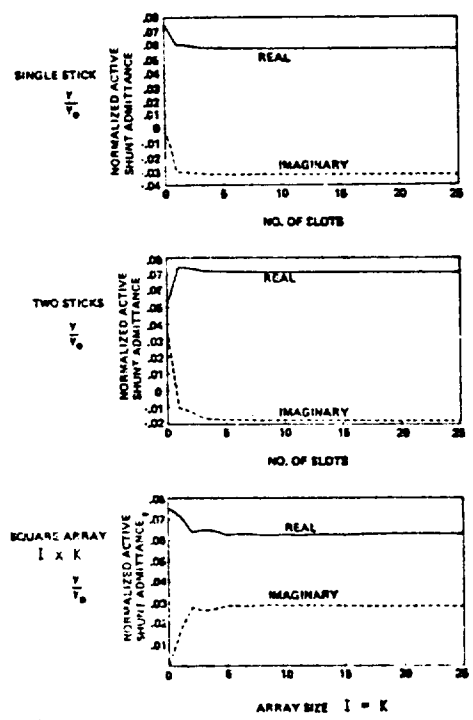


Figure 3: Estimate of Mutual Coupling in SPS Slotted Waveguide Array

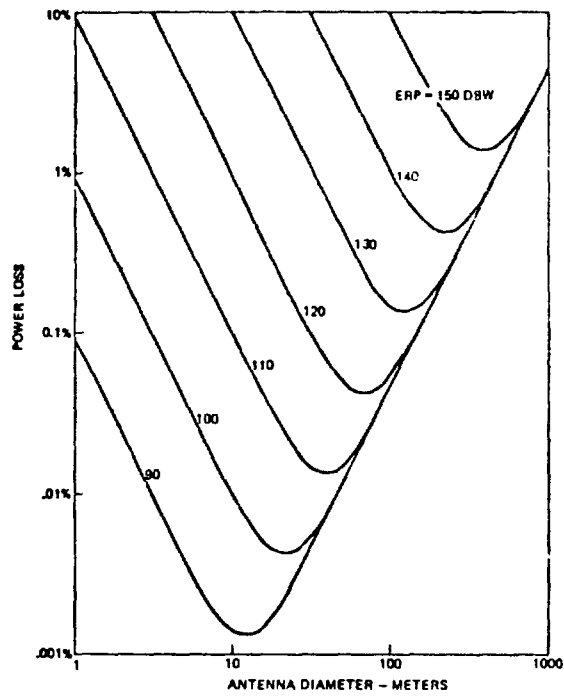


Figure 4 System Power Loss Vs. Pilot Transmit Antenna Diameter and ERP Required

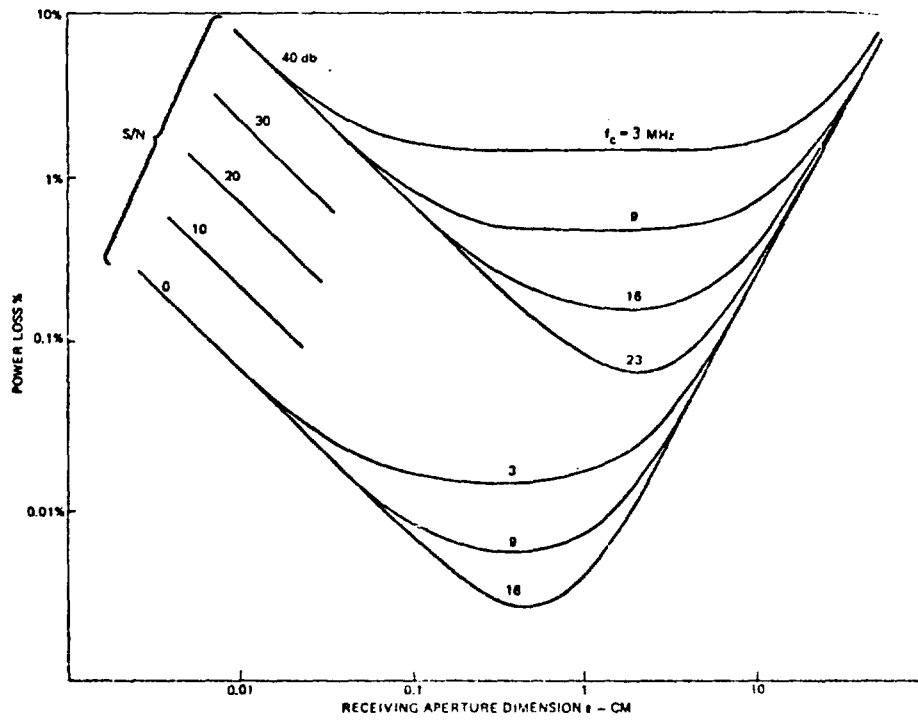


Figure 5 : Total System Loss Vs. Receive Aperture

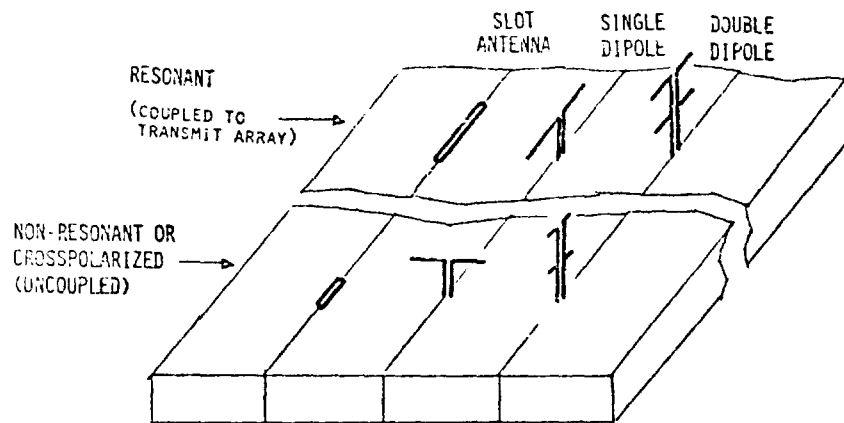


FIGURE 6: POTENTIAL SPS PILOT-LINK RECEIVING ANTENNA CONFIGURATIONS.
 THE DOUBLE DIPOLE CONFIGURATIONS AFFORD PARTIAL NOISE
 CANCELLATION.

METHOD FOR PRECISION FORMING OF LOW-COST, THIN-WALLED SLOTTED WAVEGUIDE ARRAYS FOR THE SPS

William C. Brown
Raytheon Company

Presented at the RADIATING ELEMENTS SESSION OF THE SPS MICROWAVE SYSTEMS WORKSHOP
January 15-18, 1980, Lyndon B. Johnson Space Center, Houston, Texas

ABSTRACT

A method for the precision-forming of thin-walled, slotted-waveguide arrays has been devised. Models have been constructed with temporary tools and evaluated. The application of the method to the SPS requirements is discussed.

Introduction

The method for forming thin-walled slotted waveguide arrays that will be described grew out of a necessity to narrow down the broad range of estimated cost for slotted waveguide arrays in ground based arrays. In most items that are designed for automated production the cost of the material is the dominant element of cost. Therefore the use of thin material is attractive because of the large reduction in material cost. Then, if a rapid, inexpensive method of fabrication can be devised, the cost of the slotted waveguide arrays will be low and can be accurately estimated.

Such a fabrication method had been devised in principle by the author. An opportunity then arose to build working models of the design as part of a contract with JPL for the improvement of microwave beamed power technology, using a slight modification of their electrical design for such an array.

The working models that were made from 0.020 inch material were mechanically so strong and the fabrication technique so well adapted to even

thinner material that the potential for a slotted waveguide array made from 0.005 inch or even thinner material for the SPS applications is very good.

Early estimates of the mass of a slotted waveguide array for the 1 kilometer diameter transmitting antenna for the SPS were based on the use of 0.020 inch thick aluminum material and these estimates may still persist and show up in current estimates of mass for the SPS. An array based on the use of 0.005 inch material in place of the 0.020 inch would save nearly 2.5×10^6 kilograms of material. Savings in transportation costs alone would be 250 million dollars if transportation costs were only \$100 per kilogram.

The fabrication of thin-walled guides can also be accomplished with great precision. Tolerances of $\pm 2-3$ mils should be possible.

Finally it appears, as shown in Figure 1, that the arrays can be relatively easily fabricated in space from rolls of aluminum foil which represents an ideal packing factor for transportation purposes.

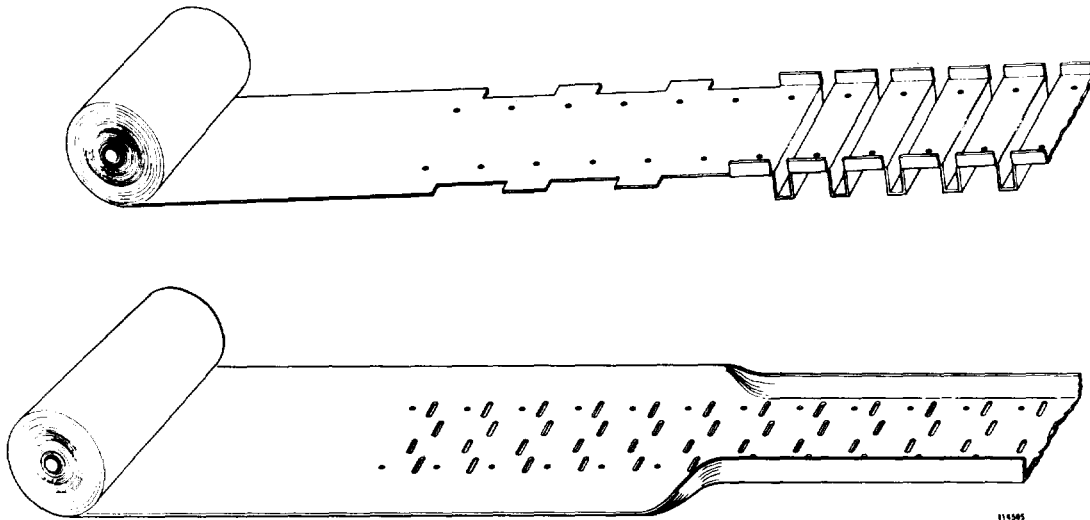


Figure 1. Proposed Method for Precision Forming and Assembly of Low-Cost, Thin-Walled, Slotted Waveguide Arrays for the SPS.

Description of Fabrication Method

The slotted waveguide array as shown in Figure 1 consists basically of a folded top plate whose corrugations contribute the three sides of the waveguide and a bottom plate into which the radiating slots are punched. The two sections then flow together and are joined to each other either by resistance spot welding or by laser beam welding to form the finished assembly shown in Figure 2.

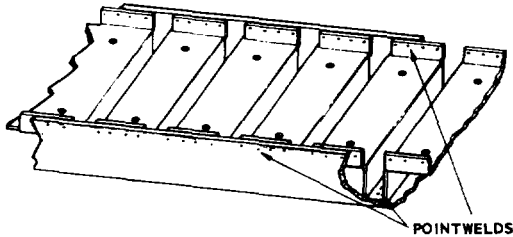


Figure 2. Finished Assembly.

The holes which are punched into the material are spaced accurately from each other and serve to accurately locate the material in the bending fixture which is also accurately machined and ground. The holes also serve to jig the top and bottom halves to each other for accurate assembly.

The method as originally proposed by the author utilized a third piece in the assembly that joined the top and bottom at their ends. An improvement to simply eliminate the end plate by the upward fold of the end of the top and bottom pieces as shown in Figure 1 is the suggestion of R.M. Dickinson.

It is possible that the broad faces of the waveguide members, both top and bottom, may need some stiffening to avoid bending and "oil canning". The thin flat channels that are proposed to house the phase and amplitude references and auxiliary power lines perform this function on the slotted surface. The unslotted surfaces could be embossed to stiffen them.

The individual slotted waveguides in the array are fed from a feed waveguide shown in Figure 3 as the transverse waveguide. Transfer of energy is made through diagonal slots between the feed waveguide and radiating waveguides. The feed waveguide is attached to the array by means of pop rivets.

Construction and Evaluation

Two 8 x 8 (8 slots in 8 waveguides) arrays were constructed from 0.020 inch aluminum with the use of temporary tooling of a simple nature. The $\frac{1}{4}$ inch separation between waveguides that is necessary in the forming process and which have become attractive as a region in which to mount solid state devices and through which to run cables made it necessary to adjust the dimensional specifications of the JPL design which was designed for a different fabrication method.

The slotted face plate, folded waveguide section, and the end channels were assembled to each other by spot welding. Back and front view of the finished assembly are shown in Figures 3 and 4.

In the absence of any antenna testing range a method was evolved to test the array by electrically probing each slot for amplitude and phase, as shown in Figure 5. This arrangement gave the phase and

amplitude information tabulated in Table I. When readings around the outside are disregarded because of edge effects, the rms phase and amplitude percentage deviation of the remaining sections are 6.22° and 10% respectively. With the outer elements included the phase deviation is 8.89°.

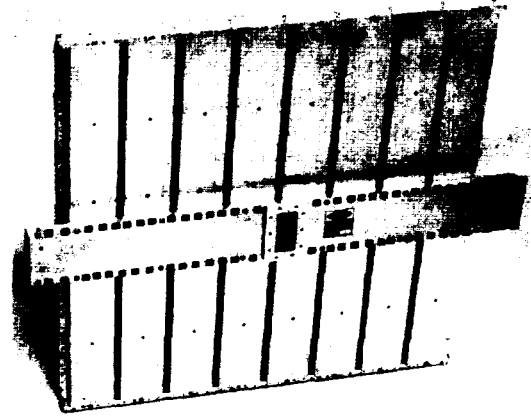


Figure 3. Back View of the 8 x 8 Slotted Waveguide Array as Constructed from 0.020 Inch Aluminum Sheet Throughout and Assembled by Means of Spot Welding.

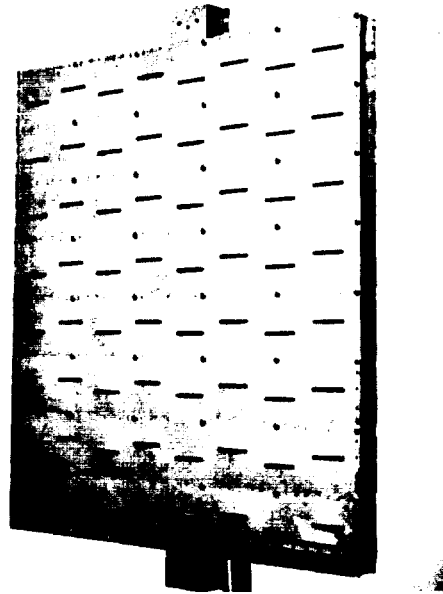


Figure 4. Front View of the 8 x 8 Slotted Waveguide Array as Constructed from 0.020 Inch Aluminum Sheet Throughout and Assembled by Means of Spot Welding.

Finally, the antenna range data taken by JPL on the array that was made for them as a portion of the contractual work effort for them is presented in Figures 6 and 7.

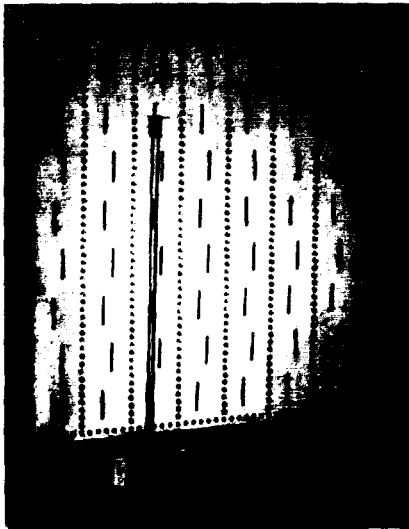


Figure 5. Probe Arrangement for Measuring Phase and Amplitude of Microwave Power Radiated at Individual Slots. The Phase and Amplitude Sensed by the Probe were Compared by Means of a Hewlett-Packard Network Analyzer with the Amplitude and Phase of the Power Input to the Single Waveguide Feed to the Slotted Waveguide Array.

TABLE I
Matrix Array of Amplitude and Phase Information on Thin Metal Slotted Array #1

Col		1	2	3	4	5	6	7	8
Row									
1	Phase	105	100	107	110	103	96	93	105
	Amp	.53	.57	.67	.70	.64	.61	.62	.62
2	Phase	104	84	80	82	91	94	79	90
	Amp	.61	.51	.59	.67	.71	.72	.59	.40
3	Phase	94	80	88	89	85	85	94	106
	Amp	.45	.58	.63	.71	.64	.58	.56	.56
4	Phase	105	79	80	73	80	89	72	94
	Amp	.61	.56	.60	.73	.73	.69	.65	.40
5	Phase	120	81	86	76	70	85	84	120
	Amp	.50	.60	.59	.72	.68	.52	.58	.50
6	Phase	96	80	74	83	92	90	79	91
	Amp	.68	.53	.57	.68	.72	.69	.60	.39
7	Phase	89	73	83	82	80	86	91	104
	Amp	.49	.60	.67	.69	.61	.60	.54	.55
8	Phase	100	86	90	93		96	88	160
	Amp	.59	.60	.53	.63		.70	.57	.45

Overall array is an 8 x 8 matrix

"Internal" array is a 6 x 6 matrix

Test data obtained by dipole probe placed in front of each radiating slot.

RMS of phase deviation of internal array is 6.22°.

RMS of phase deviation of overall array is 8.89°.

RMS of amplitude variation of internal array is 0.0628 from a mean value of 0.627.

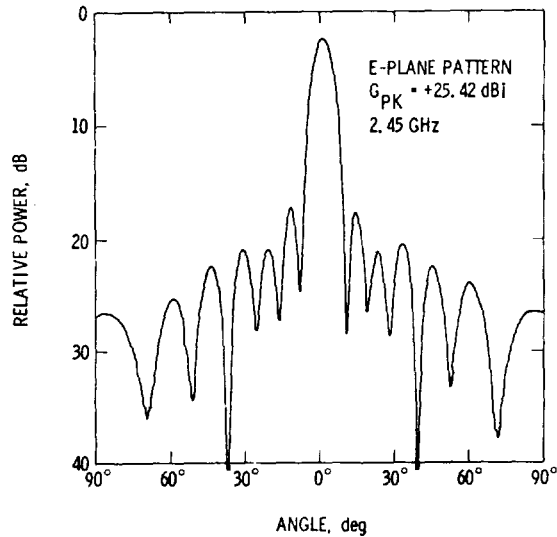


Figure 6. Antenna Pattern for 8-Slot x 8-Stick Slotted Waveguide Antenna.

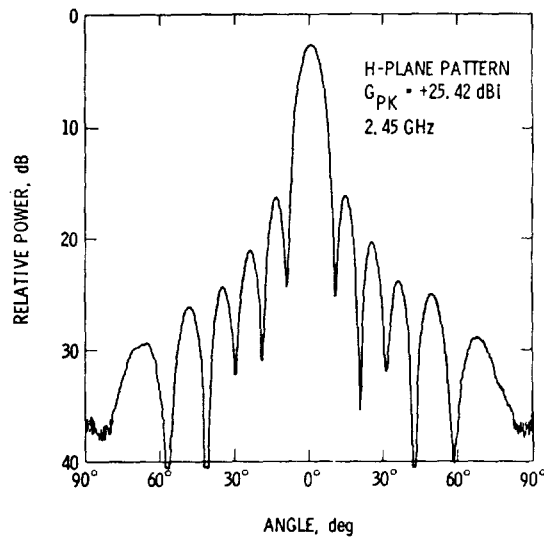


Figure 7. Antenna Pattern for 8-Slot x 8-Stick Slotted Waveguide Antenna.

CONSIDERATIONS FOR
HIGH ACCURACY RADIATION EFFICIENCY
MEASUREMENTS FOR THE
SOLAR POWER SATELLITE (SPS) SUBARRAYS

D. J. Kozakoff, J. M. Schuchardt and C. E. Ryan

Georgia Institute of Technology
Engineering Experiment Station
Atlanta, Georgia 30332

INTRODUCTION

The relatively large apertures to be used in SPS [1], small half-power beamwidths, and the desire to accurately quantify antenna performance dictate the requirement for specialized measurements techniques. The subject matter presented herein is under investigation as part of a program at Georgia Tech to address the key issues*.

The objectives of the program include the following:

- 1) For 10-meter square subarray panels, quantify considerations for measuring power in the transmit beam and radiation efficiency to $\pm 1\%$ (± 0.04 dB) accuracy.
- 2) Evaluate measurement performance potential of far-field elevated and ground reflection ranges and near-field techniques.
- 3) Identify the state-of-the-art of critical components and/or unique facilities required.
- 4) Perform relative cost, complexity and performance tradeoffs for techniques capable of achieving accuracy objectives.

The precision required by the techniques discussed below are not obtained by current methods which are capable of $\pm 10\%$ (± 0.4 dB) performance. In virtually every area associated with these planned measurements, advances in state-of-the-art are required.

ERROR SOURCES

In general, the RF and physical environment and the electronic instrumentation all contribute to the overall measurement error. Ideally, the RF source is stable in amplitude and frequency, the transmitted wave arrives at the receiver as a true plane wave free of objectionable reflections, and the atmospheric effects are negligible. The receiver must be ideal and error free, and the gain antenna reference is accurately known. In the real world, one must deal with the errors which occur as the instrumentation departs from the ideal performance listed above.

For SPS subarray antenna pattern measurements, the critical error sources have been quantified into four categories shown in Table 1. The objective of this investigation is controlling these error sources to yield an overall gain uncertainty of ± 0.04 dB. Because of the large size of an SPS subarray (81.67-wavelengths at 2.45 GHz), antenna range effects are given

*Contract NAS8-33605

the largest allowance in the error budget. The errors allocated to transmitter/receiver sources require advances in state-of-the-art of associated microwave electronics. However, even with currently available equipment, because of single frequency operation, and the fact that receiver and transmitter are phase-locked and thermally stabilized, errors can be accurately controlled. Use of a microcomputer will permit error compensation of such factors as the nonlinearity of receiver and detector.

Controlling the antenna structure for measurement will require developing a cradle assembly that will hold the antenna rigid. Preliminary weight estimates indicate approximately 2.5 tons for a prototype subarray assembly. Ambient temperature, solar energy and wind effects can be controlled somewhat by selecting the measurement time period. However, since several thousand 10-meter apertures may need to be measured during the course of the SPS program, unique test facilities are anticipated. For instance, shielding from the adverse external parameters listed above can be achieved through use of a large dome radome.

Antenna measurements can be made with the test antenna either receiving or transmitting because of the reciprocity theorem. However, in the case where the SPS array is transmitting and the goal is to determine power in the transmit beam via beam integration, unique problems arise. Figure 1 illustrates one measurement concept being considered.

FAR-FIELD MEASUREMENT CONCEPTS

The predominant error contributors for far-field measurements are 1) field nonuniformity due to ground reflection, 2) gain loss due to quadratic phase error (near-field effects), and extraneous reflections. The National Bureau of Standards has investigated error budgets associated with far-field measurements [2]. For SPS, an adopted far-field error subbudget is shown in Table 2. The large size of an SPS subarray dictates a far-field criteria of greater than $6 D^2/\lambda$ to maintain quadratic phase error loss below 0.01 dB.

Field nonuniformity can be controlled via an elevated range concept where the receive antenna null is placed at the midpoint reflection point as depicted in Figure 2. Tradeoff calculations indicate the required tower heights for elevated range distances greater than $6 D^2/\lambda$ are not practical, however, consideration for a mountain top to mountain top range with an elevation of 600 feet and a measurement range of 7 miles appears very attractive.

Consideration was given to use of a ground reflection range facility. Here, transmit and receive tower heights are selected so that the reflection from the ground adds in phase to the direct ray path. A negative feature is that a relatively large range is required to obtain a sufficiently flat amplitude wavefront over the vicinity of the test antenna. Figure 3 relates the transmit and receive tower heights as a function of range. Under the constraint of a minimum and maximum tower height of 20 and 100 feet, respectively, and minimum range of 3 miles based on near-field criteria; the shaded area indicates regions where satisfactory operation may be obtained. The criteria for a sufficiently flat amplitude wavefront over the test zone is currently under investigation. Initial calculations indicate the performance of a 4-mile ground reflection range with receive and transmit tower heights of 30 and 70 feet, respectively, provided a wavefront within 0.1 dB over a 10-meter zone, but only with use of high efficiency absorber barricades at the midrange point.

POSITIONER CONSIDERATIONS

The large weight handling requirement (2.5 tons minimum)*, and small angular accuracy requirements, indicate that the positioner is a potential problem area based on units currently available. It has been determined that the positioner must be able to resolve a sample within 0.0016 degrees corresponding to a 19 bit encoder to resolve the beam power within a ± 0.04 dB accuracy.

A survey was made of available antenna positioners, and is summarized in Table 3. The positional accuracy of off-the-shelf positioners is on the order of 0.005 degrees. Available positioner data indicate positioning of anything larger than the 10-meter subarray will not be possible based on the weight projections.

The fractional power in the beam based on a uniformly illuminated 10-meter square aperture is plotted in Figure 4. Here, it is seen that the main beam (± 0.312 degrees) encompasses approximately 79 percent of the transmitted energy.

Based on these results, a concept was devised providing desired scan performance as illustrated in Figure 5. Here, a small angle positioner (SMAP) provides very accurate scan capability over a ± 1.5 degree sector for the purpose of beam integration. The larger gimbal arrangement provides coarse positioning over the complete ± 20 degree sector. Positioner hardware providing greater angular scan does not currently exist. From the plot of fractional beam power (Figure 4) approximately 89% of the total radiated power is accounted for within $\pm 1.5^\circ$ scan; over 99% of the power is radiated in the ± 20 degree sector.

NEAR-FIELD MEASUREMENTS

Near-field techniques utilize a calibrated probe antenna to measure the amplitude and phase of the field close to the antenna aperture. Two orthogonally-polarized probes, or a single linear-polarized probe oriented in the vertical and horizontal directions are used, together with a probe compensation technique [8, 9] to obtain the complete radiation characteristics of the antenna under test (AUT). This measurement procedure requires an automated facility capable of reading the measured data in digital form for the required computer processing. The planar near-field measurement technique is particularly attractive for SPS since the SPS subarray does not have to be moved during the measurement, i.e. only the probe antenna is moved.

Recent work at Georgia Tech has demonstrated that accurate antenna patterns can be obtained via near-field techniques [4, 5]. The National Bureau of Standards has shown that for planar near-field scanning, the near-field derived patterns are more accurate than far-field measured patterns when considering all error sources involved [6].

Martin Marietta [3] has implemented an indoor planar near-field measurements facility capable of measurement of antennas up to 50-foot diameter. The benefits of this facility include all weather operation, a thermally controlled environment (maintained within 2°F), and an RF anechoic environment. RCA has also implemented an indoor planar near-field facility for acceptance testing of the AN/SPY-1 phased array antenna for the AEGIS system [10].

*This weight estimate is based on using either conventional aluminum waveguide (without klystrons) or ultra-thin aluminum waveguide with klystrons included.

Near-field measurements can also be implemented by employing cylindrical or spherical probe scanning. However, in the spherical technique it is necessary to move the AUT while holding the probe fixed. In the case of SPS, spherical near-field scanning cannot be used because of the difficulty of gimbaling the heavy subarray in order to scan over a full sphere. However, planar and cylindrical scanning concepts are applicable. A planar scan concept is shown in Figure 6 and a cylindrical concept in Figure 7. Either system has potential to be implemented outdoors, however, the effects of thermal changes on scanning mechanism and instrumentation and the fact that an outdoor facility is subject to environmental conditions, makes an indoor near-field facility far more attractive and practical.

Tradeoff studies at Georgia Tech have suggested that the planar near-field concept has potential for array measurements of an SPS mechanical module (30 square meters). Problem areas to be resolved include computer requirements and the complexity of scanning over a much larger surface with acceptable precision. A previous study performed by Georgia Tech for NASA indicated that the cylindrical near-field technique is attractive for the measurement of electrically and physically large ground station antennas [11].

Previous studies at Georgia Tech have considered the cost tradeoffs of far-field measurements versus a near-field measurement [8, 11]. The results of these investigations for both large phased array and large reflector antennas demonstrate that costs are less for the near-field facility, and that the projected measurement accuracy is superior to that which could be obtained on a high quality far-field antenna measurement range.

However, the capital investment and operating costs of the near-field facility are functions of the required measurement accuracy. For example if the on-axis antenna gain is to be determined to within 0.01 dB, the measurement probe axial position accuracy must be within 0.1 wavelength, i.e. 0.048 inches for the SPS. Also, the scan width-to-diameter ratio must be at least 1.5. Thus, this requirement has a direct effect on the mechanical design of the near-field measurement system.

In order to obtain a complete representation of the antenna pattern from a planar or cylindrical near-field scan, the field is normally sampled at $1/2$ wavelength intervals along the linear scan dimension. If the AUT is electrically large, the required Fourier transform processing can become burdensome. However, it has been shown that the sample spacing can be increased by almost an order of magnitude if only the main-beam and first sidelobes are to be defined [4, 11].

In order to obtain accurate polarization information on the antenna pattern, the polarization characteristics of the measurement probe must be carefully characterized over the maximum possible dynamic range. Work at RCA [7] has also indicated that careful probe polarization design is necessary too if a very accurate gain determination is required. For instance, assuming an SPS antenna polarization ratio of 30 dB, a probe polarization ratio of 20 dB will result in a gain measurements error of approximately 0.25 dB. Thus, a very stringent requirement is placed on probe polarization ratio; a requirement of 30 dB, or better, is anticipated.

CONCLUSIONS

Because of the large electrical size of the SPS subarray panels and the requirement for high accuracy measurements, specialized measurement facilities are required. Most critical measurement error sources have been identified for both conventional far-field and near-field techniques. Although the adopted error budget requires advances in state-of-the-art of microwave instrumentation, the requirements appear feasible based on extrapolation from today's technology.

Additional performance and cost tradeoffs need to be completed before the choice of the preferred measurement technique is finalized.

REFERENCES

1. "Solar Power Satellite Concept Development and Evaluation Program," U.S. Department of Energy and NASA Report, October 1978.
2. "Accuracy Considerations in the Measurement of the Power Gain of a Large Microwave Antenna," M. Kanda, 1974 IEEE/AP-S Symposium, Georgia Tech, Atlanta, June 1974.
3. "Near-Field Pattern Measurement Facility," C. E. Kirchoff, 1979 Antenna Applications Symposium, U. of Illinois, September 1979.
4. "Probe Compensated Near-Field Measurements Basic Theory, Numerical Techniques, Accuracy," W. M. Leach, Jr., E. B. Joy and D. T. Paris, IEEE/AP-S Symposium, Georgia Tech, June 1974.
5. "Automated Near-Field Measurements to Obtain Far-Field Patterns of Aperture Antennas and Phased Arrays," H. A. Ecker, et al, IEEE/AP-S Symposium, Georgia Tech, June 1974.
6. "Upper Bound Errors in Far-Field Antenna Parameters Determined From Planar Near-Field Measurements: Part 1-Analysis," A. D. Kaghjian, National Bureau of Standards Technical Note 667, October 1975.
7. "Automated Near-Field Test Set for Phased Array Production," D. Staiman, 1979 Antenna Applications Symposium, U. of Illinois, September 1979.
8. "Correction of Near-Field Antenna Measurements Made with an Arbitrary But Known Measuring Antenna," D. M. Kerns, Electronics Letters, Vol. 6, May 1970.
9. "Plane Wave Scattering Matrix Theory of Antenna and Antenna-Antenna Interaction: Formulation and Application," D. M. Kerns, Journal of Research of the Nation Bureau of Standards, Vol. 80B, No. 1, January 1976.
10. "Implimenting a Near-Field Antenna Test Facility," W. A. Harmening, Microwave Journal, Vol. 22, No. 9, September 1979
11. "A Study of the Application of Near-Field Measurements for NASA Requirements," B. J. Cown, C. E. Ryan, Jr., A. L. Bridges and J. D. Adams, Final Engineering Report, Contract NAS5-2234, Georgia Institute of Technology, March 1976.

TABLE 1
MEASUREMENTS ERROR BUDGET

ERROR SOURCE	ERROR COMPONENTS	ALLOWABLE VALUE IN ERROR BUDGET	COMMENTS
ANTENNA RANGE	FIELD UNIFORMITY	.037 dB	AN ADEQUATE GAIN STANDARD HAS NOT YET BEEN IDENTIFIED REFERENCE RECEIVER MUST BE USED TO NORMALIZE EFFECTS OF ATMOSPHERE
	QUADRATIC PHASE ERROR		
	EXTRANEIOUS REFLECTIONS		
	STANDARD GAIN ANTENNA UNCERTAINTY		
STRUCTURAL/ ENVIRONMENTAL	ATMOSPHERIC EFFECTS	.01 dB	WIND LOADING/THERMAL CAN BE CONTROLLED BY RADOME OVER TEST ANTENNA
	SPS ANTENNA RIGIDITY/STABILITY		
	POSITIONER ERROR		
TRANSMITTER	WIND LOADING THERMAL	.01 dB	PHASE LOCKED TECHNIQUES AND TEMPERATURE STABILIZATION MUST YIELD AMPLITUDE STABILITY OF 0.007 dB
	AMPLITUDE STABILITY		
RECEIVER	FREQUENCY STABILITY	.01 dB	ATTENUATOR CALIBRATED TO 0.005 dB S/N RATIO MUST EXCEED 40 dB THROUGH ENVIRONMENTAL CONTROL DETECTOR CALIBRATION CAN EXCEED 0.005 dB VSWR KEPT BELOW 1.05
	PRECISION ATTENUATOR UNCERTAINTY		
	REFERENCE INPUT PHASE/ AMPLITUDE ERRORS		
	SIGNAL TO NOISE RATIO		
	FREQUENCY STABILITY		
	DYNAMIC RANGE		
DETECTOR LINEARITY VSWR			

TOTAL RSS = .04 dB

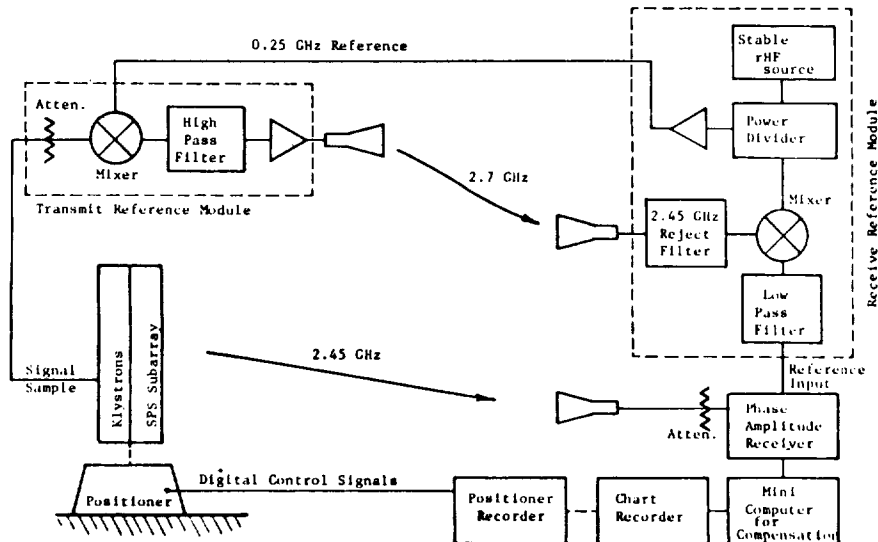


Figure 1. Equipment Configuration for Antenna Measurements.

TABLE 2
 ANTENNA RANGE MEASUREMENTS
 ERROR SUB-BUDGET

<u>ERROR COMPONENT</u>	<u>ALLOWABLE VALUE</u>	<u>COMMENTS</u>
Field Uniformity	0.015 dB	Maximum amplitude taper at edge of SPS subarray approx. 0.04 dB
Quadratic Phase Error	0.010 dB	Requires range greater than $6 D^2/\lambda$
Standard Gain Antenna Uncertainty	0.020 dB	Gain standard needs to be developed
Atmospheric Effects	0.005 dB	Atmospheric effects cancelled by reference
VSWR	0.005 dB	VSWR loss calibrated out
Extraneous Reflections	0.025 dB	Extraneous reflections -57 dB down
RSS Subtotal	0.037 dB	

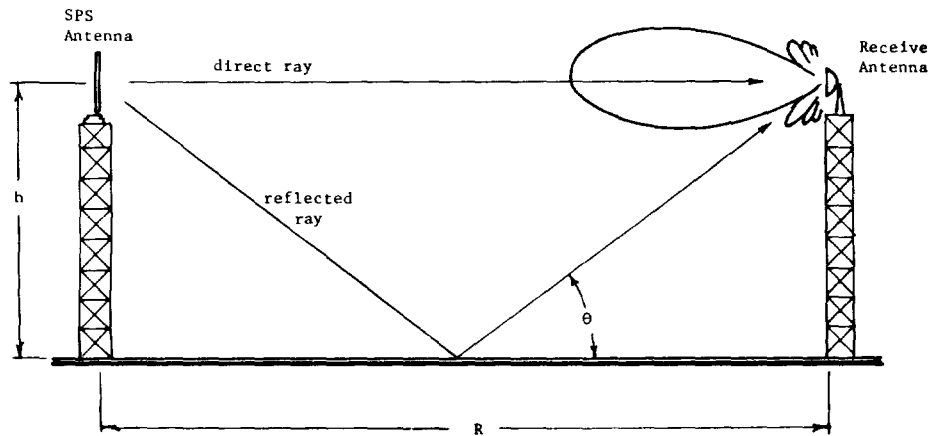
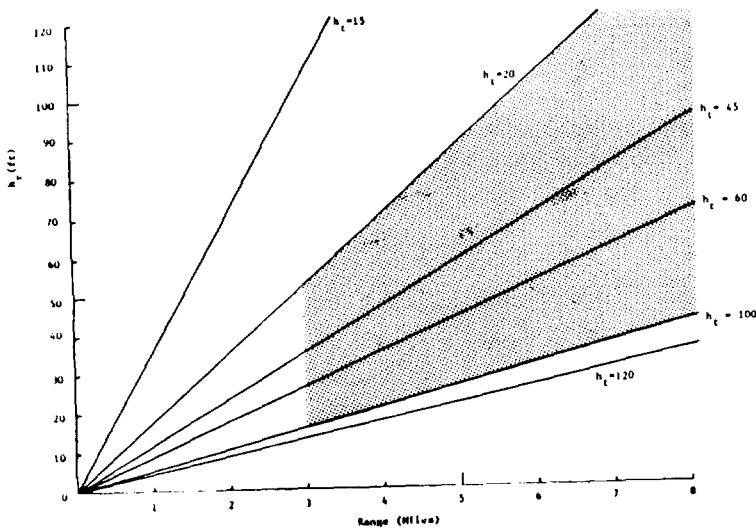


Figure 2. Elevated Antenna Range.



Note: Darkened area is allowable operating region.

Figure 3. Relation Between Receive Antenna Height (h_r), and Transmit Antenna Height (h_t) for a Ground Reflection Antenna Range.

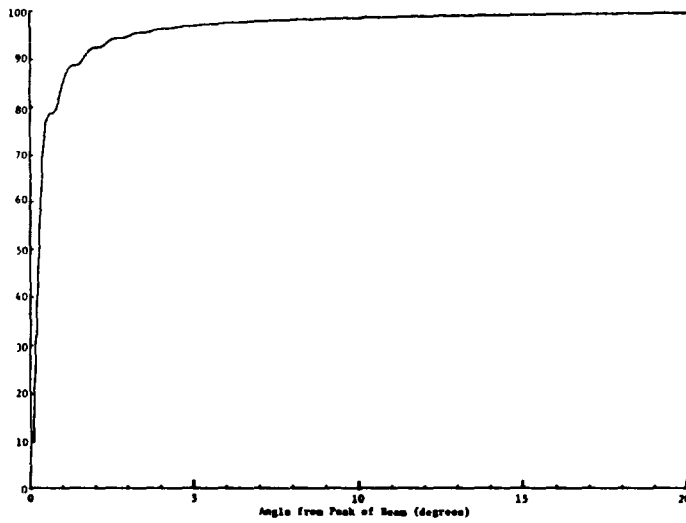


Figure 4. Fractional Beam Power for SPS Subarray Pattern.

Figure 5. Antenna Positioner Mechanism For Far-Field Pattern Measurements.

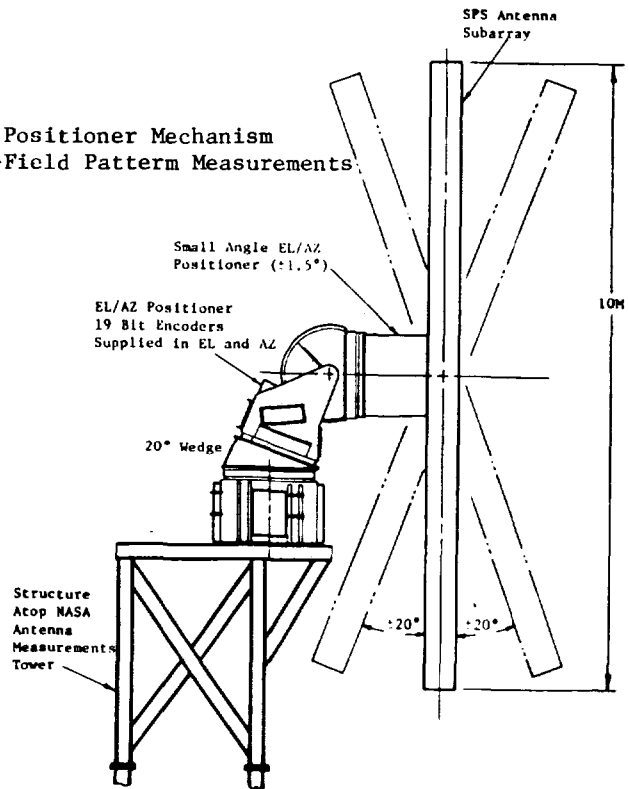


TABLE 3
SUMMARY OF POSITIONER PERFORMANCE

Scientific Atlanta Series**	Maximum Moment (Kft-lb)	Estimated Moment Arm* (ft)	Maximum Subarray Wt.		Cost***		
			Klbs	Tons	Elev./Az.	SMAP	Total
85	150	9.5	15.8	7.9	\$ 440K	\$400K	\$ 840K
45	75	7.5	10	5	\$ 111K	\$100K	\$ 211K

* Elevation over azimuth plus SMAP configuration.

** NOTE: the series 85 has a maximum vertical load limit of 25 tons.

*** November 1979 estimates.

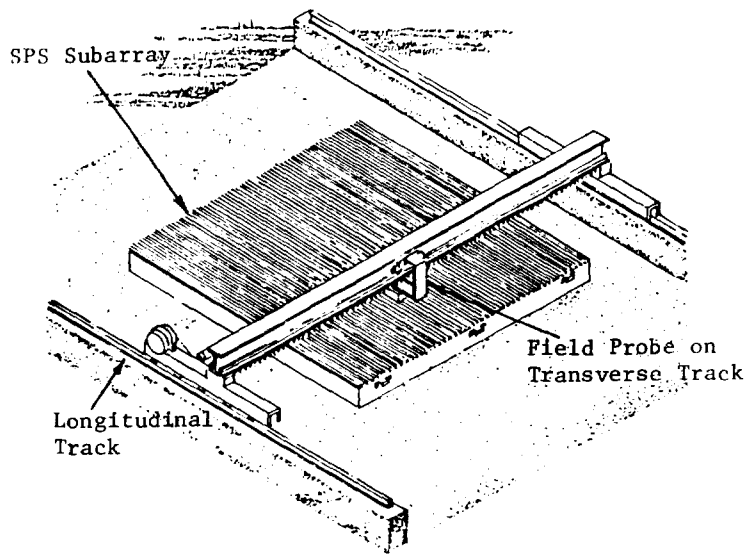


Figure 6. Planar Scanner Concept for Near-Field Measurements.

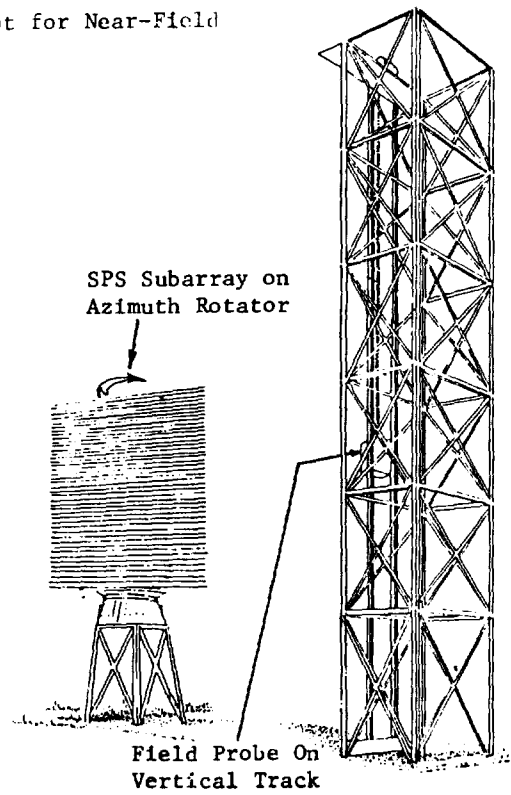


Figure 7. Cylindrical Scanner Concept for Near-Field Measurements.

CONCLUSIONS PRESENTED AT THE RADIATING ELEMENTS SESSION

1. Radiating Element Efficiencies - Low CTE (coefficient of thermal expansion) materials are required in order to obtain the required radiating efficiency of 96%
2. Type of Radiator - For large power blocks the most efficient radiator is a planar slot subarray with waveguide feed techniques.
3. Polarization - Linear polarization is preferred for simplicity and analyses show that Faraday rotation does not produce a significant loss.
4. High Voltage Breakdown - High voltage breakdown is not expected to be a problem at nominal geosynchronous orbital conditions. However, further study is required to determine the extent to which the SPS satellite produces an atmosphere.
5. Performance Measurements - Improved highly accurate measurement techniques and instrumentation will be required to verify system performance.

REMAINING ISSUES - PRESENTED AT THE RADIATING ELEMENTS SESSION

1. Practical efficiency design goal
 - a. Mass manufacturing tolerances vs. efficiency
 - b. Cost vs. efficiency
2. Suitable low CTE (coefficient of thermal expansion) material
 - a. Performance improvements
 - b. Effects of power level, multipacting, thermal cycling
 - c. Type of CTE material
3. Pilot signal reception
 - a. Shared aperture - diplexer: isolation, loss, transmit η loss
 - b. Separate aperture - filter: isolation, loss, transmit η loss
4. RF measurement accuracies
 - a. High efficiency measurements
 - b. Statistical analysis - desirable/feasible

SECTION VI
RECTENNA SESSION

Chairman: Richard M. Dickinson
NASA, Jet Propulsion Laboratory

THE HISTORY OF THE DEVELOPMENT OF THE RECTENNA

William C. Brown
Raytheon Company
New Products Center
Waltham, Massachusetts 02154

Presented at the RECTENNA SESSION OF THE SPS MICROWAVE SYSTEMS WORKSHOP
January 15-18, 1980, Lyndon B. Johnson Space Center, Houston, Texas

ABSTRACT

The history of the development of the rectenna is first reviewed through its early conceptual and developmental phases in which the Air Force and Raytheon Company were primarily involved. The intermediate period of development which involved NASA, Jet Propulsion Laboratory, and Raytheon is then reviewed. Some selective aspects of the current SPS rectenna development are examined.

Introduction

The chairman of this session believes that the perspective given by a history of the development of the rectenna would be of value to those now becoming involved with the application and further development of the rectenna for the SPS. He has asked me to present this history because he is aware that I have been closely and continuously involved with the development of the rectenna since its inception in 1963.

The concept and development of the rectenna arose in response to the need for a device that could be attached to a high altitude atmospheric platform and absorb and rectify microwave power from a microwave beam pointed at the vehicle. After the initial development of the rectenna under Raytheon and Air Force sponsorship for this purpose the rectenna development was carried on further and in a different direction by the author himself. In 1968, NASA became interested in the rectenna and its development in the context of transferring power from one space vehicle to another. This was followed by NASA's interest in the device for the receiving end of a system that would transfer electrical power from geosynchronous orbit to the earth.

Throughout this time period of 17 years, the development of the rectenna has been heavily disciplined by the various applications for which it has been considered. The result has been the accumulation of a large amount of experience which covers many facets of interest, including electrical design and performance, various physical formats, methods for accurate efficiency measurement and validation, life test data, and other items. Its development has also been characterized by contributions from many individuals whose involvement has been in two different areas. The first area is related to technical contributions. The second area is related to sponsorship. The development of the rectenna could not have proceeded very far without the encouragement and support of individuals within and outside the government who have understood the significance of free space power transmission by microwaves and the relevance of the rectenna development to this concept.

In presenting this history the author is treating the early conceptual and developmental phase as an interaction between many technological forces and developments, and people, which is the true nature of history. The history of the intermediate period is identified with the work supported by MSFC, JPL, LeRC and that was largely carried out by Raytheon. It is presented in a more summarized fashion with the

presentation focused on technological improvements and refinements. A final section is devoted to what might be considered as technological forecasting which is a projection of the past history combined with the subjective view of the author as to the impact of current and future technological and sociological events.

Early History of the Rectenna

The early development of the rectenna must be examined in the context that its conception and development grew out of the needs for a satisfactory receiving terminal for a microwave power transmission system. In this context we must take into account the factors which gave rise to an interest in the concept of microwave power transmission itself.

The first serious thought about power transmission by microwaves grew out of the development of microwaves for radar in which power was concentrated in relatively narrow beams as contrasted to the "broadcast" mode associated with low frequency radio. However, the element that really gave substance to the concept and distinguished it from the situation that existed when Hertz first demonstrated wireless power transmission with narrow beams using parabolic reflectors and spark gap generators, were newly developed electron tubes that could generate relatively large amounts of power at high efficiencies.

Still, there was no active postwar activity on microwave power transmission until it became recognized that with new approaches microwave generators could be developed to produce levels of CW microwave power about 100 times greater than from generators then available.^{1,2,3} Concurrent with this recognition was the inference that one of the potential useful applications of microwave power transmission would be microwave powered high altitude atmospheric platforms for communication and surveillance purposes.

This recognition stimulated Raytheon, under the guidance of Ivan Getting, Vice President for Engineering, to perform an in-depth study of such a platform in a helicopter format and to make a proposal to the Department of Defense in 1959 to develop such a vehicle.⁴ The reason why this is important in the development of the rectenna is that for the first time it became widely recognized that there was no efficient means of converting the microwave back into DC or low frequency electrical power at the receiving end of the system. This stimulated the Air Force to award several contracts to study this problem. One of these investigations that was to become a key element in the development of the rectenna was awarded to Purdue University and involved the use of

semiconductor diodes as power rectifiers.⁵

While this development at Purdue was proceeding, the development of super power microwave tubes had been started at Raytheon under the sponsorship of the Department of Defense and had achieved CW power outputs of over 400 kW at an efficiency exceeding 70% at a frequency of 3.0 GHz. Recognizing the potential application to free space power transmission the author had persuaded Raytheon Company to support the development of a close-spaced thermionic diode as a rectifier and the demonstration of a complete microwave power transmission system.⁶ Such a demonstration using the close-spaced thermionic diode and the physical arrangement of Figure 1 was successfully made in May 1963 with a power output of 100 watts which was used to drive a DC motor.⁷ Among those witnessing the demonstration was John Burgess, Chief Scientist at the Rome Air Development Center, who saw the potential of a microwave powered atmospheric platform for line of sight communication over long distances.



Figure 1. First experiment in the efficient transfer of power by means of microwaves at the Spencer Laboratory of Raytheon Company in May 1963. In this experiment microwave power generated from a magnetron was transferred 5.48 meters and then converted with DC power with an overall efficiency of 16%. A conventional pyramidal horn was used to collect the energy at the receiving end and a close-spaced thermionic diode was used to convert the microwaves into DC power of 100 watts. The collection and rectification arrangement was directive and not very efficient.

To encourage the chief scientist's interest the author privately constructed a small helicopter whose rotor was driven by a conventional electric drill motor supplied with power by a cable and demonstrated that it could carry aloft one of the closely spaced thermionic diodes. This demonstration was a major factor in motivating the chief scientist to set aside

discretionary funds for the development and demonstration of a small microwave powered platform. These funds became available in July of 1964, a year later.

Meanwhile it had become evident that the receiving arrangement used in Figure 1 had serious flaws for use in a microwave powered platform. The horn as a collecting element was much too directive for the expected roll and pitch of a vehicle and its collection efficiency was also poor. The close-spaced thermionic diode rectifier also proved to be a very short lived device. It was at this point that the author met by chance a college friend, Thomas Jones, in the Boston airport. Jones had become the head of the Electrical Engineering Department at Purdue University and told the author about the work going on there on the use of semiconductor diodes as microwave power rectifiers. The author immediately made a trip to Purdue and met Roscoe George, who had been carrying out most of the research activity. Professor George has been using dense arrays of closely spaced diodes within an expanded waveguide and had achieved as much as 40 watts of DC power output from microwaves in the 2 to 3 GHz range of frequency with respectable efficiencies.⁸ Although he had not made any measurements with free space radiation, he had shown how the microwave semiconductor diode, previously ignored as a power rectifier because of its very low individual power handling capability, could be combined in large numbers to produce reasonable amounts of DC power. In the absence of any other successfully developed microwave power rectifier the author was obviously drawn to the semiconductor diode approach. However, the use of George's dense arrays within a waveguide attached to a receiving horn would not solve the low collection efficiency and directivity of the receiving horn itself.

It was from this dilemma that the concept of the rectenna arose. The proposed solution was to take the individual full wave rectifiers out of the waveguide, attach them to half wave dipoles, and put a reflecting plane behind them. Once conceived⁹ the development of the rectenna, driven by its need for the proposed microwave powered helicopter, proceeded rapidly. Professor George was employed as a consultant to proceed with this approach and to make measurements on the characteristics of such a device.

With the arrangement of 28 rectenna elements shown in part in Figure 2 a power of 4 watts of DC power at an estimated collection and rectification efficiency of 50% and a power of 7 watts at an estimated efficiency of 40% were achieved.¹⁰ Of primary importance was the highly non-directive nature of the aperture (Figure 3) that had been anticipated because of the termination of each dipole antenna in a rectifier which effectively isolated the elements from each other in a microwave impedance sense except for the secondary effect of the mutual coupling of the dipoles. This feature of the rectenna that distinguishes it from the phased array antenna is of the greatest practical importance.

Although this achievement may be considered as the first major milestone in rectenna development the very small power handling capacity of the diodes limited the power output per unit area to values unsuitable for a helicopter experiment. For the helicopter experiment George suggested vertical strings of diodes separated by approximately a half wavelength, but the power density was still much too low. Placed close to each other in a plane to obtain the necessary power density, the impedance of the diode plane was very low and most of the power was reflected. The author solved this problem by placing a matching

network in front of it consisting of a plane array of rods spaced at an appropriate distance from the plane of the diode array. The final helicopter rectenna is shown in Figure 4. It was comprised of 4480 IN82G diodes, and had a maximum power output of 270 watts which was more than enough to power the helicopter rotor. The weight of the array was about three pounds or about 11 pounds per kilowatt of DC output.^{11,12}

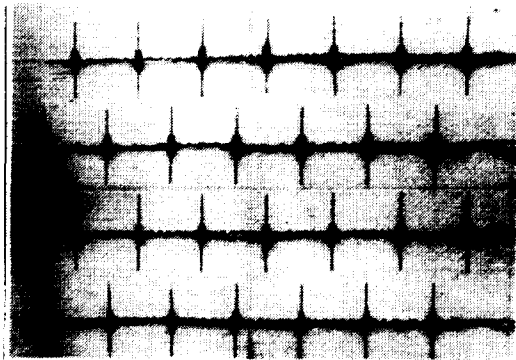


Figure 2. The first rectenna. Conceived at Raytheon Company in 1963, it was built and tested by R. George of Purdue University. Composed of 28 half-wave dipoles spaced one-half wave-length apart, each dipole terminated in a bridge-type rectifier made from four IN82G point-contact semi-conductor diodes. A reflecting surface consisting of a sheet of aluminum was placed one-quarter wavelength behind the array.

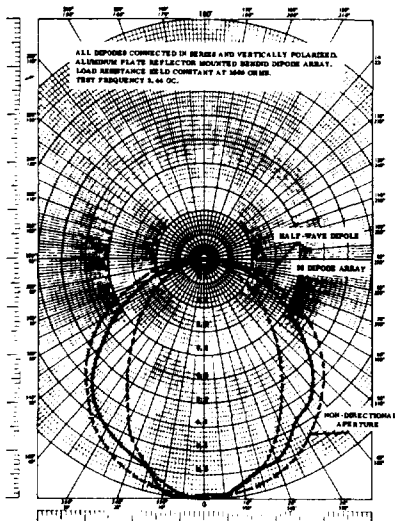


Figure 3. Directivity of the Half-Wave Dipole Array Shown in Figure 2. Directivity was essentially the same about both axes of rotation. Array has slightly less directivity than single half-wave dipole.

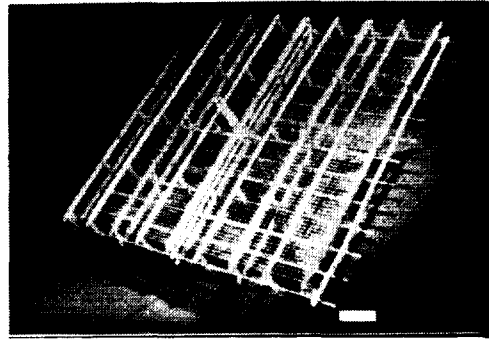


Figure 4. The special rectenna made for the first microwave-powered helicopter. The array is 0.6 meters square and contains 4480 IN82G point-contact rectifier diodes. Maximum DC power output was 270 watts.

A microwave power helicopter flight with this string type rectenna was made on July 1, 1964 prior to the start of work effort on an Air Force contract, to demonstrate continuous flight for ten hours. The Air Force contract was the basis for needed refinements and several notable demonstrations, including the specified ten hour continuous flight of the vehicle.^{11,12} Figure 5 shows the helicopter in flight. It was necessary, of course, to use laterally constraining tethers to keep the helicopter on the microwave beam but this limitation was later removed by a study and experimental confirmation that the microwave beam could be used successfully as a position reference in a control system in an automated helicopter which would keep itself positioned over the center of the beam.¹²

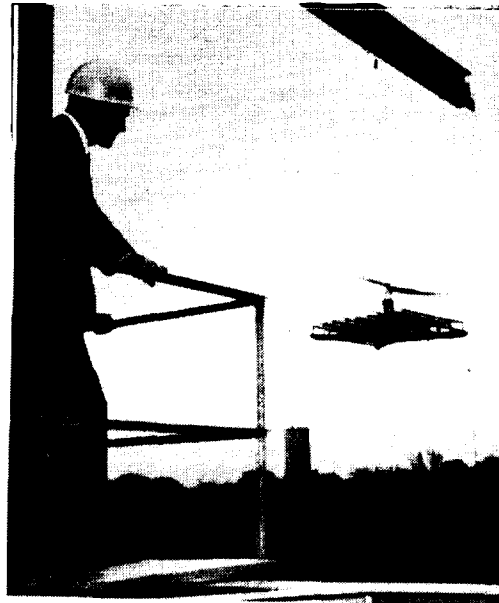


Figure 5. Microwave powered helicopter in flight 18.28 meters above a transmitting antenna. The receiving array for collecting the microwave power and converting it to DC power was made up of several thousand point contact silicon diodes. DC power level was approximately 200 watts. The date of the demonstration was October 1964.

The development of the string type rectenna (Figure 6) is of more than historical significance because it represents an approach in which large numbers of rectifying diodes can be spread over a surface to accommodate a high power density influx of microwave radiation or to operate in the vacuum of space where it may be desired to decrease to a minimum the mass required to transport heat from the diode sources to the heat sinks, in all probability passive radiators. The current status of microwave diodes (1979 technology) is such as to minimize the need for the "string-type" or equivalent arrays. Most applications currently envisaged do not call for incident microwave radiation of a density level beyond what the half wave dipole array with the greatly improved diodes can handle.

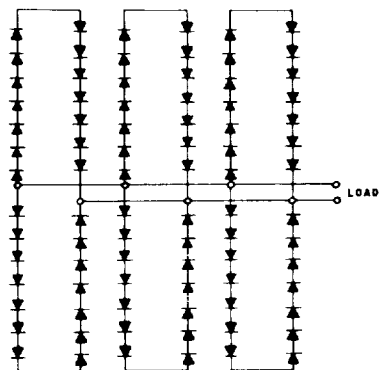


Figure 6. Schematic Drawing Showing Arrangement of Dipoles and Interconnections within a Diode Module used in Helicopter rectenna.

As the first airborne vehicle to stay aloft from power derived from any kind of an electromagnetic beam, it excited considerable interest. A demonstration to the mass media in October 1964 resulted in considerable exposure both in the press and on TV. Probably as a result of this, the author received a letter from a representative of Hewlett Packard Associates enclosing some newly developed Schottky barrier diodes which were indicated to be a substantial improvement over the point contact diodes that had been used. Tests made on the individual diodes (Type 2900) indicated that indeed they were much more efficient and would have more power handling capability. This combined with their smaller size made them of a great deal of potential interest.

Unfortunately, the Air Force elected not to further develop the microwave powered platform. It did, however, support the successful development and demonstration of a helicopter which would automatically position itself over the center of a microwave beam.¹²

In the time period from 1965 until 1970 there was no direct support of rectenna development from either government or industry. However, a substantial amount of development work on the rectenna was carried out by the author using personal funds and time during the 1967 to 1968 time period. This work was primarily aimed at incorporating the improved Schottky-barrier diodes into a very light weight rectenna structure that reverted back to the format of half wave dipoles terminated in a full-bridge rectifier. The resulting array is shown in Figure 7. The array, with a mass of only 20 grams, produced 20 watts of power output for an improvement in the power to mass

ratio of a rectenna by a factor of five. However, the rectenna of Figure 7 was also important in that it was used to make a demonstration of microwave power transmission that may have been an important factor in the decision by MSFC to continue with the development of microwave power transmission and the rectenna.

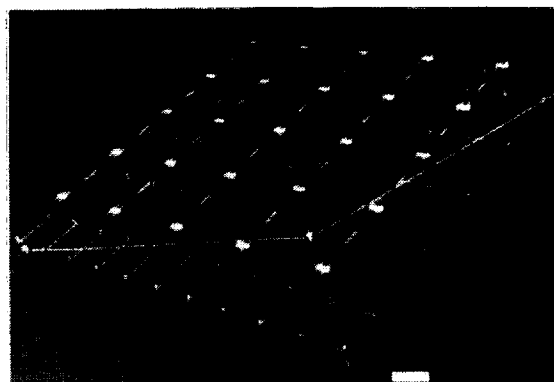


Figure 7. Greatly improved rectenna made in 1968 from improved diodes (HP2900) which became commercially available in 1965. The 0.3 meter square structure weighed 20 grams and delivered 20 watts of DC output power.

Development Under MSFC Sponsorship

The interest in the rectenna at MSFC is believed to have grown out of an interest of Associate Director Ernest Stuhlinger in some kind of free space power transmission within a space based community that would contain a collection of physically separated satellites. A country wide survey of technical approaches to this problem made by William Robinson of MSFC identified the work that had been done on microwave power transmission at Raytheon. At his and Dr. Stuhlinger's suggestion a demonstration was given to Dr. Werner von Braun and his entire staff. In the kind of demonstration that would probably not be permissible today the author set up a three foot parabolic reflector at one end of the long table as the source of a microwave beam of about 100 watts. At the other end of the table the author held the rectenna of Figure 7 now attached to a small motor with a small propeller on it. The microwave beam was used to supply power to the motor and the author would interpose his body between the source and the rectenna to demonstrate that the power was coming from the microwave beam.

Interest within MSFC resulted in setting up a small in house facility for laboratory effort under W.J. Robinson and a contract with Raytheon for a system study in 1969. Initially the system study did not involve any supportive technology development. It soon became evident, however, that a barrier to any further interest at MSFC in microwave power transmission lay in demonstrating a minimal overall system efficiency. The contract was hastily amended to permit Raytheon to construct the hardware for an overall efficiency measurement to be made at MSFC.

The system, shown in Figure 8, was hastily put together and demonstrated at MSFC in September 1970. The specified minimal overall efficiency of 19% was achieved with a measured efficiency of 26%.¹³ This demonstration focused interest upon further increasing the efficiency of the rectenna and of the

overall system. Over the next four years there was a succession of improvements in overall system efficiency, primarily because of improvements in both the collection and rectification efficiency of the rectenna. The focus in this time period was upon the development of the technology rather than upon an application. However, it is believed that the emergence of the solar power satellite concept in the 1968 to 1974 time frame and its need for high efficiency exerted considerable influence upon the drive for better efficiency from all parts of the microwave power transmission system.

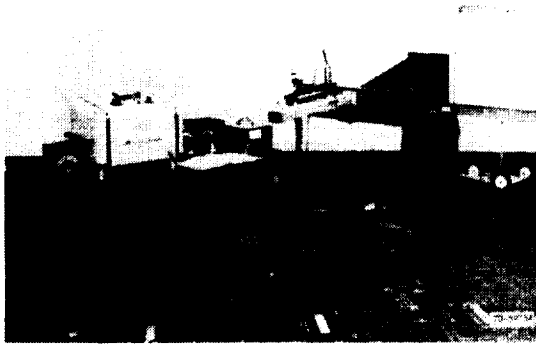


Figure 8. Test set-up of microwave power transmission system at Marshall Space Flight Center in September 1970. The magnetron which converts DC power at 2450 MHz is mounted on the waveguide input to the pyramidal horn transmitting antenna. The rectenna in the background intercepts most of the transmitted power and converts it to DC power. Ratio of DC power out of rectenna to the rf power into the horn was 40.8%. Overall DC-to-DC efficiency was 26.5%.

The MSFC demonstration of September 1970 indicated a number of deficiencies in the system including a rectenna collection efficiency of only 74% versus the theoretical maximum of 100%. This low collection efficiency was associated with improper spacing of the rectenna elements from each other in the rectenna array. The elements were therefore spaced more closely to each other in a hexagonal format, (Figure 9) and, in addition, the DC output of each rectenna element was terminated in a separate resistor to obtain a much greater range of data on the behavior of the rectenna. With the changed geometry the collection efficiency was increased to about 93%.

The decision to terminate each rectenna element in a separate resistor involved a change in the manner in which the DC power was collected and instrumented. The output of each rectenna element was brought back through the reflector plane where it could be directly monitored with DC meters. This arrangement provided such an enhanced capability to study and understand the performance of the rectenna that it was retained in the further development of it. (See Figure 10 for an adaptation to a later MSFC rectenna.) The construction however is not economical and is not recommended for most applications.

It was during this period that an arrangement to separate the measurement of the collection efficiency from the rectification efficiency of the rectenna was developed. The individual rectenna element was placed

at the end of a section of waveguide that was expanded into a small horn with an aperture of about 100 square centimeters. A metallic reflecting plane was placed behind the rectenna element and this plane also was used to seal the end of the waveguide so that no microwave power could leave the closed system. This made it possible to accurately measure the DC output power and the microwave power absorbed by the element and thus to accurately measure an efficiency, defined here as the rectification efficiency. Such an efficiency, of course, includes any circuit losses in the rectenna element itself. The test fixture environment in which the rectenna element was placed simulated to a first approximation the environment of the surrounding rectenna into which the rectenna element would eventually be placed. This test arrangement was a key factor in reducing costs for the development of the rectenna.

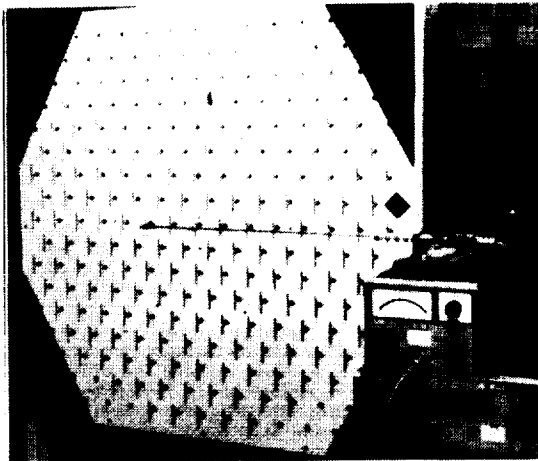


Figure 9. Close up view of rectenna used in measurements of overall system (DC to DC) efficiency. There were 199 elements in a four foot diameter hexagonal array. Rectenna was illuminated with a near gaussian shaped beam with a power density at the center about forty times that at the edges. The probe in front is used to measure the standing wave pattern in space. Probe measurements indicated that after suitable adjustment of DC load resistance and spacing of elements from the reflecting plane a reflection of less than 1% could be obtained, indicating an absorption efficiency approaching 100%. Although overall rectenna efficiency is generally difficult to measure because of edge effects and difficulty of measuring power density in the beam the unique aspects of the test facility made it possible to estimate overall capture and rectification efficiency of 82% for the rectenna within a $\pm 2\%$ error.

The collection efficiency of the rectenna has always been difficult to measure. The termination of a large aperture horn with a large number of rectenna elements, an arrangement which would seem to logically follow the test arrangement for a single element, loses its validity for collection efficiency because many modes are set up within the horn if there is any dissymmetry at all in the rectenna arrangement. Most of the power in these modes gets absorbed in the elements themselves and very little flows back into the throat of the horn and into the waveguide where any measurement of reflected power could be made. The best way to measure collection efficiency is to measure the standing wave pattern directly in front of the center of freely

exposed rectenna of sufficient area to minimize diffraction effects from the edge. The measurement is made more valid if the impinging beam has a gaussian distribution, the reflection factor is small and the reflected wave also assumed to be gaussian. These conditions prevail in the arrangement of Figure 11.

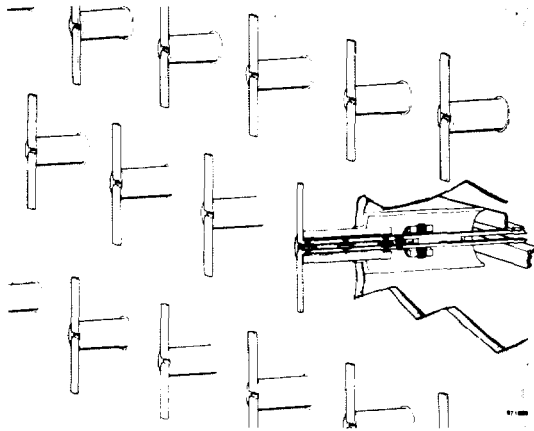


Figure 10. Sketch of the Marshall Space Flight Center rectenna which was constructed in spring of 1974. Cutaway section of rectenna element shows the two section input low pass filter, the diode, and a combination tuning element and by-pass capacitor.

Because the diode rectifier is such an important element in the collection and rectification process, a search for diodes which would improve the efficiency and power handling capability of the rectenna has been a continuing procedure. In 1971, Wes Mathei suggested that the Gallium Arsenide Schottky-barrier diode that had reached an advanced state of development for Impatt devices might be a very good power rectifier and provided a number of diodes for testing.¹⁶ These devices were indeed much better. Their revolutionary behavior in terms of higher efficiency and much greater power handling capability rapidly became the basis for the planning of improved rectenna performance.

The knowledge of the superior performance of this device was coincident with the advancement of the concept of the Satellite Solar Power Station by Dr. Glaser of the A.D. Little Co.¹⁷ The earliest investigation of a rectenna design for this concept indicated that the economics of its construction would be crucial and that mechanical and electrical simplicity of the collection and rectification circuitry would be of paramount importance. This factor, combined with the fact that no harmonic filters had existed in previous rectenna element designs but would be necessary in any acceptable microwave power transmission system, motivated a completely new direction of rectenna element development. This new direction was the development of a rectenna element employing a single diode in a half-wave rectifier configuration with wave filters to attenuate the radiation of harmonics and to store energy for the rectification process.

The construction of such a rectenna element and its insertion into a DC bus collection system is shown in Figure 10. This rectenna element was used in the last phase of the MSFC sponsored work at Raytheon to construct a rectenna 1.21 meters in diameter which was illuminated by a gaussian beam horn (Figure 9). The combined collection and rectification efficiency of this rectenna was measured at $82 \pm 2\%$. The overall DC to DC efficiency was measured at 48%.

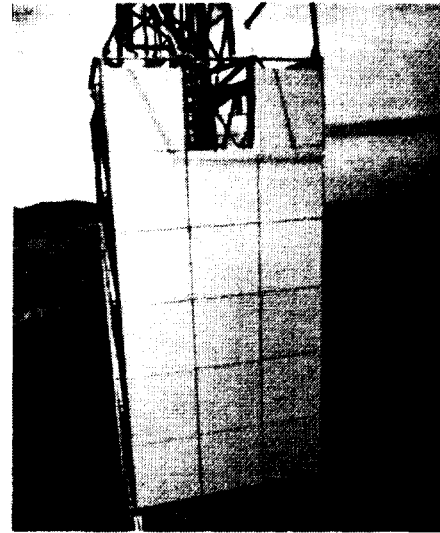


Figure 11. Photo of 24.5 Square Meter Rectenna erected in 1975 at the Venus Site of the Goldstone Facility of the Jet Propulsion Laboratory. Power was transferred by microwave beam over a distance of 1.6 km and converted into over 30 kW of cw power which was dissipated in lamp and resistive load. Of the microwave power impinging upon the rectenna, over 82% was converted into DC power. The rectenna consisted of 17 subarrays, each of which was instrumented separately for efficiency and power output measurements. Each rectenna housed 270 rectenna elements, each consisting of a half-wave dipole, an input filter section, and a Schottky-barrier diode rectifier and rectification circuit. The DC outputs of the rectenna elements were combined in a series-parallel arrangement that produced up to 200 volts across the output load. Each subarray was protected by means of a self-resetting crowbar in the event of excessive incident power or load malfunction. Each diode was self-fused to clear it from short-circuiting the array in the event of a diode failure.

Development Under JPL Sponsorship

By 1973 the solar power satellite concept (then the SSPS) had become an important enough consideration to interest the Office of Applications within NASA to support the development of the microwave power transmission portion of the system. Although it would have been logical to continue the effort at MSFC because of their initial involvement, MSFC indicated that the subject matter was outside of their main interests and that they did not wish to pursue its development further. As a result both JPL and LeRC became involved in efforts that involved the demonstration and further development of the rectenna, and the rectenna became increasingly identified with the SPS.

The JPL activity was involved with the demonstration of the transfer of power over a distance of one mile and at a DC power level of 30 kilowatts, nearly two orders of magnitude greater than had been accomplished in the laboratory. (Figure 11)^{18,19} This work effort was carried out in the 1974 to 1975 time period and has undoubtedly been the most important contribution to the establishment of confidence within the NASA and aerospace community in the feasibility of microwave power transmission. Although the emphasis

was upon demonstration rather than technology development it did provide some opportunity for additional development, those aspects involving the interface with the useful load on the output side of the array, life test data and improvement and certification of overall efficiency. An unfortunate aspect of the demonstration was that for risk minimizing purposes the uneconomic three level construction of dipoles, reflecting plane, DC power and bussing was retained. However, later work with LeRC featured the development and testing of the economic two level construction.

From the rectenna development point of view the JPL activity included the following accomplishments:

- Demonstrated the parallel-series connection of the DC output power from parallel rows of rectenna elements.
- Developed plated-heat-sink GaAs Schottky-barrier diodes with carefully controlled thickness of epitaxial layer to maximize efficiency.
- Demonstrated "fail-safe" nature of the diodes. If a diode should short out the adjacent parallel connected diodes force enough current through the package of the shorted diode to burn out a one mil diameter wire which acts as a fuse in the package.
- Demonstrated the value of crowbars in protecting diodes from load faults and from excessive incident microwave power but also the desirability of complementing them with capacitors placed across the output terminals of the diode array to absorb short duration spikes of output power from any cause.
- A mechanical design of the rectenna element itself that was much improved over the element developed under MSFC sponsorship.
- The initiating of life test on 199 rectenna elements and diodes arranged in groups that were exposed to different values of incident microwave power.
- Improved the setup in Raytheon's laboratory to demonstrate high overall (DC to DC) system efficiency and then provided certification of the data upon which the calculation of an overall efficiency of 54% was based.²⁰ The rectenna that was used in this experiment is shown in Figure 9. The overall collection and rectification efficiency of the rectenna was found to be $82 \pm 2\%$ in this experiment.

Development Under LeRC Sponsorship

Lewis Research Center carried out two activities for the Office of Applications having to do with the rectenna. One, carried out in 1974 and 1975 was a broad study of the entire microwave power transmission system for the SPS. Various approaches to the collection and rectification problem were investigated. Investigation included an examination of all rectifier approaches and all receiving antenna approaches. The rectenna approach was found to be unique in the solution of this problem.²¹

The other LeRC activity dealt exclusively with the improvement of the rectenna²² and made important contributions as follows:

Improvements in Efficiency

Improvements in rectenna element efficiencies to values slightly in excess of 90% were achieved. These

efficiencies were with DC outputs in excess of 4 watts, which is above that currently planned for the SPS. However, notable improvements were made in efficiency at low power densities with improved diodes and higher impedance rectenna elements. The results are shown in Figure 12. Further, directions in which to obtain higher efficiency, particularly at the lower power levels, were discovered.

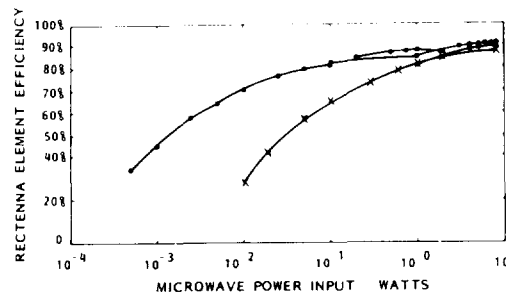


Figure 12. A summary of the efficiencies achieved with new diode in various new rectenna configurations as a function of power level, compared with performance of a standard element used in the JPL Goldstone rectenna and shown as the lower curve.

Improvement in Confidence in Collection and Rectification Efficiency Measurements

A considerable improvement in the confidence of efficiency measurements on the rectenna element was established by equating the microwave power absorbed by the rectenna element to the sum of the DC power output, the losses measured in the diode, and the circuit losses as measured experimentally and by computer simulation. The losses in the diode were measured by a unique substitution method developed at Raytheon and explained in reference 22. The balancing of microwave power input and total power output, as shown in Figure 13, is a good check on the measurement of microwave power input which is traceable to a 100 milliwatt microwave standard at the Bureau of Standards through a secondary standard sent there for calibration, and a calibrated 20 dB directional coupler with which the secondary standard is applied to the test set for the rectenna element.

Mathematical Modeling and Computer Simulation

The mathematical modeling of the rectenna element and simulating its performance on a computer was successfully carried out. Although other computer modeling had been successfully carried out,²² this was the first time that the computer program modeling was for the same rectenna element on which accurate experimental measurements of circuit and diode losses had been made.

The computer simulation generally gave results that confirmed the experimental results, as may be seen from an examination of Figure 13, but upon occasion indicated differences which have led to investigations to resolve the differences. For example, the diode losses were first computed on the basis of the theoretical design of the diode and found to be less than those measured. It was found that the forward voltage drop as measured by DC voltage measurements was greater than that predicted from theory leading to the conclusion that the ohmic contact

is not purely ohmic but retains some Schottky barrier characteristics which contribute to the voltage drop.

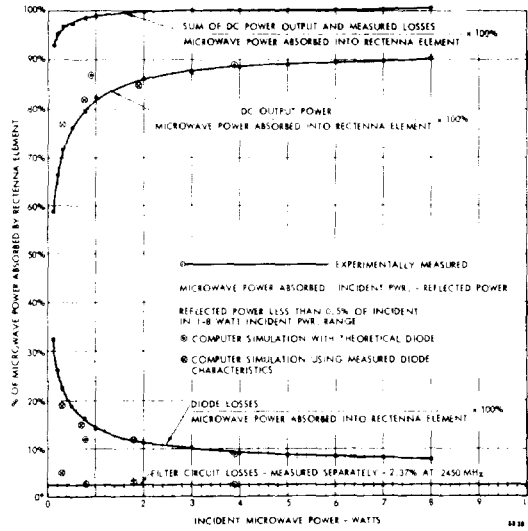


Figure 13. The DC power output, losses in the microwave diode, and losses in the input filter circuit are shown as a percentage of the microwave power absorbed by the rectenna element as a function of incident microwave power level. The sum of all of these is then compared with the absorbed microwave power. Comparison with computer simulation computations is also shown.

A typical set of diode losses as obtained from the computer simulation may be of interest. Total losses were 13.03% of the input power of which 2.08% was skin loss, 2.52% loss in the diode series resistance in the forward conduction period, 1.23% loss in the non-conducting portion of the cycle, and 7.22% loss in the Schottky junction itself. The total losses observed experimentally were 12.8%, an agreement that is probably better than can be justified.

Development of Improved Diodes

The power loss represented by the voltage drop in the Schottky barrier is an important loss in the diode, and it is the major one when the operating power level is low, even when the impedance level of the circuit is raised to minimize these losses. GaAs Schottky barrier diodes commonly use platinum as a barrier metal because it behaves better than other materials for use of the diode as an Impatt device. Tungsten has a lower work function than platinum and would be preferable in a rectenna element. Such diodes were developed and indeed found to have lower loss and to be more suitable for rectenna element application.

Suppression of Harmonic Energy

A means of reducing harmonic energy radiated from the dipole antenna was investigated. A shorted line $\frac{1}{4}$ wavelength long placed across the terminals of the dipole appears as an open circuit to the fundamental but as a short circuit to the second harmonic. The power in the second harmonic is therefore reflected back into the rectenna element. It was found that this technique will reduce the second harmonic level by as much as 25 dB but the impact of the

harmonic reflection upon the overall efficiency needs more evaluation. The technique can be incorporated with no additional cost into the rectenna element in the two-plane format. The third harmonic may be treated in a similar fashion but it is necessary to complicate the physical format of the rectenna element to incorporate it.²²

Development of a Rectenna Design that is Both Environmentally Sound and is Suited to Low Cost High Speed Production

The development of basic technology for the rectenna for the full scale SPS is well advanced, but the adaptation of this basic technology to a rectenna that is environmentally sound and that can be made at low cost in large volume production was recognized as an area of special study. Effort on this part of the program resulted in the outline of a mechanical design based upon the two-plane rectenna system in which all of the important elements of the rectenna, including the bussing of DC power, are carried out in the foreplane. This foreplane is shown schematically in Figure 14. In effect this design reverts back to some of the earliest rectennas but with greatly improved components and better understanding. A mechanical design of the entire rectenna coupled with the fabrication and electrical testing of a portion of the foreplane was carried out. The overall mechanical design is shown in Figure 15 while the electrically operative foreplane portion is shown in Figure 16.

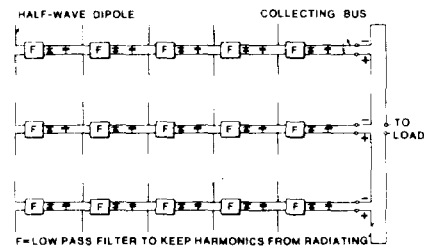


Figure 14. Interconnection arrangement of half-wave dipoles, wave filters, rectifier circuits, and collecting buses in the foreplane of a two-plane rectenna system.

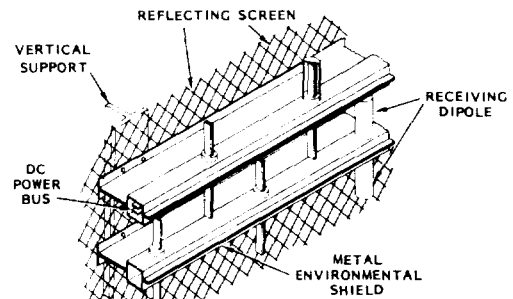


Figure 15. Proposed design of Rectenna motivated by environmental protection and cost considerations. In this design the environmental shield becomes an important load-bearing member of the structural design.

The foreplane shown in Figure 16 was thoroughly evaluated for performance. A special arrangement made it possible to test each of the five foreplane elements in the single rectenna element test fixture while all five remained within the foreplane assembly. The average efficiency of the elements was 88%. To determine its compatibility within a large array of elements

the foreplane of Figure 16 was inserted into the 199 element array shown in Figure 17. A careful check was made on any effect it might have had on the performance of the rectenna as a whole, by means of reflection measurements of the kind shown in Figure 9 and by comparison of the power obtained from the five element array with the sum of the power from the five standard rectenna elements it replaced. From the almost imperceptible impact that was noted, it was concluded that the rectenna design depicted in Figures 15 and 16 is electrically satisfactory.

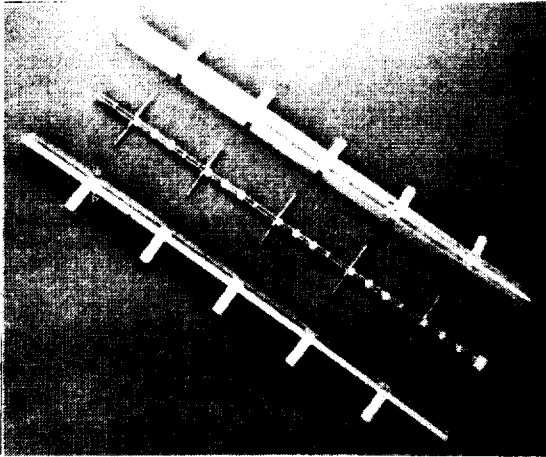


Figure 16. Basic core structure design of the foreplane illustrating the joining of individual rectenna elements to each other to form a linear, easily-fabricated structure performing the functions of DC power bussing and microwave collection and rectification.

Assessment of Life of Rectenna Element

Figure 18 provides a summation of the life test data taken up to a total of slightly over 800,000 diode hours. It is noted that there were no failure of diodes in rectenna elements operated at DC power levels below 6 watts. Even those failing at higher power levels may have been associated with infant or operator-induced failures. There was only one unequivocal self-induced life failure of a diode and that occurred in the group operating at 6 to 8 watts of DC power output.

All of the diodes that were used were the plated-heat-sink GaAs Schottky barrier diodes that were made as part of the effort under the JPL supervised program at Raytheon. The life test was made possible because of the availability of the complete microwave power transmission system and the 199 element rectenna shown in Figure 9. With this arrangement there is a distribution of power density over the rectenna by a factor of about 40.

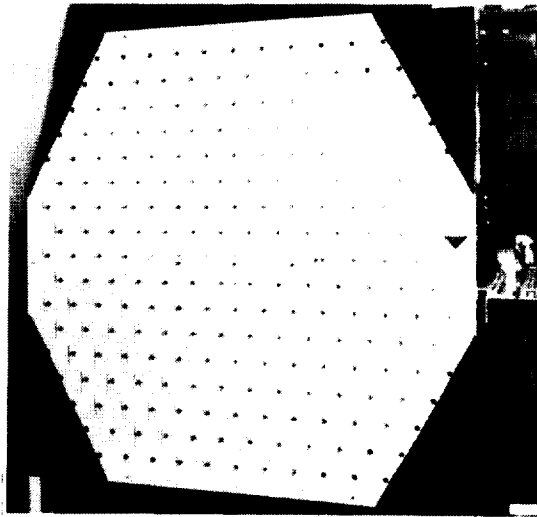


Figure 17. The test set-up for checking the foreplane type of rectenna array. The five element foreplane structure is placed at the center of the larger rectenna array as shown. The DC output is dissipated in a resistive load. The collected power from the foreplane can then be compared with the power that would have been collected from the five elements that it replaced. Reflected power measurements were also made with the probe arrangement shown in Figure 9.

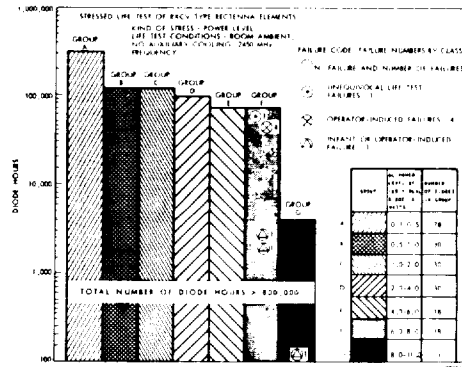


Figure 18. Diode Life Test Results Using Rectenna shown in Figure 9. Rectenna contains 199 rectenna elements which are subjected to a wide range of incident power.

Recent Developments and Future Trends

The SPS rectenna design approach of Figure 15 was structurally analyzed in considerable detail by the author.²³ Material requirements and costs were estimated. To save on material, which is the chief element of cost, airframe design practices should be used, and extensive scaled wind tests should be performed in the early design stages to forestall excessive design safety factors for wind loading.

A set of studies leading to additional understanding of the rectenna have been sponsored by Johnson Space Center, with R.J. Gutmann of RPI being the principal investigator for a number of these.²⁴

The most recent trend in rectenna development is the thin-film printed-circuit rectenna for high altitude atmospheric platform and space use. It is not believed to be suitable for the SPS rectenna because of its fragility and higher cost per unit area than the rigid construction of Figure 15. Its application to the high altitude platform, however, may lead to a better general understanding and acceptance of microwave power transmission in the SPS.

Bibliography

1. Brown, W.C., and G. Perloff, "High Power CW X-Band Amplitron," 1960 IRE International Conv. Record, vol. VIII, pt. 3, pp. 52-55.
2. Brown, W.C., "The Amplitron, A Super Power Microwave Generator," Electronic Progress, Raytheon Company, Burlington, Mass., July-August 1960.
3. Brown, W.C., "A Survey of the Elements of Power Transmission by a Microwave Beam," 1961 IRE International Conv. Record, vol. IX, pt. 2, pp. 93-106.
4. "Raytheon Airborne Microwave Platform (RAMP) System" Technical Proposal prepared for U.S. Air Force, May 21, 1959.
5. Sabbagh, E.M., et al., "Microwave Energy Conversion," WADD Tech. Rept. No. 61-48, pt. II, op. cit., Nov. 1961.
6. Brown, W.C. "Thermionic Diode Rectifier" in Okress, Microwave Power Engineering. Academic Press, Vol. II, pp. 295-298.
7. Brown, W.C., "Experiments in the Transportation of Energy by Microwave Beam," 1964 IEEE International Conv. Record, vol. XII, pt. 2, pp. 8-17.
8. George, R.H., "Solid-State Rectifiers" in Okress, Microwave Power Engineering. Academic Press Vol. II, pp. 275-293.
9. U.S. Patent No. 3,434,678, March 25, 1969, W.C. Brown, et al.
10. Brown, W.C., and George, R.H., "Rectification of Microwave Power" in "Microwave Power Engineering;" IEEE Spectrum. October 1964, pp. 88-92.
11. W.C. Brown, "Experimental Airborne Microwave-Supported Platform," Tech. Rept. RADC-TR-65-188, 1965.
12. W.C. Brown, "Experiments Involving a Microwave Beam to Power and Position a Helicopter," IEEE Trans. Aerospace Electron, System, vol. AES 5, pp. 692-702, Sept. 1969.
13. W.J. Robinson, "Wireless Power Transmission in a Space Environment" J. Microwave Power, vol. 5, December 1970.
14. W.C. Brown, "Progress in the Efficiency of Free-Space Microwave Power Transmission", Journal of Microwave Power, Vol. 7, No. 3, pp. 223-230.
15. W.C. Brown, "Free-Space Microwave Power Transmission Study, Combined Phase III and Final Report", Raytheon Report No. PT-4601, Sept. 1975. NASA Contract No. NAS-8-25374.
16. W.C. Brown, "The Technology and Application of Free-Space Power Transmission by Microwave Beam", Proceedings of the IEEE, vol. 62, No. 1 Jan. 1974, pp. 11-25.
17. P.E. Glaser, "Power from the Sun: Its Future", Science, Vol. 162, pp. 857-861, Nov. 22, 1968.
18. R.M. Dickinson, "Evaluation of a Microwave High-Power Reception-Conversion Array for Wireless Power Transmission", Tech. Memo 33-741, Jet Propulsion Lab, Cal. Inst. Tech. Sept. 1, 1975.
19. "Reception - Conversion Subsystem (RXCV) for Microwave Power Transmission System", Raytheon Report No. ER75-4386, JPL Contract No. 953968, Sept. 1975.
20. R.M. Dickinson, W.C. Brown, "Radiated Microwave Power Transmission System Efficiency Measurements", Tech. memo 33-727 Jet Prop. Lab. Cal. Inst. Tech, March 15, 1975.
21. "Microwave Power Transmission System Studies" Raytheon Contractor Report ER75-4368 NASA CR-134886, December 1975.
22. W.C. Brown, "Electronic and Mechanical Improvement of the Receiving Terminal of a Free-Space Microwave Power Transmission System", Raytheon Contractor Report PT-4964 NASA CR-135194, Aug. 1977.
22. J. Nahas, "Final Report, Simulation and Experimental Studies of Microwave-to-DC Energy Conversion Systems", Prepared for NASA, Lewis Research Center, under Grant No. NSG-3070.
23. SPS System Evaluation Phase III Study Document - Executed by Boeing, Raytheon, General Electric Boeing D180-24635-1.
24. R.J. Gutmann, J.M. Borrego "Solar Power Satellite Rectenna Design Study" Contract NAS 9-15453, December, 1978.

RECTENNA SYSTEM DESIGN
 G. R. Woodcock, Boeing Aerospace Company
 R. W. Andryczyk, General Electric

1.0 INTRODUCTION

The function of the rectenna in the solar power satellite system is to convert the downcoming microwave power beam to electrical grid power. Due to its large physical size (a typical rectenna site is a 10 KM x 14 KM ellipse) and element composition (many repetitive components), the projected cost savings of automatic mass production are of prime importance. Control of the satellite power beam and its distribution also takes place at facilities on the rectenna site. These critical functions have minor cost impacts and are not treated in this document.

The fundamental processes at the rectenna consist of rectifying the incident r.f. field into d.c. current using Schottky barrier diodes, filtering the rectified output, combining it and processing it to higher voltages for distribution. Hierarchical combination and processing of currents is done several times to integrate the relatively low power per diode to electrical grid power magnitudes. Provisions for power control for equipment protection and load management exist at each step in the hierarchy.

2.0 RECEIVING ANTENNA OPTIONS

Figure 1 illustrates the basic design choices based on the desired microwave field concentration prior to rectification and on the ground clearance requirement for the rectenna structure. For an optimized system, these parameters depend on positions within the site, local terrain and incident r.f. field. For purposes of the present study, a non-concentrating inclined planar panel with a 2 meter minimum clearance configuration was selected as representative of the typical rectenna.

3.0 RECEIVING ELEMENT OPTIONS

Figure 2 illustrates some of the options that have been considered for receiving antenna elements. Dipoles in various implementations represent the most straightforward way of receiving a linearly polarized incident field compatible with the slotted waveguide transmitting array, and are relatively easy to analyze. However, other options, including elements that receive circularly polarized fields, have been considered.

Figure 3 shows capture area as a function of element width and length for a number of different types of elements. A trade study of diode power for maximum rectification efficiency (5-10 watts per diode) as opposed to long life with passive cooling (<5 watts per diode) suggests a power level per diode of somewhere between 1 and 5 watts. (See Table 1).

TABLE 1: SINGLE DIODE RECTENNA (DIPOLE) ELEMENT

Element Power Level (Watts)	Equivalent Power* Density mW/CM ²	Achieved Element Efficiency %	Projected Element Efficiency %
8	160	91	91
1	20	88	90
0.5	10	86	88
0.2	4	84	86
0.1	2	82	85

*Proposed Power Density at SPS Rectenna Center - 23 mW/CM²

Proposed Power Density at SPS Rectenna Edge - 1 mW/CM²

The baselined modified half-wave dipole, with a capture area of 70 CM² (typical) will provide between 1-2 watts of power per diode at the center of the rectenna (23 mW/CM²) indicating good efficiency. More directional elements or dipole arrays must be used as we go out to the rectenna edge ($\approx 1 \text{ mW/CM}^2$); for instance, a 4 x 4 dipole array would again provide 1 watt per diode. Care must be exercised not to select too large an array which would pose problems of directional reception and increased losses in the r.f. collection lines. The design chosen integrates the dipoles and their associated power and microwave circuitry inside an aluminum environmental shield and support structure which readily lend themselves to mass production methods.

4.0 BASELINE RECTENNA DESCRIPTION

A representative rectenna design at a 35° latitude is described, characterized by a 5 GW Gaussian tapered beam with a peak incident microwave power of 23 mW/CM². Power is collected out to the point where the interception efficiency is 95%. The basic receiving element of the baseline rectenna is a dipole above a ground plane. The dipole assembly also contains a filtering and matching circuit to match the dipoles to the incoming wave with a reflection coefficient of better than -20 db. It is assumed that all dipoles are identical throughout the rectenna. The number of dipoles in the rectenna is approximately 1.3×10^{10} in a 7.9 CM = .64 λ triangular array format.

Component designs for the rectenna are varied to most effectively match the incident power flux in ten rings. Basically, all microwave system components of a given type are similar within a ring. However, power bussing and control segmentation at the 5-10 mW power level and above extends across ring boundaries. Local d.c. voltages on the panels are designed not to exceed +3.25 KV.

Due to the power density variation over the rectenna aperture, a single type of radiating element or a single type of rectifier cannot provide optimum conversion efficiency. Either a number of radiating element types or a number of diode types must be provided. Presently, one single type of diode is assumed which is operated with four different types of antenna elements. It is assumed that besides the dipole element already described, these antenna elements are formed by using the basic dipoles in arrays containing 2, 4, or 8 dipoles. The corresponding assemblies are called Type 1,2,3, and 4 receiving arrays. There are approximately 7.654×10^9 arrays (diode assemblies) in the overall antenna.

The array assemblies are combined into panels which are the smallest assembly units from the fabrication point of view. 10 m² was selected for the panel area, with a N-S plane dimension of 3 m and E-W plane dimension of 3.33 m. Figure 4 shows a typical panel assembly in the center of the rectenna. It is assumed that all panel sizes are identical. This requires 7,060,224 panels in the rectenna. There are four different types of panels, corresponding to the four different types of receiving arrays. Although the dipoles and diodes are identical for all panels, the combining-matching-filtering circuits and the diode wiring represent four types. Table 2 summarizes the characteristics of the panels.

Ring	$\frac{mW}{\text{cm}^2}$	$\frac{W}{\text{Panel}}$	$\frac{V}{P_{DC} \text{ Panel}}$	Dipoles	Diodes	$\frac{V}{V_{DC} \text{ Diode}}$	$\frac{W}{P_{DC} \text{ Diode}}$	$\frac{V}{V_{DC} \text{ Panel}}$	$\frac{A}{I_p \text{ Panel}}$	$\frac{\text{ohm}}{P_{DC} \text{ Panel}}$
1	23.33	2333	1738.8	43 x 43 = 1849	1849	17.96	.9398	772.3	2.25	1100
2	18.76	1876	1375.2	1849	1849	16.11	.7437	692.7	1.98	1100
3	14.38	1438	1043.3	1849	1849	14.11	.5642	606.7	1.72	1100
4	11.42	1142	828.1	2x10x31 = 1860	930	17.73	.8904	545.6	1.50	1136
5	8.67	867	625.6	1860	930	15.44	.6727	478.6	1.31	1136
6	6.72	672	468.1	1860	930	13.59	.5033	421.3	1.11	1136
7	5.34	534	365.4	1860	930	12.12	.3929	375.7	.973	1136
8	4.24	424	292.1	4x21x22 = 1848	462	15.32	.6322	337.0	.866	1152
9	3.49	349	236.5	1848	462	13.90	.5119	305.8	.773	1152
10	3.14	314	214.0	8x15x15 = 1800	225	18.90	.9511	283.5	.755	1100

TABLE 2:
RECTENNA
PANEL
CHARACTERI-
ZATION

Units are combined from panels in such a manner that nominally 1,000 panels are in one unit and the N-S dimension of a unit is always $32 \times 3.662 = 117.18$ m, which means that the number of panel rows in the N-S plane is always 32. This allows a standardization of the unit layouts to a minimum of seven types. Figure 5 shows the overall layout of the rectenna with the ring boundaries and the number of units within each ring. Note that the N-S dimension of the units are standardized to 117.18 m everywhere within the rectenna and only the E-W dimension of the units varies from ring to ring.

The last assembly which is formed at DC is called "group". This brings the power output into the 5-10 MW range. In order to keep the voltage levels relatively low, groups are formed from the units by parallel connections only. The power from the unit output is brought to group centers, or blocks, where the DC to AC inverters are located, by relatively long transmission lines that are parallel-connected at the group centers only. Blocks handle approximately 70 MW of power each.

Selection of the layout for the rectenna AC system between the individual DC/AC converters and the bulk power transmission system depends on the location and the power levels of the DC/AC converters as well as on the needs of the bulk power transmission system. A one-line diagram for the rectenna AC system in which the DC output from the dipoles is collected into 40 MW DC/AC converter stations is shown in Figure 6. The 40 MW converter station output is transmitted by underground cable to 200 MW transformer stations where the voltage is stepped up to 230 kV, then collected in 1,000 MW groups and transformed to 500 kV for interphase with the bulk transmission system. The switchyards are shown arranged as reliable "breaker and a half" schemes where single contingency outages may be sustained without loss of power output capability. The selection of the voltage level for the ultimate bulk power transmission interface with the utility grid, as well as the possibility of interconnecting two or more of the 1,000 MW switching stations together should be optimized based on detailed information about the connecting utility system. The solution, shown in Figure 6, integrated in a utility system with a control structure, as indicated in Figure 7, is one of several possible choices.

Availability calculations for the baseline rectenna design (Figure 8) were performed, the results of which are that 80% of the rated satellite power is available 96.8% of the time, and that scheduled no-power periods total only 208 hours per year.

To define the requirements for a given specific situation, load flow and system stability studies are required. It is likely, however, that the SPS power system would be far more stable than a conventional power plant of the same rating. This would mean that the transmission distances could be increased for a given line loading without need for as much series compensation as in conventional power plants.

When substantial amounts of power are to be transported for distances of 400 miles or more, the consideration of a high-voltage DC (HVDC) as the transmission load is often indicated. The HVDC system is ideally suited for long distance bulk power transport since it does not suffer from stability effects and can even be used to improve the stability of the AC system to which it is connected. The DC system is asynchronous and can easily transmit power between independent power systems such as those of the Eastern and the Western United States. HVDC technology is advanced and the systems have been well received. A 6,300 MW system in Brazil is currently in the proposal stages with full scale operation scheduled for 1985. It appears that a DC system or a combination of DC and AC systems could be applied to the Solar Power Satellite system with few difficulties.

5.0 SCATTERING AND RADIO FREQUENCY INTERFERENCE

The microwave transmission link must meet a stringent standard of electromagnetic cleanliness which states that out-of-band power must be more than 150 db down from the link power. Even though stray power reflected from and/or radiated by the

rectenna generally travels in an upward direction, there are enough scattering mechanisms for harmonics from the diode rectifier and associated noise to warrant the serious question of meeting this requirement. Some of the approaches and their implications are summarized in Raytheon data of Table 3 below.

TABLE 3: APPROACHES TO DECREASE HARMONIC RECTENNA RADIATION

<u>Approach</u>	<u>Expected Improvement in 2nd, 3rd and 4th Harmonics</u>	<u>Implications</u>
o More filter sections of current design	Approx. 14 db per section	o No physical room, 1% loss for each section.
o Stub lines to short higher harmonics at dipole terminals	~30 db	o Mechanical tolerance problem. o 2nd harmonic reduction easily added. o 3rd and higher harmonics require added width to core section. o Less than 1% decrease in circuit efficiency. o Could degrade the electronic efficiency
o Incorporate stub lines as part of filter sections	~60 - 80 db	o Mechanical tolerance problem. o Requires additional width of core section. o Some circuit efficiency degradation. o Could degrade the electronic efficiency.
o Full wave rectification	~15 db	o Doubles or quadruples number of diodes. o Greatly complicates electrical circuit and mechanical construction.

In the baseline design, two low pass filter sections which attenuate the second and higher order harmonics by over 25 db separate the rectifier from the outside world. More filter sections add approximately 17 db more suppression, each at a cost of approximately 1% efficiency loss. Other alternatives, also with an efficiency penalty, are to use stub line filters or full wave rectification. All of these approaches have mechanical configuration problems that, while solvable, will increase rectenna diode array assembly costs. Given these difficulties, it may become necessary to seek SPS-assigned bands at the first few harmonic frequencies.

Another type of scattering which affects system design is Fresnel edge diffraction from the rectenna panel edges. A slight overlapping of panels can reduce these losses but does increase total panel area and cost. The expected capture loss and resultant efficiency loss is estimated at between 1 to 2%.

6.0 RECTENNA SYSTEM OPTIMIZATION

Optimization of a rectenna system design to minimize costs is carried out at several levels. It is always desirable from the cost per unit power standpoint to transmit as much power through the transmission link as the ionospheric medium and beam pattern constraints will allow. The rectenna should be increased in size until the incremental rate of return from sales of the intercepted power are marginal. Such a procedure is illustrated in Figure 8 where the incremental revenue per square meter is balanced by the incremental cost per unit rectenna area at the optimum.

Much of the cost of the rectenna is in the structural support material required to support it against wind drag and snow loads. Different types of rectenna panels were considered. The baseline design chosen is an intermediate between the inexpensive but draggy flat panels and the more expensive, low drag panels which have circuit topology problems. The present rectenna panel support structure evolved from stiff edge-supported panels to a hierarchical more centrally supported frame which uses much less material.

7.0 RECTENNA CONSTRUCTION

Construction of the rectenna is, by necessity, highly automated. Starting with prefabricated dipole assembly components, a dipole machine (Figure 9), manufactures completed dipole/diode assemblies at a high rate. These are then combined with other prefabricated parts to manufacture receiving element sticks. The sticks, metal frame and ground plane are then tack-welded together to form panels (Figure 10).

The completed panels are then taken to the rectenna site where specialized equipment, shown on Figure 11, prepares the site through the emplacement of panel support arches. The panels are then lowered on the support arches, fastened and connected electrically.

There must, of necessity, be some rather conventional construction at the rectenna for the grid power system and the pilot beam transmitter(s), but these constitute only a small fraction of the construction cost.

8.0 RECTENNA COST

The rectenna investment and maintenance cost breakdown for the baseline design is indicated in Table 4.

TABLE 4: SPS RECTENNA COST BREAKDOWN PER MAJOR TASK

<u>Task</u>	<u>Labor</u>	<u>Eqmt.</u>	<u>Material</u>	<u>Freight</u>	<u>Total</u>
Initiate Site Preparation	503	301	4,479	255	3,402
Complete Site Preparation	1,400	1,047	18,780	884	~15,446
Foundation and Supporting Structure	24,550	64,093	182,842	32,181	303,666
Manufacture and Install Panels	24,296	145,134	928,664	3,455	1,101,549
TOTAL (\$'s in Thousands)	50,752	210,575	1,088,247	36,775	1,386,349

Land costs are excluded, but are typically less than 5% of the anticipated cost for typical sites considered. If desired, the land underneath the rectenna may be used for factories or intensive agriculture.

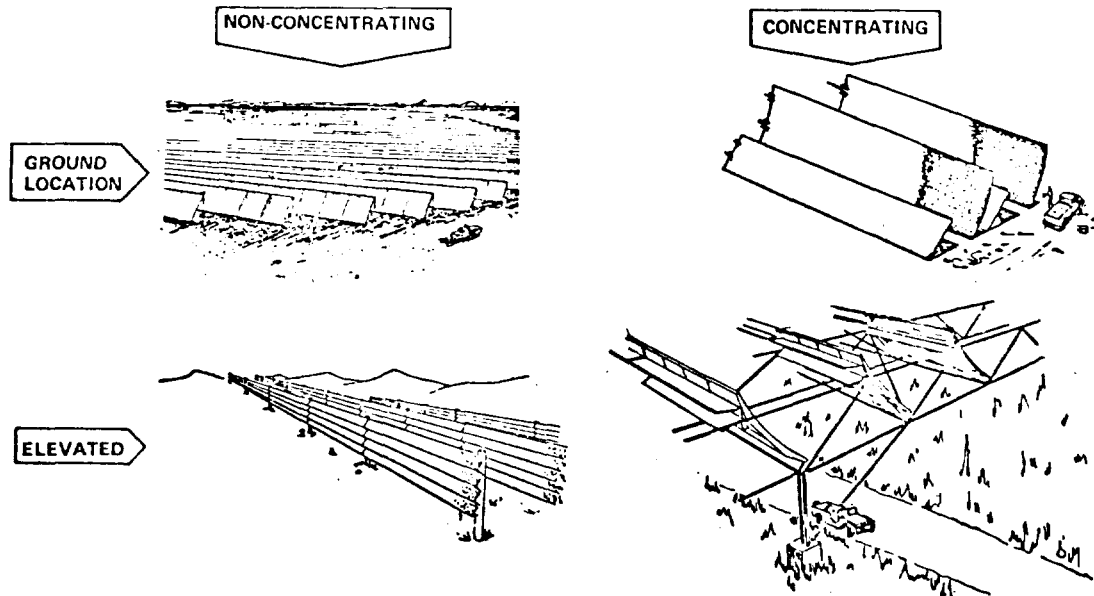


Figure 1: Potential Rectenna Configurations

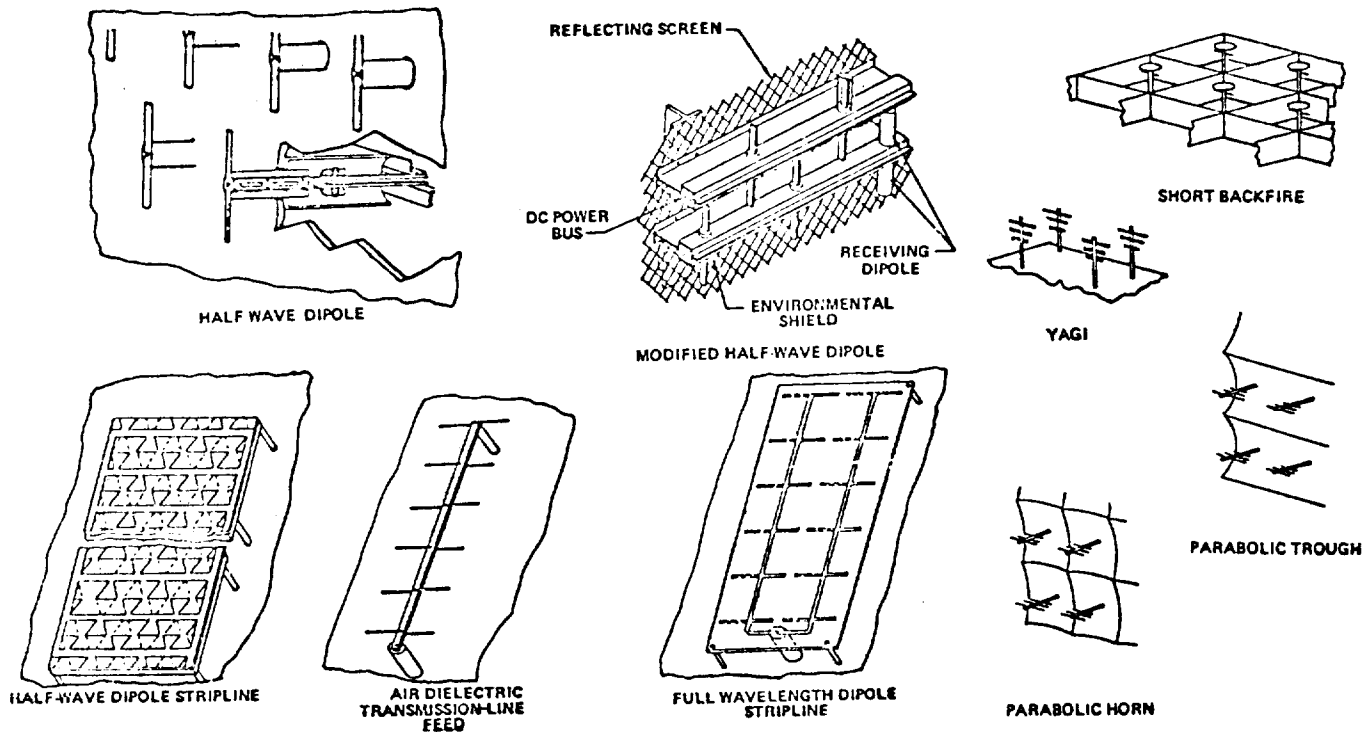


Figure 2: Rectenna Receiving Element Options

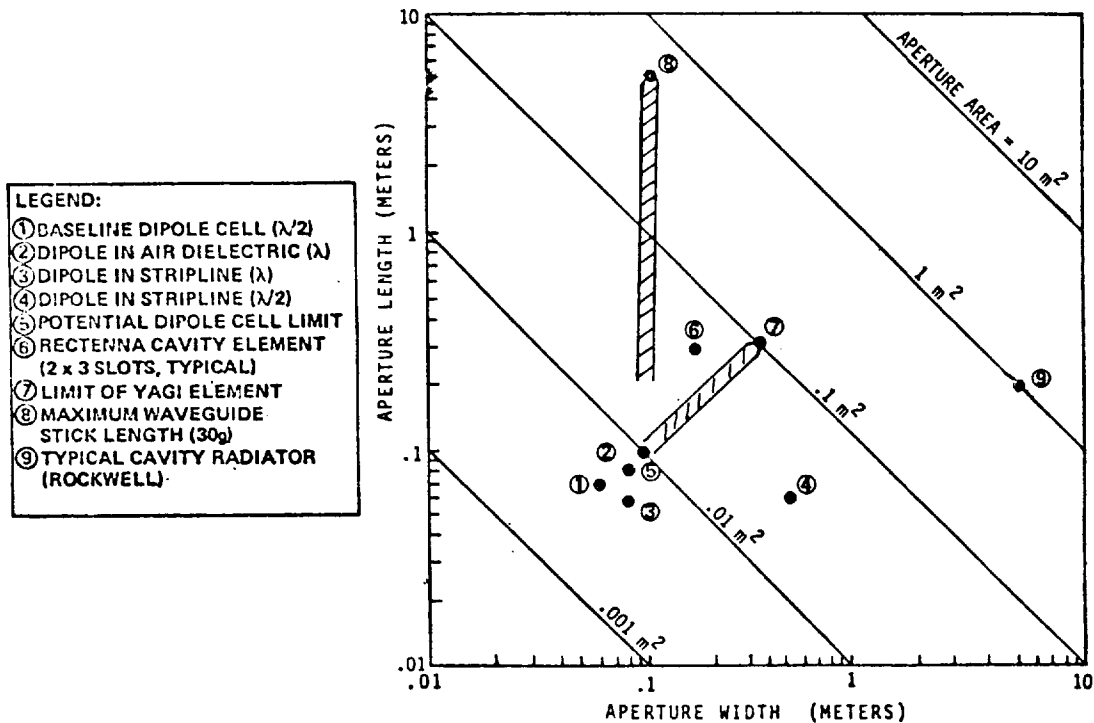


Figure 3: Rectenna Element Capture Areas

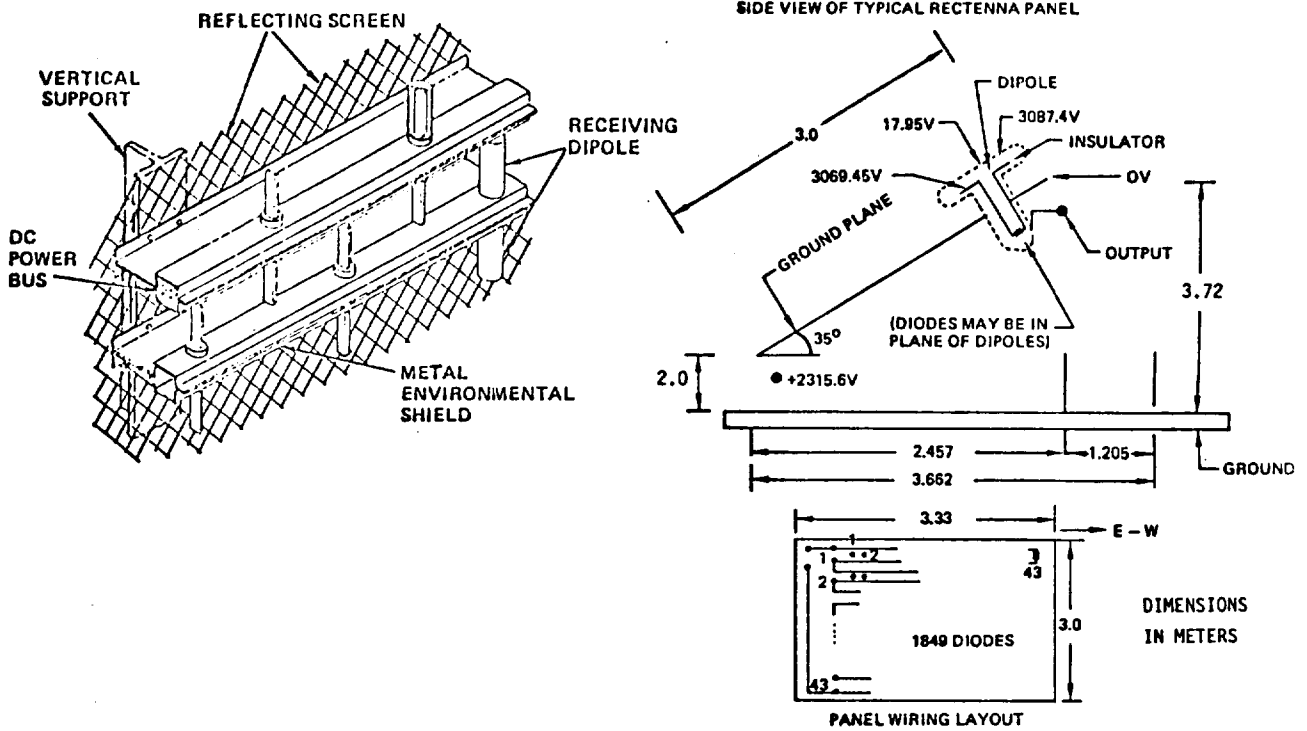


Figure 4: Typical Panel Configuration at Rectenna Center

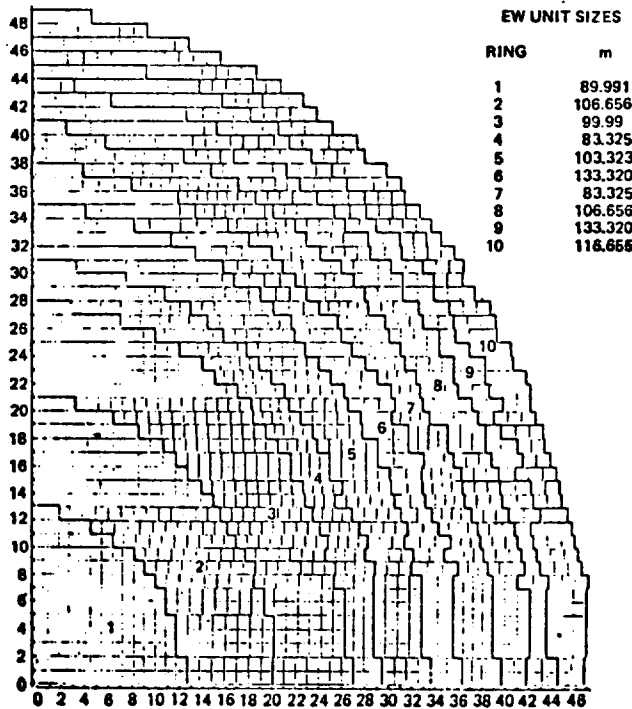


Figure 5: Rectenna Ring and Unit Boundary Map

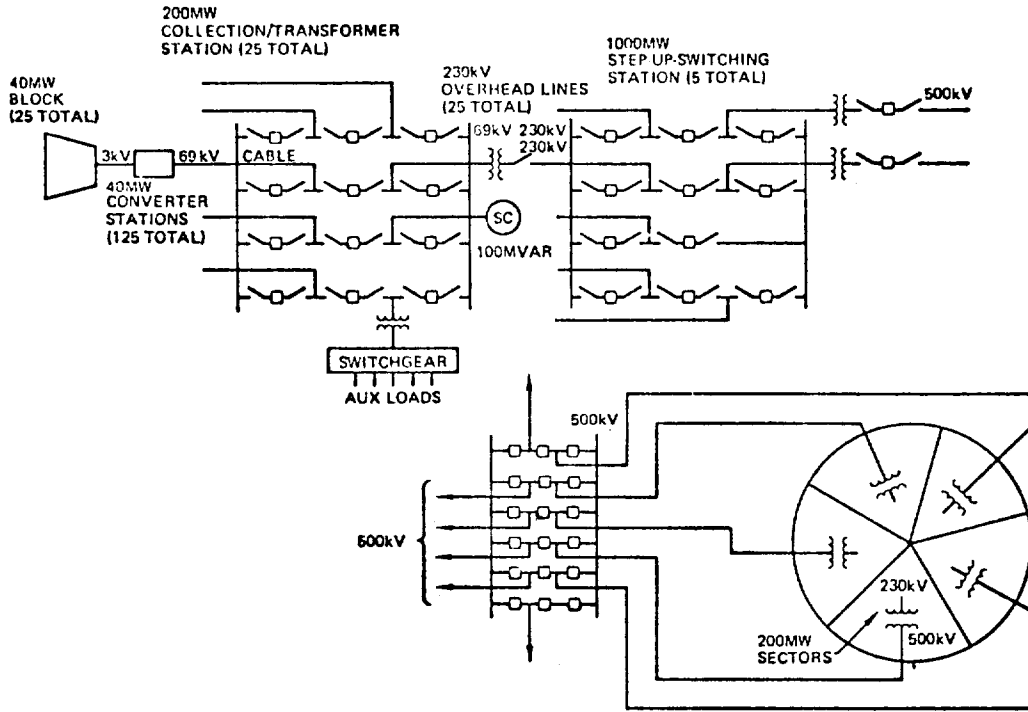


Figure 6:
Grid
Connection
Approach

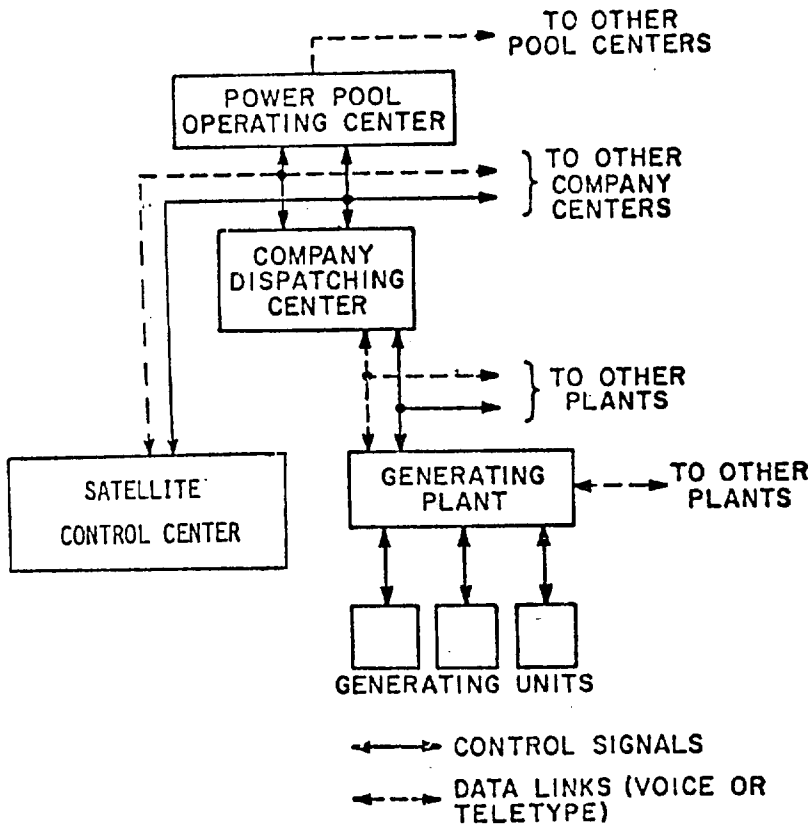


Figure 7:
Utility System
Control Structure

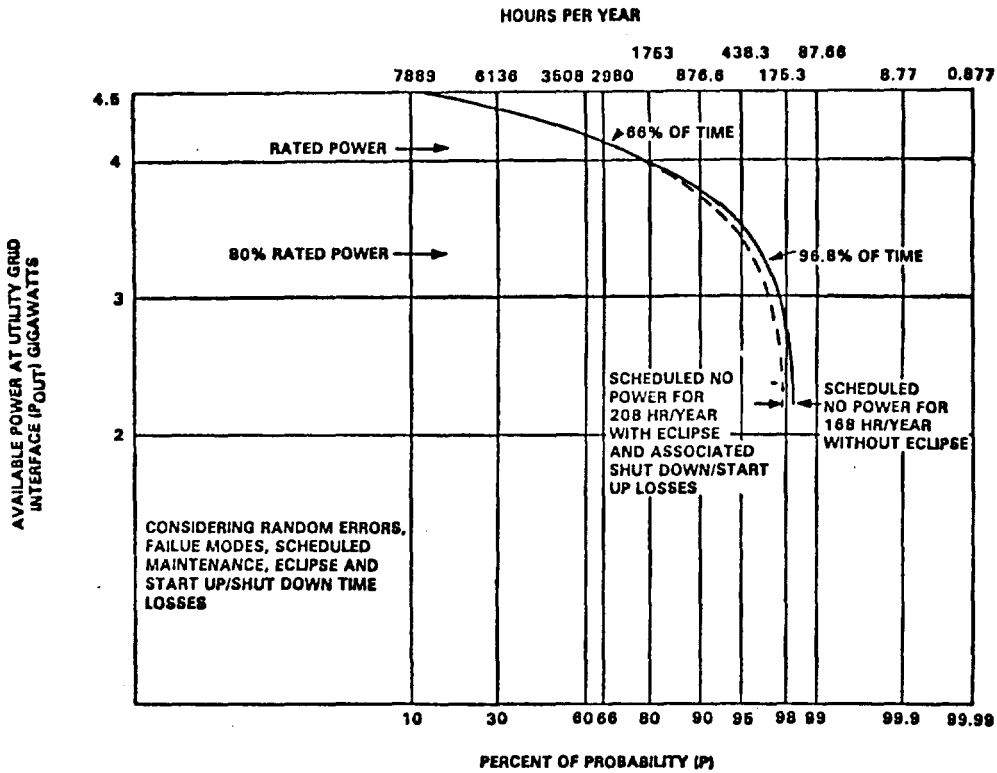
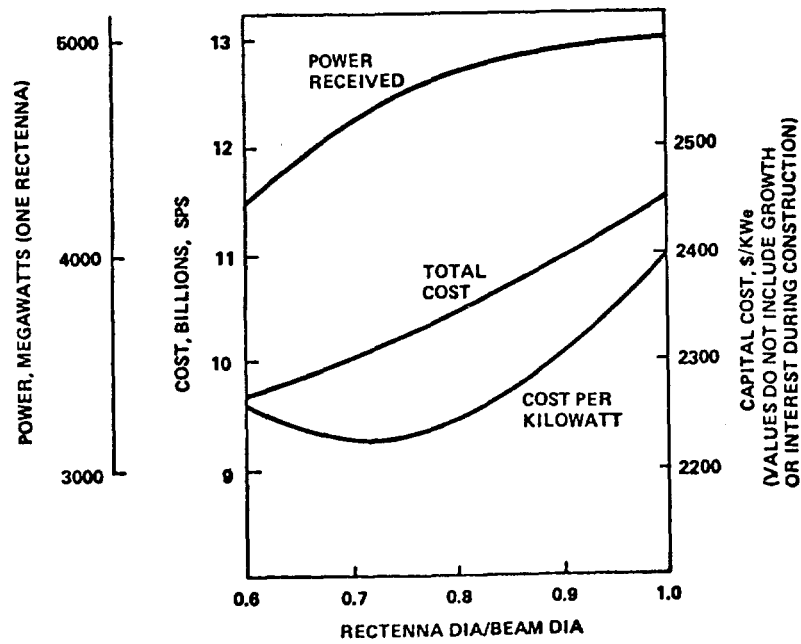


Figure 8: SPS Power Availability

SPS-1388



(Note: Beam diameter is the entire main lobe to the first null.)

Figure 9: Rectenna Size Optimization

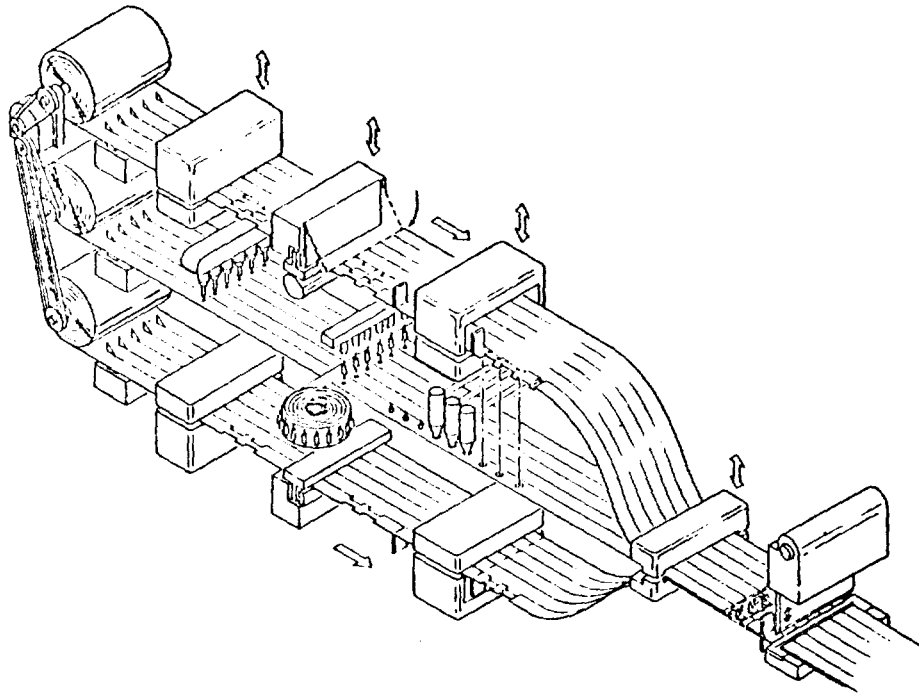


Figure 10: Dipole Machine

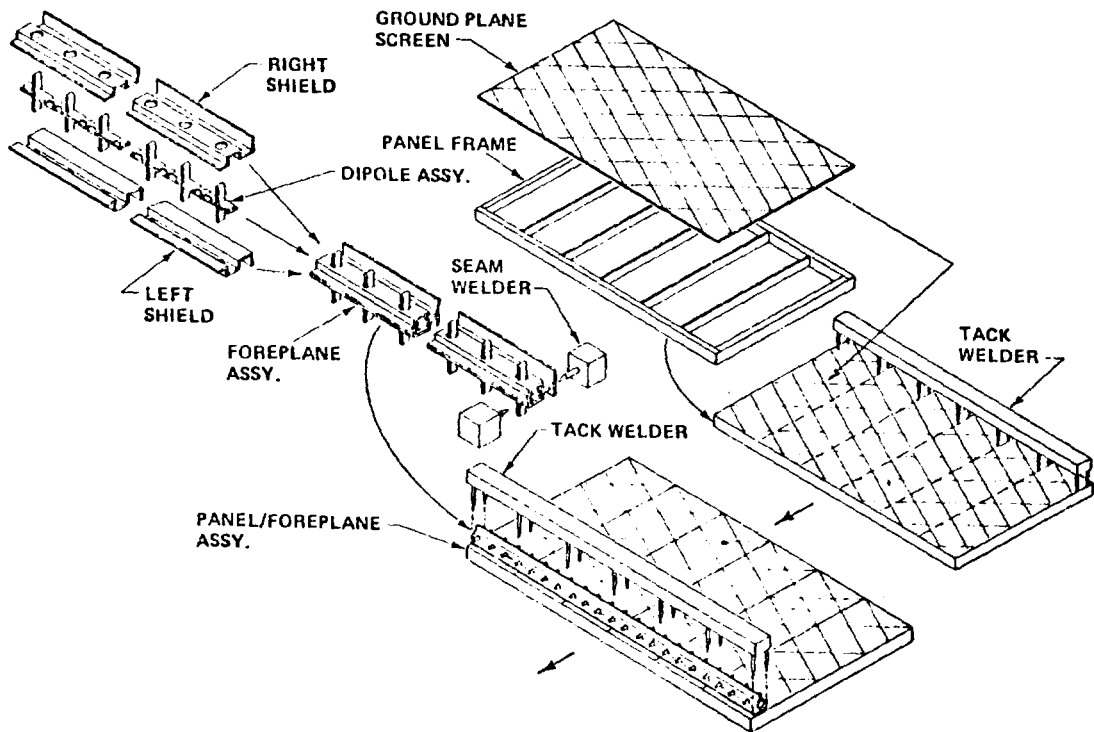


Figure 11: Rectenna Panel Fabrication Sequence

Rectenna Session: Micro Aspects
Dr. Ronald J. Gutmann
Rensselaer Polytechnic Institute

There are two micro aspects of the rectenna design which will be addressed in this presentation: evaluation of the degradation in net rectenna RF to DC conversion efficiency due to power density variations across the rectenna (power combining analysis) and design of Yagi-Uda receiving elements to reduce rectenna cost by decreasing the number of conversion circuits (directional receiving elements). The first of these micro aspects involves resolving a fundamental question of efficiency potential with a rectenna, while the second involves a design modification with a large potential cost saving. These tasks were investigated under contract with JSC during 1978.

Power Combining Analysis

In the rectenna, numerous rectifier circuits share a common DC load to achieve useful power levels. The rectifier outputs can be combined in series and/or parallel to enhance the voltage and/or current level respectively, with previous rectennas designed with first stage parallel combining followed by series combining.

A fundamental question in this receiving, rectification and power combining process is caused by the power taper of the incident microwave beam. The incident power density can vary by 10 dB over the rectenna area since a high percentage of the transmitted microwave power needs to be collected and the power beam sidelobe level must be kept reasonably low. Since the output (DC terminal) characteristics of the rectifier are power dependent, rectifiers at different power levels that share a common DC load cannot be operated at optimum conditions. With individual rectifiers near 90% maximum efficiency, the resultant efficiency degradation could be significant. In this work the efficiency degradation that results when an array of microwave power rectifiers shares a common DC load was evaluated for the first time.

In analyzing the degradation, we assume that the output load line or volt-ampere (V-I) characteristics of each of the rectifying circuits to be *combined* are known. This V-I characteristic can be determined by either

a circuit analysis of the rectenna element, by a computer simulation or by direct measurement of the output voltage and current for several load resistances. It is assumed that the V-I characteristics are a function of some parameter θ of the rectenna element (in our case incident RF power). Given the V-I characteristics, it is possible to determine the operating point for maximum power output.

In Fig. 1 we show the V-I characteristics of two dissimilar rectenna elements as well as the points at which each of them deliver maximum power if operating independently. The same figure shows that if the elements are operated in parallel (common output voltage) or in series (common output current), they will not operate at their optimum power output and their combined power output will be less than if operated independently. We have developed expressions for the power combining inefficiency (reduction in output power compared to collected power assuming each rectifier operated in its own optimum DC load) for both series and parallel combining.^(1,2)

In order to evaluate the power combining inefficiency an accurate output equivalent circuit model of the conversion circuitry is needed. This was obtained using two independent approaches. First, an approximate closed form circuit model of the rectifier was developed assuming an ideal diode and lossless circuit elements. The output load line was then obtained analytically. Second, a more precise computer simulation model was used, and the output equivalent circuit was obtained by varying the DC load resistance and plotting the resultant output load line.

We have shown that assuming an ideal diode, the circuit indicated in Figure 2A has yielded 100% conversion efficiency if $L_3 - C_3$, $L_5 - C_5$ etc. form odd harmonic parallel resonant circuits, C_1 series resonates the resultant inductive impedance at the fundamental frequency and $R_L = (\pi^2/8) R_S$.^(1,2) Figure 2B indicates the more exact computer simulation model, a reasonable representation of the actual circuitry used in experimental rectennas. The models and the resulting load lines will be discussed further in the presentation.

When using these models and various assumed power density variations, we find that parallel combining is marginally better than series combining and that the closed form analytical model slightly underestimates the power

combining inefficiency compared to the computer simulation results. Assuming a uniform power density distribution, the power combining inefficiency is 1.0% when the ratio of maximum to minimum power density is 2.0 to 1.0, reducing to 0.3% if the ratio is 1.4 to 1.0. This has an important effect on the design of the rectenna DC power combining network, favoring ring combining rather than row combining particularly near the rectenna edge.

Directional Receiving Elements

A principal advantage of the rectenna concept for the receiver in free-space microwave power transmission systems is that the effective receiver pattern is sufficiently non-directional (i.e. beamwidth sufficiently large) that receiver steering is not required. However in evaluating the requirements for a solar power satellite (SPS) with a small orbit eccentricity in a near zero inclination geostationary orbit, it became apparent that the half wave dipole separated by $\approx 0.2 \lambda$ from a conducting ground plane has a more non-directional pattern than needed. That is the beamwidth of the receiver pattern at which 1% of the incident power is not received (0.04 dB beamwidth)* is much larger than the off normal incidence due to orbit considerations. Since the rectenna cost is projected to be $\sim 25\%$ of the total system cost, consideration of more directional receiving elements is clearly desirable.

In most applications fewer RF to DC conversion circuits (favoring directional elements) and power beam pointing requirements (favoring non-directional elements) are expected to dominate the directionality issue. An additional factor with the present GaAs Schottky diode rectifiers and present SPS design values is that higher RF to DC conversion efficiency is possible at higher power levels (power density limited by nonlinear interactions in ionosphere and possibly biological factors), thus favoring somewhat more directional elements. An additional disadvantage to directional receiving elements are more stringent requirements for a stable rectenna structure and precise element tolerances.

In considering alternate receiving elements at the modest gain enhancement considered desirable, we focused on the Yagi-Uda element because of

* Since efficient power transmission is paramount in the SPS application, a 1% beamwidth is more applicable than either the 3 dB or 1 dB beamwidth used in many microwave applications.

its simplicity. Including proximity effects in an actual array configuration was beyond the scope of our program. Instead we utilized antenna performance of isolated Yagi-Uda arrays in arriving at the expected electrical performance depicted in Table 1.^(1,3)

Based upon this electrical performance we designed three and six element Yagi-Uda arrays, with and without ground plane reflector, in both conventional baseline construction and in printed circuit form. Design of three element Yagi-Uda elements without ground planes are depicted in Fig. 3. These designs will be discussed further in the presentation.

The resultant costs obtained are in our investigation presented in Table 2, the trend toward lower cost with increased rectenna element gain being apparent. As expected, the cost reduction per unit rectenna area varies between the ratio of element densities (dependent upon effective area of each receiving element) and the square root of this ratio (dependent upon linear density of element rows). The net result is clear: THERE IS A LARGE RECTENNA COST SAVING POSSIBLE BY UTILIZATION OF MORE DIRECTIONAL RECEIVING ELEMENTS LIKE YAGI-UDA ELEMENTS. In a typical SPS rectenna there would be $\sim 75 \text{ km}^2$ area, so that a cost reduction of $\$/\text{m}^2$ is equivalent to a 75 million dollar reduction in capital costs. Thus savings of 300 to 450 million dollars per rectenna may be possible with the more directional Yagi-Uda element (capital costs in 1978 dollars).

The comparison between conventional construction and printed circuit implementation is less apparent. The printed circuit estimates are based upon less detailed design, but these results do not indicate a substantial reduction with printed circuit implementation. Only if socket and DC buss bar cost can be reduced will a large cost advantage result. These may be possible with careful structural designs requiring less material usage and low cost manufacturing, 5 mm diameter aluminum buss bars being assumed in our work. However, the conversion efficiency of printed circuit implementations will be somewhat lower, so baseline construction definitely seems preferred.

We have shown that more directional receiving elements are expected to lower rectenna costs in free-space microwave power transmission systems such as the SPS where the microwave power beam is relatively stationary with respect to the rectenna. Yagi-Uda receiving elements are considered

most desirable when moderate gains of perhaps 8 to 14 dB (with respect to an isotropic radiator) are optimum. Yagi-Uda antennas become undesirably awkward at higher gain, and alternatives such as short back-fire antennas should be considered. However it is believed that higher gain may result in unrealistically stringent power beam-rectenna alignment requirements in the SPS.

References

1. R. J. Gutmann and J. M. Borrego, "Solar Power Satellites Rectenna Design Study: Directional Receiving Elements and Parallel-Series Combining Analysis", Rensselaer Polytechnic Institute Report under Contract NAS9-15453 with NASA Johnson Space Center, December 1978.
2. R. J. Gutmann and J. M. Borrego, "Power Combining in an Array of Microwave Power Rectifiers", IEEE Trans. Microwave Theory and Techniques, MTT-27, December 1979.
3. R. J. Gutmann and R. Gworek, "Yagi-Uda Receiving Elements in Microwave Power Transmission System Rectennas", Journal of Microwave Power, 14, September 1979.

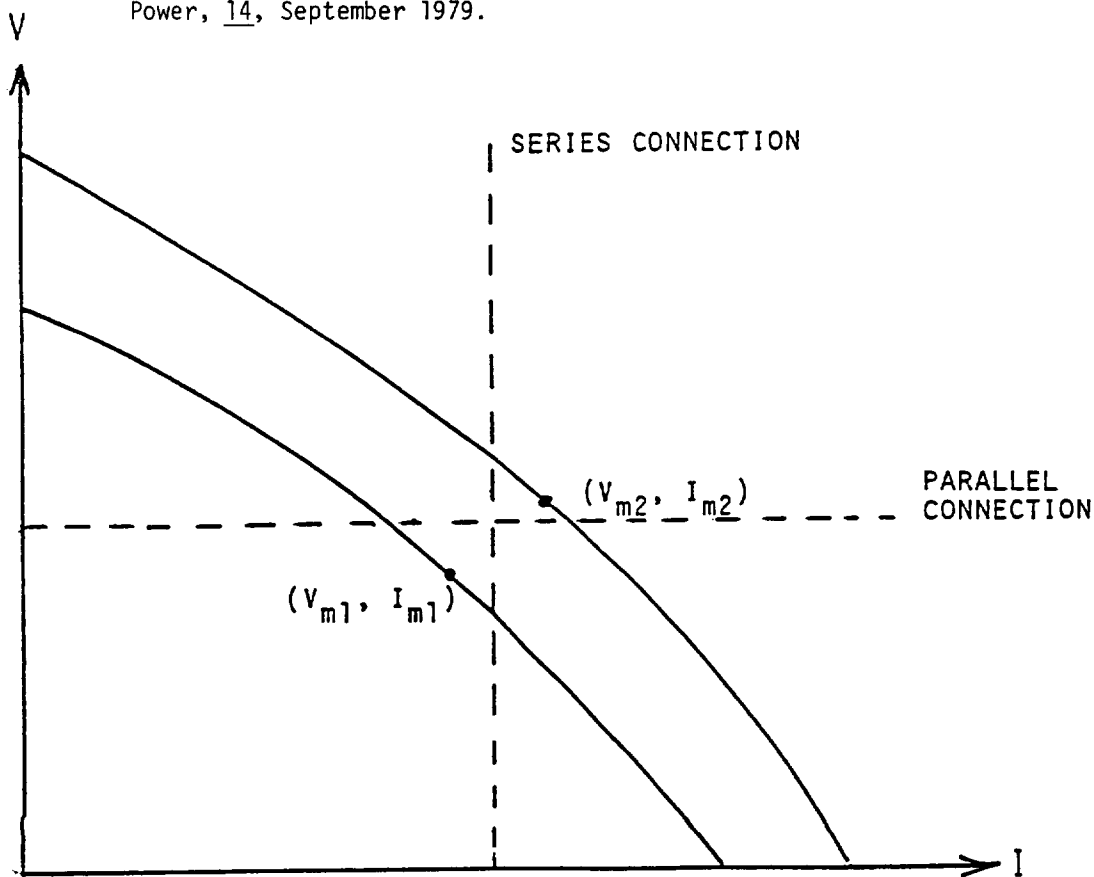


Figure 1 Output Load Line for Two Different Rectifiers

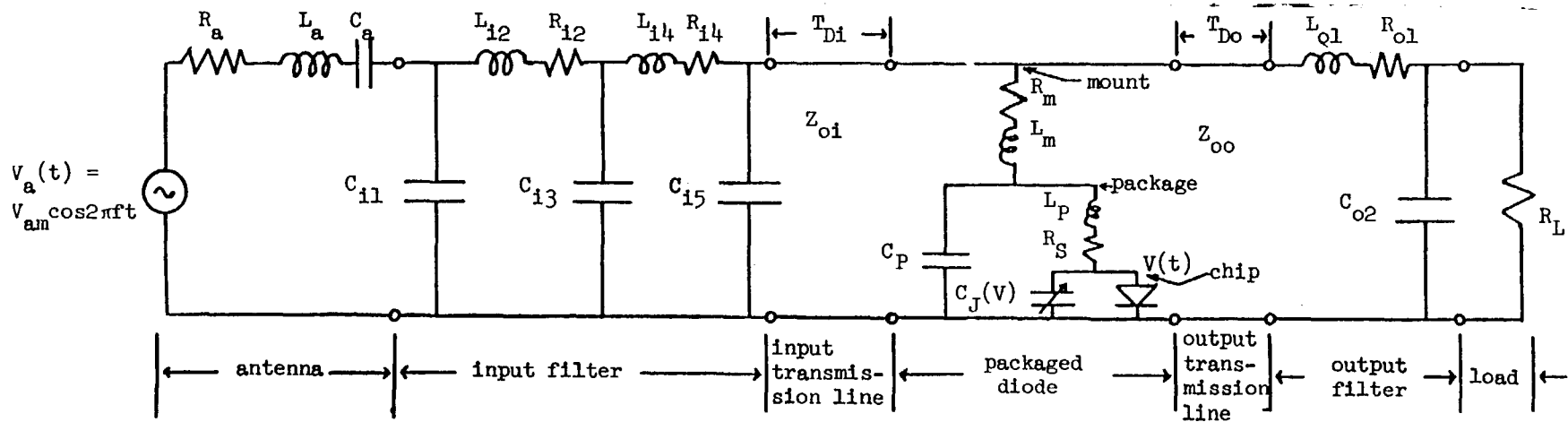
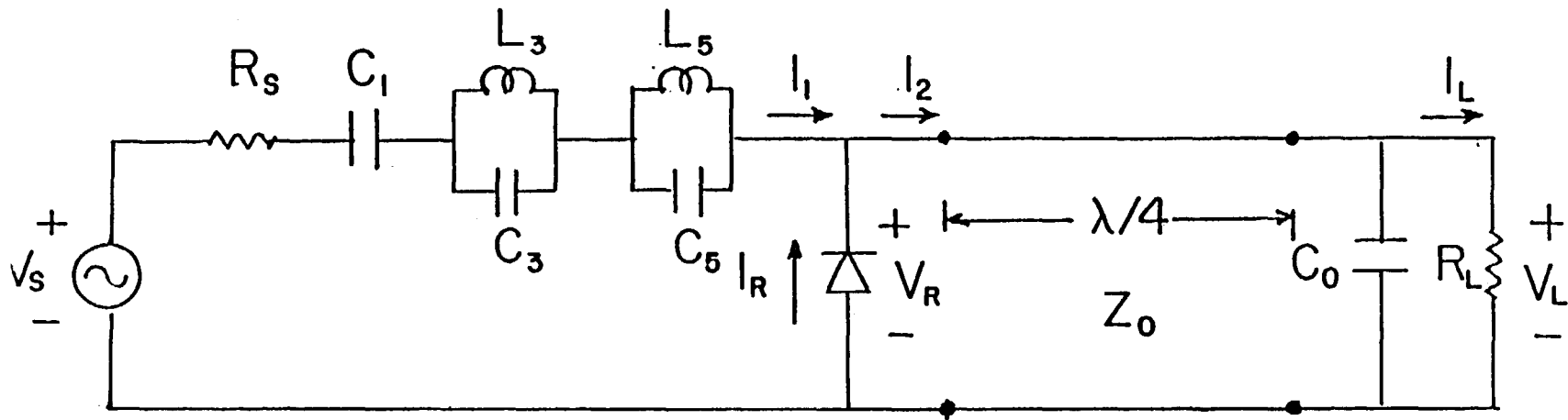
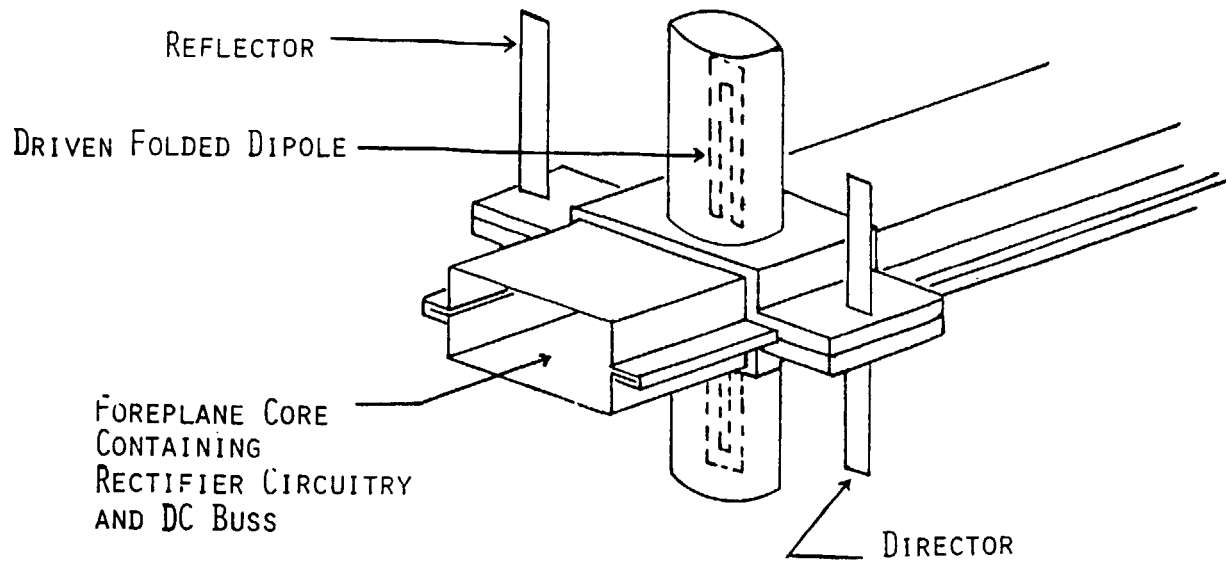


Figure 2 Equivalent Circuit Models for Microwave Rectifier
 (A) Ideal Circuit Model
 (B) Realistic Circuit Model of Baseline Rectifier



297

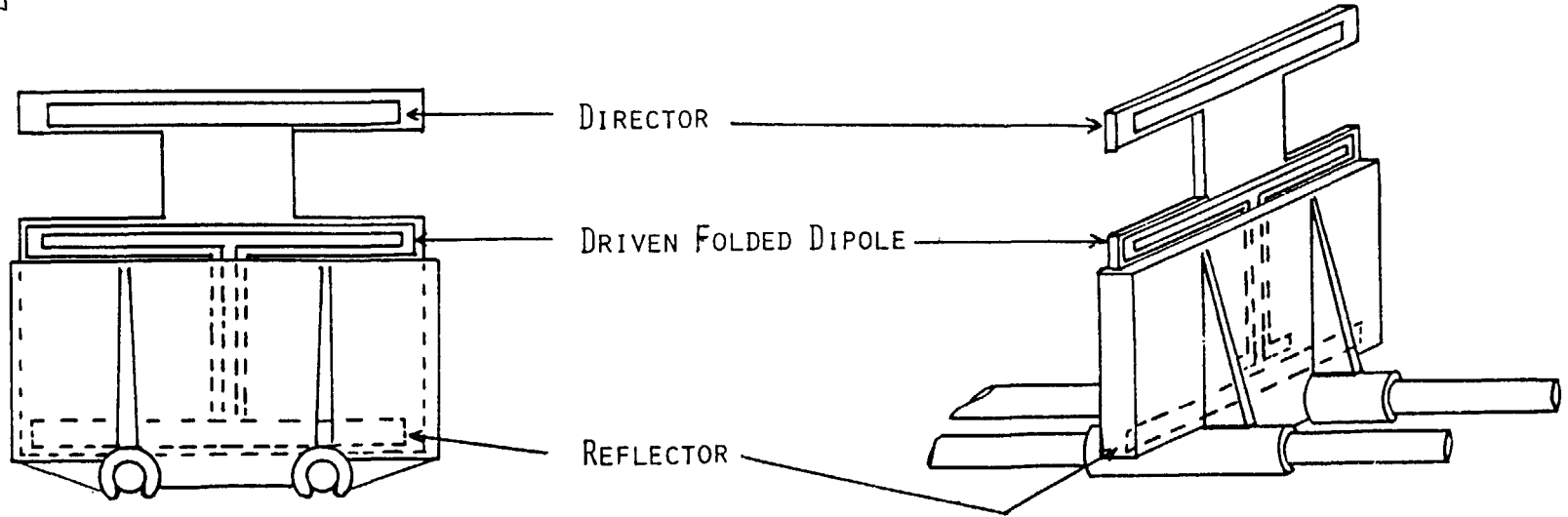


Figure 3 Three Element Yagi-Uda Receiving Array
 (A) Baseline Construction
 (B) Printed Circuit Construction

Table I

Expected Optimal Performance of Yagi-Uda Receiving Elements

	<u>Gain (wrt Isotropic) dB</u>	<u>F/B Ratio dB</u>	<u>Receiving Element Reduction Factor*</u>
3 Element-Low F/B ratio	11	5	2.82
3 Element-Moderate F/B ratio	10	15	2.24
3 Element-High F/B ratio	8.5	25	1.58
6 Element-Low F/B ratio	14	5	5.62
6 Element-Moderate F/B ratio	13	15	4.47
6 Element-High F/B ratio	11.5	25	2.82

298

* Relative to 6.5 dB Half-Wave Dipole Separated by $.20\lambda$ from a Conducting Ground Plane

A. Printed Circuit Board Implementation

(costs are given in $\$/m^2$)

	<u>Half-wave Dipole with ground plane</u>	<u>3 element Yagi with ground plane</u>	<u>without ground plane</u>	<u>6 element Yagi without ground plane (average size)</u>
Element Density ($\frac{\text{elem.}}{m^2}$)	192	81	123	57
Socket	\$.92	\$.39	\$1.12	\$.52
DC buss bar	2.78	1.81	2.23	1.55
Printed Circuit Board	.24	.24	.42	.44
Ground Plane	<u>1.91</u>	<u>1.91</u>	<u>.00</u>	<u>.00</u>
Cost/ m^2	\$5.85	\$4.35	\$3.77	\$2.51
Diodes at \$.01 each	<u>\$1.92</u>	<u>\$.81</u>	<u>\$1.23</u>	<u>\$.57</u>
Total Cost/ m^2	\$7.77	\$5.16	\$5.00	\$3.08

B. Conventional Type Construction

(costs are given in $\$/m^2$)

	<u>Half-wave Dipole with ground plane</u>	<u>3 element Yagi with ground plane</u>	<u>without ground plane</u>	<u>6 element Yagi without ground plane</u>
Element Density ($\frac{\text{elem.}}{m^2}$)	192	81	123	57
Coreplane Core	\$3.13	\$1.47	\$2.09	\$1.09
Aluminum Shield/ Structural Member	2.14	1.40	.92	.64
Yagi-Uda Additions	.00	.30	.71	.76
Ground Plane	<u>1.91</u>	<u>1.91</u>	<u>.00</u>	<u>.00</u>
Cost/ m^2	\$7.18	\$5.08	\$3.72	\$2.49
Diodes at \$.01 each	<u>1.92</u>	<u>.81</u>	<u>1.23</u>	<u>.57</u>
Total Cost/ m^2	\$9.10	\$5.89	\$4.95	\$3.06

Table 2 Rectenna Cost Estimates (excluding rectenna frame)

A THEORETICAL STUDY OF MICROWAVE BEAM ABSORPTION BY A RECTENNA

James H. Ott
James S. Rice
Donald C. Thorn

Novar Electronics Corporation, Barberton, Ohio

ABSTRACT

The results of a theoretical study of microwave beam absorption by a Rectenna is given. Total absorption of the power beam is shown to be theoretically possible. Several improvements in the Rectenna design are indicated as a result of analytic modeling. The nature of Rectenna scattering and atmospheric effects are discussed.

INTRODUCTION

A workable Solar Power Satellite system will depend upon the efficient free-space transmission of energy to earth via an environmentally benign microwave beam. The "Rectenna", a large array of dipole devices which captures and rectifies microwave power from satellites, embodies an emerging technology pioneered by William C. Brown¹ of Raytheon. Brown² and Richard Dickinson³ of JPL have reported tests on experimental Rectenna arrays which have achieved microwave to dc conversion efficiencies exceeding 50%. However, classical antenna theory tells us that an isolated dipole must re-radiate as much energy as it delivers to a properly matched load. Because of a frequently expressed concern over whether or not this antenna theory was in contradiction with experimental Rectenna results, Novar Electronics Corporation undertook the task of developing a theoretical model which describes the absorption of a microwave beam by a very large Rectenna. In view of the size and scope of the SPS program, it is important to theoretically determine whether a rectenna array of the reference system design can totally absorb the power beam—that is, produce no scattering. In addition, it is desirable to study the microwave absorption process in order to provide a theoretical model for the simulation of design improvements and, because of concerns about possible electromagnetic interference from the rectenna, to obtain additional insights into the rectenna's scattering properties.

Novar's work demonstrates not only that the theoretical absorption limit is in fact 100% but that the number of elements required for total absorption per unit area can be greatly reduced, significantly reducing the cost of the Rectenna. Results further indicate that Rectenna panels can be made to totally absorb at any angle of incidence by adjusting reflector and element spacing and load impedance. This suggests a flat or terrain conforming Rectenna eliminating the need for the "billboard" or "Venetian blind" design and essentially conforming to the terrain. Also, the screen reflector should be able to be replaced by parasitic reflector dipole elements.

Deviations from conditions required for total absorption give rise to scattering, and the resulting losses due to variations from design center values for several parameters are shown. The directionality of fundamental and harmonic scattering from a Rectenna is described. Among the factors causing scattering that were studied are microwave beam depolarization and amplitude fluctuations caused by disturbances in the atmosphere. Included in this category is "diffracted signal enhancement", the diffractive effects of large objects flying over the Rectenna, which can be expected to cause transient signal increases as large as 9 dB which must be taken into account in the rectenna design.

Because of the difficulty in trying to analyze a large array of interacting dipoles using mutual impedance analysis, it was necessary to develop another type of mathematical model descriptive of the microwave

power absorption process. Two such models were derived from Maxwell's equations. These models quantify conditions for total absorption of the power beam by a Rectenna and provide values for scattering losses due to deviations in each condition.

CURRENT SHEET RECTENNA MODEL

The first model is based on the current sheet equivalency of a large planar array above a reflector as shown in Figure 1. The current sheet has the properties of resistive absorbers described by Jasik⁴ and Kraus⁵. The model is mathematically characterized by an expression for the fraction of an incident plane wave's power that is reflected from the sheet.

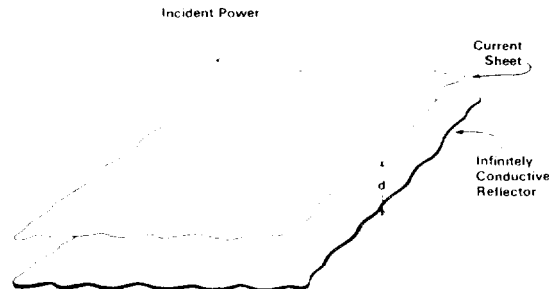


FIGURE 1
CURRENT SHEET RECTENNA MODEL

This expression, which agrees with Jasik, and for which no derivation could be found in the literature, is determined as follows. First, Maxwell's equations are solved to obtain general expressions for the electric and magnetic fields in the region above the current sheet and in the region between the current sheet and the reflector surface.

Next, the boundary conditions are satisfied at the infinitely conductive reflector surface and then at the current sheet as the thickness of the current sheet is allowed to become very thin. This yields expressions for the waves at the surface of the current sheet. The expressions are then solved simultaneously for the power reflection coefficient, the fraction of power reflected by the current sheet. It is expressed by either Equation 1a or 1b, following, depending upon the polarization of the incident wave.*

*Polarization is defined by the relationship of the incident wave's electric field vector, \underline{E} , to the plane of incidence, the plane determined by rays in the directions of propagation of the incident and reflected waves. When \underline{E} is parallel to the plane of incidence, the wave is said to be parallel polarized. When \underline{E} is perpendicular to the plane, the wave is said to be perpendicular polarized. (Any other polarization can be decomposed into a combination of parallel and perpendicular polarization.)

Parallel Polarization

$$|r_{\parallel}|^2 = \frac{\left(\frac{\sqrt{\mu}f}{R_0} \cos\theta - 1\right)^2 + \cot^2\left(\frac{2\pi d}{\lambda} \cos\theta\right)}{\left(\frac{\sqrt{\mu}f}{R_0} \cos\theta + 1\right)^2 + \cot^2\left(\frac{2\pi d}{\lambda} \cos\theta\right)} \quad (1a)$$

Perpendicular Polarization

$$|r_{\perp}|^2 = \frac{\left(\frac{\sqrt{\mu}f}{R_0} \sec\theta - 1\right)^2 + \cot^2\left(\frac{2\pi d}{\lambda} \cos\theta\right)}{\left(\frac{\sqrt{\mu}f}{R_0} \sec\theta + 1\right)^2 + \cot^2\left(\frac{2\pi d}{\lambda} \cos\theta\right)} \quad (1b)$$

where:

- R_0 is the resistance of the current sheet in ohms per square*,
- θ is the angle of incidence of the received wave as measured from the normal,
- d is the separation between the current sheet and reflector,
- λ is the wavelength,
- μ and ϵ are the permittivity and permeability, respectively.

The expressions above demonstrate that total absorption is theoretically possible for normal incidence ($\theta = 0$) when $d = \lambda/4$ and $R_0 = \sqrt{\mu}f = 377$ ohms for free space. The power reflection coefficient and reflected power as functions of deviations in R_0 , d , or θ from those values required for total absorption at normal incidence are shown in Figure 2.

The model further predicts that a Rectenna can be designed for total absorption for beam angles off normal incidence.† This leads to the possibility of a Rectenna that can be built to lie flat on the ground and be essentially "terrain conforming". This type of Rectenna array has several advantages over the "billboard" or "venetian blind" construction of the reference system: 1) much less excavation is required, 2) there is the potential to suspend the elements and reflector screen above farms, buildings, etc., and 3) less scattering is anticipated because there are no "billboard" edges to cause diffraction of the power beam.

This current sheet Rectenna model provides a "macroscopic view" of the microwave absorption process. Novik has developed a second model which provides an insight into the role played by the individual Rectenna elements. Moreover it provides an independent theoretical confirmation of the ability of the Rectenna to totally absorb the power beam.

WAVEGUIDE RECTENNA MODEL

The second model quantifies the electromagnetic modes (field configurations) in the immediate vicinity of a Rectenna element in the Rectenna array and gives limits for the element spacing which permit total power beam absorption by preventing unwanted modes from propagating (scattering). This model is based on the properties of a special waveguide described by Wheeler⁶ in his analysis of certain aspects of a large planar array. Specifically, the waveguide has

special "imaging" characteristics and has the ability to allow only plane wave propagation. The waveguide is rectangular in shape with a probe (monopole) inserted through the middle of one of the walls. However unlike "conventional" waveguides, the two walls parallel to the monopole are nonconductive and "magnetic" ($\mu = \infty, \sigma = 0$), with the other two walls being perfectly conductive ($\sigma = \infty$). When we solve the equations describing the nature of wave reflections at

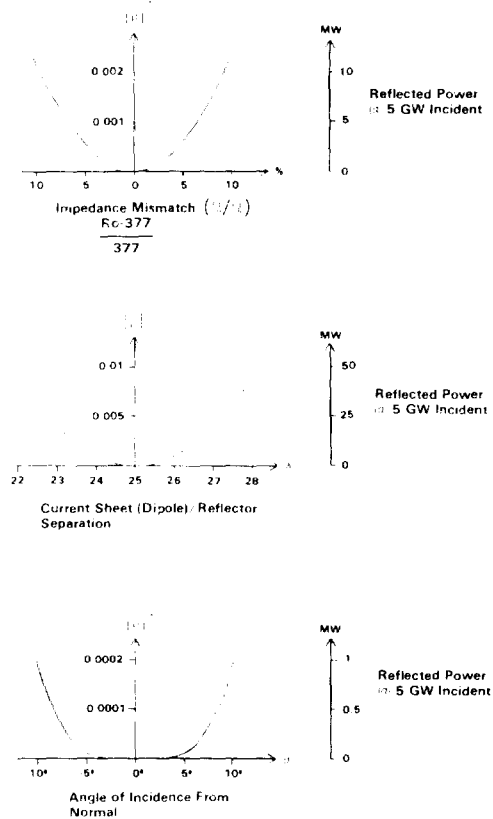


FIGURE 2
POWER REFLECTION COEFFICIENT AND REFLECTED POWER LEVEL OF THE CURRENT SHEET RECTENNA MODEL AS A FUNCTION OF VARIOUS PARAMETERS

*Resistance per square is the resistance between opposite edges of a square slab of resistive material and therefore is independent of the size of the square.

†With λ fixed, and given any θ , there is an R_0 and d such that $|r|^2 = 0$.

the walls, it is found that a monopole in this type of waveguide, which we will call a "mixed-wall" waveguide, produces an infinite array of image dipoles with currents of identical magnitude and phase as depicted in Figure 3.* Conversely, an infinite array of identical dipoles with currents of identical magnitude and phase can be replaced by a single monopole in a mixed-wall waveguide to analyze the behavior of a dipole as illustrated by Figure 4. Since the power beam is nearly uniform in power density over quite a large area, dipoles within a fairly large arbitrarily selected area of the Rectenna will have currents nearly uniform in magnitude and phase which can be closely approximated for that area by an infinite array. Thus the behavior of a dipole which defines the center of this area can be accurately modeled by the behavior of a monopole in a mixed-wall waveguide.

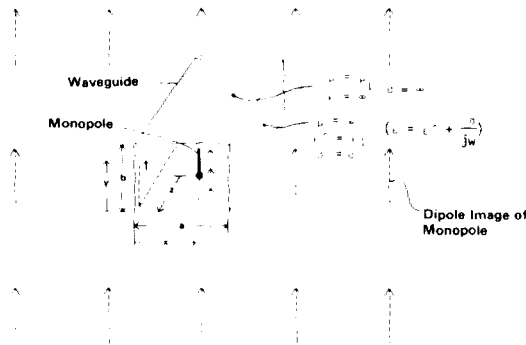


FIGURE 3
IMAGING PROPERTIES OF MIXED-WALL
WAVEGUIDE WITH MONOPOLE

The first step in analysis of this monopole's behavior is to determine what modes can propagate in the mixed-wall waveguide† and under what conditions. We want the TEM mode to be the only mode that can propagate. This TEM mode is the same field configuration as that of the power beam, i.e., a plane wave. If other modes propagate, scattering is taking place. Since the side walls of a mixed-wall waveguide as shown in Figure 3 are non-conductive and "magnetic", the mixed-wall waveguide is similar to a strip-line for the TEM modes. Thus this waveguide will support the TEM mode at the power beam frequency independent of the waveguide dimensions.

Next, the properties of the mixed-wall waveguide for the higher order modes are derived in order not only to determine the conditions required for their evanescence but also to allow us to describe the near fields around the monopole. To do this, Maxwell's equations are solved to obtain wave equations which are then modified by mathematical decomposition to put them into an efficient form for solution. The wave equations are then solved to obtain general equations for the magnetic and electric fields in the mixed-wall waveguide. These equations are functions of pairs of integers, one integer of which is associated with the "a" dimension in Figures 3 and 4, and the other with "b". Specific values for the inte-

gers in a pair defines a mode. The higher order modes have either transverse magnetic or transverse electric fields.‡ These are respectively designated the TM_{fg} and the TE_{gm} modes, where f and n are 0,1,2,3,...; g and m are 1,2,3,....

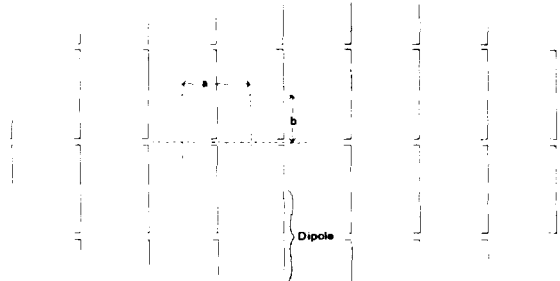


FIGURE 4
SECTION OF INFINITE ARRAY OF DIPOLES MODELED BY
A MONOPOLE IN A "MIXED-WALL" WAVEGUIDE

Inspection of the mode equations shows that the lowest cutoff frequency for higher order TM modes is associated with TM_{01} and that for the TE modes is the TE_{10} . This means that at a given frequency the smallest critical dimensions for propagation are associated with those two modes. The next larger critical dimension is associated with the TE_{20} .

The TE_{10} mode is actually non-existent in our mixed-wall waveguide/monopole configuration because it is not generated when the monopole is located in the center of this special type of waveguide.** This results in the critical dimensions for higher mode

*Analogous to the study of optical reflections from mirrors, the "method of images" shows that the fields within the mixed-wall waveguide boundaries are the same as though there was no waveguide but only the monopole and an infinite number of identical magnitude and phase images.

†Modes, which are the various field configurations that can exist within a waveguide, have the property that for a given frequency they are evanescent (non-propagating) for waveguide dimensions less than certain critical values, which are called "cutoff" dimensions, and can propagate for any dimensions greater than those values. Each mode has its own set of cutoff dimensions. Conversely, for a given set of waveguide dimensions, there is a critical frequency for each mode (called the cutoff frequency) below which the mode is evanescent and above which it can propagate.

‡Transverse means no component in the $\pm z$ direction in Figure 3.

**Note that "mode-hopping", the generation of modes due to waveguide imperfections, is not a problem here because the waveguide is assumed to be ideal.

propagation being determined by the TM_{01} and the TE_{20} . Specifically, for evanescence of all higher modes, those critical dimensions restrict the waveguide dimensions to be less than one wavelength in the "a" direction and less than one half wavelength in the "b" direction. (This is equivalent to a Rectenna element spacing of just under one wavelength.)

The total electric field, \underline{E} , and the total magnetic field, \underline{H} , in the mixed-wall waveguide are each sums of the various field configurations or modes that exist in the waveguide. Now \underline{E} and \underline{H} are vector sums of respective field components in the x, y, and z directions of Figure 3. Thus for "+z directed" field components, \underline{E} and \underline{H} can be represented by the equations given in Table I, where A_{mn} and B_{fg} are respectively the maximum amplitudes of H_z and E_z , K_{00} is the maximum amplitude of the H field of the TEM wave. The α 's and β 's at the bottom of the table are respectively the real and imaginary parts of the expressions shown for the γ 's. The terms involving double summations represent the "sums of the higher order modes". The leading terms in the equations for E_y and H_x are the equations for the TEM mode. If the higher order modes are evanescent, then the double summation terms are components of the fields associated with reactive power.

If a reflector or shorting plate is inserted in the waveguide behind the monopole, as shown in Figure 5, the situation is equivalent to the infinite array of dipoles in Figure 4 being backed by a reflector. A set of equations analogous to those in Table I can then be generated for the "-z directed" field components of the waves reflected from the shorting plate. Summing the +z and -z directed field components in the neighborhood of the monopole gives rise to a set of equations of the same form as those in a conventional waveguide backed by a shorting plate. These equations establish matching requirements on the monopole and load impedances and spacing of the monopole from the shorting plate so that the non-evanescent wave does not propagate back up the waveguide toward the source. Since it is well known that a probe in a conventional waveguide backed by a shorting plate can totally absorb all power flowing down the waveguide⁷, it is therefore expected that a probe (monopole) in a mixed-wall waveguide can also totally absorb all power flowing down that type of waveguide. Therefore total absorption of the plane wave power beam by a dipole in a Rectenna is expected when the separation between dipoles is within limits dictated by the mixed-wall waveguide model's dimensions which restrict propagation in that waveguide to the TEM mode.

Since the waveguide dimensions which restrict propagation to the TEM mode is less than λ in the "a" direction and less than $\lambda/2$ in the "b" direction of Figures 3 and 4, and since the separation between the centers of the dipoles is "a" by "2b" as can be seen from Figure 4, then the maximum allowable separation of the centers of dipoles for total absorption of a plane wave, for the rectangular grid configuration of Figure 4, is just under one wavelength.

$$\begin{aligned}
 H_z &= 0 + \sum_{m=1}^{\infty} \sum_{n=0}^{\infty} A_{mn} \sin \frac{m\pi x}{a} \cos \frac{n\pi y}{b} e^{-\alpha_{mn} z} \\
 E_z &= 0 + \sum_{f=0}^{\infty} \sum_{g=1}^{\infty} B_{fg} \cos \frac{f\pi x}{a} \sin \frac{g\pi y}{b} e^{-\alpha_{fg} z} \\
 E_x &= 0 + \sum_{m=1}^{\infty} \sum_{n=0}^{\infty} \frac{j\omega\mu n\pi}{k_{cmn}^2} A_{mn} \sin \frac{m\pi x}{a} \sin \frac{n\pi y}{b} e^{-\alpha_{mn} z} \\
 &\quad + \sum_{f=0}^{\infty} \sum_{g=1}^{\infty} \frac{-\alpha_{fg} f}{k_{cfg}^2} B_{fg} \sin \frac{f\pi x}{a} \sin \frac{g\pi y}{b} e^{-\alpha_{fg} z} \\
 E_y &= \frac{\mu}{r} K_{00} e^{-j\beta_{00} z} + \sum_{m=1}^{\infty} \sum_{n=0}^{\infty} \frac{j\omega\mu m\pi}{k_{cmn}^2} A_{mn} \cos \frac{m\pi x}{a} \cos \frac{n\pi y}{b} e^{-\alpha_{mn} z} \\
 &\quad + \sum_{f=0}^{\infty} \sum_{g=1}^{\infty} \frac{\alpha_{fg} g\pi}{k_{cfg}^2} B_{fg} \cos \frac{f\pi x}{a} \cos \frac{g\pi y}{b} e^{-\alpha_{fg} z} \\
 H_x &= K_{00} e^{-j\beta_{00} z} + \sum_{m=1}^{\infty} \sum_{n=0}^{\infty} \frac{\alpha_{mn} m\pi}{k_{cmn}^2} A_{mn} \cos \frac{m\pi x}{a} \cos \frac{n\pi y}{b} e^{-\alpha_{mn} z} \\
 &\quad + \sum_{f=0}^{\infty} \sum_{g=1}^{\infty} \frac{j\omega\epsilon g\pi}{k_{cfg}^2} B_{fg} \cos \frac{f\pi x}{a} \cos \frac{g\pi y}{b} e^{-\alpha_{fg} z} \\
 H_y &= 0 + \sum_{m=1}^{\infty} \sum_{n=0}^{\infty} \frac{-\alpha_{mn} n\pi}{k_{cmn}^2} A_{mn} \sin \frac{m\pi x}{a} \sin \frac{n\pi y}{b} e^{-\alpha_{mn} z} \\
 &\quad + \sum_{f=0}^{\infty} \sum_{g=1}^{\infty} \frac{j\omega\epsilon f\pi}{k_{cfg}^2} B_{fg} \sin \frac{f\pi x}{a} \sin \frac{g\pi y}{b} e^{-\alpha_{fg} z} \\
 \gamma_{mn} &= \alpha_{mn} + j\beta_{mn} = \sqrt{k^2 - \left(\frac{m\pi}{a}\right)^2 - \left(\frac{n\pi}{b}\right)^2} = \sqrt{k^2 - k_{cmn}^2} \\
 \gamma_{fg} &= \alpha_{fg} + j\beta_{fg} = \sqrt{k^2 - \left(\frac{f\pi}{a}\right)^2 - \left(\frac{g\pi}{b}\right)^2} = \sqrt{k^2 - k_{cfg}^2} \\
 \beta_{00} &= k = \frac{2\pi}{\lambda}
 \end{aligned}$$

TABLE I

**ELECTROMAGNETIC FIELD EQUATIONS
FOR A MIXED-WALL WAVEGUIDE**

Equations shown are for total "+z directed" portion of the field components in a mixed-wall waveguide. With appropriate sign changes, equations express the "-z directed" components.

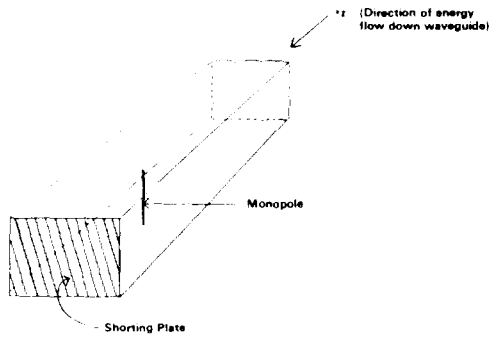


FIGURE 5
MONOPOLE IN MIXED WALL WAVEGUIDE
BACKED BY SHORTING PLATE

ELEMENT DENSITY

The existence of non-evanescent higher order modes corresponds to the existence of grating lobes. Analysis of the generation of grating lobes indicates that the maximum separation between dipole centers for avoidance of grating lobes with the triangular grid configuration used in the Reference System is just under 1.15λ . It is understood that the present separation between dipole centers in the Reference System is just under 0.6λ . The number of Rectenna dipole-diode elements needed for total power beam absorption can be significantly reduced over the number needed for the Reference Systems as shown below.

	NUMBER OF DIPOLE-DIODE ELEMENTS REQUIRED (NORMAL INCIDENCE)
Reference System Design	18 billion
Triangular Grid Configuration With Maximum Allowable Dipole Spacing	4.5 billion
Rectangular Grid Configuration With Maximum Allowable Dipole Spacing	5.2 billion

In addition, greater diode efficiency is indicated when the number of Rectenna dipole elements is reduced since the power density per diode is higher.

PARASITIC REFLECTING DIPOLES

Total absorption of energy by the monopole in a conventional waveguide requires that the shorting plate in the waveguide be approximately a quarter wavelength behind the monopole. This distance is also expected to be proper for the mixed-wall waveguide. Since the shorting plate corresponds to the Rectenna reflector, and since it is expected that the shorting plate can be replaced by a parasitic reflecting mono-

pole as can be done easily in a conventional waveguide and still totally absorb the energy traveling down the waveguide, then the Rectenna reflector should be replaceable by parasitic dipole elements, as depicted in Figure 6.

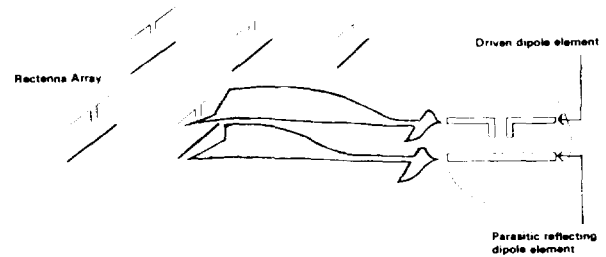


FIGURE 6
RECTENNA WITH PARASITIC REFLECTING
DIPOLE ELEMENTS

HARMONIC FILTER

None of the preceding analysis permits the dipole terminals to see a non-linear load for total absorption. What is required in a Rectenna element for total absorption is a harmonic filter, as depicted in Figure 7, that presents a linear load to the dipole terminals at the fundamental frequency such that the load voltage and current seen by the dipole are pure sinusoids not in phase quadrature, i.e. that the linear load has a real component.

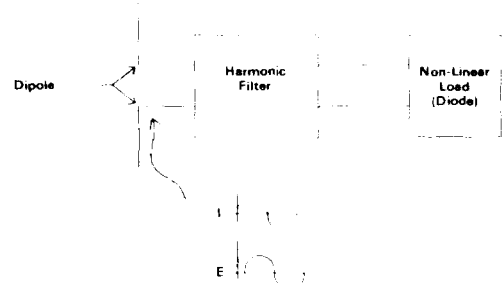


FIGURE 7
RECTENNA ELEMENT HARMONIC FILTER

FUNDAMENTAL SCATTERING

Specular scattering of the power beam, depicted in Figure 8, is expected to result from most deviations in the Rectenna's parameters. The smaller the deviation anomaly, the broader will be the specular lobe. Single, isolated element failures (short or open diodes) will appear to radiate as isotropic sources above a reflector.

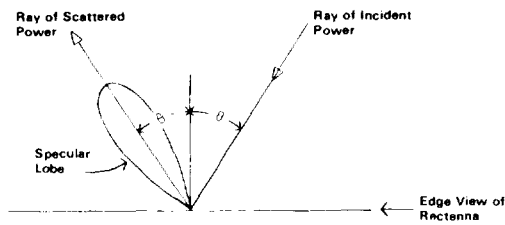


FIGURE 8
DEPICTION OF SPECULAR SCATTERING
FROM FACE OF RECTENNA
Frequency is the power beam fundamental

HARMONIC SCATTERING

The Rectenna dipole-filter-diode assembly and power bus are expected to be most significant sources of harmonic scattering. The harmonic energy will be concentrated in grating lobes, as shown in Figure 9. Random Rectenna imperfections will broaden the lobes.

ATMOSPHERIC EFFECTS

Atmospheric phenomena cause polarization shifts and amplitude fluctuations in an electromagnetic wave at microwave frequencies 8,9,10,11,12,13. However, only infrequent depolarizing events up to 20 dB (1% scattered power) have been observed in microwave down-link transmissions with greater than 10 meter apertures. Based on these observations, depolarization is not expected to be a significant source of scatter.

Amplitude fluctuations cause scattering by disrupting the uniform illumination of the Rectenna. In addition, this disruption of the RF power level from design values for the diodes causes impedance mismatches resulting in further scattering. Existing earth-space propagation measurements to date¹³

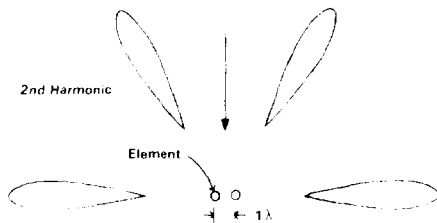


FIGURE 9a
EXAMPLE OF ELEVATION OF HARMONIC RADIATION

Figure depicts 2nd harmonic scattering for normal incidence of power beam when the element spacing is equal to λ at the fundamental frequency.

indicate a maximum of 0.1 dB amplitude fluctuations for 2-3 GHz at elevation angles above 20° (which would cause insignificant scattering).

There are factors which impair the application of previous earth station measurements to the SPS. In all studies found, there is significant aperture averaging. The minimum aperture area for those studies is about $5000\lambda^2$ as compared to about $1\lambda^2$ or so of each "independent" receiving element in the Rectenna. This indicates that the amplitude fluctuations may be appreciably greater than 0.1 dB for the Rectenna. Another factor is that the measurement data, taken at C and S bands, were obtained from modulated signals. Most deep fades are frequency sensitive. Therefore for modulated signals, which have their power spread over a spectrum of frequencies, the observed amplitude fluctuations would be expected to be less than those of the monochromatic SPS power beam.

As of this writing, Novar Electronics Corporation intends to receive, at its earth station located in Summit County, Ohio, special monochromatic calibration signals from RCA's new F3 Satcom* in order to observe aperture averaging effects and monochromatic signal fading characteristics. Aperture areas of approximately $1200\lambda^2$ and on the order of $1\lambda^2$ will be used to comparatively receive the signals (which are transmitted for satellite installation test purposes to determine EIRP contours).

*Scheduled to be stationed in orbit at the end of December, 1979

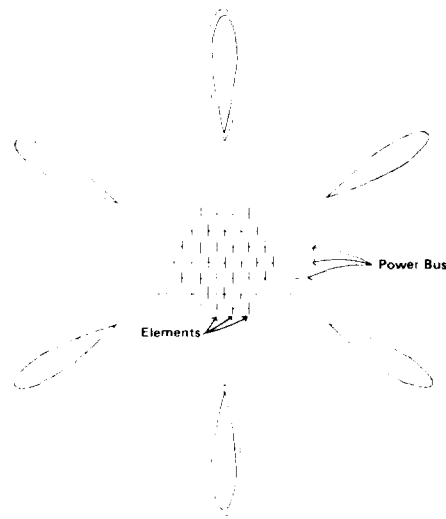


FIGURE 9b
AZIMUTHS OF HARMONIC RADIATION

"Dotted" lobe due to power bus.

FIGURE 9
GRATING LOBE NATURE OF HARMONIC
SCATTERING FROM A RECTENNA

DIFFRACTED SIGNAL ENHANCEMENT

A large object flying through the power beam over the Rectenna causes diffraction patterns to be generated at the Rectenna as depicted in Figure 10. Preliminary experimental evidence has been obtained. Depending on the size and shape of the object, increases in signal levels as large as 9 dB are possible. Therefore, Rectenna diodes should have tolerance to the resulting spot-transient signal enhancement to protect against overvoltage transients from fast aircraft and also against diode overheating from slower objects.



FIGURE 10
DIFFRACTION ENHANCEMENT AT RECTENNA
CAUSED BY OBJECT FLYING THROUGH THE
POWER BEAM

CONCLUSIONS

Analytic modeling shows that it is theoretically possible for a Rectenna to totally absorb microwave energy, i.e., produce no scattering. The number of elements required is significantly less than indicated in the Reference System. The Rectenna can be designed for total absorption at off-normal angles of incidence and it is expected that the Rectenna's reflecting screen can be replaced with parasitic reflecting dipoles.

Further space-earth transmission studies are required. The application of existing data to the SPS is impaired because these were from measurements of modulated signals received by large aperture antennas.

REFERENCES

1. W. C. Brown, "The Technology and Application of Free-Space Power Transmission by Microwave Beam," Proceedings of the IEEE, Vol. 62, No. 1, January 1974, pp. 11-25.
2. W. C. Brown: "Optimization of the Efficiency and Other Properties of the Rectenna Element," 1976 IEEE MTT-S International Microwave Symposium Digest of Technical Papers, pp. 142-144.
3. R. M. Dickinson: "Performance of a High-Power 2.388-GHz Receiving Array in Wireless Power Transmission Over 1.54 km", 1976 IEEE MTT-S International Microwave Symposium Digest of Technical Papers, pp. 139-141.
4. H. Jasik (Ed): Antenna Engineering Handbook, McGraw-Hill Book Company, 1961. (The Salisbury screen is described in Sec. 32, page 36.)
5. J. D. Kraus: Electromagnetics, McGraw-Hill Book Company, Inc., 1953. (The "Space cloth" is discussed, starting on page 407.)
6. H. A. Wheeler: "The Radiation Resistance of an Antenna in an Infinite Array or Waveguide" Proc. I.R.E. Vol. 36, No. 4, April 1948, pp. 478-487. (Introduces concept of waveguide to image interchange) (Gives radiation resistance of each element of an infinite rectangular array on the basis of a special waveguide.) (States ability of individual antenna in guide with reflector to have 100% absorption.)
7. J. C. Slater: Microwave Transmission. McGraw Hill Book Company, Inc., 1942 (Good basic treatment including a careful discussion of the limitation of "impedance" in waveguides. Discusses dipole-waveguide connection on page 296.)
8. R. R. Taur: "Ionospheric Scintillation at Frequencies Above 1 GHz" Cosmat Technical Review, Vol. 4, No. 2. Fall, 1974.
9. J. P. Basart, G. K. Miley, and B. G. Clark: "Phase Measurements with an Interferometer Baseline of 11.3 km" IEEE Trans. on Antennas and Propagation. Vol. AP18, No. 3, May 1970, pp. 375-379. (Provides a good insight into phase variations due to the atmosphere.)
10. D. J. Fang: "Attenuation and Phase Shift of Microwaves due to Canted Raindrops" Cosmat Technical Review Vol. 5, No. 1. Spring, 1975.
11. D. J. Fang and J. Jih: "A Model of Microwave Propagation Along an Earth Satellite Path" Cosmat Technical Review Vol. 6, No. 2. February 1976.
12. M. C. Thompson, Jr. and H. B. James: "Antenna Aperture Size Effect on Tropospheric Phase Noise" IEEE Transactions on Antennas and Propagation Vol. AP. November, 1966. pp. 800-802.
13. R. K. Crane and D. W. Blood: "Handbook for the Estimation of Microwave Propagation Effects--Link Calculations for Earth-Space Paths (Path Loss and Noise Estimation)" Environmental Research & Technology, Inc. Technical Report No. 1, p. 7376 - TRI, June 1979.

In addition to the publications listed above, the authors gratefully acknowledge the assistance provided in personal communications from R. K. Crane, D. J. Fang, P. W. Hannan, R. K. Moore, R. R. Taur, and H. A. Wheeler.

RECTENNA ARRAY MEASUREMENT RESULTS

Richard M. Dickinson
Telecommunications Science and
Engineering Division Staff
Jet Propulsion Laboratory

ABSTRACT

The measured performance characteristics of a rectenna array are reviewed and compared to the performance of a single element. It is shown that the performance may be extrapolated from the individual element to that of the collection of elements.

Techniques for current and voltage combining have been demonstrated. The array performance as a function of various operating parameters is characterized and techniques for overvoltage protection and automatic fault clearing in the array have been demonstrated. A method for detecting failed elements also exists.

Instrumentation for deriving performance effectiveness is described. Measured harmonic radiation patterns and fundamental frequency scattered patterns for a low level illumination rectenna array are presented.

INTRODUCTION

Prior to a definite commitment for a significant application of Beamed RF Power, performance characteristic data must be obtained for use by design engineers and systems analysts. The operating performance of a rectenna array under various conditions of load, RF power input level, temperature, polarization, angle of incidence, state of maintenance, and frequency is required. Fundamental performance factors are the transfer efficiency, relating dc power output to available RF power input, and the level and distribution of scattered fundamental and emitted harmonic radiation from the array. Secondary performance factors are the output voltage and converter temperature. The existing measured performance data on rectenna arrays will be reviewed and recent results will be discussed.

MEASURED RECTENNA ARRAY PERFORMANCE

High efficiency (greater than 50%) rectenna array characteristics were documented in Ref. 1, for the condition of highest collection-conversion efficiency performance associated with a demonstration of overall system end to end dc transfer efficiency. The array consisted of 199 half wave gallium arsenide Schottky barrier diodes connected to half wave dipoles through a two section low pass filter projecting through a flat solid ground plane. The elements were arranged in a triangular lattice whose outline configuration was a hexagon. The collecting area per element was about 52 cm². The incident flux density ranged from 203 mW/cm² to 2.5 mW/cm² in a gaussian distribution over the aperture of the array. (A 19 dB taper.) The dc load collection consisted of 21 separate concentric rings of adjustable resistances tailored to the ring radius. A one tenth wavelength dipole probe in front of the array measured about 1.11 to 1 VSWR on axis under matched conditions.

The peak collection-conversion efficiency of an individual element was measured as $87 \pm 1.5\%$, whereas the average efficiency of the entire array at approximately 0.5 KW output dc power was 82.7% of the available RF power incident upon the array (not counting the estimated 4% spillover energy). The array transfer efficiency decreased less than 2% for a 16.7% decrease in RF input power level.

The next large rectenna array was tested at Goldstone, CA (Ref. 2) and consisted of 4590 elements arranged in 17 subarrays of 270 elements each arranged in a triangular grid pattern. The subarrays were grouped in a three column arrangement with the top center subarray absent, as shown in Fig. 1. Fig. 2 and 3 are of the array performance characteristics and capabilities for use of the instrumented output data. The measured performance can in general be accurately predicted from general transmission line reflection coefficient theory as concerns the load variations, and the polarization and angle of incidence performance follows array theory. Computer models (Ref. 3, 4) for the diode and associated RF circuitry are able to predict the element performance as a function of the input RF amplitude, however, the array performance is poorer than predicted in most cases, by a few percent. This may be due to the effects of mutual coupling in the array, which are not modeled in a single element analysis. Nevertheless, over a 10 dB range of input power density, the rectenna array performance may be adequately predicted within a few percent, based upon measured diode characteristics.

Figure 4 compares the transfer efficiency performance of a single element, the average element in a subarray of 270 elements, and the average element in an array of 4590 elements over a 6 dB range of RF power density input. The performance of a large array may be extrapolated with confidence from the single element.

CURRENT AND VOLTAGE COMBINING AND PROTECTION

Figure 5 shows the wiring diagram of one of the 270 element subarrays. By insulating the dc buss from the subarray frame the paralleled rows of rectenna element outputs may be seriesed in order to raise the output voltage, while still presenting an adequate output impedance level to the individual element.

The subarray rows are self-clearing of short circuited diode faults by the fusing open of the one mil diameter gold bond wires in the packaged diodes under the combined short circuit current developed by 45 rectennas in parallel. The failed elements may be detected while operating by the increased reflected power at a VSWR probe over the element, or alternatively while the array is inoperative, by briefly individually illuminating each element while monitoring the dc output (termed "sniffing").

Overvoltage protection from loss of load, excessive RF input level or interruption of input, was accomplished in the Goldstone tests by the self actuated crowbar in Fig. 5. A voltage limiter would be less traumatic for the load than a crowbar however.

INSTRUMENTATION

Fig. 5 also shows the isolated load central element for a subarray, that is used to provide a measure of the input RF power flux density. An RF shielded thermistor is employed to measure the temperature of the central buss bar in the subarray. Calibrated shunts and precision voltage dividers

were employed to sample the output current and voltage levels. A fixed track, movable probe positioned in front of the subarray to measure the reflected power would be an expensive, but useful instrument to monitor the subarray performance under various operating conditions. It could be integrated into a sniffing and maintenance positioning assembly perhaps, that travels over the array surface.

SCATTERED FUNDAMENTAL AND RADIATED HARMONIC CHARACTERISTICS

Figure 6 shows a 42 element rectenna array undergoing pattern recording of its emitted harmonics as a function of various operating parameters. Figures 7 and 8 show the measured harmonics and the scattered fundamental patterns for certain conditions. These patterns are typical for a wide range of parameters. The significant facts are that the scattered fundamental is distributed over a broad range of angles, and that the fourth harmonic is of higher magnitude than the third harmonic. The array was underexcited due to equipment limitations, with the peak RF to dc conversion efficiency being only 35%, however the results are expected to be applicable to a normally functioning array. Future designs will probably require more filtering of harmonics in order to control them and permit the array to meet applicable radio regulations (Ref. 5). The scattered fundamental frequency radiation may be controlled to a degree by varying the dc load value, the incident flux density level, or the dipole to ground plane spacing, each of which affects the impedance match of the array, and thus provides a potential parameter for control of the reflected fundamental magnitude. Figure 9 shows the variation in efficiency and dc power output for a particular subarray as the spacing is varied.

The RF frequency could also be varied to effect an impedance match. Figure 10 shows the bandwidth measurements for the 42 element array for two different illumination conditions. Such a design characteristic would have to be integrated with the harmonic filter design also.

CONCLUSIONS AND RECOMMENDATIONS

Adequate theory and design information exists that has been compared with full scale measurements, to provide engineers and systems analysts with the characterization of rectennas performance to within the order of a couple of percent. Particularly for high power level of incident flux density applications. The data for scattered fundamental and emitted harmonics could use some theoretical modeling to gauge the preliminary measurements. Also, bandwidth analysis and modeling for degraded modes such as partially obscured apertures and inadequate maintenance or repair need to be undertaken to round out the rectenna complete characterization.

Refinements such as automatic feedback control of rescattered fundamental by changing the ground plane spacing or load, frequency, or incident power density should be studied to evaluate their effectiveness and life cycle cost in meeting applicable radio regulations.

It should be stated that the above conclusions are based principally on measured results of half wave dipole arrays, and some of the conclusions are applicable to other elements such as yagis, only if the same array characteristics can in practice be achieved. The stipulation applies to any high gain element array.

Better harmonic filtering and active dc load management within a tapered density array along with an efficient and effective overvoltage limiter need to be developed, along with rapid repair techniques also. Long life environmental protection is still a continuing requirement for certain applications, along with light weight and waste heat dissipation for space and high altitudes.

REFERENCES

1. Dickinson, R., and Brown, W., Radiated Microwave Power Transmission System Efficiency Measurements, Technical Memorandum 33-727, Jet Propulsion Laboratory, Pasadena, California, May 15, 1975.
2. Dickinson, R., Evaluation of a Microwave High-Power Reception-Conversion Array for Wireless Power Transmission, Technical Memorandum 33-741, Jet Propulsion Laboratory, Pasadena, California, September 1, 1975.
3. Nahas, J., "Modeling and Computer Simulation of a Microwave-to-dc Energy Conversion Element," IEEE Trans. Microwave Theory Tech., Vol. MTT-23, No. 12, December 1975, pp. 1030-1035.
4. Brown, W., "Optimization of the Efficiency and Other Properties of the Rectenna Element," 1976 IEEE MTT-S International Microwave Symposium Digest of Technical Papers, pp. 142-144.
5. Edition of 1976 Radio Regulations Published by the General Secretariat of the International Telecommunications Union, Geneva, 1976.

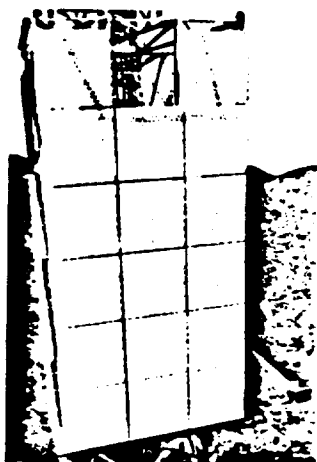


Fig. 1. The RXCV Array

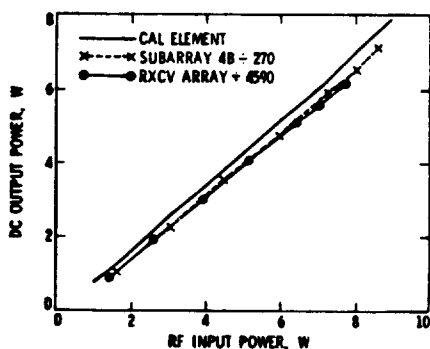


Fig. 4. Transfer Efficiency Performance Comparison

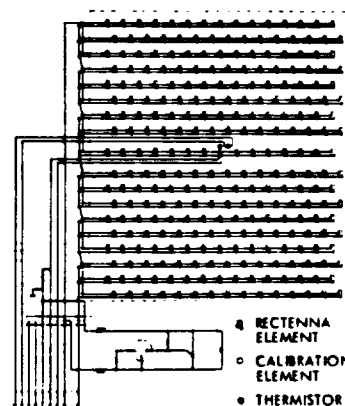
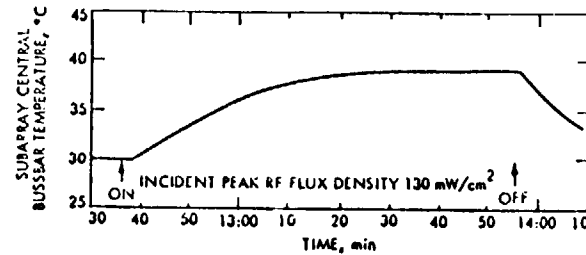
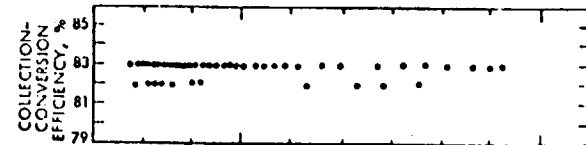
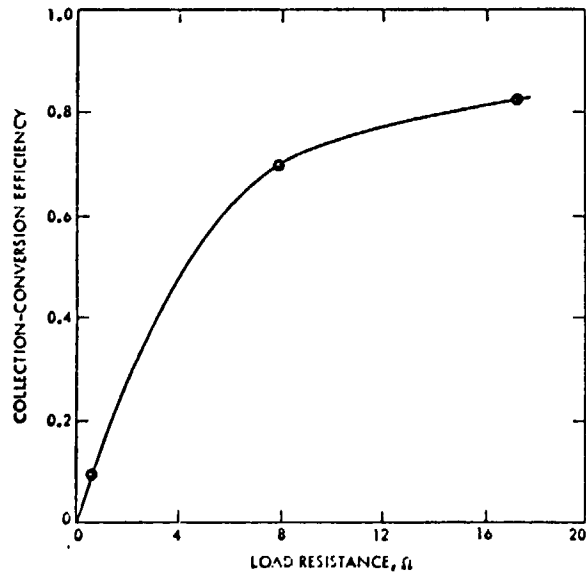
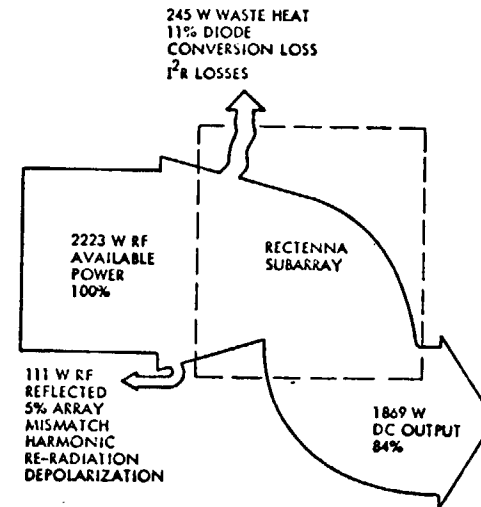
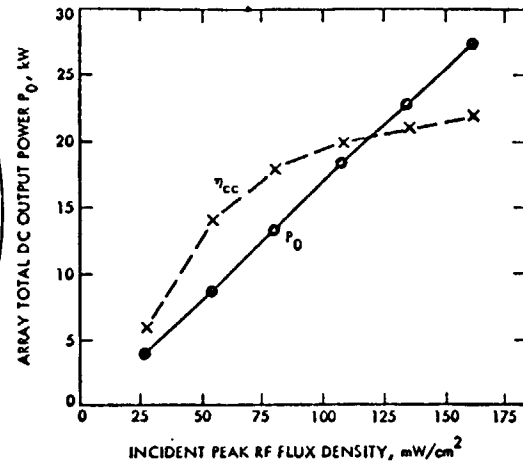
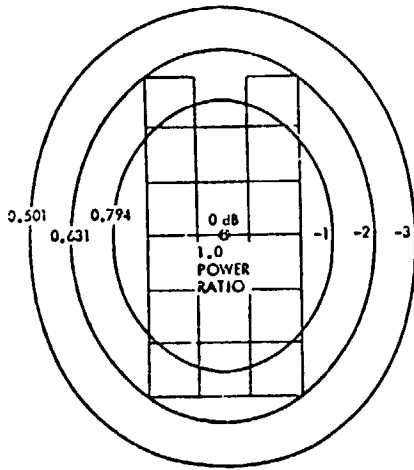


Fig. 5. Subarray Wiring Diagram

MICROWAVE RECEPTION-CONVERSION ARRAY PERFORMANCE I

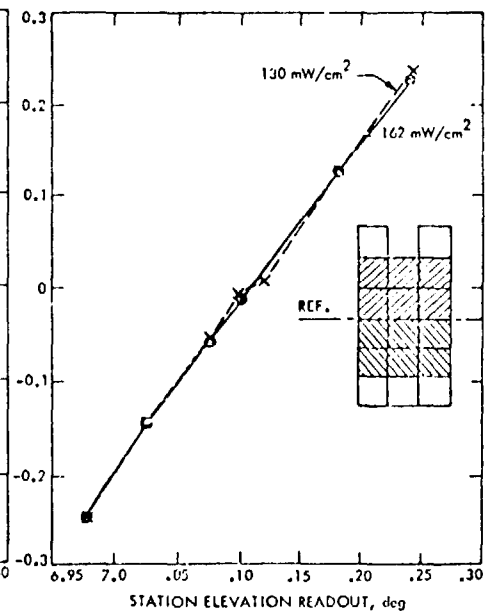
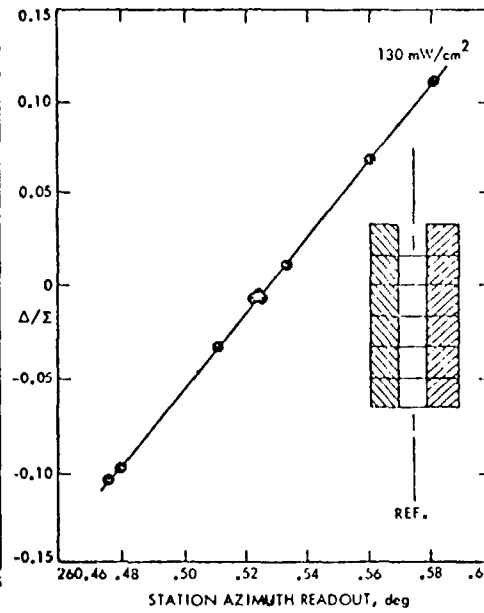
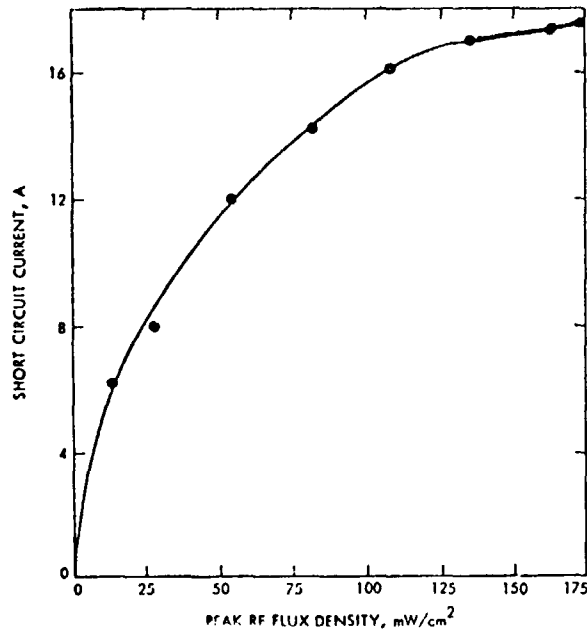
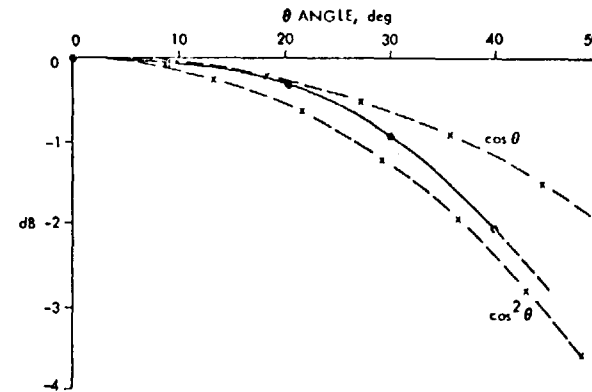
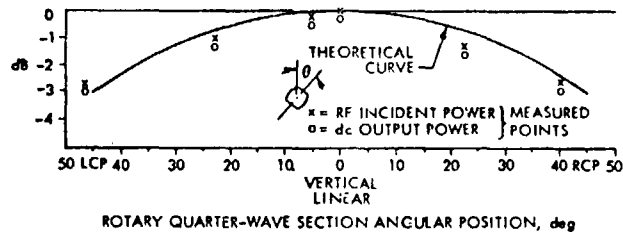
311



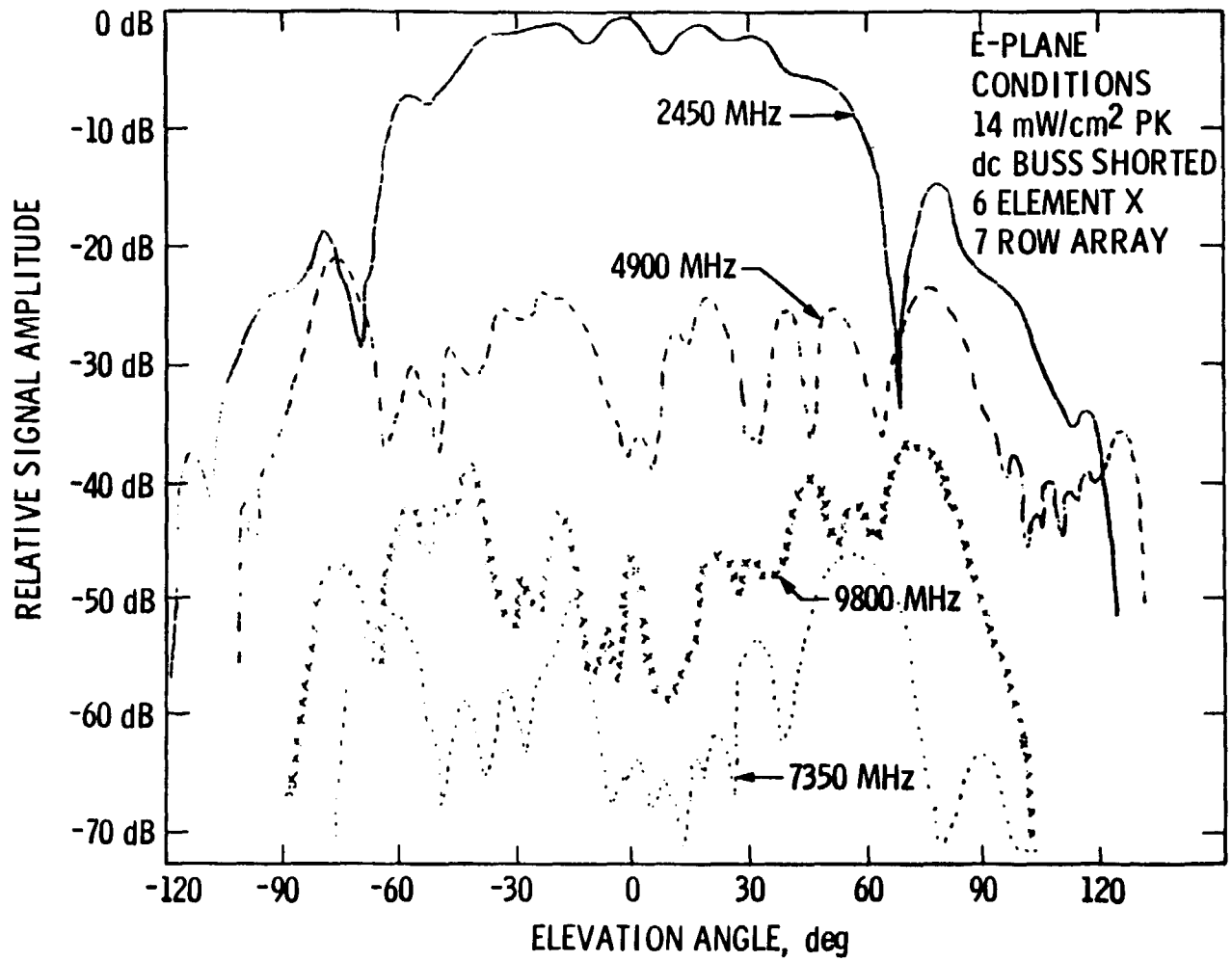
1-20-76 RMD

MICROWAVE RECEPTION-CONVERSION ARRAY PERFORMANCE II

312

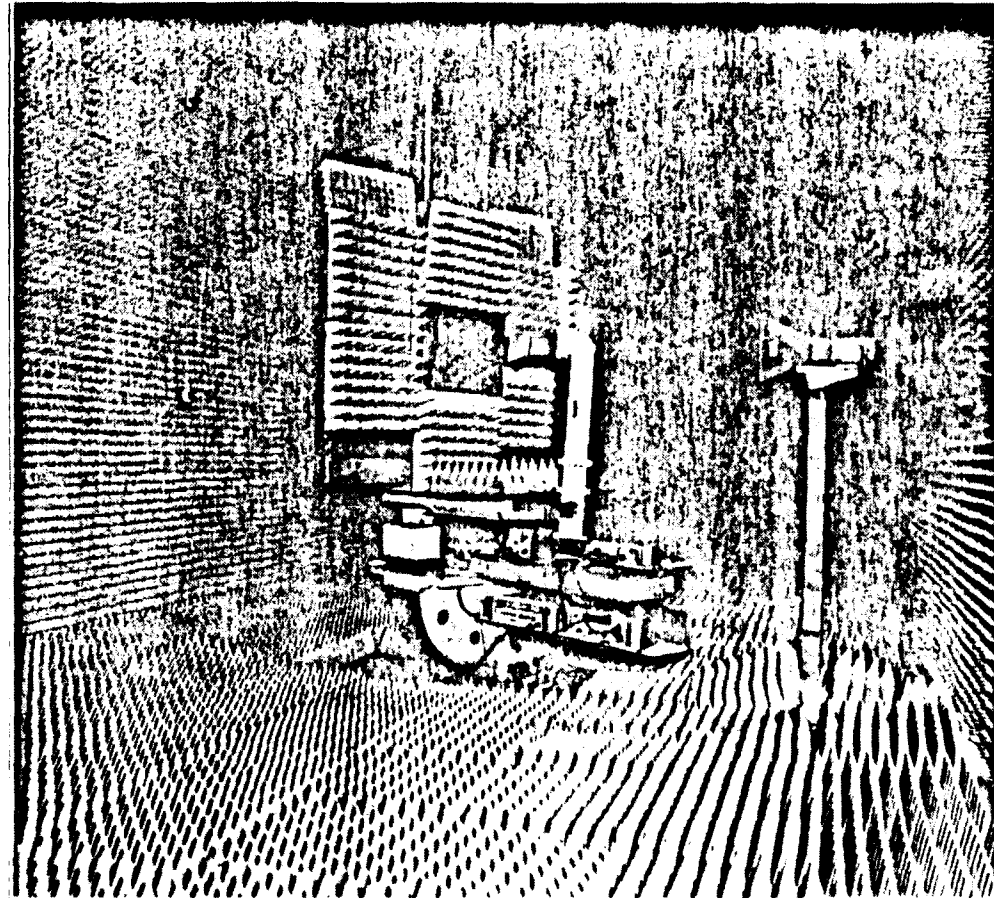


BEAMED RF POWER TECHNOLOGY RECTENNA RESCATTER AND EMISSIONS



BEAMED RF POWER TECHNOLOGY

RECTENNA SUBARRAY FUNDAMENTAL SCATTER & HARMONIC EMISSION RADIATION PATTERNS



SPS ASSESSMENT REVIEW

BEAMED RF POWER TECHNOLOGY

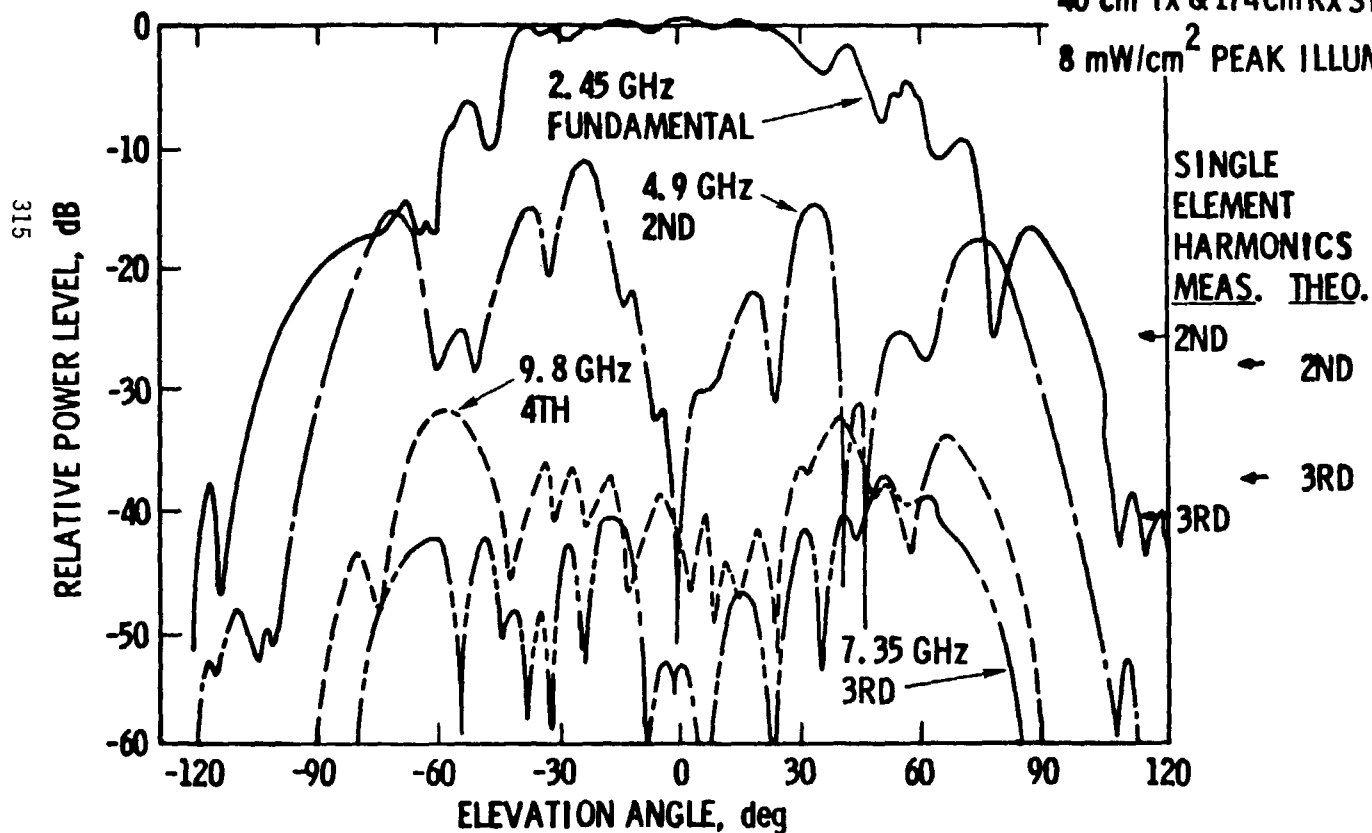
RECTENNA RESCATTER AND EMISSIONS

E-PLANE CONDITIONS

$R_L = 15 \Omega$ /ROW 6 x 7 SUBARRAY

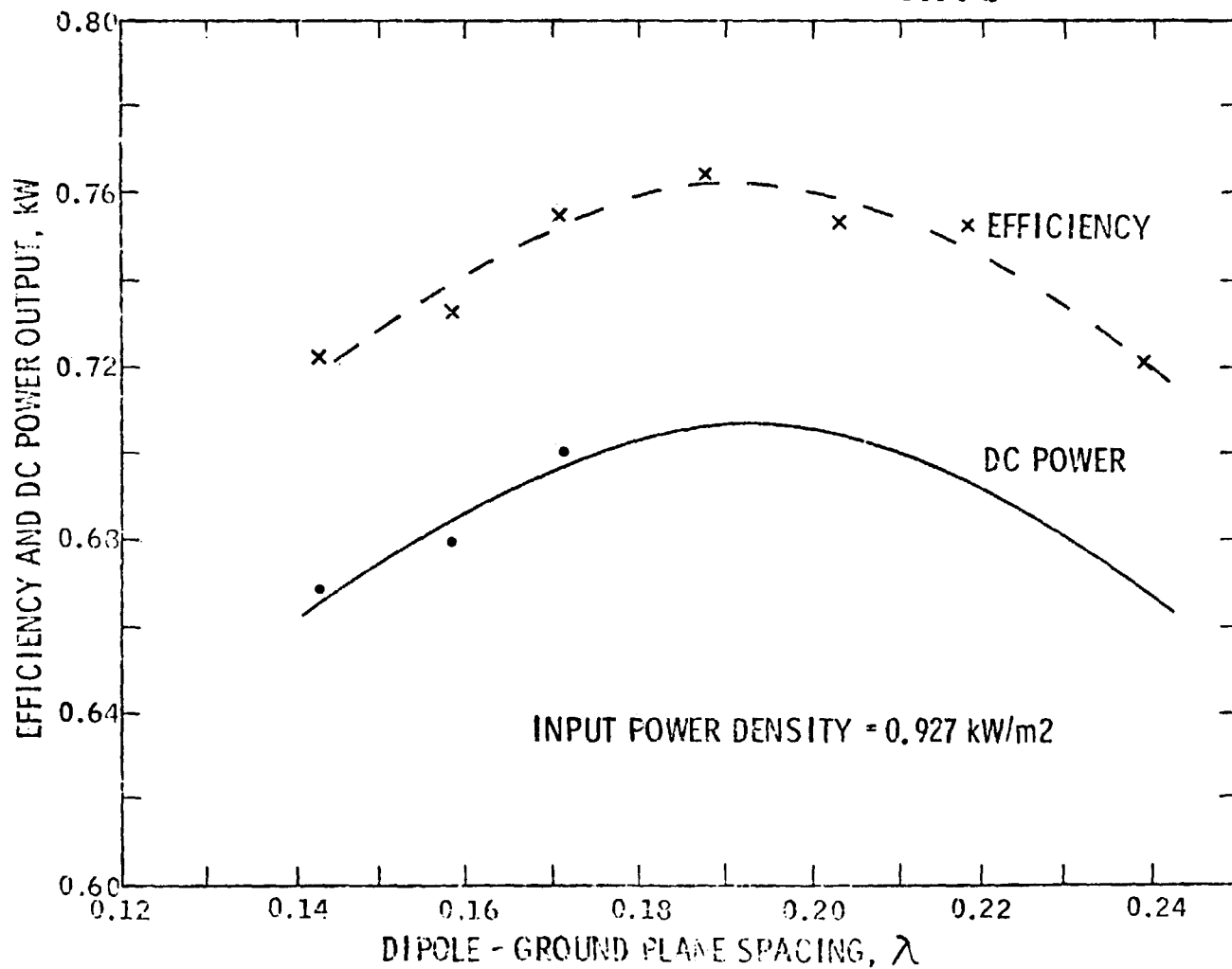
40 cm Tx & 174 cm Rx SPACING

8 mW/cm² PEAK ILLUMINATION



POWER OUTPUT AND EFFICIENCY VS GROUND PLANE SPACING

316



CONCLUSIONS PRESENTED AT THE RECTENNA SESSION

1. Concept - The rectenna concept (individual antenna elements feeding directly into a rectifying circuit) has been shown by analysis and research to be the most technically effective and economically feasible RF-to-DC power converter for providing electrical power.
2. Harmonic Suppression - RF filtering will be required for harmonic suppression in the rectenna.
3. Higher Gain Antenna Elements - In areas of low power density higher gain antenna elements can increase conversion efficiency and reduce the parts count.
4. Collection Techniques - Analysis of rectenna collection techniques indicates that parallel and series combining inefficiencies are nearly identical.
5. Power Combining - It is preferable, from the standpoint of combining inefficiencies, to combine rectenna power in concentric rings rather than in continuous rows.
6. Demonstration - High power output at a long range with high combined collection/conversion efficiency has been demonstrated with a rectenna design that is tolerant to angle of incidence, temperature, polarization, flux density levels and load resistance magnitude changes.

System Definition studies have integrated microwave system requirements into a typical rectenna array. The conclusions resulting from these studies and the characteristics of a typical array are discussed below.

1. Rectenna Configuration
 - a. The RF collecting array consists of a group of serrated flat panel subarrays of vertically polarized half-wave dipoles ($\sim 111/m^2$), tilted with respect to the earth's surface so as to be perpendicular to the incoming RF beam. (Total area perpendicular to the beam of 78.5 km^2).
 - b. An 80% optically transparent, steel mesh with less than 1% RF leakage is employed as the ground plane.
2. Incident RF Energy
 - a. The normal incident RF energy is gaussian distributed across the rectenna with a peak intensity of 23 mW/cm^2 .
 - b. Studies to date have only considered rectenna configurations which receive RF energy from one SPS satellite.
3. Rectenna Area - The rectenna collecting area is to extend to the normal incident flux density level of 1 mW/cm^2 . (Approximately 5 km radius E-W, variable with latitude in N-S direction) and the rectenna is to be fenced to exclude transient intrusion.

4. Type of Rectifiers - Half wave Schottky barrier Ga-As diodes are preferred as RF-to-DC rectifiers.
5. Efficiencies - The collection efficiency is projected to be 88% and the conversion efficiency is 89%.
6. Costs -
 - a. The currently estimated rectenna cost is a large part of the total SPS program cost (approximately 20%).
 - b. The rectifier is the largest cost element in the rectenna.

1

REMAINING ISSUES - PRESENTED AT THE RECTENNA SESSION

1. Reradiation characteristics
 - a. Nominal and failure modes
 - b. Fundamental and harmonics
 - c. Cost/efficiency tradeoff to reduce reradiation
2. Manufacturability vs. cost
 - a. Mass manufacturing techniques of rectenna
 - b. Component mass manufacturing costs (diode)
3. Rectenna array efficiency (over varying power density levels)
 - a. Match dipole/diode combination (different diodes)
 - b. Parallel dipoles into same diode
 - c. Higher gain antenna element (Yagi-Uda, slotted wave guide)
4. RF measurement accuracies
 - a. High efficiency measurements
 - b. Statistical analysis - desirable/feasible
5. Environmental protection vs. loss in efficiency
 - a. Hail, wind, lightning, rain, sand
6. Diffraction at top edge of rectenna panels
 - a. Passive vs. active techniques to resolve
 - b. Terrain following rectenna vs. serrated rectenna vs. cost

SECTION VII

SOLID STATE CONFIGURATIONS SESSION

Chairman: Woolsey Finnell
NASA, Marshall Space Flight Center

MICROWAVE POWER
TRANSMISSION SYSTEM
WORKSHOP

SESSION ON SOLID STATE

BY WOOLSEY FINNELL/MARSHALL SPACE FLIGHT CENTER

INTRODUCTION

"Why should we study a solid state SPS" is a valid question and one that we do not have a complete system answer for at this time. The first chart is an attempt to list some of the reasons a solid state SPS should be investigated. Solid state is no magical solution to SPS designs but it does attack three very important aspects of SPS - the potential for low cost through mass manufacturing techniques that are well established, reliability, and essentially maintenance free operation. Solid state was not considered in the original Raytheon study for LRC in 1975 on the microwave system. Low efficiency and power levels of a kilowatt or larger made them unattractive for SPS. NASA decided to investigate the possibility of a solid state design that incorporated a much lower device power requirement. A design was developed requiring 120W devices or amplifiers which appeared more reasonable but still very difficult for S-band.

The next step was to determine if solid state devices could potentially be highly efficient. An analytical approach was selected to investigate this potential. Dr. Roulston of Waterloo University performed the analysis and indicated there were no fundamental limitations on the efficiency of solid state devices. Further study by the systems contractors and NASA has produced two concepts that will be given a more detailed systems analysis. These concepts produced amplifier power requirements of 5 to 30 watts. One concept simply substituted a solid state

antenna for the reference Klystron antenna. The other concept produced an entirely new SPS conceptual design and was called a solar cell solid state sandwich design. Both of these designs will be discussed by other summaries in this section. However, it should be noted that all solid state designs have thus far been characterized by larger antennas, smaller rectennas, and less delivered power than the SPS reference concept. There is no solid state reference concept at present because of the systems analysis on solid state concepts is not complete. Much data has been generated by numerous sources on the solid state concepts. The following summaries in this section are just representative of the study effort. Thus far Rockwell, Boeing, Raytheon and RCA have been directly involved in the solid state studies. The last two charts list the preliminary conclusions and issues related to this solid state study effort. Solid state continues to be a viable alternative to the reference Klystron concept and is included in the six year planning document (Ground Based Exploratory Development - GBED) now being finalized.

MSFC SOLID STATE ACTIVITY

WHY SOLID STATE

- o HIGHER RELIABILITY THAN TUBES
(- 10^6 HOURS VS. 10^4 HOURS)
- o TECHNOLOGY BASE
- o POTENTIAL FOR LOW COST
- o SYSTEM COSTS OPTIMIZES AT LOWER POWER OUTPUT
AT UTILITIES (1.0-1.5 GW)
- o POTENTIAL FOR REDUCING FRONT END COST
- o MORE EASILY ADAPTABLE TO FLIGHT/GROUND TEST
- o START-UP - SHUT-DOWN

SOLID STATE CONCLUSIONS

1. Solid state SPS concepts have not had the same depth of systems definition as the reference concept; however, preliminary results indicate the following.
 - a. The system sizing parameters optimize such that lower power is delivered to the utility grid.
 - b. The transmit antenna is larger primarily because of the thermal limitations.
 - c. The rectenna land requirement is smaller.
 - d. Weight per delivered kilowatt is projected to be more.
 - e. Maintenance projections are better because of the higher reliability.
2. Type of Power Amplifier - Based on studies to date, the GaAs FET is the preferred solid state power amplifier.
3. Antenna Unit Costs - Solid state antennas will have high parts count similar to the solar array, and therefore unit costs are a critical item.
4. Mitigating Designs - Conceptual designs have to some degree mitigated the issues of thermal and low voltage power distribution.
5. Items of Concern - Techniques of phase distribution, (possibly to more points on the array), and power distribution (on the end mounted configuration more DC-to-DC converters are required) are major items of concern in the solid state concept.
6. Technology - Associated technology development is more likely for solid state due to the advancing technology base.
7. Continued Investigation - Based on current findings, continued investigation of solid state concepts and issues is warranted.

SOLID STATE ISSUES

- Efficiency
- Operating Temperature
- Low Voltage Distribution
- Harmonic Noise Suppression
- Power Combining
- Subarray Size
- Monolithic Technology
- Life Time
- Mutual Coupling
- Amplifier gain
- Input to Output Isolation
- Charge Particle and **UV** Radiation Effects

MODIFIED REFERENCE SPS WITH SOLID STATE TRANSMITTING ANTENNA

G. R. Woodcock, B. R. Sperber, Boeing Aerospace Co.

1.0 INTRODUCTION

The motivations for considering solid state microwave power amplifiers for the solar power satellite transmitting antenna have been the possibilities of greatly increased system reliability due to elimination of electron tube cathodes, a lower mass per unit power and transmitting array area due to the high power densities obtainable in semiconductors (the active region of a power GaAs FET has a power density exceeding 10^{15}W m^{-3} !), and, probably, cost savings due to development of small hardware items that can be handled by individuals instead of organizations.

In order to provide a fair assessment of where we stand today with regard to solid state SPS technology, the design described here is close to that of the NASA/DOE reference and is implemented using today's solid state technology with only a small "push." The small push is raising the efficiency of DC-RF conversion from the .68 obtained by RCA in 1975 to somewhat over .8 of the solid state SPS. This is generally considered feasible by semiconductor industry representatives.

Other solid state SPS configurations can yield somewhat better performance. However, these generally do not provide as fair a vehicle for comparison with the reference and usually also incorporate somewhat more advanced technologies.

2.0 SOLID STATE MICROWAVE POWER AMPLIFIER TECHNOLOGY

Currently a wide variety of solid state devices suitable for use as microwave amplifiers exist. These include bipolar and field effect transistors, many types of two-terminal devices (tunnel, Gunn, IMPATT, BARITT and TRAPATT diodes) and electron bombarded semiconductors (EBS). (EBS have been included as being solid state since the electron beam only supplies a small control current, with the bulk of the supply current staying in the semiconductor.) For those active devices with over two terminals, there are several classes of circuit configurations that the active devices may be used in. Finally, there is a growing number of commonly used solid state materials out of which components may be fabricated, using several types of process at each step of the fabrication.

State of the art power-added efficiency, gain and single device power as a function of frequency for various types of CW microwave output solid state devices are shown on Figures 1 through 3. As technology evolves the curves will move towards the upper right-hand corners of the graphs.

Given the results of Figure 1, it would appear that there is no hope of achieving efficient solid state DC-microwave conversion in the near future. All the two terminal devices have efficiencies less than .36, which is so low as to make their use for SPS impractical. Most of the three terminal devices are not much better. However, in the case of three-terminal devices, the classes of amplifiers presently used (Classes A and B for GaAs FETs and Class C for bipolar transistor amplifiers) inherently limit their efficiency. Other classes of amplifiers, summarized on Figure 4, can have efficiencies approaching unity.

In fact, to achieve the desired efficiencies of .8 or greater requires that the devices be used in "switched mode" types of amplifiers, which attain high efficiency by minimizing the I-V product time integral over the operating cycle. This generally requires device switching times about a factor of ten less than the RF period. Experimental amplifiers with efficiencies of over 90% have been built at frequencies above 100 MHz. NASA-sponsored microwave amplifier studies have recently been initiated to determine the feasibility of high efficiency at microwave frequencies.

Because of the many high frequency components in the waveforms characteristic of fast switches, efficient switching amplification devices must have large bandwidths. This leads to different device noise properties than those at the narrowband SPS reference system klystron tubes. While the switching amplifiers do have frequency selective output circuits that transform the switched waveform into a sine wave, these will not be nearly as selective as a 5-cavity klystron. However, the solid state design will benefit due to its small module size giving a larger ground footprint than that of the larger klystron module.

Achieved device gains vs frequency are shown on Figure 2. There is a striking difference between small-signal and power gain for FETs. At the SPS frequency of 2.5 GHz bipolars have about 8 db gain while GaAs FETs yield around 10 db. In general, GaAs FETs have several db more gain than bipolars throughout the spectrum. As for the other devices, IMPATTs can have gains of over 20 db and electron beam semiconductors are projected to yield about 20 db. The low gain of Static Induction Transistors (SITs) at 1 GHz eliminates them from consideration at present, although they appear to have great potential for further development due to their high power bandwidth product.

The power per device is an important SPS parameter since the number of devices which can be efficiently combined in a module is limited by circuit losses and the power per module determines the RF power density per unit transmitting array area. The single device power chart (Figure 3) shows that silicon bipolar transistors, GaAs FETs and multi-mesa IMPATTs can all handle powers above 10 watts, which is an adequate power level for SPS application. Of the devices considered here, only E-beam semiconductor devices are capable of generating a power level of 100 watts per device which would be adequate for one device per radiating element. For the other devices, power combining will be necessary.

The fundamental failure modes in semiconductor devices are wearout failure modes that tend to be concentrated at surfaces, both internal and exposed, and are generally electrochemical in origin. In the case of the internal surfaces, transport of species to and away from interfaces eventually degrades contacts. In the case of external surfaces, impurities can come in from outside to form compounds and high electric fields can cause breakdown.

EBS cathodes presently have an expected lifetime of 2×10^5 hours, over an order of magnitude less than that required for a 30-year satellite, so they appear unsuitable. The two remaining solid state amplifier candidates are GaAs FETs and Si bipolar transistors. Si bipolar lifetimes are limited by electromigration of emitter finger metallizations due to localized high current densities. This gives relatively sudden and complete hard (open or short circuit) failures, whereas GaAs FETs seem to suffer from contact degradation which decreases performance gradually.

Of the three terminal devices, GaAs Field Effect Transistors (FET's) and Si-bipolar transistors provide approximately equal power capability at 2.45 GHz and appear potentially feasible for SPS use. GaAs FET's were selected as the preferred DC-RF conversion devices because they have higher gain than silicon bipolars, higher power added efficiencies, roughly equal power capabilities at 2.5 GHz and lower device metallization current densities leading to better expected reliabilities. GaAS FET's for SPS application could be fabricated separately and mounted in hybrid fashion or combined with other components on larger GaAS chips in integrated circuits. The latter alternative is preferred because of its significantly lower costs in mass production, although it does entail somewhat more development. For conservatism and in consideration of the fact that efficient "switched mode" amplifiers require gain at frequencies higher than the fundamental, the maximum single device powers in the solid state baseline design satellite were chosen to be 7.5 watts. For devices like this, a reasonable operating voltage is 15 volts.

A current small signal GaAS FET lifetime versus temperature curve is shown on Figure 5. There is currently no lifetime data on power GaAS FET's in the literature. When it appears, it is likely to be somewhat worse than Figure 5, but Figure 5 probably represents lifetimes achievable with development of the relatively new GaAs FET technology. It should be noted that solid state devices fail with log-normal statistics. Since the SPS failure criterion is loss of 2% the transmitting array with no maintenance, the mean time to failure required for the device is about a factor of ten more than the SPS life. Thus the average junction temperature for SPS GaAS FET's should be no higher than 140°C.

Figure 6 shows current and projected GaAS FET costs with an estimated 70% production rate improvement curve (i.e., units produced at the rate of $2n$ per year cost 70% as much as units produced at the rate of n per year). For the anticipated projected rates, the cost per unit power for GaAS FET's are nearly the same as the projected cost per unit power for klystrons. In practice, integrated circuits with several stages of driver amplifiers and other circuitry will be incorporated with the power amplifier. Since production costs are roughly equivalent to chip size and the output FET is anticipated to use approximately 70% of the total semiconductor area, the above cost estimates are adequate to first order.

3.0 SOLID STATE ANTENNA MODULE INTEGRATION

Cost effective integration of the low power, low voltage solid-state devices into mass producible antenna array elements represents the prime challenge in solid-state microwave power transmitter design. The "natural" array element size of about a wavelength squared and radiative cooling considerations for the peak microwave density areas at the transmitting array center yield 11 devices per λ^2 at an anticipated 5.5 kW m^{-2} radiated microwave power per unit area. For central array modules of the modified reference solid-state SPS both a small module size and combining of several devices were used to get the 4-FET $.6\lambda \times .6\lambda$ microstrip cavity combining module shown in Figure 7.

To avoid the power combining losses associated with circuit hybrids, the power from 4 solid-state amplifiers is combined by direct coupling of each amplifier's output to the radiating antenna structure. The resulting savings in transmitter efficiency range from 4% to 10%, depending upon the configurations being compared. The selected power-combining antenna consists of a printed (metallized) microstrip circuit on a ceramic type dielectric substrate which is backed by a shallow lightweight aluminum cavity which sums the power of four microwave sources. The antenna behaves like two half wavelength slot-line antennas coupled together via a common cavity structure. Feedback is taken from sampling probes in the module

cavity and used to correct for amplifier phase errors. This insures that the insertion phase of each module is identical even though the power amplifiers are fabricated to relatively loose (low cost) insertion phase requirements.

The modules are fabricated by starting with metallized (microstrip) 25 mil thick alumina dielectric cards which are attached to a 7.5 mil thick aluminum sheet metal carrier. A 7.5 mil thick stamped aluminum back plate is then attached, covering the substrate and all circuit components. This back cover defines the antenna cavity as well as shielding the otherwise exposed electronic components on the substrate. The high thermal conductivity of the aluminum components and of the alumina substrate allows the module's waste heat to spread to all surfaces as evenly as possible.

For the lower power density areas of the array an alternate dipole radiator module configuration is proposed. (See Figure 8.) This module design is approximately a third the mass per unit area of the 4-FET cavity radiator module because it has nearly no ceramic and significantly less metallization.

4.0 ANTENNA INTEGRATION

Variations of the basic cavity radiator and dipole radiator modules have been used to define a 1.42 km diameter transmitting antenna with a 9.54 db 10-step Gaussian taper similar to that of the reference SPS. Since its peak transmitted power per unit area is $\frac{1}{4}$ that of the reference satellite, its grid output power is half that of the reference, or 2.5 Gw.

Antenna quantization scheme specifications are summarized on Figure 9. There are seven basic module types of varying mass. As the 4-FET cavity radiator and 2-FET dipole module powers are reduced the module masses may also be reduced by removing superfluous metal not required for lateral thermal conduction. The 2-FET cavity radiator can also take advantage of reduced dielectric mass. No claim is made that these designs are optimized; they represent hopefully conservative estimates for likely module configurations.

To reduce I^2R power bussing losses the 15 volt modules must be connected in a series-parallel arrangement. The connection hierarchy selected for the $(.6\lambda \text{ by } .6\lambda)$ cavity radiator modules has four modules in parallel to form units called rows. Twelve rows are connected in series to form strings. Three strings in parallel make up a panel, which is the least replaceable unit. One hundred forty-four panels in a 12×12 series-parallel matrix form subarrays of the same size $(10m \times 10m)$ as in the current baseline, with a subarray voltage drop of 2.16 kv. Two subarrays are connected in series to give a 4.32 kv distribution voltage.

In the case of subarrays using the slightly larger $(.6\lambda \times .8\lambda)$ dipole moduler the hierachy is the same except that the rows only have three modules in parallel.

A reliability assessment of the described cavity radiator module subarray hierarchy as a function of probability of amplifier failure, Q , is summarized in Figure 10. In case only one amplifier failure per row is permitted, string failures will cause 2% rf power reduction (with 50% probability) in 22 years for an amplifier MTBF of 3.5×10^6 hours. The random failures at this time cause an additional 0.8% of amplifiers to have failed so that the total rf power reduction at this time is 2.8%. If two amplifier failures per row are allowed, the power loss due to string failures of 2% and random amplifier failures of 3.2% together

result in a subarray power loss of 5.2% after 63 years. These results indicate that, for the SPS requirement of less than 2% rf converter failures in a 30 year period, the objectives of maintenance-free operation are achievable. This provides encouragement for further effort to address the issues of series-parallelizing such large strings.

An additional reliability feature beyond those considered in the assessment of all the module designs for string protection is the use of an external high temperature resistor which is shunted in to dissipate the nominal module power when the power amplifier in a module becomes open-circuited. By making the resistors small filaments a visual indication of failure is provided.

Although the failure reliability aspects of the above series-parallel configuration appear workable, other valid questions remain. The modules each have separate inputs that must be kept from coupling to neighboring outputs over the power supply lines. This is believed feasible but has not yet been experimentally demonstrated. Also, in a real system startup and shutdown transients are experienced. There must be kept from "rattling around" in the series-parallel matrix and selectively blowing out modules. Protection against these transients is believed assured if all the modules present similar impedances to the power line and have some over-voltage protection.

5.0 SATELLITE CONFIGURATION

A trade study done to decide on the preferred power distribution system to the 4.32 kv subarray pairs from the solar array compared directly bussed DC, high voltage AC and high voltage DC with DC-DC converters. The results are shown on Figure 11 in the form of conductor and power loss make-up array mass as a function of conductor temperature. Direct DC won out despite a low power bussing efficiency of .73. However, it should be noted that should power converter technology improvements result in 25% power converter mass reductions, high voltage DC with DC-DC converters would be the preferred option.

Satellite efficiency and sizing, done in a fashion similar to the NASA/DOE reference SPS design, clearly shows the impact of the buss losses on Figure 12.

The completed 2.5 GW modified reference SPS configuration is shown on Figure 13. The technology of the non-microwave subsystems is the same as the reference except for elimination of the antenna yoke by using linear actuators between the antenna edge and the rotary platform and the use of a pentahedral main satellite bay structure. Both changes reduce satellite mass somewhat.

Figure 14 gives a mass and cost summary. Total mass per unit transmitted power is up 30% from the reference because of DC bussing and DC-microwave conversion inefficiencies, with costs tracking. A second pass through the design, concentrating on increasing power bussing efficiency to achieve mass reductions, might reduce this difference but it is unlikely to erase it.

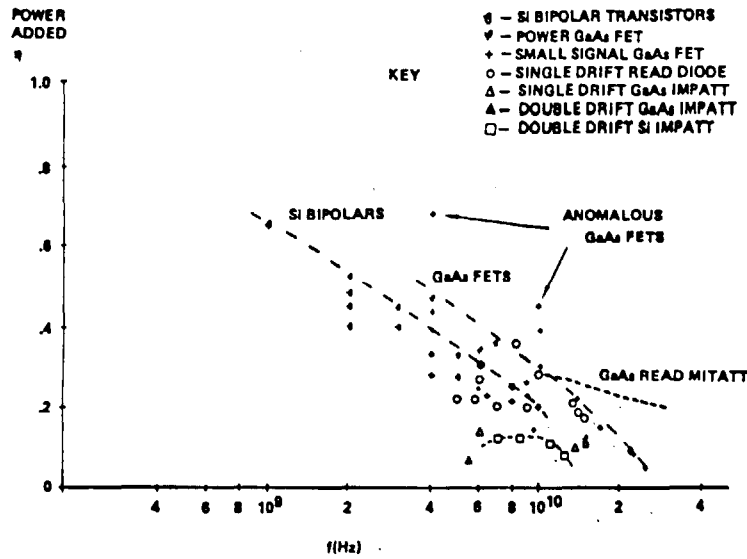


Figure 1. CW Solid State Device Efficiency vs Frequency—1978

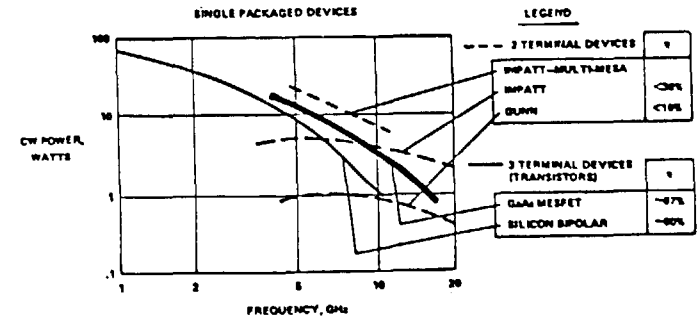


Figure 3. Solid State CW Power vs Frequency—1978

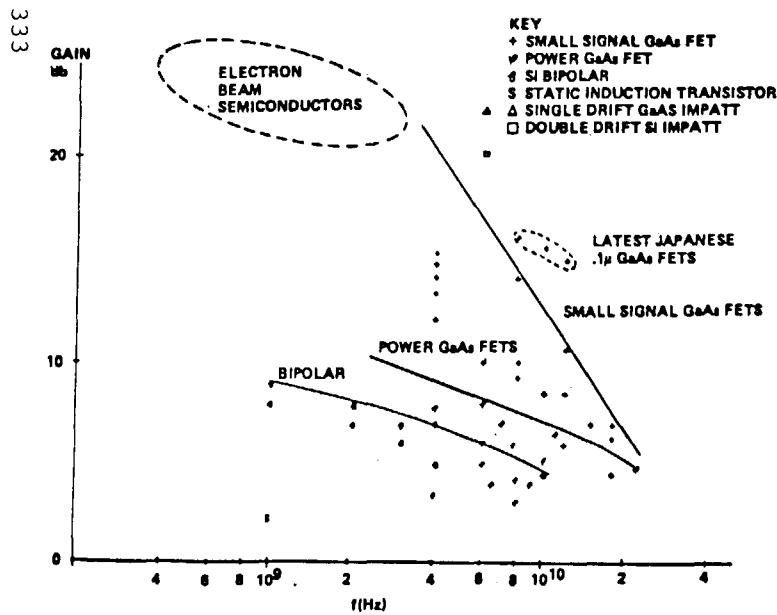


Figure 2. Solid State Device Gain vs Frequency—1978

Figure 4. Characteristics of Various Amplifier Classes

Amplifier Class	Maximum Power-added Efficiency for Sine Wave Output	Typical Efficiency Values Achieved	@ Frequency	Duty Cycle at Maximum Efficiency	Active Device Saturated ?	Active Device Cut Off ?
A	.5	.3	@ 1 GHz	1.0	No	No
B	.783	.5	@ 1 GHz	.5	No	Yes
C (Unsaturated)	.896	.6	@ 2.5 GHz	.3	No	Yes
Switched Mode Amplifiers	D	1.0	@ 10 MHz	.5	Yes	Yes
	E	1.0	@ 100 MHz	.5	Yes	Yes
	F	1.0	@ 10 MHz	.5	Yes	Yes
	S	1.0	@ 100 KHz	Variable >> 1	Yes	Yes
Multivoltage	1.0	.8	@ 10 MHz	Variable	Yes	Yes
			@ 100 KHz	Variable	Yes	Yes

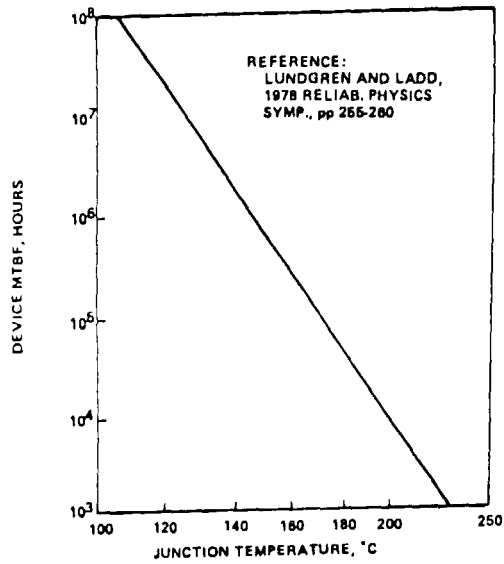


Figure 5. Small Signal GaAs FET Lifetime vs Junction Temperature

334

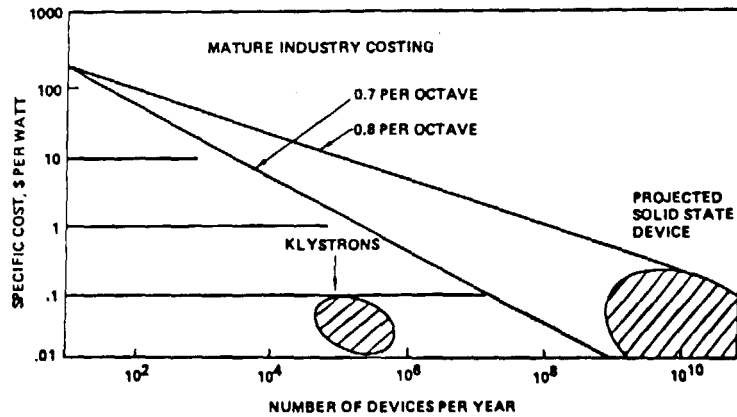


Figure 6. Projected GaAs FET Costs

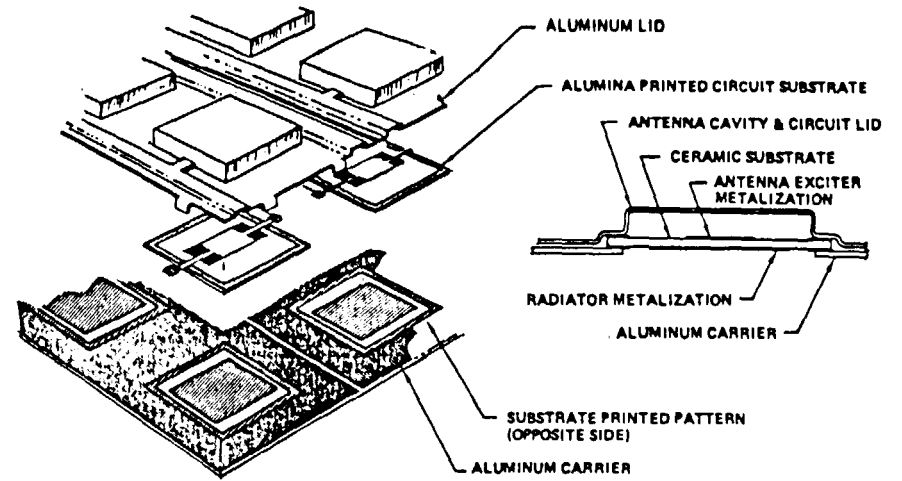


Figure 7. Solid State Combiner-Radiator Module

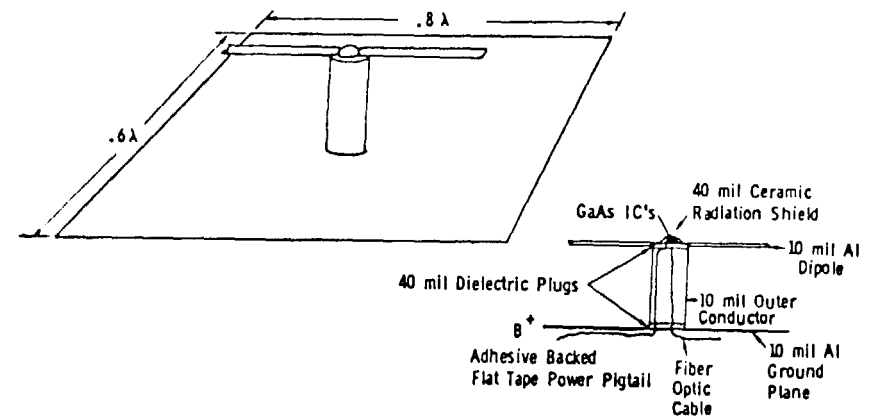


Figure 8. Solid State Dipole Radiator Module

STEP	OUTSIDE RADIUS (m)	STEP AREA (m ²)	NUMBER OF SUBARRAYS	MODULE TYPE	MODULE POWER (W)	(P/A) _{RF} (Kw m ⁻²)	(M/P) _{RF} (kg km ⁻¹)	STEP MODULE MASS (T)	NO. FETS (M)
1	124.8	48,970	456	High Power 4-FET, Cavity Radiator (4.06 kgm ⁻²)	28.7	5.50	.742	200	37.82
2	249.6	146,830	1,360	"	24.0	4.45	.917	600	112.80
3	322.4	130,820	1,208	Reduced Power 4-FET Cavity Radiator (3.58 kgm ⁻²)	19.2	3.56	1.006	468	100.20
4	384.8	138,640	1,280	"	16.0	2.97	1.207	496	108.17
5	457.6	192,680	1,784	2-FET Cavity Radiator (3.06 kgm ⁻²)	12.8	2.37	1.289	590	73.99
6	520.0	191,680	1,776	2 FET Dipole (1.47 kgm ⁻²)	12.8	1.78	.826	582	55.24
7	561.6	141,390	1,312	"	9.6	1.33	1.101	208	40.81
8	582.4	74,795	696	"	8.5	1.18	1.244	110	21.65
9	644.8	238,950	2,208	1 FET Dipole (1.47 kg m ⁻²)	6.4	.89	1.652	351	34.34
10	707.2	264,880	2,448	"	4.3	.59	2.476	389	38.07
TOTALS			14,528					3,694	621.09

Figure 9. Solid State Transmitting Antenna Quantization

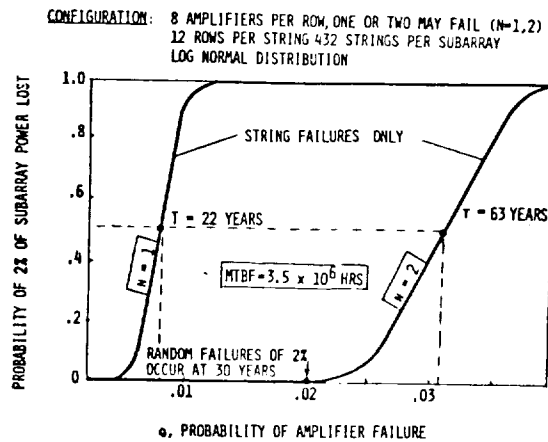


Figure 10. Solid State SPS Array Center Subarray Reliability

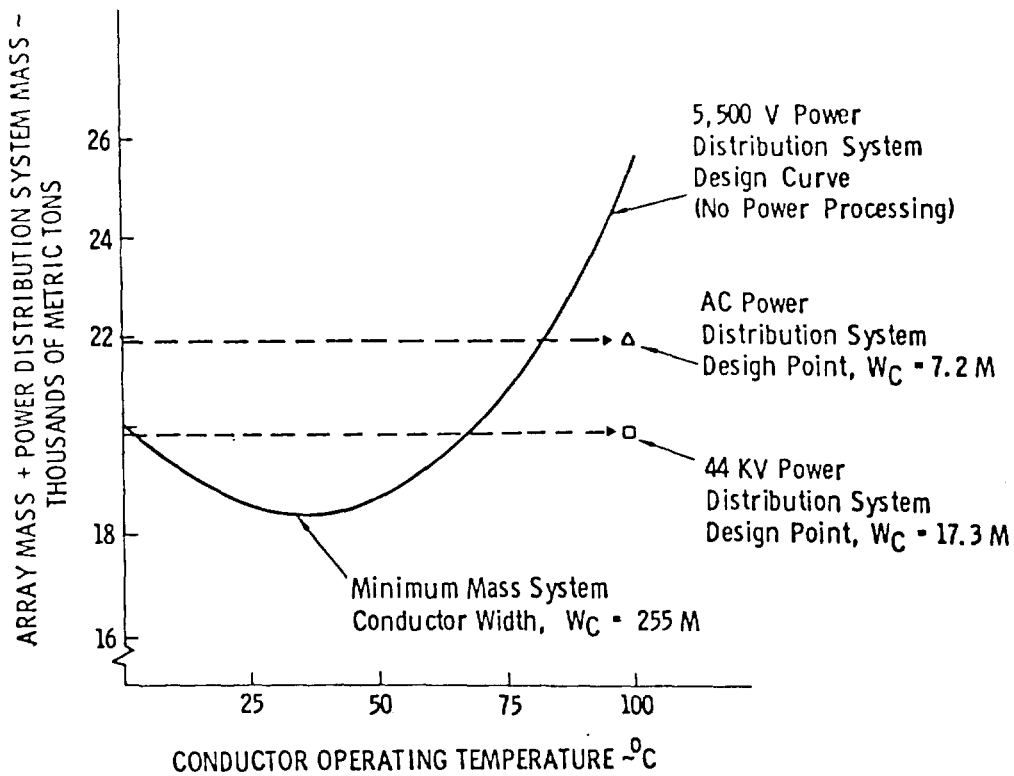


Figure 11. Power Distribution System Analysis

<u>ITEM</u>	<u>EFFICIENCY</u>	<u>MEGAWATTS</u>	
Array Mismatch			
Array Mismatch	.965	6050	Ideal Array Output
Main Bus I ² R	.729	5838	
Antenna Distr	.97	4256	Total Antenna Input
DC-RF Conversion	.8	4128	
Waveguide I ² R	N/A	3303	Total RF Radiated Power
Ideal Beam	.965	3303	
Inter-Subarray Losses	.976	3187	
Intra-Subarray Losses	N/A	3110	
Atmosphere Loss	.98	3110	
Intercept	.95	3048	
Rectenna RF-DC	.89	2896	Incident on Rectenna
Grid Interface	.97	2577	
	<u>.413</u>	<u>2500</u>	Net to Grid

TOTAL ARRAY OUTPUT 6050 MW
 TOTAL SOLAR ARRAY AREA = 33.8 km²

Figure 12. Solid State SPS Efficiency and Sizing

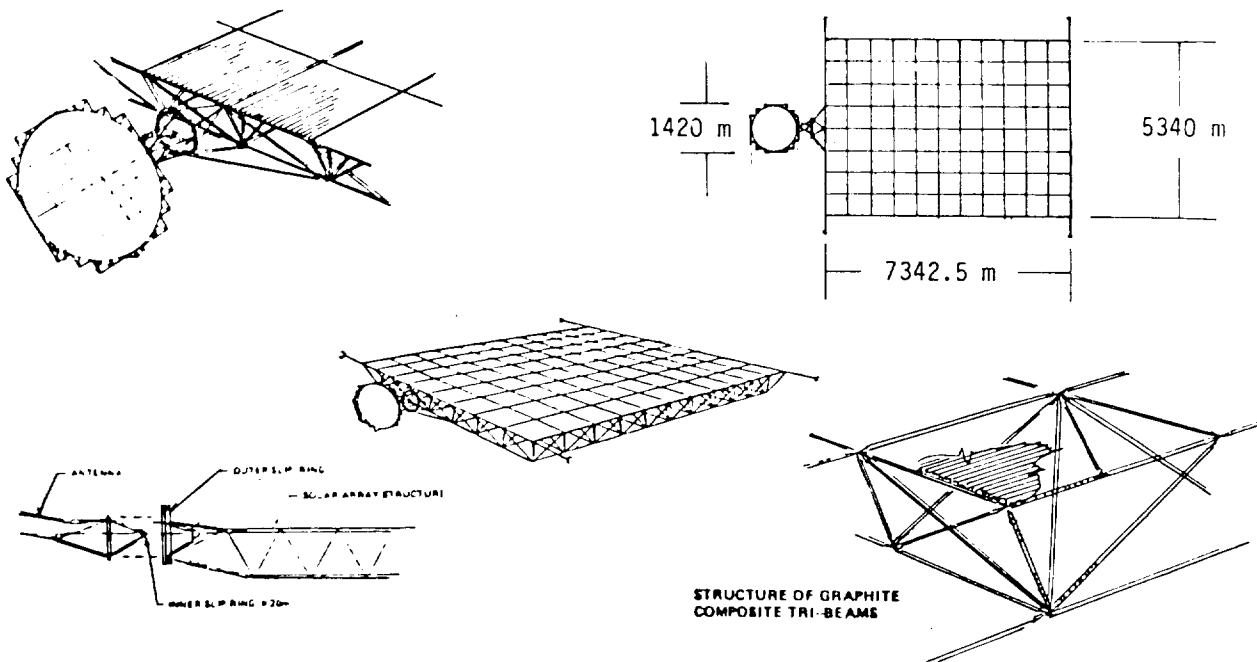


Figure 13. 2.5 Gw Solid State SPS Configuration

	<u>MASS (MT)</u>	<u>ESTIMATING BASIS</u>	<u>(COST (\$M))</u>
1.1 SPS	<u>35,204</u>		<u>4,541</u>
1.1.1 ENERGY CONVERSION	<u>22,087</u>		<u>2,350</u>
1.1.1.1 STRUCTURE	<u>2,851</u>	Detailed Estimate	275
1.1.1.2 CONCENTRATORS	(0)	Not Required	(0)
1.1.1.3 SOLAR BLANKETS	14,409	Scaled from Reference	1,355
1.1.1.4 POWER DISTRIB.	4,400	Detailed Estimate	530
1.1.1.5 THERMAL CONTROL	(0)	Allocated to Subsystems	(0)
1.1.1.6 MAINTENANCE	427	Scaled from Reference	190
1.1.2 POWER TRANSMISSION	<u>6,365</u>		<u>1,134.5</u>
1.1.2.1 STRUCTURE	460	Scaled from Reference	38
1.1.2.2 TRANSMITTER	4,480	Detailed Estimate	888.5
SUBARRAYS			
1.1.2.3 POWER DISTR. & COND.	1,262	Scaled from 1.1.1.4	124
1.1.2.4 PHASE DISTR.	25	Scaled from Reference	51
1.1.2.5 MAINTENANCE	20	Docking Ports Only	20
1.1.2.6 ANTENNA MECH. POINTING	118	Scaled by Mass x Area	13
1.1.3 INFO MGMT & CONTROL	<u>145</u>	Scaled from Ref.	<u>73</u>
1.1.4 ATT. CONT. & STA.KP.	<u>146</u>	Scaled From Ref	<u>110</u>
1.1.5 COMMUNICATIONS	<u>0.2</u>	Same as Ref.	<u>8</u>
1.1.6 INTERFACE	<u>113</u>	Est. Based on Simplification	<u>46.3</u>
1.1.7 GROWTH & CONTINGY.	<u>6,348</u>	Same % as Reference	<u>819</u>

Figure 14. Solid State SPS Mass and Cost Summary

SPS SOLID STATE ANTENNA POWER COMBINER
G. W. Fitzsimmons, Boeing Aerospace Company

1. INTRODUCTION

Solid state dc-rf converters offer potential improvements in reliability, mass and low voltage operation, provided that anticipated efficiencies in excess of 80% can be realized. Field effect transistors offer the greatest potential in the SPS frequency band at 2.45 GHz. To implement this approach it is essential that means be found to sum the power of many relatively low power solid state sources in a low-loss manner, and that means be provided to properly control the phase of the outputs of the large number of solid state sources required.

To avoid the power combining losses associated with circuit hybrids it was proposed that the power from multiple solid state amplifiers be combined by direct coupling of each amplifier's output to the radiating antenna structure. The resulting savings in transmitter efficiency ranges from 4% to 10% depending upon the configurations being compared. The selected power-combining antenna consists of a unique printed (metalized) microstrip circuit on a ceramic type dielectric substrate which is backed by a shallow lightweight aluminum cavity which sums the power of four microwave sources. The antenna behaves like two one-half wavelength slot-line antennas coupled together via their common cavity structure. A significant feature of the antenna configuration selected is that the radiated energy is summed to yield a single radiated output phase which represents the average insertion phase of the four power amplifiers. This energy may be sampled and, by comparison with the input signal, one can phase error correct to maintain the insertion phase of all solid state power combining modules at exactly the same value. This insures that the insertion phase of each SPS power combining antenna module is identical even though the power amplifiers are fabricated to relatively loose (low cost) insertion phase requirements.

The concept, illustrated in Figure 1, shows two solid state power amplifier modules with two outputs each at 5 watts delivering power to the antenna. The power amplifiers derive their input from an integrated circuit which performs the function of phase error correction so that each module has the same insertion phase. The phase error correction circuit employs two probes to sample the phase of the of the radiated power. This phase is then compared with that at the module input. A ceramic substrate is proposed to dissipate the heat of the power amplifiers via radiation. The high thermal conductivity of the ceramic substrate and of the aluminum cavity and ground plane will spread the heat so that all surfaces will participate in the cooling process.

The material that follows describes an initial program to verify the suitability of this concept for SPS. An appropriate microstrip antenna is being developed which will be evaluated when driven from four solid state power amplifiers.

2. EXPERIMENTAL VERIFICATION PROGRAM

The objective of the program is to demonstrate the suitability of a 2.45 GHz power combining microstrip slot-line antenna, when fed by four solid state

amplifiers, to the needs of a solar power satellite. The program entails the design and fabrication of a four feed microstrip antenna and a stripline antenna phasing network which will be integrated with four transistor amplifiers to demonstrate that the total solid state module (amplifiers plus antenna) will operate as an efficient power combining-radiating system. The antenna developed will be evaluated for gain, pattern and efficiency on the antenna range with and without the amplifiers. The amplifiers will be connected directly to the antenna without benefit of isolators so that their interaction via the antenna will be unimpeded. The combined output power of the amplifiers will be approximately 1/2 watt.

Figure 2 contains a sketch of the power combining microstrip antenna to be evaluated. The dielectric substrate is metalized on both sides. The underside, within the cavity, contains the four microstrip feed lines which are coupled to the two radiating slots on the top side via two narrow slotlines. In order to feed the antenna, two of the rf inputs are required to be 180° out of phase with the remaining two. An antenna feed network is thus required which will provide the four 0°-180° equal amplitude outputs.

The antenna feed network, the power amplifiers and the microstrip antenna will be connected as indicated in Figure 3a. The four cables connecting the amplifiers and the antenna are required to have equal electrical lengths as are the cables connecting the antenna feed network and the amplifiers. This is necessary to retain proper phasing of the antenna.

3. EXPERIMENTAL PROGRAM STATUS

3.1 FEED NETWORK

Three solid state antenna module feed networks have been assembled and measurements on all have been made. Two of the feed networks are needed to accomplish the antenna range tests. The stripline feed network, (Figure 4a), consists of two 0°-180° rat race ring hybrids fed by a single in-phase two-way power divider. The circuit metalization pattern was etched into the top circuit cover plate as a label for the finished feed. Figure 4b contains a photograph of the automatic network analyzer being used to measure the feed network performance.

The insertion loss and insertion phase measurements over a 500 MHz bandwidth indicate (Figure 5) that at the design frequency, the insertion loss of all ports is nearly equal. The insertion phase error window at 2.45 GHz is 1.5° wide, or ± .75°. The measured results for all feed networks at 2.45 GHz are as follows:

Serial No.	Phase Balance	Loss Balance	Insertion Loss	Isolation & Return Loss
001	± .73°	± .03 dB	.154 dB	25 dB
002	± .39°	± .03 dB	.189 dB	25 dB
003	± .81°	± .015 dB	.172 dB	25 dB
GOAL	± 1°	± .05 dB	.2 dB	20 dB

The measured insertion phase to all ports of each network deviate from a mean value by less than one degree, which was the design goal. The measured loss was less than 0.2 dB for each of the units over and above the 6.02 dB that results from the four way power division. This value will be used again when the antenna efficiency is calculated. A more important parameter is loss balance, which is so small that it is hardly measurable ($\pm .03$ dB). Thus, the power delivered to all ports is within 0.7% of the mean value.

The isolation between the feed network output ports is greater than 25 dB for all units. This minimizes the interaction between amplifiers in the final configuration, by preventing reflected power from the input of each amplifier from reaching the input of one or more of the other amplifiers. Thus, the amplifiers are operated as if they were each driven from an isolated source. This is a particularly good operating procedure where one is primarily interested in how well the power combining antenna performs, and in how well the solid state amplifiers interact with each other within the antenna circuitry.

The impedance match realized at each port results in a VSWR < 1.12 , with a return loss greater than 25 dB. In actual operation, a low output VSWR and good isolation is only available if the input power to the feed network is derived from a well-matched source.

3.2 POWER AMPLIFIERS

The four 2.45 GHz power amplifiers have been supplied by Tron-Tech, Inc. of Eatontown, N. J. and, to date, have only been evaluated under small signal conditions. (Table 1) As can be seen, the amplifiers meet many of the specifications and are out on others. More tests are scheduled to determine how the amplifiers perform under the required drive condition needed to yield 1/8 watt of output power. Until these additional tests are completed, it is premature to speculate on the degree of suitability of the four amplifiers.

Table 1. AMPLIFIER SPECIFICATIONS & SMALL SIGNAL MEASURED VALUES

Parameter	Specification	Measured by Boeing (small signal)
Frequency	2.45GHz	2.45GHz
Power out @ 1 dB gain compression	+21 dBm	Not measured
Gain	6 dB min.	7.76 dB - 8.18 dB
Gain match	$\pm .5$ dB max.	$\pm .21$ dB
VSWR in:	2.5:1 max.	3.65:1 (one unit)
out:	1.5:1 max.	1.66:1 (two units)
Phase match	$\pm 5^\circ$ max.	$\pm 2.4^\circ$
Phase control	$\pm 10^\circ$ min.	$\pm 2^\circ$ by varying B^+ according to Tron-Tech.
Gain Control	by varying B^+	Installed separate loss cont. which yields ± 1.5 dB according to Tron-Tech.
Infinite VSWR save at full power	340	verified by Tron-Tech.

The amplifiers were specified to be fail-safe under conditions of infinite VSWR at all phases. This was required to insure that the amplifiers wouldn't fail during test. Such a failure would preclude the collection of antenna data with the amplifiers attached. Since the amplifiers are designed to operate Class A, the small signal data exhibited in Table 1 may not change very much under large signal tests.

3.3 RADIATING ELEMENT

A four feed microstrip antenna has been developed which appears suitable for the task at hand. It evolved through a series of steps which began with a microstrip to slot-line coupler and graduated from a single feed slot line antenna to a dual fed slot-line antenna and finally, the four feed design illustrated in Figure 3b. Figure 3b shows the metalization pattern (actual scale) on each side of the microstrip dielectric substrate. The four microstrip lines (shown shaded) cross under and couple their energy to the four narrow slotlines which transport the signal to the wide radiating slots (shown in black). The antenna substrate is 2.6 inches square and is backed by a 2.5" x 2.5" x 0.30" cavity, which couples the radiating slots together.

The antenna, when fed by the feed network described earlier, exhibits a bandwidth at the 15 dB return loss points of approximately 100 MHz. A preliminary pattern taken with the antenna on the range is shown in Figure 6. The peak gain as measured is approximately 8 dB; however, not accounting for 0.43 dB of feed network and cabling losses. The pattern is well behaved with the first sidelobes approximately 23 dB down. A second "cleaned-up" model will now be fabricated to initiate full range testing with and without the power amplifiers.

4. TEST PLAN

The primary purpose of the antenna range testing is to determine the efficiency of the four feed antenna with and without the amplifiers. The efficiency is derived by dividing the antenna gain G by the antenna directivity D . The antenna gain will be determined by a 3-antenna method in which antenna spacing is measured to better than 1/2%. This method is expected to yield gain accuracies of ± 0.3 dB.

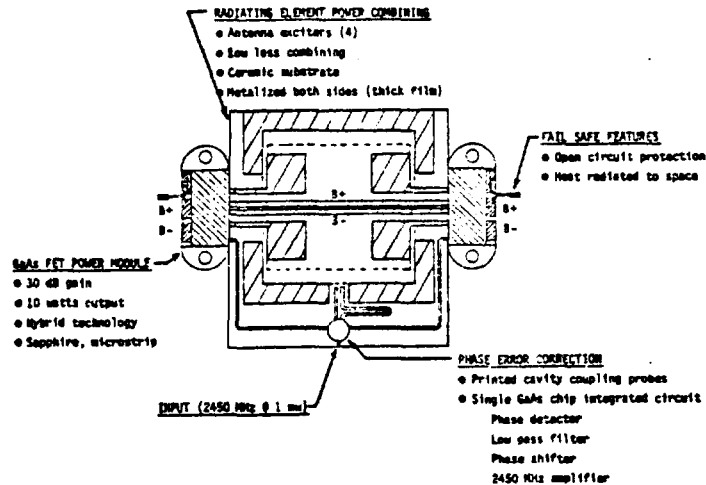
The antenna directivity D is defined as the ratio of the peak radiated power to the average isotropic radiated power (average power radiated over the unit sphere). To arrive at the average isotropic radiated power, one must measure and total up the radiated power over the spherical surface with the unknown antenna at its center, and average that value by dividing by the number of measurements. Typically, a $2^\circ \times 2^\circ$ cell is employed which requires 16,200 measurements. The error associated with the directivity measurement is approximately $\pm .25$ dB.

The antenna feed system insertion loss will be measured on the automatic network analyzer (HP 8542B), which is periodically certified by Hewlett-Packard using standards traceable to NBS to an accuracy of ± 0.15 dB ($\pm 3.51\%$) for devices of low insertion loss. Thus, when the feed system insertion loss is

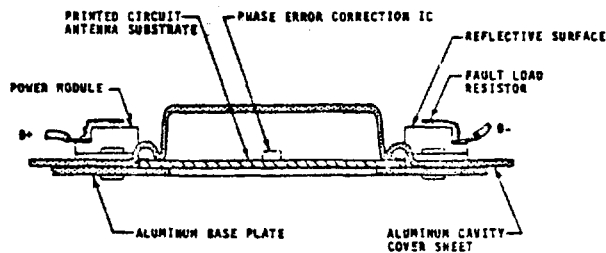
subtracted from the measured gain, the feed system measurement uncertainty will be added to the previously stated uncertainties. The RSS value of the combined efficiency is thus, $\pm \sqrt{(.30)^2 + (.25)^2 + (.15)^2} = \pm .42\text{db} = \pm 10\%$

Cross-polarized radiation for the SPS application is considered wasted power, and therefore, it will also be measured and included when determining the antenna efficiency.

With the basic antenna characterized for gain, pattern and efficiency, antenna range measurements will then be made with the solid state power amplifiers inserted and operating with a combined output power of approximately one-half watt. The measurement of interest is the difference between the range received power with and without the inclusion of the solid state power amplifiers. The difference should be equal to the gain of the amplifiers. This difference will verify the degree in which the antenna sums the available power of the four amplifiers. Pattern measurements will also be taken to compare with those taken without the power amplifiers. As a final test to verify the entire procedure, the integrated amplifier-antenna system will be tested for directivity and gain, and the overall efficiency will be calculated.

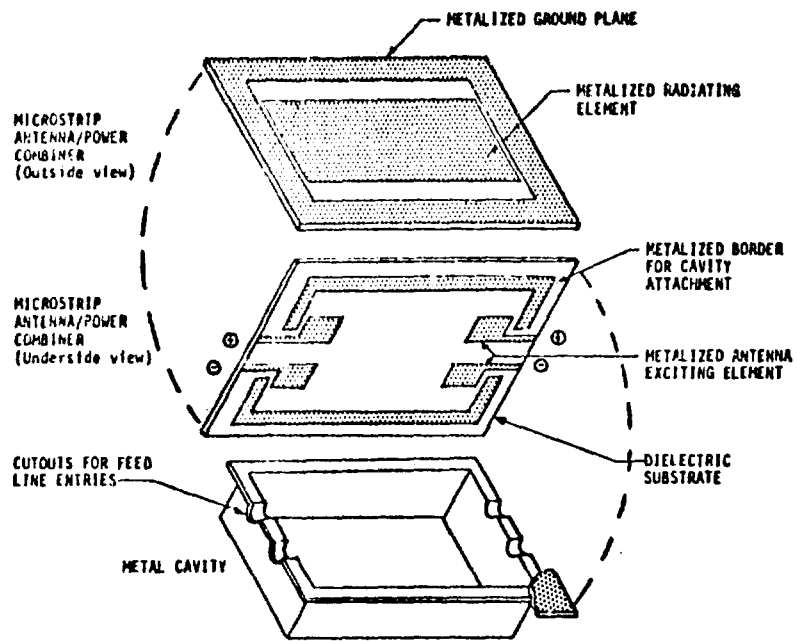


(a) PLAN VIEW

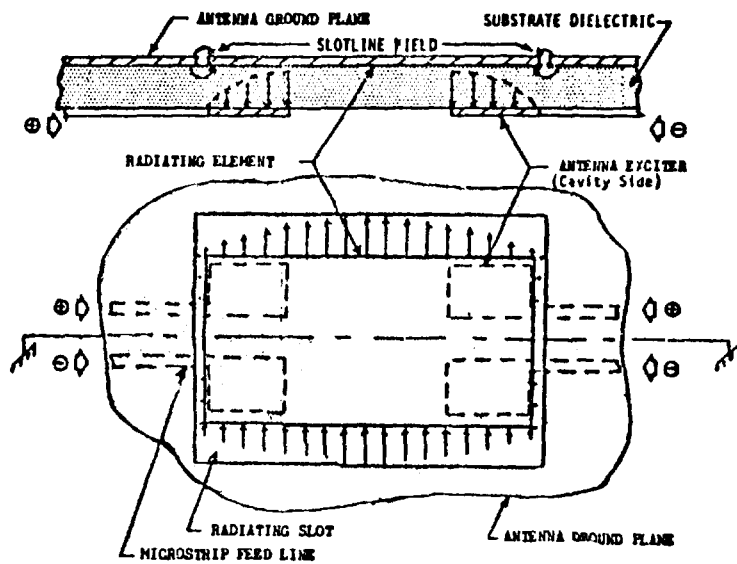


(b) CROSS SECTION

FIGURE 1 SOLID STATE POWER COMBINING MODULE CONCEPT (20 WATTS)



(a) BREAK-A-WAY VIEW



(b) "E" FIELD PROFILE

FIGURE 2 POWER COMBINING MICROSTRIP SLOTLINE ANTENNA

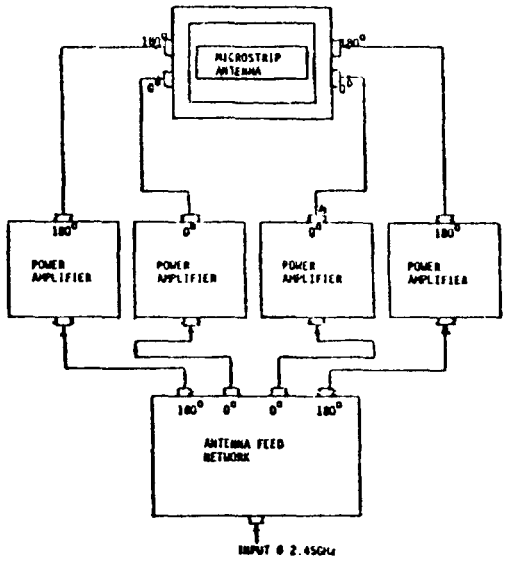


FIGURE 3a POWER COMBINING ANTENNA, FEED NETWORK & POWER AMPLIFIER BLOCK DIAGRAM

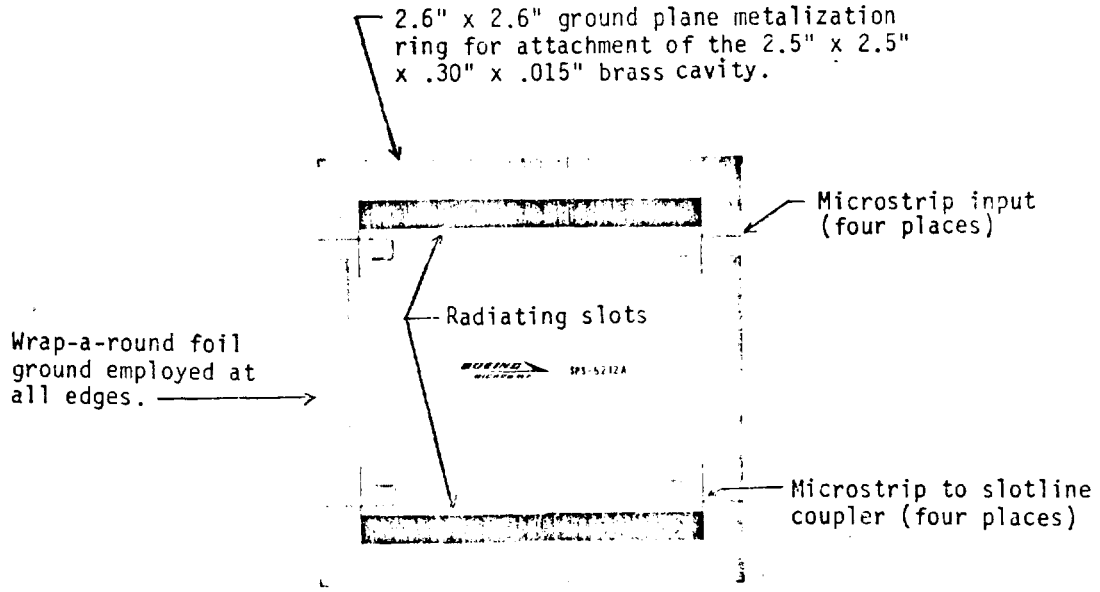


FIGURE 3b COPPER METALIZATION PATTERN FOR FOUR FEED MICROSTRIP ANTENNA

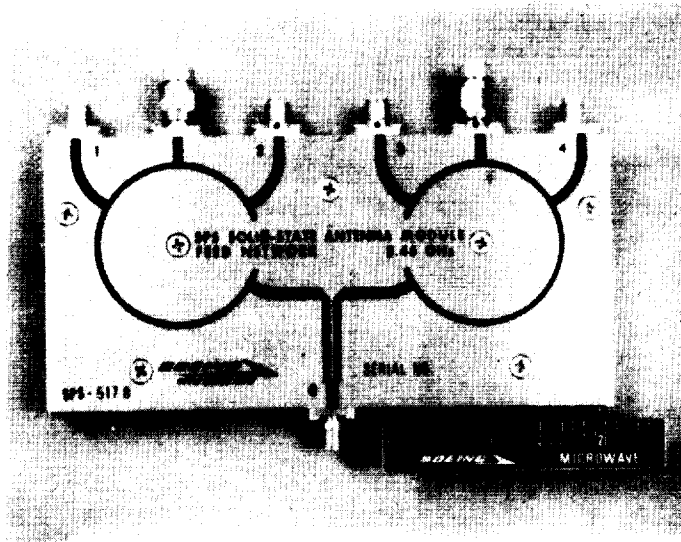


FIGURE 4a STRIPLINE FEED NETWORK

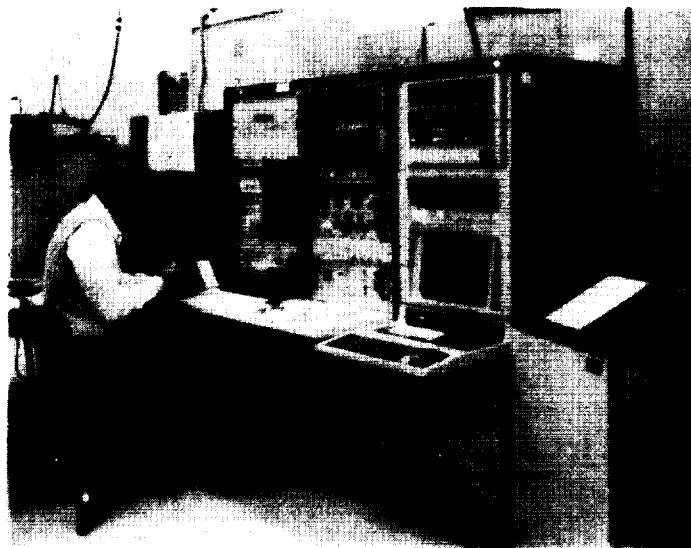
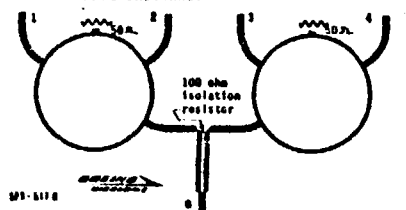
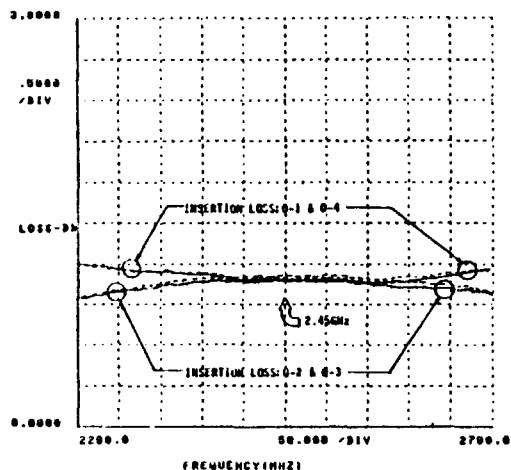


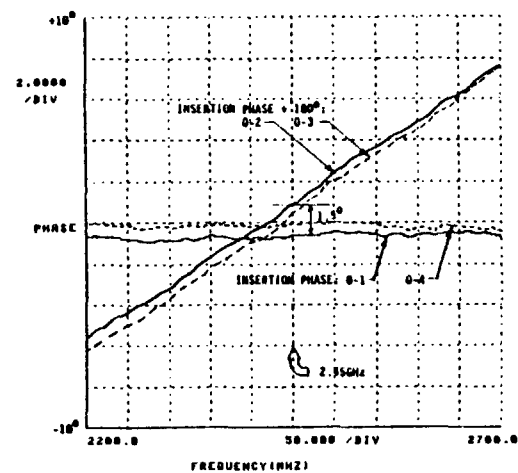
FIGURE 4b AUTOMATIC NETWORK ANALYZER

THE BOEING CO. GWF SEPTEMBER 10, 1979
 SPS SOLID-STATE ANTENNA MODULE FEED NETWORK
 NETWORK 2.48 GHz
 SPS-317B, SER. #01



INSERTION LOSS

THE BOEING CO. GWF SEPTEMBER 10, 1979
 SPS SOLID-STATE ANTENNA MODULE FEED NETWORK
 NETWORK 2.48 GHz
 SPS-317B, SER. #01



INSERTION PHASE

FIGURE 5 INSERTION LOSS AND INSERTION PHASE VERSUS FREQUENCY FOR THE STRIPLINE FEED NETWORK.

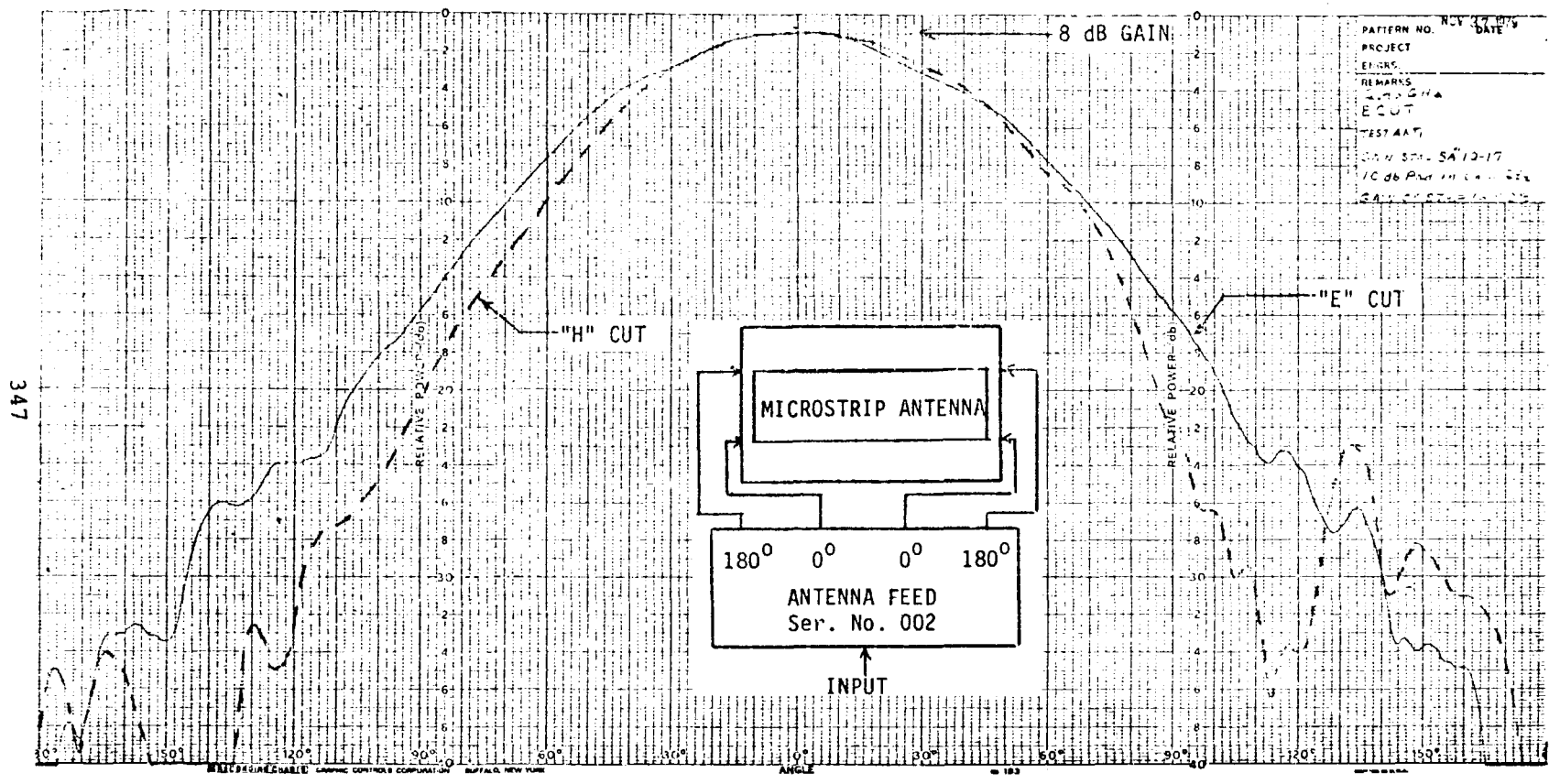


FIGURE 6 ANTENNA RANGE GAIN PATTERN FOR THE FIRST POWER COMBINING MICROSTRIP ANTENNA (FEED NETWORK NO. 2)

SOLID STATE SYSTEMS CONCEPTS

By K. G. Schroeder, I. K. Petroff/Rockwell International

1.0 INTRODUCTION

This paper describes two prototype solid-state phased array systems concepts for potential use in the Solar Power Satellite (SPS). In both concepts, the beam is centered on the rectenna by means of phase conjugation of a pilot signal emanating from the ground. Also discussed is on-going solid-state amplifier development.

The basic systems concepts are now described in more detail.

2.0 OVERVIEW OF SOLID-STATE ARRAY CONCEPTS

Two different solid-state array concepts are being developed at this time: The End-Mounted Space System (Figure 1) and the Sandwich (Figure 2). Both concepts use the same element and spacing, but in the end-mounted system 36-watt amplifiers are mounted on the ground-plane, whereas in the sandwich the amplifiers are elevated to the dipoles, and their waste heat is dissipated by beryllium oxide discs. The feed lines are underneath the ground-plane, and a coaxial transmission line is carried all the way to the amplifier input. (See section on RF Signal Distribution). Figure 4 in Section 4 shows the sandwich dipole layout in close-up view.

3.0 SOLID-STATE PHASE CONTROL

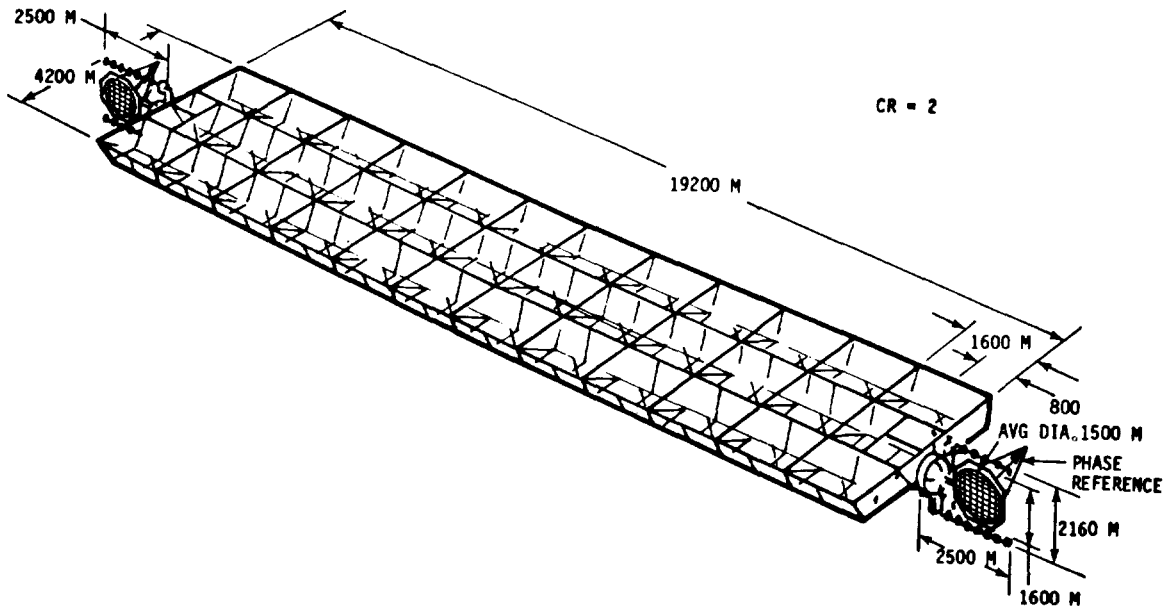
3.1 REFERENCE PHASE DISTRIBUTION

Phase conjugation at the 10 meter by 10 meter subarray is used to steer the beam. The reference phase signal is distributed over the spacetenna aperture via a radio link. Figure 3 illustrates this method giving a perspective view of the top of the aperture. Two important features are: (a) the phase reference signal originates from a single transmit location at the rear of the aperture; and (b) phase reference and pilot antennas are orthogonally polarized with respect to the power dipoles to avoid feedback loops. Instead of an endfire (e.g., "Cigar") array, broadside arrays can be used for reference and pilot pick-up. Both configurations shall be considered in more detail in future studies.

The phase reference signal is distributed as follows:

From the shaped-beam illuminator antenna an RF signal is distributed over a cone with maximally 90 degrees beamwidth. All reference pick-up antennas see approximately the same signal strength. The local oscillator and driver amplifier is redundant. Large variations in aperture flatness can be compensated modulo 2π since bandwidth is of no concern for the reference phase signal. The phase at each subarray pick-up point is normalized with respect to a perfectly flat

FIGURE 1. END-MOUNTED SOLID STATE CONCEPT (REF. 1)

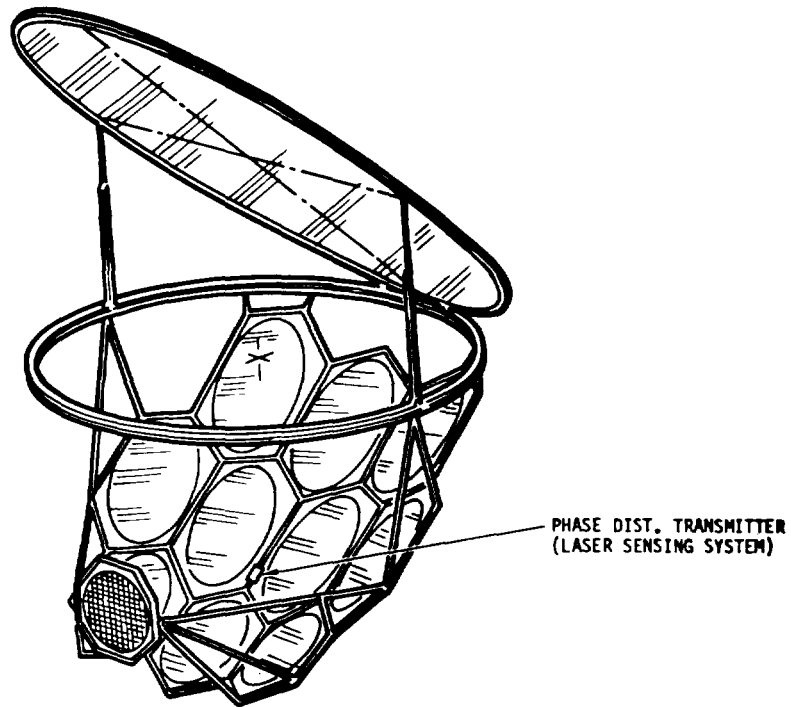


END-MOUNTED SOLID-STATE CONCEPT CHARACTERISTICS

- o GaAs SOLAR ARRAY
- o GEOMETRIC CR = 2.0
- o DUAL END-MOUNTED MICROWAVE ANTENNAS
- o AMPLIFIER BASE TEMPERATURE = 125°C
- o AMPLIFIER EFFICIENCY = 0.8
- o ANTENNA POWER TAPER - 10dB
- o ANTENNA DIAMETER = 1.35 km
- o POWER AT UTILITY INTERFACE = 2.61 GW PER ANTENNA
(5.22 GW TOTAL)
- o RECTENNA BORESIGHT DIAMETER = 7.51 km PER RECTENNA

Ref. 1) After: G. M. Hanley, SPS Concept Definition Study (Exhibit D),
First Performance Review - 10 October 1979.

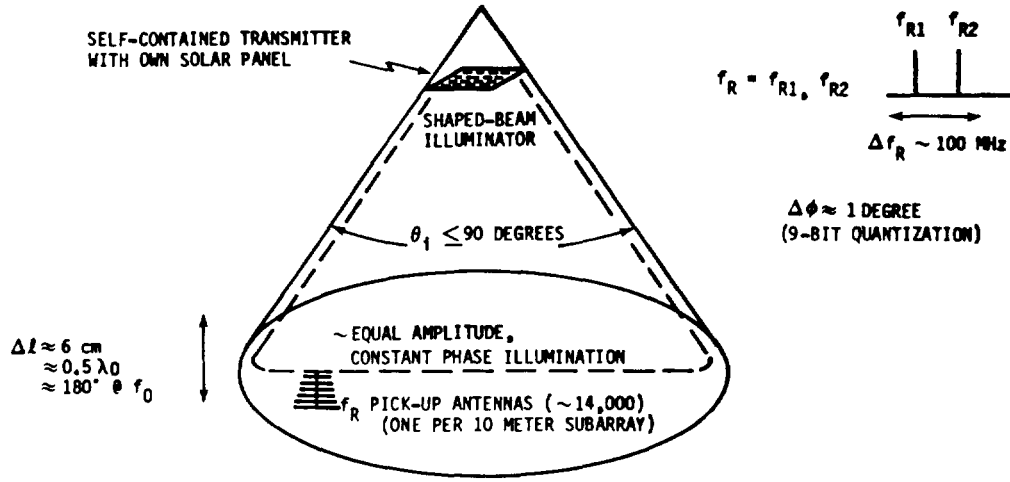
FIGURE 2. SOLID STATE SANDWICH CONCEPT RECOMMENDED FOR POINT DESIGN
(REF. 1)



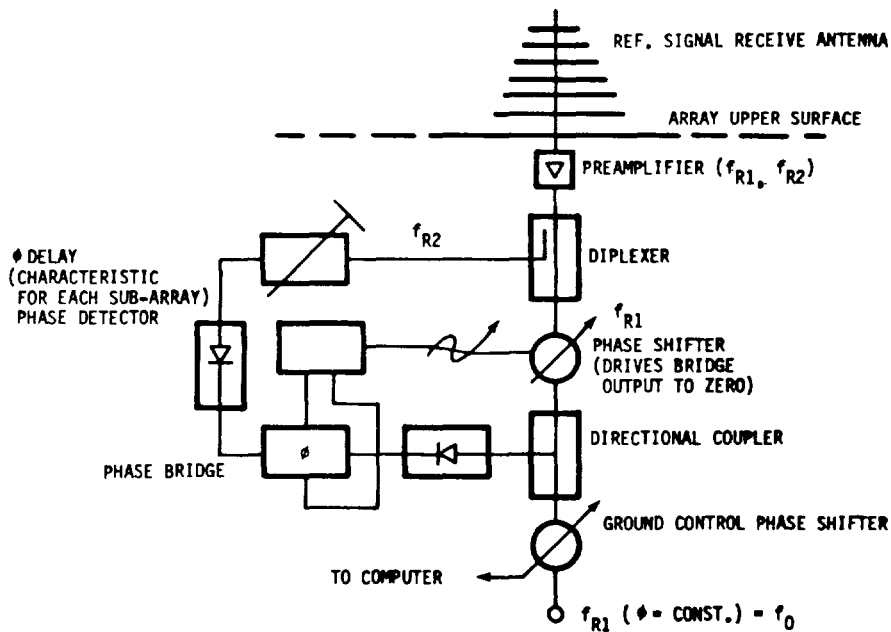
RECOMMENDED SOLID-STATE SANDWICH CONCEPT CHARACTERISTICS

<u>CHARACTERISTIC</u>	<u>PRIMARY</u>	<u>SECONDARY</u>
SOLAR ARRAY TYPE	GaAs	MULTI-BANDGAP
EFFECTIVE CR	6	5 TO 6
SOLAR ARRAY TEMP. ($^{\circ}\text{C}$)	200	200
AMPLIFIER BASE TEMP. ($^{\circ}\text{C}$)	125	125
AMPLIFIER EFFICIENCY	0.8	0.8
ANTENNA TAPER RATIO (dB)	0	0
ANTENNA DIAMETER (Km)	1.77	1.64 TO 1.58
POWER AT UTILITY INTERFACE (GW)	1.26	1.47 TO 1.54
RECTENNA BORESIGHT DIA. (Km)	5.10	5.39 TO 5.68

FIGURE 3. PHASE REFERENCE SIGNAL DISTRIBUTION SYSTEM AND REFERENCE SIGNAL CONTROL LOOP



NOTE: PICK-UP ANTENNA ORTHOGONALLY POLARIZED WITH RESPECT TO POWER BEAM
 TOTAL ISOLATION $I_T \geq 40 + 60$ dB ≥ 100 dB
 CROSS POL FRONT-TO-BACK RATIO (CAN BE MADE >100 dB)



uniform aperture by means of a servo loop shown in the bottom part of Figure 3. For each subarray center location, a phase delay differential ("reference standard") is computed which occurs for the two generating frequencies f_{R1} and f_{R2} if the receiving antenna is located on a perfect plane. These delays can be calculated, and tuned in the lab to fractions of a degree. The output of the phase bridge then drives a phase shifter until the path delay differential equals that of the reference standard.

Since this circuit is used at every subarray, the subarray center points are electrically normalized to show $\phi = \phi_0$ constant across the entire array. This provides the conjugation circuit with the required reference phase.

3.2 RETRODIRECTIVE BEAM CONTROL

A retrodirective control circuit which compensates for pilot-generated beam shifts (without ionospheric effects) is the Chernoff circuit, with additional isolation added by (a) separating the pilot and power frequency paths, (b) using orthogonally polarized radiating elements; and (c) providing the remaining isolation in separate bandpass filters. The total required filter isolation is 70 dB, according to preliminary pilot system calculations.

This pilot system is predicated on ~ 100 dBw pilot power. The proposed implementation of this pilot system consists of a circular array of low to medium-gain elements placed at the periphery of the rectenna, on top of utility poles if necessary to avoid interference from the power collection and transmission system.

The system provides vastly improved reliability over a single-dish, concentrated amplifier pilot system, and also provides such a wide power tube when the near-field beam enters the ionosphere that certain ionospheric effects will be mitigated. If ionospheric tests show that delay compensation through the ionosphere is required, a three-tone pilot system will be used as described in the Phase Control Session.

3.3 RF SIGNAL DISTRIBUTION SYSTEM

The current baseline distribution system for the conjugated RF signal is the same for both solid-state concepts.

Seven levels of corporate divisions provide equiphase feeding to the 16,384 elements in each 10m x 10m subarray.

The salient features of this distribution network are: weight of 0.67 million kilograms for the total array using UT-47M; 250°C temperature capability; approximately 10dB ohmic loss (in addition to 42dB splitting loss). All layers of coax are pressed together behind the ground-plane, and very little thermal resistance is presented to the heat being radiated rearward from the ground-plane in the end-mounted concept, and toward the ground-plane (from the solar cells) in the sandwich concept. The composite heat transfer will be established by the spacing between the ground plane and the solar cells in the case of the sandwich.

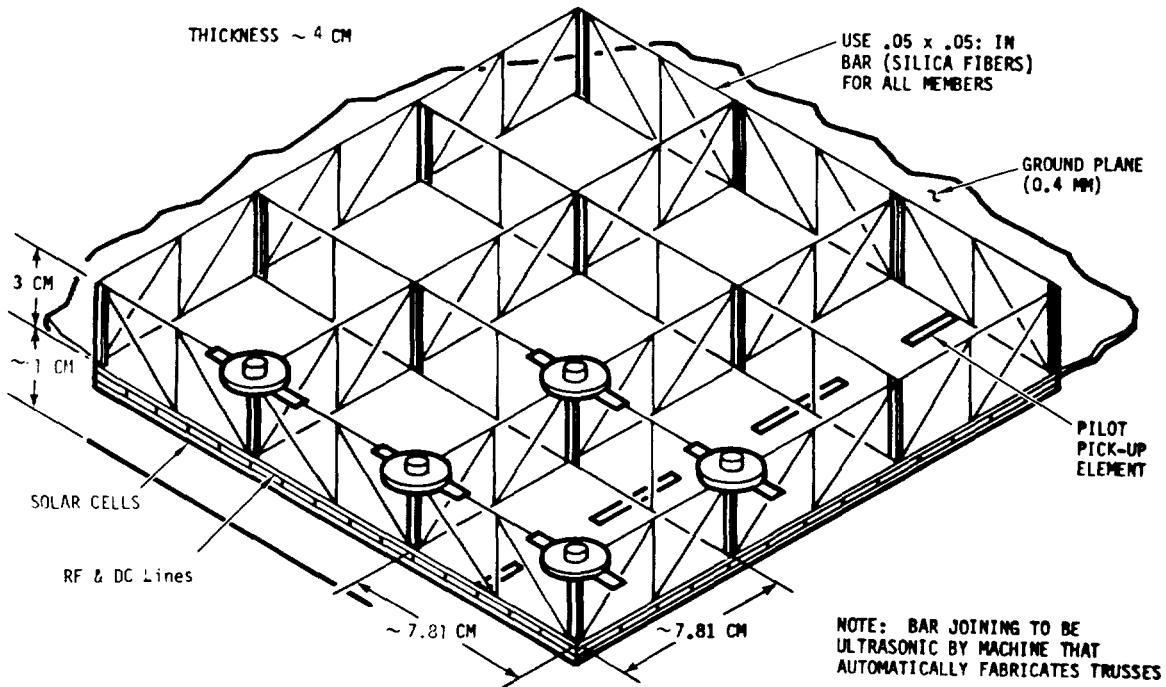
4.0 SOLID-STATE RADIATORS

A number of elements have been considered for the reference phase pick-up and pilot-tone pick-up elements: Helices; disc-on-rod antennas; yagis; dipole arrays; slot arrays; patch-type microstrip arrays; and arrays of various other strip-type radiators.

For the power radiators, all of the above array elements (except for high-gain end-fire arrays) have been considered but thin dipoles were selected because a) they lead to a minimum power requirement for the amplifier module; b) provide the necessary heat removal characteristics, and c) yield maximum reliability.

Figure 4 shows the dipole layout selected for the sandwich concept. The pilot pick-up slots are interspersed, but the power dipoles can be removed from this section if additional isolation is required, and/or space is required for the conjugation circuit.

FIGURE 4. SANDWICH ANTENNA WITH DIPOLES OVER GROUND PLANE



5.0 SOLID-STATE POWER AMPLIFIERS

The assessment of solid-state devices for r-f conversion in the SPS microwave power transmission system has included to date both an analytical effort and an amplifier development program.

5.1 Analytical Studies

The analytical study was carried out for Rockwell International at the University of Waterloo, Canada. The first phase of the study consisted of a computer simulation of bipolar transistors, in Class C and Class E type circuits. Both silicon and GaAs bipolar transistors were modelled. In the second part of the study, GaAs MESFETs were modelled in Class B and Class C circuits. Work is currently in progress to obtain Class E results.

The study was undertaken as an evaluation of transistors for the microwave space power system. The goal was the determination of transistor fabrication parameters suitable for power conversion efficiencies of at least 80% with power gains of at least 10 dB.

5.2 Bipolar Transistor Simulation

The simulation is carried out by using two basic programs. The first program generates a circuit model of the transistor, from inputs consisting of the impurity profile and lifetimes, plus geometry data. The second program is a circuit analysis program where the device model is incorporated into the desired external circuit. The results of the bipolar transistor analysis indicated that GaAs devices perform better at high temperatures with respect to efficiency than Si devices of similar geometrical parameters as shown in Figures 5 and 6. A comparison of Class C with Class E operation for the silicon transistor at 27⁰C, shows that at high power levels (20 watts) the saturated Class-C mode gives the best results (Figure 7), while at lower power levels (10 watts) Class C gives better results at gains below 13 dB and Class E performs better at higher gains, (Figure 8).

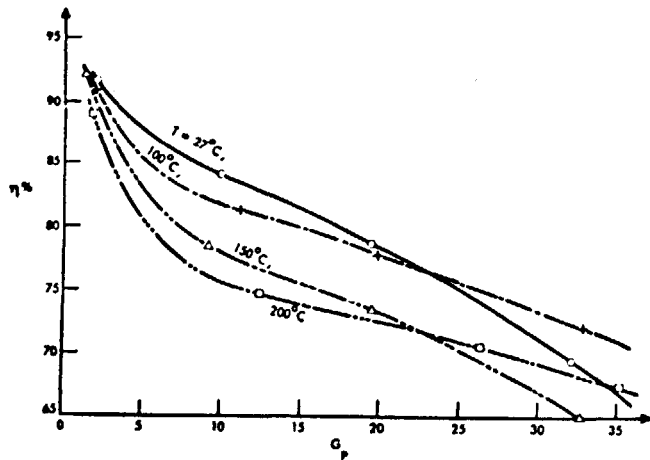


FIGURE 5. Results of High Temperature Study for the Silicon Transistor at 2.45 GHz

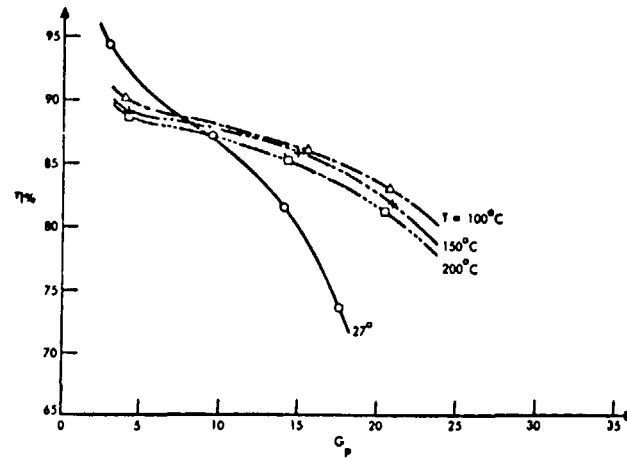


FIGURE 6. Results of High Temperature Study for the GaAs Transistor at 2.45 GHz

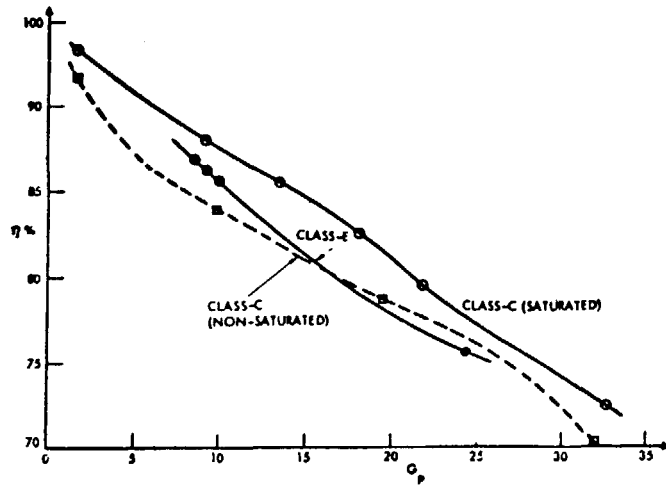


FIGURE 7. Efficiency vs Power Gain at 2.45 GHz and High Power Level for Silicon

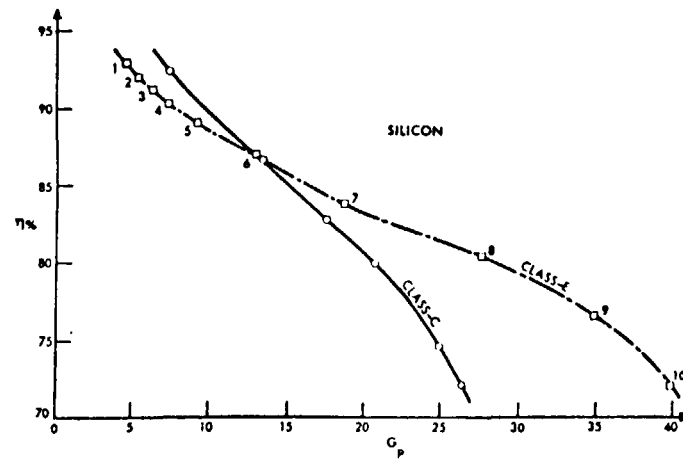


FIGURE 8. Efficiency vs Power Gain at 2.45 GHz and Low Power Level for Silicon

5.3 GaAs MESFETs Simulation

This study, currently in progress, follows the procedure used for the bipolar transistor simulation. A circuit model is generated by an appropriate program and is fed into the circuit analysis program. The devices modelled, so far, were basic one-cell structures, with low overall power output capability. The power output, power gain and efficiency obtained for the five structures modelled so far are shown in Figure 9. This figure shows plots of power added efficiency versus P_{out}/P_{max} for each device, where the three values shown correspond to conduction angles of 80° , 120° and 180° . The dashed lines indicate a mode of operation which cannot be attained physically, because the gate source voltage exceeds the breakdown voltage for that transistor.

6.0 POWER AMPLIFIER DEVELOPMENT

The goal of the power amplifier development program is to demonstrate that efficient operation at a 5 to 10 watt power level can be achieved with off the shelf GaAs power FETs and to show that the performance can be improved with optimized devices of similar type. The high efficiency power amplifiers are being developed for Rockwell International by RCA and will be discussed in a subsequent presentation.

GaAs devices were selected because of data showing that GaAs performs better than silicon at the temperatures likely to be encountered in the SPS environment. Several transistor structures should be investigated to establish possible trade-offs with respect to power level, comparative efficiencies and reliability. Schottky barrier FETs are the first choice for testing at the experimental level in view of the high degree of activity in their development due to their use as power devices at microwave frequencies.

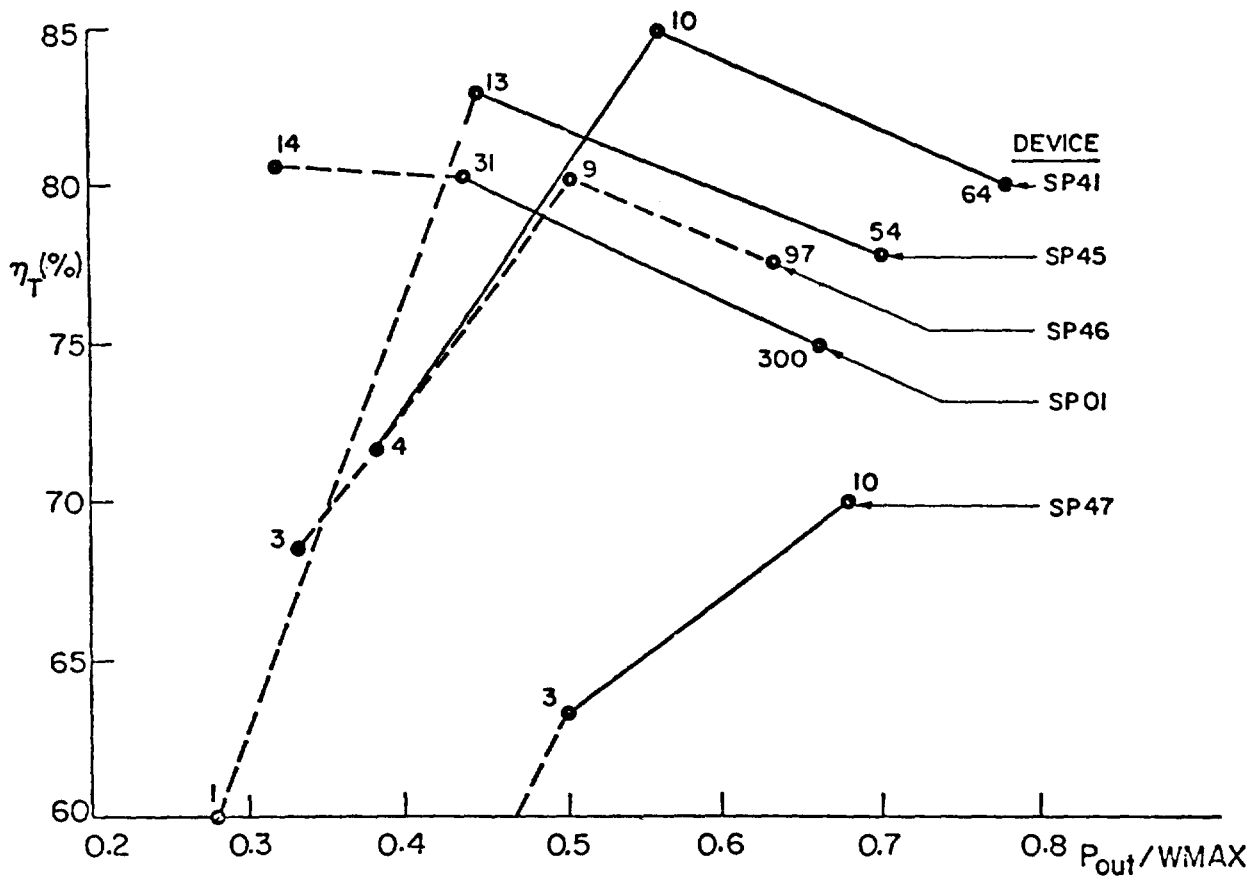


FIGURE 9. Total Efficiency vs (Output power/Wmax) for Sinusoidal Drive at 2.45 GHz for Five Different FETs. NOTE: The numbers indicate power gains.

SOLID STATE DEVICE TECHNOLOGY FOR SOLAR POWER SATELLITE*

By David G. Weir/RCA

NASA, Johnson Space Center sponsored a program, "Analysis of S-Band Solid-State Transmitters for the Solar Power Satellite," based on the assumption that a high-efficiency solid-state SPS transmitter may be feasible.

The objectives of the study were to:

- o expand the understanding of the SPS transmitter concept and relate it to the possible utilization of solid-state (rather than thermionic) elements in the antenna array;
- o explore the need for technology development in the areas of devices, circuits, and interface configurations for a solid-state antenna array;
- o recommend specific technology advancement programs that could impact future SPS designs.

An additional task, added toward the end of the program in agreement with the Technical Monitor, was to construct a sample solid-state amplifier, based on existing gallium arsenide FET devices, so that power, gain, and efficiency relationships could be experimentally explored.

The study was designed to explore independently aspects of the devices, the circuits, and the overall antenna system. Only toward the end of the investigations were these three elements brought together to provide an overall view of the solid-state antenna concept and to recommend follow-on technology investigation programs.

DEVICE INVESTIGATIONS

For any system configuration, devices providing the maximum possible power at the highest possible efficiency would obviously be desirable. In practice, however, power must be traded off against efficiency, with efficiency the paramount parameter. When these factors are considered, gallium arsenide rather than silicon appears to be the favored material for the SPS application; the device used would be some kind of field-effect transistor of the type that combines high efficiency and relative ease of fabrication.

Thermal and electrical designs for both Schottky-barrier and junction-type FETs were presented at the conclusion of the study. Their purpose, rather than serve as device designs to be actually developed, was to highlight the considerations likely to influence the choice of future programs. No clearcut preference of one over the other was discerned at that point in the study. Devices providing 4 watts at greater than 80% power-added efficiencies were considered feasible.

*RCA presentation at NASA, Johnson Space Center, Houston, TX, 17 January 1980.

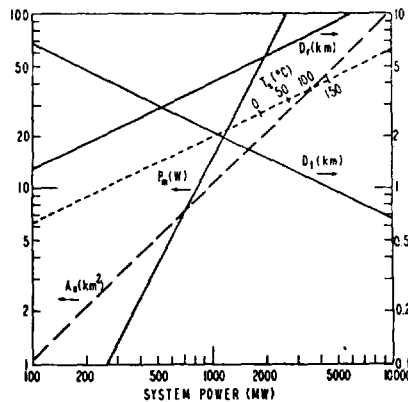
An actual amplifier stage was constructed with commercially available devices. It provided 3 watts of output power at an efficiency of 58% -- results considered very good indeed. The unit was delivered to JSC at the conclusion of the study.

One of the important recommendations of this part of the study was the undertaking of a follow-on experimental and theoretical program to ascertain the factors contributing to high-efficiency operation of microwave FETs. Previous experience with specialized large-signal computerized equipment pointed to the benefits of using this apparatus for the recommended follow-on study program.

ANTENNA SYSTEM INVESTIGATIONS

The Reference System (DOE/NASA Report, October 1978) served as a basis for the first phase of the antenna system investigations.

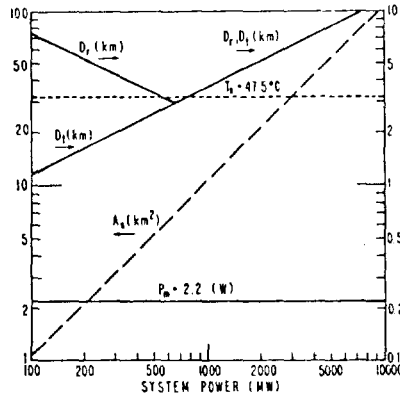
If it is attempted simply to replace the thermionic devices contemplated in the Reference System by clusters of solid-state devices whose power is combined to form equivalent transmitting elements, penalties in voltage-distribution losses, power combining losses, and thermal problems must be seriously considered. From detailed analyses performed during our study, it soon became apparent that a solid-state replacement program of this nature, while it may contribute toward the overall reliability of the system, would fall short in terms of the operational parameters -- particularly in terms of a Factor of Merit measured in watts per kilogram.



SPS design nomograph - 10-db taper.

At that point in the study, again with the concurrence of the Technical Monitor, emphasis was placed on a concept that considered direct conversion of sunlight into microwave power-generating modules, thereby obviating the need for voltage distribution altogether and essentially solving the thermal problems. Some specific problem areas peculiar to this approach were addressed in

the study -- e.g., the relative orientations of the solar array and the microwave antenna, the spacing of the antenna elements and, most importantly, the near-field properties of such an antenna.



SPS design nomograph - uniform distribution.

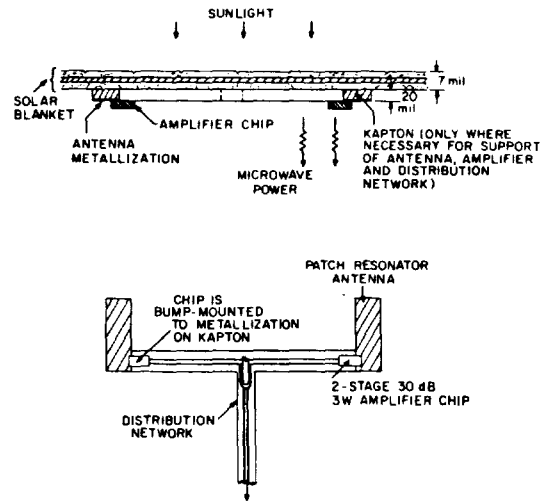
It was concluded that this type of system has Factor of Merit (W/kg) advantages over the Reference System, and that a tubular beam can indeed be created; a judicious choice of phase tapers made it possible to smooth power variations over the rectenna. Computer simulations of this type of antenna beam were performed at the conclusion of the study. Recommendations for adapting this approach, after further study, were made.

We recommended that studies aiming at a fuller understanding of the factors affecting high-efficiency operation of microwave FETs and the circuitry associated with them be vigorously pursued. Large-signal waveform analysis of FET operation was identified as a necessary factor of these studies.

MODULE INVESTIGATIONS

The module study quickly yielded the (not unexpected) notion that the efficiency of the power module is the most important design parameter, since it impacts very strongly the overall SPS cost in terms of dollars per watt of output power. Here again power combining losses and primary power distribution problems pointed toward the concept of the solar-powered module; an analysis of the practical power limits placed the module somewhere between 0.5 and 30 watts, with the power-vs-efficiency tradeoff pointing toward an optimum value of 1.5-3 watts.

Two design concepts were shown in which modules were placed on a $1.3\text{-}\lambda \times 1.3\text{-}\lambda$ grid, with 16-module clusters controlled by a single receiver module and providing 50 watts of transmitter power per cluster. As was the case with the device designs, both module designs (a "high Q" version and a "patch resonator" approach) were meant to represent the approach rather than be specific.



Patch - resonator design.

The most important recommendation resulting from the module study was a strong indication that any future efficiency optimization attempt should consider the device-module interface as part of the problem. Thus the large-signal waveform analysis recommended for the device studies should be combined with similar analyses for the module circuitry.

CONCLUSIONS AND RECOMMENDATIONS

The JSC study program yielded the following conclusions:

- o It does not appear prudent to simply replace the thermionic microwave power converters in the Reference System by equivalent clusters of solid-state devices.
- o On the other hand, real benefits can be obtained if the system architecture takes full advantage of the operating parameters of solid-state microwave devices. This leads to a concept of direct utilization of the solar-panel-generated power by low-power microwave amplifiers (the so-called SMART concept).
- o The postulated 80% power-added efficiency of the microwave amplifiers appears ultimately achievable. Gallium arsenide FETs are the logical device candidates for this service.

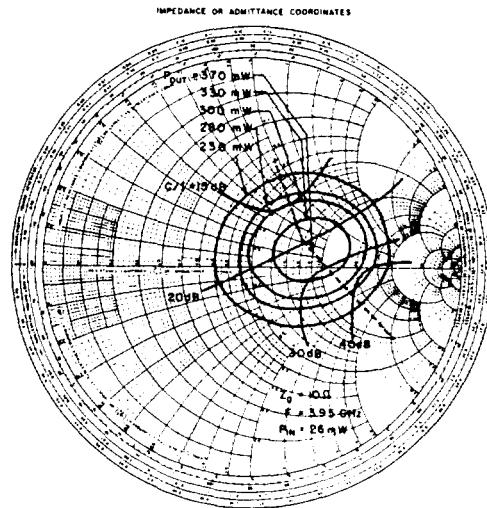
SPS SOLID-STATE AMPLIFIER

NASA, Marshall Space Center through Rockwell International, is presently sponsoring the "SPS Solid State Amplifier Development Program."

This program represents an extension of the effort performed as part of the JSC study: its main purpose is to gain a better understanding of the factors contributing to the high-efficiency performance of GaAs FETs. Large-signal waveform analysis techniques are a major investigative tool in the program.

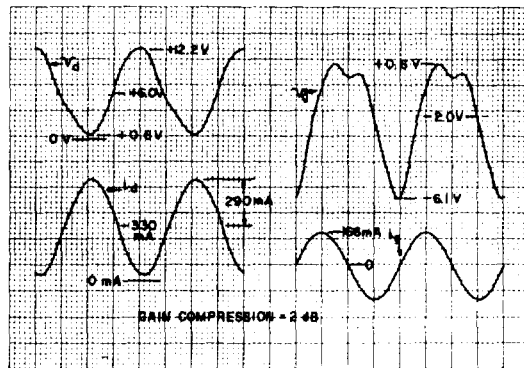
The program is divided into two consecutive tasks, with present effort still under Task A. This calls for the demonstration of an amplifier having an output power of 5 watts, a gain of 8 dB, and a power-added efficiency of 50%. In Task B the power output, gain, and efficiency to be demonstrated are increased to 10 watts, 10 dB, and 65%, respectively. To date a survey of available devices from a total of six domestic and foreign manufacturers of GaAs FETs was made, and circuits using various devices are being built and analyzed as the transistors are received. While "Class E" operation was and continues to be of interest for the SPS application because of its potential for very high efficiency, it is by no means certain that such mode of operation can be obtained at microwave frequencies, and the work under the program is not restricted to multipole operation of the FETs.

As previously mentioned, computer-aided analysis techniques are used extensively in the program, not only in the normal small-signal device characterization mode, but also to define the available tradeoffs under large-signal operating conditions. Examples of such techniques are the automatic plotting of circles of constant efficiency, constant gain, constant power output, and constant intermodulation distortion on special instrumentation which exists at RCA Laboratories.



Microwave CAD large-signal analysis.

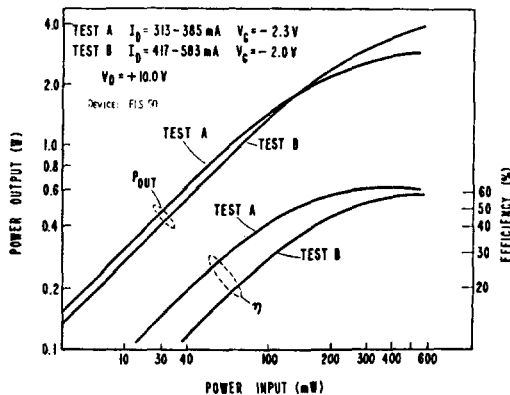
In addition, we have demonstrated a technique for synthesizing current and voltage waveforms under FET amplifier full operating power. This approach is also a powerful analytic tool in our investigation.



Full-power-measured voltage and current waveforms.

While the effort is still in progress and any attempts at projections of final results (even in Task A) are still considered premature, some very significant findings have already been made. When optimized for maximum efficiency at the SPS frequency, a power amplifier stage using a transistor designed for 12 GHz operation yielded 71% power-added efficiency, a very impressive figure that exceeds the requirements of Task B.

This result was obtained at a power output close to 1 watt and a gain in excess of 11 dB. The mode of operation may be described as an inverted Class AB, since the drain current is highest at low rf drive and lowest at full rf drive -- the rf voltage turns off the device during a substantial fraction of the rf cycle, hence the high efficiency. However, when the same type of operation was attempted with a transistor of the same manufacturer (but rated at somewhat lower power output at 12 GHz), low efficiency was observed at 2.45 GHz, but at a power output much closer to the rated value. These results are presently



Test results - max. power and max. efficiency tuning.

under intensive investigation. The current and voltage waveform analyses are expected to shed some light on the hitherto unexplained aspects of this type of FET performance.

Both Task A and Task B will make use of power-combining circuits in the final amplifier configuration. A study of such circuits is included in the program.

SOLID-STATE SPS TECHNOLOGY FORECAST

Solid-State Technology is in a period of rapid growth in both the microwave and the signal-processing areas. Specific applications of this technology in a variety of spaceborne systems occur with increasing frequency and effectiveness. The roots of this great interest in solid-state devices, components, and integrated circuits have been, on the one hand, the commercial computer industry and its integrated-circuit logic components and, on the other, the military-systems interest in microwave solid-state devices. This trend is quite independent of the SPS concept. Thus the SPS will reap tremendous benefits from the very large investments made in this technology, investments that are certain to continue in the future.

The directions of technology research pertinent to the SPS concept span the entire gamut of fields familiar to the solid-state industry--materials, devices, circuits, processing methods, and automated test procedures. In the semiconductor materials area, gallium arsenide is presently the most important compound for microwave applications, while ternary and quaternary materials are being investigated for use, particularly at the higher microwave frequencies. The silicon-on-sapphire technology is likely to provide the SPS solid-state antenna with an excellent technology base for substrate materials.

New device concepts, in addition to the FET which presently appears to be the best candidate for amplifiers at the SPS frequency, are the vertical FET, the power MOS transistor, the SIT, and matrix transistors, all of which are in advanced stages of exploration at the present time.

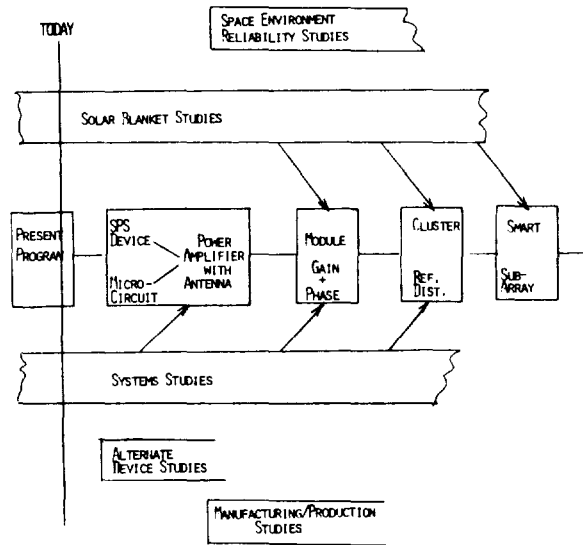
The most important area in circuit development is the return, after a hiatus of some years, to the concept of microwave lumped-circuit design. Lumped circuits designed for microwave frequencies extend FET operation to very high microwave frequencies. At 2.45 GHz, they permit extreme miniaturization of the amplifiers, making large distributed antenna arrays feasible.

Finally, modern processing methods -- e.g., ion-beam milling and plasma etching -- are likely to extend the techniques of the integrated-circuit chips to microwave circuits, while the selective implantation of impurities by means of ion implantation and laser annealing techniques point toward the fabrication of monolithic components directly on semi-insulating gallium arsenide.

These comments are not intended to imply that the SPS components -- both for signal-processing and for conversion to microwaves -- will not require specific and vigorous development. The attached diagram is a rough indication of the various microwave components which require study, development, and refinement in manufacturing techniques. We feel that the two most important areas requiring immediate attention are the following:

- o THE CONFIRMATION THAT A SMART-TYPE SOLID-STATE ANTENNA IS INDEED WORTHY OF SERIOUS CONSIDERATION AND SHOULD THEREFORE FORM PART OF THE MAIN-STREAM OF SPS STUDIES.

o THE INITIATION OF A SOLID-STATE POWER AMPLIFIER DEVELOPMENT PROGRAM AIMED SPECIFICALLY AT HIGH-EFFICIENCY SPS APPLICATION. THIS EFFORT SHOULD INCLUDE THE ACTIVE DEVICE AND THE MICROCIRCUIT MATCHING, INCLUDING ANTENNA, IN A SINGLE PACKAGE.



PROGRESS REPORT ON SOLID STATE SANDWICH CONCEPT

- DESIGNS, CONSIDERATIONS AND ISSUES -

Owen E. Maynard

Raytheon Company, Equipment Division

Presented At

Solid State Configurations Session of the SPS Microwave Systems Workshop
15-18 January 1980

Lyndon B. Johnson Space Center, Houston, Texas

ABSTRACT

Progress in analysis and design of solid state approaches to the SPS Microwave Power Transmission System is reviewed with special emphasis on the Sandwich concept and the issues of maintenance of low junction temperatures for amplifiers to assure acceptable lifetime. Ten specific issues or considerations are discussed and their resolution or status is presented.

Introduction and Background

Investigations of Microwave Power Transmission System (MPTS) concepts by Raytheon in the past have not addressed solid state approaches due primarily to the problem of trying to achieve long life (30 years) in an application where high power density and limited waste heat dissipation capabilities are inherent.

Solid state amplifier efficiencies for the current technology are too low (50% to 70% range) requiring 50 to 30% of the DC power to be radiated as waste heat while keeping junction temperatures within acceptable limits. Recent projections of solid state amplifiers have indicated that the efficiency may be as high as 80%, requiring 20% of the DC power to be radiated as waste heat reducing the problem by a factor close to 2.

Solid state amplifiers operate at low voltage, 20 V, compared to 20 kV to 40 kV for tubes and the DC power transmission and conditioning system weights, complexities and cost for known overall system concepts were of major concern for kV power distribution systems and incredible for low voltage systems. The solid state sandwich concept, where the DC power distribution is a simple grid interface with the static microwave portion of the sandwich, is such that investigation of the solid state approach became of considerable interest.

Results have been encouraging and the concept is considered to warrant further and more in-depth investigation. The critical outstanding issues include the need for demonstration of the high efficiency for the amplifiers. When this is accomplished, the issues and considerations discussed herein become important.

Results of Investigation by Raytheon for NASA-MSFC

Raytheon's investigation has included the following tasks:

1. Definition and Math Modeling of Basic Solid State Microwave Devices
2. Initial Conceptual Subsystem and System Design
3. Sidelobe Control and System Selection
4. Assessment of Selected System Concept
5. Parametric Solid State MPTS Data Relevant to SPS Concept

An efficiency goal for the DC to RF amplifiers of 80% has been established. Although this has not been demonstrated it is considered to be a realistic goal and is therefore the basis for the investigation. Parametric data for 75% and 85% are included.

Conceptual subsystem and system design investigations resulted in the following:

- (a) 1.95 km diameter transmitting antenna having uniform power density of 500 W/m^2 (RF);
- (b) 4.5 km beam diameter or minor axis rectenna having maximum power density of 23 mW/cm^2 ;
- (c) Free space sidelobes $< 0.1 \text{ mW/cm}^2$ for 2nd and further out sidelobes;
- (d) First sidelobe above 0.1 mW/cm^2 out to the fenced minor axis of 9.2 km;
- (e) Subarray size 32 x 32 elements 3.2m x 3.2m;
- (f) Microwave subsystem for spacetenna weight of $\sim 3 \text{ kg/m}^2$;
- (g) DC to DC efficiency of 0.51;
- (h) Total transmitted power of $\frac{\pi \times 1.95^2}{4} \times 500 \times 10^6 = 1.493 \times 10^9 \text{ W RF}$
- (i) DC power into antenna = $\frac{1.493 \times 10^9}{.99 \times .99 \times .8 \times .96 \times .98} = \frac{1.493 \times 10^9}{.738}$

$$= 2.02 \times 10^9 \text{ W DC}$$

- (j) Power out of rectenna to power grid = $1.49 \times 10^9 \times .98 \times .825 \times .89 \times .97$
= 1.04×10^9 W DC
- (k) Antenna concept is one amplifier/transmitting antenna element (narrow bandwidth) with element printed on tape $1/4 \lambda$ from ground plane. Receiving antenna elements are wide bandwidth and are orthogonal to the transmit elements to minimize adverse coupling.
- (l) Waste heat is passively radiated to deep space from pyrographite radiators having $\epsilon = 0.8$ and $\alpha = 0.05$ thermal control coatings. Waste heat (500 W/m^2) from the photovoltaic array is assumed to add to the heat load on the microwave side.
- (m) Single step taper at the transmitting antenna was investigated to determine sensitivity for reduction of 2nd sidelobe. Significant reduction is achievable with single step.
- (n) Further parametric investigations indicate that the RF power per element may be increased from 5 W/element to 6, thus permitting a significant reduction in spacetenna diameter for the same power density on the ground.
- (o) Further detailed investigation of the concept is warranted.

Issues/Considerations

The issues and considerations along with their resolution and status, shown in the attached table, have evolved during the investigation. Each of them will be discussed in turn in the oral presentation and copies of the visual aids will be made available.

SUMMARY AND CONCLUSIONS
SOLID STATE SANDWICH CONCEPT ISSUES AND RESOLUTION SUMMARY

<u>ISSUES/CONSIDERATIONS</u>	<u>RESOLUTION/STATUS</u>
LOW VOLTAGE DISTRIBUTION	FURTHER REFINEMENT REQUIRED TO MINIMIZE WEIGHT AND CONTROL THERMAL LEAKAGE
HARMONIC AND NOISE SUPPRESSION	FREQUENCY ALLOCATION NEEDS AT HARMONICS SHOULD BE CONSIDERED OR CONSIDER SPREAD SPECTRUM AND ACTIVE SUPPRESSION
SUBARRAY SIZE	3M X 3M MAY BE CLOSE TO OPTIMUM, FURTHER STUDY OF IMPLEMENTATION REQUIRED
MONOLITHIC TECHNOLOGY	MONOLITHIC APPROACHES APPLY AND REQUIRE TECHNOLOGY DEVELOPMENT FOR MINIMIZATION OF COST AND WEIGHT
LIFETIME	LIFETIME AFFECTED BY JUNCTION TEMPERATURE LIMITS AND CHARGED PARTICLE RADIATION REQUIRING TECHNOLOGY DEVELOPMENT IN BOTH AREAS
MUTUAL COUPLING	IMPLEMENTATION BY PRINTED DIPOLES SPACED FROM GROUND PLANE WITH BALUN IN CIRCUITRY AND CLOSE ELEMENT SPACING TO MINIMIZE DETRIMENTAL MUTUAL COUPLING EFFECTS
INPUT TO OUTPUT ISOLATION	ORTHOGONAL DIPOLES, OFFSET FREQUENCIES AND FILTERING PROVIDE SATISFACTORY ISOLATION OF TRANSMIT FROM RECEIVE SIGNALS
CHARGED PARTICLE RADIATION EFFECTS	GaAs IS CURRENTLY BEST TECHNOLOGY (REQUIRES MORE ADVANCEMENT IN "MECHANISMS" OF FAILURE)
TOPOLOGICAL CONSIDERATIONS	REQUIRED FUNCTIONS CAN BE IMPLEMENTED IN SANDWICH CONCEPT. FURTHER DETAILS AT SUBARRAY BOUNDARIES REQUIRED.
SIDELOBE SUPPRESSION	SINGLE STEP EDGE TAPER MAY BE REQUIRED.

CONCLUSIONS PRESENTED AT THE SOLID STATE CONFIGURATION SESSION

1. Solid state SPS concepts have not had the same depth of systems definition as the reference concept; however, preliminary results indicate the following.
 - a. The system sizing parameters optimize such that lower power is delivered to the utility grid.
 - b. The transmit antenna is larger primarily because of the thermal limitations.
 - c. The rectenna land requirement is smaller.
 - d. Weight per delivered kilowatt is projected to be more.
 - e. Maintenance projections are better because of the higher reliability.
2. Type of Power Amplifier - Based on studies to date, the GaAs FET is the preferred solid state power amplifier.
3. Antenna Unit Costs - Solid state antennas will have high parts count similar to the solar array, and therefore unit costs are a critical item.
4. Mitigating Designs - Conceptual designs have to some degree mitigated the issues of thermal and low voltage power distribution.
5. Items of Concern - Techniques of phase distribution, (possibly to more points on the array), and power distribution (on the end mounted configuration more DC-to-DC converters are required) are major items of concern in the solid state concept.
6. Technology - Associated technology development is more likely for solid state due to the advancing technology base.
7. Continued Investigation - Based on current findings, continued investigation of solid state concepts and issues is warranted.

REMAINING ISSUES - PRESENTED AT THE SOLID STATE
CONFIGURATION SESSION

1. High RF-DC conversion efficiency ($\geq 80\%$)
2. Gain and power output
3. Power combing
4. Low voltage distribution
5. Reliability/temperature tradeoffs
6. Phase stability and control
7. Unit costs
8. Amplifier RFI (noise, harmonics)
9. Monolithic technology
10. Mutual coupling
11. Input to output isolation
12. Charged particle and UV radiation effects

1. Report No. NASA CP-2141	2. Government Accession No.	3. Recipient's Catalog No.	
4. Title and Subtitle Solar Power Satellite Microwave Power Transmission and Reception		5. Report Date December 1980	
		6. Performing Organization Code	
7. Author(s) Coordinator R. H. Dietz		8. Performing Organization Report No. S-503	
		10. Work Unit No. 953-36-00-00-72	
9. Performing Organization Name and Address Lyndon B. Johnson Space Center Houston, Texas 77058		11. Contract or Grant No.	
		13. Type of Report and Period Covered Conference Publication	
12. Sponsoring Agency Name and Address National Aeronautics and Space Administration Washington, D.C. 20546		14. Sponsoring Agency Code	
		15. Supplementary Notes	
16. Abstract This volume contains papers presented at six technical sessions of the Solar Power Satellite (SPS) Workshop on Microwave Power Transmission and Reception, together with conclusions and remaining issues presented at the General Session. The meetings were held at the Lyndon B. Johnson Space Center, January 15-18, 1980, as part of the technical assessment process of the DOE/NASA SPS Concept Development and Evaluation Program. All aspects of SPS microwave power transmission and reception were addressed including studies, analyses, and laboratory investigations. The six technical sessions covered Microwave System Performance, Phase Control, Power Amplifiers, Radiating Elements, Rectenna, and Solid State Configurations.			
17. Key Words (Suggested by Author(s)) Antenna design Ionospheric disturbances Wave propagation		18. Distribution Statement Unclassified - Unlimited Subject Category 44	
19. Security Classif. (of this report) Unclassified	20. Security Classif. (of this page) Unclassified	21. No. of Pages 370	22. Price* \$10.50